

Thermal mass enhancement for energy saving in UK offices

Thomas Whiffen

MEng

Thesis submitted to the University of Nottingham
for the degree of Doctor of Philosophy

July 2016

*“Innovation is found on the boundary,
keep challenging the boundaries.”*

Abstract

UK government targets have set out energy-efficiency as a central strategy to meeting carbon reduction targets. End-use energy in the commercial sector accounts for 26% of building energy consumption. Space heating and cooling alone account for 33% of commercial building energy consumption. Low-energy technologies capable of moderating space temperatures offer energy efficient enhancement to commercial buildings. From literature, both sensible and latent thermal energy storage (TES) systems have demonstrated low-energy cooling capabilities. This work builds on the TES studies to date, investigating novel sensible, latent and combined active TES systems.

Following energy in buildings context, literature review, and research planning, enhancements to an industrial sensible active-TES system were investigated. A prototype active-TES system was designed, modelled and constructed under industrial guidance, then tested under fixed laboratory conditions. In laboratory conditions the WVHC (water-cooled and ventilated hollow core) performance was limited due to the volume of water in the closed water system; therefore under fixed operation strategies the VHC (ventilated hollow core) system outperformed the WVHC systems (seasonal COP of 8.1 compared to 0.5). Subsequently, control strategies were investigated to optimise the water cooling capabilities. Under optimised control the WVHC system demonstrated greater benefit than the VHC system, offering a seasonal COP of 10.6.

To deepen the investigation, the WVHC system was isolated from the room; the thermal response being modelled and tested under increasing thermal loads. The basic VHC system delivered 55W/m^2 of cooling. With open loop cool-water supply ($7\text{-}9^\circ\text{C}$) the WVHC achieved theoretical cooling over 135W/m^2 . COP figures for the VHC system (10.4-11.3) outperformed the WVHC (1.4-3.8) due to constant water flow in operation. When modelled in a room scenario, the VHC system maintained room comfort temperatures under thermal loads up to 200W/m^2 , equivalent to 35W/m^2 soffit heat flux.

Although demonstrating benefit, the embedded pipes required for the WVHC prototype were not feasible on a building level retrofit. A suitable retrofit PCM enhancement to the active-TES system was therefore investigated, initially through CFD modelling. A prototype of the optimal design was subsequently constructed and tested under laboratory conditions. The unit achieved 104W/m^2 and 61W/m^2 cooling with respective air velocities of 2.5 and 1.5m/s. The prototype was charged with a novel, bio-based PCM following differential

scanning calorimetry (DSC) assessment of a sample. The total TES capacity of the 25kg unit was 0.42 kWh.

To conclude the work, the prototype PCM unit was fitted to the VHC system (VPHC) and laboratory tested. Energy saving performance was compared against VHC and WVHC performance, as well as a reference chamber without hollow core (NoHC). Under laboratory diurnal-swing conditions the VHC, WVHC and VPHC systems saved, on average, 0.4, 1.1 and 0.8 kWh per day respectively, against the NoHC reference chamber. Under twelve-hour fixed-occupancy conditions without AC backup, the VHC, WVHC and VPHC systems reduced the temperature, on average by 2.9, 5.7 and 3.9°C respectively against the NoHC reference.

Using the modelling software IES, the chamber configurations were modelled and annual energy savings figures generated. From these figures, an economic assessment was carried out for a UK context. The WVHC system offered the greatest twenty year return on investment (£690,000 savings based on the moderate economic forecast for a 3,000m² single-storey building). The VPHC system was investigated for viability to the UK's non-domestic 'Green Deal' scheme. Based on the modelled energy savings and economic model, a price of £300 per PCM unit was required to achieve the 'golden rule' of five year payback.

Acknowledgements

Thank you to Christ Jesus, my saviour, redeemer, restorer, re-newer and inspirer. Thank you for making this work possible, working all things together for good and giving me grace to endure to the end. I gladly give my life to you and all I have done and ever hope to do. Be glorified in this place and in this work. Receive my worship as an offering wholly devoted to you. By your grace, let something arising from here bring an everlasting blessing to humanity.

To all those on earth who helped make this possible. Thank you to Prof. Riffat for his faith in me initially, his tireless work to secure funding and his on-going support to see this PhD through to completion. Thank you to all the other academic support I have received from staff in the Dept. of Architecture and the Built Environment (DABE). Thank you to Dr Tetlow for getting me started, thank you to Dr Su for refining my modelling, thank you to Dr Zheng for aiding my CFD work, thank you to Hu and Happiness for their assistance with the DSC work.

The author would like to thank J.Whiffen, Dept. Architecture and Built Environment, Tarmac Building Products, the Mark Group, Actimass Ltd and the Technology Strategy Board for their research funding. Without their willingness to support this work and their keen interest in the outcome, a successful PhD would not have been possible.

Thank you to all the other members of the DABE family for their immeasurable assistance in making these plans possible. Thank you to Zeny, Lyn and all the administrative support team, thank you to Dolly, Jonny, Andy and D.Taylor for interpreting my drawings and turning them into reality. Thank you to James, Tony, Scott and Malcom for their help with materials preparation, room construction and heavy lifting. Thank you to all those who helped with the big lifts!

Thank you to all the other members of the University of Nottingham who have broadened my experience whilst studying for this PhD. Thank you to Prof. Gillott for the opportunities to demonstrate labs and take Creative Energy Homes tours. Thank you to Dr Guzman and Dr Rodrigues for their assistance on conferences and presentations. Thank you to Dr Speight, Helen and all the MOOC team for the most fun I've had on a video conference.

Thank you to my friends throughout Nottingham. Thank you to Rev. and Mrs Hammond for their vision, faith, prayers, hospitality and friendship. Thank you to Mr and Mrs Payne who made starting this journey a joy, and filling my stomach each day. Thank you to Mr and Mrs Jackson whose friendship and hospitality have provided great nourishment. Thank you to all

my other friends at Saviour's Church in the Meadows; thank you for the times of worship, prayer, laughter, inspiration and tasty meals.

Thank you to my wider friends and family around the globe. Thank you to Ginny and Phil for funding an invaluable trip to California in my first year. Thank you for your care and support. Thank you for fun weeks and weekends away. Thank you for coming to our wedding and sharing in my life. Thank you to all those who have helped proof read my work. Thank you to Dr Garrett-Glass for putting up with my creative grammar and providing some rough polish. Thank you to Paul, Richard, Ella, Philip and Anna for all your contributions and time.

Thank you to all those who have inspired me, to all who wrote declarations and prayers for my office wall, and to all who worshipped at Bethel and around the world, by doing so you shifted the atmosphere at my desk. Thank you to my grandfather, William, my great-uncle, David and my grandpa, Douglas. Your life testaments inspire me each day to not hold back and pursue the plans God has for me.

Thank you to my parents, for starting this journey and giving me strength when I had none. Thank you for my Dad, Richard, who has always encouraged me to live an abnormal life. Thank you to my Mum, Jean, who funded this work initially. Thank you to my new parents-in-law Paul and Penny, for your love, care and devotion, especially to Martha.

Thank you Martha, my love, I cherish the time we have together and have valued your willingness to listen, serve, endure this time, to love me and look ahead. Thank you for your endless prayers and support. I delight to adventure with you. Let the adventure go on.

Finally, thank you to all those who prayed; my success is your success. Run with perseverance the race marked out for you, looking to Jesus the founder and perfecter of faith.

Table of Contents

| | |
|--|------|
| Abstract..... | i |
| Acknowledgements..... | iii |
| List of Figures | xi |
| List of Tables | xvii |
| Nomenclature | xxi |
| 1. Introduction | 1 |
| 1.1 Background | 1 |
| 1.2 Energy Context..... | 3 |
| 1.2.1 Energy Figures..... | 3 |
| 1.2.2 Governmental Measures | 4 |
| 1.3 Building Context..... | 6 |
| 1.3.1 Energy Usage..... | 6 |
| 1.3.2 Standards for Thermal Comfort and Energy Efficiency in Buildings | 11 |
| 1.3.3 Current State of Low Energy Technology in Service-sector Buildings | 13 |
| 1.4 Summary | 17 |
| 2 Literature Review..... | 19 |
| 2.1 Introduction | 19 |
| 2.2 Sensible Thermal Energy Storage Review | 20 |
| 2.2.1 Passive Thermal Mass | 20 |
| 2.2.2 Thermally Active Building Systems (TABs)..... | 20 |
| 2.2.3 Modelling of Sensible TES Systems..... | 27 |
| 2.2.4 Underground Thermal Energy Storage Systems (UTES) | 30 |
| 2.3 Latent Thermal Energy Storage Review | 31 |
| 2.3.1 Background | 31 |
| 2.3.2 Design Considerations..... | 37 |
| 2.3.3 Built Environment Applications | 55 |
| 2.3.4 PCM Modelling..... | 61 |

| | | |
|-------|---|-----|
| 2.3.5 | Barriers to PCM Utilisation..... | 64 |
| 2.3.6 | Further Applications..... | 67 |
| 2.4 | Thermal Energy Storage Contrast | 68 |
| 2.4.1 | Technology Contrast | 68 |
| 2.4.2 | Cost Contrast..... | 71 |
| 2.5 | Conclusions | 72 |
| 2.6 | Research Work Scope | 73 |
| 2.6.1 | Scope for Further Work | 73 |
| 2.6.2 | Hypothesis..... | 74 |
| 2.6.3 | Research Aim | 75 |
| 2.6.4 | Research Objectives..... | 75 |
| 2.6.5 | Thesis Overview | 76 |
| 3 | Active Thermal Mass Design and Model..... | 79 |
| 3.1 | Introduction | 79 |
| 3.1.1 | Scientific Background..... | 80 |
| 3.1.2 | Methodology..... | 81 |
| 3.1.3 | Contributions to knowledge | 82 |
| 3.1.4 | Chapter aims | 82 |
| 3.2 | Prototype Design | 83 |
| 3.2.1 | Prototype Design..... | 83 |
| 3.2.2 | Laboratory Rig Design | 86 |
| 3.3 | Active Thermal Mass Modelling..... | 87 |
| 3.3.1 | Modelling Background | 88 |
| 3.3.2 | Modelling Methodology..... | 89 |
| 3.3.3 | Modelling Guide..... | 101 |
| 3.3.4 | Annual Performance Investigation Method | 111 |
| 3.3.5 | Results and Discussion | 113 |
| 3.3.6 | Summary of Findings..... | 122 |

| | | |
|-------|---|-----|
| 3.4 | Conclusions | 124 |
| 4 | Active Thermal Mass Testing | 127 |
| 4.1 | Introduction | 127 |
| 4.1.1 | Methodology..... | 128 |
| 4.1.2 | Contributions to knowledge | 128 |
| 4.1.3 | Chapter aims | 129 |
| 4.2 | Prototype Construction & Installation | 130 |
| 4.2.1 | Prototype Construction Method..... | 130 |
| 4.2.2 | Chamber Fitting and Installation..... | 133 |
| 4.2.3 | Rig Capabilities, Limitations and Assumptions | 136 |
| 4.2.4 | Summary of Findings..... | 137 |
| 4.3 | Ventilated Thermal Mass Prototype Testing | 139 |
| 4.3.1 | System Enhancement Investigation..... | 139 |
| 4.3.2 | Variable Operating Conditions Twenty-four hour Test | 156 |
| 4.4 | VHC Model Validation..... | 169 |
| 4.4.1 | Validation Method | 169 |
| 4.4.2 | Validation Initial Results..... | 170 |
| 4.4.3 | Validation Summary..... | 172 |
| 4.5 | Conclusions | 174 |
| 5 | Sensible Thermal Mass Component | 177 |
| 5.1 | Introduction | 177 |
| 5.1.1 | Contributions to knowledge | 178 |
| 5.1.2 | Chapter aims | 179 |
| 5.2 | CFD Investigation | 180 |
| 5.2.1 | Modelling methodology..... | 180 |
| 5.2.2 | Simulation Parameters..... | 184 |
| 5.2.3 | Simulation Procedure..... | 186 |
| 5.2.4 | Mesh Independent Study..... | 186 |

| | | |
|-------|--|-----|
| 5.2.5 | Modelling Assumptions..... | 188 |
| 5.2.6 | Results..... | 189 |
| 5.2.7 | Discussion..... | 198 |
| 5.2.8 | Summary of Findings..... | 205 |
| 5.3 | Laboratory Investigation..... | 206 |
| 5.3.1 | Methodology..... | 206 |
| 5.3.2 | Results and Discussion..... | 212 |
| 5.3.3 | Summary of Findings..... | 218 |
| 5.4 | Performance Comparison and Validation..... | 220 |
| 5.4.1 | Initial Comparison..... | 220 |
| 5.4.2 | Table of Differences..... | 222 |
| 5.4.3 | Laboratory Data Calibration..... | 224 |
| 5.4.4 | Re-Modelling..... | 227 |
| 5.4.5 | Summary of Findings..... | 232 |
| 5.5 | Optimum Operating Method Generation..... | 233 |
| 5.5.1 | System Hierarchy..... | 233 |
| 5.5.2 | Maximum Theoretical Cooling Capacity..... | 233 |
| 5.5.3 | Optimum Operating Method..... | 234 |
| 5.6 | Room Model..... | 236 |
| 5.6.1 | Method..... | 236 |
| 5.6.2 | Model..... | 236 |
| 5.6.3 | Simulation Results..... | 243 |
| 5.6.4 | Discussion..... | 250 |
| 5.6.5 | Summary..... | 251 |
| 5.7 | Conclusions..... | 252 |
| 6 | PCM Component..... | 257 |
| 6.1 | Introduction..... | 257 |
| 6.1.1 | PCM..... | 258 |

| | | |
|-------|---|-----|
| 6.1.2 | Investigation context | 258 |
| 6.1.3 | Contributions to knowledge | 259 |
| 6.1.4 | Chapter aims | 259 |
| 6.2 | PCM Component Modelling..... | 260 |
| 6.2.1 | Methodology..... | 260 |
| 6.2.2 | Results and Discussion | 270 |
| 6.2.3 | Summary of Findings..... | 280 |
| 6.3 | PCM DSC Analysis..... | 282 |
| 6.3.1 | Method | 282 |
| 6.3.2 | Results and Discussion | 284 |
| 6.3.3 | Summary of Findings..... | 287 |
| 6.4 | Prototype PCM Diffuser Design and Construction..... | 288 |
| 6.4.1 | Design..... | 288 |
| 6.4.2 | Construction..... | 290 |
| 6.4.3 | Additional Diffusers..... | 296 |
| 6.5 | Prototype PCM Diffuser Proof of Concept Testing | 298 |
| 6.5.1 | Method | 298 |
| 6.5.2 | Results and Discussion | 300 |
| 6.5.3 | Summary of Findings..... | 312 |
| 6.6 | Conclusions | 313 |
| 7 | Pilot Scale Testing | 317 |
| 7.1 | Introduction | 317 |
| 7.1.1 | Contributions to knowledge | 318 |
| 7.1.2 | Chapter aims | 319 |
| 7.2 | Pilot Scale Prototype Testing | 320 |
| 7.2.1 | Installation Methodology..... | 320 |
| 7.2.2 | Test Method..... | 326 |
| 7.2.3 | Results and Discussion | 330 |

| | | |
|-------|--|-----|
| 7.2.4 | Summary of Findings..... | 347 |
| 7.3 | Economic Analysis..... | 350 |
| 7.3.1 | Economic Analysis Method..... | 351 |
| 7.3.2 | Modelling Method..... | 355 |
| 7.3.3 | Results..... | 357 |
| 7.3.4 | Summary of Findings..... | 363 |
| 7.4 | Conclusions..... | 364 |
| 8 | Conclusions..... | 369 |
| 8.1 | Introduction..... | 369 |
| 8.2 | Major Findings..... | 371 |
| 8.3 | Recommendations..... | 374 |
| 8.4 | Further Work..... | 376 |
| 8.5 | Concluding Remarks..... | 379 |
| 8.6 | Publications..... | 380 |
| 8.6.1 | Journal Papers..... | 380 |
| 8.6.2 | Accepted Abstracts..... | 380 |
| 8.6.3 | Conference Participation..... | 380 |
| 9 | References..... | 383 |
| 10 | Appendix A..... | 393 |
| | Theoretical 3-day Long simulation..... | 393 |
| | 4acph B(2) Investigation..... | 395 |
| 11 | Appendix B – Instrument Accuracy and Measurement Errors..... | 397 |

List of Figures

| | |
|--|----|
| Figure 1.1 - Technologies required to reduce CO ₂ emissions by 2050 [2] | 2 |
| Figure 1.2 - UK 2012 final energy consumption by sector (in Mtoe) [4] | 4 |
| Figure 1.3 - Final global energy consumption by sector and building energy mix in 2010 [8] ... | 6 |
| Figure 1.4 - Global Building Energy Flows in 2011 [10] | 7 |
| Figure 1.5 - Building Energy Consumption Breakdown [10] | 8 |
| Figure 1.6 - Worldwide office energy flows in 2011 [10]..... | 9 |
| Figure 1.7 - Service-sector Built Environment End-use Energy Breakdown in EJ for 2011 [10] | 11 |
| Figure 1.8 - Predicted Percentage of Dissatisfied (PPD) over various room temperatures and seasons (Winter/Transition Period and Summer) [12]..... | 12 |
| Figure 1.9 - Technologies commissioned in 2012/13 [14] | 14 |
| Figure 2.1 - Diurnal Temperature Cycle for TABS application [12] | 21 |
| Figure 2.2 - Thermal Active Building System (TABS) [24] | 23 |
| Figure 2.3 - Typical Hollow Core Air Network [33] | 24 |
| Figure 2.4 - Termodeck Slab Schematic | 24 |
| Figure 2.5 - 24 hour Hollow Core Operation [33] | 25 |
| Figure 2.6 - E.Fry Building Temperature Profiles | 26 |
| Figure 2.7 - Hybrid Radiant Floor System [42] | 27 |
| Figure 2.8 - Three Systems Simulated by [47] | 29 |
| Figure 2.9 - AHU Control Strategy for the Systems in Figure 2.8 [47] | 30 |
| Figure 2.10 - Comparison of Energy Storage Technologies [53]..... | 31 |
| Figure 2.11 - Change in Enthalpy versus Temperature for Water at 1atm..... | 33 |
| Figure 2.12 - Water Phase Transition Curve [59]..... | 33 |
| Figure 2.13 - Phase Transition Curve [52]..... | 34 |
| Figure 2.14 - Change in Temperature required to store 5,000kJ [60] | 35 |
| Figure 2.15 - Temperature vs Time graph displaying the different rates of heat transfer in Paraffin and Paraffin/EG[69]..... | 36 |
| Figure 2.16 - Incorporated PCM Design Flow Chart | 38 |
| Figure 2.17 - Design Flow Sheet..... | 39 |
| Figure 2.18 - Classification of Thermal Energy Storage Materials [63, 65]..... | 43 |
| Figure 2.19 - PCM Classification Tree [61] | 44 |
| Figure 2.20 - Melting Enthalpy and Temperature for a range of PCMs [62] redrawn from [59] | 46 |

| | |
|--|-----|
| Figure 2.21 - Melting Temperature versus Enthalpy for known PCMs with melting points between 0 and 35°C..... | 47 |
| Figure 2.22 - Comparison of Energy Stored and Released during a 24 hour period | 68 |
| Figure 2.23 - Comparison of Thickness Required to store 5,700kJ over 10°C [59] | 68 |
| Figure 2.24 - Variation of Concrete to A22H PCM mass ratio with respect to temperature change..... | 70 |
| Figure 2.25 - Current work on TES in Buildings [129] with proposed scope added in dashed orange | 73 |
| Figure 3.1 - Prototype Cutaway Drawing..... | 84 |
| Figure 3.2 - Simplified Rig Design..... | 86 |
| Figure 3.3 - Energy Balance Block Diagram..... | 90 |
| Figure 3.4 - Validation Performance: 24hr Summer Simulation..... | 100 |
| Figure 3.5 - Graphical Representation of Model..... | 101 |
| Figure 3.6 - Excel Heat Balance Time Step Model User Interface..... | 102 |
| Figure 3.7 - AHU Specification Menu | 103 |
| Figure 3.8 - Schematic and Menu options for AHU Configuration | 104 |
| Figure 3.9 - Schematic and Menu options for 'InDirect' AHU Operation | 105 |
| Figure 3.10 - Schematic and Menu options for 'Fan Only' AHU Operation | 106 |
| Figure 3.11 - Schematic and Menu options for 'NoSlab' Slab Configuration..... | 106 |
| Figure 3.12 - Schematic and Menu options for 'Slab' Slab Configuration | 107 |
| Figure 3.13 - Schematic and Menu options for 'Water' Slab Configuration | 107 |
| Figure 3.14 - Schematic and Menu options for 'VSlab&Water' Slab Configuration | 108 |
| Figure 3.15 - Schematic and Menu options for 'ConstFan' Night Cool option | 109 |
| Figure 3.16 - 3-D Drawing of the Theoretical Office with WVHC system highlighted | 111 |
| Figure 3.17 - Theoretical Office Plan..... | 112 |
| Figure 3.18 - Seasonal Performance (a) COP, (b) COP with Heat Recovery, (c) nCOP, (d) nCOP with Heat Recovery..... | 116 |
| Figure 3.19 - Simulated Annual Room Temperature Profiles | 118 |
| Figure 3.20 - Simulated Thermal Performance | 119 |
| Figure 3.21 - Simulated Energy Performance | 121 |
| Figure 3.22 - Normalised COP Performance | 122 |
| Figure 4.1 - Prototype under construction | 130 |
| Figure 4.2 - Outlet and Cross-over with embedded Thermocouples | 131 |
| Figure 4.3 - Additional Cast Concrete Layer..... | 131 |

| | |
|--|-----|
| Figure 4.4 - Air Shutters and Pipe Network | 132 |
| Figure 4.5 - Rotated, Raise and Installed Prototype Slab..... | 133 |
| Figure 4.6 - Fan, Water, Heating and Temperature Sensing Systems Installed..... | 134 |
| Figure 4.7 - Insulated Chamber..... | 134 |
| Figure 4.8 - Heater time schedule..... | 140 |
| Figure 4.9 - PassiveHC Temperature Profile | 143 |
| Figure 4.10 - 10VHC Temperature Profile..... | 144 |
| Figure 4.11 - 32VHC Temperature Profile..... | 144 |
| Figure 4.12 - 10WVHC Temperature Profile | 145 |
| Figure 4.13 - 32WVHC Temperature Profile | 145 |
| Figure 4.14 - Chamber Temperature Profiles for Constant Operation Systems..... | 147 |
| Figure 4.15 - Average Slab Temperature Profiles for constant operating conditions | 148 |
| Figure 4.16 - Heat transfer rate between slab and chamber | 151 |
| Figure 4.17 - COP Chart for Constant Operation Systems | 153 |
| Figure 4.18 - Temperature Profiles for Variable Operation Conditions..... | 159 |
| Figure 4.19 - 10WVHCpman Temperature Profiles | 160 |
| Figure 4.20 - 32WVHCa21pman Temperature Profiles | 160 |
| Figure 4.21 - 32WVHCa20p22.5 Temperature Profiles..... | 161 |
| Figure 4.22 - 32WVHCa20.5p21.5 Temperature Profiles..... | 161 |
| Figure 4.23 - Average Chamber Temperatures for Variable Operating Condition Tests..... | 162 |
| Figure 4.24 - Average Slab Temperatures for the Variable Operating Conditions Scenarios.163 | |
| Figure 4.25 - 24hr Variable Conditions Heat Transfer Rate | 164 |
| Figure 4.26 - 8hr Variable Conditions Heat Transfer Rate | 165 |
| Figure 4.27 - COP Chart for Variable Operating Conditions | 166 |
| Figure 4.28 - 10VHC Initial Comparison Temperature Profiles..... | 170 |
| Figure 4.29 - 10VHC Scenario Validation Updated Temperature Profiles | 171 |
| Figure 4.30 - 10VHC Scenario Validation Temperature Profiles | 172 |
| Figure 5.1 - Schematic diagram representing the modelling method | 180 |
| Figure 5.2 - (a) Typical 3 Core Slab, (b) Typical 4 Core Slab and (c) Prototype Air Slab | 182 |
| Figure 5.3 - (a) Prototype Pipe Network and (b) Simplified Embedded Pipe Network | 183 |
| Figure 5.4 - Prototype Air Slab at 0.22m/s air velocity and with 50W/m ² Soffit Heating | 190 |
| Figure 5.5 - Water Cooled Prototype Slab with 0.58m/s water velocity and 50W/m ² soffit heating | 191 |

| | |
|--|-----|
| Figure 5.6 - Air Prototype Slab with 0.22m/s air velocity under (a) 10W/m ² (b) 20W/m ² (c) 40W/m ² and (d) 50W/m ² ceiling soffit heat flux | 192 |
| Figure 5.7 - Internal wall and soffit temperature contours and (a) Water Pipe network, (b) Air Network with Air velocity of 0.22m/s and of (c) 0.88m/s all with a -50W/m ² heat flux on the Soffit..... | 194 |
| Figure 5.8 - Outer slab wall temperature contours of (a) Water Pipe network, (b) Air Network with Air velocity of 0.22m/s and of (c) 0.88m/s all with a -50W/m ² heat flux applied to the Soffit..... | 195 |
| Figure 5.9 - Heat Flux Contours of the Air Cooled Prototype Slab with Air Velocity of 0.22m/s and Soffit Heat Flux of 50W/m ² | 196 |
| Figure 5.10 - Soffit Temperature versus Soffit Heat Flux where Slab is cooling the Room | 198 |
| Figure 5.11 - Chart of Soffit Temperature versus Soffit Heat Flux where Slab is heating the Room..... | 198 |
| Figure 5.12 - Cross section of WVHC component Rig | 207 |
| Figure 5.13 - Insulated Palette with (a) Heat Mat and (b) Prototype Slab | 207 |
| Figure 5.14 - Air system with (c) 32W Fan, (d) AC Unit and (e) connecting duct | 208 |
| Figure 5.15 - Water System Installation..... | 208 |
| Figure 5.16 - Insulated Slab..... | 209 |
| Figure 5.17 - Slab 5 Temperature Profiles for each System with 50W/m ² Load | 212 |
| Figure 5.18 - Prototype Slab Heat Balance | 213 |
| Figure 5.19 - Heat Balance Graph for 50W/m ² Scenarios..... | 215 |
| Figure 5.20 - Final Slab Temperature against Heat Load Plot..... | 217 |
| Figure 5.21 - Effective thermal load (eLoad) against final average slab temperatures..... | 226 |
| Figure 5.22 - Updated Geometry Model and Mesh..... | 230 |
| Figure 5.23 - Room model with slab ceiling..... | 237 |
| Figure 5.24 - Medium-coarse and ultra-fine meshed room model | 242 |
| Figure 5.25 - Room model velocity vector isographic frame view..... | 243 |
| Figure 5.26 - Room inlet velocity vector frame view | 244 |
| Figure 5.27 - Slab air network velocity vector frame view | 244 |
| Figure 5.28 - Velocity contours (l) front on at a mid-point cross section and (r) whole room volume from the right side | 245 |
| Figure 5.29 - Room model isotherms with inlet velocity at 2m/s and floor heat flux at 75W/m ² | 246 |
| Figure 5.30 - Sizing graph: Internal thermal load against room temperature..... | 250 |

| | |
|--|-----|
| Figure 6.1 - 10kg Constant Mass Models of Configurations (A-D)..... | 261 |
| Figure 6.2 - 30mm Cross Section Models (A-D) | 262 |
| Figure 6.3 - Example of the first three CFD monitors reviewed | 266 |
| Figure 6.4 - Examples of the final two monitors reviewed over the twenty-four hour CFD simulations..... | 267 |
| Figure 6.5 - Air Temperature vs Time Chart..... | 271 |
| Figure 6.6 - PCM Liquid Fraction vs Time..... | 272 |
| Figure 6.7 - Heat Flux vs Time Chart | 273 |
| Figure 6.8 - PCM Liquid Fraction Comparison | 276 |
| Figure 6.9 - Heat Flux of Differing PCM | 276 |
| Figure 6.10 - PCM Liquid Fraction for B(2) Model under Different Conditions | 279 |
| Figure 6.11 - Chart of Heat Flux against Time for B(2) models under different conditions ... | 279 |
| Figure 6.12 - (a) SDT Q600 DSC-TGA and (b) Accompanying PC..... | 282 |
| Figure 6.13 - Alumina Crucibles, Temperature Probe and Furnace Entrance | 283 |
| Figure 6.14 - DSC Test for Energain® Sample..... | 284 |
| Figure 6.15 - DSC Test for X25..... | 285 |
| Figure 6.16 - X25 DSC Curve..... | 286 |
| Figure 6.17 - Diffuser Specifications Cross Section (in mm) | 288 |
| Figure 6.18 - PCM Diffuser Prototype Sketch (in mm)..... | 289 |
| Figure 6.19 - Modified PCM Diffuser Dimensions following mis-delivery (in mm) | 291 |
| Figure 6.20 - (a) Upper Layer of Diffuser Cut (b) Spacers between Lower Layer and Angled Base..... | 292 |
| Figure 6.21 - (c) Diffuser with undrilled tabs, (d) Lower Layer with Drilled Tabs and (e) Mild Steel Diffuser Attachment | 292 |
| Figure 6.22 - (f) Leak Testing Lower Tray, (g) Measuring Honeycomb and (h) Fitting Honeycomb..... | 293 |
| Figure 6.23 - (i) Lower Tray PCM Weight Before and (j) After Charging, and (k) Upper Tray Weight Before and (l) After Charging | 294 |
| Figure 6.24 - (m) Charged Lower Tray, (n) Embedded Thermocouple | 294 |
| Figure 6.25 - (o) Fully Charged X25 Diffuser | 295 |
| Figure 6.26 - (p) and (q) Diffuser Fitted inside Thermal Chamber and (r) Attached AC Duct Cooling Thermal Chamber | 295 |
| Figure 6.27 - Inert Celotex Diffuser..... | 296 |
| Figure 6.28 - Energain(r) Diffuser..... | 297 |

| | |
|---|-----|
| Figure 6.29 - Tested Diffusers (a) No PCM, (b) X25, (c) Energain(r)..... | 298 |
| Figure 6.30 - Thermal Chamber | 299 |
| Figure 6.31 - Chamber and Thermocouple Setup (dimensions in mm) | 300 |
| Figure 6.32 - Three hour Temperature Profiles without internal load | 301 |
| Figure 6.33 - Three Hour Temperature Profiles with internal Load of 50W/m ² | 302 |
| Figure 6.34 - AC-only Cooling-Saving Profiles | 303 |
| Figure 6.35 - Air Inlet (A2) Temperature Profiles during Chamber Heating | 304 |
| Figure 6.36 - A6-A2 Temp Profiles during Chamber Heating..... | 305 |
| Figure 6.37 - Chamber cooling Temperature profiles (PCM heat benefit | 307 |
| Figure 6.38 - Temperature Profiles with 0 and 50W/m ² Loads | 308 |
| Figure 6.39 - Saturated Heat Temperature Profiles..... | 310 |
| Figure 6.40 - Fully dissipated heat Temperature Profiles | 311 |
| Figure 7.1 - Constructed Test Chambers..... | 321 |
| Figure 7.2 - Slab and Frame Before and After the Lift Procedure..... | 322 |
| Figure 7.3 - Room B Temperature Sensors | 323 |
| Figure 7.4 - Temperature and Flow Meter Sensors wired into the DT500 Data Taker | 323 |
| Figure 7.5 - Installed Heat mat (l) and AC Units in Room A (c) and Room B (r)..... | 324 |
| Figure 7.6 - Diffuser Clip Extensions secured with Wooden Wedge | 325 |
| Figure 7.7 - Fitted Diffuser in Room A..... | 325 |
| Figure 7.8 - VHC Peak Period Temperature Profiles | 331 |
| Figure 7.9 - WVHC Peak Period Temperature Profiles..... | 332 |
| Figure 7.10 - VPHC Peak Period Temperature Profiles | 332 |
| Figure 7.11 - Temperatures for First 8hours..... | 333 |
| Figure 7.12 - VHC Temperature Profiles for the Diurnal Swing Tests..... | 335 |
| Figure 7.13 - WVHC Temperature Profiles from the Diurnal Swing Tests | 336 |
| Figure 7.14 - VPHC Temperature Profiles from the Diurnal Swing Tests..... | 336 |
| Figure 7.15 - First 8 'occupied' hour temperature profiles for diurnal swing tests | 338 |
| Figure 7.16 - Fixed-occupancy Ambient Temperature Profiles | 344 |
| Figure 7.17 - Fixed-occupancy Room A Temperature Profiles..... | 345 |
| Figure 7.18 - Fixed-occupancy Room B Temperature Profiles..... | 345 |
| Figure 7.19 - IES Laboratory Chamber Model..... | 356 |
| Figure 7.20 - Comparison NPV for each TES technology against Time (years) under moderate financial conditions | 361 |
| Figure 8.1 - TES technology tree [129] with thesis contributions added (orange)..... | 371 |

List of Tables

| | |
|--|-----|
| Table 1.1 - Service sector energy breakdown figures in EJ for 2011 [10] | 10 |
| Table 1.2 - Good Practice and Typical Office Energy Usage Figures taken from CIBSE Guide F Table 20.9 [9] | 13 |
| Table 2.1 - Desirable PCM Properties [53, 61, 74] | 40 |
| Table 2.2 - Commercially available PCMs with melting range between 21 and 28°C [63, 85, 86] | 49 |
| Table 2.3 - Properties of MicroPCM Slurry and Components [26] | 54 |
| Table 2.4 - Equation 2.5 Nomenclature Key | 62 |
| Table 2.5 - Energy Density Comparison | 70 |
| Table 3.1 - Slab based thermocouple locations for Figure 3.1 | 85 |
| Table 3.2 - Additional Hollow Core Parts Required | 86 |
| Table 3.3 - Annual Performance Simulation Parameters | 114 |
| Table 3.4 - Average Annual Comfort..... | 119 |
| Table 3.5 - Average Annual Energy Consumption | 120 |
| Table 4.1 - Instrument Accuracy | 137 |
| Table 4.2 - Constant system operating test conditions | 141 |
| Table 4.3 - U-Value inputs for Figure 4.16 | 151 |
| Table 4.4 - Energy Performance Data for Enhancement Scenarios..... | 153 |
| Table 4.5 - Variable Operating Test Conditions | 157 |
| Table 4.6 - U-value components [136, 137]..... | 164 |
| Table 4.7 - Variable Condition Energy Performance Data | 166 |
| Table 4.8 - Validation Boundary Conditions | 169 |
| Table 4.9 - Optimum Coefficients and Percentage differences of data..... | 172 |
| Table 5.1 - Boundary Conditions for CFD Simulations | 185 |
| Table 5.2 - Output Parameters | 185 |
| Table 5.3 - Mesh Parameters | 187 |
| Table 5.4 - Mesh Independent Results | 188 |
| Table 5.5 - Summary of Key Cooling Results at Steady State | 197 |
| Table 5.6 - Hollow Core Heating Coefficients (k) | 201 |
| Table 5.7 - Cooling Technology Recommendations..... | 203 |
| Table 5.8 - Industry Expected Performance Recommendations | 204 |
| Table 5.9 - Compiled Experiment Conditions Investigated..... | 210 |
| Table 5.10 - Exhaustive Experiment Conditions for each Scenario Investigated..... | 211 |

| | |
|---|-----|
| Table 5.11 - Air, Water, Slab and Insulation Physical Properties..... | 213 |
| Table 5.12 - Complete Heat Balance Summary | 214 |
| Table 5.13 - COP Figures at different Heat Loads | 216 |
| Table 5.14 - Laboratory Final Temperatures..... | 217 |
| Table 5.15 - Performance Coefficients..... | 217 |
| Table 5.16 - Modelling Final Temperatures | 221 |
| Table 5.17 - Laboratory Final Temperatures..... | 221 |
| Table 5.18 - Performance Coefficient Comparison..... | 222 |
| Table 5.19 - Table of Identified Differences..... | 223 |
| Table 5.20 - Effective Thermal Load Final Temperatures | 225 |
| Table 5.21 - Effective thermal load (eLoad) performance coefficients | 226 |
| Table 5.22 - 20VHC Conditions and Final Slab Temperatures..... | 227 |
| Table 5.23 - 32VHC Conditions and Final Slab Temperatures..... | 228 |
| Table 5.24 - WHC Conditions and Final Slab Temperatures | 228 |
| Table 5.25 - Performance Coefficient Comparison under same conditions..... | 229 |
| Table 5.26 - Matched Geometry Final Slab Temperature Comparison | 230 |
| Table 5.27 - Updated Geometry Performance Coefficients | 231 |
| Table 5.28 - Average COP Figures | 233 |
| Table 5.29 - Maximum Theoretical Cooling Capacity | 234 |
| Table 5.30 - Optimum Operating Conditions and System Hierarchy..... | 235 |
| Table 5.31 - Room model boundary conditions..... | 238 |
| Table 5.32 - Overview of certain terms for Equation 5.8, Equation 5.9, Equation 5.10 and Equation 5.11 | 239 |
| Table 5.33 - Radiant independence model boundary conditions..... | 240 |
| Table 5.34 - Radiant independence model simulation results | 240 |
| Table 5.35 - Mesh parameters..... | 241 |
| Table 5.36 - Mesh independence results..... | 242 |
| Table 5.37 - Room simulation results | 247 |
| Table 5.38 - Side wall semi-transparent temperature gradients for each room model scenario | 248 |
| Table 5.39 - Central plane temperature gradients for each room model scenario..... | 249 |
| Table 6.1 -10kg Constant-Mass Models Dimensions..... | 263 |
| Table 6.2 - Thirty-millimetre Cross-sectional Models Dimensions | 263 |
| Table 6.3 - Summary Ratios for 10kg Constant-Mass Models | 264 |

| | |
|---|-----|
| Table 6.4 - Volume multipliers and summary ratios for the thirty-millimetre cross-section models..... | 264 |
| Table 6.5 - Mesh Parameters..... | 268 |
| Table 6.6 - PCM Temperature under differing Mesh Parameters..... | 268 |
| Table 6.7 - Time-step Independence Settings..... | 269 |
| Table 6.8 - Time-step Independence Results..... | 269 |
| Table 6.9 - Iteration Independence Results..... | 270 |
| Table 6.10 - Power Output..... | 274 |
| Table 6.11 - PCM Properties..... | 275 |
| Table 6.12 - Cooling Capacity Data (18-28°C)..... | 277 |
| Table 6.13 - Different Test Conditions..... | 278 |
| Table 6.14 - A22H Power Output at Different Conditions..... | 280 |
| Table 6.15 - X25 Power Output at Different Conditions..... | 280 |
| Table 6.16 - Literature and Laboratory DSC Data..... | 286 |
| Table 6.17 - Cooling Power with flow rate of air at 1.5m/s..... | 306 |
| Table 6.18 - Chamber Cooling (PCM heating Benefit)..... | 307 |
| Table 7.1 - Pilot-scale test chamber Test Log..... | 327 |
| Table 7.2 - Peak-cooling-demand Test Conditions..... | 328 |
| Table 7.3 - Diurnal-swing Test Conditions..... | 329 |
| Table 7.4 - Fixed-occupancy Test Conditions..... | 330 |
| Table 7.5 - Day one Peak Temperature Delay..... | 339 |
| Table 7.6 - Day two Peak Temperature Delay..... | 339 |
| Table 7.7 - Energy Consumption Figures for Week Long Tests..... | 341 |
| Table 7.8 - COP Comparison across the test conditions and systems..... | 342 |
| Table 7.9 - Average Occupied Temperature Difference..... | 346 |
| Table 7.10 - Data Inputs for Electrical Supply..... | 346 |
| Table 7.11 - Daily Savings based on diurnal swing results..... | 347 |
| Table 7.12 - Capital Costs..... | 351 |
| Table 7.13 - IES Model Construction..... | 356 |
| Table 7.14 - Daily Savings based on diurnal swing results..... | 358 |
| Table 7.15 - Moderate Projection: Energy Price Rise by 9.8% annually; Interest Rate at 5%.358 | 358 |
| Table 7.16 - Optimistic Projection: Energy Rise 11.1%Annually; Interest at 2%. | 358 |
| Table 7.17 - Conservative Projection: Energy Rise 8.5%Annually; Interest at 10%. | 359 |
| Table 7.18 - Moderate Projection: Energy Price Rise by 9.8% annually; Interest Rate at 5%.360 | 360 |

| | |
|--|-----|
| Table 7.19 - Optimistic Projection: Energy Rise 11.1%Annually; Interest at 2%. | 360 |
| Table 7.20 - Conservative Projection: Energy Rise 8.5%Annually; Interest at 10%. | 361 |
| Table 7.21 - Internal Rate of Return | 362 |
| Table 11.1 - Instrument Accuracy | 397 |

Nomenclature

| Symbol | Term | Units |
|-----------|--|----------------------|
| a | Latent Heat Factor | - |
| A | Area | m^2 |
| acph | Air changes per hour | <i>per hour</i> |
| b | melting width | - |
| C_{eff} | Effective Heat Capacity | J/kgK |
| C_p | Specific Heat Capacity | J/kgK |
| C_s | Solid State Specific Heat Capacity | J/kgK |
| d (or D) | diameter | m |
| D_{opt} | Optimum Wall thickness | M |
| E | Energy | J |
| EJ | Exa-Joules (10^{18} Joules) | |
| f | friction factor | |
| g | gravitational constant | m^2/s |
| h | Average Heat transfer coefficient | W/m^2K |
| h | height | m |
| h | Specific Enthalpy | J/kg |
| H_f | Latent heat of formation | kJ/kg |
| H_v | Latent heat of vaporisation | kJ/kg |
| I | Irradiance | W/m^2 |
| k | performance coefficient (or conductivity) | (W/mK) |
| l (or L) | length | m |
| M | Mass | kg |
| \dot{m} | Mass flow rate | kg/s |
| Mtoe | Million tonnes of oil equivalent | |
| N | Number of air changes | - |
| p | Partial pressure | Pa |
| P | power | W |
| Q | Energy | J or kJ or kWh |
| q | Flux | J/s or W |
| r | constant | |
| Re | Reynolds Number | |
| T | Temperature | $^{\circ}C$ |
| t | Time | <i>Seconds</i> |
| u | Initial velocity | m/s |
| U | Overall Heat Transfer Coefficient | W/m^2K |
| V | Volume | m^3 |
| v | velocity | m/s |

| | | |
|------------|-------------------|-------------------------|
| W | Work done | <i>J or kWh</i> |
| x | length | |
| α | | |
| β | Liquid Fraction | - |
| Δ | Change in | - |
| ϵ | emissivity | <i>m</i> |
| η | efficiency | |
| μ | viscosity | <i>Pa.s</i> |
| π | Pi | - |
| ϕ | Mass Fraction | - |
| ρ | Density | <i>kg/m³</i> |
| τ | Time Period | <i>Seconds</i> |
| ν | Dynamic viscosity | <i>Pa.s</i> |

Chapter 1: Introduction

The case for low-energy cooling

1. Introduction

1.1 Background

Throughout human history, the never-ending pursuit of knowledge has led to countless breakthroughs and innovation. From our ancient roots, the exponential accumulation of discovery, development and delivery have seen humanity subdue the planet; making even extreme locations on earth inhabitable environments. Each innovation has enabled new expectations for life: industrialised farming secured food supplies; the industrial revolution enabled mass transportation and increased output; and the current information age has created instantaneous-worldwide access.

With each new age, new possibilities arise; what were distant dreams of our ancestors become considered a basic human right for our children. The benefit to human wellbeing and societal development continues to accelerate. The acceleration of human civilisation, fuelled by ambition, only stops when the side effects of development become toxic to further development. It is at such a juncture that society finds itself today.

Population growth, industrialisation of developing nations, access to worldwide knowledge, increasing levels of welfare, economic growth and human ambition put increasing demands on our natural world. Sustainability, the buzz word of the 21st century, seeks to satisfy all these drivers and carve a viable path. Sustainability aims to create a future where societal and economic growth persists unhindered by the limited bounds of the environment.

Although still egocentric, to accomplish this sustainable future, care and consideration regarding the side effects of development have become paramount. Increasing efficiency of material acquisition, processing, delivery and use has become essential. The need for sustainability persists throughout society to reduce our impact on natural cycles. The energy cycle remains a pressing need for sustainable innovation. The United Kingdom coalition government (of 2010-2015), in The Energy Efficiency Strategy 2012 [1], set out energy-efficiency as a key strategic objective to decarbonise the UK, maintain secure energy supplies and increase the productivity of businesses.

Worldwide, increasing numbers of political and non-governmental organisations have set out low-carbon energy strategies on a national and international level. Central to these plans is a reduction in greenhouse gas emissions. Figure 1.1, from the International Energy Association's (IEA) Energy Technology Perspectives 2010 publication [2], highlights the major technologies capable of achieving significant CO₂ emission reductions by 2050. Shifts in end-use actions account for 53% of CO₂ reduction strategies; improving end-use fuel and electricity efficiency contribute 38%, more than double the 17% contribution made from renewables [2]. To establish a sustainable future will require a holistic approach with all technologies and stakeholders contributing to carbon reductions and energy savings.

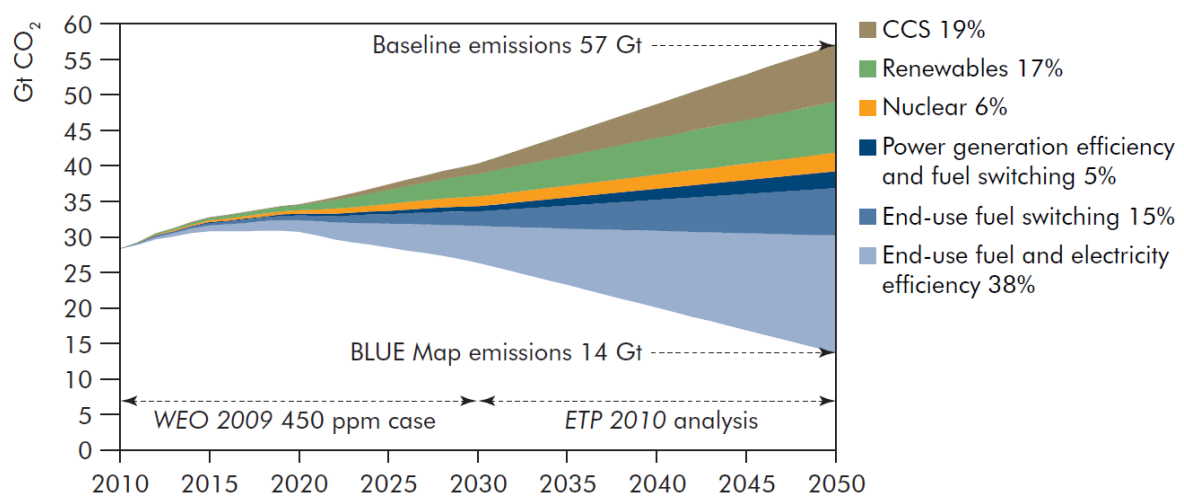


Figure 1.1 - Technologies required to reduce CO₂ emissions by 2050 [2]

1.2 Energy Context

Intrinsic to developed society and fundamental to human quality of life is readily available energy. On-demand electricity has become a basic human right in developed nations; powering essential and luxury daily activities alike. Despite the growing infrastructure, during and since the industrial revolution, modern challenges have arisen in the energy sector. Spurred on by the 1997 Kyoto Protocol and subsequent international summits, the case for climate-change mitigation has drawn attention to the negative effects of society's energy-rich CO₂-emitting habits (oil fuelled transportation, coal powered electricity generation, etc).

As climate-change science gathered evidence, political calls for innovation in the energy sector were noted; as many developed nations sought energy independence. The goal to secure a stable supply was strengthened through the 1970s energy crises, where oil costs rose to over 35\$ per barrel in the US (based on the value of dollars in the year 2000) [3]. In the UK today, although supply remains stable through international trade deals, the volatile political climates ensconcing Russia and the Middle East continue to motivate governments to obtain further energy security [1].

Further to the environmental and political drivers, sufficient investment in renewable generation and associated infrastructure offer economic benefits. Once established, an energy network where fuel is negated and electricity generated from naturally available renewable energy will reduce energy costs. Establishing expertise in the field also offers export opportunities. Currently, further work is required to reduce the cost of infrastructure and enhance the economic case for holistic renewable energy generation.

There is undoubtable evidence to suggest securing a sustainable energy supply-chain and infrastructure will bring holistic (social, environmental and economic) benefit. The human impact on climate change can be reduced, benefiting at-risk societies and the political and social security of a nation's wellbeing secured; all whilst avoiding variable fuel costs and harnessing available energy. Central to achieving sustainable energy infrastructure is satisfying the ever-increasing demand imposed by worldwide population growth. The built environment sits at the heart of this conundrum, seeking to house and facilitate ever-improving quality of life without overstressing nature's capability to provide.

1.2.1 Energy Figures

In 2012, European Union (EU) member states accounted for 1,683.5Mtoe (70.5EJ) of gross inland energy consumption [4]. The UK, accounting for 12.6% of the EU population,

accounted for 12.0% of the energy consumed throughout the EU (202.3Mtoe or 8.5EJ). After distribution and losses the final UK energy consumption in 2012 was 134.0Mtoe (5.6EJ). Figure 1.2 conveys the sector breakdown of UK energy consumption. Industry, transport and household consumption accounts for over 86% of national consumption. The service sector accounts for 12% of final energy consumption. Agriculture, fishing and others account for the remaining 2%. Consumption within the domestic and commercial built environment (household and service sectors) amounted to 55.8Mtoe in 2012 (41.6%) [4].

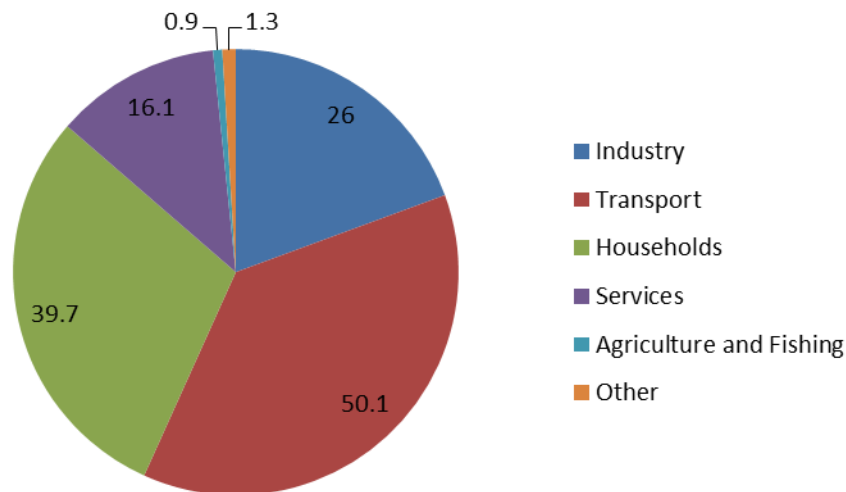


Figure 1.2 - UK 2012 final energy consumption by sector (in Mtoe) [4]

Between 1973 and 2000 energy consumption rose by 68.4% within the commercial sector, in contrast to a 70.2% rise in the transport sector [5]. Energy intensity (energy consumption divided by contribution to gross domestic product (GDP)) has not improved since the late 1980s, suggesting a lack of energy efficiency improvement. The commercial output from the commercial sector has rapidly grown, however energy consumption has increased at a similar rate. Trends at the turn of the millennia suggested a doubling of office floor space every twenty-five years in the UK. Additionally, UK offices are increasingly being fitted with chiller technologies in response to overheating cases, leading to increased end-use energy demand from the commercial sector.

1.2.2 Governmental Measures

In the UK, following the oil shocks of the 1970s, the Department of Energy first issued policies to reduce energy demand [1]. Since the Kyoto Protocol was first signed efforts to overcome inhibiting market-forces and initiate a sustainable revolution have been taken. The UK

government has continued to introduce new legislation; set legally binding targets for industry sectors and significantly fund research in the sustainable energy technology field.

In the past decade the UK government passed the UK Climate Change Act 2008, implementing Kyoto emission targets. In 2009 the Energy Performance Certificate (EPC) became mandatory in the UK to fulfil the EU Energy Performance of Buildings Directive. The directive required all buildings to have certificates characterising their energy performance and emission ratings at the point of construction, sale or every ten years. The intended purposes of the scheme were to enable buyers to select dwellings based on their energy efficiency, and make investors aware of the energy related risks of their assets [6].

The Energy Act 2011 aims at reducing fossil-fuel dependency and energy demand. In the UK the Department for Energy and Climate Change continues to spearhead delivery of the government's target to reduce carbon emissions by 80% by 2050 [7].

Amidst the targets, the 2010-15 coalition government set out detailed strategic plans to deliver a low-carbon future. The UK government's Energy Efficiency Strategy 2012 [1] targeted solutions for the commercial and industrial sectors as well as domestic dwellings. The government saw investment in energy efficiency as offering holistic benefit. Commercially, by growing expertise and innovation in the UK, greater exploitation of export markets could open up. Socially, energy efficiency was a mainstay in the government's strategy for reducing fuel poverty. Environmentally, a reduction in energy demand will reduce overall emissions.

The strategy projected the policy package would save 163TWh in 2020 and 217TWh in 2030, against business as usual projections. The EU has set out a 20% primary energy reduction by 2020 against 2007 business as usual projections [1]. The UK government has recognised the need for reducing end-use energy demand and implementing widespread efficiency measures. They also recognised the global opportunity, economically and academically, to lead the world in energy-efficient measures.

1.3 Building Context

Globally, the building sector was the largest end-use energy sector in 2010, based on final energy consumption figures in Figure 1.3 [8]. Assessment by the International Energy Agency (IEA) projects a 50% rise in energy demand within the building sector by 2050, in business as usual models. It was identified that with stringent building codes and energy-efficient retrofit aggressively encouraged, a 25% (40EJ) reduction in energy demand is possible against business as usual projections [8].

Although needed across all sectors, the need for implementation of end-use energy-reduction measures is essential within the built environment. Within the last fifteen years, the sustainable building strategy in the UK has shifted from a renewable generation focused approach to a fabric first approach; that seeks to minimise whole-life energy requirement from the initial design and construction stages. Recognising the need for industry guidance, the Chartered Institute of Building Service Engineers (CIBSE) launched their Guide F on Energy Efficiency in Buildings in 2012 [9].

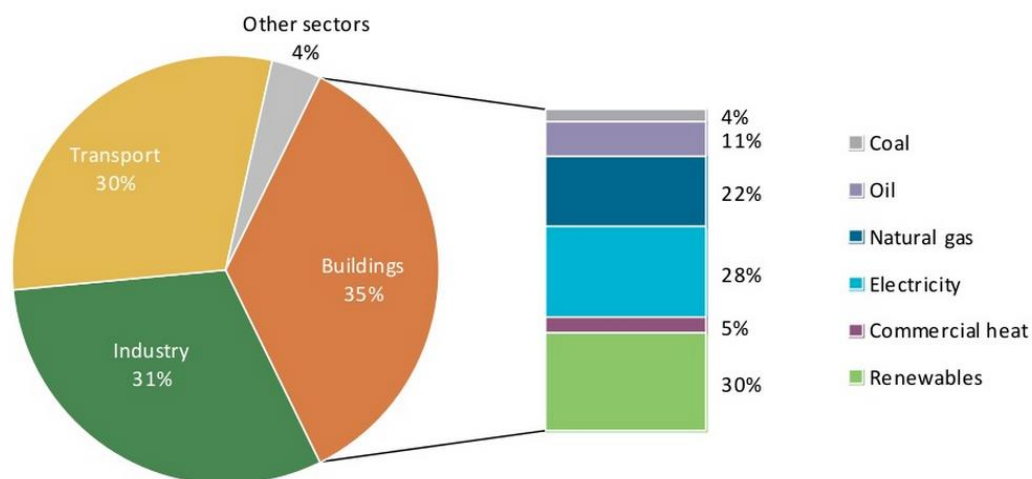


Figure 1.3 - Final global energy consumption by sector and building energy mix in 2010 [8]

1.3.1 Energy Usage

1.3.1.1 Buildings

Assessments made by the International Energy Agency (IEA), demonstrate the energy flows in the building sector across the world in 2011. Figure 1.4 charts the findings demonstrating the fuel makeup, sector usage and end-use purpose. In total 543EJ of energy are produced worldwide during 2011 with 348EJ consumed as end-use energy, of which 118EJ are consumed within the built environment [10].

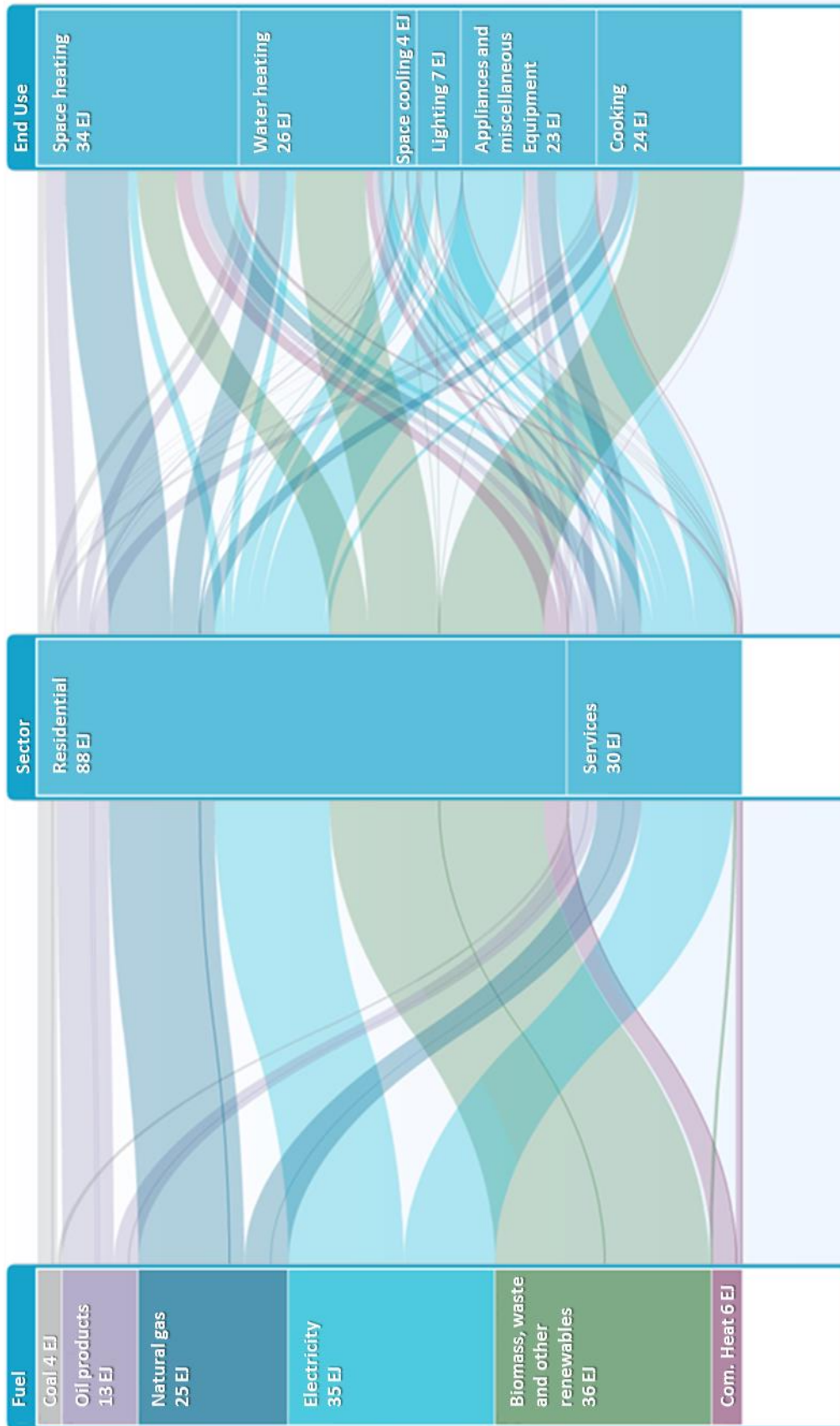


Figure 1.4 - Global Building Energy Flows in 2011 [10]

Taking the figures from Figure 1.4 and representing them as a percentage, Figure 1.5 charts the energy usage breakdown. As a percentage, space heating and cooling accounts for 33% (38.4EJ) of all building energy consumption.

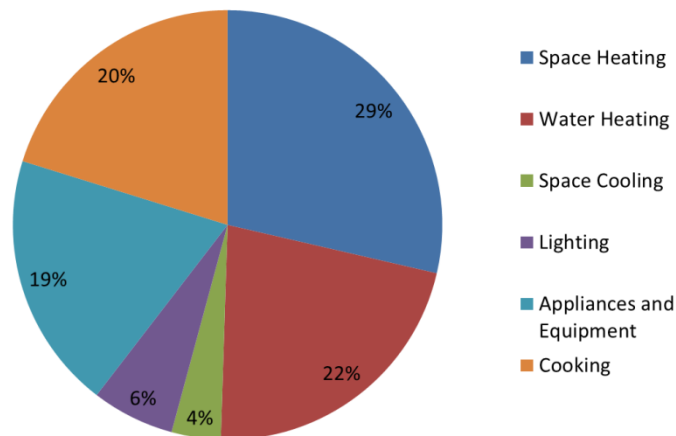


Figure 1.5 - Building Energy Consumption Breakdown [10]

1.3.1.2 Service Sector Buildings

The service sector accounts for 26% of building energy consumption, 9% of worldwide consumption; therefore differences made across the service sector built environment can have a real effect on the overall global-energy consumption figures. In the UK commercial building sector this equates to approximately 0.5EJ per year [4, 10]. The figures presented in Figure 1.6 represent the energy flows based on fuel source and end-use for the global service sector in 2011.

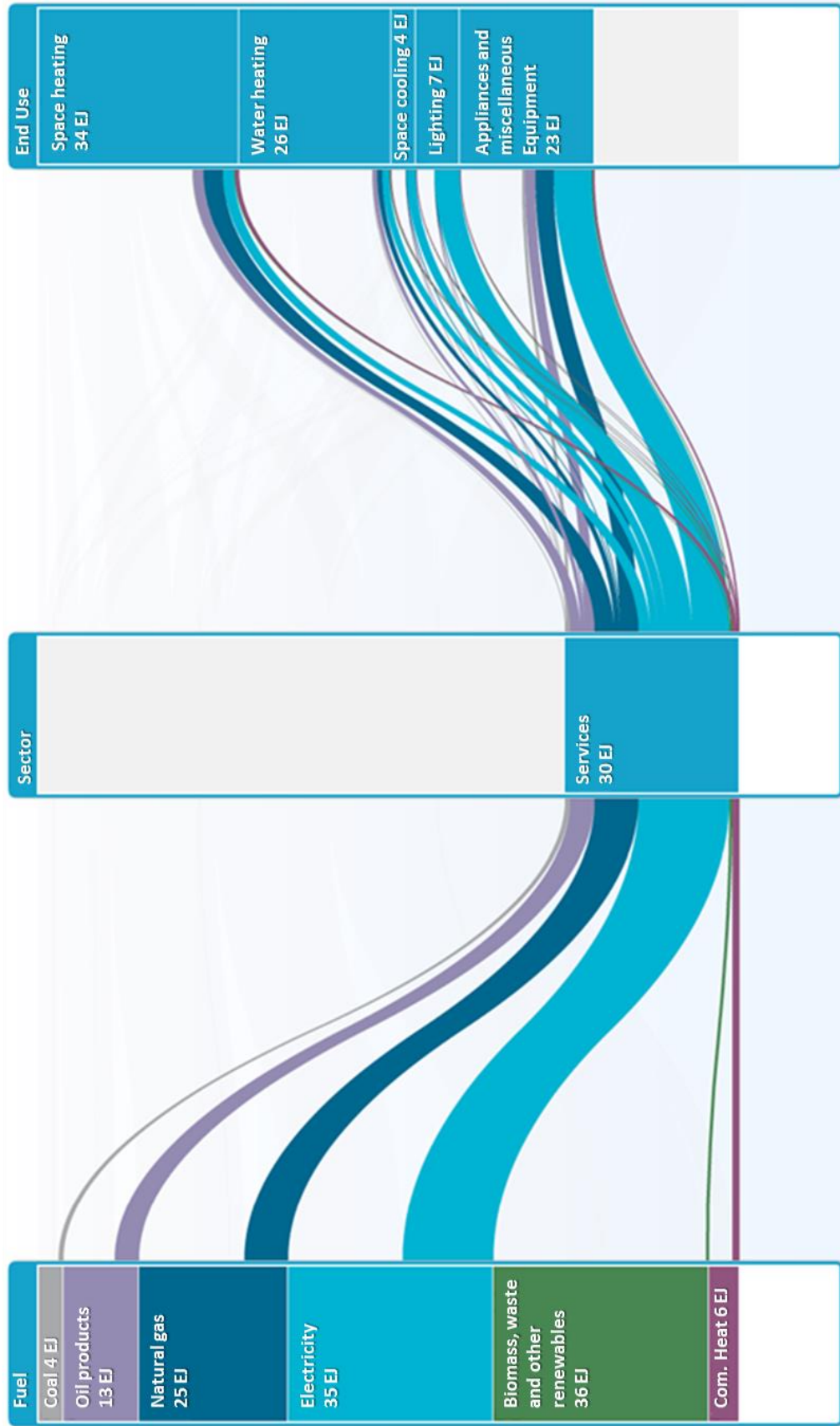


Figure 1.6 - Worldwide office energy flows in 2011 [10]

Worldwide, in 2011, 43% of energy consumed in the service-sector built environment was supplied from fossil fuels; with renewables accounting for 3% in the fuel mix. In total, the overall energy consumed in offices was 30.3EJ in 2011 (Table 1.1).

Table 1.1 - Service sector energy breakdown figures in EJ for 2011 [10]

| Service Energy Consumption | | | | | |
|-----------------------------------|----------------------|----------------------|----------------------|-----------------|---------------------------------|
| (all units in EJ) | <i>Space Heating</i> | <i>Water Heating</i> | <i>Space Cooling</i> | <i>Lighting</i> | <i>Appliances and Equipment</i> |
| Total | 8.3 | 3.6 | 1.9 | 4.2 | 12.3 |
| Coal | 0.3 | 0.2 | 0 | 0 | 0.5 |
| Oil | 1.8 | 0.7 | 0 | 0 | 1.8 |
| Natural Gas | 3.3 | 1 | 0.3 | 0 | 3.1 |
| Electricity | 1.9 | 1.2 | 1.6 | 4.2 | 6.3 |
| Renewables | 0.2 | 0.3 | 0.02 | 0 | 0.3 |
| Commercial Heat | 0.8 | 0.2 | 0 | 0 | 0.3 |

Assessing the end-use energy demand, 41% of commercial sector energy is consumed by appliances and equipment. Growing dependency on smart network-connected electronics, where data is available all the time, is putting an increasing demand on service sector energy supply. From Figure 1.7, 33% of end-use energy is consumed through space heating and cooling. The demand for energy supply to facilitate modern commercial and service sector infrastructure continues to rise, putting extra stress on energy markets and the environment. To meet the government climate change targets, energy-efficient measures throughout the service-sector built environment are essential.

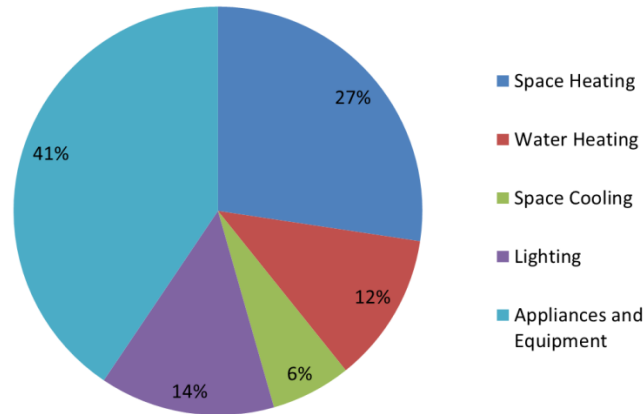


Figure 1.7 - Service-sector Built Environment End-use Energy Breakdown in EJ for 2011 [10]

1.3.2 Standards for Thermal Comfort and Energy Efficiency in Buildings

Commercial buildings create a synthetic environment within an external climate to facilitate business operations. In 2011, 10.2EJ were used worldwide to maintain thermal comfort within commercial buildings [10]. The international standard, ISO 7730, for thermal comfort defines thermal comfort as, “that condition of mind which expresses satisfaction with the thermal environment.” However, since each individual preferences differ, indices were developed to predict the percentage of dissatisfied (PPD) occupants and determine a standard for building thermal comfort [11].

The curves displayed in Figure 1.8 were generated using the PPD approach, in accordance with ISO 7730 [11]. During winter and transitional periods (Wi/Tp), room temperature should be maintained between 21 and 24.5°C, to remain below the 6% PPD threshold. During summer months (Su), the maximum comfort temperature increases to 26°C. In extremes, maintaining a PPD of less than 20%, the temperature range may vary between 18 and 28°C depending on employee seasonal dress.

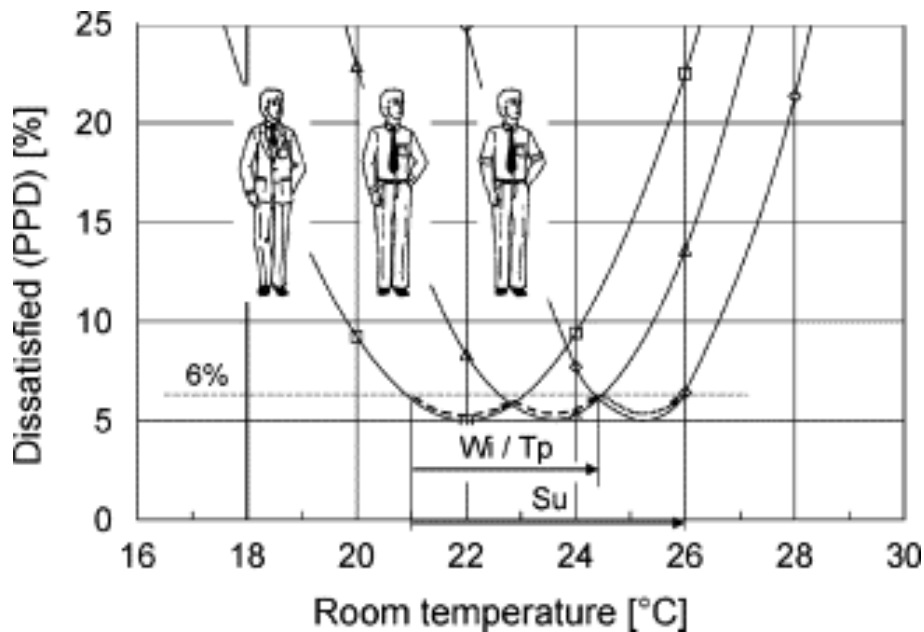


Figure 1.8 - Predicted Percentage of Dissatisfied (PPD) over various room temperatures and seasons (Winter/Transition Period and Summer) [12]

To accommodate the twin drivers of building thermal comfort and energy efficiency within the UK, CIBSE released the third edition of their Guide F – Energy Efficiency in Buildings [9]. In it CIBSE set out energy-efficient design guidance for the UK building industry. CIBSE state that, “an energy efficient building provides the required internal environment and services, with minimum energy use, in a cost effective and environmentally sensitive manner.” In response to legally-binding government targets on greenhouse-gas emissions, the building service engineer guide outlines implementation principles to ensure low-energy demand; energy-efficient buildings are designed and delivered within the UK.

The purpose of the energy efficient design strategy is to provide thermal comfort and acceptable air quality with minimum use of energy. The design strategy set out in the guide [9] notes the increasing part ventilation plays in building energy losses, due to improved levels of insulation reducing conduction losses. The energy-efficient design strategy, therefore, majors on ventilation network measures:

- 1) Air tight envelope
- 2) Minimum air changes necessary
- 3) Passive solutions before active solutions
- 4) Efficient plant equipment
- 5) Energy recovery
- 6) Reduce duct losses
- 7) Effective controls

As well as design strategy methods, the guide offers benchmark energy figures as displayed in Table 1.2. Taken from CIBSE Guide F, Table 1.2 outlines good and typical practice energy consumption figures for different office systems within the UK commercial building stock [9]. Based on the figures in Table 1.2, the energy demand from an Air Conditioning (AC) system (combining cooling and fan, pumps and controls demand) should be 44 kWh per m² per year, for a good practice energy-efficient system; 91 kWh per m² per year for a typical system.

Table 1.2 - Good Practice and Typical Office Energy Usage Figures taken from CIBSE Guide F Table 20.9 [9]

| System | Delivered energy for stated office type / (kW·h·m ⁻²) per year | | | | | | | |
|-------------------------------|--|---------|---------------|---------|---------------|---------|---------------|---------|
| | Type 1 | | Type 2 | | Type 3 | | Type 4 | |
| | Good practice | Typical | Good practice | Typical | Good practice | Typical | Good practice | Typical |
| Gas/oil heating and hot water | 79 | 151 | 79 | 151 | 97 | 178 | 107 | 201 |
| Catering gas | 0 | 0 | 0 | 0 | 0 | 0 | 7 | 9 |
| Cooling | 0 | 0 | 1 | 2 | 14 | 31 | 21 | 41 |
| Fans, pumps and controls | 2 | 6 | 4 | 8 | 30 | 60 | 36 | 67 |
| Humidification | 0 | 0 | 0 | 0 | 8 | 18 | 12 | 23 |
| Lighting | 14 | 23 | 22 | 38 | 27 | 54 | 29 | 60 |
| Office equipment | 12 | 18 | 20 | 27 | 23 | 31 | 23 | 32 |
| Catering electricity | 2 | 3 | 3 | 5 | 5 | 6 | 13 | 15 |
| Other electricity | 3 | 4 | 4 | 5 | 7 | 8 | 13 | 15 |
| Computer room | 0 | 0 | 0 | 0 | 14 | 18 | 87 | 105 |
| Total gas or oil | 79 | 151 | 79 | 151 | 97 | 178 | 114 | 210 |
| Total electricity | 33 | 54 | 54 | 85 | 128 | 226 | 234 | 358 |

Note: Type 1: cellular naturally ventilated; Type 2: open plan naturally ventilated; Type 3: 'standard' air conditioned; Type 4: 'prestige' air conditioned

1.3.3 Current State of Low Energy Technology in Service-sector Buildings

In 2013, 10% of UK greenhouse-gas emissions were produced in service-sector buildings [13]. The UK energy-efficiency market sat at £17.6billion, supporting 136,000 people. Thus the economic and environmental case for energy-efficient investment in service-sector buildings is profound. A major obstacle noted in the sector arises due to the relationship between landlord and tenant. Landlords rarely see the effects of energy bills, so are unpersuaded to install energy-efficient technologies; whilst tenant leases typically last less than five years, requiring retrofit energy-efficient technologies to have rapid paybacks to make the economic case compelling. Increased government-backed support is required to promote the UK non-domestic Green Deal scheme, and incentivise the uptake of energy efficiency.

In 2013 the UK the commercial property market was worth approximately £717 billion, with 51% of organisations renting office space [13]. Industry wide, 74% of businesses have commissioned some level of energy-efficiency technology retrofit. Amongst large corporations nine out of ten have commissioned work; whilst only six out of ten SMEs have

commissioned projects [14]. Figure 1.9 charts the wide range of energy-efficient technologies commissioned during 2012/13.

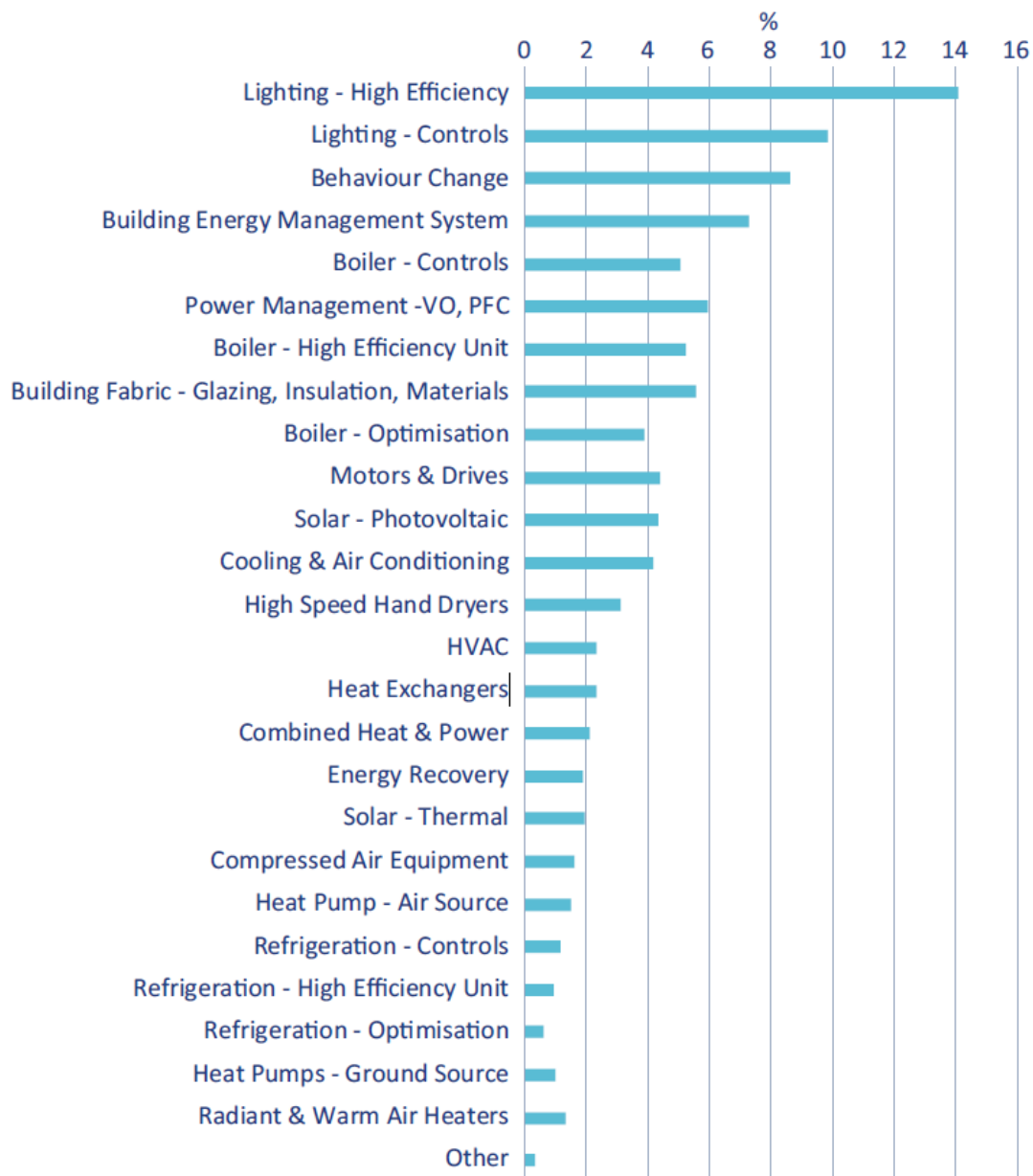


Figure 1.9 - Technologies commissioned in 2012/13 [14]

Work done by Housin [8] suggests the two leading technologies for the reduction of building energy demand, within the EU, are advanced building envelopes (for cold regions) and heat pumps. The work also suggests the leading political measures to be enacted are; a deep renovation of existing buildings and zero-energy new buildings as standard. The work encourages further research into the development of heat pump and thermal storage technology, as well as integration of buildings using smart grid technology.

To achieve government targets, and bring down associated carbon emissions, the sustainable building methodology within the UK built environment has seen a shift in the last fifteen years. In the early 2000s, sustainable buildings targeted renewable energy generation; whilst today sustainable building design favours a fabric first approach, akin to the German PassivHaus standard. High levels of insulation and smart energy management place very little energy demand on the grid.

1.3.3.1 Overheating Problem

Although highly energy efficient when considered at the design stage, super-insulated air-tight retrofit in highly-glazed densely-populated buildings has caused cases of operative temperatures exceeding thermal-comfort standards for unacceptably long periods. In an effort to provide thermally-efficient buildings, some internal environments have exceeded comfort regulations. Various studies [15-20] have investigated overheating in super-insulated buildings, presenting the problems faced.

Roberts [15], projects that overheating in buildings is likely to increase as the effects of climate change increase and insulation continues to play a significant role in energy efficient designs. CIBSE Guide A quantifies overheating in buildings when internal temperatures exceed 28°C for 1% of occupied hours.

1.3.3.2 Energy Efficient Overheating Mitigation Solutions

Various commercially-available passive-solutions to overheating exist, whilst others are still at the conceptual stage. Roberts [15] highlights innovative adaptive shading systems: electrochromatic glazing and thermochromic glazing, amongst the solutions to overheating currently under development. Traditionally brise soleil systems and external shading have sought to reduce excess thermal gain.

Research assessing the relationship between thermal comfort and productivity found occupants were more tolerant of high temperatures when they had available to them a form of control [21]. The 'adaptive comfort theory', though not solving overheating, enables productivity through extreme operative temperatures. Behavioural change in occupants offers a significant opportunity for energy-efficient enhancements.

Building energy management systems (BEMS) enable the smart control of energy flows throughout the building. For active systems, such as mechanical ventilation with heat recovery (MVHR) systems, monitoring room thermal loads and temperature set points can provide adequate ventilation and cooling, without oversizing the plant equipment.

Further research suggests additional thermal-mass systems as offering overheating mitigation solutions for light-weight constructions. Chiu [18] sets out a system that utilises cool night temperatures as a heat sink to dissipate thermal-energy requirements within the occupied space. Phase Change Materials (PCM) offer energy-dense thermal-mass suitable for light-weight structures, however modelling is unconvincing and systems should be applied with caution [15]. Active thermal-mass systems, integrated in a BEMS, offer the energy-efficient benefits of both night cooling and smart plant management. Such systems offer the benefit of utilising existing building fabric to offset office cooling demand and mitigate overheating.

1.4 Summary

The international built environment accounted for 35 per cent of global energy demand in 2010 and is forecasted to rise significantly in coming years. Energy intensity has not reduced despite continued expansion of commercial sector buildings. Therefore, energy-efficient technologies have become a central strategy in the UK government's sustainability agenda. Thermal energy storage (TES) technologies have been identified as an energy-efficient thermal regulation technology. A detailed investigation into the state of the art of TES technologies has therefore been undertaken in the next chapter. The investigation focuses on built environment applications, uptake barriers and the fundamentals of novel PCM for lightweight TES.

Chapter 2: Literature Review

Thermal Energy Storage Technology – A State of the Art

2 Literature Review

2.1 Introduction

As introduced in *Chapter 1*, thermal energy storage (TES) is capable of low-energy office cooling, inhibiting overheating. TES achieves this through offsetting electrical demand from day to night periods. Effective storage and release systems can be designed for a given purpose or with built in adaptability and control. Whilst energy storage systems alone will not establish energy security, effective coupling with renewable energy generation and insulation will significantly reduce end-use energy demand. Through reduction of end-use energy, TES technology contributes towards sustainable energy security and emission reduction targets.

This chapter investigates the academic and commercial work published to date in the areas of both sensible and latent TES, with specific attention on applications in the built environment. Focus is given to technologies suitable for low-energy UK offices. Attention is also given to reviewing the modelling work done in the field of TES. The chapter concludes

with a capability contrast between sensible and latent TES and suggests suitable areas of innovative research.

2.2 Sensible Thermal Energy Storage Review

The principles of sensible TES have been used in buildings since their origins. Buildings were traditionally designed to keep inside spaces conditioned passively, away from the external climate. With the introduction of cheap electricity and air-conditioning technology this trend faded and lightweight construction was favoured. The rebirth of interest in thermal-mass technologies in the last thirty years has seen a reverse of this trend [22].

2.2.1 Passive Thermal Mass

Following a similar mechanism as storage heaters, the thermal mass of a building can be utilised to provide residual heating or cooling [23]. During summer months, the thermal mass absorbs heat generated in the room and creates a buffer from solar gain. The application is limited during consecutive hot days; where the external temperature exceeds the desired internal temperature. In this situation, the available TES limit (thermal capacity) is reached. The heat stored will then be released into the internal space, causing the temperature to rise to uncomfortable levels, an effect labelled 'overheating'.

Similarly, the building's thermal mass offers protection from the cold until all heat from the thermal mass has been lost to the external environment. The thermal mass will then absorb internal heat, cooling the room. Insulation, typically material with low thermal conductivity, reduces the effects of external temperature fluctuations on internal temperatures; increasing the effectiveness of thermal mass applications. Passive thermal mass systems are limited by surface heat-transfer and therefore require incorporation at the design stage [22].

Many TES systems exhibit good performance as alternative insulators. The heat generated is stored and released as required, offering internal temperature control. The benefits of TES are often more desirable during cooling requirements when insulated spaces are liable to overheating. Active-TES systems remove excess heat from the building, maintaining thermal comfort, via a dynamic heat-transfer fluid. Commonly air or water, the active fluid transfers energy between the thermal mass and connected environments.

2.2.2 Thermally Active Building Systems (TABS)

Thermally active building systems (TABS) utilise the intrinsic thermal mass of a building by incorporating air or water networks into the mass. By embedding a fluid network into the thermal mass, the active heat transfer area is increased; improving performance. Further, the

conditioning of the active fluid, through connected plant equipment, enables temperature control of the thermal mass, and subsequently the internal building envelope [12].

Figure 2.1 demonstrates the typical temperature fluctuation and operation of the thermal mass in TABS. From point (1) to (3) internal gains from occupant behaviour and solar gains accumulate thermal energy in the room, and subsequently the thermal mass. The thermal mass moderates the temperature by absorbing heat energy at the heat transfer surface. Once unoccupied, the room can be cooled by activating the cooling system in the thermal mass until the required set point is reached ready for next day operation (points (4) to (5)). Between the points (2) and (3) a 1°C difference is observed between the air temperature (2' to 3') and room temperature (2 to 3) due to the additional heat transferred through convection. Once cooled (4) the additional convective fraction is negligible [12]. The dip between (2) and (3) occurs due to activation of the TABS fluid.

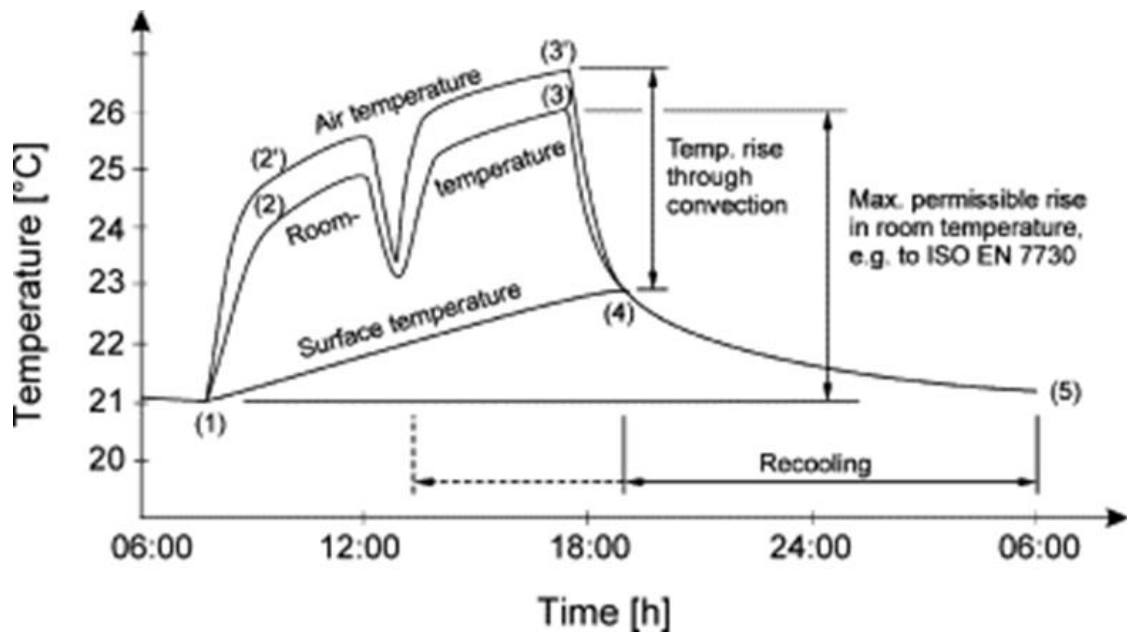


Figure 2.1 - Diurnal Temperature Cycle for TABS application [12]

Thermal-mass efficiency, in temperature control, is limited by heat exchange area; traditionally the external surfaces of the mass. Due to typically low thermal conductivities of building materials, discharge of heat stored is slow; especially with the typically small temperature differences in building applications. Integrating an active system, through channels in the thermal mass, increases heat exchange area and heat transfer efficiency. Typically air or water is used as thermal fluid to enhance performance though further refrigerants are alternatively used.

2.2.2.1 *Water Driven*

Water driven systems embed a matrix of pipes in the thermal mass. These pipes connect to a closed loop water heating system. Water passes through the mass, removing or radiating heat. Heat transfer rate to the thermal mass is increased with pipe contact area; however heat transfer to the room remains limited by the active thermal mass external surface [24, 25].

Room heating rates can be increased by operating a higher temperature difference between the room and mass. Thermal mass acts to dissipate heat, protecting the room from temperature spikes. Thermal capacity is enhanced by water removing excess heat from the slab during extended hot seasons. This type of cooled-ceiling, or chilled-ceiling, technology [26] makes the residual thermal mass active.

Buildings with installed water driven TABS have enabled energy-efficient cooling as far back as the 1990's. Meierhans [27] documents the performance of a slab-cooled water-driven system. The system utilises night-cooling via an air to water heat exchanger situated in a Swiss building. Numerous research papers modelling TABS have been carried out. Hauser [28] simulated annual performance of a building with and without a water driven TABS installed. The system generated annually 60kWh/m^2 (at an average of 6.8W/m^2) of cooling. Feng [29] investigated the benefits of radiant cooling versus air displacement methods. It was found that with a standard air temperature difference of 10°C up to $130\text{-}140\text{W/m}^2$ could be cooled.

Lehman [12] investigated a method for design and sizing a water driven system. To size TABS, Lehman found that a combined approach, based on average and peak cooling demands, was required. The work concluded that during cooling operation, short periods of operation with a 'low' supply temperature enable reduced operating costs and avoid continual pumping duty. Basu [30, 31] conducted a review of methods for sizing TABS. The models in ISO 11855 offer models that can be implemented at early design stage in quasi-steady state cooling load models.

Work by Weitzmann [24] determined the optimum position of the PEX water pipes for control of a hollow core slab as thermal mass was embedded 50mm above the soffit surface. The optimum pipe position resolves two useful parameters: maximum cooling capacity is achieved the closer the pipes are to the soffit surface; however the activation of the thermal mass is reduced in these instances. To make use of the slab's cooling capacity pipe distance from the slab is preferred. Figure 2.2 conveys the experimental testing conducted of PEX

water pipe at optimum depth in the hollow core slab. The work focused on water driven systems, but highlighted the benefits of investigating the system with ventilation and different thermo-active components.



Figure 2.2 - Thermal Active Building System (TABS) [24]

2.2.2.2 Air Driven

Air driven TABS rely on a mechanical-ventilation pathway through building structural elements. The popular Termodeck [32] system utilises ventilation air as the thermal fluid. Concrete hollow core absorbs heat from the room, whilst pre-conditioned ventilation air passes through the hollow core; before being released into the room, as characterised in Figure 2.3 and Figure 2.4. Invented in the late 1970's a steady stream of computational and experimental research has been carried out on the industrial system [33].

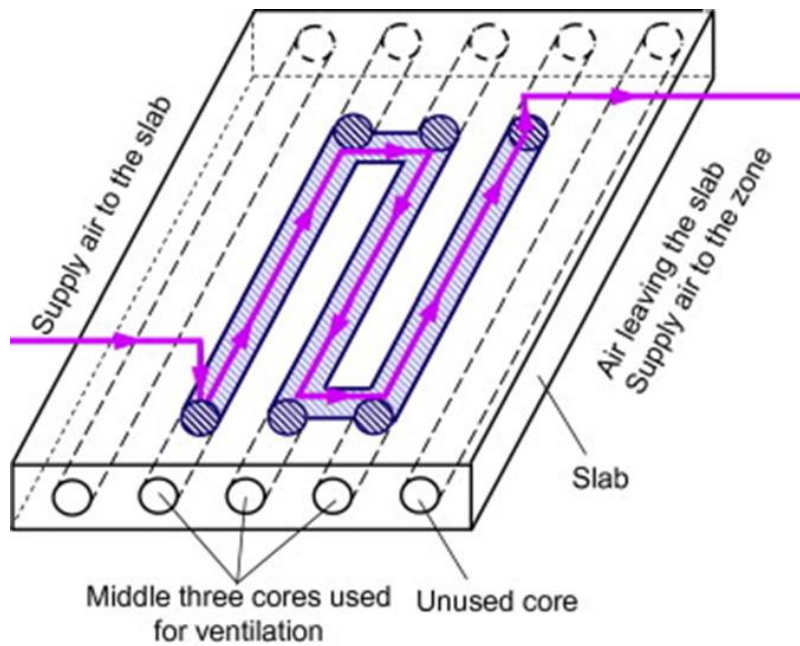


Figure 2.3 - Typical Hollow Core Air Network [33]

The ventilation air serves to maintain hollow core and room temperature. Air passing through the hollow core en-route to the room increases the heat exchange area, whilst also enabling room temperature control through recycled heat. Heat transfer from the thermal mass to room is no longer limited by the ceiling surface area, since pre-treated ventilation air conditions the room also [34].

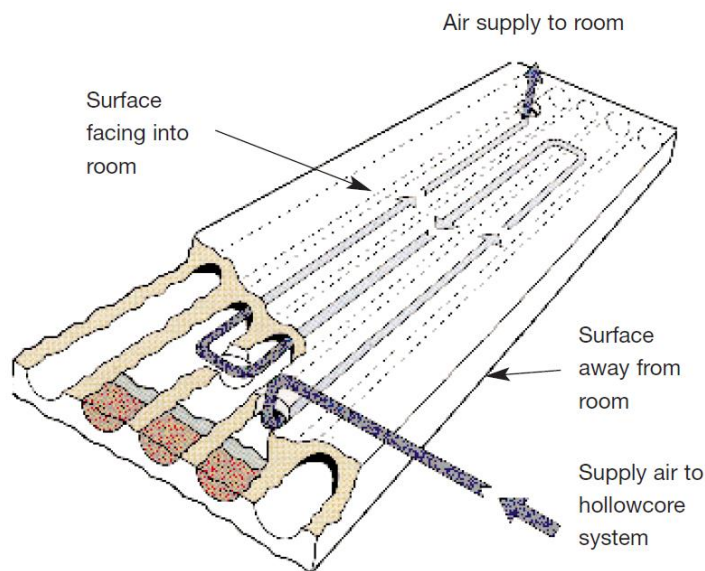


Figure 2.4 - Termodeck Slab Schematic

During hot spells, night ventilation flushes the residual heat from the hollow core thermal mass. This extends the operation envelope and ensures room temperatures never exceed

the national standard office temperature hours [35]. Night ventilation operation limits the applicability of the technology to buildings with intermittent occupancy patterns. The temperature profiles, in Figure 2.5, demonstrate the twenty-four hour operation the ventilated TES undertakes; maintaining comfort temperatures during occupied hours, and then discharging the thermal energy stored during night hours.

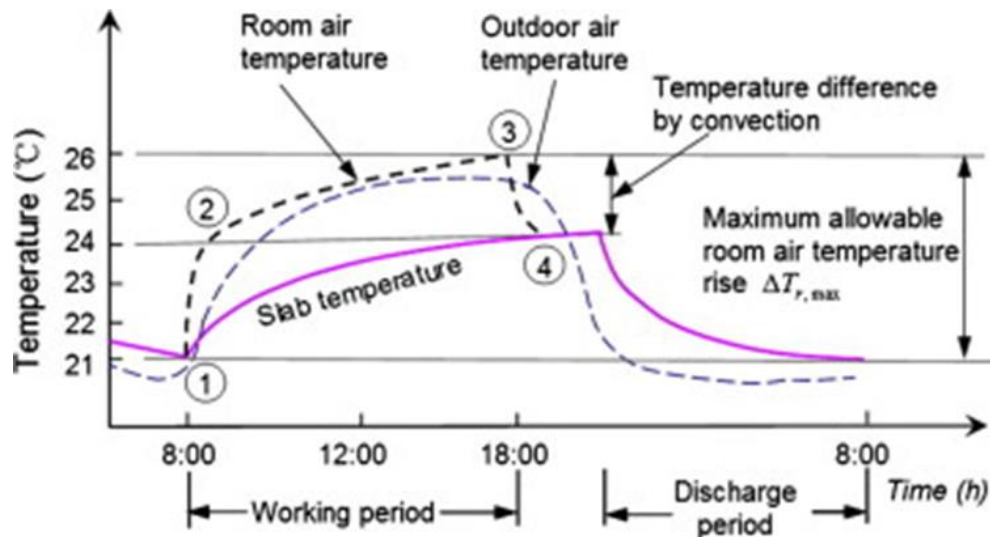


Figure 2.5 - 24 hour Hollow Core Operation [33]

Commercial studies, to date, have focused on building performance reviews; whilst most academic interest has sought to characterise performance through computational modelling. Ren [36] used a simplified combined resistance or lumped-parameter method to model the hollow core network. The work suggested that the heat transfer coefficient around the bend in the air network was fifty times greater than in the straight duct. However modelling by Barton [37], using a two-dimensional finite-difference model, found minimal effect on overall heat transfer due to the air network bends. Suggestion by Green [38] of additional internal baffles, to enhance heat transfer, was made following validated computational fluid dynamic (CFD) and laboratory investigations on a two core slab.

A three-year investigation by Winwood [32, 39, 40] used a CFD model of the hollow core to characterise the performance under ventilated conditions. The work culminated in a full building assessment offering suggestions to improve the building's annual operation [39]. Figure 2.6 charts the effect of the Termodeck system on the cooling of the Elisabeth Fry building, UK [41]. The internal daily temperature cycle movement demonstrates the slab heating during the day coupled with night cooling. Since early days of the technology, control strategies for each building have been developed to optimally manage the internal comfort with maximum energy efficiency.

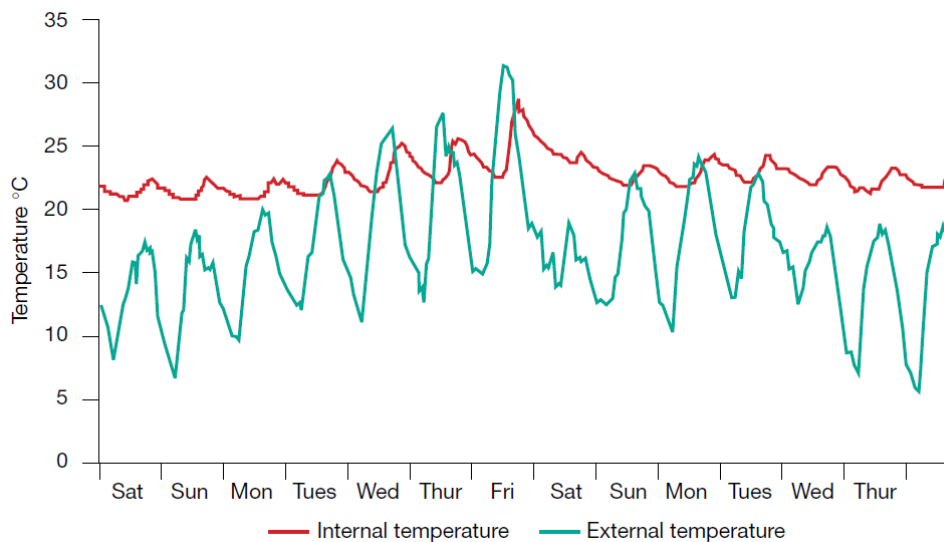


Figure 2.6 - E.Fry Building Temperature Profiles

2.2.2.3 Hybrid System

In the past few years, Chae [42] published a thermal evaluation of a hybrid radiant-cooling system (Figure 2.7). The system incorporates concentric layers of air and water passing through the building fabric. Investigation was carried out using CFD modelling and found the fabric cooling could be achieved by the water stream; whilst the air supplied the required room ventilation. The proposed system offered 2.1°C cooler temperatures following night ventilation cooling. As designed the system proposed using cooling water to temper the air and slab, separating any water-slab interaction. The system builds on water driver TABS technology (which offers radiant room cooling), whilst additionally seeking to temper inlet air through the TABS and subsequently offer additional displacement air cooling.

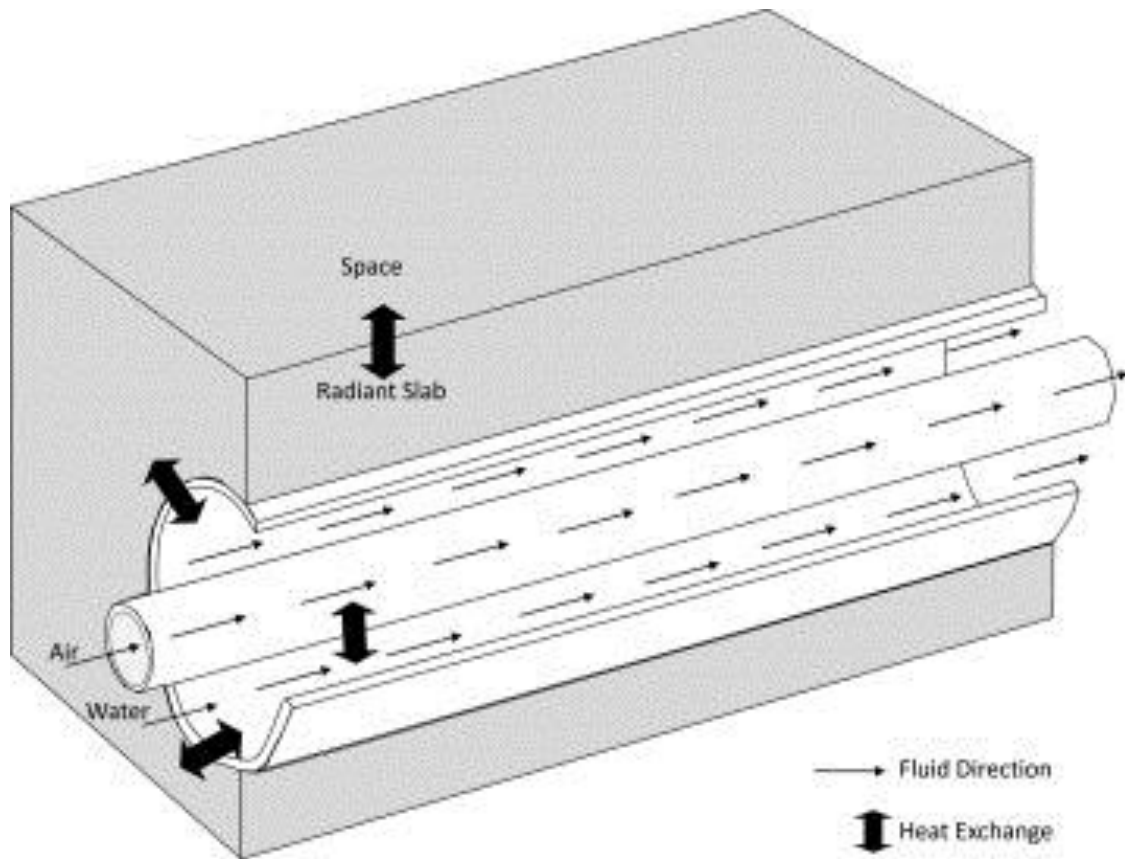


Figure 2.7 - Hybrid Radiant Floor System [42]

2.2.3 Modelling of Sensible TES Systems

Modelling of Sensible TES (STES) systems has been carried out extensively. Since 1974 until 2013 the air-driven hollow-core systems have been modelled. Xu [33] reviewed the work to date revealing performance of the technology has been simulated, amongst others, following black box [43], simplified finite element [44], finite difference [37], CFD [40], RC [36], mathematical numerical [45, 46] and computational modelling methods [47].

Winwood [40] validated a CFD model for a (fabric energy storage) FES-slab to understand performance under different air conditions and air paths. Corgnati [48] used Simulink® to study reduced summer cooling demand for an Italian-Mediterranean climate using a ventilated hollow core (VHC) system. They concluded that night ventilation can help when reducing summer cooling demand.

Work by Karlstrom [49] used FEMLAB modelling, with cross validation against literature results and experimental measurements from Weitzmann [24], to estimate hybrid performance. Under water only operation, as in [24], the soffit thermal load was 51.7W/m^2 in [49] and 50.0W/m^2 in [24]. Complex radiation and convection heat transfer was noted

from the model scenarios investigated but no heat transfer rates were reported for an active hybrid system.

Chae [47] carried out Energy Plus modelling of a ventilated hollow core (VHC) system in a whole building simulation. Unlike previous modelling, the system included air conditioning (AC) units and appropriate control. The work investigates three system configurations displayed in Figure 2.8. The secondary heating, ventilation and air conditioning (HVAC) and air handling unit (AHU) system control strategies that supplement the VHC system are conveyed in Figure 2.9. The work was validated against equations developed by [50]. Using unoccupied ventilation, a reduction of almost 29kWh per day (12W) was reduced from the cooling-coil demand.

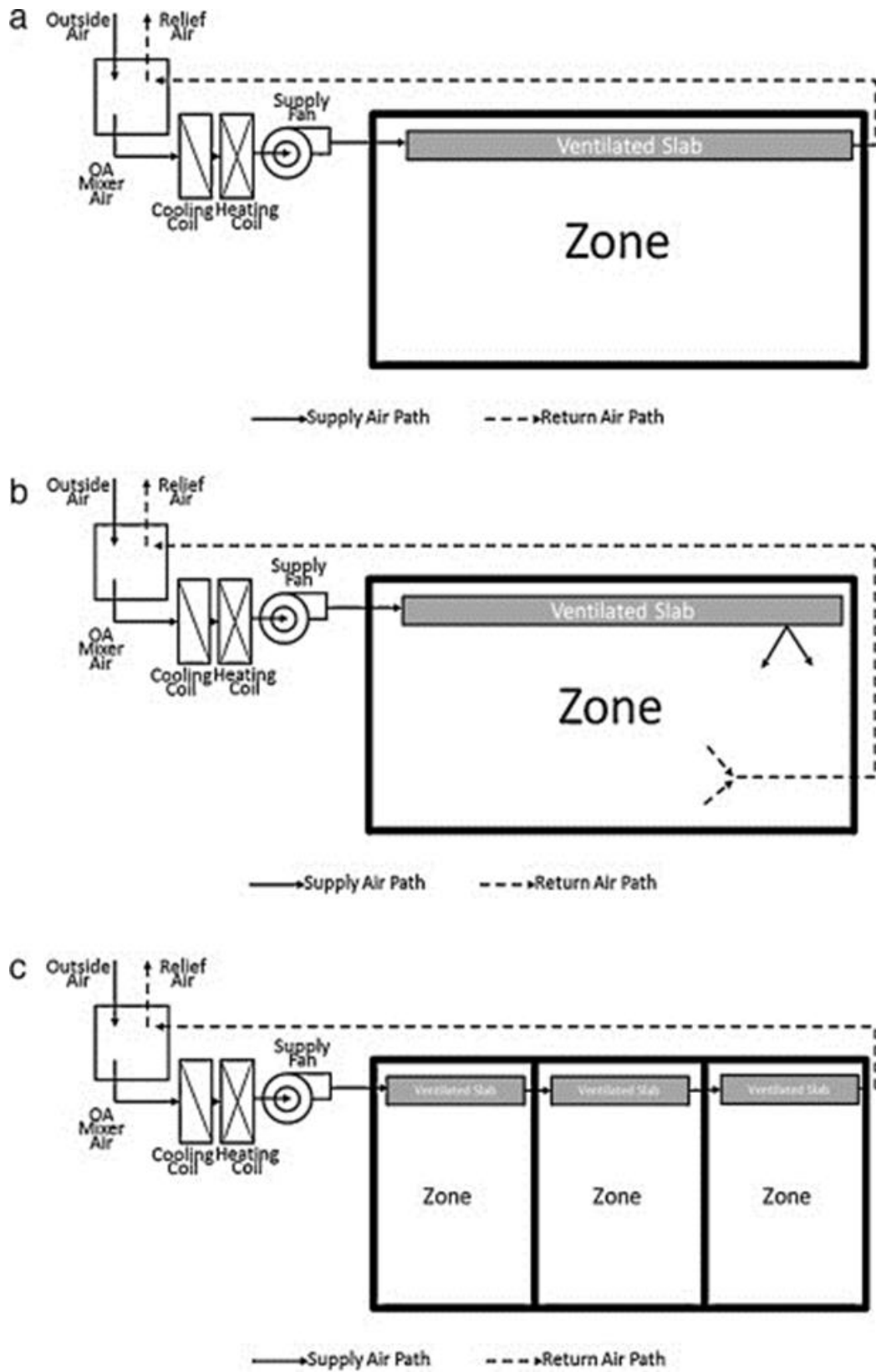


Figure 2.8 - Three Systems Simulated by [47]

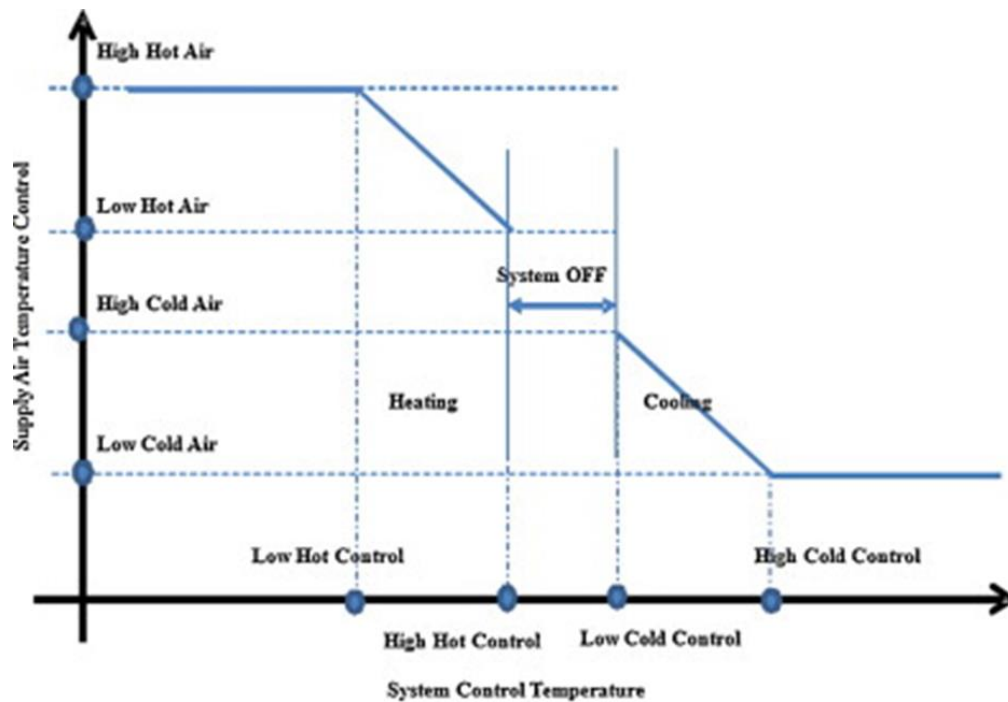


Figure 2.9 - AHU Control Strategy for the Systems in Figure 2.8 [47]

2.2.4 Underground Thermal Energy Storage Systems (UTES)

Another form of STES utilises the vast heat density available in the earth's ground water systems. Aquifer thermal energy storage (ATES) systems are operated as open loop systems, pumping ground water through the system. In summer, the water acts as coolant and the groundwater temperature in the aquifer gradually increases, typically from 9°C to 12°C, to 15°C to 20°C, in Dutch systems. In winter this warm water acts as low grade heating and the temperature in the aquifer drops to between 5°C and 10°C [51].

Alternatively, borehole thermal energy storage (BTES) systems operate in a closed loop function. Heat-transfer fluid extracts heat from the ground water and is pumped back to the buildings above. No groundwater is transported, allowing systems to operate at more extreme temperatures than the ATES systems [51]. Further systems have been designed in collaboration with solar water heaters. These systems endeavour to store the heat generated in the hot summer months for use in the cold winter months [52].

2.3 Latent Thermal Energy Storage Review

Latent thermal energy storage (LTES) has attracted a great deal of interest for its high thermal density (thermal capacity per kilogram), relative to STES materials, by exploiting the latent heat of fusion. This section focuses on the current state of phase change material (PCM) technology, and its application within the built environment due to the technology's high TES capability. Using data taken from [53], Figure 2.10 compares the performance of PCM technology verses traditional energy storage, such as lead-acid batteries. PCM offers high energy storage density, surpassed only by chemical storage in hydrogen and methanol, demonstrating its high suitability as a main contributor towards energy efficiency.

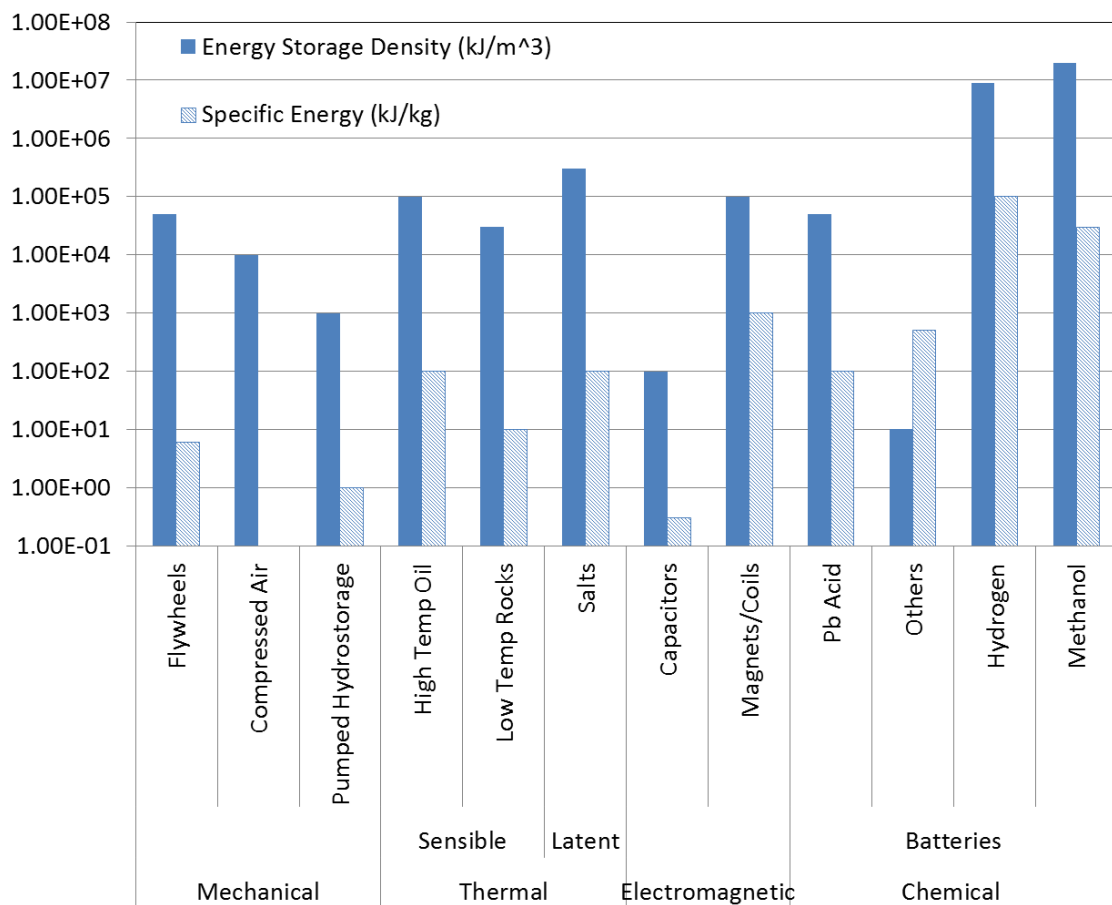


Figure 2.10 - Comparison of Energy Storage Technologies [53]

2.3.1 Background

The most well-known and abundant phase change material is ice, however every chemical compound will change phase at a given temperature and pressure. Ice has been used as coolant as far back as the beginnings of civilisation. The relatively low (0°C) melting point however limited the applicability of ice water systems in built environment applications. Early research into PCM for TES was carried out by the University of Delaware in the 1970s.

The PCM was incorporated with solar collectors to store heat [53]. For these early applications a wide range of melt temperatures was utilised. In modern built environment applications the useful melting temperature range has been reduced more narrowly around the comfort temperature (22°C – 26°C) [54].

2.3.1.1 Social Case

The call for innovation and application of PCM in the built environment has been spurred on by the growing 'green' movement. With calls for cuts on carbon emissions, without standard-of-life varying, the market for smart sustainable technology grows ever bigger. Interest has been ignited in the search for efficient thermal batteries and buffers ensuring the maximum usage of available heat. Thermal buffers can also shift the peak-electrical load of a building into off-peak times of the day, cutting electrical bills by making use of night-time tariffs.

PCM boasts impressive potential for applications within the built environment, due to their ability to absorb relatively high levels of heat with little change in temperatures. Applications have been explored widely from supplementary insulation in building materials [55], to active materials replacing refrigerants in naturally ventilated air conditioning units [56].

Cold storage, as touched on by Tay [57] and reviewed in depth by Akio [58], makes use of PCM to store 'coolth' (the ability to absorb heat) and thus shift cooling demands, levelling a building's energy consumption across a twenty-four hour period. This shifting, offsets high electrical demand times and utilises reduced-tariff electricity, saving consumers money whilst maintaining thermal comfort.

2.3.1.2 Scientific Case

The science behind PCMs high energy density is due to the latent heat of fusion. When a substance changes phase, that is to melt, evaporate, condense, solidify or sublime, a vast amount of energy is absorbed or released; despite no significant change in measured temperature [53]. This change in energy as phases change is down to the difference in intermolecular bonds in the material that varies in each phase.

Taking water as an example of the energy stored and released during phase change, Figure 2.11 and Figure 2.12 [59] outline the relationship between temperature and energy. Three stages of sensible heating occur; when the material is in a stable phase. At transition temperatures (melting and boiling points) latent heating occurs where an excessive amount of energy is released or absorbed, with little to no temperature change. The latent heat of

fusion, utilised in PCM systems, is significant, almost equal to that of the entire liquid heating section.

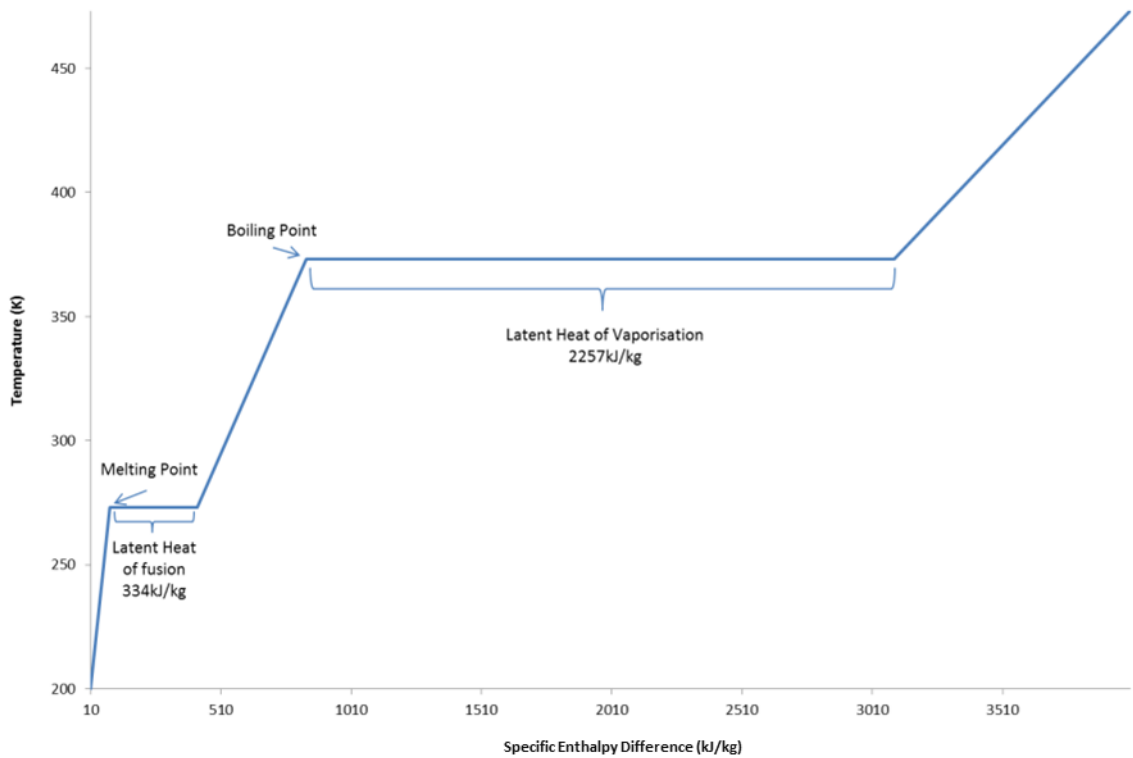


Figure 2.11 - Change in Enthalpy versus Temperature for Water at 1atm

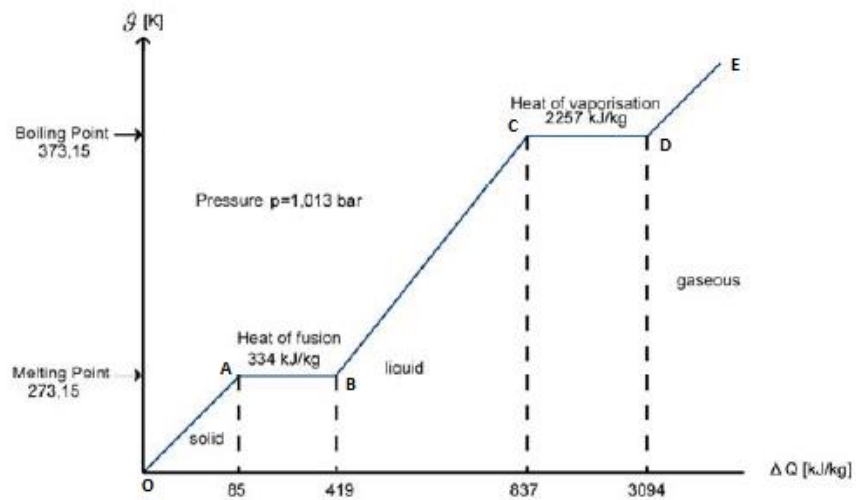


Figure 2.12 - Water Phase Transition Curve [59]

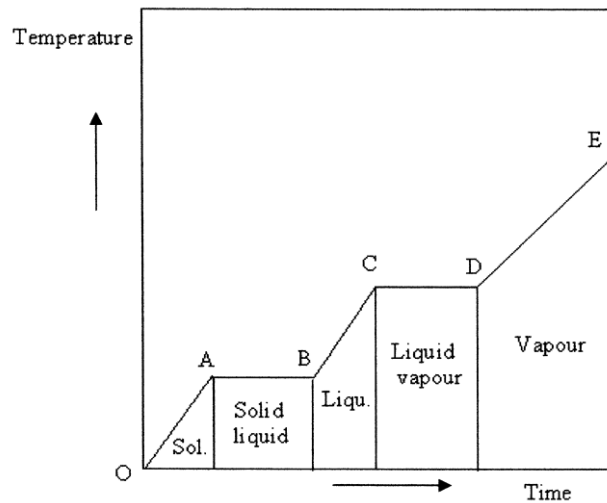


Figure 2.13 - Phase Transition Curve [52]

During the sloped sections of Figure 2.13 (OA, BC, DE) the material is undergoing sensible heating, thus the energy change is a function of temperature change, specific heat capacity and the mass. During the flat sections (AB, CD), where temperature is constant, latent heating is occurring. Here the energy change is simply a function of the material's mass and latent heat of transformation [52].

For materials with unknown changes in energy the total energy for the system can be calculated with the Equation 2.1 below, where subscripts refer to points on the temperature time curve in figure 2.13. This equation combines the sensible and latent heat equations to determine the overall change in energy. Cooling is modelled using the same equation as heating, only with opposite results. Ideal PCM will undergo complete even transitions offering the cooling and heating duty depending on initial state. Dincer et al [53] explains in further detail the theory behind the curve.

Equation 2.1

$$\Delta Q = m \left[\int_{T_O}^{T_A} c_{ps}(T)dT + \Delta H_f + \int_{T_B}^{T_C} c_{pl}(T)dT + \Delta H_v + \int_{T_D}^{T_E} c_{pv}(T)dT \right]$$

Any latent heating system will utilise both sensible and latent heating during its operation. As seen in the latent heat transition graph, operation at temperatures either side of the transition temperatures will drive sensible heating in the PCM. For detailed understanding of PCM applications a good foundation in thermodynamics, crystallisation, heat transfer and even fluid dynamics is desirable. A growing understanding of crystalline growth within PCM capsules is aiding modelling.

A comparison of the heat storage capabilities of various materials was carried out [60] with the results graphed in Figure 2.14 below. The temperature change required to store 5,000kJ of energy, with a starting temperature of 25°C, was recorded with the PCM paraffin-wax exhibiting the lowest temperature change. Based on the temperature rise and initial temperature the water also underwent phase transition. The two thermal fluids remained in liquid phase and the sensible thermal masses tested remained as solids. Further work [60] demonstrated paraffin wax to have the highest energy storage density (kJ/kg) of the materials tested, exhibiting ten times the performance of concrete and rock.

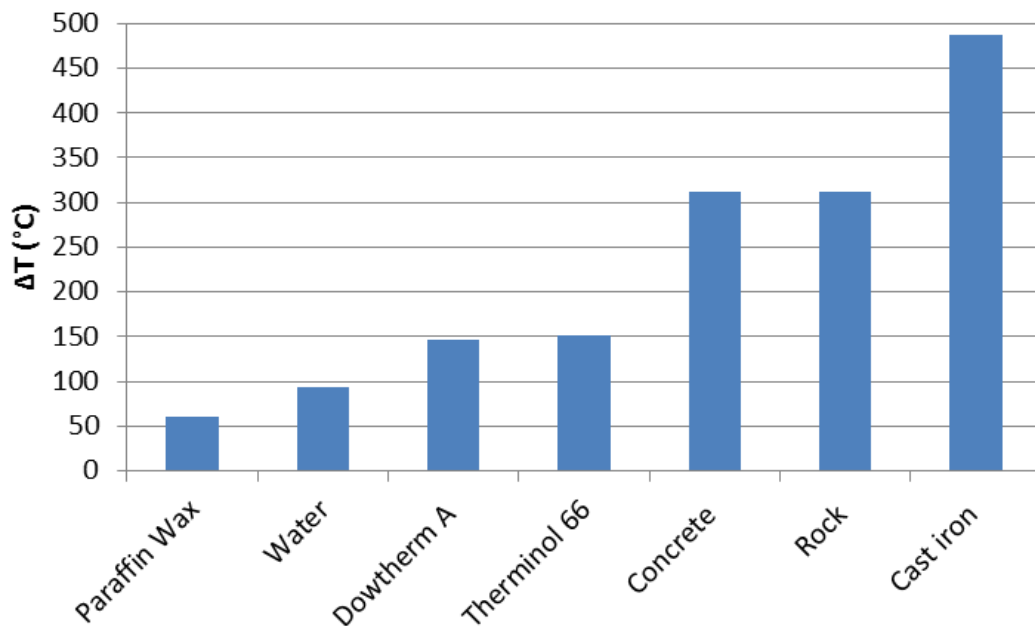


Figure 2.14 - Change in Temperature required to store 5,000kJ [60]

2.3.1.2.1 Thermal Analysis Methods

The thermal properties of any thermal energy storage system are a clear way of quantifying performance and comparing methods [61]. Thus a variety of analytical methods have been developed to characterise the thermal properties of pure PCM and phase change incorporated building materials (PCIBM) [62-65]. The most commonly used to determine the thermal energy storage capabilities of a sample material are discussed below.

2.3.1.2.1.1 Differential Scanning Calorimetry (DSC) [66]

DSC is a thermal analytical technique that measures the amount of heat required to keep a substance at a given temperature [61]. Tests are then continued across a temperature range that increases linearly with time [67]. PCM samples are tested against a reference sample (with known thermal properties). The product of a DSC test is a curve displaying the heat flux

verses temperature or time. It is possible from the DSC curve produced to identify the crystallisation and melting temperatures of the tested substance along with the size of latent heat. The drawbacks of DSC are the accentuated super-cooling effects reported due to the small sample sizes and thus poor nucleation effects [68].

2.3.1.2.1.2 Differential Thermal Analysis (DTA)

DTA follows a similar method to DSC though keeps the heat flux constant and monitors the variation in temperature, T , between the reference and test samples. Various thermal properties can be calculated from the temperature difference between reference and sample [61]. Buddhi et al [68] constructed a simple variation of DTA that tested samples with an accuracy of 5% of the then traditional DSC tests. By keeping the heat flow constant DTA can produce Time versus Temperature graphs, illustrating the heat transfer rate via conduction of the test sample through a variety of temperatures [69]. Figure 2.15 displays the form of a DTA graph. Similarly to DSC the small sample sizes used in testing may misrepresent the thermo-physical performance of a given material when operating in bulk units [70]. Further limitations of DSC and DTA exist in the large expensive rigs and their inability to measure multiple samples simultaneously [70].

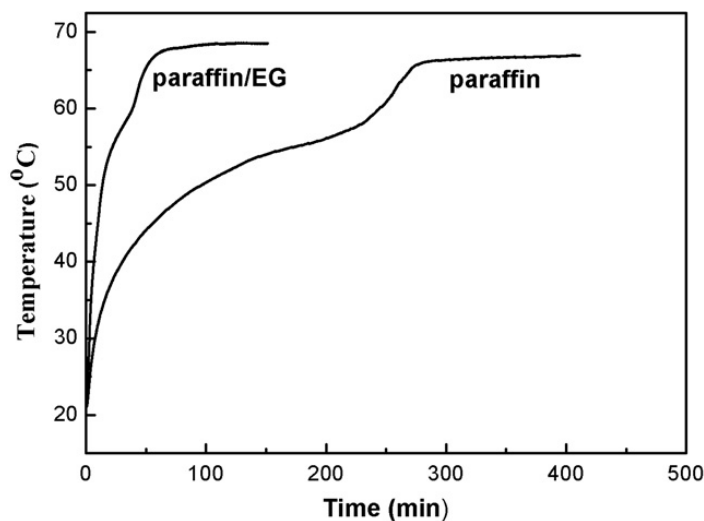


Figure 2.15 - Temperature vs Time graph displaying the different rates of heat transfer in Paraffin and Paraffin/EG[69]

2.3.1.2.1.3 T-History Method

A number of research groups have developed a simpler method with comparative results to traditional methods [61]. Initially developed by [70] the test samples are placed in test tubes equipped with thermocouples connected to a data logger. The samples are heated and cooled in water baths for a set period of time. From temperature verses time curves the

thermal properties of the sample can be obtained. [70] reported an accuracy of approximately 10% with literature data for the samples tested. The process has since been refined by [71] and [72] to correct some assumptions in the initial method and widen the operation envelope. By keeping the system and operation constant the heat input to the sample is constant. Thus this method could be considered to follow the same principles as DTA. Despite this simple method many still rely on DSC and DTA to characterise the performance of the heat storage technology though the T-history method may provide a useful method for characterising bulk PCM, giving a more realistic representation of applied performance.

2.3.2 Design Considerations

The Incorporated PCM (IPCM) design process is inherently iterative. When incorporating PCM in a given design, various specifications need to be outlined as to what properties the potential PCM should exhibit (temperature change, chemical stability, etc). For any application the initial requirements of a TES unit are: (1) the operational temperature envelope for the unit, and (2) the required heat load to maintain the specified temperature. The required heat load will be dependent on the heat transfer of external heat [60].

Following the two initial requirements a selection of available PCM displaying the most suitable combination of specified properties is identified. Having selected the most suitable material, the encapsulation method (discussed further in Section 2.3.2.4) must be selected along with the layout and orientation of the PCM. This decision is made before or after the PCM choice, depending on whether the design application allows variation of encapsulation method.

Once potential PCM, encapsulation and configurations are conceived the design's heat-transfer capabilities are optimised for the application design specification. Further optimisation and design modifications may be required to meet the design specification and budget before the most suitable option is chosen.

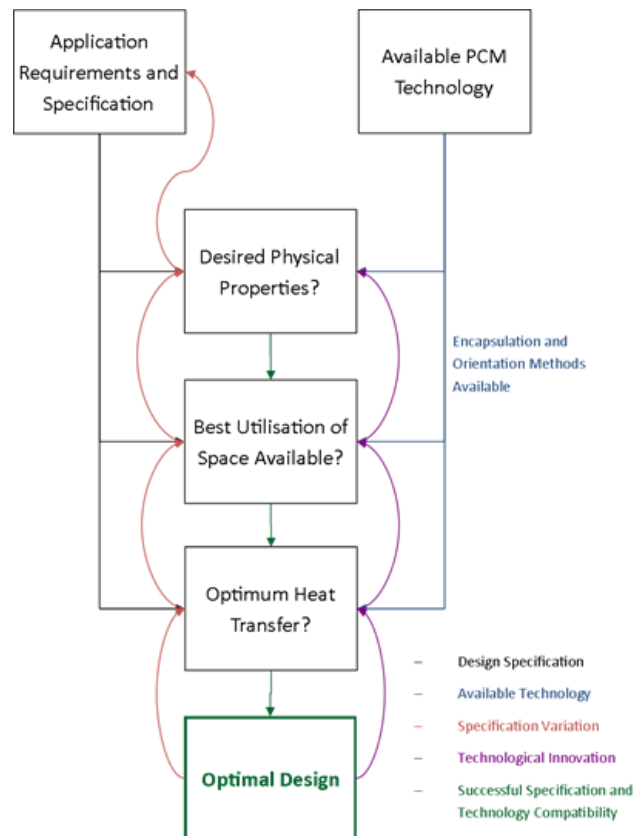


Figure 2.16 - Incorporated PCM Design Flow Chart

Figure 2.16 puts this multi-stage iterative design process into a simple flow chart. At each design stage there are two inputs, the *design specification* and *available technology*. If the availability matches the specification then the process can move onto the next design stage. If there is incompatibility at any stage two potential variables can be explored to find a solution; either minor *specification variation* or the development of *technological innovation*. Once compatibility is reached the design process may progress until the *optimal design* is reached.

2.3.2.1 PCM Design Methodology

The multi-stage iterative design flow chart in figure 2.16 was developed by the author upon reviewing the state of design procedures available. Alternative design procedures from literature are reviewed below and comparisons drawn.

Figure 2.16 presents a good tool for walking through the design stages when introducing a new PCM product to market. Methods similar to this have been used numerous times in early PCM research to characterise a new material, though without flowcharting the process. Figure 2.17 serves as a design tool for incorporating known PCM into various applications. With the exception of the *technological innovation* step, where stages of figure 2.17's

process would be utilised, figure 2.16 works to find the best solution within the known data region.

After the theoretical modelling of a system; workable experimental tests must always be undertaken to confirm the validity of the numerically optimal design. The final branch in figure 2.17 outlines this practical process. Dolado [73] recently conducted uncertainty propagation analysis to offer a band of theoretical results, useful when validating practical results.

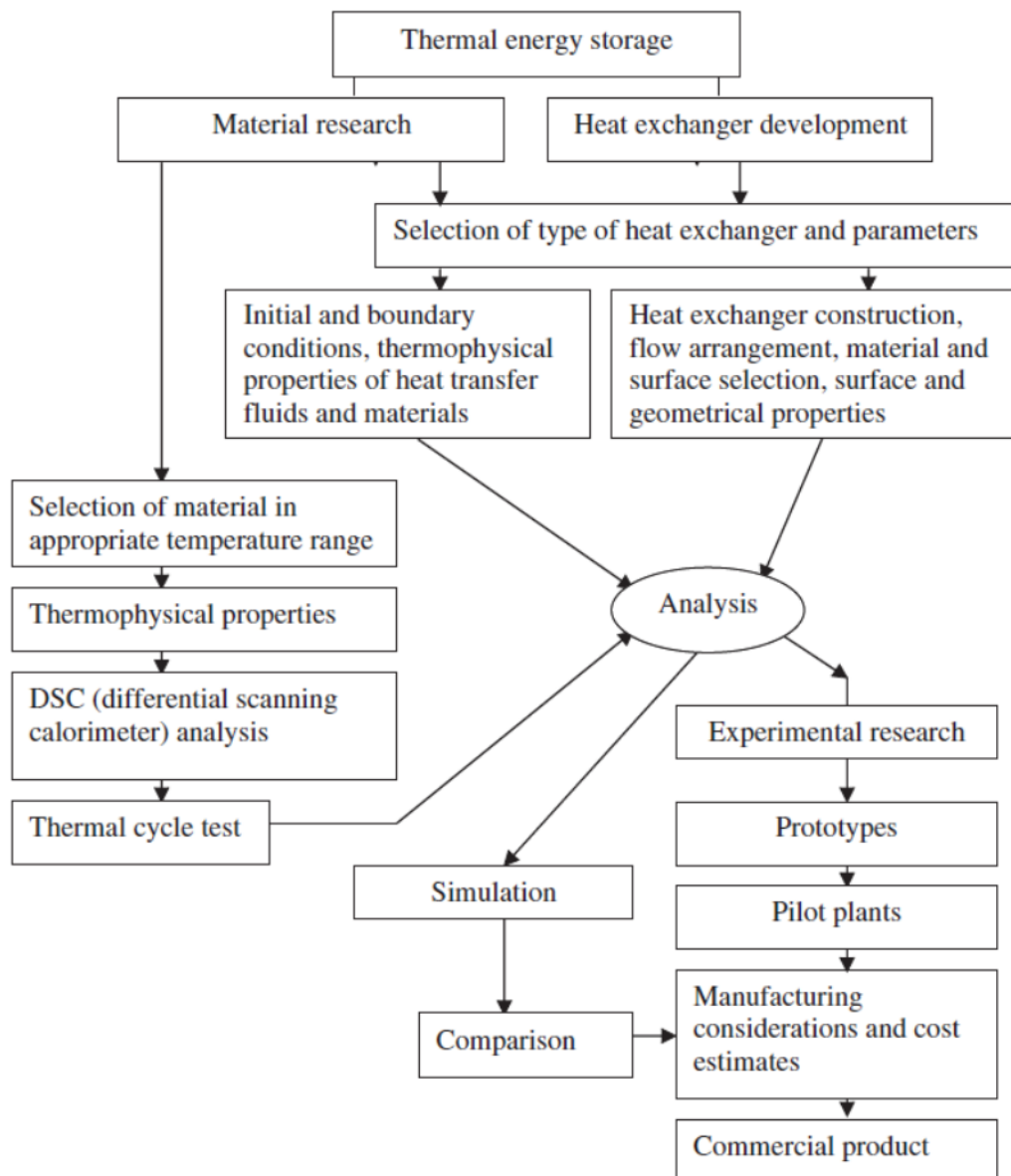


Figure 2.17 - Design Flow Sheet

2.3.2.2 Desirable Properties

In the search for potential PCM, the desirable properties first need to be ascertained to qualify which materials would benefit from further research and development. Zhou [61] highlighted three key properties for any potential PCM, that of, “suitable melting temperature, desirable heat of fusion and thermal conductivity as specified by the practical application”. Dincer [53] identifies seven important criteria and combined with further desirable features summarised from [74] are shown in Table 2.1 followed by a brief justification of desirability.

Dincer [53] adds further ‘technical’ criteria to the desirable property list asserting that simplicity, applicability, effectiveness, compactness, compatibility, viability and reliability all aid the desirability of a potential PCM. These ‘technical’ criteria are quantified through the determining of the tabulated properties below.

Table 2.1 - Desirable PCM Properties [53, 61, 74]

| Thermodynamic | Kinetic | Chemical | Economic |
|---|---------------------------------|--|----------------------|
| (1) Melting temperature in desired range | (1) High nucleation rate | (1) Completely reversible freeze melt cycle | (1) Low cost |
| (2) High latent heat of fusion per unit mass | (2) High rate of crystal growth | (2) Chemical stability | (2) Widely available |
| (3) High thermal conductivity | | (3) High freeze melt stability | |
| (4) High specific heat and high density | | (4) Non corrosive | |
| (5) Small volume changes on phase transition | | (5) Nontoxic, non-flammable and non-explosive material | |
| (6) Complete melting | | | |
| (7) Small vapour pressure at operating temperatures | | | |

2.3.2.2.1 Thermodynamic

- (1) The key property that governs initial selection of chemicals for their applicability is their melting point. The melting point is where the latent heat of fusion is released, thus to utilise this energy storage capacity the PCM must undergo phase change (melt) in the desired operating temperature range.

- (2) Favourable PCMs with large latent heat of fusions per unit mass (less material stores a given amount of energy) offer greater heat storage capabilities for applications, increasing their relative effectiveness [53].
- (3) High thermal conductivity is desirable in many applications to enable swift charging and discharging of heat using minimal temperature differences.
- (4) High specific heat and high density aid the storage of heat during sensible heat storage system phases and increase the heat storage potential per unit volume [63].
- (5) Small volume changes when the PCM undergoes phase transition ensure simple storage capabilities and eliminate containment problems. When PCM is contained in slurry small phase changes ensure minimal effects on viscosity variation and operational pumping loads.
- (6) Complete melting ensures PCM is only ever present in homogeneous phases. Avoiding solid liquid separation and thus maintaining stability throughout operation cycles.
- (7) Having a minimal vapour pressure at operation temperatures avoids chemical leakage, loss of material and flammability risks.

2.3.2.2.2 Kinetic

- (1) PCMs with high nucleation rates avoid super cooling and ensure consistent freezing and melting points are maintained.
- (2) The desired high rate of crystal growth is commonly dependant on nucleation rate and enables fast release of energy when PCM returns to its solid state.

2.3.2.2.3 Chemical

- (1) It is necessary for long term stability that the freeze/melt cycle is completely reversible ensuring no loss of heat storage capacity through numerous cycles.
- (2) Again to enhance stability, it is necessary that the chemical make-up does not vary through the physical phase transition.
- (3) Degradation should be avoided throughout a large quantity of freeze/melt cycles to maintain consistent long term predictable performance.
- (4) The PCM should be noncorrosive towards surrounding materials to ensure safe and stable operation of the system.
- (5) Similarly toxicity, flammability and an explosive nature should all be avoided to ensure safe and stable operation.

2.3.2.2.4 Economic

- (1) The bottom line of any commercially viable technology will favour products with low associated costs.
- (2) To keep costs low the PCM should be abundant, accessible and require minimal synthesis to make it ready for fabrication.

It is desirable to find suitable materials that exhibit strong characteristics in all properties identified in the desired operation range. As with any optimisation this ideal is rarely found, therefore analysis and optimisation of the key and flexible parameters are required to identify the optimum material.

For building applications optimum melting point varies between 0°C and 35°C depending on specific application. The bulk of the materials reviewed here will have their melting point around the comfort temperature of 22°C. As recorded in [61], [75] determined that to maximise the benefits of a diurnal PCM cycle the PCM melting point should be 1°C to 3°C higher than the average room temperature, though various sources [76-78] concluded that the optimum temperature varied slightly from [75]. Equation 2.2 and Equation 2.3 were developed by [79] to calculate optimum melting temperature.

Equation 2.2

$$T_{m,opt} = \bar{T}_r + \frac{Q}{ht_{stor}}$$

Equation 2.3

$$\bar{T}_r = \frac{t_d T_d + t_n T_n}{t_d + t_n}$$

Where \bar{T}_r is the average room temperature calculated from Eqn. 2.3, where T is temperature, t is time and the superscripts d and n refer to day and night. Q is the total heat absorbed per room surface area, h is the average heat transfer coefficient between wall surface and surroundings and t_{stor} is the storage time.

Better PCM's with low temperature melting points have a heat of fusion above 200kJ/kg, though many commercially available PCMs have a heat of fusion between 100 and 200kJ/kg [61]. After thermal storage at operating temperature the most important aspect of PCMs is their long term stability [63].

2.3.2.3 Materials and Properties

2.3.2.3.1 Classification

It has been reported by Regin et al [60] that Lane [80] reviewed in the order of 20,000 chemical materials with a view of identifying those with a melting point in the region between 10°C and 90°C. Most potential PCM can be grouped into the classification tree below. After determining a chemical's latent heat potential, it is classified based on the particular phase-change that occurs in the operation temperature envelope. The four possible transition groups are gas-liquid, solid-gas, solid-liquid and solid-solid. Of the transition groups solid-liquid has shown the most promise [61] though solid-solid transitions attracted some initial interest they were discounted due to the relatively small enthalpy observed.

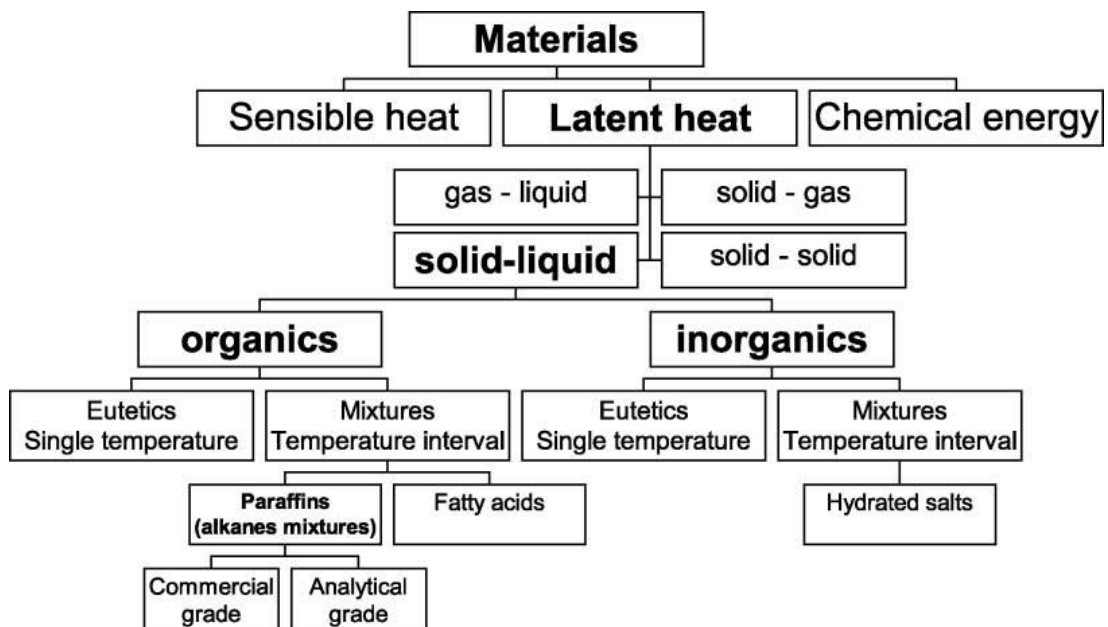


Figure 2.18 - Classification of Thermal Energy Storage Materials [63, 65]

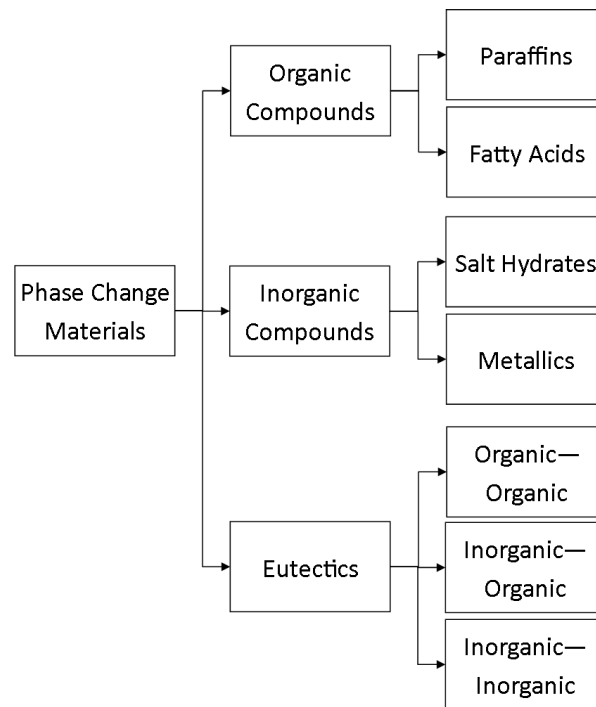


Figure 2.19 - PCM Classification Tree [61]

Figure 2.18, redrawn from [61], best illustrates the classification stages for solid-liquid PCM. There is slight discrepancy in the classification of eutectics, hence the differences in classification diagrams. As Figure 2.19 suggests, some of most promising PCM for building applications is that of organic paraffin.

2.3.2.3.1.1 Ice

The most well-known and abundant phase change material is ice, however every chemical compound will change phase at a given temperature and pressure. Early phase change research explored the application of ice systems for effective cooling. The relatively low (0°C) melting point limited the applicability of ice systems and the performance has since been surpassed. Thus a wide range of organic, synthetic and eutectic chemicals have been identified with melting temperatures nearer the region of a buildings comfort temperature.

2.3.2.3.1.2 Organic

The organic classification largely includes fatty acids and paraffins with the later attracting increased attention. They make for attractive PCM due to their:

- Wide and variable melting point range
- Relatively high heat of fusion
- No super cooling
- Chemically stable and recyclable

- Good compatibility with other materials (for mixtures)

The disadvantages of paraffins versus alternative PCM is their low thermal conductivity (around 0.2W/mK), their relatively large volume change and their flammability risk [61]. Research has presented methods to alleviate the disadvantages through the addition of high thermal conductivity materials and fire retardant additives [63].

2.3.2.3.1.3 *Inorganic*

Of the inorganic materials, hydrated salts have received the most attention exploring their particular application in solar heating systems. Inorganic salts are favourable as PCM due to their:

- High heat of fusion
- High thermal conductivity (around 0.5W/mK)
- Low volume change
- Low cost

The disadvantages holding back inorganic salts are their poor nucleation rates which cause super-cooling and their corrosive nature; both of which hamper the stability of the PCM and its supporting system [61]. To avoid super-cooling, nucleating agents are added; whilst arranging PCM in a thin layer increases stability [63].

2.3.2.3.1.4 *Eutectics*

Eutectics are mixtures of chemical compounds, either crossing the organic-inorganic divide or made up solely of either class, that all undergo phase transition at similar temperatures [52]. These mixtures are developed to offer specific melting points, thus have a great advantage in their sharp melting temperatures [61]. These synthesised materials also boast high volumetric storage densities. The current stumbling block for eutectic mixtures is the lack of available thermo-physical data. With greater understanding of these properties the true potential of eutectic mixtures can be ascertained.

Figure 2.20, redrawn from [59], graphs the range of available materials with low temperature (-100-200°C) melting points against their relative melting enthalpies (latent heat of fusion). It serves as a good initial comparison to understand the different PCMs available and their respective properties.

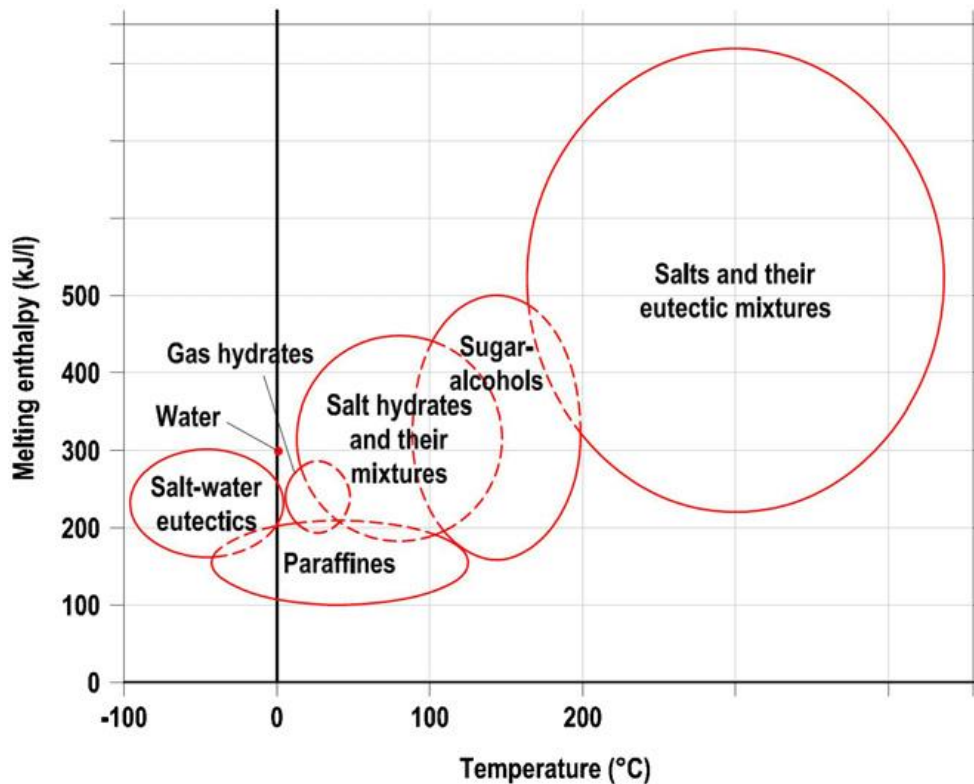


Figure 2.20 - Melting Enthalpy and Temperature for a range of PCMs [62] redrawn from [59]

2.3.2.3.2 Thermal Properties

To date numerous potential PCMs have been identified. Various authors have listed extensive thermal properties of such PCMs with [63] including all known materials with melting points in the temperature range from -10 to +100°C. For the purpose of building thermal comfort applications however the useful temperature range lies between 0 and 35°C. Their thermal properties are presented in Figure 2.21 below. On the chart each marker type represents a different data source ([52]square, [63]diamond & triangle, [64]circle, [65]cross and [81]dash). In figure 2.21 each colour represents a different classification;

- Blue – Organics (eg. Paraffins)
- Orange – Inorganics (eg. Salt Hydrates)
- Red – Inorganic Eutectics (eg. Salt Mixtures)
- Green – Organic Eutectics (eg. Fatty Acid mixtures)

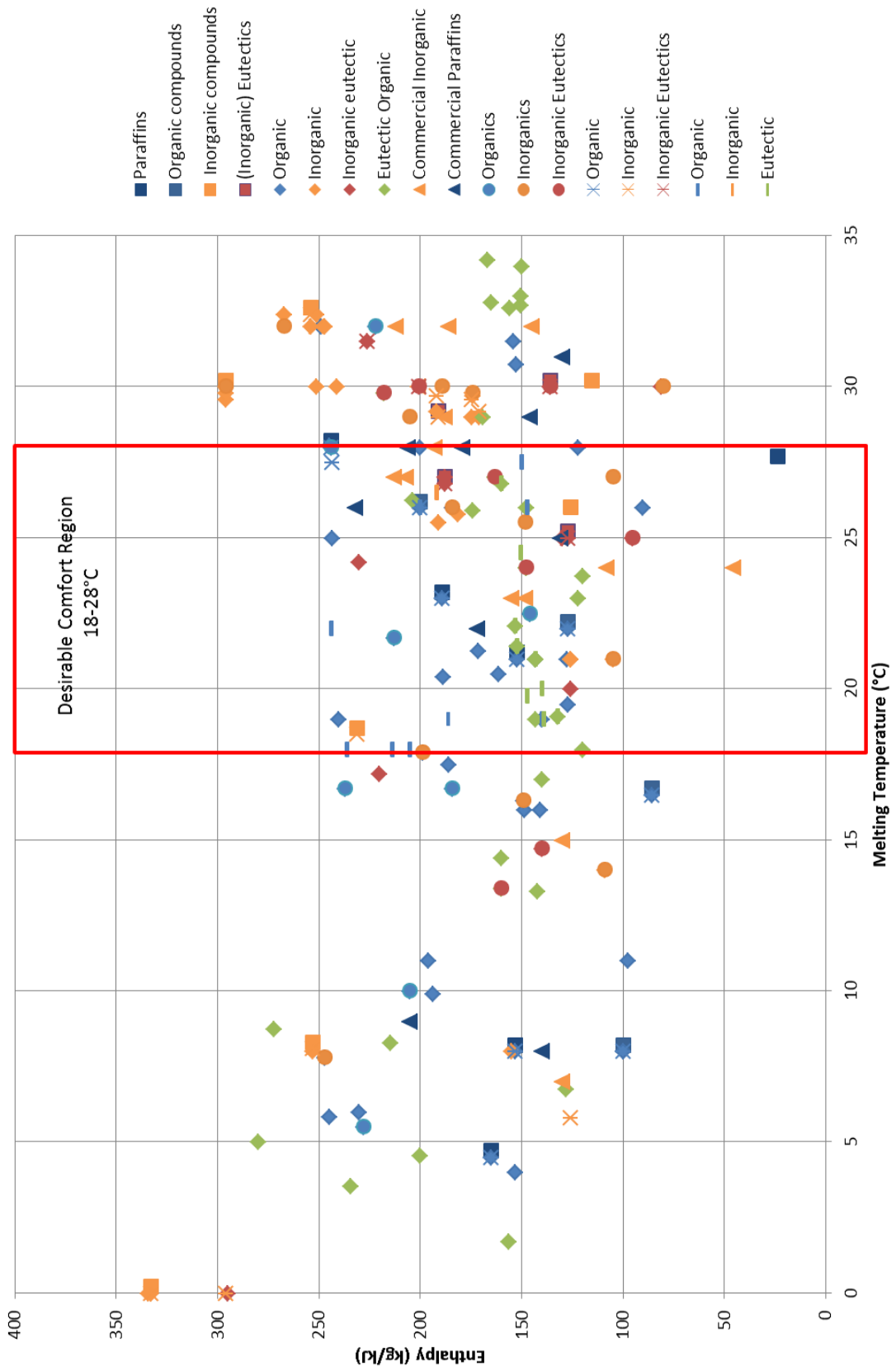


Figure 2.21 - Melting Temperature versus Enthalpy for known PCMs with melting points between 0 and 35°C

From figure 2.21, it is clear that the PCM with highest enthalpies are the salt hydrates. Within the desirable comfort region paraffin based organics offer the highest fusion enthalpies in the given region.

2.3.2.3.3 Commercial Materials

Various PCMs are available commercially from a range of suppliers. Table 2.2 lists the thermal properties of PCMs available with a melting point between 18 and 28°C. Rubitherm specialises in paraffin based PCM production for application as thermal storage medium [82]. The melting points of their products range from -10 to 100°C.

EPS Ltd (PCM Products) specialises in PCM and other environmental chemicals and services. They have a wide variety of containers and applications to house the PCM or can fill any given container with the specified PCM. The PCM can operate in the temperature range from -114°C to 164°C. Depending on the operational temperature range the PCM is made up of a mix of non-toxic salts and organic compounds [83].

BASF offers Micronal® PCM, PCM contained in micro acrylic capsules. The Micronal® PCM is suitable for mixing in fluid substances (paints or adhesives) or more densely in powder form, suitable for inclusion in construction mixes to produce 'melting' dry walls. Micronal® PCM targets building applications offering products with a range of melting temperatures in the human comfort region, 21 - 26°C [84].

Further manufacturers include Teap, Cristopia, Climator, Mitsubishi Chemical, Doerken, Merck and, as of 2013, Croda. Of these manufacturers the melting temperatures of PCM offered range from -50 to 118°C [53]. Table 2.2 captures commercially available PCM within the 22-28°C temperature range.

Table 2.2 - Commercially available PCMs with melting range between 21 and 28°C [63, 85, 86]

| Material | Type | Melting Point | Heat of Fusion | Thermal Conductivity | Company Source |
|--------------|--------------|---------------|----------------|----------------------|--------------------|
| | | (°C) | (kJ/kg) | (W/mK) | |
| CT21 | Bio-based | 21 | 176 | 0.18 | Croda |
| S21 | Salt hydrate | 22 | 170 | 0.54 | PCM Products |
| A22 | Paraffin | 22 | 145 | 0.18 | PCM Products |
| A22H | Paraffin | 22 | 216 | 0.18 | PCM Products |
| RT 20 | Paraffin | 22 | 172 | 0.88 | Rubitherm GmbH |
| S23 | Salt hydrate | 23 | 175 | 0.54 | PCM Products |
| A23 | Paraffin | 23 | 145 | 0.18 | PCM Products |
| Climsel C 23 | Salt hydrate | 23 | 148 | - | Climator |
| E23 | Salt hydrate | 23 | 155 | 0.43 | EPS Ltd. |
| Climsel C 24 | Salt hydrate | 24 | 108 | 1.48 | Climator |
| TH 24 | Salt hydrate | 24 | 45.5 | 0.8 | TEAP |
| A24 | Paraffin | 24 | 145 | 0.18 | PCM Products |
| CT25 | Bio-based | 25 | 186 | 0.21 | Croda |
| S25 | Salt hydrate | 25 | 180 | 0.54 | PCM Products |
| A25 | Paraffin | 25 | 150 | 0.18 | PCM Products |
| A25H | Paraffin | 25 | 226 | 0.18 | PCM Products |
| RT 25 | Paraffin | 25 | 131 | 0.88 | Rubitherm GmbH |
| A26 | Paraffin | 26 | 150 | 0.21 | PCM Products |
| RT 26 | Paraffin | 26 | 232 | - | Rubitherm GmbH |
| STL 27 | Salt hydrate | 27 | 213 | 1.09 | MitsubishiChemical |
| S27 | Salt hydrate | 27 | 183 | 0.54 | PCM Products |
| S27 | Salt hydrate | 27 | 207 | - | Cristopia |
| AC 27 | Salt hydrate | 27 | 207 | 1.47 | Cristopia |
| RT 27 | Paraffin | 28 | 179 | 0.87 | Rubitherm GmbH |

2.3.2.4 Encapsulation

As introduced above, central to PCM integration is the method of encapsulation. Encapsulation is the process of encasing the PCM to avoid leakage and subsequent performance losses. Various companies have utilised different methods. EPS specialise in adaptable macro encapsulation solutions [83]. Rubitherm have developed in situ bulk storage solutions [82] whereas BASF have cornered the market in the most adaptable form, microencapsulation [84]. To achieve heightened performance PCM encapsulation technology continues to be refined. In each encapsulation method it is important that the PCM and container-material have no chemical interaction to maintain long-term stability and avoid corrosive mixes [63].

2.3.2.4.1 Direct Application

Early research into PCM incorporation focused largely on direct incorporation and direct immersion. For direct incorporation, PCM in either liquid or powdered form is directly added to the bulk building material mix during production. The attraction of the technology is its simplicity; however problems with leakage and material compatibility hinder widespread applicability [61].

Direct immersion techniques involve dipping prefabricated building materials in liquid PCM. The building material surface absorbs the PCM material via capillary elevation. Due to the exposed nature of the PCM on the material surface significant leakage occurs during the life time of the technology [61].

2.3.2.4.2 Bulk Storage

Bulk storage encases the PCM in a large heat exchanger tanks. This method can be highly cost effective since little processing of the materials is required to prepare them for operation. Issues have arisen around poor thermal conductivity causing fluctuating performance. Effective methods of improving heat transfer through agitation and increased surface area have been explored [60].

2.3.2.4.3 Macro-Encapsulation

Macro-encapsulation houses PCM in solid moveable containers. Cabeza et al. [63] contains figures of macro-encapsulation methods offered commercially by EPS and TEAP. PCM is encapsulated in various containers ranging in size from ten centimetres to a few meters [83]. In each application the standard units are then fitted within a wider system to ensure maximum heat transfer. These macro-encapsulation units are anti-corrosive and thus can house inorganic PCM. As with bulk storage methods, poor heat transfer throughout the contained PCM causes solidification on the edges. The large scale makes incorporation in building applications difficult [61].

2.3.2.4.4 Microencapsulation

Microencapsulated PCM (MicroPCM) contains PCM particles (the core), a few microns in diameter, in a sealed membrane (the shell). Methods for incorporating MicroPCM in applications range from uniform sealing in a solid matrix to suspension in a heat transfer fluid (HTF). Most modern applications of PCM favour MicroPCM [81] because of the high surface area to volume ratio, compared to macro-encapsulated systems. Keeping this ratio greater than macro-encapsulated alternatives reduces the effects of the typically poor thermal conductivity, though this is highly dependent on the thermal conductivity of the membrane

shell. In MicroPCM internal volume changes are tolerated by the shell and avoid bulk volume change.

BASF's Micronial® PCM uses MicroPCM technology, encapsulating a paraffin core with a vinyl membrane [84]. Key to MicroPCM technology is compatibility and stability of the core and shell. Typically the shell membrane will be made from a high molecular weight polymeric film that maintains the structure of the particles and ensures no material leakage when in the liquid phase. Good stability and minimal structural strength losses upon concrete incorporation have been reported [61]. The use of MicroPCM in building materials has alleviated the leakage losses seen with the direct incorporation method.

PCM can be micro-encapsulated through a range of methods, both physical and chemical. Physical encapsulation methods include pan coating, air-suspension coating, centrifugal extrusion, vibration nozzle and spray drying. PCM is physically encapsulated via interfacial polymerisation, in-situ polymerisation and matrix polymerisation [81]. MicroPCMs are categorised based on their core structure and shell deposition process:

- Mononuclear – a single core with a single surrounding shell.
- Polynuclear – multiple cores surrounded with a single shell.
- Matrix Encapsulation – core material is distributed homogeneously throughout the shell material.

Many MicroPCMs are produced following a four stage process: emulsification, coacervation, cross-linking and filtration [53].

2.3.2.4.5 Shape-Stabilized PCM

PCM dispersed homogeneously throughout a supporting material, such as high density polyethylene (HDPE) or silicone, form a stable composite material. This composite material boasts high thermal conductivity, high stability and the ability to maintain solid shapes throughout the phase change process [61].

2.3.2.4.6 Slurry

There are two methods reported for transporting PCM in thermally active fluids (slurries) that of microencapsulation (MicroPCM) and direct mixing of paraffin in water by use of immiscible fluids [26, 53]. In MicroPCM slurries the core PCM is encapsulated by a molecular vinyl coating allowing for expansion without leakage into the slurry. These encapsulated balls exist in suspension in the thermally active fluid.

Paraffin directly mixed in water makes use of appropriate surfactants to enable the solubility of paraffin in water [87]. Further work to understand the melting and solidification process in water is required to enable wider application of paraffin water slurries. Initial investigations show promise in comparison to MicroPCM slurries offering reduced cost, simpler production and more efficient heat transfer [87]. Stability of the mixture is questionable and requires further techniques to maintain a consistent density of paraffin throughout the liquid. Lu [87] suggests some methods including constant mixing and thickening addition.

For both methods the use of slurries opens new capabilities for PCM applications as thermally active fluid. By making use of their relatively high energy densities the PCM slurries rival traditional coolant fluid applications. Careful consideration of the slurry transport medium will aid the thermal performance of the suspended MicroPCM [88]. Their functionality as fluids also enables transport to and from active centres through traditional liquid pumping methods.

2.3.2.5 Heat Transfer

Whilst the previous stages in the design process refine what technology is available, the specifics of the technology to meet the performance objectives will only be found as heat transfer capabilities are considered. The rate of heat transfer is governed by various physical properties [60], both of the PCM and heat transfer medium, the structural arrangement and operation of the PCM system.

It has been reported that *all manners of heat transfer* are present in the operation of a PCM system. *Convection* occurs within the heating fluid, between the fluid and external surfaces and between the heating fluid and PCM containers. *Conduction* carries heat through PCM containers and throughout the encapsulated PCM. Depending on the system *radiation* may occur from the container surface. When modelling packed bed systems the effective conductivity and total heat transfer coefficient are most often used to express general thermodynamic performance [60].

2.3.2.5.1 Modelling Heat Transfer

To model the performance of PCM systems requires a good understanding of the PCM transition process, heat transfer and fluid flow. Thus various different research teams have endeavoured to produce replicable formulae. Regin *et al* [60] catalogues many of the mathematical models that have been developed for modelling the heat transfer in various PCM systems. There are two methods, those of the single model and double model; the

difference arising due to the apparent physical transformation that occurs during phase change.

Further, difficulties in modelling have occurred due to the thermal gradients that occur within encapsulated PCM. During heat extraction the liquid core solidifies first on the outer boundaries of PCM. This solidification creates a crystalline PCM shell that must be permeated for the centrally contained heat to be extracted. Since the thermal conductivity of PCM is typically low this crystalline layer can significantly impede heat transfer and thus limit the system. For this reason many commercial systems have produced lower than expected performance during the product lifetime.

Limitations of modelling methods are still numerous and the applicability of a model varies widely on a specific system due to the diversity of PCMs and applications. [60] discusses many of the modelling limitations and the methods being explored to increase the models accuracy. Dolado et al [73] investigated a theoretical model carrying out uncertainty propagation analysis on various inputs. The findings increased the realistic nature of model results thus enhancing the model's credibility.

Tay et al [57] proposed a simplified design method characterising the PCM performance in effectiveness of number of transfer units (ϵ NTUs), the design method commonly applied in traditional heat exchanger design. Building upon experimental validation of PCM thermal storage units (TSUs) [89], thermal resistance of a PCM system [90] and a simplified slurry crystallisation model [91] the methodology for quantifying ϵ NTUs was undertaken. ϵ NTU was found to predict performance within 23% of experimental data. Greatest accuracy was found with higher heat transfer area. Whilst accurate under cylindrical shell and tube setups further investigation was required for application in wider environments. The method is however suitable for designing storage systems based on required temperature conditions.

2.3.2.5.2 Enhancement

Use of PCM in bulk systems has suffered from poor heat transfer due to their relatively low thermal conductivity; worse in paraffin based systems [61]. Various studies have therefore been carried out to enhance the heat transfer capabilities through bulk PCM. Conductive heat transfer was increased by use of metal foams, aluminium powders, carbon fibre and expanded graphite structures [87, 92].

Early enhancement of macro-encapsulated PCM was achieved through the design of a packed bed system [60]. Here increased voidage and surface area to volume ratio provided

better heat transfer. Heat transfer was still found to be limited within each container during crystallisation due to the solid layer formed on the boundary. Additions of metal fins, aluminium honeycomb and additives have been tested to increase conductivity however the cost and incompatibility with certain PCM have prohibited their progress [69].

Expanded graphite (EG) has shown great potential for enhancement of paraffin based systems [69]. EG demonstrates high thermal conductivity, high stability, good compatibility and lower density than metal promoters. Expanded graphite impregnated with paraffin PCM to form a mixture of 92wt% PCM produced minimal loss of latent heat whilst speeding up the conduction rate by over 250 minutes [69]. Work by Zhang et al [69] has developed EG in a more economical and environmentally neutral means through microwave irradiation.

The use of microencapsulated and emulsion based PCM slurries improve heat transfer by taking advantage of convective heat transfer along with the minimal conduction [92]. Heat transfer is therefore not limited to the poor rates of conductive heat transfer reported in bulk PCM [87]. In small scale applications, such as emulsion based PCM slurries, heat transfer effects can vary heavily due to the increased impact of surface interactions and thus increase the undesirable effects of super-cooling [93].

Figures taken from Wang et al [26] in Table 2.3 show the promising enhancement when MicroPCM was suspended in slurry. A 60% loss of latent heat is the main drawback, reducing the heat storage density, though significant enhancement of specific heat (80%) and thermal conductivity (32%) increase the capability of MicroPCM as a heat transfer medium.

Table 2.3 - Properties of MicroPCM Slurry and Components [26]

| Material | Density | Specific Heat | Thermal Conductivity | Latent Heat |
|---|---------------------------|----------------------|-----------------------------|--------------------|
| | <i>(kg/m³)</i> | <i>(J/kgK)</i> | <i>(W/mK)</i> | <i>(kJ/kg)</i> |
| MicroPCM particle (solid) | 829 | 1789 | 0.382 | 196 |
| MicroPCM particle (liquid) | 819 | 2153 | 0.203 | - |
| MicroPCM slurry (mass fraction(ϕ)) | | | | |
| $\phi = 0.1$ | 987 | 3945 | 0.575 | 19.6 |
| $\phi = 0.2$ | 976 | 3707 | 0.551 | 39.2 |
| $\phi = 0.3$ | 933 | 3470 | 0.528 | 58.8 |
| $\phi = 0.4$ | 911 | 3232 | 0.505 | 78.4 |

2.3.2.6 Cost Optimisation

After meeting the technical requirements, and before technology is commercialised, the final stage is the financial cost. The economic impact, commonly quantified in payback period, will be optimised against environmental and technical performance. Operation of the whole PCM incorporated system will be reviewed against competing technologies. If extra expense is required for innovative technology, the technical benefits (felt either through increased comfort or financial and environmental savings) must far outweigh the increased capital investment to overcome the risk adverse industry. The price of commercially available PCM varies from of 0.4 to 7.4 £/kg (0.5 to 10 €/kg) [63, 94].

2.3.3 Built Environment Applications

A great deal of PCM thermal energy storage applications in the built environment have been tested, largely academically, though a growing number of industries are expressing interest in PCM capabilities. Some products have made it to market and are listed in this section along with the trials.

Traditional interest in building applications has targeted an increase of thermal performance of light weight, building materials such as wallboard, concrete and insulation. More recently the development of PCM slurry has widened the scope of applications utilising PCM not only as heat storage medium, but also heat transfer fluid in air conditioning and cooled ceiling systems [81].

A list of capable PCM enhanced building applications was outlined by Dincer et al [53]:

- Cool TES, storing night cooling for use in day
- Incorporated into building structure
- Tempering heating and cooling water
- Providing night time heating and daytime preheating
- Solar hot-air heating system
- Domestic hot water preheater
- Solar hot water baseboard
- Off peak electricity usage
- Adsorption AC (with concentrated solar)

Whilst this list is not comprehensive it illustrates the wide variety of potential applications where PCM can be utilised throughout the built environment.

2.3.3.1 Wallboard

Wallboards are commonly used throughout the built environment making them a suitable candidate for PCM incorporation [81]. PCM incorporated wallboard provides TES throughout the natural framework of the building, increasing the traditionally low thermal capacity. A PCM incorporated system enables passive solar heating and off-peak cooling.

Early studies by Pieppo et al [75] recognised that simply adding PCM to walls and using passive solar heating offered savings of 5-20% on heating costs. Such savings may offer too slow a payback time. Performance however will be governed by PCM melt temperature, latent heat capacity per unit area, effectiveness of incorporation method, climate conditions and direct solar gains. Most studies focus on improving the controllable factors; those of PCM selection and incorporation [81].

Using PCM mixed with gypsum and shape-stabilised incorporations natural indoor temperature swing was reduced by 46% and 56% respectively [95]. Shape-stabilised systems proved to be more thermally effective with better utilisation of latent heat. Various other wallboard incorporation methods have been reported, including combining vacuum insulation panels with PCM. Reduction of temperature swings, overheating and lower temperature walls were commonly reported of wallboard systems [81].

Commercially National Gypsum has produced Thermalcore – ‘melting’ dry wall that incorporates BASFs MicroPCM particles into the dry wall mixture [96]. The dry wall panels make use of diurnal temperature swings to maintain temperate room climates whilst shifting electric duties to off-peak periods.

In work by Peippo et al. [75] equations to calculate the optimum wall thickness and phase change temperature were produced and subsequently been summarised by Zhou et al. [61]. Developed alongside equations for optimum melting temperature the optimum wall thickness was calculated from Equation 2.4.

Equation 2.4

$$D_{opt} = \frac{t_n h}{\rho \Delta H} (T_{m,opt} - T_n)$$

Where D_{opt} is the average optimum wall thickness; T is temperature, t is time and the superscripts d and n refer to day and night; h is the average heat transfer coefficient between the wall surface and surroundings; ρ is the PCM density and ΔH is the latent heat of fusion.

$T_{m,opt}$ is the optimum melt temperature calculated from Equation 2.2 (in the 'Desirable Properties' section).

De Gracia et al. [97] developed a method for calculating the thermal properties of composite building materials and subsequently studied the performance of PCM impregnated gypsum wallboard. It was found that PCM impregnated wallboard exhibited approximately 25-30% higher heat capacities and U-values. This increase results in a doubling of the thermal lag time measured [97]. The predicted payback of fatty acid mixture (30% PCM enhanced wallboard) had a payback time of between nine and seventeen years depending on the climatic conditions, assuming PCM cost of £2.3/kg (\$1.5/kg (US Dollars) at 2010 exchange rate) [62].

2.3.3.2 Concrete

Similarly to wallboard, different methods of incorporation have been tested, from direct incorporation to the more modern incorporation of MicroPCM matrix. Through direct application of PCM to 19mm floor panels energy savings of 24% were found by static analysis under Denver building conditions [62].

From experimental tests it was found that emission savings of 1-1.5kgCO₂/m² per year could be achieved using PCM enhanced concrete in Mediterranean conditions [81]. Tygai et al. [81] found that after a few consecutive hot days, where night cooling could not effectively cool the PCM, typical high heat storage capacity was lost. Various other arrangements of PCM concrete enhancement can be found in [81] to maximise stability, thermal performance and avoid leakage.

Scepticism around PCM enhanced concrete looms, due to the already high thermal mass of concrete, in comparison to lighter weight building alternatives such as wallboard. Never the less PCM enhanced concrete boasts an overall heat capacity of 8,000kJ/m²K; ten times that of PCM enhanced wallboard [62]. The relatively high cost of PCM however still hinders this step change in performance.

2.3.3.3 Ceilings and Floors

Various configurations of PCM incorporated ceiling fabrications have been designed [98, 99], utilising passive solar heating coupled with night cooling of the PCM [61]. When connected to passive solar heating the heat is stored until required, commonly when no external solar heating is available.

It has been found that passive PCM ceiling installations have suffered with overheating, resulting in incomplete diurnal phase change. It is often in these extended cold or hot days that extra heat duty is required, but the passive PCM is unable to cope. In conjunction with BASF, dynamic PCM radiant ceiling panels charged with PCM were coupled with geothermal heat sinks and passive solar heating to maintain effective PCM radiative heat management throughout the seasons [84].

PCM incorporation in underground floor systems makes use of heat discharge to the earth during the day shifting electrical consumption to the night rates. Shape-stabilised PCM incorporated into underground ductless heating systems has demonstrated good feasibility, though other underground systems have only marginal economic benefits [61].

A PCM incorporated concrete mix was added to the soffit of a pre-fabricated concrete hollow core deck [100]. It was found that the poor thermal conductivity of the PCM soffit layer inhibited the passive cooling of the sensible TES hollow core.

2.3.3.4 Insulation

Investigations into PCM incorporated cellulose and PU-foam insulators have found that 40% of wall-generated peak-load cooling was reduced. When fitted to attic insulation peak summer temperatures were reduced from 43°C to 32°C [62].

2.3.3.5 Shutters and Window Blinds

Research into PCM incorporated blinds reported 10°C reduction in blind temperature and a three hour time delay. 2°C reduction of room temperature was also achieved through the ZAE Bayern prototype. The incorporation of PCM in blinds uses minimal PCM for considerable effect on room temperature, in comparison to traditional incorporations. Comparative heat transfer losses are also greatly reduced by utilising solar radiation for heat gain avoiding the effects of typically poor convective or conductive coefficients[66].

As with the majority of building applications, applying the PCM within the building envelope provides a high thermal inertia, increasing the effectiveness of standard building modules. PCM shutters were modelled by Soares et al [101] to absorb heat through solar gain during the day and release the stored energy through the night. Due to low thermal-diffusivity of PCM the optimum PCM quantity was found to be directly related to the distance from metal fins, the modelled heat transfer surface. The modelling found that optimum utilisation of PCM storage occurred when complete phase change took place during a twenty-four hour cycle.

Further, Soares et al [101] found an optimal winter operation temperature of 20°C for Coimbra, Portugal. Using n-octadecane their results showed a daily heat cycle of 2,501kJ; surpassing the performance of a similar design of concrete by approximately 66%. Using SOLATHERM data they concluded that optimum winter design could be calculated for any given location.

2.3.3.6 Cooled Ceilings

The invention of PCM slurries, either through microencapsulation or emulsification, has introduced a new range of active PCM building applications. Building on existing water cooled ceiling (WCC) technology Wang et al [26] explored the incorporation of MicroPCM slurries as heat transfer fluid. Their work also reviewed and determined various numerical equations for modelling MicroPCM slurries for use as thermally enhanced fluids in WCC operations.

The mathematical model produced suggested that CC employing MicroPCM slurries could effectively offset the cooling demand to low cost night tariffs. The model developed is reported as being capable of helping building designs under various climatic conditions that would economise on storage tank size and pump capabilities [26].

[102] investigated a ventilated PCM ceiling unit made up of 27% PCM to maximise night ventilation benefits. The inlet air of 29.5°C was cooled to between 22 and 24°C during the eight hour test period. With air velocities of 2 and 3m/s the heat flow from the PCM registered 45 and 73W/m², respectively, after one hour. After eight hours of operation the panel heat flow exhibited 35 and 55W/m², respectively. During the diurnal laboratory tests not all the PCM was melted. Further design optimisation via computational modelling was put forward to maximise the daily PCM melt fraction.

2.3.3.7 Air Conditioning Systems

Further use of MicroPCM slurries as a heat transfer medium has seen the material incorporated in AC units. Here the slurry can operate in its dual function, that of heat storage and transfer. The high thermal capabilities of the slurries enable reductions in heat transfer area and thus AC units on the whole [88].

Cool-Phase[®], by Monodraught, has developed a system suitable for heating office spaces. The units claim 90% energy savings by efficiently recycling the waste heat in the exhaust air [56]. The 'thermal batteries' containing the PCM drives the summer cooling and winter heating. The installations are suitable for retrofit and have reduced over heating in office space

significantly. The six to ten kWh of energy storage contained in typical Cool-Phase® units can reduce AC consumption by up to 90%, according to Monodraught.

Systems utilising TubeICE, by PCM Products, have incorporated the PCM filled plastic tubes into ceiling voids or ventilation ducts. Around room comfort temperature, a single tube of available TubeICE can store 0.14 kWh of energy storage [103].

Chiu [18] used TRNSYS to model a PCM heat exchanger as part of a ventilation network. The work identified a 3.6kW cooling demand during peak-cooling-demand periods. An active LTES system maintained acceptable indoor comfort range at less than half the conventional AC operational cost. Future study advised optimising the energy system management to increase the economic benefits of the night cooling concept.

Work by [104, 105] investigated a novel PCM cooling system utilising ventilation air. Heat discharge of the PCM module was improved through non-integration within the building fabric, by increasing ventilation rates around the unit. Through modelling 34% annual energy savings were predicted based on UK office annual cooling loads.

2.3.3.8 Problems and Solutions in Building Applications

For many of the building application systems, limitations of PCM incorporation are apparent in extended weather windows. Passive PCM applications, where the material is used simply to increase the thermal capacity of the building material, suffer significant reductions in performance when diurnal melt cycles are not completed. Application of PCM in domestic buildings tested at the University of Nottingham struggled to solidify for extended periods during the summer [106]. PCM operating without phase transition operates under sensible heating, therefore losing the potential attraction of PCM incorporation.

Dynamic PCM applications, such as pumped MicroPCM slurry, can avoid such susceptibility due to temperature dissipation throughout the MicroPCM bulk storage tank. In these situations a larger heat buffer, commonly situated in the ground, ensures temperature variation is less affected by solar radiation. Recent work investigating ventilated PCM systems demonstrates potential, yet requires optimisation for full benefits to be realised [104].

Further widening of the operating envelope will help extend the likelihood of diurnal PCM transition. Thus in design stages, it is imperative to select a PCM with suitable melt temperature for the given application. Incorporation of various PCM with different melt temperatures may increase the effectiveness of the material. Ultimately, where diurnal

phase transition still struggles, PCM may need to be coupled with traditional AC units to ensure maximum comfort for building users.

2.3.4 PCM Modelling

Dutil et al [107] highlighted that the immaturity of PCM computer modelling continues to hinder the widespread incorporation of PCM within the construction industry. There is a lack of standard testing procedures and apparatus. Until this improves, research results will continue to be uncertain and optimum designs and materials obscured. Such variation in methods hinders industrial take up, as real world performance is unknown. Further, a lack of standardized methodology has made the ratifying of mathematical models inconsistent.

Dutil noted that studies show that incorporating PCM into building materials improved energy-efficiency by 10 – 15%. A careful review of modelling assumptions was proposed to understand the variation on the predicted effectiveness of PCM. Work is being undertaken to populate a database to aid consistent research, though is as yet inaccessible [107]. Further, the investigation led by Dutil suggested characterisation of composite encapsulated PCM performance was needed along with a refinement of modelling systems.

As yet, despite academic efforts, methods for modelling PCM incorporation into building simulation have not yet been standardised [92, 107]. To date PCM modelling has been carried out through three generic methods. Numerical analysis (with bespoke models based on the first and second laws of thermodynamics) characterises the effect of the phase-change process theoretically [108]. Secondly computational fluid dynamics (CFD) (using finite element methods) investigate PCM performance with the phase-change process modelled as a ‘mushy’ zone [109, 110]. Finally, more recently, building simulation software has become available that models specific commercial PCM products and PCM layers [111-114]. Typically a finite difference method is used within the energy simulation to determine the PCM effect [114].

2.3.4.1 PCM Mathematical modelling Methods

Propagation analysis by Dolado [73] validated a numerical PCM-air heat exchanger model (calculated from physical properties and equations characterising the heat flow) against experimental data. Traditionally PCM models use thermal conductivity alone to determine heat transfer through the PCM. Lin Qiu [115] studied the convection component of heat transfer within the CFD model. They found through CFD modelling that the liquid region represented reality and the natural convection increased as liquid fraction increased.

Verma [108] conducted a review of PCM modelling methods grouping the work done into First and Second Laws of Thermodynamics. First Law models, supported by validated experimental evidence, were reported. Common assumptions across the models analysed include the omitting of super-cooling and that heat transfer is conduction controlled. To date the level of experimental analysis validating the second law modelling methods requires further undertaking.

Developed from Gaussian distribution theory, and building on background work by Kim and Athienitis [116, 117], Darkwa [118] developed PCM first law numerical characterisation through an effective heat capacity calculation. The equation was used for performance investigation of PCM wallboard. From the PCM physical properties of latent heat, melt temperature, melt width and specific heat capacity; an effective heat capacity was calculated across the melting range. From this equation theoretical enthalpy curves can be plotted for novel PCM and thermal performance quantified in numerical models.

Equation 2.5

$$\int_{T_1}^{T_2} c_{eff} = c_s + a e^{-0.5\left(\frac{T-T_m}{b}\right)^2}$$

Table 2.4 - Equation 2.5 Nomenclature Key

| | |
|-----------------------------|--|
| c_{eff} | Effective Heat Capacity (J/kgK) |
| c_s | Specific Heat Capacity in Solid State (J/kgK) |
| a | Latent Heat Factor |
| T | Temperature (K) |
| T_m | Melt Temperature (K) |
| b | Melting Width (Standard Deviation, Function of Purity) |

2.3.4.2 PCM CFD Modelling

Fundamental analysis of PCM performance can be carried out on a localised level, using finite element software such as ANSYS Fluent. This is useful for fundamental studies, but becomes complex when simulating integrated HVAC technologies in a building context. Gowreesunker [119] used coupled TRNSYS-CFD simulation to monitor both the thermal air flow effects inside an airport terminal in CFD, and the HVAC PID in TRNSYS.

Within the Fluent CFD package, phase change models can be constructed using the *solidification/melting mode* [109]. The mode is designed to solve fluid flow problems using an

enthalpy-porosity method, where material porosity is equal to the liquid fraction. For the majority of PCM applications, except PCM slurry, the PCM is stationary; therefore porosity and pull velocities available in the *solidification/melting mode* are obsolete. The mode is limited to setting one set of physical properties for a material covering both the liquid and solid states.

The energy equations central to the simulation take into account both sensible and latent heat for materials modelled, deriving the portion of latent heat released from the liquid fraction. Liquid fraction, β , during the transition 'mushy' zone is calculated from Equation 2.6 [109].

Equation 2.6

$$\beta = \frac{T - T_{solidus}}{T_{liquidus} - T_{solidus}}$$

Shatikian [110] used Fluent 6.0 to investigate an aluminium finned PCM heat sink using a reduced computational domain to characterise the complete system. The work characterised the melting profiles of PCM in vertically portioned heat sink systems.

2.3.4.3 PCM Simulation Programs

BASF have developed their own software, PCM express, for modelling their patented Micronial® PCM within the built environment [120]. The software offers a crude estimation of temperature and energy savings based on building inputs. Commercial products incorporating Micronial® PCM can be simulated in the program. This software does not enable simulation of novel PCMs or PCM products.

To date most academic research into PCM systems within the built environment has been carried out using TRNSYS or Energy Plus. Through the *PCM wall plug-in* it is possible to model PCM as a wall construction within TRNSYS [112]. Two methods are enabled: either user specified physical properties or selection of commercially available technologies. The software is designed to simulate transient thermal performance in buildings [121]. TRNSYS uses a step function and finite difference model to represent the phase change performance transition. Work by Oyeleke [121] used DSC data to validate TRNSYS inputs.

The building simulation software, ESP-r, which was developed for building research purposes, uses a special materials facility to enable PCM inclusion in building models. The facility makes use of the effective heat capacity method to include the latent properties in the software energy balance models [122].

A bespoke plug-in has been developed for PCM modelling of DuPont's commercial product Energain® in TAS [106]. IES, in conjunction with Monodraught, have developed a module suitable for modelling their Cool-Phase® technology [111]. However, to date, IES have not developed a fully adaptable PCM plugin suitable for modelling PCM retrofitted as part of the construction fabric. With the exception of *PCM Express*, where most commercial technologies featuring Micronal® PCM can be modelled, building performance comparison between PCM technologies requires knowledge and comparable modelling in different building simulation engines.

Energy Plus, free building simulation software developed by the United States government (NREL), contains the functionality to model PCM within any construction layer, using a finite difference method [123]. Energy Plus is solely a thermal simulation engine. To enhance usability a Google Sketchup plugin was developed by NREL (the National Research Energy Laboratory). Further, the commercial software Design Builder utilises the Energy Plus engine for thermal simulations. Within Design Builder, Bio-PCM® saved enthalpy curves enable performance simulation of the Bio-PCM® commercial range. Additional PCM enthalpy curves can be specified to enable further simulation of novel PCM products [114].

2.3.5 Barriers to PCM Utilisation

Though young, PCM technology continues to mature through academic innovation and industrial implementation. Significant barriers to their widespread use within the built environment still remain. This section addresses the performance, modelling, industrial and economic barriers facing PCM.

2.3.5.1 Performance Limitations

The high-energy-storage densities reported are only effective within the PCM transition temperature envelope. For many of the building application systems, limitations of PCM incorporation are apparent in extended weather windows. Passive PCM applications, where the material is used simply to increase the thermal capacity of the building material, suffer significant reductions in performance when diurnal-melt cycles are not completed. Application of PCM in residential buildings tested at the University of Nottingham struggled to solidify for extended periods during the summer, negating the latent benefits [106].

[81] has shown that where diurnal phase-change has not been achieved, the thermal performance drops significantly; with the material exhibiting only sensible energy storage behaviour. Careful selection of PCM can minimise this drawback [61, 62].

Dynamic PCM applications can avoid such susceptibility due to temperature dissipation throughout the MicroPCM bulk storage tank. In these situations a larger heat buffer, commonly situated in the ground, reduces solar gain. Despite the dynamic benefits, the micro-capsules in MicroPCM slurries suffer from shearing through pumping; inhibiting the system applicability. Other solutions have incorporated moving an alternative heat-transfer fluid between PCM plates [56].

Further widening of the operating envelope will help extend the likelihood of diurnal PCM transition. Thus for best performing design, it is imperative to select a PCM with suitable melt temperature for the given application. Incorporation of various PCM with different melt temperatures may increase the effectiveness of the material. Development of MicroPCM slurries and other enhancements is widening the scope for PCM applications, helping to overcome the thermal-capacity and conductivity limitations. Continued research in this and conductive dopants will continue to increase the technical capabilities of PCM.

In many building applications, PCM competes against existing AC and insulation systems. To truly rival such established technologies, superior performance and at least comparable cost must be achieved. To date, PCM performance has required supplementary AC and insulation to guarantee desired comfort levels; due to the uncertainty of diurnal phase transition. Performance must be enhanced to compete with established alternatives. Integration with building energy management systems may enable PCM to compete with existing AC technologies.

2.3.5.2 Modelling Limitations

Increasingly building simulation is used to test and determine theoretical performance of novel technologies. As highlighted by Dutil et al [107] further characterisation of PCM performance and review of modelling assumptions will increase confidence in modelled performance. Progress has been achieved through the utilisation of the Energy Plus engine within commercial software Design Builder as well as the development of bespoke PCM products within IES and TAS.

2.3.5.3 Industrial Barriers

The lack of viable examples hinders the widespread application of PCM technology in the architecture and HVAC industries [107]. Growing case studies are available, largely in the Far East; however the conservative building industry is still reluctant to adopt fresh technologies. So it is likely that the long term safety and performance will have to be closely monitored

before widespread introduction. Further high profile installations at BRE and Whitehall in the UK are aiding commercial interest [124].

One institution in Germany, RAL PCM, has endeavoured to set standards for PCM quality and production control. To alleviate associated anxieties around PCM incorporation in the HVAC industry, a consortium of leading PCM manufacturers founded the *Quality Association PCM* to set quality standards for the emerging industry.

2.3.5.4 Economic Barriers

High construction costs, long payback times and uncertain green benefits all hold back significant incorporation of green technology [125]. Based on figures from Mehling [66] current to 2008 European fuel prices, it was deemed that two hundred full storage cycles would be required to save the amount of energy it would cost for initial PCM investment. This optimistic estimate excluded cost of containment or operational costs and assumed the stored heat was available free. From this brief analysis Mehling concluded that under current energy prices, the widespread incorporation of PCM was economically uncompetitive.

As socio-economic climates shift and fuel prices increase, a more detailed cost benefit analysis will be required, incorporating the overall Coefficient of Performance (COP) or Energy Efficiency Ratio (EER) of the specific PCM system. In such analysis the technological advantage (and thus perceived value) of the systems can be weighed up against the added cost to offer a cost benefit.

In an effort to open the door to investment, Menassa [125] developed an effective model for presenting the economic case of sustainable investment to building stakeholders and investors. The work took into account the product life cycle and perceived benefits; presenting results as an alternative net present value (NPV).

In 2008, Alanne [126] concluded PCM was, “not ready for commercial seasonal heat storage use,” based on work by the Australian Government. It issued a cost target of approximately 42£/kWh (57€/kWh on 2008 rates) for thermal energy technologies. For PCM technologies to be commercial competitive this cost target must be achieved.

Introducing new PCMs and operational methods requires a considerable economic shift, before the technology becomes a major constituent in the built environment market. The perceived advantage of the technology’s benefits must significantly outweigh the added cost for the technology to be accepted. Strong drivers from world governments towards greener

building standards are however, helping to overcome the traditional scepticism of new ideas and giving momentum to new technologies.

2.3.6 Further Applications

Despite reticence in the built environment industry, PCMs attractive properties also make it suitable for various applications outside of the built environment market. Most applications utilise PCM for one of two properties, thermal protection (inertia) or thermal storage. In the first case the typical low conductivity of PCM aids suitability, whilst the same property hinders the performance of many thermal storage applications [60].

Further uses of thermal protection (outside of the built environment applications) include thermal storage of solar energy, heating and sanitation of hot water and thermal protection of food and medical transport. Further medical applications include operating tables, and hot and cold therapies. Automotive applications are found in and out of the vehicle with PCM used to cool engines and maintain thermal comfort inside [60].

Dincer et al [53] lists further applications including PCM applied in refrigeration cooling system. The PCM reduces temperature fluctuation and increases efficiency, in personal and large-scale electronics. When used as a cooling medium, PCM can cool gas turbine inlet air, increasing turbine efficiency. One further study identified PCM incorporated in the desalination process; it is reported as having doubled the system water production per unit area.

Coupling PCM with thermoelectric units in satellites has produced a means of producing power during the hours of darkness. Catalytic converters have been developed incorporating PCM to release heat and increase the activation rates of the converters. MicroPCM has been successfully incorporated into fibres enabling PCM enriched clothing for applications in cold or hot climates [60].

2.4 Thermal Energy Storage Contrast

2.4.1 Technology Contrast

The significant thermal storage enhancement that PCM offers over traditional building materials is clearly shown in Figure 2.22. Figure 2.23 [59] illustrates this difference by the thickness required to store approximately 5,700kJ over a 10°C temperature range. The results demonstrated in figure 2.22 and figure 2.23 are only effective over the PCM transition temperature, outside of this temperature envelope the material would operate only under sensible heating.

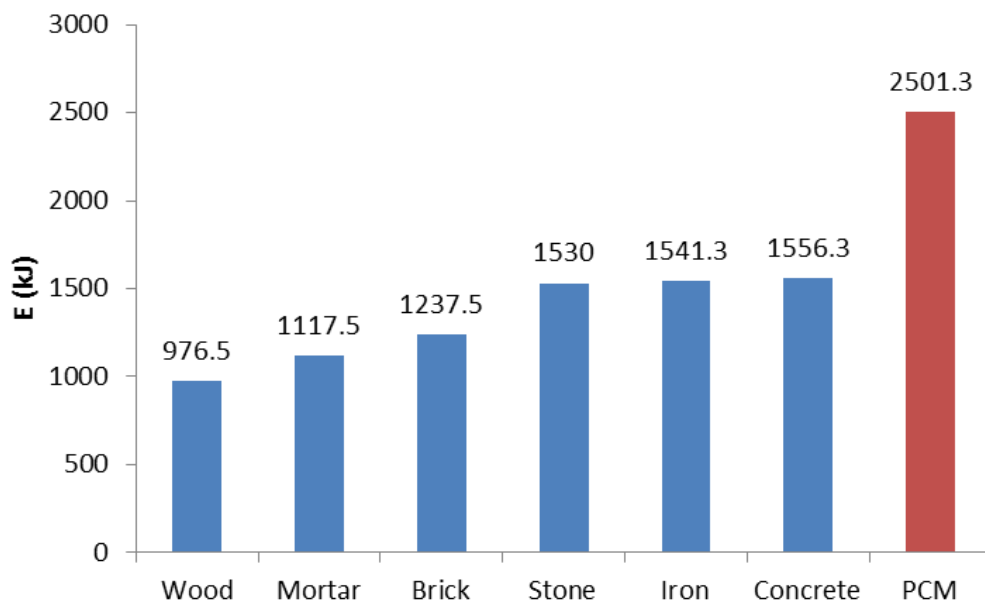


Figure 2.22 - Comparison of Energy Stored and Released during a 24 hour period

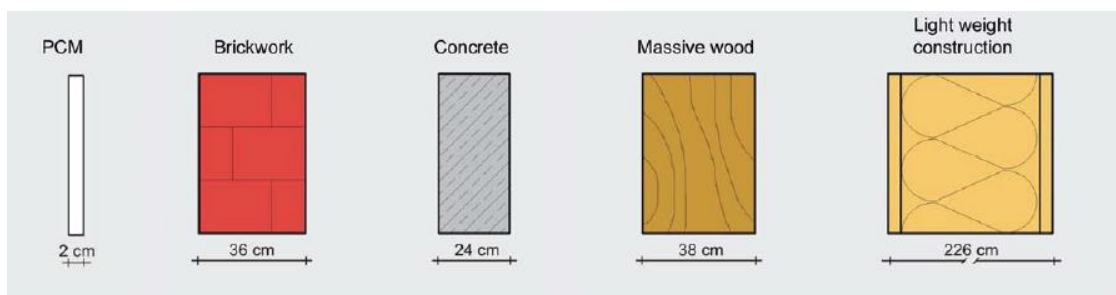


Figure 2.23 - Comparison of Thickness Required to store 5,700kJ over 10°C [59]

When Wang et al [26] studied the incorporation of MicroPCM slurry in cooled ceiling technology the results were compared against an ice-water alternative. MicroPCM slurry and the ice-water system had COP values of 4.0 and 2.2 respectively. Both systems effectively

offset the cooling to night periods; however the ice-water systems consumed 72% more energy than MicroPCM slurry and water systems due to increased pumping rates.

Dincer et al [53] details various case studies of effective integration and operation of PCM based thermal energy storage systems both for cooling and heating including a large district heating facility in Japan. One case in Rueil Malmaison Central Kitchen, France, supplies over 12,000 school dinners throughout the Parisian suburbs resulting in high peak cooling demands. The PCM tank designed has been used to reduce the peak electrical demand by over 80%. The benefits of these similar PCM cooling systems include; maintenance free operation (with reduced running cost), quick temperature response, standby capacity, flexibility and impressive environmentally neutral operation [53].

Figures typically contrasting PCM energy storage capabilities against traditional thermal energy storage medium, such as concrete or water, contrast latent heat energy storage only against a given temperature change within the sensible energy storage media. Since PCM contain both latent and sensible heat a brief mathematical investigation was undertaken to review the combined latent and sensible energy storage capabilities of two high performing, commercially available PCM, against concrete and water. The numerical investigation assessed the combined energy storage over a range of temperature changes (ΔT) (row 1 in Table 2.5).

Physical properties for concrete, PCM Products A22H, CrodaTherm25 (CT25) and water were presented in table 2.5. The mass of the samples was adjusted to offer the same quantity of energy storage as 10kg of CT25. Energy density was subsequently calculated and results reported in table 2.5. For the 10°C temperature range, more than twenty times the mass of concrete is required to store the same amount of energy. The PCM investigated offers five to six times the energy density of water.

Table 2.5 - Energy Density Comparison

| | Concrete[64] | PCM(CT25)[85] | PCM(A22H)[86] | Water | |
|-------------------------------|--------------|---------------|---------------|---------|--------------|
| Temperature Change | 10 | 10 | 10 | 10 | <i>K</i> |
| Specific Heat Capacity | 880 | 2100 | 2850 | 4184 | <i>J/kgK</i> |
| Latent Heat | 0 | 186000 | 216000 | 0 | <i>J/kg</i> |
| Mass | 235.2 | 10 | 8.5 | 49.5 | <i>kg</i> |
| Energy Stored | 2070000 | 2070000 | 2070000 | 2070000 | <i>J</i> |
| Energy Density | 8.8 | 207 | 244.5 | 41.8 | <i>J/kg</i> |

Following this initial comparison, the temperature change was varied between 5 and 50°C (row 1 table 2.5). It was assumed that the entire latent heat portion would be utilised in the two PCMs, over each temperature change. To compare PCM performance variation against concrete, the mass ratio (concrete mass divided by the A22H PCM mass to store the amount of energy) was plotted against the temperature change in Figure 2.24.

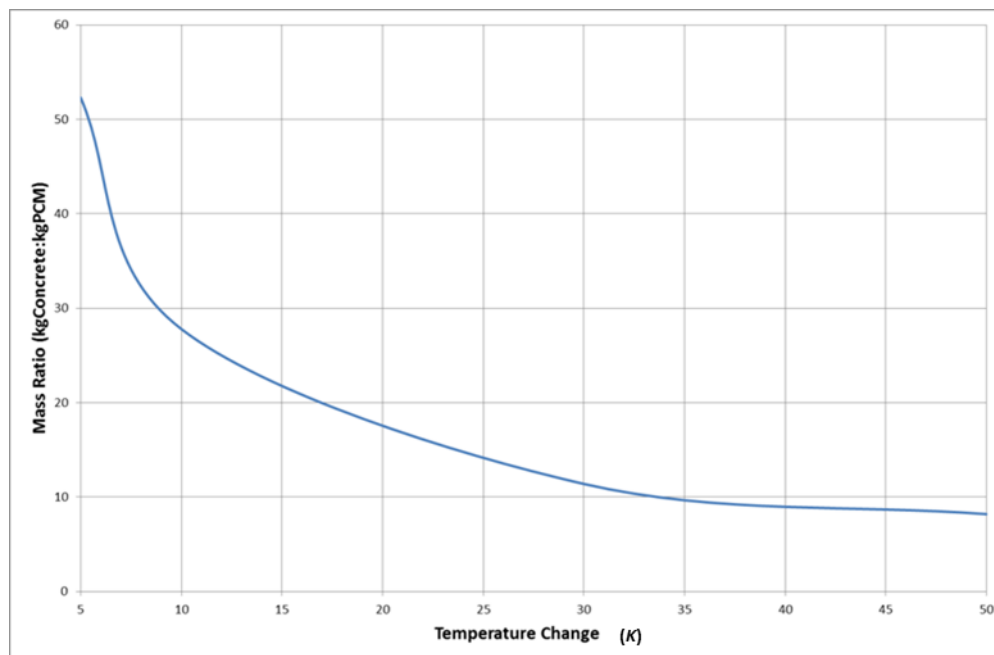


Figure 2.24 - Variation of Concrete to A22H PCM mass ratio with respect to temperature change

Figure 2.24 graphs how the concrete to A22H PCM mass ratio varies with respect to temperature. Under a small temperature change ($\Delta T=5K$), assuming the full latent effect is utilised, the PCM is capable of storing the same amount of energy as a concrete mass fifty times greater. Noticeably, as the allowable temperature change increases the significance of

the latent heat is reduced. With a 50K temperature change, a mass of concrete eight point two times greater than the PCM is required to store the same amount of heat.

2.4.2 Cost Contrast

PCM cost ranges from £2 per kilogram, for salt hydrates, up to as much as £9.6 per kilogram for pre-packaged systems [127]. In contrast concrete costs approximately £0.09 per kilogram. Using the energy density figures from Table 2.5; concrete, CT25 and A22H offer respective cooling capabilities of 0.011, 0.017 and 0.022 pounds (£) per kilojoule. Despite the greater energy density of PCM, the low relative cost of concrete means that for PCM the energy cost is 150-200% that of concrete [128]. In contrast against the TES commercial cost target of 41.56 £/kWh [126] the PCM reviewed, CT25 and A22H, achieve 55.48 and 73.80 £/kWh respectively.

2.5 Conclusions

Research and implementation of TES technologies have consistently demonstrated energy savings, and the ability to offset cooling demand; benefiting from reduced night-time temperatures and energy costs. PCM has demonstrated impressive TES capabilities and heat transfer impedance within the transition temperature range. These qualities have been tested in a wide variety of applications with a growing number of incorporated building products profiting from increased thermal capacity.

Organic PCM, especially paraffin, has become the favoured material in industry; avoiding the toxicity and sub-cooling problems evident in inorganic PCM. The low-thermal-conductivity of organic PCM has been effectively combatted through incorporation of conductive enhancers, such as expanded graphite, or through increased surface area to volume ratio via microencapsulation and suspension in slurry. Flammability risks have been minimised with fire retardant doping. A fresh avenue of research has opened in recent years with the development of MicroPCM slurries. This technology, though still in its infancy, has the capability not only to store heat, but also transport it, operating as an effective thermally active fluid.

A wealth of understanding and applications of passive PCM has been established; utilising PCM capability to impede heat transfer, insulate any given environment; or to function as thermal batteries by storing heat. The performance of Cool-Phase[®] demonstrates the real world capability within PCM technology to achieve efficient temperature control. PCM technology continues to mature with growing numbers of commercial products available. Despite this energy storage costs still exceed the cost target of £41.56/kWh.

2.6 Research Work Scope

2.6.1 Scope for Further Work

From the thorough review carried out there remains significant scope for academic investigation in the field of TES within the built environment. Enhancements to sensible TES systems have been investigated through air or water driven TABS [129]. Further cooling performance, in high need buildings, or during peak-seasons may benefit from the combination of an active air and water system. Work comprehending the theoretical and experimental performance of a combined (water and air) system would be of interest (Figure 2.25). Appropriate control systems have contributed greatly to the energy-efficiency improvement of air-based TES systems; therefore investigation of control strategies for a combined will offer performance benefit.

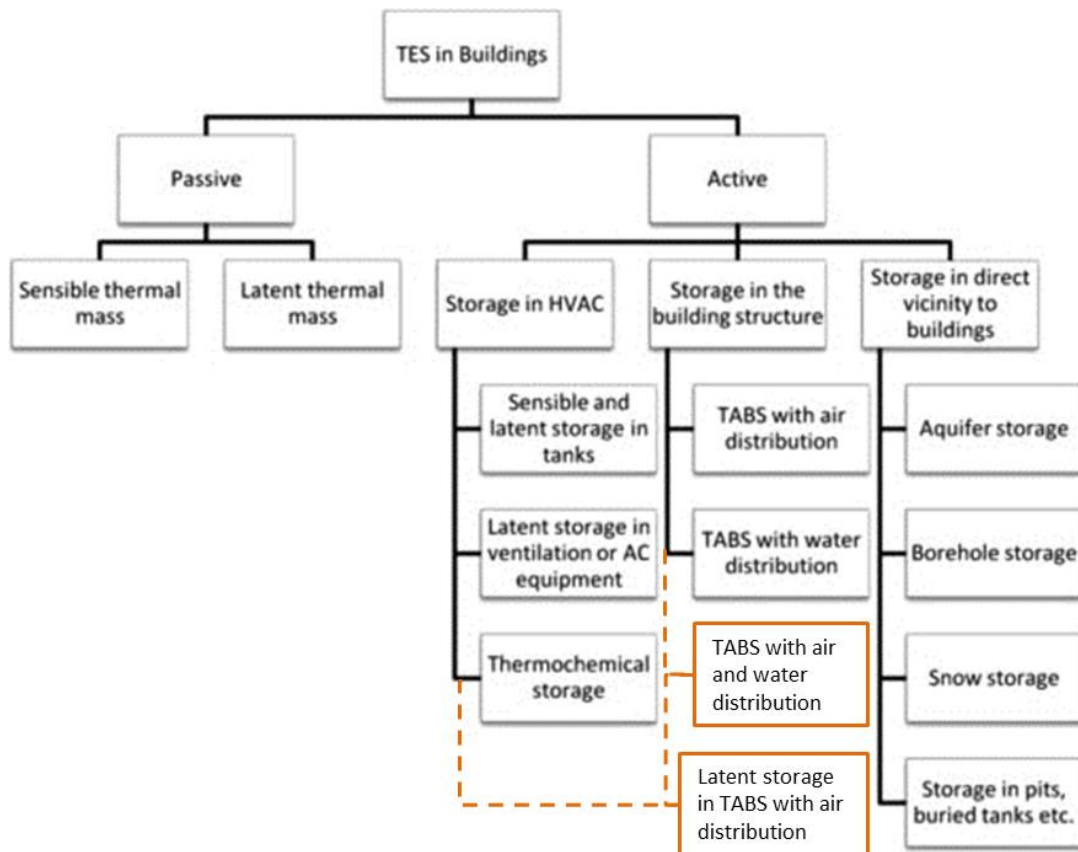


Figure 2.25 - Current work on TES in Buildings [129] with proposed scope added in dashed orange

Low cost, high latent heat, chemically inert, stable PCM (such as CrodaTherm™); that have been independently characterised, are the future of successful PCM integration into commercial built environment applications. Testing, characterisation and economic assessment of novel PCM would therefore be of benefit to further knowledge and stimulate the uptake of commercial PCM. Further work investigating TES modelling methods to

determine suitable methods, strength test existing methods, analyse previous assumptions and develop robust modelling methods, would be of benefit.

To date, PCM additions to sensible TES systems have been largely passive; through direct addition to building materials, screed layers or in finishing materials. The promise of active PCM systems have been investigated as standalone additions to HVAC systems [129]. The commercial success of active sensible TES systems suggests the modelling and experimental investigation of active hybrid sensible and latent TES systems is an interesting avenue of investigation. Understanding the relative benefits of latent TES over traditional sensible TES and the appropriate application for maximum benefit is of further interest.

2.6.2 Hypothesis

The energy and building contexts outlined in *Chapter 1*, illustrate the clear need for energy efficient buildings. The UK has initiated an, “*Energy Efficiency Strategy*,” targeting greenhouse-gas emission reductions and the growth of expertise in energy efficiency [1]. Achieving energy efficiency in commercial-sector buildings requires technologies that can deliver thermal comfort, using the minimum amount of energy, whilst offering competitive return-on-investment. Solutions exist, however others require further research and development to be trustworthy and cost-effective.

From the thorough examination of literature, conducted in *Chapter 2*, thermally active building systems (TABS) offer a low-energy solution for maintaining indoor thermal comfort. The investigation conducted also identified growing academic and commercial interest in the field of phase change materials (PCM), an emerging technology suitable for smart thermal energy storage (TES) systems within the built environment.

Building on the successful TES research work carried out to date, the research work conducted in this thesis aims to further existing knowledge, and offer an energy-efficiency technological and commercially viable solution through the exploration of the following hypothesis:

This thesis proposes to investigate the hypothesis that: enhanced active-thermal mass systems, which utilise the building envelope and PCM retrofit additions, are cost-effective energy-efficient thermally-comfortable technologies, suitable for UK offices.

2.6.3 Research Aim

The research conducted in this thesis aims to:

- Identify thermally-comfortable, energy-efficient and cost-effective enhancements to an air-based concrete hollow-core TES system, utilising emerging PCM technology.

The investigation will be laboratory led to provide real data suitable for characterisation. The enhancements to be investigated are water and air thermal fluids passing through the TES system and, a retrofit system featuring PCM. The focus on laboratory led research will enable the characterisation and validation of subsequent models following this thesis work.

2.6.4 Research Objectives

The research objectives below serve to achieve the research aim above.

- Develop an air-based TES system suitable for laboratory testing and water-pipe addition.
 - Identify a suitable air-based TES system,
 - Understand performance limitations and,
 - Design and construct water-pipe development of air-based system.
- Investigate benefit for water-pipe enhancement through the use of mathematical modelling, CFD and laboratory testing. Enhancement via improved thermal fluid will be considered, along with increased surface transfer area and viable PCM retrofit additions.
 - Modelling of air and open-loop water system under seasonal office conditions.
 - Design and construction of prototype rig, including thermal chamber to contain the raised TES system.
 - Testing of the prototype cooling capability with respect to water (closed-loop) and air control strategies.
 - CFD modelling of air and water TES systems to find steady-state cooling performance.
 - Component laboratory testing of air, water and, air and water TES system operations under steady-state thermal conditions.
- Research, design and develop a suitable PCM retrofit enhancement to the air-based TES system.

- Conduct CFD simulations of potential PCM retrofit additions to identify the most cost-efficient design.
- Characterise the physical properties of the favoured PCM through DSC analysis.
- Design and construct preferred PCM retrofit design.
- Characterise PCM retrofit system cooling performance through isolated component laboratory testing.
- Design and fabricate test chambers for office condition replication with and without the enhanced TES system. Each test chamber will be required to vary and measure temperature inside and out.
- Investigate, at a pilot scale level, the cooling and energy saving benefit of the water and PCM TES system enhancements.
 - Install TES system and enhancements to test chamber,
 - Fit thermoregulation and measuring equipment,
 - Conduct *fixed*, *diurnal swing* and *peak period* tests and,
 - Generate cooling and energy saving data for each enhancement under given conditions; useful for validating future enhancement models.
- Conduct economic assessment of the enhanced TES system to determine the cost effective nature of the system and suitability for the UK's non-domestic 'Green Deal' scheme.

2.6.5 Thesis Overview

To ascertain the capability of enhanced thermal-mass as an energy-efficient thermal-comfort technology, with particular focus on the UK office context, this investigation has followed the work scope outlined in this thesis overview. The work has begun in *Chapter 1*, outlining the need for this research through the sustainable drivers and legislative context; in which built environment energy-saving technologies demonstrate their capabilities for aiding the achievement of wider UK sustainability targets.

In *Chapter 2*, having highlighted the wider capabilities of energy storage, this work details the state of the art of thermal energy storage (TES). Particular detail was offered in the field of latent thermal energy storage (LTES) technology, and the modelling practices of typical LTES phase change materials (PCM) within the built environment. This has defined the scope for further developments in the field, enabling the identification of a research hypothesis.

Building on the context, state of the art and hypothesis, the main body of the work, *Chapters 3-7*, undertook a proof-of-concept; through investigation of the capabilities and enhancements of a novel active thermal-mass system. The early work (*Chapters 3-5*) investigated sensible TES systems; designing, modelling and testing a novel pilot-scale TES prototype, featuring the active water and air enhancement. Further, (*Chapter 6*) the work analysed a PCM retrofit system, for integration with the active-TES system. In culmination (*Chapter 7*) a combined sensible and latent TES investigation, brought the findings from two fields together. The enhanced active thermal mass prototype was investigated for energy saving, temperature reducing and economic benefit.

Central to these enhancements was the addition of thermal mass through PCM incorporation. The active thermal-mass system was further enhanced through the investigation of low-energy heat management systems for the harnessing, transportation and storage of heat. Additionally, the development of a suitable control-strategy enabled highly-efficient cooling of high-intensity office spaces (*Chapter 4*). Further to the technical proof-of-concept, commercial and comfort considerations were discussed and concluded with an economic analysis (*Chapter 7*).

As a result of major funding from UK industry, this post-graduate research work has maintained a continual furthering of technological innovation in a high demand field. The industrial partners were keen to explore diversifications to their product base. As such, the contributions to knowledge presented within this thesis are both novel and relevant within the sustainable built environment sector. Commercial development and product launch have been realised, arising directly from the work conducted.

Chapter 3: Active Thermal Mass Design and Model

Prototype Design and Performance Modelling

3 Active Thermal Mass Design and Model

3.1 Introduction

Ventilated hollow core (VHC) is an established energy efficient technology within the built environment [130]. Similarly the use of thermally activated building systems (TABS) has demonstrated energy efficient temperature management through the embedding of water pipes as part of hollow core systems [131]. Similarly, computational simulation of chilled ceilings in conjunction with PCM thermal storage tanks has demonstrated energy saving potential [26].

The work reviewed in *Chapter 2* reveals the capability of thermal energy storage (TES) systems to satisfy internal thermal comfort and make significant energy and financial savings, up to 90% AC energy savings for leading latent TES systems [132]. To assess the scope for TES enhancement, and satisfy the first research objective of this work, a prototype VHC system will be identified, designed and simulated in this chapter.

Following initial design, characterisation of a suitable VHC system will be predicted through numerical modelling. The modelling will aim to comprehend its performance, control strategy, and energy saving benefits over passive thermal mass systems. The results of the modelling aim to highlight the areas where alternative thermal fluids and ventilated PCM thermal mass systems may provide benefit.

During the modelling understanding of the performance benefits of water incorporated hollow core (WHC) and combined water and ventilated hollow core (WVHC) will be investigated. The investigation in this chapter served as a building block for further detailed active thermal mass investigation. Through this process understanding of control strategy and WVHC prototype design was obtained. The conclusions from this chapter have informed subsequent detailed modelling and laboratory trials.

3.1.1 Scientific Background

The fundamental effectiveness of TES systems to function as energy-efficient thermal conditioning relies on the principles of thermodynamics and heat transfer. Thermally massive buildings, where the building structure is made of heavy weight material, are able to moderate day and night temperatures through the high specific heat capacity and low thermal conductivity coefficients. Thermally massive buildings moderate the internal temperature but offer no control over the temperature of the mass and internal space.

Active TES systems pass ventilation air through the building mass to improve heat transfer and system control. The control of the system is therefore governed by the properties of the internal air flow and surrounding thermal mass. On a time (0) to time (1) level the condition of the air flow and mass can be calculated from:

Equation 3.1

$$Q_{slab} = m_{slab}c_{p,slab}(T_{slab,1} - T_{slab,0})$$

Equation 3.2

$$q_{air} = \dot{m}_{air}c_{p,air}(T_{air,1} - T_{air,0})$$

The overall heat transferred in the air networks can be calculated using the overall heat transfer coefficient (U), the contact area (A) and the air inlet and outlet temperatures in the equation below:

Equation 3.3

$$q_{internal} = UA(T_{air,out} - T_{air,in})$$

The overall heat transfer coefficient (U) is calculated for the thermal fluid's physical and fluid flow properties, for example material viscosity, turbulent flow and dimensionless numbers (Re , Nu and Pr). Work by Green [38] details these relationships in an active TES (VHC) context.

To enhance an active TES system, improvements in control or capacity are cited. Control is improved through heat transfer changes, for example: increased temperature difference or increased fluid flow. To improve capacity greater mass or additional mass with a greater specific heat capacity is added. It is therefore required that an air-based TES system be constructed capable of control and capacity enhancements.

3.1.2 Methodology

Based on the scientific background and the state of the art there revealed potential to improve upon traditional active TES systems, either through capacity or control modifications. The purpose of this chapter is to develop an air-based active TES prototype, capable of available enhancements. Initially the prototype will be enhanced through embedding of water pipes. Through water activation the control of the slab is increased, due to the improved heat transfer properties. Effective PCM enhancement will be considered in later chapters to add thermal capacity.

3.1.2.1 Design Prototype system

Following the modelling, and having recognised enhancement opportunities, the prototype system will be designed and constructed as follows:

1. Outline prototype requirements
2. Design system and test rig

3.1.2.2 Model Prototype TES system

To enable the construction and enhancement of the active TES prototype, numerical modelling will be conducted. The aim is to reveal the areas where enhancement is of particular value. The method for numerical modelling will be conducted as below:

1. Construct a heat and mass balance numerical model to simulate the VHC performance
2. Validation of system performance against commercial proprietary software
3. Prediction of VHC annual performance
4. Construction and prediction of WHC and WVHC annual performance
5. Summary of enhancement opportunities

3.1.3 Contributions to knowledge

Having completed the methods outlined above, numerous valuable contributions to knowledge have been achieved:

- Benefits of water and air driven TES systems has offered energy-efficient thermal regulation of internal spaces, offering cooling capacity up to 60 to 70W/m² [24]. In super-insulated hi-tech offices, greater cooling can be required. This work therefore investigates the scope of combining water and air driven TES to provide high levels of energy-efficient heat dissipation.
- An initial understanding of how a combined WVHC system performs, both numerically and practically was sought. The ability to model water and air based hollow core (WVHC) system was established in summer 2012. The work conducted here was built upon in a 2012 draft industry design guide [133], followed by an approved method for modelling which was established subsequently in January 2014 by IES [134].

3.1.4 Chapter aims

- 1) Design a prototype hollow core sample featuring air and water networks, suitable for thermal testing.
- 2) Develop a modelling tool to simulate the performance of the combined water and air activated thermal mass system.
- 3) Simulate appropriate scenarios using the modelling tool to estimate performance.
- 4) Identify suitable opportunities for TES enhancement.

3.2 Prototype Design

Amidst legislation driving low carbon design and implementation within the construction industry, ventilated hollow core (VHC) has proven its worth as a sustainable temperature stabiliser for commercial office environments [130]. Likewise cooled ceiling technology and TABS have demonstrated great potential in offering an alternative to under floor heating [131]. This work has therefore been undertaken to determine the viability and potential performance of a combined ventilated and water cooled radiative thermal mass temperature control technology (WVHC).

As identified the novel nature of a combined WVHC system requires design, construction and installation of a pilot scale prototype test rig. The prototype rig was required to replicate the established air based performance of typical active hollow core systems such as Termodeck and Actimass [34]. As a start point under floor heating guidelines were followed for the construction of the water addition [25]. Performance would be measured based on energy consumption and temperature profiles. This section details the design, construction and installation process that has been carried out to enable the prototype's familiarisation testing.

3.2.1 Prototype Design

The prototype required the inclusion of both an air and water network embedded in the thermal mass. The first discovery identified that, unexpectedly, neither had been constructed in the sample slab. The ordered embedded water pipes were simply inserted one inch into the slab and wedged in place for exhibition. Similarly, the typical air networks used in industrial systems were not drilled. Further, upon assessment it was found that two metal pins running the full depth of the slab reduced the core length of four of the cores by a quarter.

In order to maintain rig prototype performance through the air network in line with industry operation standards it was necessary to ensure the final air temperature and slab temperature are equal $\pm 1^\circ\text{C}$ when the air leaves the air network [34]. Due to the restriction of the air path length and the operation standard, all six cores were utilised in the air network.

Aware of the demonstration hollow core limitations, prototype scope design drawings were developed. Figure 3.1 shows the intended WVHC design complete with thermocouple locations. The dotted lines are the pre-drilled hollow core channels. The red crosses in green

circles represent the cross overs between cores. The cores and crossovers make up the air network. Purple crosses, A_{1-6} , denote the position of thermocouples measuring the temperature in the air stream. The black arrow demonstrates the air flow direction through the network and finally out of the green circle with small red-cross into the room.

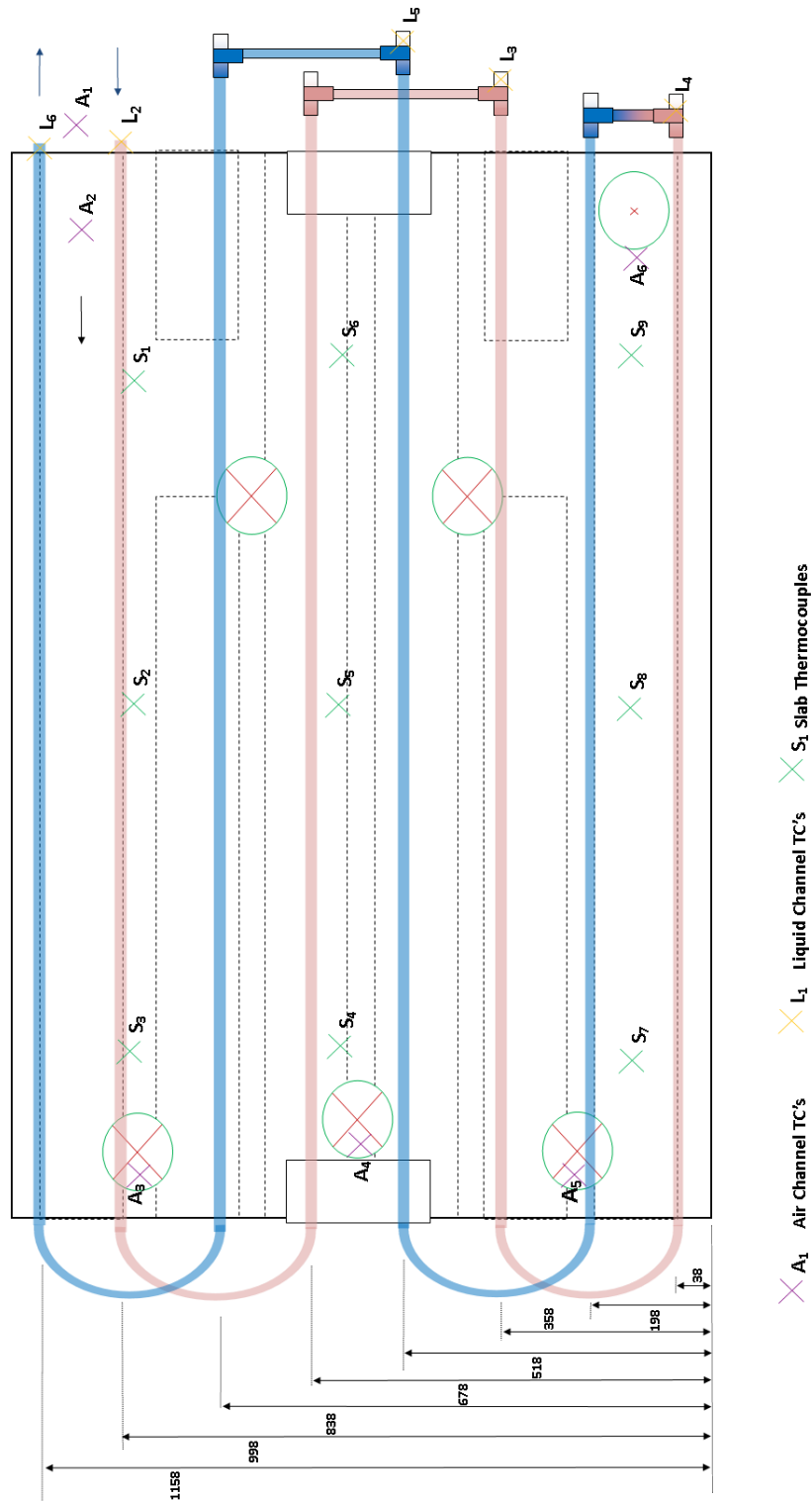


Figure 3.1 - Prototype Cutaway Drawing

The blue and red lines represent the water pipe system. The blue arrows denote the water flow direction. The pipes are connected following a double serpentine method to enable even heat transfer distribution across the slab. The water pipes pass through the concrete slab eight times spaced as shown in figure 3.1. Their measurements are in millimetres. Yellow crosses, L_{2-6} , mark the position of thermocouples measuring the temperature in the liquid stream.

The green crosses mark the points where thermocouples, S_{1-9} , measure the temperature of the concrete. These were positioned 50mm deep in accordance with the figures in Table 3.1. The concrete and air thermocouples are embedded into the concrete slab whilst the liquid thermocouples are inserted into the pipes at the right end of the slab. In total nineteen thermocouples were specified to monitor and characterise the thermal performance of the hollow core prototype.

Table 3.1 - Slab based thermocouple locations for Figure 3.1

| Sensor | Horizontal | Vertical |
|----------------------------------|-------------------|-----------------|
| Distance from bottom left corner | | |
| S1 | 1295 | 940 |
| S2 | 740 | 949 |
| S3 | 260 | 955 |
| S4 | 330 | 593 |
| S5 | 790 | 615 |
| S6 | 1296 | 617 |
| S7 | 163 | 123 |
| S8 | 714 | 115 |
| S9 | 1209 | 103 |

To accomplish the preparation and construction, the rig required additional parts and further construction stages. Table 3.2 documents the additional parts required to convert the hollow core slab into a WVHC functional prototype.

Table 3.2 - Additional Hollow Core Parts Required

| Part Required | Quantity | Source | Purpose |
|------------------------------|------------------------|---------------|---|
| UFH Water Pipe | 25m | UFH Warehouse | To carry the liquid through the slab. Sufficient structural strength to be embedded in concrete and handle temperature variation through testing. |
| Cross Over Plates and Outlet | 5 and 1 | TBP | Seal the cross overs once drilled and maintain outlet diameter through additional concrete layer. |
| Concrete | 100 litres of concrete | Lafarge | To construct the additional 50mm of depth necessary to embed the pipes. |
| Thermocouples | 20+ K-Type | RS | To measure the temperature in the slab, air, water and room throughout the experimentation. |

3.2.2 Laboratory Rig Design

To gain understanding of the prototype operation and provide novel contributions to knowledge a suitable laboratory rig was designed to test the capabilities of the innovative WVHC system. Interest from industry had centred on enhancing the cooling capabilities of VHC systems during peak periods. Further, findings from the Excel Model highlighted greater scope for enhancement during spring and summer conditions. Therefore rig design focused on replicating conditions requiring slab cooling rather than heating.

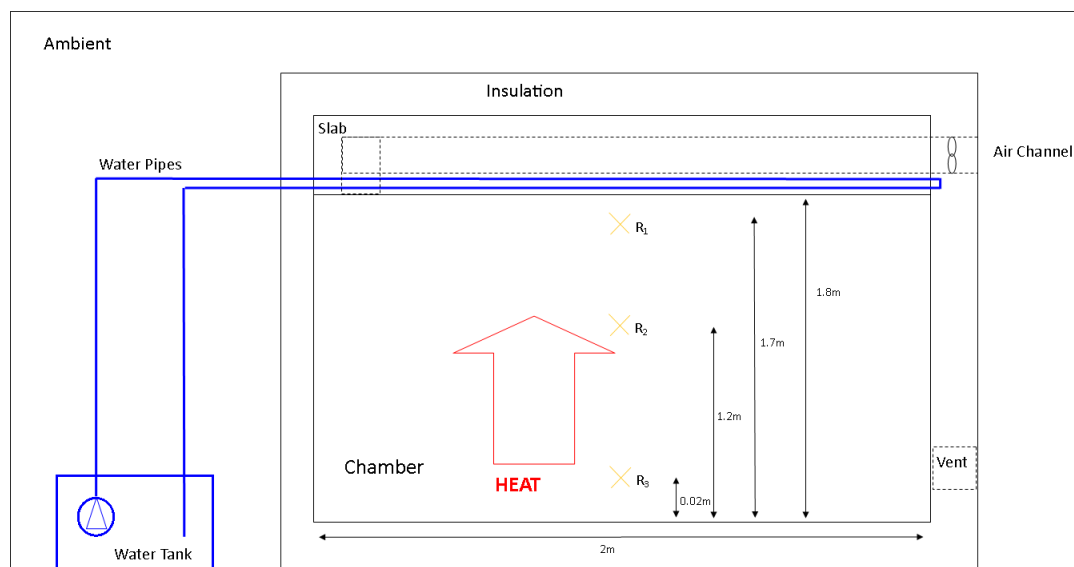


Figure 3.2 - Simplified Rig Design

Figure 3.2 displays the simplified rig design. The WVHC prototype system was mounted as the ceiling soffit of a suitably insulated test chamber – replicating standard VHC practice. Air entered through the ‘Air Channel’ fan, and exited through the ‘Vent’. Internal gains were modelled by an internal heater with room temperature sensors (R_{1-3}) positioned vertically in the middle of the chamber. Evidence from [24, 135] reveals most internal room temperature variation in chilled ceiling systems is observed vertically, with differing characteristics at elevations below half a metre, at approximately one metre and close to the ceiling. The air surrounding the chamber was at ambient laboratory temperature (typically between 15 – 18°C during ‘occupied’ periods). The water tank contained thirty-five litres of ambient temperature water, pumped at 4 l/min.

To simulate a typical office cooling demand scenario twenty-four hour simulations were to be carried out with eight hours of occupied heating, followed by sixteen hours of unoccupied simulated conditions. Temperatures were monitored throughout the twenty-four hour period.

The internal room heater provided radiant heat to ensure convective heat transfer was provided by the fan installed in the WVHC system only. Cooling was provided through the combined ventilation and water activated hollow core. Temperature sensors in the prototype system, chamber and ambient spaces provided data for temperature profile analysis. Energy meters connected to the heater, fan and pump provided energy consumption information.

Before construction initial modelling was conducted to predict the theoretical performance of the WVHC design.

3.3 Active Thermal Mass Modelling

Precedence for computational modelling of VHC systems has been set as far back as 1998 [36] with a comprehensive review published in 2014 [33]. In 2013 work by Chae [47] included AHU strategy in VHC performance modelling for the first time. Karlstrom [49] built on research by Weitzmann [24] to model WHC and WVHC performance but no performance figures were published for the combined system. The modelling conducted in this section goes beyond the previous slab only models, where air-concrete boundary heat exchange is given the major focus. The model formed in this chapter brings together the mathematical models from previous elements of the system to give overall system performance. The model also includes control strategies and AHU performance, capable of predicting annual performance.

For the purpose of this investigation, to obtain understanding of WVHC performance, a ventilated thermal mass heat-balance model was developed. The model functioned as a time-step heat-balance model with the balance for the previous time-step forming the inputs for the next. The time-step numerical model was used to predict the innovative system performance under seasonal conditions. Excel was used to conduct the calculations due to the graphical display, making tracking system performance variation against time simple.

External and internal temperature profiles, generated via early simulations using the bespoke Excel based *Thermal Mass Temperature Control Simulator*, were validated against the industry used building simulation software, *Equa*. Following a pilot scale scenario, the *Simulator* modelled the twenty-four hour British summertime performance of each configuration. The restrictions made on this initial scenario limited the scope of the results generated. Each technology being contrasted suffered from suboptimal performance and the minimal time frame simulated gave only a brief understanding of performance.

Therefore, from the model developed this investigation compares the annual performance of ventilated hollow core (VHC), water activated hollow core (WHC) and a combined ventilated and water activated hollow core (WVHC) radiative thermal mass temperature control technologies in a typical small UK office.

3.3.1 Modelling Background

The modelling purpose was to produce a model that predicts the comparative performance of ventilated hollow core (VHC), water activated hollow core (WHC) and a combined air and water activated hollow core (WVHC) systems. To quantify system performance, Coefficient of Performance (COP) figures and temperature profiles were generated for seasonal UK operation.

Figure 3.5 shows a cross-section of the generic office room represented in the Excel simulation model. During VHC, WHC and WVHC operation a simple AHU system services the room with preheated or precooled air and then recycles exhaust air through a thermal wheel. Water pipes pump mains water through the slab and out to drain. There is no water recycle or heat recovery in the water side of the model. Heat generation in the room replicates occupancy behaviour and solar gains. AHU, slab and heat generation variations are specified in the model.

3.3.2 Modelling Methodology

To develop understanding of the function, capability and operation of the system a bespoke Excel based heat balance time step model was developed. Equa, due to its use within the industry, was used as reference software to verify the Excel model.

The Excel model constructed was based on iterative time step, steady-state heat transfer functions. The hollow core technology was modelled over a one room office, of a user specified size. Further user specifications dictated occupancy patterns, target room set points, minimum air exchanged and operating technology and strategy. The model generated a temperature profile for key temperatures, as well as key figures such as energy consumption and Coefficient of Performance (COP) for the simulation's total time duration.

3.3.2.1 Energy Balance

Figure 3.3 graphically represents the energy balance that is solved for each time period. Each term is introduced below. Q , in figure 3.3, represents the energy in the stream at each given subscript location. Most energy terms are calculated from respective temperatures (T) of the stream. These temperatures are calculated on a time step basis. W , in figure 3.3 represents work done in heating or cooling carried out by the AHU or slab.

3.3.2.1.1 Time Period and Duration

The model calculates the following balance for each time period, τ (seconds). The model calculates a fixed 1,870 time periods. Total time for the model is varied through time period multiplied by total time steps (1,870). To specify a certain total time, divide the total duration (seconds) by 1,870. For example for twenty-four hour (86,400 second) duration calculate $86,400/1,870$, giving 46.2 second duration for each time period in a twenty-four hour model.

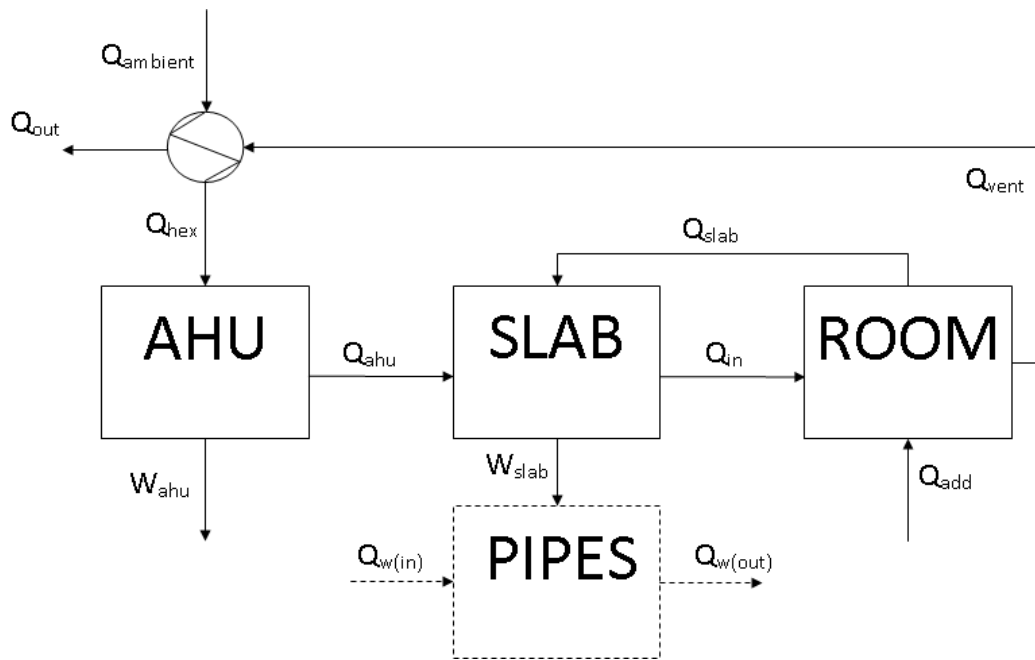


Figure 3.3 - Energy Balance Block Diagram

3.3.2.1.1.1 $Q_{ambient}$ and T_{amb}

Since all energy values were given in relative terms rather than absolutes the initial energy, ($Q_{ambient}$) was not calculated, however ambient temperature (T_{amb}) taken from an average Equa summer weather data and adjusted seasonally, was the start point for calculations. Included in the Excel model was a theoretical average twenty-four hour temperature data for the UK. From the Equa weather file a half hour average was found and adjustments made for each season.

3.3.2.1.1.2 Q_{hex}

Heat transferred through the heat recovery heat exchanger (thermal wheel) was modelled with a minimum of 75% efficiency and since $T_{room} = T_{vent}$, T_{hex} was calculated (Equation 3.4).

Equation 3.4

$$T_{hex,1} = 0.75(T_{room,0} - T_{amb,1}) + T_{amb,1}$$

Since 75% of the available energy in the extract vent was transferred to the inlet channel, the energy recovered by the thermal wheel (W_{wheel}) was calculated from the energy transferred to the inlet air stream (Equation 3.5).

Equation 3.5

$$W_{wheel} = \dot{m}c_{p,air}(T_{hex} - T_{amb})\tau$$

3.3.2.1.1.3 *Wahu*

Equation 3.6

$$W_{ahu} = \dot{m}c_{p,air}(T_{hex} - T_{ahu})\tau$$

The work by the AHU was the energy required to heat or cool the inlet air from T_{hex} to T_{ahu} (Equation 3.6). Energy to power the fan was calculated separately as 'Fan Energy'. T_{ahu} was established based on the model's operation mode. In 'Direct' and 'InDirect' operation modes T_{ahu} was a function of the user defined room set point temperatures, however in 'FanOnly' operation mode, temperature rise was set to 1.1K above T_{amb} (the 1.1K rise occurring through the fan).

The mass flow rate of air, \dot{m} (kg/s), was a product of the user specified 'air changes per hour', air density and room volume (Equation 3.7).

Equation 3.7

$$\dot{m} = \frac{V \times \rho \times change/hr}{3600}$$

The time period, τ (secs), was specified by the user and the heat capacity, $c_{p,air}$ (J/kgK), was taken from data.

3.3.2.1.1.4 *Qahu and Tahu*

Q_{ahu} and T_{ahu} were calculated from the specified AHU operation mode.

3.3.2.1.1.5 *Tslab and Wslab and Qin*

The temperature of the slab was initially specified at 23°C but subsequently calculated from the heat transferred from air or water and internal room space. A two-stage calculation was carried out for each time step (time period). Firstly that of the internal heat transfer from fluid (air or water) to the slab and secondly that of the soffit surface transfer between room and slab.

3.3.2.1.1.6 *Wslab*

The work by the slab was considered as the combined heat transfer, both heating and cooling, carried out by the slab from the internal and external flows. Thus the sum of $Q_{internal}$ and $Q_{external}$ equals W_{slab} .

3.3.2.1.1.7 *Slab $q_{internal}$*

Equation 3.8

$$q_{internal} = UA\Delta T_{LMTD}$$

Equation 3.9

$$\Delta T_{LMTD} = \frac{(\Delta T_i - \Delta T_o)}{\ln\left(\frac{\Delta T_i}{\Delta T_o}\right)} = \frac{(T_{ahu} - T_{slab}) - (T_{in,theo} - T_{slab})}{\ln\left(\frac{(T_{ahu} - T_{slab})}{(T_{in,theo} - T_{slab})}\right)}$$

The internal heat transfer (q_{internal} (W)) (Equation 3.8) was governed by the heat transfer coefficient, U ($\text{W}/\text{m}^2\text{K}$). For air passing through the slab this figure was taken as $4.55\text{W}/\text{m}^2\text{K}$ from the inverse of the general thermal resistance from industrial design [136]. For the water system the U value was taken as $29.4\text{W}/\text{m}^2\text{K}$, again taken from the inverse of the industry calculated thermal resistance, R ($\text{m}^2\text{K}/\text{W}$) [137].

The heat transfer surface area, A , was the surface of the hollow core channels for the air system and the water pipes for the water based system. Each core was modelled as a continuous cylinder to approximate surface area (Equation 3.10).

Equation 3.10

$$A = \pi dl$$

The log mean temperature difference, ΔT_{lmtd} (K), modeled the change in temperature difference between the slab and heat transfer fluid throughout the length of the system (Equation 3.9). During this calculation the slab temperature (T_{slab} (K)) was taken from the previous time step iteration. T_{ahu} was calculated from the work done in the AHU.

Since the slab outlet/room inlet temperature (T_{in}) was unknown before completing the calculation a theoretical T_{in} , $T_{\text{in,theo}}$, was estimated based on a weighted average of the air inlet and slab temperatures. Firstly the energy density ratio of the thermal fluid (air or water) passing through the slab in any given time period to slab was generated (Equation 3.11).

Equation 3.11

$$EDRatio = \frac{m_{slab}c_{p,slab}}{m_{air}c_{p,air}\tau}$$

From this figure the weighted average calculation predicted $T_{\text{in,theo}}$ (Equation 3.12).

Equation 3.12

$$T_{in,theo} = \frac{EDRatio \times T_{slab} + T_{ahu}}{EDRatio + 1}$$

Thus the internal heat transfer to and from the slab (q_{internal} (W)) could be calculated (Equation 3.13 & Equation 3.14). This heat flux, multiplied by the time period, τ (secs), was then used to calculate the slab outlet/room inlet air temperature (T_{in}) and the resultant slab temperature (T_s (K)).

Equation 3.13

$$q_{\text{internal}}\tau = Q = m_{\text{slab}}c_p(T_{s,1} - T_{\text{slab},0})$$

Equation 3.14

$$q_{\text{internal}} = \dot{m}_{\text{air}}c_p(T_{\text{in}} - T_{\text{ahu}})$$

In water based systems the air temperature from the AHU was passed straight into the room without affecting the heat transfer to the slab. For combined water and air systems the heat flux from each fluid was combined and that heat transfer was applied to the slab.

3.3.2.1.1.8 Slab q_{external}

In the model, the resulting T_{slab} , from the internal heat transfer calculation was taken as the input temperature for the surface heat transfer equations, which adjust the temperature for the external flows. Secondly the slab temperature was affected by the convective and radiative heat flows between the slab surface and the room. A second T_{slab} calculation for each time period included the room interaction heat transfer effects. Using derived equations from an ASHRAE study [138], room temperature control radiation and convection heat transfer were governed by Equation 3.15 and Equation 3.16.

Equation 3.15

$$q_{\text{rad}} = 5 \times 10^{-8}[T_{\text{room},0}^4 - T_{s,1}^4]$$

Equation 3.16

$$q_{\text{conv}} = 2.12[T_{\text{room},0} - T_{s,1}]^{1.31}$$

In each case the heat transfer was given in W/m^2 . The convection equation proved to be stable only for room cooling (where $T_{s,1} < T_{\text{room},0}$) therefore a simplified q_{conv} equation was used to maintain stability for both heating and cooling. Brief study showed little effect in the overall room temperature profiles with the simplified equation (Equation 3.17).

Equation 3.17

$$q_{\text{conv}} = 2.12[T_{\text{room},0} - T_{s,1}]$$

From the combined heat transfer per meter squared, the effect on the slab temperature was calculated from Equation 3.18, Equation 3.19 and Equation 3.20.

Equation 3.18

$$Q_{external} = mc_p(T_{slab,1} - T_{s,1})$$

Where:

Equation 3.19

$$Q_{external} = (q_{rad} + q_{conv})\tau A$$

And rearranged to give the new slab temperature, $T_{slab,1}$ (K), thus the whole calculation became:

Equation 3.20

$$T_{slab,1} = T_{s,1} + \frac{Q_{external}}{m_{slab}c_p}$$

3.3.2.1.1.9 Q_{in} and T_{in}

The air temperature leaving the slab and entering the room (T_{in} (K)) was calculated from Equation 3.21.

Equation 3.21

$$Q_{in} = q_{internal}\tau = \dot{m}_{air}c_p(T_{in} - T_{ahu})\tau$$

Equation 3.21 was then rearranged to make temperature, T_{in} , the subject (Equation 3.22).

Equation 3.22

$$T_{in} = T_{ahu} + \frac{Q_{in}}{\dot{m}_{air}c_p\tau}$$

When non slab systems were modelled, T_{in} was equal to T_{ahu} ; and where water and air slab systems were modelled Q_{in} was purely the air component of $q_{internal}$.

3.3.2.1.2 $Q_w(in)$ and $Q_w(out)$

3.3.2.1.2.1 Water Outlet Temperature, $T_{w,out}$

The actual water outlet temperature ($T_{w,out}$) was calculated from the theoretical $q_{internal}$ (Equation 3.23).

Equation 3.23

$$Q = q_{internal}\tau = \dot{m}_{water}c_{p,water}(T_{w,out} - T_{w,in})$$

The water mass flow rate, \dot{m}_{water} (kg/s), was user specified, as was the water start temperature ($T_{w,\text{in}}$). $c_{p,\text{water}}$ was taken from data thus $T_{w,\text{out}}$ was calculated from the rearranged heat capacity calculation above (Equation 3.23). The model did not contain a water recycle and it was assumed constant fresh water at the user specified temperature enters the embedded pipe network.

3.3.2.1.3 Room Temperature, T_{room}

There were three components to the room temperature calculation at each time period. In each component the initial temperature was taken from the outcome of the previous temperature, with the first component taking a start temperature from the outcome of the previous time step.

3.3.2.1.3.1 Q_{slab} effect on Room Temperature (T_r)

The energy transferred between the slab and the room was governed by q_{external} and consisted of convective and radiative heat transfer components. The room temperature (T_r (K)) was calculated from a similar equation as the resulting slab temperature (Equation 3.24).

Equation 3.24

$$T_{r,1} = T_{\text{room},0} + \frac{Q_{\text{external}}}{\rho_{\text{air}} V_{\text{room}} c_p}$$

3.3.2.1.3.2 Q_{in} effect on Room Temperature (T_{rm})

Secondly T_{rm} , the resultant room temperature calculated as a function of the temperature of the additional air that has entered through the AHU and/or slab during time period, τ , was calculated simply as an average mix temperature. The air was considered well mixed and therefore uniform in temperature and T_{rm} calculated as in Equation 3.25.

Equation 3.25

$$T_{\text{rm},1} = \frac{T_{\text{in},1} V_{\text{air}} \dot{\tau} + T_{r,1} V_{\text{room}}}{\rho_{\text{air}} V_{\text{air}} \dot{\tau} + V_{\text{room}}}$$

3.3.2.1.3.3 Q_{add} effect on Room Temperature (T_{room})

The final component was the resultant temperature from solar gains and occupancy behaviour as specified in the model dashboard. The heat transferred to the room was made up of two components: heat transferred due to occupancy behaviour (q_{occ} (kW)) and heat transferred due to solar gains (q_{sol} (kW)). User specified variations in these two measures were required. Data for the impact of each aspect was taken from an air conditioning sizing guide [139].

The addition of all these factors resulted in an overall heat addition for each time period (Equation 3.26).

Equation 3.26

$$Q_{add} = (q_{occ} + q_{sol})\tau$$

This heat transferred made up the final room temperature calculation (Equation 3.27) for each time step (T_{room}).

Equation 3.27

$$T_{room,1} = T_{rm,1} + \frac{Q_{add}}{\rho_{air}V_{room}c_p}$$

The parameters required for specification consisted of number of occupants, total wattage of electrical equipment and the total wattage of lights. Each occupant accounted for 0.12kW, each watt of electrical equipment accounted for 0.001kW and each watt of lighting for 0.0013kW of required cooling. During the user specified occupied hours these added heat loads impacted on the room temperature in a combined calculation with the heat gained through solar gains.

The heat gained through solar gains (q_{sol}) was calculated from the user specified room window arrangements and annual season. Each square metre of south facing window's accounted for 0.25 and 0.38kW with and without blinds respectively. Each square metre of north facing window's accounted for 0.05 and 0.07kW with and without blinds respectively. A seasonal day factor that acted as a simple multiplier varied between 0 to 1 during summer months, from 0 to 0.8 during autumn and spring months and between 0.6 to -0.2 during winter months. Aside from this negative factor during winter nights no other losses were accounted for in the model and the room was assumed to have perfect insulation.

3.3.2.1.4 Qvent

The resulting air temperature leaving the room was considered equal with the room temperature due to the assumption that the room temperature was uniform and well mixed. It was further assumed that air left the room at the same rate it entered, thus room pressure remains constant. All extract or inlet fan power was included in a separate fan power calculation.

3.3.2.2 COP Calculation

Equation 3.28

$$COP = \frac{W}{Q}$$

In its simplest form the COP is a measure of system efficiency. Commonly used in heat pumps but applicable for other heat recovery and cooling technologies, the COP figure represents the amount of cooling energy provided by the system (W) divided by the energy consumed by, or inputted to, the system from the energy source (Q) (Equation 3.28) [9]. Thus, for example, a COP of 3.5 indicates that for every 1kWh of electricity supplied 3.5kWh of cooling energy was provided through the given technology. Work, herein, refers to the thermal work or effective cooling or heating energy provided by either the slab or the thermal wheel.

The COP calculation in the Excel model measured the energy efficiency of the technology being tested by dividing the thermal work done (cooling or heating) by the slab by the sum of the electrical energy input required. Two COP figures were reported, one that includes the energy recovered through the thermal wheel (Equation 3.30) and the other that just measured the energy efficiency of the slab against the various electrical components in the system (AHU heating and cooling coils, fan and pump) (Equation 3.29). These were average COP figures.

Equation 3.29

$$COP = \frac{\sum W_{slab}}{\sum Q_{ahu} + \sum Q_{fan} + \sum Q_{pump}}$$

Equation 3.30

$$COP_{wheel} = \frac{\sum W_{slab} + \sum W_{wheel}}{\sum Q_{ahu} + \sum Q_{fan} + \sum Q_{pump}}$$

Q_{ahu} , W_{wheel} and W_{slab} were already calculated above. Q_{fan} and Q_{pump} were calculated as introduced below.

3.3.2.2.1 Qfan

The fan power (W) was calculated from the specific fan power of 2W/l/s, common in industrial systems [34], multiplied by the air flow rate derived from the user specified air changes and room volume. The resulting fan energy (Q_{fan} (kWh)) was calculated from the time period, τ (secs), and an assumed efficiency of 80%. The total Q_{fan} throughout the simulation duration was calculated through simple summation. Fan operation can be

adjusted in the 'Inputs' dashboard to operate in 'night cooling', 'constant fan' or 'occupied only' modes. In the latter a minimal flow rate was passed during unoccupied hours.

3.3.2.2.2 Q_{pump}

In water based systems the energy required to pump water through the system was calculated from the water flow rate, system dimensions and fluid properties. The pump power (P_{pump} (W)) was calculated from Equation 3.31.

Equation 3.31

$$P_{\text{pump}} = v\rho gh$$

Where v was volumetric flow rate (m^3/s), ρ was water density (kg/m^3), g was acceleration due to gravity (assumed constant at $9.81\text{m}/\text{s}^2$) and h was the equivalent height lost (m) due to friction calculated from Equation 3.32.

Equation 3.32

$$h = f \left(\frac{L}{D} \right) \left(\frac{V^2}{2g} \right)$$

L was the pipe length (m), D the pipe diameter (m), V the mean fluid velocity (m/s), g ($9.81\text{m}/\text{s}^2$) and f the dimensionless moody friction factor calculated from equations, calculated from the friction factor graph for laminar and turbulent flows. During laminar flow ($Re < 1000$):

Equation 3.33

$$f = \frac{64}{Re}$$

Where:

Equation 3.34

$$Re = \frac{\rho VD}{\mu}$$

μ was the dynamic viscosity of the fluid (Pa.s). In turbulent conditions ($Re > 4000$) the moody friction factor was calculated as from Equation 3.35.

Equation 3.35

$$f = \left[1.14 + 2 \log \left(\frac{D}{\varepsilon} \right) \right]^{-2}$$

ϵ was the emissivity (m), approximately $3 \times 10^{-6} m$ for plastic pipe. Due to the size of pipes and the expected flowrate, fluid flow was typically turbulent thus in the model it was assumed that for transition flows ($1000 < Re < 4000$) the moody friction factor were modelled as laminar (Equation 3.33).

Pump energy was thus calculated from the pump power multiplied by the time step, τ , and pump efficiency, η , assumed 90%. The pump energy required during each time step was added together throughout the total simulation time, for use in the COP calculation.

3.3.2.3 Verification Process

After design the Excel based thermal mass simulator performance was verified through a comparative method, against a reference model constructed in the Scandinavian building simulation software, Equa. Equa was chosen for the reference model due to its use in industry by ventilated hollow core engineers. Due to Equa being proprietary software that was not available for this investigation, the Excel model was constructed and used following verification.

The reference model was simulated as a well-insulated, single storey, single room cubical space with dimensions of 2 by 1.5 by 1.16m. A 0.375m thick slab was placed above the windowless room with additional energy duties set at $10 W/m^2 K$ and $20 W/m^2 K$ for lights and equipment respectively. Performance was simulated over a twenty-four hour UK summer period with inlet and extractor fans maintained at a constant flow rate of $7 l/s/m^2$. Weather data for the validation simulation was taken from the Equa model's ambient temperature profiles for the twenty-four hour period referenced.

Equa ceiling soffit and room temperature twenty-four hour profiles were plotted alongside Excel simulated room and slab temperature twenty-four hour profiles in Figure 3.4. The greatest variation was observed between slab and soffit temperatures in the Excel and Equa models respectively. Much discrepancy in these figures was due to the modelling assumption in the Excel model of uniform slab temperature. The Equa model specifies the temperature modelled at the ceiling surface whereas the Excel model took the temperature as a uniform average throughout the slab.

Following U-value adjustment, the comparative room temperatures shown in figure 3.4 demonstrated close matching of the Equa and Excel simulated room temperature performance. Despite slight time delay in peak matching due to temperature averaging, a variation of less than $0.5^\circ C$ was evident throughout all but the last three hours of the

simulation. With this close fit in room temperature simulation, the Excel model was verified suitable for VHC simulation.

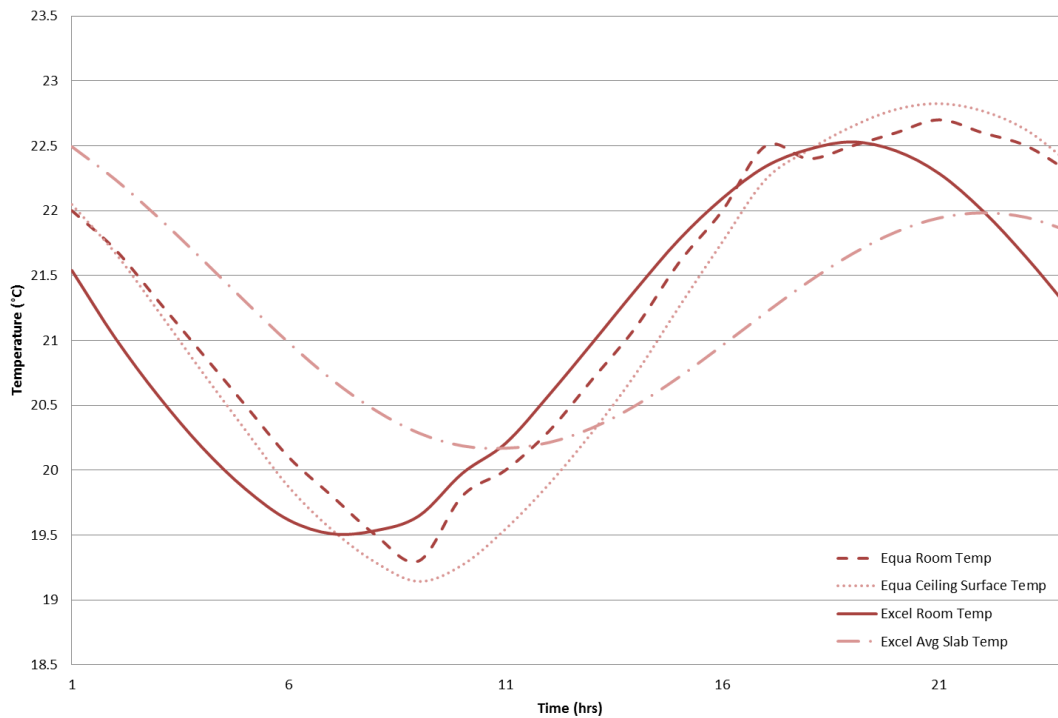


Figure 3.4 - Validation Performance: 24hr Summer Simulation

3.3.2.4 Limitations and Assumptions

The weather data calculation method was limited. Based on seasonal relationships with the Equa summer design conditions, weather data temperature profiles have been calculated in thirty-minute averages. When plotted against Equa simulations this showed a lag time in simulated temperatures. Only weather profiles for twenty-four hour UK seasonal design-days were generated within the model, therefore limiting the scope of testing. The method for calculating annual performance based on the individual seasonal design days was therefore also limited. Breadth and depth of temperature profiles could be improved through inclusion of real weather data.

The calculation of $T_{in,theo}$ was based on estimations. These estimations affect the level of heat transfer. By using the Energy Design Ratio an informed estimation was used to minimise error caused. System efficiencies were assumed at 75% for the thermal wheel, 80% for fan and 100% in the AHU heating and cooling processes. The water pump has an assumed efficiency of 90%.

Throughout the model it was assumed that mass volumes of air, water or concrete have a uniform temperature at each time step. Perfect insulation was assumed throughout

therefore all heat lost occurred from mechanical ventilation and energy inefficiencies through the system. Some heat loss occurred through the winter night, included in the solar gain function.

3.3.3 Modelling Guide

The simulator was designed to model the thermal performance of a single storey office where temperature was controlled by differing thermal mass utilisation strategies. Within the model there were a variety of hollow core arrangements and plant control (AHU) options available (Figure 3.5). This pictorial guide enables better understanding of what each configuration represented.

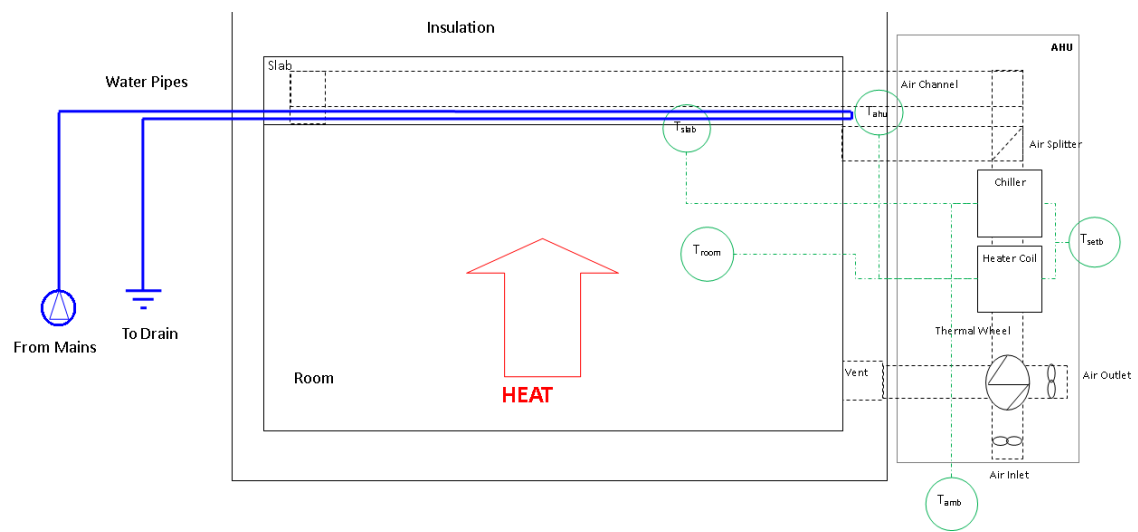


Figure 3.5 - Graphical Representation of Model

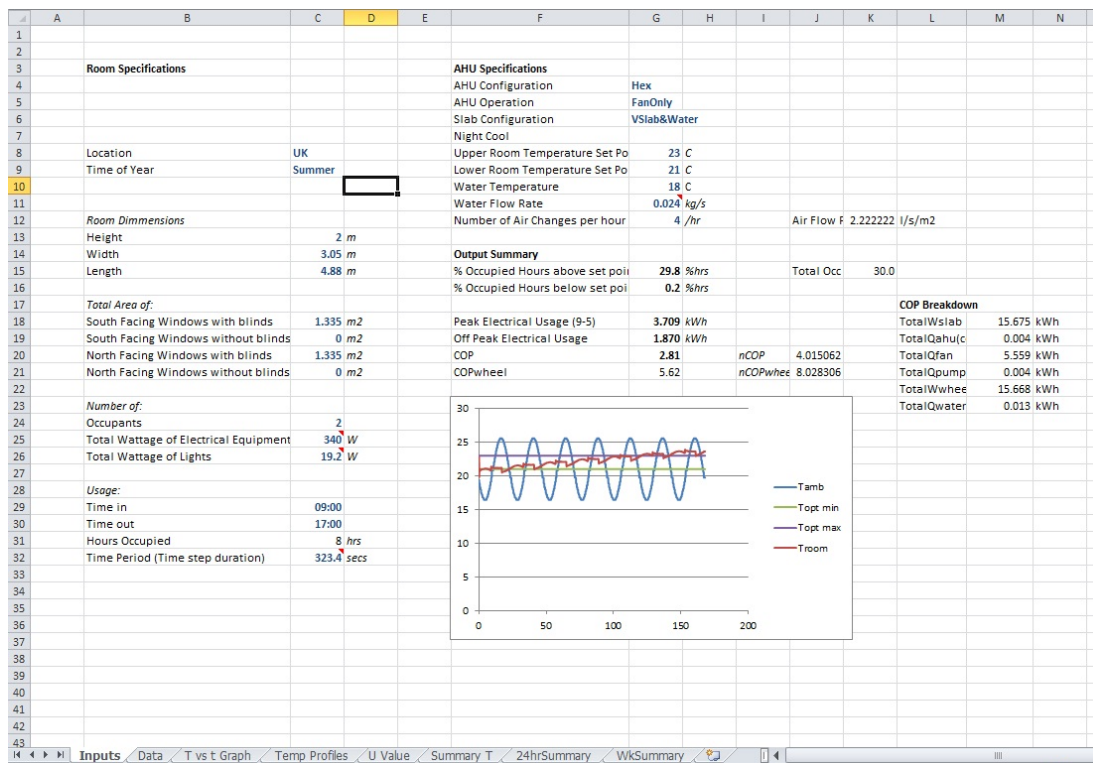


Figure 3.6 - Excel Heat Balance Time Step Model User Interface

When the model was opened, all the parameters, in the 'Inputs' Sheet, were set as per Figure 3.6 shown above. The calculation behind each input (blue writing) is explained in section 3.3.2 Modelling Methodology. Definitions, available options and what they represent are explained in this section. The configurations of the hollow core and accompanying AHU were adjusted based on the pre-set inputs in the 'AHU Specifications' section. These appear in a drop down list when the cell was selected.

On the 'Inputs' tab, figure 3.6, the all necessary inputs and variables were specified to set up the desired scenario. Each blue figure required a user specification that adjusted the internal model calculations, whilst the output summary and incorporated temperature profile demonstrated the technology performance in the test conditions.

3.3.3.1 Inputs

Location: The model was only suitable for modelling UK temperature profiles. Expansion of weather data would increase the applicability to other locations beyond the UK.

Time of Year: Selection ranges from the four seasons and sets the ambient temperature profile data within the model. Annual Performance Investigation enables a year round calculation and a breakdown of performance in each season.

Room Dimensions: Specify the room being modelled. The model only accommodates cuboid shaped rooms. If the space being modelled consists of alternative geometry then an equivalent room volume should be modelled.

Window Area: The total area of North and South windows and whether they were covered by blinds should be specified. This input affected the solar gain calculation thus for East and West facing windows the area should be halved between the North and South sections to offer an approximation.

Occupancy: The expected occupancy behaviour was modelled from the 'Number of' and 'Usage' parameters. The number of occupants and equipment wattage was required for internal room thermal gains. Guides for typical computer and light wattage were available as inbuilt model cues. The usage hours dictate the typical occupied working hours. The model assumed each day was a work day with no weekend parameter available.

Time Period: (time step duration): This was integral to the overall time span of the model. 46.2 seconds would model twenty-four hours and 323.4 seconds would model one week (seven days). Further explanation was included in the Section 3.3.2.

AHU Specifications: The second column of inputs detailed the required variables regarding the particular technology being modelled.

| | |
|---------------------------|---------|
| AHU Specifications | |
| AHU Configuration | NoHex |
| AHU Operation | FanOnly |
| Slab Configuration | Slab |
| Night Cool | |

Figure 3.7 - AHU Specification Menu

In the top middle of the 'Inputs' sheet, under the 'AHU Specifications' title, the following four categories help to define the various configurations and operation modes available to be modelled within the Excel model. They were separated into 'AHU' and 'Slab' variations. 'AHU' considered all of the technology preceding the slab whilst the 'Slab' referred to the exact configuration of hollow core soffit in operation for the simulation.

Any available setting could be combined with any other set up, however the AHU operations 'Direct' and 'InDirect' were designed to work in conjunction with slab

configurations ‘Slab’ and ‘VSlab&Water’. These control systems have been designed to mimic performance of typical ventilated hollow core installed in buildings across the UK. The ‘SetPointMatch’ offers a theoretical ideal temperature management system designed to be used with the ‘NoSlab’ slab configuration. AHU Configuration and Night Cool variations can be combined to match the user’s specifications.

3.3.3.1.1 AHU Configuration

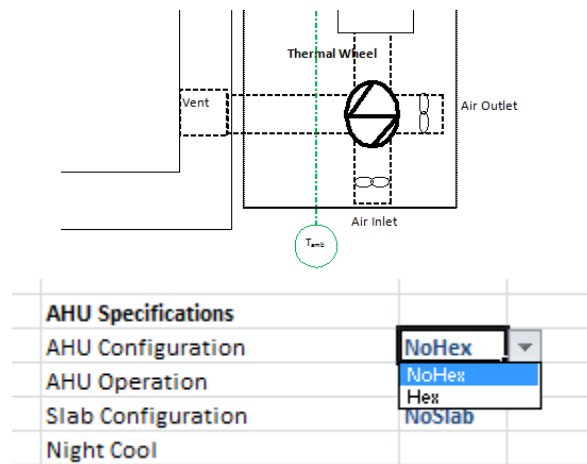


Figure 3.8 - Schematic and Menu options for AHU Configuration

This option refers to the thermal wheel as shown in Figure 3.8. The thermal wheel was setup as a heat exchanger (Hex) that exchanges the heat from the outlet air with the heat from the inlet air. Two options were available within the model, either ‘NoHex’ or ‘Hex’ meaning no heat exchanger (thermal wheel) or heat exchanger respectively. When no heat exchanger was present the outlet air was simply exhausted into the atmosphere without any effect on the inlet air. When a heat exchanger was present 75% of heat was transferred between the inlet and outlet air streams.

3.3.3.1.2 AHU Operation

Four options were available to the user; ‘FanOnly’ – where the model sends ambient air +1.1°C into the system, ‘Direct’ and ‘InDirect’ – where the AHU heaters and coolers were controlled in accordance with building management control strategies [34]. The ‘Direct’ mode has a wider temperature threshold around the set point. Finally ‘SetPointMatch’ operated the AHU heaters and chillers to output air at the mean specified room temperature set point to simulate perfect temperature control.

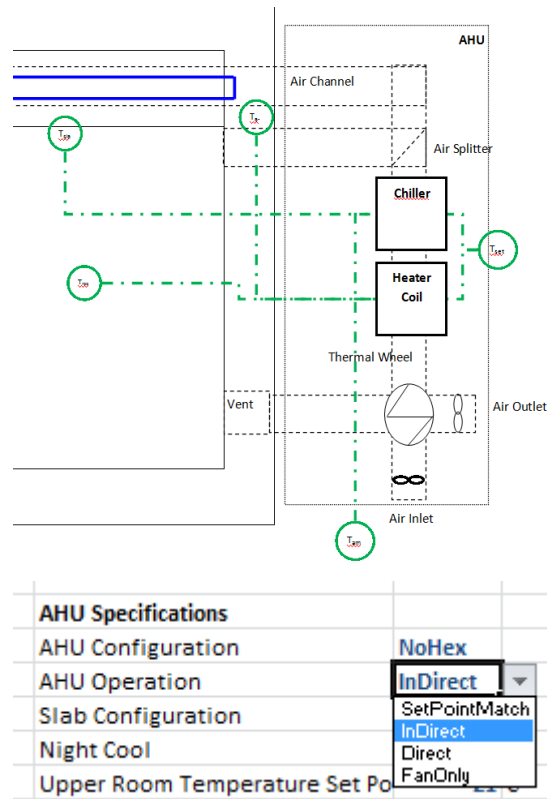


Figure 3.9 - Schematic and Menu options for 'InDirect' AHU Operation

The 'AHU Operation' parameter sets the operation method of the Heater and Chiller within the AHU. There were four control options available. The first three options represented an AHU setup as shown (Figure 3.9) above with heater, chiller and fan. The variation between the options was based on the heater and chiller control methods. 'SetPointMatch' operates as a theoretical perfect air heater/cooler that will heat or cool ambient inlet air to the set temperature (T_{set}).

'Direct' and 'InDirect' were the most complex AHU control strategies. Depending on the room temperature's (T_{room}) relationship to T_{set} , and the available heating or cooling in the slab temperature (T_{slab}), the heater and cooler within the AHU would heat or cool T_{amb} as required.

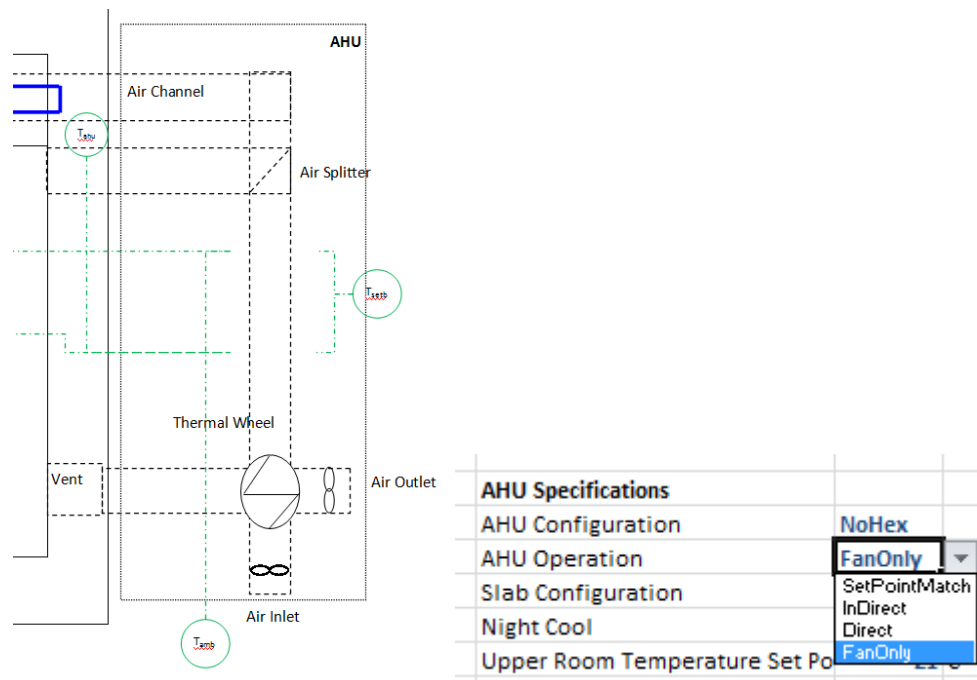


Figure 3.10 - Schematic and Menu options for 'Fan Only' AHU Operation

The final and simplest option, 'Fan Only', represented an AHU unit void of a heater or chiller (Figure 3.10). The air stream would pass through the fan, through a heat exchanger if selected and subsequently into either the room or hollow core as desired. In this setup the AHU had no ability to carry out any supplementary heating or cooling on the air inlet stream.

3.3.3.1.1.3 Slab Configuration:

There were four options for slab configuration:

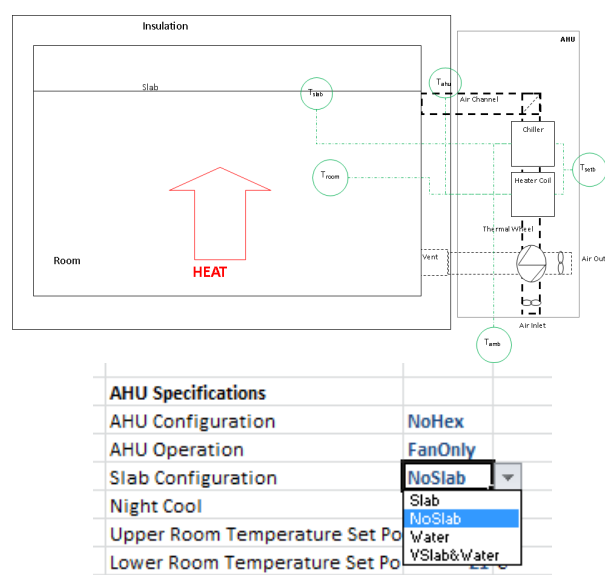


Figure 3.11 - Schematic and Menu options for 'NoSlab' Slab Configuration

1. 'NoSlab' – the model sends air straight from the AHU to the room bypassing slab channels, although a passive soffit remains (Figure 3.11),

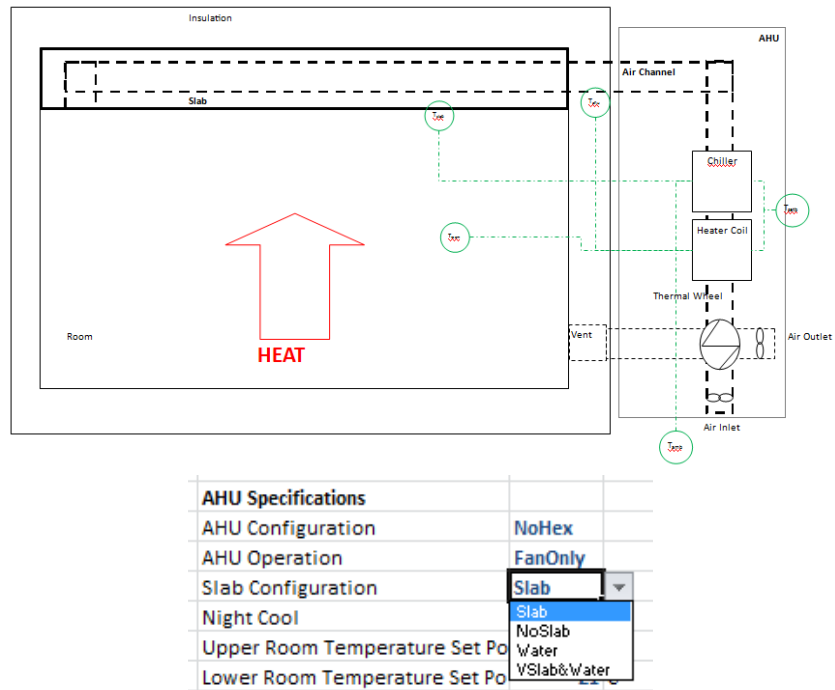


Figure 3.12 - Schematic and Menu options for 'Slab' Slab Configuration

2. 'Slab' – the model sends air through the hollow core network, calculating the heat transfer between the air from the AHU and the slab before modelling air mixing in the room (Figure 3.12),

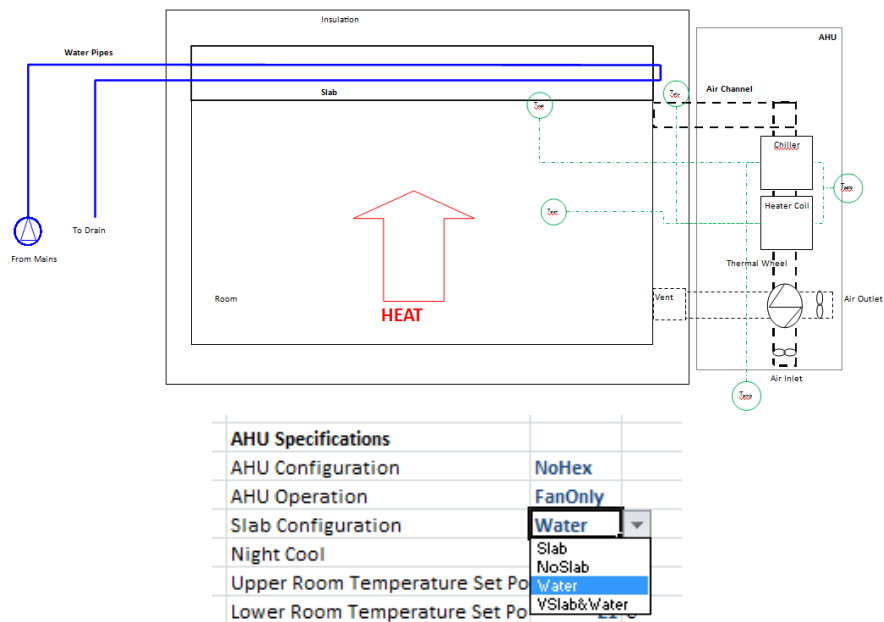


Figure 3.13 - Schematic and Menu options for 'Water' Slab Configuration

3. 'Water' – models a hydrated slab only with air passed straight from the AHU into the room whilst the water cools or heats the slab and the slab in turn affects the room temperature passively (Figure 3.13) and,

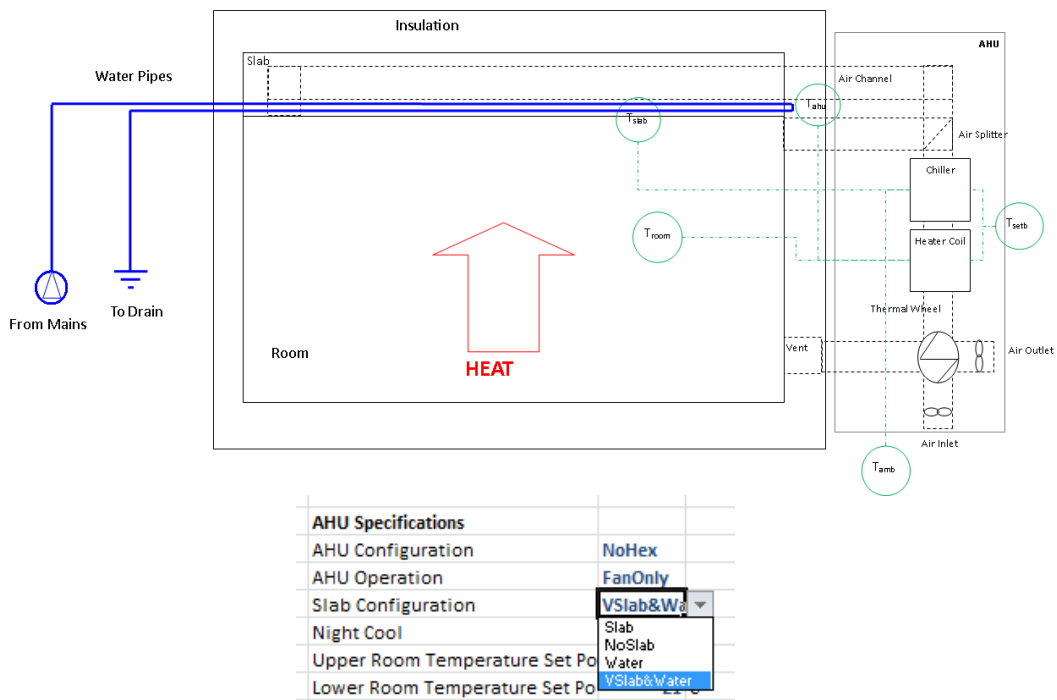


Figure 3.14 - Schematic and Menu options for 'VSlab&Water' Slab Configuration

4. 'VSlab&Water' – models a combined ventilated and hydrated slab modelling internal air channels and water pipes in the hollow core system (Figure 3.14).

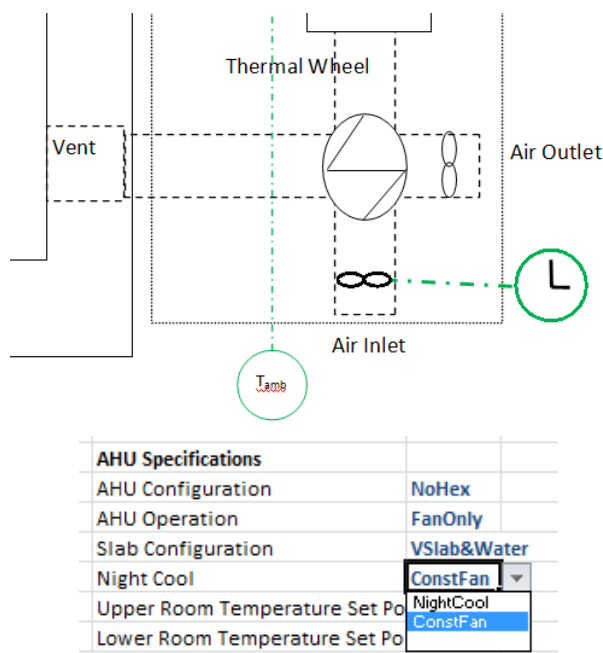
3.3.3.1.1.4 **Night Cool:**

Figure 3.15 - Schematic and Menu options for 'ConstFan' Night Cool option

The 'Night Cool' parameter contains three options for fan control into the AHU (Figure 3.15). The first option, 'NightCool', blows air through the AHU and subsequent slab configuration at the specified fan speed during occupied hours. During unoccupied hours the fan speed was increased to a set maximum of twenty-five air changes per hour, providing the ambient temperature was lower than the desired set temperature. This mode was designed to be operated with 'Slab' and 'VSlab&Water' slab configurations for use in ventilated hollow core scenarios.

The second option 'ConstFan' maintains a constant fan speed throughout the duration of the simulation, whether occupied or not the fan will maintain a constant speed.

The final option was a blank option, ''. This will maintain specified fan speed during occupied hours and reduce the fan speed to a minimum of one air change per hour (acph) during unoccupied hours to reduce overall energy consumption.

Temperature Set Point: The upper and lower temperature set points were the guide that the AHU control system and the output analysis operate to.

Water Temperature: The water system operates as an open mains-water system in the model, thus the initial water set point was specified and can be adjusted arbitrarily for heating or cooling.

Water Flow Rate: The water flow rate affects the required pumping power.

Number of Air Changes per Hour: This details the required air changes either as specified in CIBSE guides or in accordance with technology requirements [34, 140]. From this parameter and the room volume the air flow rate was calculated. A guide figure of resulting volumetric flow rate was provided.

3.3.3.2 Outputs

AC Output Summary: The summary offered the key outputs from the model giving an idea of the technology's relevant performance.

%Occupied Hours Above/Below Set Point: This measure gives a crude calculation of thermal comfort within the modelled space through the duration of the simulation.

Electrical Usage: These measures demonstrate the capabilities of the technology modelled to reduce electricity consumption and offset peak demand into low-tariff time periods.

COP: The coefficient of performance (COP) conveys the energy efficiency of the system. The figure was calculated from the energy absorbed or released by the slab, divided by the amount of energy consumed by the system. The COP figure here constitutes the average COP of both heating and cooling (Equation 3.36).

Equation 3.36

$$\text{Average COP} = \frac{\sum W_{slab}}{\sum Q_{ahu} + \sum Q_{fan} + \sum Q_{pump}}$$

COP_{wheel}: The COP_{wheel} figure includes the energy recycled through the thermal wheel in the COP calculation to give a complete figure for the whole system, rather than solely the energy efficiency of the slab (Equation 3.37).

Equation 3.37

$$\text{COP}_{wheel} = \frac{\sum W_{slab} + \sum W_{wheel}}{\sum Q_{ahu} + \sum Q_{fan} + \sum Q_{pump}}$$

COP Breakdown: This gives a breakdown of the terms making up the COP calculation to give the user an understanding of where the energy in the system was being consumed and re-used.

Temperature Profile: A small temperature profile chart was also generated to demonstrate the room temperature fluctuations with respect to ambient temperature and temperature set points. The y-axis measures temperature in degrees Celsius with the x-axis measuring time in hours.

Further outputs and temperature versus time charts were able to be generated and a separate performance summary was generated in the 'Summary' tab. As stated initially in this document, this model has been designed to model seasonal UK performance of existing and novel thermal mass based building temperature control technologies during a specified time period. Further widening of the scope to predict annual performance, alternative locations or technologies requires further revisions of the Excel model.

3.3.4 Annual Performance Investigation Method

Through aggregating seasonal performance, the Excel model could be used to simulate annual performance. This section introduces a brief investigation conducted using the Excel model tool to determine annual performance and identify opportunities for enhancement.

3.3.4.1 Scenario

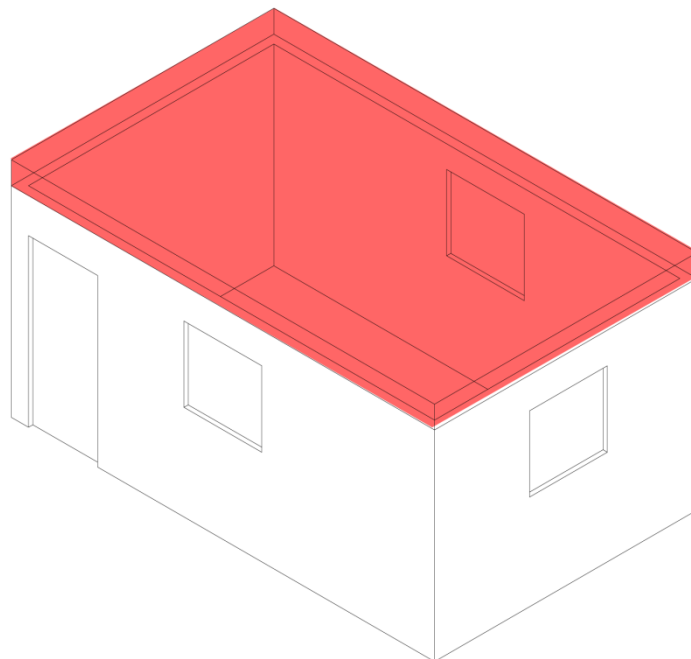


Figure 3.16 - 3-D Drawing of the Theoretical Office with WVHC system highlighted

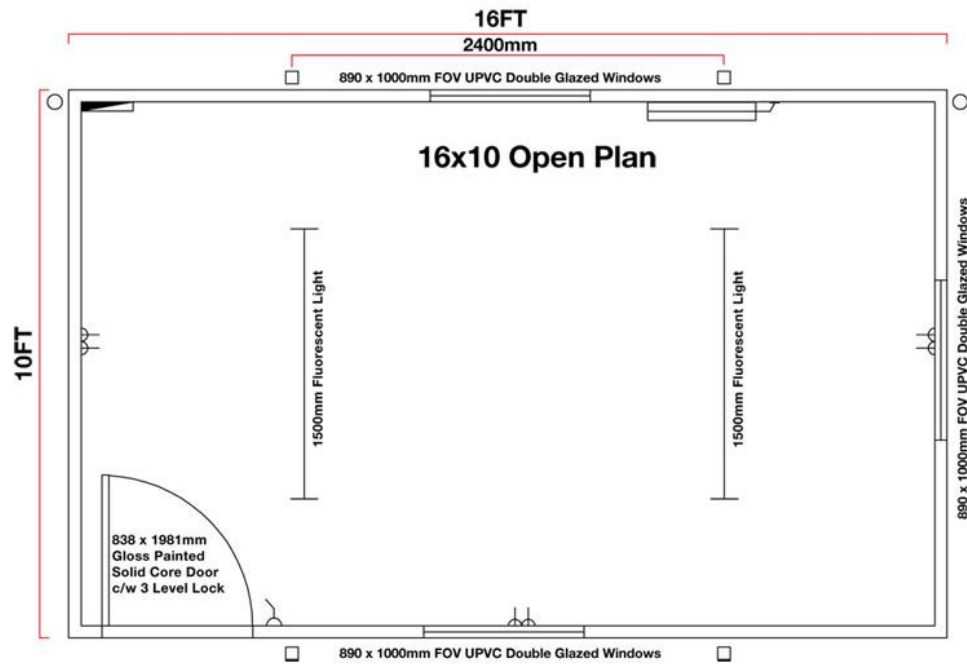


Figure 3.17 - Theoretical Office Plan

The investigation was based on a 4.88m (16ft) by 3.05m (10ft) by 2m single story office (Figure 3.16). The office houses a total of three windows on the North, East and South side of the office each 0.89m by 1m (0.89m^2) (Figure 3.17).

The office was occupied between 9am and 5pm, seven days a week, by two computer operators and had two fluorescent light fittings. It was perfectly insulated and air tight, save for the forced ventilation through the thermal mass system. Mechanical ventilation delivered four air changes per hour (acph). Room temperature controls were set to 21°C (minimum) and 23°C (maximum).

To generate an estimation of annual performance four simulations were run, one typical week in each season (generated from seven consecutive seasonal design days). Performance from each seasonal simulation was converted to an annual performance assuming thirteen spring, summer, autumn and winter design-weeks.

The water flowrate for all simulations was set to 0.024kg/s from Underfloor Heating Calculator Manual [141]. The U-value was set to $20.74\text{W/m}^2\text{K}$ based on the validation work with Equa. The initial slab temperature was set at 21°C . As standard the WVHC system was operated in 'Fan Only' mode, therefore no additional preheaters or coolers were configured for the simulations.

3.3.4.2 System Configurations

Two base cases (1 & 2) were simulated to contrast the hollow core system (3, 4 & 5) performance against:

1. **HtrClr** – for the first base case temperature was controlled by a simple air heater-cooler system without any additional thermal mass.
2. **PassiveHC** – the second base case operated as a passive hollow core slab. Ambient ventilation air bypassed the hollow core air network.
3. **VHC** – traditional ventilated hollow core system (VHC) operated in accordance with typical industry used control strategies [34]. All seasons were operated in ‘Fan Only’ mode without additional heating or cooling.
4. **WHC** – building on early commercial [133] control strategies, water activated hollow core (WHC) was simulated. For the winter, spring and autumn design weeks the water temperature was set to 18°C to provide additional heating. During the summer design week the water temperature was set at 14°C. Water was pumped continually through occupied periods. Minimum ventilation air was directed to the room bypassing any air network.
5. **WVHC** – a novel water and air ventilated hollow core (WVHC) system was simulated combining the VHC and WHC conditions. The winter, spring and autumn water temperature was set to 18°C and summer water temperature set to 14°C. Water was pumped continually through occupied periods whilst the fan operated in accordance with the commercial control strategy [34]. Air was passed through the hollow core air network before entering the room. No further heating or cooling was conducted on the air stream.

3.3.5 Results and Discussion

3.3.5.1 Water Controlled Hollow Core Investigation Discussion

Simulations of the water controlled hollow core (WHC) investigated the effect of water temperature variation. A suitable temperature for each season to achieve energy efficient thermal stability was targeted. Higher water temperatures offered greater thermal stability through winter months but the energy cost to achieve this was excessive so a reduced temperature was considered optimum. When WHC is required to heat, a water loop with heat recovery is advised. To offer cooling demand an open loop mains water system is advised.

The water control system was not fully optimised. Minimal control was established during the annual performance investigation. Open loop mains water was pumped through the slab during all occupied hours despite at certain times (when $T_{slab} < T_{opt}$ and $T_w < T_{slab}$) this having a negative effect on the technologies thermal comfort performance.

3.3.5.2 Annual Performance Investigation

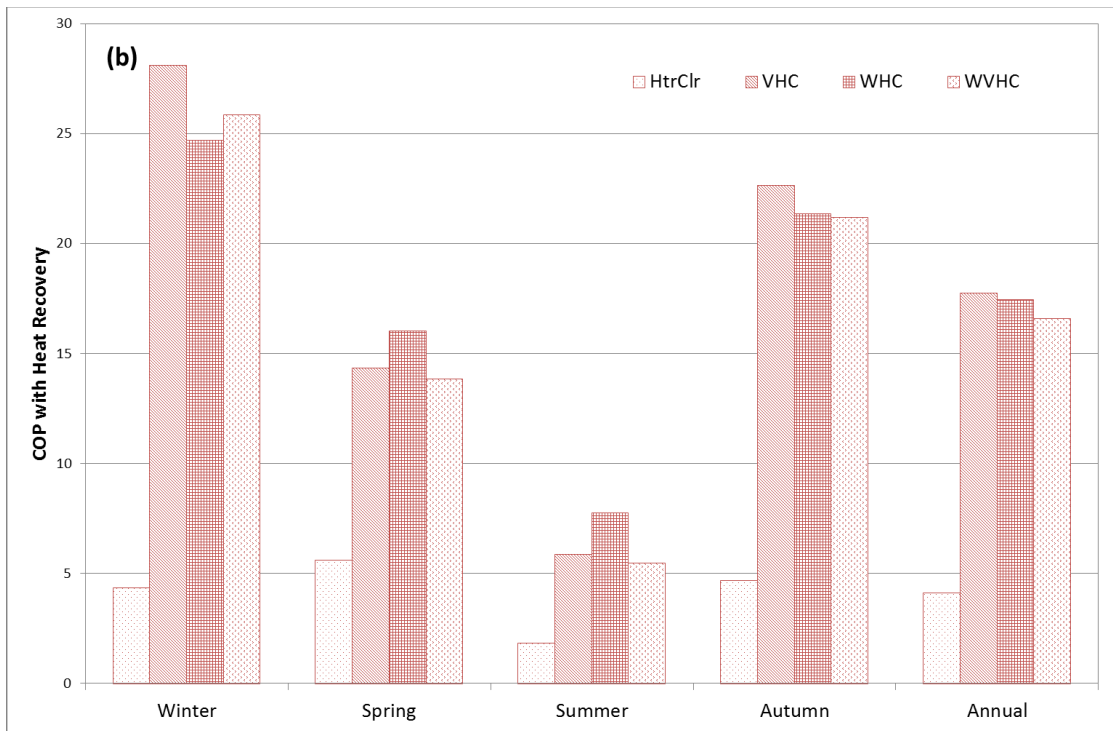
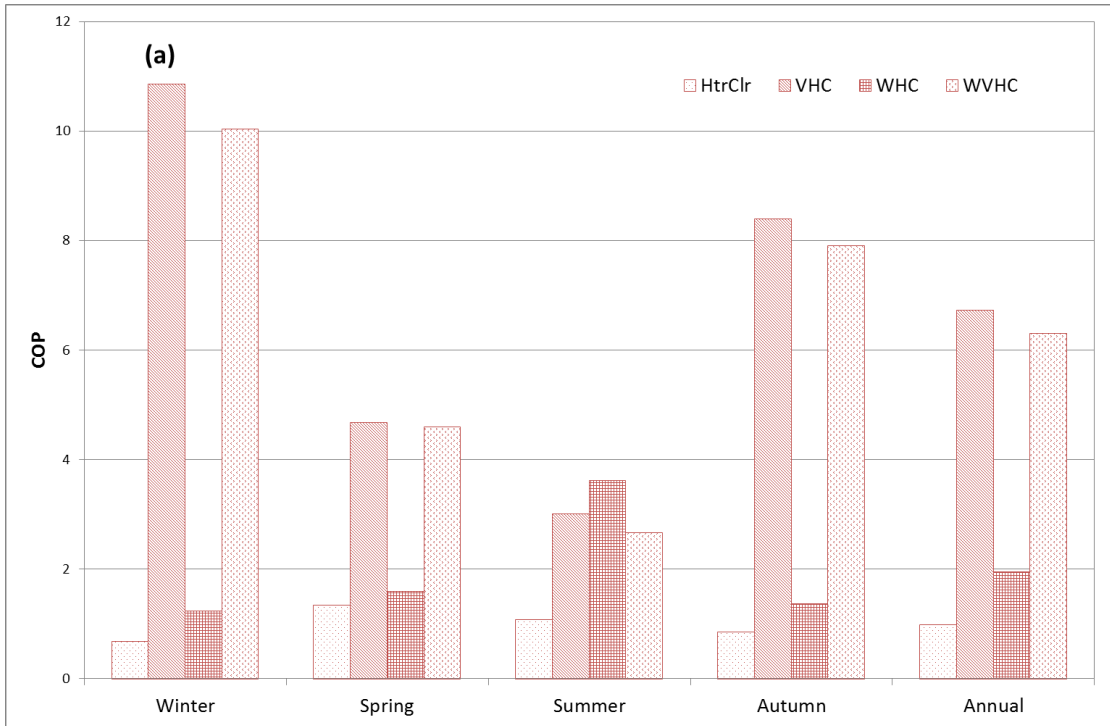
To review performance of each system the following parameters (Table 3.3) were specified for each simulation carried out in the Annual Performance Investigation.

Table 3.3 - Annual Performance Simulation Parameters

| Technology | Season | AHU Operation | Slab Technology | Night Cool | Water Temp. °C | Water | Air | Air |
|-------------------|--------|------------------|--------------------|---------------|----------------------|----------------------|---------------------|------------------------------------|
| | | | | | | Flow Rate kg/s | Changes Per hour | Flow Rate l/s/m ² |
| Heater/ Cooler | ALL | SetPointMatch | NoSlab | off | n/a | n/a | 7.2 | 4.0 |
| Passive HC | ALL | FanOnly | NoSlab | off | n/a | n/a | 4.0 | 2.2 |
| VHC | ALL | FanOnly | Slab | off | n/a | n/a | 4.0 | 2.2 |
| WHC | Winter | FanOnly | Water | off | 18 | 0.024 | 4.0 | 2.2 |
| | Spring | | | | 18 | | | |
| | Autumn | | | | 18 | | | |
| WVHC | Summer | FanOnly | V&Water | off | 14 | 0.024 | 4.0 | 2.2 |
| | Winter | | | | 18 | | | |
| | Spring | | | | 18 | | | |
| | Autumn | | | | 18 | | | |
| | Summer | | | | 14 | | | |

3.3.5.3 Seasonal Performance Results

Following each simulation, seasonal performance was reviewed based on energy and thermal comfort measures COP, COP with HR, nCOP and nCOP with HR. Equation 3.38 documents the calculation for normalised (nCOP) figures, representing energy efficiency as a function of temperature control. To distinguish the performance of the system with and without heat recovery, four charts were plotted. Figure 3.18 (a) – (d) documents the seasonal performance of each performance measure.



Thermal mass enhancement for energy saving in UK offices

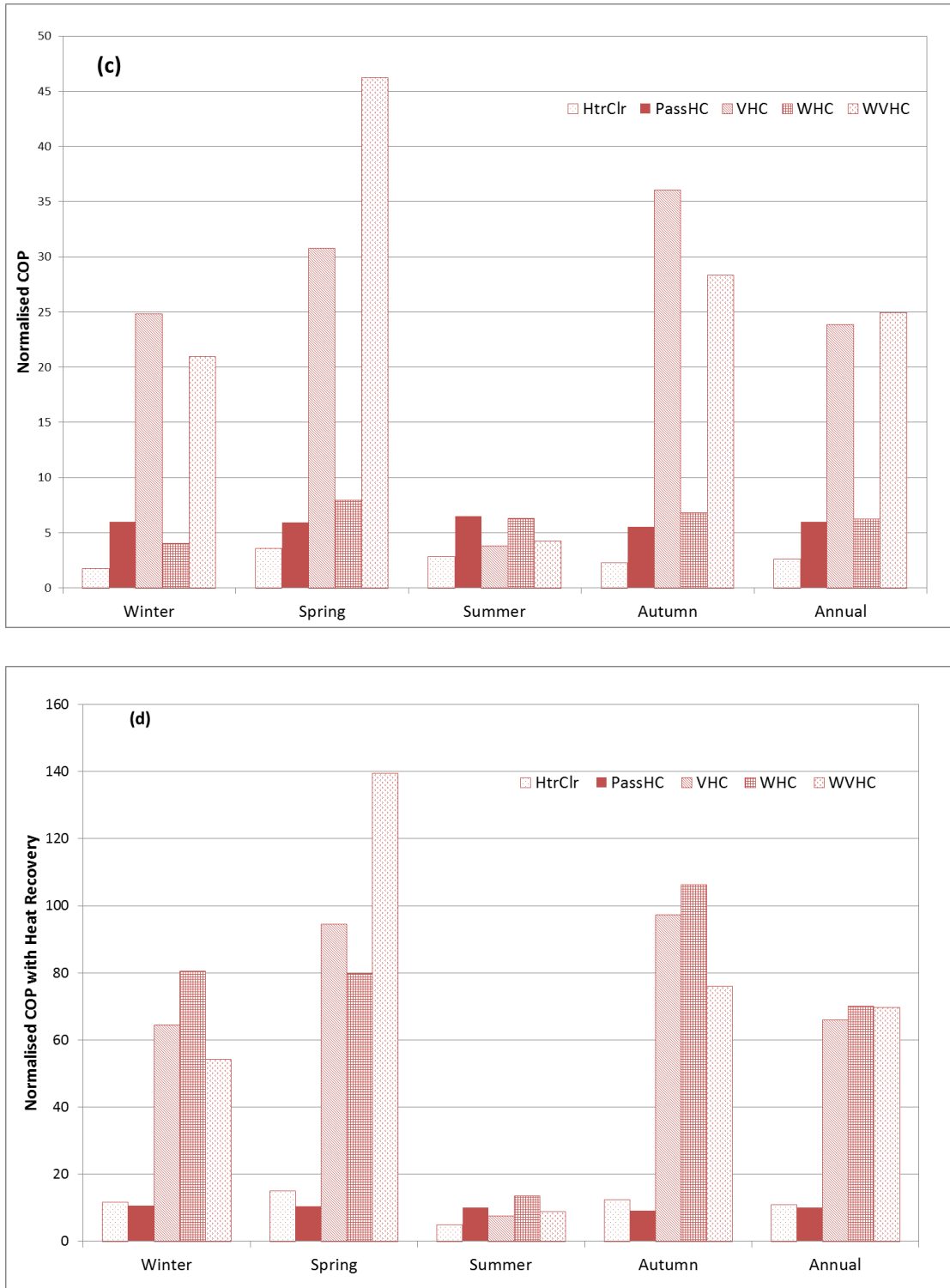


Figure 3.18 - Seasonal Performance (a) COP, (b) COP with Heat Recovery, (c) nCOP, (d) nCOP with Heat Recovery

3.3.5.3.1.1 COP

From the COP chart the VHC outperformed the base case and enhanced systems throughout winter, autumn and spring. The best summer simulated performance was achieved by the WHC system demonstrating the cooling capability of the embedded water channels. Across annual averages VHC and WVHC achieved COP figures of 6.7 and 6.3 respectively. Passive slab (PassHC) was not charted on figure 3.18 (a) and (b). PassHC achieved an annual COP of 26.1 but failed to maintain comfort conditions.

3.3.5.3.1.2 COP with Heat Recovery (HR)

When energy recovered through the thermal wheel was included in the calculation the COP_{wheel} figures generated offered more enhancement to water based systems due to the high level of heat recovery occurring in the water system. WHC achieved the highest COP_{wheel} figures for spring and summer. Winter and autumn simulations revealed a VHC system to have the greatest COP_{wheel} figure. Average annual COP_{wheel} figures for the WHC and WVHC systems were 17.4 and 16.6 respectively.

3.3.5.3.1.3 nCOP

The normalised COP (nCOP) figure generated quantified the thermal comfort and energy efficiency of each AHU and hollow core system. PassHC remained relatively constant throughout the seasons. VHC achieved the highest figures in winter and autumn whilst WVHC achieved the highest nCOP in spring. During summer PassHC and WHC offered the best nCOP figure. Across the year WVHC (25.9) achieved a 1 point gain on a traditional VHC (24.9) system.

3.3.5.3.1.4 nCOP with Heat Recovery

Analysis of figure 3.18(d) reveals the most even average annual performance of the three active hollow core systems: 65.8, 69.9 and 69.5 for the VHC, WHC and WVHC systems respectively. WHC achieved highest during winter, summer and autumn whilst WVHC achieved the highest during temperate efficiency during spring.

Based on the traditional COP figure, when the systems were considered alone, of the technologies modelled, VHC offered the most energy efficient heating and WHC the most energy efficient cooling. When combined with heat recovery in the thermal wheel the WHC and WVHC systems performance was greatly boosted. Without this, the WHC system has no energy recovery that traditionally leads to high COP values.

Advancements in the water configuration with heat storage tanks, cold water loops, plant, variable valves and pumps offer an interesting enhancement. Simple open loop mains water WHC system offers system enhancement during the summer season, VHC's worst performing season. WVHC performs best during spring time, optimising the use of temperate weather conditions. For enhancements to demonstrate their greatest worth further development of enhancements should target operation in the spring and summer conditions.

Summer season efficiencies were consistently lower than the other seasons, across the COP metrics reviewed. This underperformance reveals significant opportunity for system enhancement, to bolster the energy efficient operation of the system during the summer season.

3.3.5.4 Thermal Comfort Conditions

After simulating each season's performance based on seasonal design weeks the results were averaged across the year and the results graphed. With the exception of a PassHC all of the technologies maintained average annual occupied room temperatures close to the optimum target of 21°C, and all within human comfort levels (18-25°C) (Figure 3.19 and Table 3.4). Figure 3.20 charts the key figures from Table 3.4.

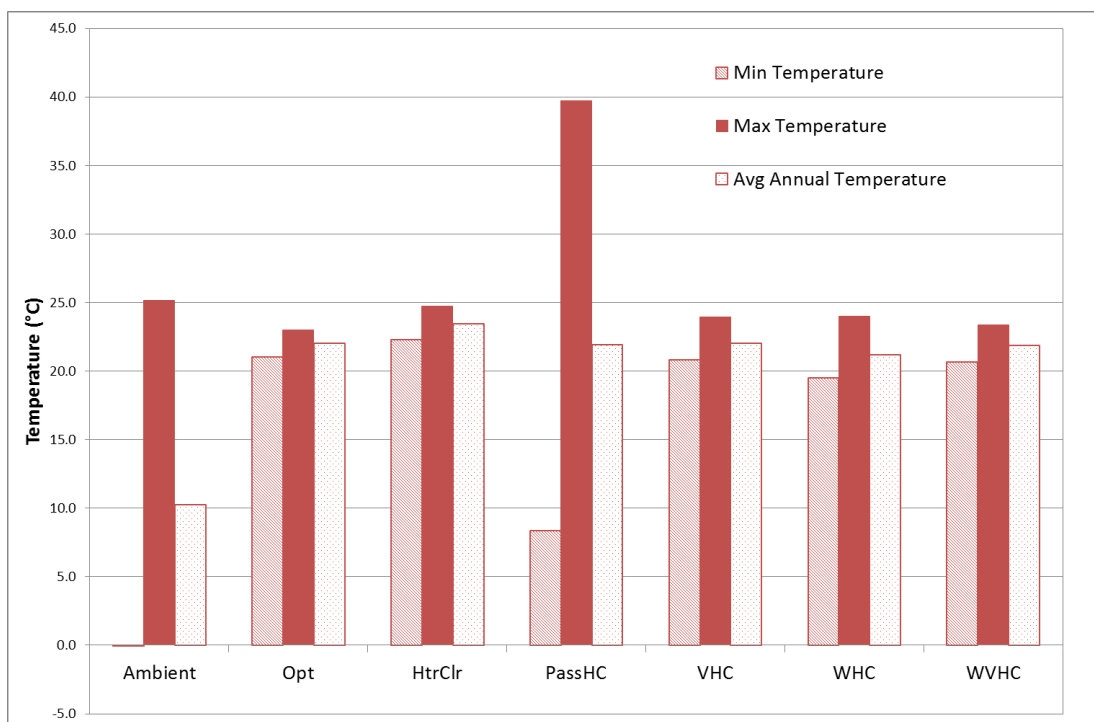


Figure 3.19 - Simulated Annual Room Temperature Profiles

Table 3.4 - Average Annual Comfort

| | | | HtrClr | PassHC | VHC | WHC | WVHC |
|---------------------------|-------------|----|--------|--------|------|------|------|
| Temperature | Min | °C | 22.3 | 8.4 | 20.8 | 19.5 | 20.7 |
| | Max | °C | 24.7 | 39.7 | 23.9 | 24.0 | 23.4 |
| | Avg | °C | 23.4 | 21.9 | 22.0 | 21.2 | 21.9 |
| | AvgDev | °C | 0.8 | 4.0 | 0.2 | 0.2 | 0.2 |
| | Occ. AvgDev | °C | 0.4 | 4.4 | 0.1 | 0.2 | 0.1 |
| Avg Time Below | | % | 98.9 | 56.0 | 10.7 | 18.5 | 7.0 |
| Avg Time Above | | % | 0.0 | 38.5 | 1.7 | 37.8 | 4.4 |
| Total Time Outside | | % | 98.9 | 94.6 | 12.4 | 56.4 | 11.4 |

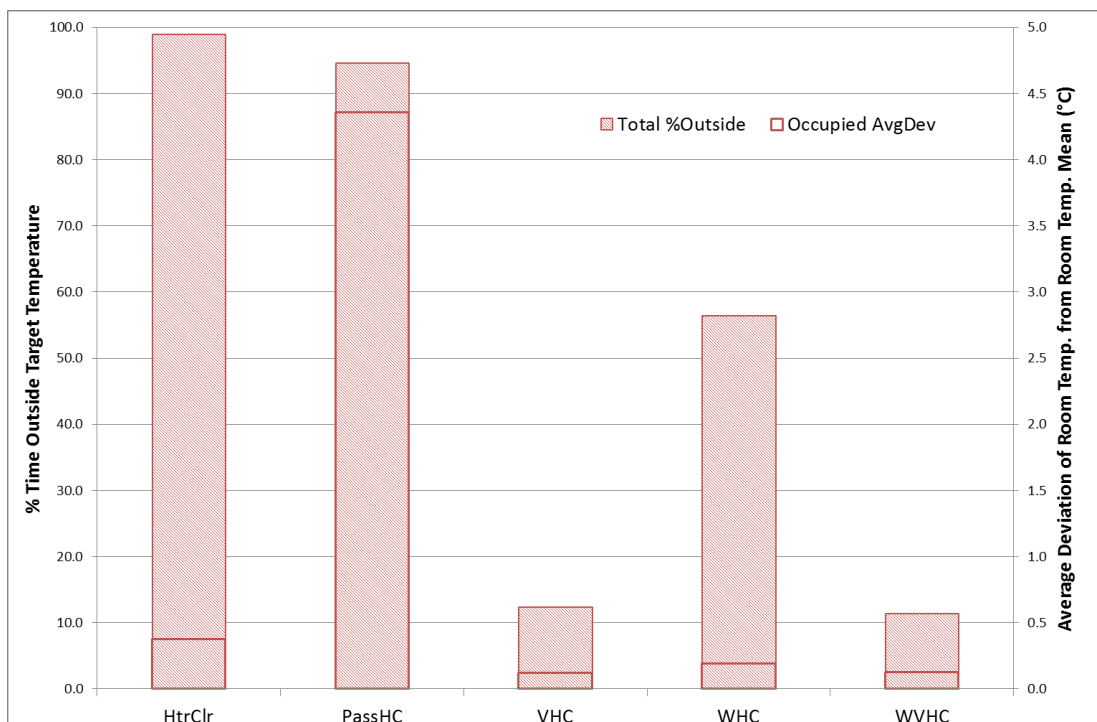


Figure 3.20 - Simulated Thermal Performance

Further to the temperature profiles, thermal comfort was monitored through two methods; the temperature exceedance method [142] where percentage time outside optimum temperature was recorded, and the average occupied room temperature deviation from the occupied room temperature mean. Since all the systems average temperatures lay within the optimum target temperature band (21-23°C), this Average Deviation metric gave a good measure of sustained thermal comfort. Ideal energy efficient thermal control technologies demonstrate low hours outside the set temperature band and low Average Deviation readings (figure 3.20 and table 3.4).

The traditional air heater-cooler (HtrClr) system struggled to efficiently keep temperature within the narrow temperature window. The passive slab (PassHC) system failed to maintain thermal comfort. All three hollow core systems performed well with the ventilation based systems recording better thermal comfort. Despite the high percentage hours outside set points these were never more than 3°C outside the optimum temperature, maintaining room temperature within acceptable human comfort temperature thresholds. Similar deviations were seen across the three hollow core systems. VHC and WVHC recorded the least hours outside the optimum target temperature band due to effective temperature moderation from the slab conditioned inlet air.

3.3.5.5 Energy Performance

Table 3.5 - Average Annual Energy Consumption

| | | HtrClr | PassHC | VHC | WHC | WVHC |
|-----------------------------|---------------|--------|--------|-------|-------|-------|
| Energy Consumed | <i>kWh/yr</i> | 1084.5 | 173.7 | 289.3 | 185.0 | 302.7 |
| COP | | 1.0 | 26.1 | 6.7 | 1.9 | 6.3 |
| COP_{wheel} | | 4.1 | 43.6 | 17.7 | 17.4 | 16.6 |
| nCOP | | 2.6 | 6.0 | 23.9 | 6.2 | 24.9 |
| nCOP_{wheel} | | 10.9 | 10.1 | 65.8 | 69.9 | 69.5 |
| Avg Time Below | % | 98.9 | 56.0 | 10.7 | 18.5 | 7.0 |
| Avg Time Above | % | 0.0 | 38.5 | 1.7 | 37.8 | 4.4 |
| Total Time Outside | % | 98.9 | 94.6 | 12.4 | 56.4 | 11.4 |

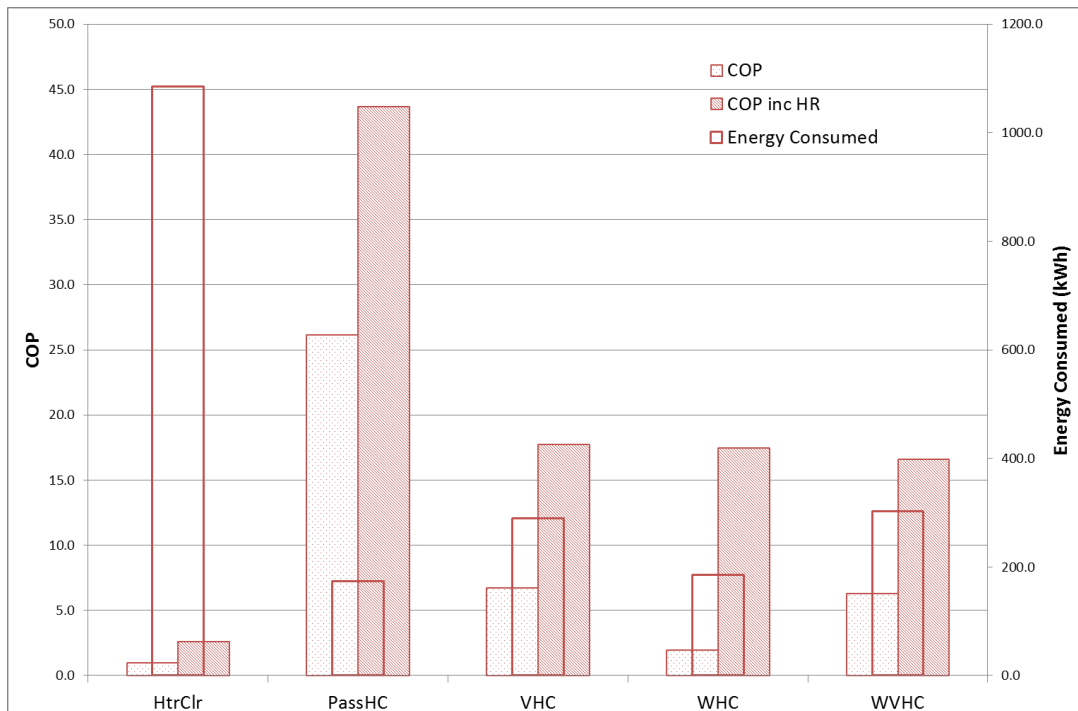


Figure 3.21 - Simulated Energy Performance

With multiple technologies demonstrating comparable average temperature control performance, the energy consumed to achieve these comfort levels was reviewed (Figure 3.21 and Table 3.5). Optimum energy performance exhibited low energy consumption figures accompanied with a high COP figure, demonstrating excellent re-use of energy. The base case air heater/cooler configuration was the least efficient method of maintaining thermal comfort as it required the most energy and reused the least. PassHC technology demonstrated the best energy efficiency, with the various hollow core technologies showing promising performance.

The two COP figures demonstrate the performance with and without the heat recovery thermal wheel. Whilst part of an effective overall system, the thermal wheel was not a direct part of the hollow core technology alone, so performance with and without its inclusion has been reported to convey the variation between hollow core technologies as well as overall air handling systems.

3.3.5.6 Normalised Performance

From the COP figures alone the PassHC performance surpassed the other technologies, however, in light of the poor thermal control exhibited by the PassHC a normalised COP (nCOP) metric was developed to offer a figure for overall energy efficient thermal control performance. The figure incorporates the traditional COP and the Average Temperature Deviation from Mean (Equation 3.38).

Equation 3.38

$$nCOP = \frac{COP}{AvgDev}$$

The figure had little value for further calculations but gave a clear representation of the technology that demonstrated both high levels of energy efficiency and thermal control.

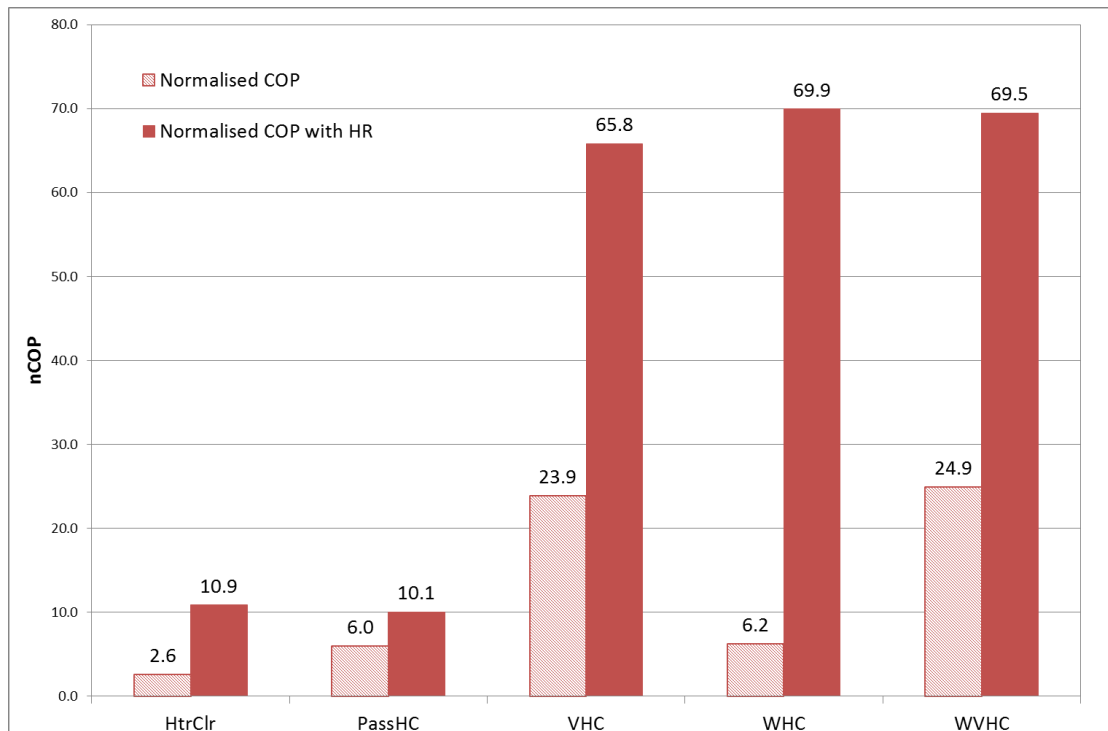


Figure 3.22 - Normalised COP Performance

From Figure 3.22, the combined technology of ventilation and water controlled hollow core offers the optimum annual energy efficient thermal control (nCOP). The nCOP figures for the PassHC system demonstrate poor overall performance. Each of the hollow core technologies surpassed the base case technologies due largely to the active recycling and storage of heat energy in the system.

3.3.6 Summary of Findings

The water control system was not fully optimised. Open loop mains water was pumped through the slab during all occupied hours despite at certain times (when $T_{slab} < T_{opt}$ and $T_w < T_{slab}$) this having a negative effect on the technologies thermal comfort performance. Water system control would improve WHC and WVHC efficiencies.

Despite the lack of control water addition offered low-energy, efficient-cooling to the slab. The cooling was most needed during peak summer periods, with WHC systems demonstrated

the greatest performance during the summer season. WVHC systems operated most efficiently during the spring season.

VHC systems were least efficient during summer seasons. This season, where slab saturation is a more likely occurrence, offers the greatest opportunity for energy efficient enhancements to the VHC system. For enhancements to demonstrate their greatest worth, further development of enhancements should target operation in spring and summer conditions.

WVHC systems offered the most sustainable thermal mass temperature control of the systems tested. Pilot scale tests should be undertaken to further validate the findings from the simulations. Economic analysis will also be required to determine the monetary benefits of fitting such a system. Further investigation is also required to establish an efficient and effective control strategy for the water based and combined technology.

A summertime alternative to VHC enhancements may be possible with appropriate incorporation of PCM. This function was not possible in this Excel model and should be investigated further.

3.4 Conclusions

The time step heat balance modelling enabled detailed understanding of VHC control strategies, system thermal response and energy efficiency. The model was constructed with the given purpose of gaining familiarisation and quantifying hollow core enhancement performance. Assumptions were made to simplify the model and enable swift generation of results. From the annual simulation results all TABS tested (VHC, WHC and WVHC) maintained year round comfort. On average 0.5°C was saved by the WVHC system over the VHC base. WHC exhibited the weakest COP figures, with VHC and WVHC comparable. Enhancement benefit was greatest during the summer season when VHC slab was saturated.

Following modelled evidence that scope for enhancement through embedded water pipes remains, the performance of the prototype system will be laboratory tested under pilot scale conditions. The prototype design was used to inform the model. Laboratory trials should be undertaken in spring and summer replicated conditions to best demonstrate the enhancement. To test and validate the model findings the designed prototype will be constructed and tested in a laboratory facility in the following chapter.

Chapter 4: Active Thermal Mass Testing

Prototype Construction and Laboratory Investigation

4 Active Thermal Mass Testing

4.1 Introduction

The modelling work in *Chapter 3* revealed the suitability for thermal energy storage (TES) system enhancements, to satisfy internal thermal comfort and make significant energy and financial savings during spring and summer seasons. To investigate the performance of TES enhancements, and satisfy the first research objective of this work, a prototype VHC system was constructed, installed and investigated, as reported in this chapter.

Detailed design and construction of a suitably integrated water and air activated VHC (WVHC) prototype was documented in part two of this chapter. Following installation some initial experimental tests were carried out on the enhanced prototype system to further understand the enhanced VHC system's thermal response and capacity.

During the laboratory testing, understanding of the performance benefits of water incorporated hollow core (WHC) and combined water and ventilated hollow core (WVHC) were investigated; with and without temperature control systems. The laboratory

investigations were conducted under fixed heating conditions, replicating internal heat gain during occupied hours.

4.1.1 Methodology

Based on the evidence from the modelled performance (section 3.3.5), scope for energy-efficient cooling enhancement was most prevalent during summer seasons where additional cooling capability was required. The purpose of this chapter was to construct an air-based active TES prototype, capable of incorporating available enhancements, and investigate the energy-efficient cooling capabilities when overheating threatens. Initially, the prototype was enhanced through the embedding of water pipes. Through water activation the control the slab was increased, due to the improved heat transfer properties.

Investigation into energy-efficient thermal regulation of TES during peak periods was undertaken by:

1. Constructing the designed prototype
2. Installing the prototype into the test chamber
3. Undertaking twenty-four hour tests observing thermal and energy performance of different system modes, when inflicted with a fixed, high level of internal gains:
 - a. Test under fixed control systems, to determine system type performance
 - b. Test under optimised control systems, to determine system performance with smart control
4. Validating the model through comparison with laboratory results

4.1.2 Contributions to knowledge

Having completed the methodology outlined above, numerous valuable contributions to knowledge have been achieved:

- Benefits of water and air driven TES systems has offered energy-efficient thermal regulation of internal spaces, offering cooling up to 60 to 70W/m² [24]. In super-insulated hi-tech offices, greater cooling is required [143]. This work therefore investigates the scope of combining water and air driven TES to provide high levels of energy-efficient heat dissipation.
- Practical understanding of WVHC system prototype design, construction and installation has been obtained and reported. It builds upon industry design guides [25, 34] to deliver a pilot scale prototype. This design highlights the novel process

undertaken, the numerous obstacles faced and overcome and the laboratory limitations.

- The laboratory investigation offers new knowledge on the performance benefits of a combined water and air activated thermal mass system (WVHC) and novel findings from an initial investigation into control strategy and temperature set-points. As highlighted [39], active TES systems benefit greatly from efficient control strategies.
- The laboratory findings also offer figures for validation of thermal models. Validation of the *Chapter 3* model offers a useful tool for assessing the performance of WVHC systems when installed in single space buildings. The laboratory figures are available for further research to develop and validate active thermal mass models.

4.1.3 Chapter aims

- 1) Prepare a pilot scale hollow core slab, suitable for thermal investigation through embedding of an air and water network, and temperature sensors – as per the designs in *Chapter 3*.
- 2) Investigate pilot scale performance under fixed conditions and varying control strategies, to understand combined WVHC performance better.
- 3) Validate the *Chapter 3* model from the test data generated.

4.2 Prototype Construction & Installation

To implement the design laid out in *Chapter 3*, and enable the laboratory prototype testing, a WVHC prototype was constructed as detailed below. The prototype was subsequently installed into the experimental chamber for investigation.

4.2.1 Prototype Construction Method

Following acquisition of the required parts the prototype construction method below, was followed.

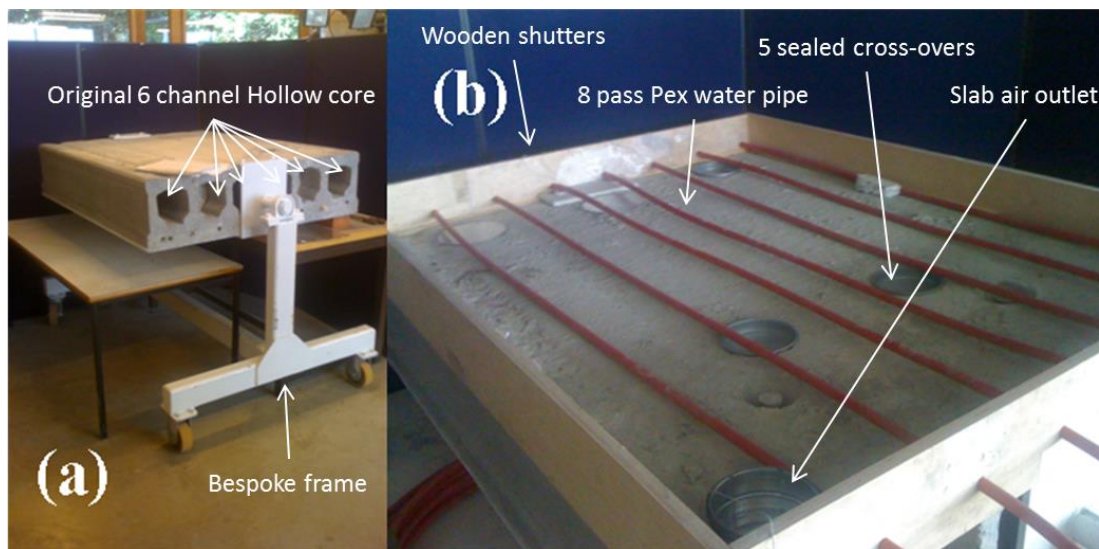


Figure 4.1 - Prototype under construction

- 1) The demonstration hollow core was positioned in the laboratory, Figure 4.1(a), for prototype enhancement as per the prototype design in *Chapter 3* (Figure 3.1).
- 2) The cross-overs and outlet, forming the designed air network, was drilled by an industry professional. The silver discs in Figure 4.1(b) were inserted to seal the internal crossovers (Figure 4.2(d)).

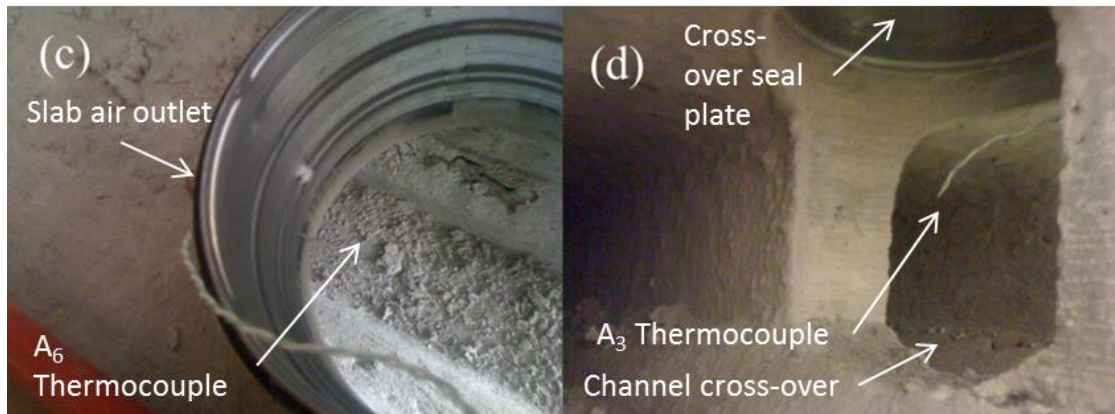


Figure 4.2 - Outlet and Cross-over with embedded Thermocouples

- 3) K-type thermocouples were inserted at the designated cross-overs and air outlet (Figure 4.2).
- 4) Wooden shutters were constructed to fit around the slab (Figure 4.1(b)). The shutters served a dual purpose; to hold the pipes in place, providing bracing to straighten them out, whilst also containing the additional cast concrete that embedded the pipes.
- 5) Four lengths of 16mm (internal diameter) by 1.5mm (wall thickness) by 4m (length) Pex UFH piping were cut, straightened and inserted through the wooden shutters (Figure 4.3 (e & f)) to follow the designed pathway (Figure 3.1).
- 6) Prior to concrete casting the hollow core slab was lowered onto a pallet for ease of casting. The hollow core thermocouples (S_{1-9}) were labelled, and then positioned on the exposed concrete surface before a 50-60mm concrete layer was added.

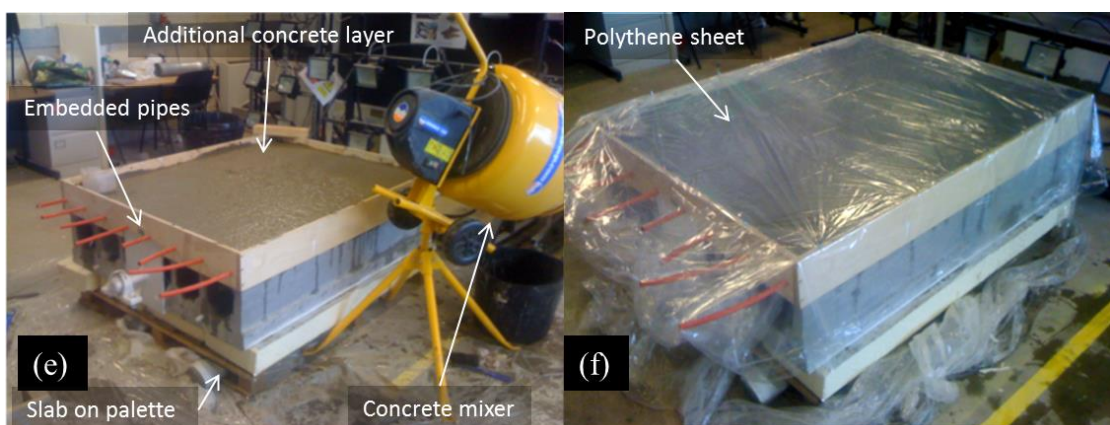


Figure 4.3 - Additional Cast Concrete Layer

- 7) A concrete-PVA mix was prepared and the 50-60mm layer added. The original concrete surface was swept and whetted prior to concrete addition. PVA was added

to the additional concrete mix to provide a suitable bond between the original and additional concrete.

- 8) The aggregate/cement concrete mix was prepared by University of Nottingham laboratory technicians and cast onto the slab surface, embedding the water pipes (Figure 4.3 (e)).
- 9) Following casting, to help the concrete cure, a polythene sheet was pinned across the setting concrete (Figure 4.3(f)).
- 10) The prototype slab was returned to its moveable stand and allowed to cure under polythene for one month.

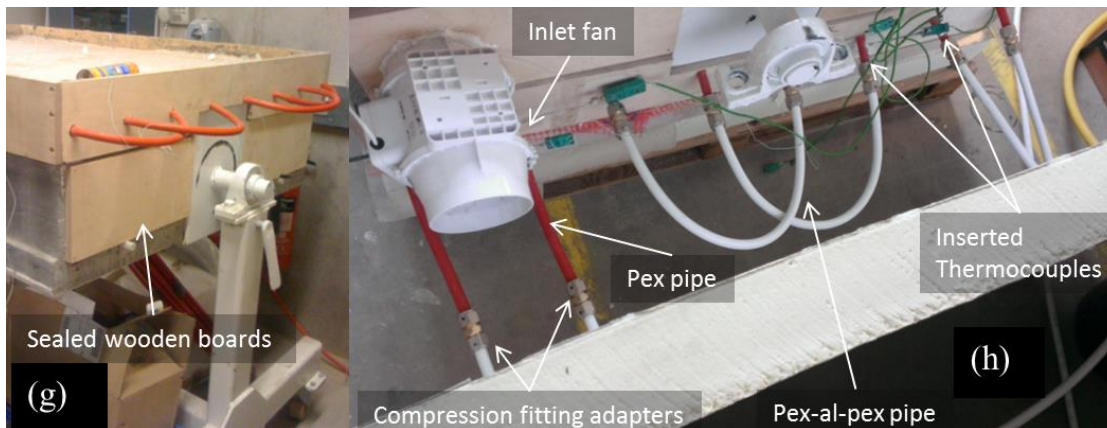


Figure 4.4 - Air Shutters and Pipe Network

- 11) Wooden boards to shut off the hollow cores and create the air network were prepared and sealed in place (Figure 4.4(g)). A hole was drilled in one board to position the inlet fan.
- 12) Initial air velocity tests were carried out to determine the relationship between the fan power and delivered velocity through the prototype air network [144].
- 13) The water pipe network was completed through the attachment of compression fitting adapters and white Pex-Al-Pex piping (Figure 4.4(h)).

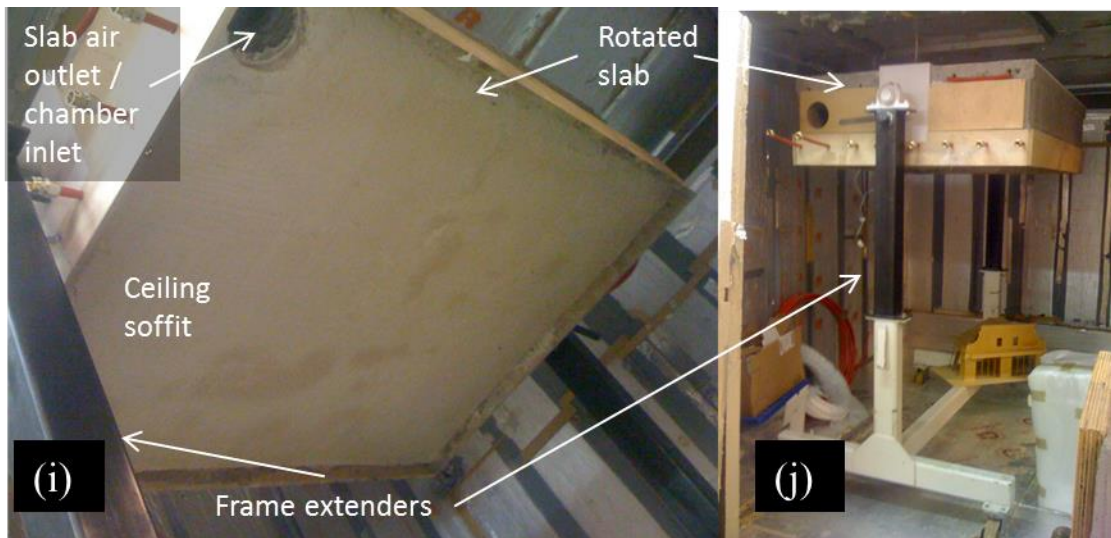


Figure 4.5 - Rotated, Raise and Installed Prototype Slab

- 14) The prepared prototype slab was subsequently *rotated* – to make the additional concrete surface the ceiling soffit (Figure 4.5(i)), *raised* – onto purpose built frame extenders (Figure 4.5 (j)), and *installed* into a prepared insulated chamber (Figure 4.5 (j)).

The chamber installation and prototype fitting process was completed in the following section.

4.2.2 Chamber Fitting and Installation

Following construction of the prototype slab and initial installation into the ambient test chamber the final system parts were installed.

- 1) Fan, water, heating and temperature measurement systems (detailed in Table 11.1) were installed (Figure 4.6).
- 2) The chamber floor, ceiling and walls were constructed from 100% re-used 80 & 100mm thick Celotex insulation (Figure 4.7) with a quoted U-value of 0.22 W/m²K [145].

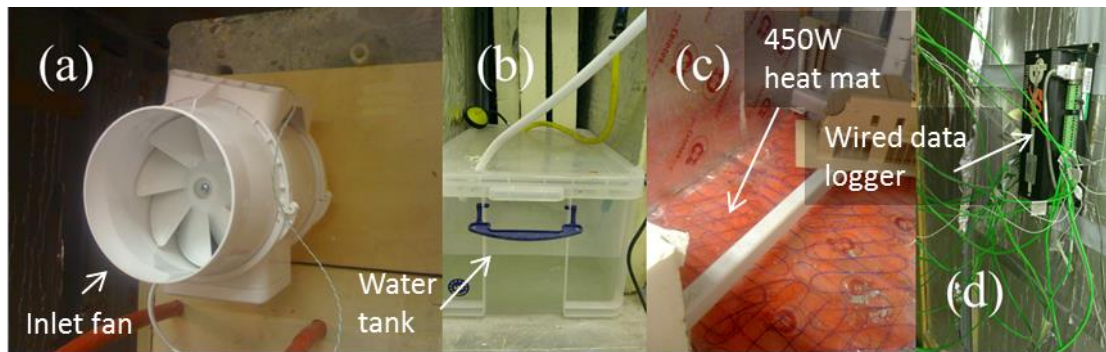


Figure 4.6 - Fan, Water, Heating and Temperature Sensing Systems Installed

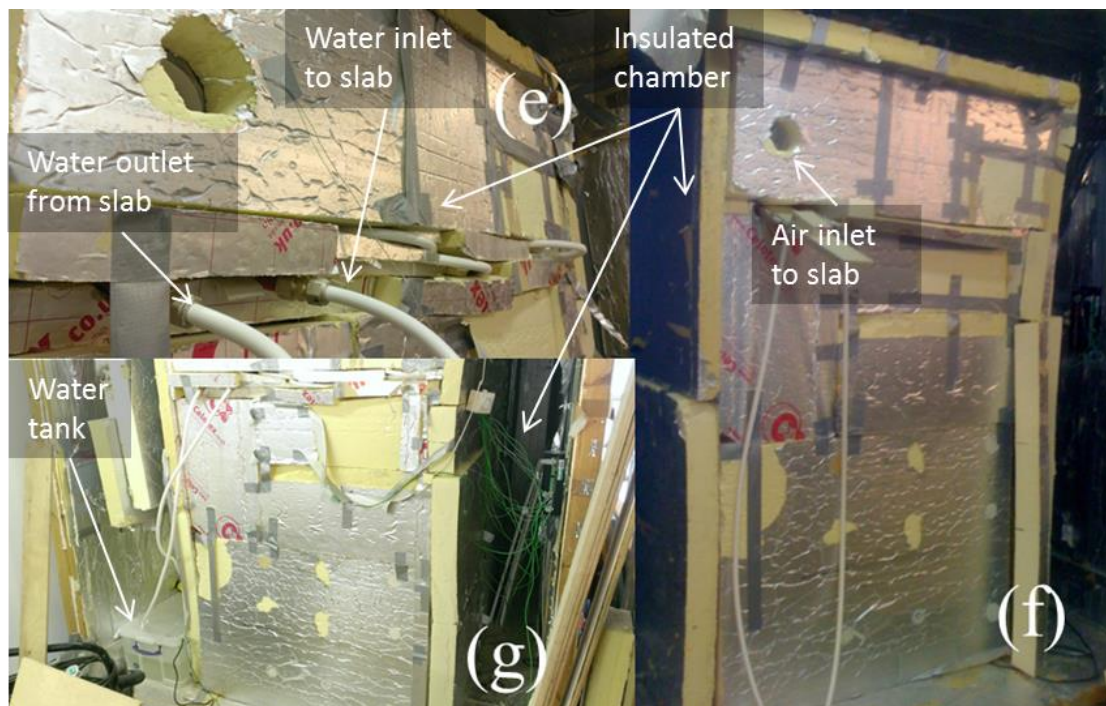


Figure 4.7 - Insulated Chamber

The installed axial-inlet fan had a theoretical maximum power of 32W. The fan was controlled using a dimmer and thermostat, enabling static and temperature controlled investigations. There was a passive outlet vent installed in the chamber, although the chamber was not perfectly air tight (so air leakage between insulation layers occurred).

To enable control of the air inlet velocity to the chamber, air velocity tests were conducted to determine the relationship between fan power (W) and average air inlet velocity. The power was fixed, using an electrical dimmer, at incremental steps between 7.3 and 33.9W. Average air inlet velocity was measured using a portable anemometer, held one centimetre from the slab outlet. Tests were conducted on two separate occasions under laboratory conditions. The data was analysed and a relationship between air velocity and fan power generated. The fan power required to deliver 4 acph, in accordance with the minimum industrial VHC

ventilation rates for high rise non-domestic offices [34, 146], was calculated at 10.3W. At this minimum power the anemometer was not sufficiently sensitive to consistently measure the air velocity, so the fan (generating the inlet air velocity) was controlled using an electrical dimmer and power meter [144].

The water system installed was powered by a 160W Conrad submersion pump. By design the pump was operated by a level switch. An additional temperature switch was installed to enable static and temperature controlled investigations. It was found that the pump did not work well with a dimmer switch, therefore the water system operated on an on/off control system only, with a delivered flow rate of 4l/min. A tank with maximum capacity of 64 litres was half filled with mains water. Temperature sensor (L_1) was inserted into the water tank (Figure 4.6 (b)) to monitor the change in temperature [147].

Liquid thermocouples (L_2 - L_5) were inserted into the red Pex pipe network. To enable this, small holes were drilled into the red Pex pipe. Thermocouples were subsequently inserted and the holes waterproofed with Sika Sikaflex EBT+ (Figure 4.4(h)).

A 450W radiant heating mat was spread across the chamber floor to replicate total heat gain (Figure 4.6 (c)). From [143] the total heat gain for offices can range from 75 to 180 W/m² depending on building type and office location. The heating mat was connected to a capable dimming switch to adjust the heat load on the room. Heat loss was calculated to comprehend actual cooling conducted by the hollow core, in the chamber. Based on known physical properties and reviewed against observed results, the calculated heat loss from the chamber was 160W – with maximum heat mat loading. Taking this into consideration the maximum heat gain replicated in the chamber, generated by the heat mat was approximated at 120W/m², (based on an internal heat gain, after fabric losses, of 290W and chamber floor area of 1.2 × 2m) [148].

The temperature measurement system consisted of Type K thermocouples, a DT500 data logger and a PC operating the DeLogger software. Nine thermocouples embedded 50mm above the hollow core soffit (S_{1-9}) monitored the slab temperature. Six thermocouples (A_{1-6}) situated in the air network monitored the air temperature from inlet, through the slab and into the chamber. Six thermocouples (L_{1-6}) monitored the water temperature in the tank, and throughout the water pipe network. Three thermocouples inside the chamber (R_{1-3}) measured the temperature at differing heights. Two thermocouples were placed opposite each other, on either side of the chamber wall (W_1 and W_0). These readings were used to

monitor temperature difference across the chamber wall. Finally one ambient temperature sensor monitored the external chamber temperature. The software was programmed to take data readings every five minutes.

The chamber was constructed out of re-used Celotex insulation. Where available 100mm insulation was used with some sections of 80mm installed as required. Silver cloth tape was used to seal the sections. An entrance way to the chamber was installed in the bottom right corner for modifications to the system and installations as required. Throughout the testing, as discoveries were made, the chamber was dismantled and rebuilt to install system upgrades.

4.2.3 Rig Capabilities, Limitations and Assumptions

The rig constructed provided the capability of investigating PassiveHC, VHC, WHC and WVHC system performance in a cooling scenario. Further investigations were possible into the performance variation with respect to static and temperature dependant control strategies.

No capability for managing the ambient conditions was available for the rig. As only one chamber was constructed it was not possible to generate figures for a room with no slab as a reference – although attempts were made by insulating the soffit surface. Heat flux could only be calculated based on available physical properties and measured temperature differences. The rig was limited to twenty-nine channels due to the working capacity of the data logger.

The water system was limited to a closed loop tank system. This significantly hampered its thermal capacity. The water pump also acted as a 160W heater in the water stream. No ability to switch between closed loop and open loop systems was available therefore intelligent operation of supplementary energy storage was not possible.

The insulation was not ideal due to the re-use of insulation. The fan was limited in its operation and the 10.3W specified power didn't always provide required flowrate. Water flowrate was monitored by a manually-read flow meter and therefore only provided instantaneous information. The energy meters were useful for setting powered devices to certain wattage, but did not record variation in power over time therefore power delivery was assumed constant.

The air path through the slab was not ideal due to shortening of four channels. The water pipe bends were not embedded into the slab so some water conditioning acted directly on the room instead of through the slab. Damage to the water pipes during rotation, raising and

installation caused some pinch points in the pipe. This will affect the water velocity through the pipe; therefore assumed uniform velocity through the pipe will differ in reality.

The construction of the rig left scope for further additional investigation into PCM incorporation through the addition to the water tank, the soffit or as internals in the chamber. Access to the hollow cores was restricted due to the boarded and insulated cores. Instrumentation accuracy was limited as per the levels found in Table 4.1.

Table 4.1 - Instrument Accuracy

| Instrument | Suitability Range | Units | Sensitivity | Accuracy | Calibration |
|--|----------------------|-------|----------------|----------|---|
| K-type Thermocouple | -100 to +250°C | °C | 41µV/°C | ±1.5°C | Ice to boiling test conducted on reference thermocouple. All other thermocouples calibrated against the reference thermocouple. |
| Turbine Flow Sensor (Gems FT-110) | 1 to 10 l/min | Hz | 55Hz per l/min | ±3% | Flow rate calibrated against time taken to fill a one litre measuring cylinder. |
| Anemometer: Skywatch® Xplorer1 | 0.8 to 41.7 m/s | m/s | - | ±3% | Compared against measurements taken by alternative anemometers in university on same apparatus. |
| Energenie Power Meter | 0.1 to 3120 W | W | - | ±2% | - |
| | 200 to 276 V | V | - | ±1.5% | |
| | 0.005 to 13 A | A | - | ±2% | |
| | 45 to 65 Hz | Hz | - | - | |

4.2.4 Summary of Findings

A prototype slab capable of testing WVHC performance was constructed with embedded pipes, air network and temperature sensors. In connection the prototype system was raised, installed, instrumented and insulated ready for testing. Piping problems were overcome with 1.5mm to 2mm interior diameter compression fitting adapters.

The slab was only mobile on the designed trolley so rig adaptations were made to secure the slab at ceiling height on the trolley. The rotation of the slab was problematic and cause pipe damage. The resulting leaks were temporarily sealed with a permanent solution installed at a

later date. When building future WVHC systems it is advisable to cast the pipes fully embedded into the system to avoid risk of damage in transportation or installation.

The size of the prototype and resulting chamber meant that no control of ambient temperature was possible due to access restrictions and technology available. Budget constraints and technology availability threatened to de-rail the installation but the system was installed ready for testing.

4.3 Ventilated Thermal Mass Prototype Testing

In the industrial pursuit of low cost energy efficient buildings ventilated hollow core (VHC) has carved out its own niche. By utilising the thermal mass of building fabric, internal room temperature can be controlled with minimal additional energy. After twenty years of successful operation this section outlines the performance of an enhanced traditional VHC system in a pilot scale test chamber at the University of Nottingham. The innovative system enables water cooled hollow core (WHC) and combined water cooled, ventilated hollow core (WVHC) testing on the novel prototype.

Within the specially constructed test chamber the 1.3 tonne hollow core prototype slab was monitored for temperature and energy flows, firstly under constant operating conditions. The aim of this investigation was to understand cooling performance and contrast system cooling efficiency through Coefficient of Performance (COP) analysis for each hollow core system. Subsequent experiments investigated the effect of temperature set point control strategies for the enhanced VHC systems.

Throughout the investigations, conclusions have been drawn from each experiment with findings summarised at the end of the section. Validation of the model reported in *Chapter 3* has been conducted at the end of this chapter. This initial experimentation served as a starting point to comprehend cooling performance and efficiency of the systems under fixed heating conditions. The results from the investigations serve as a starting point to identify suitable avenues for further detailed modelling and experimental investigation in later thesis chapters.

4.3.1 System Enhancement Investigation

4.3.1.1 Testing Methodology

Work by [24] set a precedent for investigation of pilot scale active TES systems. This work differs through the use of active TES as a roof component, instead of floor; but follows suggestions by Weitzmann to investigate alternative thermally active components. The test rig was kept deliberately simple to comprehend comparative system performance.

Having designed, constructed and installed the WVHC prototype, as outlined in the previous sections, twenty-four hour mock occupation tests were carried out to determine the cooling capacity of each active TES system. During the twenty-four hour test period the 450W heat mat was on for eight hours, to replicate heat gain in a general office. This was equivalent to an effective cooling load of 120W/m^2 [143] (Figure 4.8), following chamber heat loss.

Following this heated period, temperatures were monitored for sixteen hours to observe the temperature change through the night. Temperature readings were taken every five minutes throughout the twenty-four hour test period. Prior to each test the chamber and hollow core slab were cooled to 18°C. The ambient conditions remained between 15 and 18°C throughout the investigation.

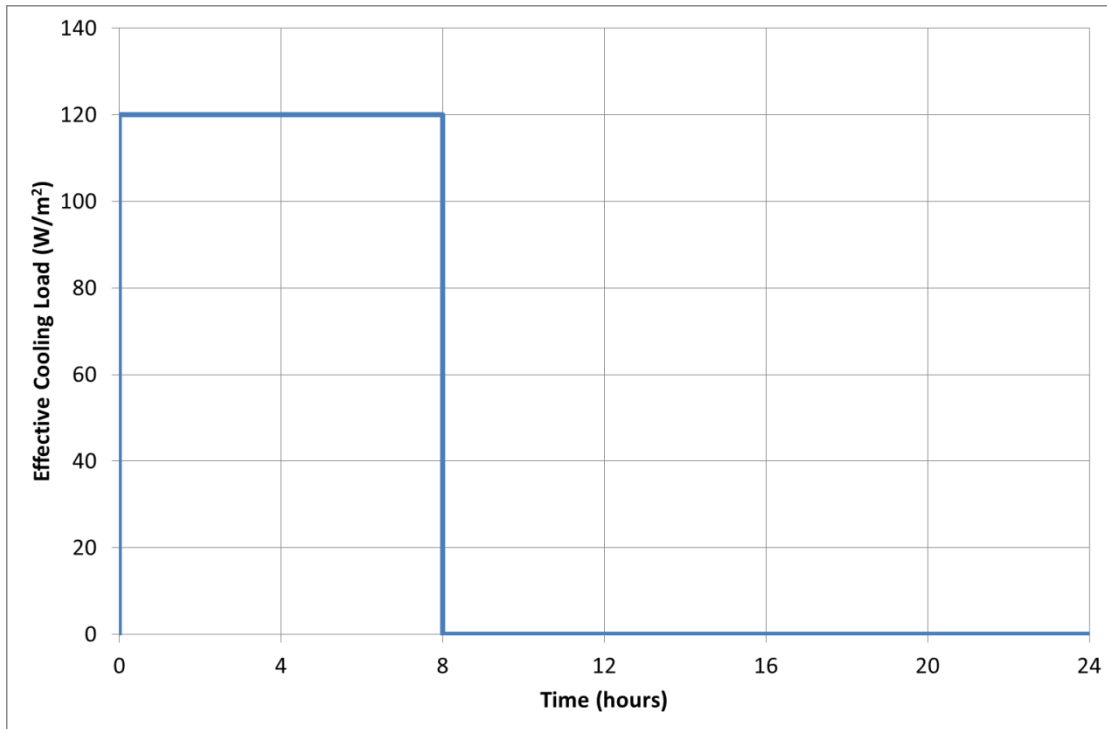


Figure 4.8 - Heater time schedule

During the initial tests fixed cooling control was tested to determine the system performance without dynamic control. In each of the five scenarios tested the initial system operating conditions were maintained throughout the twenty-four hour test period. The five system operating conditions tested can be found in Table 4.2.

Table 4.2 - Constant system operating test conditions

| Scenario | Label | Fan Operating Conditions | Pump Operating Conditions | Cooling provided by: | System operating description |
|----------|-----------|--|---------------------------|--|---|
| 1) | PassiveHC | Constant Off | Constant Off | passively from soffit heat exchange | No active system |
| 2) | 10VHC | Fixed 10W (delivering 4acph - 0.22m/s) | Constant Off | minimum forced ventilation and soffit heat exchange | fan delivering minimum air changes per hour |
| 3) | 32VHC | Fixed 32W (2.5m/s) | Constant Off | maximum forced ventilation and soffit heat exchange | fan delivering air at 2.5 m/s |
| 4) | 10WVHC | Fixed 10W (delivering 4acph - 0.22m/s) | Constant On | minimum forced ventilation, conduction from cooling water and soffit heat exchange | fan delivering minimum air change per hour and pump providing water at 4l/min |
| 5) | 32WVHC | Fixed 32W (2.5m/s) | Constant On | maximum forced ventilation, conduction from cooling water and soffit heat exchange | fan delivering air at 2.5 m/s and pump providing water at 4l/min |

10WVHC represents theoretical WHC operation with minimum fan operation due to minimum fresh air requirements for offices. With no mechanical ventilation the PassiveHC test acts as a theoretical bench mark though would not typically be installed in practice due to not meeting the minimum ventilation standards in a well-sealed office. Along with twenty-four hour room temperature profiles the respective COP and nCOP for each system was calculated following the method below.

Heat loss was calculated from Equation 4.1.

Equation 4.1

$$Power (W) = U (W/m^2K) \times A (m^2) \times \Delta T (K)$$

Where the U value for the insulation was 0.17W/m²K and the total insulated surface area of the internal room was 17.6m². The temperature differential was calculated between the internal wall and external wall temperatures from Equation 4.2 and therefore varies dependant on the wall surface temperatures.

Equation 4.2

$$\Delta T (K) = T_{wi} - T_{wo}$$

From these energy flows a COP for cooling could be generated. COP figures in this instance were used to quantify the energy efficiency of the system; therefore the COP calculation, traditionally used for heat pump technology, was adapted for energy-efficient cooling systems such as active TES. Additional heat loss was calculated empirically with an average 160W additional loss due to air changes [148]. All remaining heat was assumed to be cooled by the WVHC system, therefore the cooling can be calculated from the result of the chamber heat balance and COP can be calculated from Equation 4.3.

Equation 4.3

$$COP = \frac{\text{Useful Cooling}}{\text{Energy used by the Pump and Fan}} = \frac{\text{Heat Mat Power} - \text{Heat Lost}}{\text{Pump power} + \text{Fan power}}$$

As well as the temperature profiles, to comprehend the temperature stability achieved by the system numerically the average room temperature deviation from an ideal of 21°C was calculated (Equation 4.4), where T is the average chamber temperature and n the number of temperature readings per day.

Equation 4.4

$$AvgDev21 = \frac{\sum(|T_i - 21|)}{n}$$

As discussed in *Chapter 3*, to offer a combined measure of energy efficiency and temperature stability, a normalised COP (nCOP) figure was calculated (Equation 4.5).

Equation 4.5

$$nCOP = \frac{COP}{AvgDev21}$$

4.3.1.2 Results and Discussion

4.3.1.2.1 Scenario Profiles

The temperature profiles for each of the five scenarios have been plotted in Figure 4.9 to Figure 4.13. On the charts the ambient, air inlet to chamber, average chamber and average slab temperatures were plotted. Air inlet to chamber was akin to air outlet from slab. For the WVHC systems additional liquid inlet and outlet to slab curves were plotted. From these charts it was possible to characterise the heat transfer behaviour through the twenty-four hour investigations. Since the ambient laboratory conditions most closely represent Spring/Autumn conditions, the comfort temperature range for these transition period seasons, based on ISO 7730 [35], have been highlighted on each temperature profile.

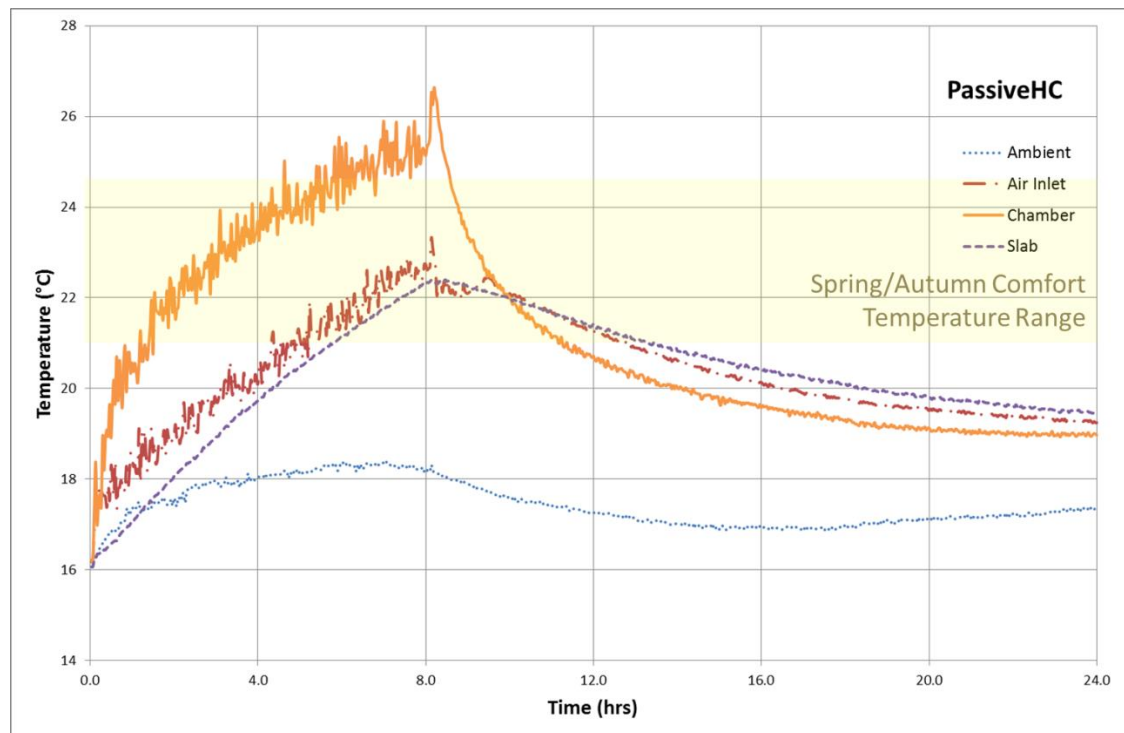


Figure 4.9 - PassiveHC Temperature Profile

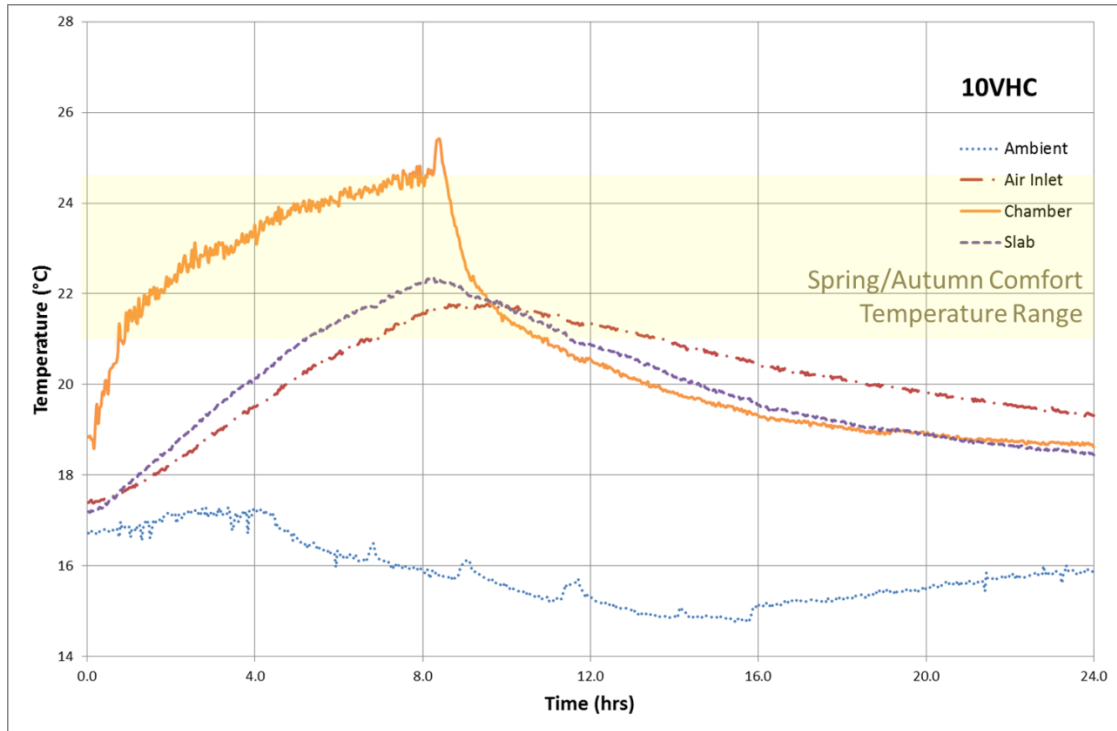


Figure 4.10 - 10VHC Temperature Profile

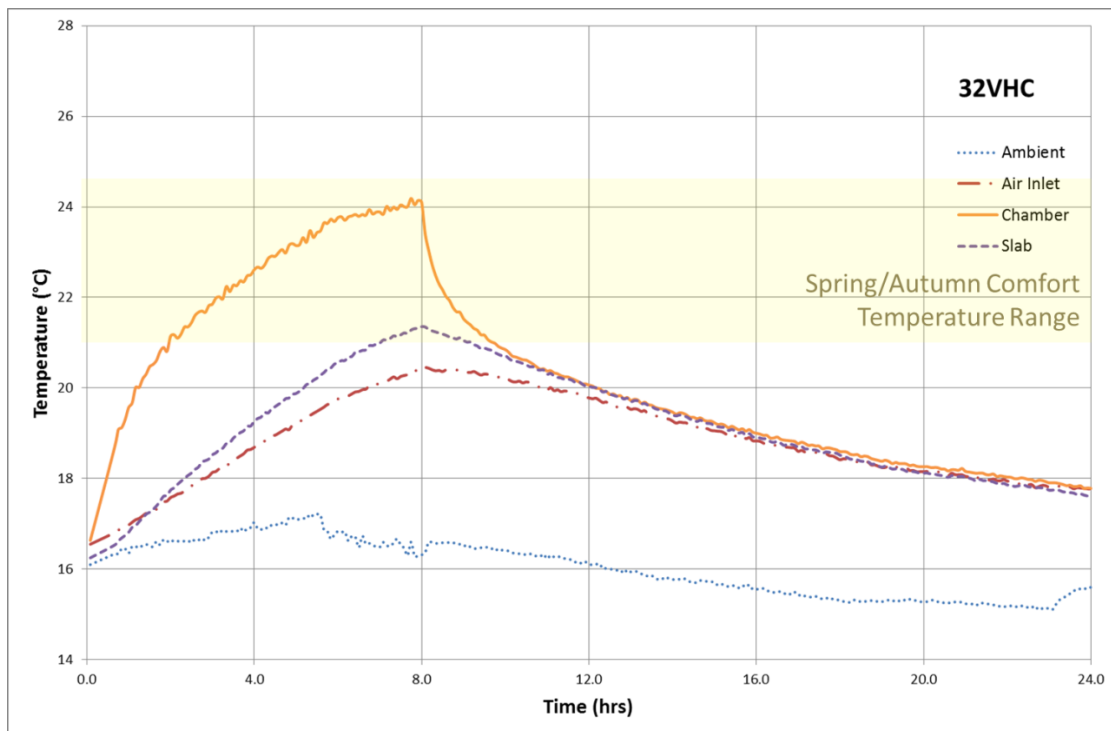


Figure 4.11 - 32VHC Temperature Profile

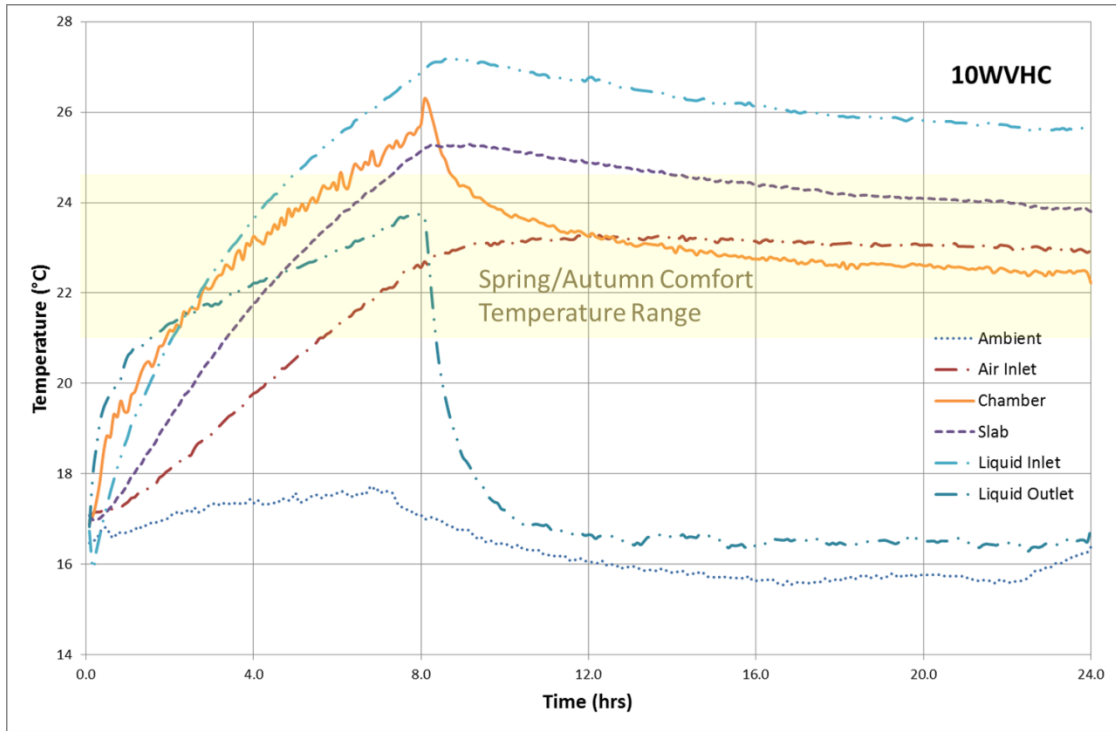


Figure 4.12 - 10WVHC Temperature Profile

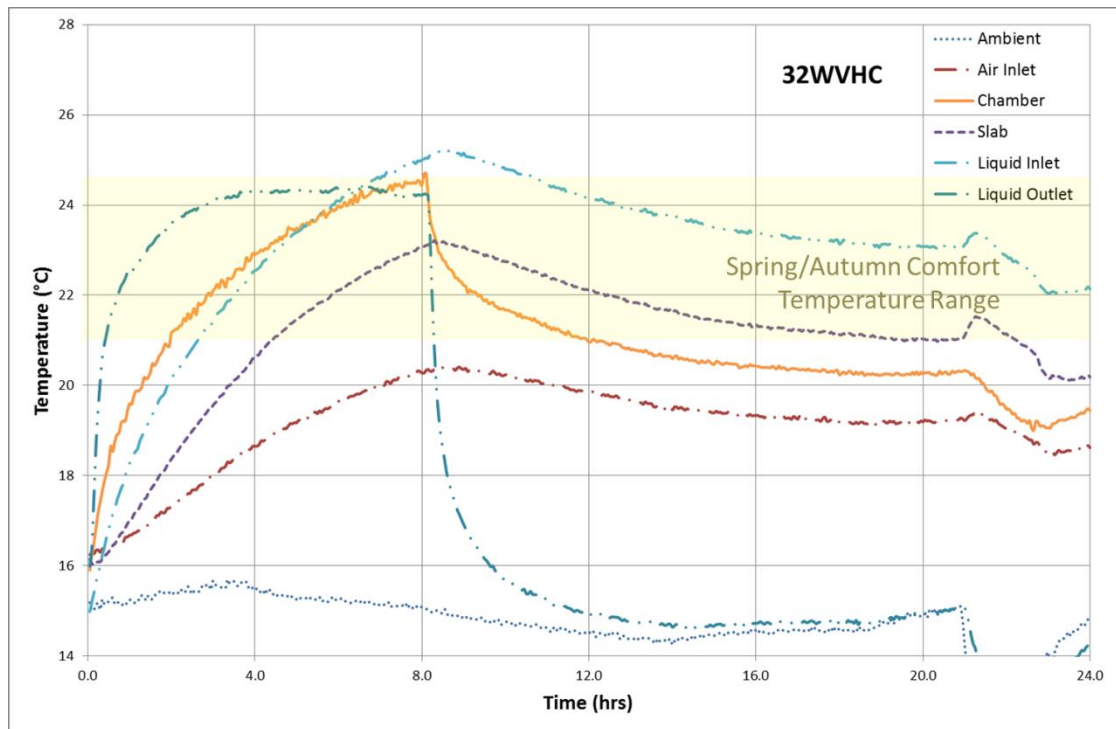


Figure 4.13 - 32WVHC Temperature Profile

In each figure (figure 4.9 to figure 4.13) temperature rise was observed during the first eight hours due to the heat gain, delivered by the radiant heat mat following the schedule in figure 4.8. At the end of the heating ('occupied') period a temperature spike was observed in the PassiveHC, 10VHC and 10WVHC systems. In each case, within thirty minutes of the heater

turning off the temperature began to reduce in all cases due to heat loss through the chamber walls. In the WVHC systems the rate of temperature reduction was stalled due to the cycling water. The water maintained slab and chamber temperature, better than the air only based systems, due to the greater specific heat capacity of water and an approximately 0.5°C temperature rise observed by passing through the pump.

The PassiveHC system saw the greatest disturbance in air temperature readings due to the lack of chamber convection currents. The benefit of ventilated hollow core was evident in the 10VHC and 32VHC profiles. Average chamber temperatures began to stabilise with air inlet temperatures to the chamber, continually offering a cooling effect to both the slab and the chamber throughout the occupied periods.

In the WVHC systems both the cooling and heating effect of dynamic heat storage in the water system was evident. During the 10WVHC system, the liquid inlet temperature heated to slab temperature in thirty minutes. For all subsequent hours the water system had a heating effect on the slab, opposed to the intended cooling effect designed. After two hours the liquid inlet temperature surpassed the chamber temperature and therefore subjected the chamber to additional heating from the water stream. This overall effect resulted in a consistent rise in chamber and slab temperature. The dynamic water storage offered some benefit by maintaining comfort conditions throughout the 'unoccupied' night period.

The 32WVHC system demonstrated an improvement on the 10WVHC system. The increased cooling capacity delivered from the air network helped to delay the water network overheating (liquid inlet temperature exceeding average chamber temperature) until the final two hours of the 'occupied' period. The water pipe network was still able to maintain the chamber temperature within comfort temperatures throughout the 'unoccupied' period. The fluctuation in temperatures during the final three hours of the 32WVHC test was due to the laboratory doors being unintentionally left open, causing the ambient laboratory temperature to drop and the rig temperature fluctuate accordingly.

4.3.1.2.2 Chamber Temperatures

In Figure 4.14, each curve represented the average chamber temperature, averaged from the three chamber thermocouple readings taken throughout the twenty-four hour test. Similar temperature changes were observed during the 'occupied' and 'unoccupied' hours. The sudden drop in the 32WVHC test (purple line) was due to the laboratory doors being open for that period. The temperature curves followed an exponential like pattern as the system approached equilibrium during each 'occupied' phase.

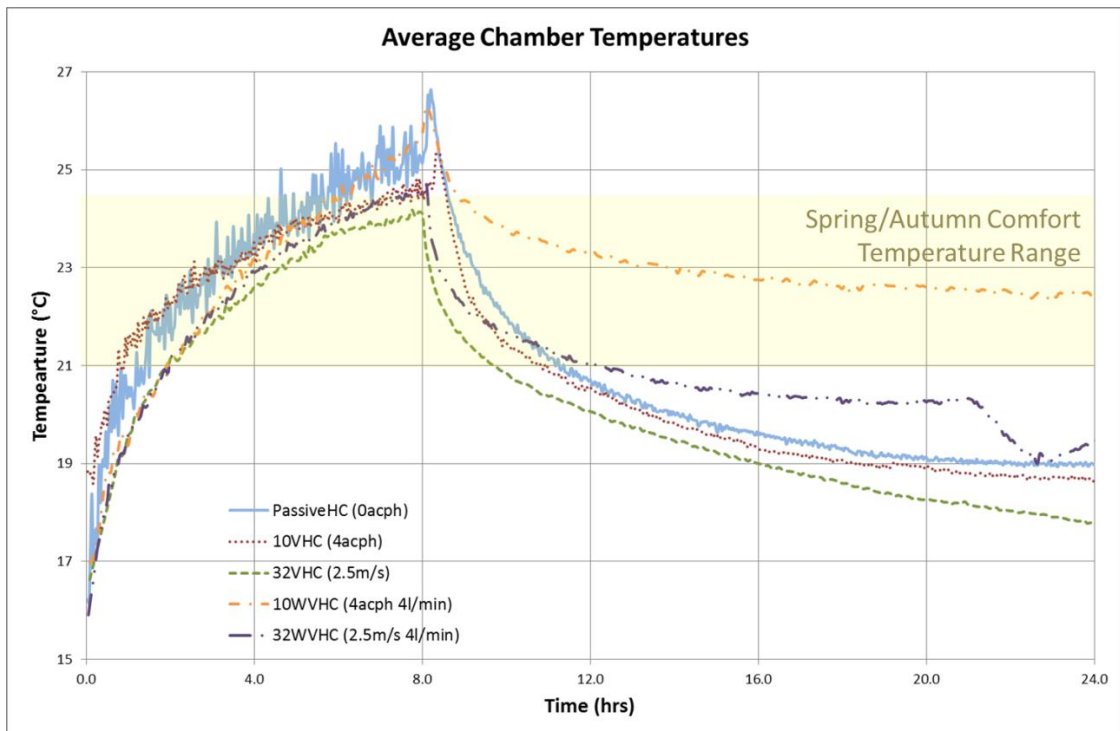


Figure 4.14 - Chamber Temperature Profiles for Constant Operation Systems

The peak temperature reached was in the PassiveHC system, attaining 26.5°C. The 10WVHC system had the next highest final occupied temperature at 26.3°C. The 10VHC system topped out at 25.3°C, the combined 32WVHC system kept room temperatures to 24.7°C whilst the system that achieved the lowest peak average room temperature of 24.2°C was achieved by the 32VHC system. In the PassiveHC, 10VHC and 10WVHC a temperature spike was witnessed immediately after the heaters were switched off. Increased ventilation systems (32WVHC and 32VHC) did not display the same phenomena. This temperature spike may be due to a localised effect akin to the urban heat island effect. At low ventilation rates the radiation stored in the concrete was released after the panel was turned off, causing a localised spike in temperature.

4.3.1.2.3 Slab Temperatures

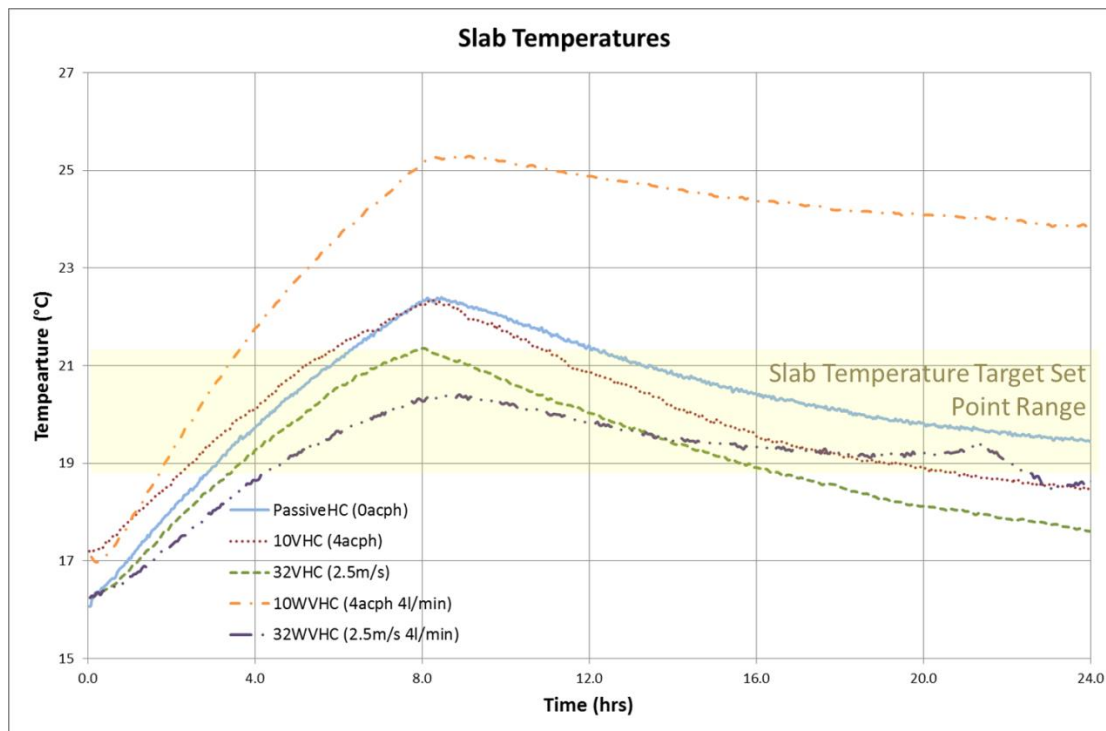


Figure 4.15 - Average Slab Temperature Profiles for constant operating conditions

Since industrial VHC systems determine their control strategies based on slab temperature a comparison temperature profile plot (Figure 4.15) was analysed for average slab temperatures during each system investigation. For the slab to sufficiently moderate chamber temperature it was required to remain between 18.8 and 21.3°C, for a previous twenty-four hour average of 15 to 20°C [34]. During this investigation only the 32VHC and 32WVHC held to this standard. At their peak PassiveHC and 10VHC reached 22.4°C and 22.3°C respectively under the intense thermal load. The 10WVHC slab temperature overheated due to the uncontrolled water cycle.

4.3.1.2.4 Temperature Observations

4.3.1.2.4.1 VHC vs PassiveHC

Firstly, by ventilating the hollow core slab a reduction of 1.5°C peak average room temperature was achieved over the passive slab system. Further benefits of ventilation were demonstrated by reduced final twenty-four hour temperature, which shows the benefits of night cooling.

Between the 10VHC and 32VHC results a reduction of 1.5°C at the end of the occupied heating period and a 1.6°C final temperature difference have been observed. From analysis of the respective slab temperatures in Figure 4.15 the 32VHC system maintained further

cooling capacity at the end of the 'occupied' period whilst the 10VHC slab had reached cooling capacity.

The increase in cooling capacity was due to the increased air flowrates. Due to the cool ambient air temperatures available the increase in fresh cool air into the room reduced room overheating. The increased flowrate similarly benefited the cooling of the slab. The greater volume of cool air passing through the slab offered greater heat capacity whilst also improving heat transfer. The increase of fan speed did however reduce the residence time of the air within the slab which restricted heat transfer between the slab and the air. This will result in the air delivery temperature into the room, out of the slab, remaining cooler in 32VHC systems.

4.3.1.2.4.2 VHC vs 10WVHC

In the early stages of the eight-hour 'occupied' heating period the WHC system achieved excellent cooling, limiting the temperature rise within the room. However, the thermal capacity of the water tank was soon saturated and caused the temperature of the slab to rise faster than the 10VHC system. This was evident from four-hours onwards, the 10WVHC line trended up whilst the VHC lines largely mitigate the heat through the addition of cooler air to the hollow core channels. In the 10WVHC tank system the removed heat was gradually recycled.

Based on the flowrate of 4l/min the total residence time was approximately twenty-six seconds, therefore the entire thirty-five litre volume of water has been once through the system within nine minutes. After which the heat removed during the first exchange was recycled into the slab, causing subsequent temperature rise. The 160W submersion pump also increased the thermal gain in the tank system.

In the VHC systems, where the hollow core slab represented the only thermal mass of the system, the temperature dropped rapidly and proceeded to fall some 6-8°C throughout the sixteen hour night period. In contrast the WVHC systems, with both slab and water acting as thermal mass were able to maintain a comfort temperature above 22°C throughout the cold night. For buildings where twenty-four-seven building occupation was required, a WVHC system may offer a suitable low energy system for continual temperature regulation.

4.3.1.2.4.3 VHC vs 10WVHC vs 32WVHC

The combined maximum fan with maximum pump 32WVHC system offered some interesting results. The shape of the room heating and cooling curves appeared to trend very similarly to

the 32VHC system initially. From the four-hour mark the increased heat recycling through the water pipe network caused the temperature in the 32WVHC system to increase more than the 32VHC. This additional heat storage was utilised as the water pumping maintained greater comfort temperatures through the night which, save for the severe drop in ambient temperature, would have delivered a final temperature of approximately 20.5°C.

From Figure 4.15 the 32WVHC system was capable of stabilising the slab temperature throughout the daily cycle. This was likely due to the heat recycling in action in the water tank based system. The water system showed a significant increase and application of thermal energy storage, transport and recycling. The 32WVHC system reached a more optimum usage of the water tank system than the 10WVHC due to the additional cooling delivered through the air network. Control systems and operation strategies for such applications require further investigation to fully release this potential.

4.3.1.2.5 Heat Transfer Rate

To compare pure thermal regulation performance, and eliminate ambient temperature differences, the heat transfer rate between slab and chamber was calculated for each time step using Equation 4.6 and Equation 4.7. The U-values were calculated from industry data sheets for the air and water flow characteristics for each system. The U-values for each system mode are displayed in Table 4.3.

Equation 4.6

$$\text{Heat Transfer Rate (W/m}^2\text{)} = U \text{ (W/m}^2\text{K)} \times \Delta T \text{ (K)}$$

Equation 4.7

$$\Delta T = \overline{T}_{slab} - \overline{T}_{room}$$

Table 4.3 - U-Value inputs for Figure 4.16

| System Mode | U-Value (W/m ² K) | Method | Ref. |
|-------------|---------------------------------|---|------------|
| PassiveHC | 6.21 | Found using an industry accredited U-value calculator for air activated thermal mass, with an average infiltration rate of 4acph. | [136] |
| 10VHC | 20.74 | Calculated from industry accredited modelling data | [136] |
| 32VHC | 71.84 | Found using an industry accredited U-value calculator for air activated thermal mass, with an average inlet velocity of 2.5m/s | [136] |
| 10WVHC | 50.19 | Calculated from industry accredited modelling data | [136, 137] |
| 32WVHC | 101.29 | Found using an industry accredited U-value calculator for air activated thermal mass, with an average inlet velocity of 2.5m/s, and water based slab calculations | [136, 137] |

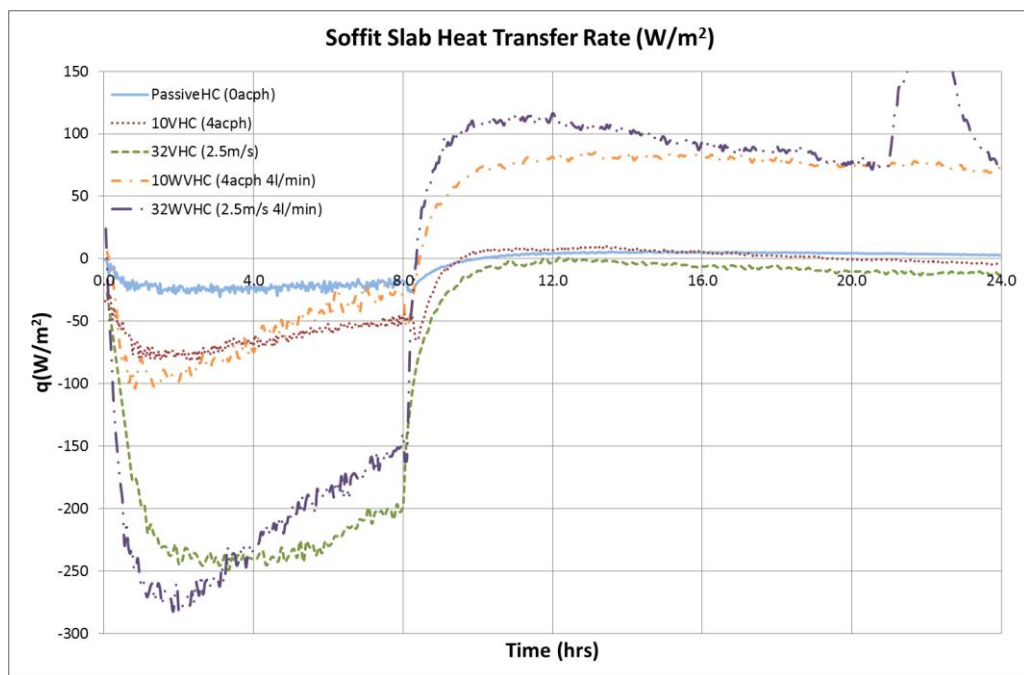


Figure 4.16 - Heat transfer rate between slab and chamber

The findings from Figure 4.16 confirm that the greatest amount of cooling was achieved by the 32WVHC system during the first three and half hours, peaking at 283W/m^2 of cooling. As the temperature difference between the water and room reduced, so did the cooling rate. After four hours the 32VHC system offered the greatest sustained level of cooling. Similarly, the contrast between 10VHC and 10WVHC reveals that for the first four hours the water enhanced system offers enhanced cooling, however after four hours the 10WVHC cooling rate declines and the 10VHC sustains a greater rate. During the 'unoccupied' period, the heating rate, evident in both WVHC systems, was generated by the circulating water, recycling the heat absorbed during the 'occupied' period.

The rate of cooling provided, during the 'occupied' period was dependent on the internal heat gain delivered. It will be interesting to observe the variation in cooling rate with respect to internal heat gain variations. This investigation will be explored in the next chapter.

4.3.1.2.6 Energy Performance

For each system energy consumption was quantified and the system COP calculated using Equation 4.3. This simple measure gives an energy efficiency ratio informing readers how much effective energy was removed for every unit of energy inputted. In the chart below COP was charted alongside nCOP, a performance quantifying figure that includes energy efficiency and thermal comfort. The nCOP was calculated as COP divided by the average deviation magnitude throughout the experiment from 21°C – the target room temperature (Equation 4.4 and Equation 4.5).

The National Calculation Methodology (NCM) [149] uses a seasonal system energy efficiency ratio (SSEER) as a metric for quantifying cooling system performance in non-domestic premises. The calculation method averages the EER for each season to offer a figure for annual energy efficiency. Depending on the system, the NCM notional efficiencies range from 1.67 to 2.25, depending on the system mode. The COP figures calculated herein were calculated under specific conditions and were not calibrated on an annual basis so direct comparison was unsuitable. The COP figures more closely represent an SSEER figure.

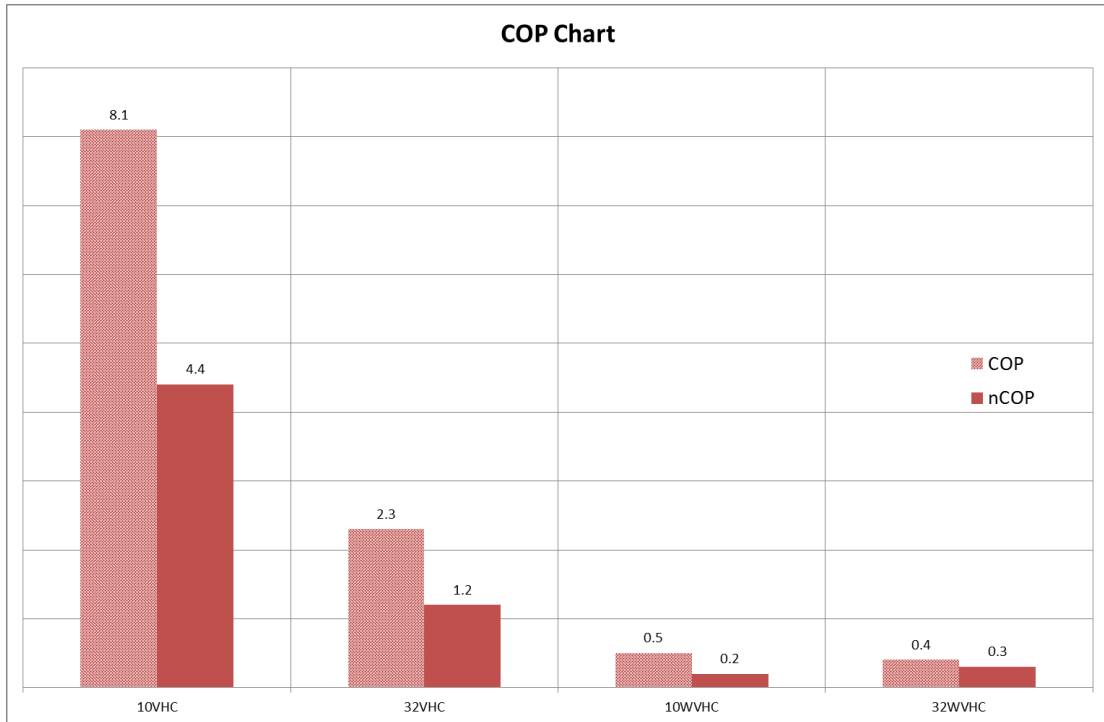


Figure 4.17 - COP Chart for Constant Operation Systems

Table 4.4 - Energy Performance Data for Enhancement Scenarios

| Test Type | Duration | Date | Dev21 | Energy Consumed | COP | nCOP |
|--------------|------------|------------|--------------------|-----------------|-----|------|
| | <i>hrs</i> | | $^{\circ}\text{C}$ | <i>kWh</i> | | |
| Passive Slab | 24 | 07/01/2013 | 1.88 | 0.00 | n/a | n/a |
| 10VHC | 24 | 12/12/2012 | 1.84 | 0.25 | 8.1 | 4.4 |
| 32VHC | 24 | 04/02/2013 | 1.94 | 0.79 | 2.3 | 1.2 |
| 10WVHC | 24 | 06/02/2013 | 2.23 | 4.09 | 0.5 | 0.2 |
| 32WVHC | 24 | 11/02/2013 | 1.26 | 4.72 | 0.4 | 0.3 |

The data in Figure 4.17 shows the greatest energy efficiency in the 10VHC system. The COP for the PassiveHC system could not be calculated since no power was consumed by the system; thus needing to divide by zero. The 32WVHC system maintained the best AvgDev21, deviating by only 1.26°C on average. However due to having the worst COP figures this minimal deviation was not sufficient to avoid it being the least efficient system. The remaining systems all generated an average deviation of 1.8-2.2°C from the 21°C set point. The nCOP figures for the first three systems charted were therefore roughly half that of their COP counter parts. All of the deviation averages demonstrate good performance since minimal average deviation from the target temperature was achieved.

The COP figures demonstrated in the VHC systems, showed excellent performance as anything above 1 was good and anything above 4 was considered excellent [133]. The

10WVHC and 32WVHC systems suffered from unnecessary work done by the pump hindering the hollow core systems cooling objective. This ongoing pumping did ensure excellent heat recycling during unoccupied night time hours. The pump cooling shows promise, however requires efficient use to ensure maximum cooling is achieved for minimal pumping energy use.

To develop the efficiency of the system and optimise the control strategy the COP must be increased whilst the average deviation decreased. To achieve this, the time the pump and fan are at maximum must be reduced to a minimum. This can be achieved simply by using temperature switches however in reality a basic fan load would also be needed to meet minimum fresh air regulations at all occupied times.

Simulation in the laboratory chamber most closely resembled autumn time operation in the Excel model. In the modelling the VHC system registered a COP of 8.4; in the testing a COP of 8.1 was recorded. Significant differences between the WHC and WVHC modelled results (1.4 & 7.9) and 10WVHC or 32WVHC results (0.5 & 0.4) occurred. The variation in water system operation from an open loop mains supply to a closed loop tank supply greatly affected resulting performance.

4.3.1.3 Summary of Findings

In summary the results from the constant conditions tests found that:

- The 32VHC system kept the room coolest during occupied heating hours (24°C).
- The 10WVHC system kept the room warmest during unoccupied night hours (22°C).
- The 32l water system's thermal capacity was rapidly saturated (in 30-50 minutes) and subsequently heated the slab.
- The 10VHC system achieved the greatest energy efficiency rating (discounting PassiveHC).
- A close match between simulated (from the Excel model autumn season) and tested COP for a VHC and 10VHC system was noted, 8.4 and 8.1 respectively.
- 10WVHC and 32WVHC systems energy efficiency and cooling performance suffered from excessive and untimely pump use.
- The active hollow core technologies operating in constant mode reduced the peak room temperature by 1.5-3°C.

The closed loop water tank system operational in the 10&32WVHC systems offered cooling initially, but due to the limited thermal mass in the thirty-two litre water tank, once the water tank temperature had surpassed comfort room temperature, continual pumping of the water loop caused the slab to be heated rather than cooled.

The water tank had a storage capacity one tenth of that of the hollow core prototype. The flow of the water, its close proximity to the slab soffit and the 160W pump in the water tank caused a rapid rise in water tank temperature. The water tank enabled shock cooling of the hollow core but was insufficient for sustained cooling periods greater than thirty minutes. With this system design the findings suggest that the most efficient use of the water cooling capacity would be to flush the contained water in the slab, taking about twenty-six seconds, intermittently.

Further improvements to the water system were possible; relocating the water tank, increasing water volume in tank or increasing tank thermal capacity with the addition of PCM. Greater cooling benefit was also possible from an open loop system with mains water, rather than a closed water loop with limited cooling capacity. Smart operation of both a closed loop and open loop system was ideal for industrial applications to offer dynamic heat storage, energy recycling and cooling. Cooling enhancement with additional thermal mass in the water tank and an open loop system was taken forward for subsequent systems.

When combined with increased fan duty (32WVHC) the overheating of the water system was almost offset. Further increase in the ratio between fan duty and pumping duty will lead toward maximising the benefits of the water cooling, whilst avoiding unwanted overheating. Since it was not possible to reduce water flowrate by dimming the pump power and the fan power was already on maximum, an increased ratio of air to water power was proposed by using intermittent pump control. System performance with variable control of the water system was investigated in the following section.

Findings suggest constant operation conditions throughout the twenty-four hour period were not the optimum way of operating these energy storage systems. These tests provide an initial bench mark of performance. Subsequent variable operating conditions were investigated based on temperature set point control.

Based on the energy efficiency and cooling capabilities of the constant conditions systems an Optimum Operation Method (OOM) is suggested utilising set point control. It is anticipated that a base operation of 10VHC accompanied by intermittent set point controlled 32VHC and

10WVHC loads to rapidly exchange the warm room air and shock cool the slab respectively offers the OOM for the system.

Following these findings variable operating conditions were tested to test the OOM hypothesis and determine suitable set point control to maximise the water, air and concrete system components. No physical water system enhancement was carried out, only additional temperature set point control, to determine the benefits of control and enable suitable comparison with the constant operating conditions investigation.

4.3.2 Variable Operating Conditions Twenty-four hour Test

Early research into air activated thermal mass in UK offices concluded that considerable performance efficiencies could be achieved through efficient control [39]. In line with this, following the constant conditions investigation it was clear that improvements to energy efficiency and comfort could be obtained through improved system control. The fan requires less power than the water pump, however the water system, until saturated, offers faster cooling of the slab. Taking this into account temperature set points for WVHC system control were sought that would optimise energy-efficient cooling.

Building upon the findings from the constant operation of the WVHC prototype performance it was deemed that the best use of the water tank cooling capacity was in bursts and the bulk of the slab activated cooling duty be carried out by the air stream. For this reason this investigation was carried out to understand which set points and variable operating conditions of the air network and water network would achieve optimum stabilisation of occupied room temperatures and increased energy efficiency.

4.3.2.1 Testing Methodology

Using the same twenty-four hour methodology as the constant operating conditions investigation, the heater was on for eight hours and then remained off for sixteen hours to allow the system to discharge (figure 4.8). Different control strategies were employed to help the enhanced thermal mass system deliver the required cooling load throughout the twenty-four hour periods. In each case temperature set-point control was employed, either triggered automatically or manually. To enable the variable operation, temperature switches were fitted to the fan and pump systems. Respective temperature set-points were investigated along with different configurations of water and air systems. Five system configurations and control strategies were investigated with performance reviewed against the 10VHC benchmark results from the previous investigation to observe the enhancement offered through set-point control.

Table 4.5 - Variable Operating Test Conditions

| Scenario | Label | Fan Operating Conditions | Pump Operating Conditions | Cooling provided by: | System operating description |
|----------|-------------------|---|---|--|--|
| 1) | VHCa21 | 21°C (on/off) set-point control (0 or 2.5m/s) | Constant Off | maximum forced ventilation and soffit heat exchange | fan delivering air at 0 or 2.5 m/s |
| 2) | 10WVHC pman | Fixed 10W (delivering 4acph - 0.22m/s) | Manually operated for 5mins every 30mins once Avg. Room temperature exceeded 21°C | minimum forced ventilation, conduction from cooling water and soffit heat exchange | fan delivering minimum air change per hour and pump providing water at 0 or 4l/min |
| 3) | 32WVHC a21pman | 21°C (on/off) set-point control (0 or 2.5m/s) | Manually operated for 5mins every 30-50mins when Avg. Room temperature exceeds 22.5°C | maximum forced ventilation, conduction from cooling water and soffit heat exchange | fan delivering air at 0 or 2.5 m/s and pump providing water at 0 or 4l/min |
| 4) | 32WVHC a20p22.5 | 20°C (on/off) set-point control (0 or 2.5m/s) | 22.5°C (on/off) set-point control (0 or 4l/min) | maximum forced ventilation, conduction from cooling water and soffit heat exchange | fan delivering air at 0 or 2.5 m/s and pump providing water at 0 or 4l/min |
| 5) | 32WVHC a20.5p21.5 | 20.5°C (on/off) set-point control (0 or 2.5m/s) | 21.5°C (on/off) set-point control (0 or 4l/min) | maximum forced ventilation, conduction from cooling water and soffit heat exchange | fan delivering air at 0 or 2.5 m/s and pump providing water at 0 or 4l/min |

From scenario to scenario the control strategies were developed in an effort to maintain comfort temperature throughout the occupied periods. This process of development was discussed in the section following, 4.3.2.2 Results and Discussion.

4.3.2.2 Results and Discussion

4.3.2.2.1 Scenario Profiles

Scenario (1), VHCa21, was based on a VHC system with an automatic 21°C temperature set point on the fan. When the chamber temperature exceeded 21°C maximum fan power was activated delivering cooling air through the slab and into the chamber. From the top right chart in Figure 4.18 the fan was off initially, then was activated once 1.5 hours into the test. Having successfully cooled the room below the 21°C set point the fan switched off for approximately twenty minutes. The chamber temperature then rapidly surpassed the temperature set point and the fan was initiated again for the duration of the occupied period. The fan was switched off thirty minutes after the 'occupied' period finished after temperatures had dropped.

Scenario (2), 10WVHCpman (Figure 4.19), sought to reduce the chamber temperature deviation and utilise the water tank cooling capacity throughout the day. Throughout this twenty-four hour test the fan was specified to a constant 10W base load delivering four acph. Additional cooling was supplied by manual operation of the pump. Throughout the 'occupied' period the user initiated the pump for five to six minutes when average chamber temperature had surpassed 21°C. The pump was then switched off for twenty-five to thirty minutes, allowing the chamber temperature to rise again. This process was repeated throughout the 'occupied' period until the water tank temperature offered no cooling benefit, at which point no further pumping was carried out. No pumping was carried out during 'unoccupied' periods.

For Scenario (3), 32WVHCa21pman (Figure 4.20), further learning from Scenario (2) was utilised in the manual strategy. During this test, in an effort to avoid exploiting the water cooling benefit early in the 'occupied' day and leaving no capacity when cooling was most required in the late afternoon, increased user set-points were employed. With the fan initiating at 21°C the pump was activated in the final three and a half hours when average chamber temperature encroached on 23°C. Water pumping was maintained until chamber temperatures reduced below 22.5°C. This strategy enabled extended water cooled periods when cooling was most required.

Following two manually operated scenarios two fully automated scenarios were investigated. For Scenario (4), 32WVHCa20p22.5 (Figure 4.21), water pump set point was maintained at 22.5°C whilst the fan set point was reduced to 20°C in an effort to ensure water cooling

capacity was not overloaded and pump power reduced during the twenty-four hour test. Both the fan and pump were switched off after the 'occupied' period.

Scenario (5), 32WVHCa20.5p21.5 (Figure 4.22), explored the effect of a narrowed comfort band, managed through automated set-point control. The aim was for the automated system to keep chamber temperature more closely controlled around the desired 21°C temperature. For this reason the respective temperature set points for the fan and pump were 20.5 and 21.5°C. As before the air delivery was limited to 0 or 2.5m/s. No basic mechanical ventilation was supplied when the chamber temperature was below 20.5°C.

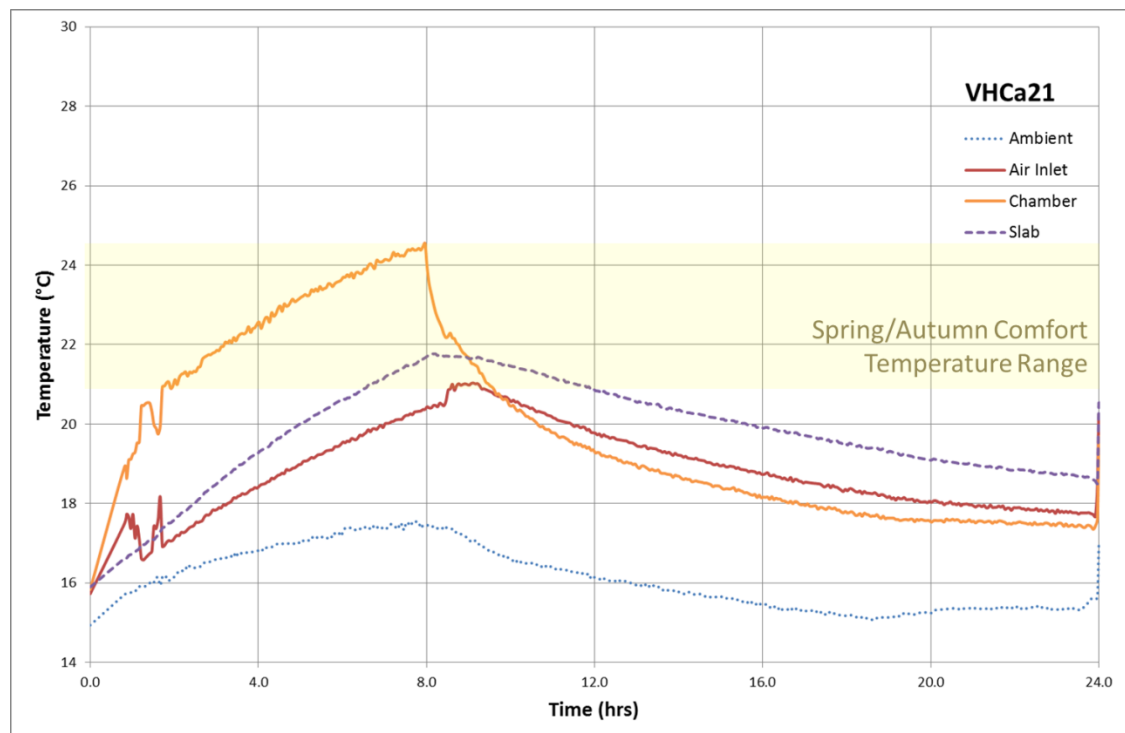


Figure 4.18 - Temperature Profiles for Variable Operation Conditions

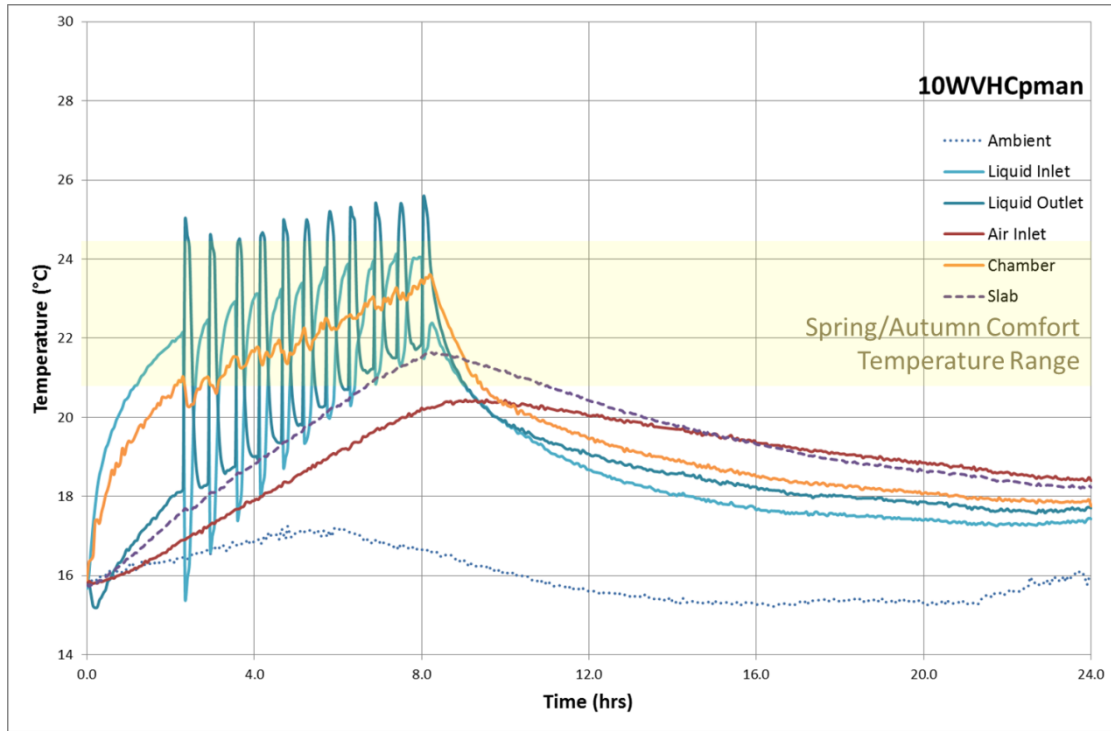


Figure 4.19 - 10WVHCpman Temperature Profiles

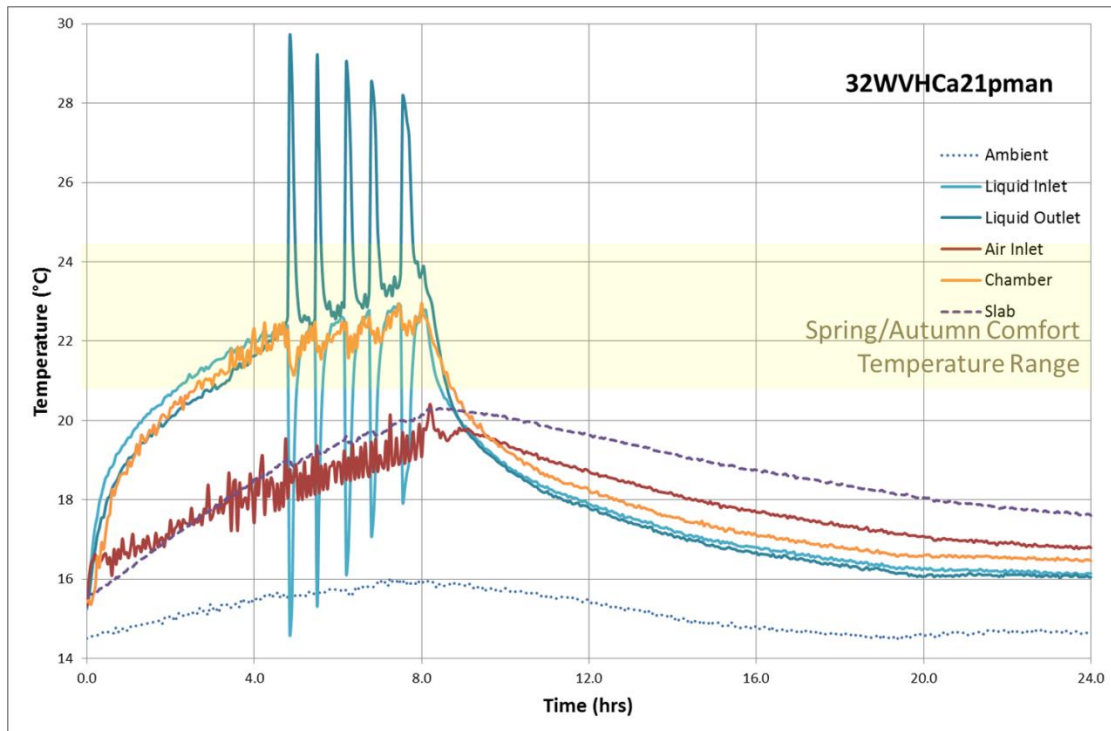


Figure 4.20 - 32WVHCa21pman Temperature Profiles

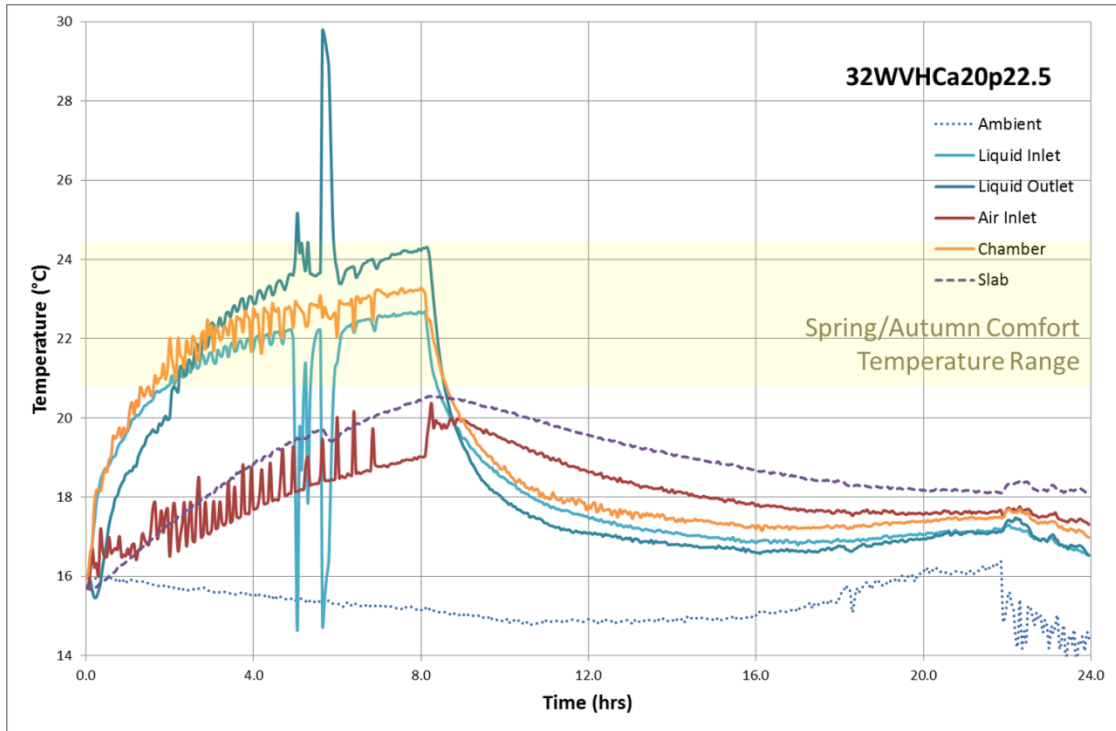


Figure 4.21 - 32WVHCa20p22.5 Temperature Profiles

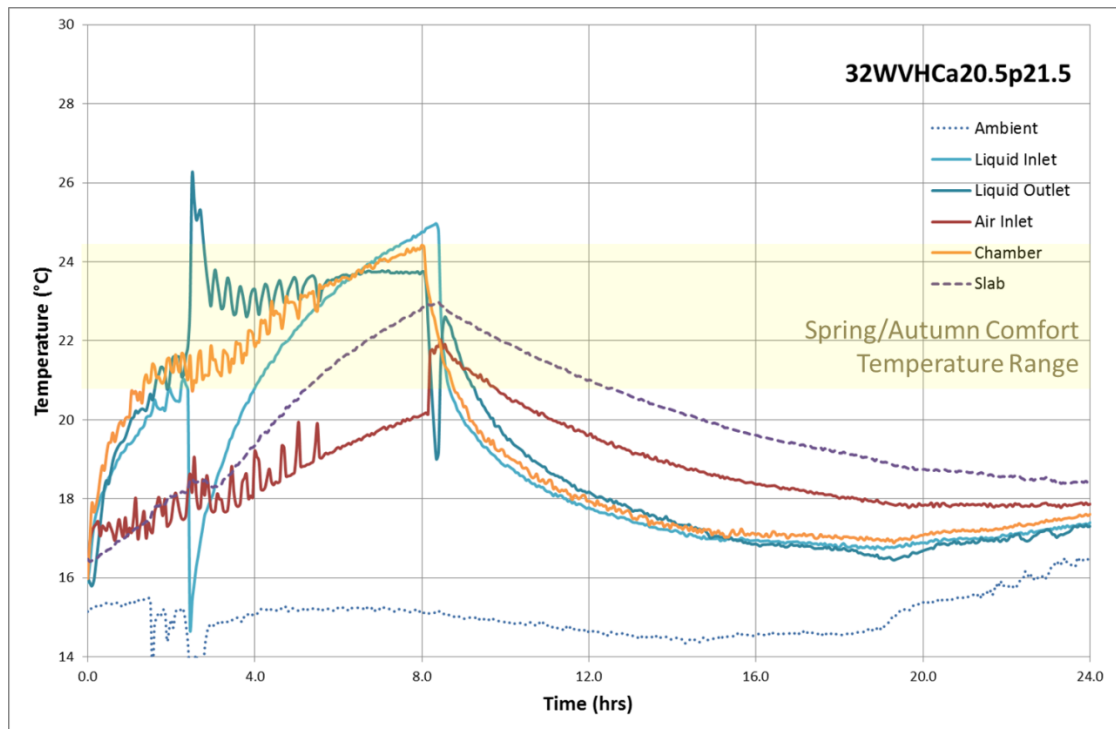


Figure 4.22 - 32WVHCa20.5p21.5 Temperature Profiles

Each of the variable condition scenarios maintained average chamber temperatures within the spring/autumn comfort temperature range for the majority of the ‘occupied’ time. The first (VHCa21) and final (32WVHCa20.5p21.5) cases peaked marginally above the maximum transition period temperature. In both cases the active cooling (air and air and water

respectively) had reached capacity early in the day. The thermal mass inertia avoided the chamber overheating. The latter 32WVHCa20.5p21.5 demonstrates that a wider band of control is required when seeking to moderate a large thermal mass. The temperature spikes in the WVHC systems demonstrate when the water was pumped around, causing a surge in temperature.

4.3.2.2.2 Chamber Temperatures

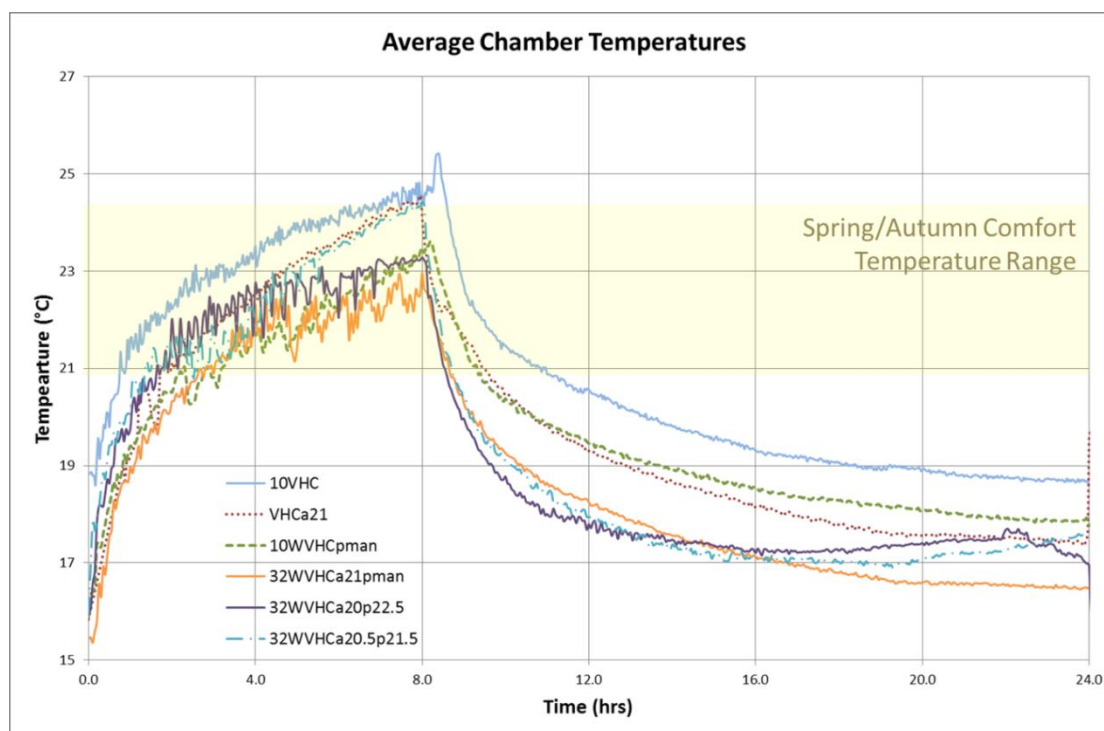


Figure 4.23 - Average Chamber Temperatures for Variable Operating Condition Tests

Figure 4.23 charts the average chamber temperatures during the twenty-four hour tests. 10VHC performance was charted to offer reference profile with final 'occupied' temperature of 25.4°C. The VHCa21 and 32WVHCa20.5p21.5 systems achieved the worst performance of the variable condition strategies both registering final 'occupied' temperatures of 24.4°C. 10WVHCpman maintained the lowest average chamber temperature until the final three hours, finally recording a peak chamber temperature of 23.6°C. The best performing automated system was achieved by the 32WVHCa20p22.5 system recording a final 'occupied' temperature of 23.3°C. User operation surpassed automated set-point control by 0.8°C at the end of eight hours of heating, registering a temperature of 22.5°C.

The performance of these set-point controlled systems demonstrates that with suitable control, efficiently utilising the contained water can maintain comfort temperatures even under extreme occupied heat loads. 32WVHCa20p22.5 and 32WVHCa21pman maximised the

use of air cooling available, only using water cooling, driven by the pump, for small durations when required. The poor performance of the 32WVHCa20.5p21.5 demonstrated that the pump activation set-point was too low for the conditions (ambient temperatures and internal heat gain) tested under. Further investigation identifying the link between optimum set-point temperatures, ambient temperatures and cooling demand would be of use commercially; aiding the design of an adaptable control strategy that could achieve optimum temperature control efficiency year round.

4.3.2.2.3 Slab Temperatures

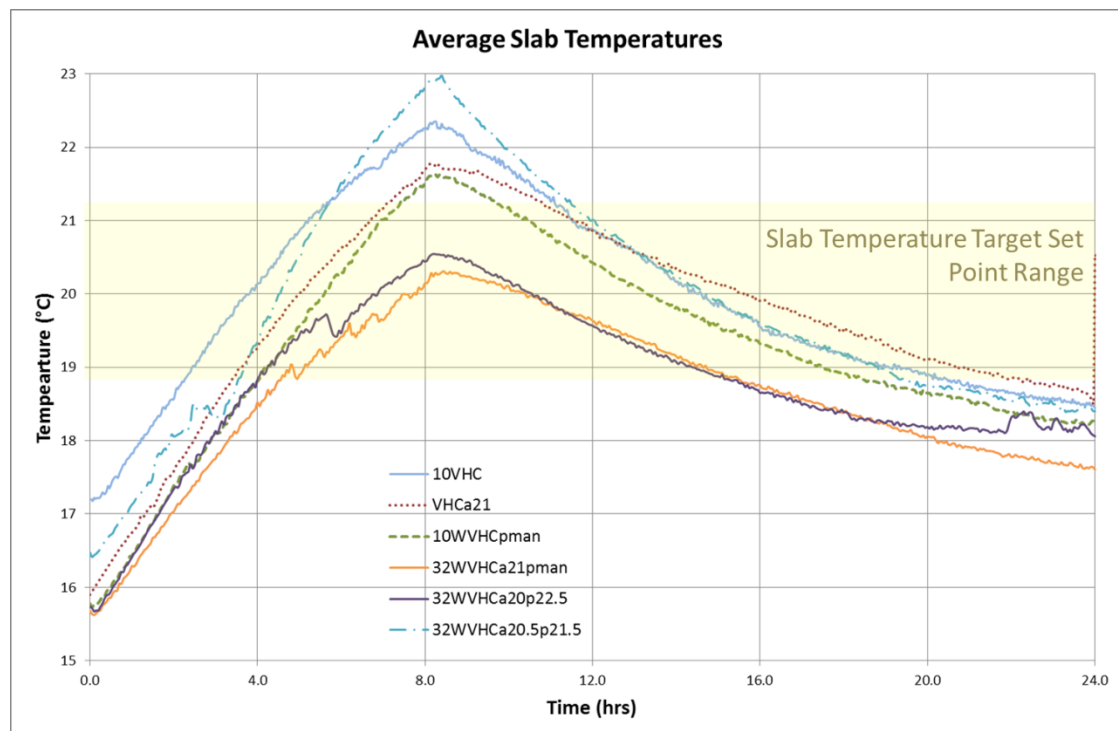


Figure 4.24 - Average Slab Temperatures for the Variable Operating Conditions Scenarios

Figure 4.24 demonstrated that only the 32WVHCa21pman and 32WVHCa20p22.5 systems maintained the average slab temperatures below the 21.3°C threshold [34]. Evidence of slab cooling from the water system intervention was clear in the final three systems, 32WVHCa21man, 32WVHCa20p22.5 and 32WVHCa20.5p21.5. In the final scenario, reducing the set-point below 22°C had an adverse effect during the final hours of ‘occupied’ operation.

4.3.2.2.4 Heat Transfer Rate

Following the same method as laid out in section 4.3.1.2.5, the overall heat transfer rate between the slab and the chamber was calculated. Since the operation of the air and water streams varied during the course of each twenty-four hour test it was not suitable for a single U-value to be used throughout the analysis. Overall U-values were calculated for each time

period as the sum of the respective U-values at the given air and water flowrates in Table 4.6. The figures were found from industry informed calculators. The results for each scenario were plotted in Figure 4.25 and Figure 4.26.

Table 4.6 - U-value components [136, 137]

| Air Stream | Water Stream |
|-----------------------------------|----------------------------------|
| 0 m/s (6.21W/m ² K) | 0l/min (0W/m ² K) |
| 4 acph (20.74W/m ² K) | 4l/min (29.45W/m ² K) |
| 2.5 m/s (71.84W/m ² K) | |

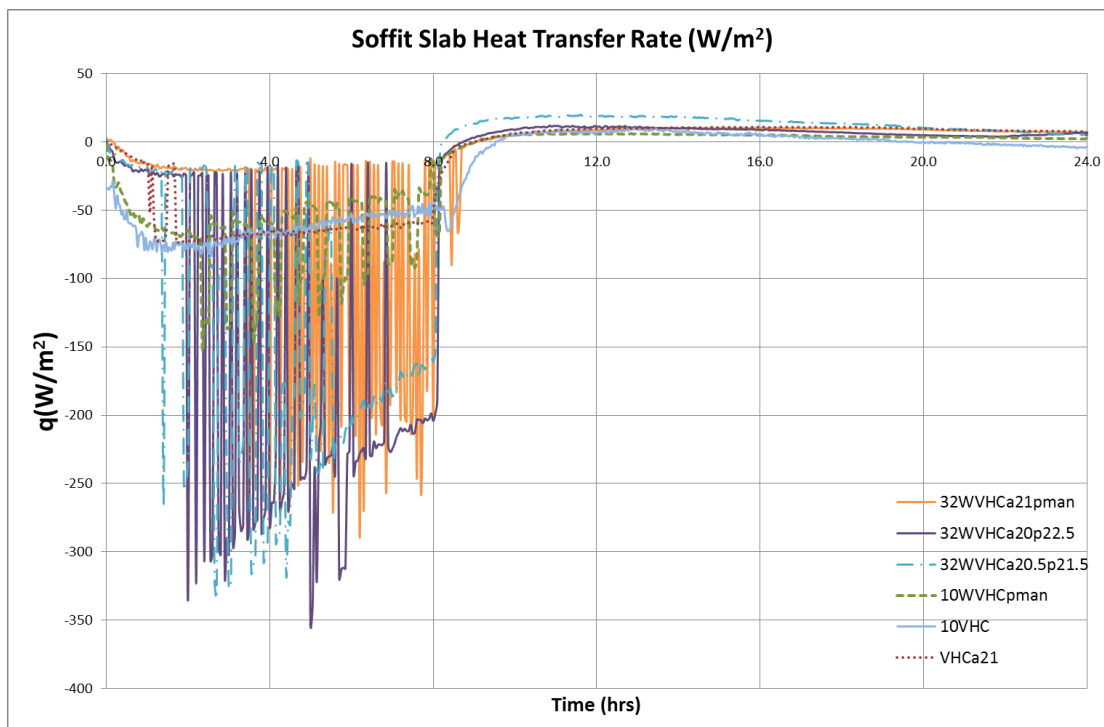


Figure 4.25 - 24hr Variable Conditions Heat Transfer Rate

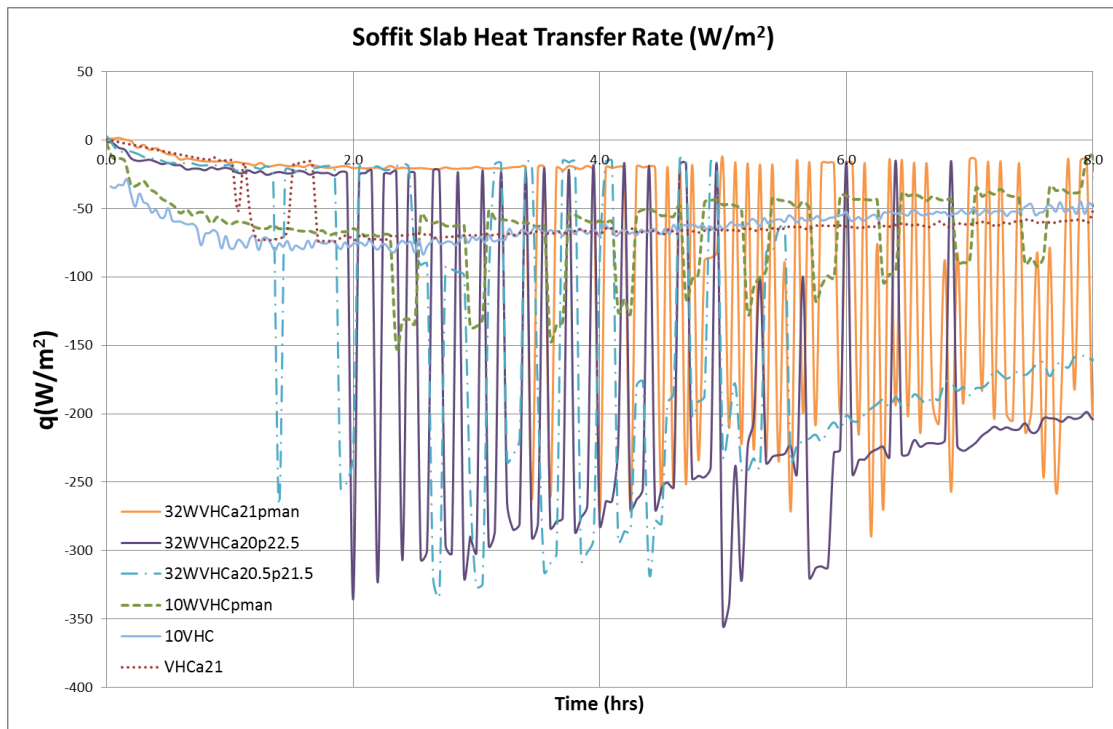


Figure 4.26 - 8hr Variable Conditions Heat Transfer Rate

Figure 4.25 portrays the varying heat transfer rate occurring during the variable conditions twenty-four hour tests. The fluctuations occur due to the switching on and off of the ventilation and water systems in the slab. To aid analysis, figure 4.26 presents the ‘occupied’ hours only. Passive cooling, before any active system was engaged peaks at 20 W/m^2 . A base load fan of 10W delivers between 50 and 80 W/m^2 of cooling. When the base load fan was coupled with the water system (10WVHCpman) an additional 50 to 75 W/m^2 of cooling was delivered to the chamber. The greatest cooling occurred during 32WVHC based scenarios. Depending on water tank temperature the cooling achieved when operating the fan and pump driven systems ranged from 160 W/m^2 to 350 W/m^2 during the eight ‘occupied’ hours.

Since the active thermal mass system was responsive to the internal heat gain, investigation into heat transfer rate variation with respect to cooling demand should be conducted.

4.3.2.2.5 Energy Performance

COP and nCOP figures were calculated for the twenty-four hour test period, following the method outlined previously in the fixed system operation period (section 4.3.1.2.6).

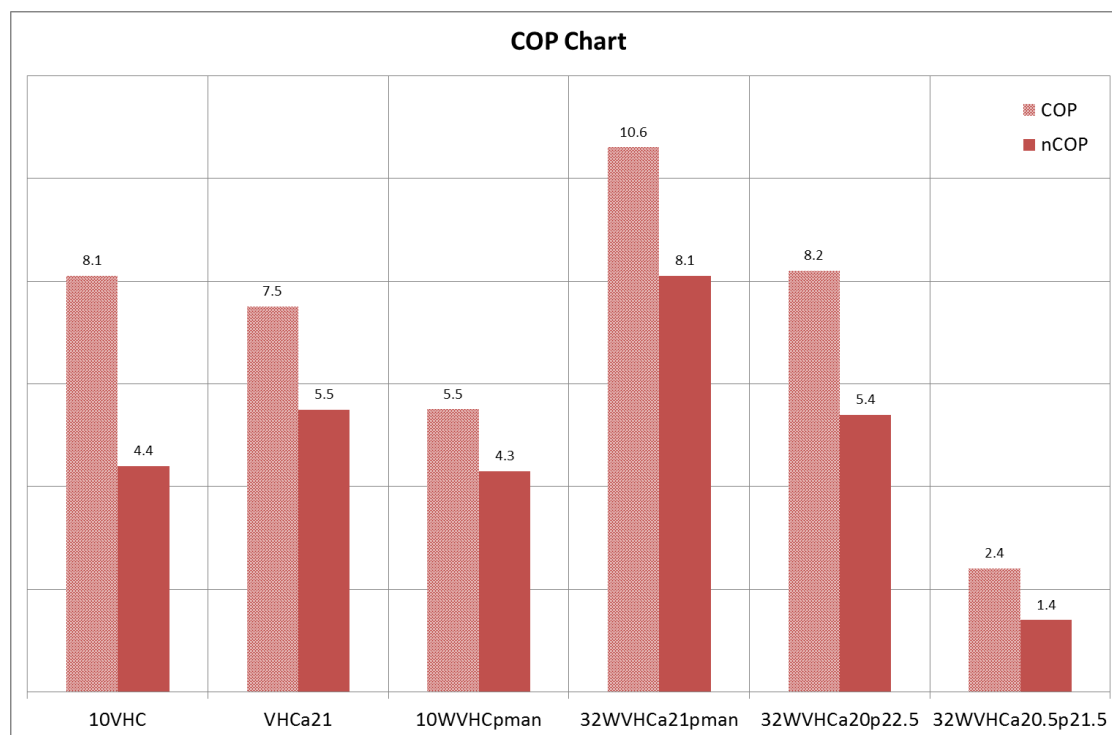


Figure 4.27 - COP Chart for Variable Operating Conditions

Table 4.7 - Variable Condition Energy Performance Data

| Test Type | Duration | Date | Dev21 | Energy Consumed | COP | nCOP |
|------------------|--------------|------------|-----------|-----------------|------|------|
| | <i>Hours</i> | | <i>°C</i> | <i>kWh</i> | | |
| 10VHC | 24 | 12/12/2012 | 1.84 | 0.25 | 8.1 | 4.4 |
| VHCa21 | 24 | 14/02/2013 | 1.38 | 0.27 | 7.5 | 5.5 |
| 10WVHCpman | 24 | 19/02/2013 | 1.28 | 0.38 | 5.5 | 4.3 |
| 32WVHCa21pman | 24 | 26/02/2013 | 1.32 | 0.20 | 10.6 | 8.1 |
| 32WVHCa20p22.5 | 24 | 05/03/2013 | 1.53 | 0.26 | 8.2 | 5.4 |
| 32WVHCa20.5p21.5 | 24 | 12/03/2013 | 1.65 | 0.88 | 2.4 | 1.4 |

All the systems maintained operating chamber temperature within 1.28-1.65°C of the targeted 21°C. This was an improvement on the fixed systems, demonstrating the importance of control. The 10WVHCpman operating method offered the closest match to the 21°C target temperature. The 32WVHCa21pman method used the least amount of energy whilst maintaining comfort temperature therefore it produced the greatest COP figure of all systems tested. A 20% energy reduction was observed between the 10VHC baseline and the best operating 32WVHCa21pman system.

4.3.2.2.6 VHCa21 vs 10VHC & 32VHC Discussion

The final chamber temperature in the VHCa21 test reached 24.5°C. In comparison with the 10VHC & 32VHC constant operation the final chamber temperature was 25.3 & 24.2°C

respectively. Comfort has been minimally affected. Comparison between COP figures demonstrated the significant energy savings achieved against the 32VHC system. Due to the VHCa21 systems reduced temperature deviation, the temperature dependant system improved the nCOP figure against both the 10VHC and 32VHC systems. The VHCa21 offered 32VHC cooling capabilities with energy consumption on a level with the 10VHC constant operation system.

4.3.2.2.7 WVHC Variable Systems vs WVHC Constant Systems and 32VHC

Of the WVHC variable systems, the 32WVHCa21pman control strategy kept chamber temperatures coolest at 22.5°C. The automated 32WVHCa20p22.5 system ensured temperatures stayed below 23.3°C. Each system maximised the cooling capacity when required to bring the greatest benefit to the slab and chamber respectively. In contrast even the well performing 32WVHC dragged chamber temperatures to 24.7°C. This 2.2°C improvement was observed whilst reducing energy usage by 95.8% against the 32WVHC system.

The best performing of the constant condition trials was the 32VHC system. Of the systems trialled this most closely represented typical industrial ventilated hollow core systems. Against this important benchmark the 32WVHCa21pman saved 1.6°C from the final chamber temperature coupled with 75% energy savings.

4.3.2.2.8 Temperature Set-points

Throughout the trials different temperature set-points were investigated. Most conclusively contrast between 32WVHCa20p22.5 and 32WVHCa20.5p21.5 revealed that the narrow set-point band was ineffective at providing energy efficient cooling operation of the hollow core prototype, under test conditions. The wider band provided both better temperature control, whilst also using less than one third of the energy. In the manual operated modes, by following the same strategy, water cooling capacity was utilised most effectively during the final heated hours.

4.3.2.3 Summary of Findings

The findings from the variable conditions investigation revealed that chamber comfort can be improved whilst greatly improving on energy savings. Using a pump temperature set-point of 22.5°C, effective use of the water tank cooling capacity, without overloading the water system was enabled. This mode of operation improved the COP figures for all water incorporated systems.

Variable fan with a temperature set-point of 21°C, VHCa21, maintained chamber temperatures equivalent to a 32VHC system whilst using a similar amount of energy as a 10VHC system. Since the fan was active through most of the heated period this benefit has been largely achieved through night time switch off.

Variable systems were capable of saving energy whilst improving comfort. The best performing variable conditions system saved 2.2°C against the best performing constant condition system, whilst using 95.8% less energy. Against the PassiveHC the 32WVHCa21pman system achieved 3.6°C maximum temperature reduction.

Further developments are possible both in terms of operational optimisation, and the water and air system design. Traditional VHC systems incorporate an AHU capable of preheating or cooling inlet air that would offer further temperature control benefit. Larger, repositioned water tanks feeding a closed loop system coupled with an on demand open loop water system fed from mains water would provide improved cooling capabilities. Alternatively the thermal capacity of the water tank and hollow core system could be improved through the addition of PCM, explored further in *Chapter 6 and 7*.

4.4 VHC Model Validation

As introduced in *Chapter 3*, a numerical model simulating VHC, WHC and WVHC performance was developed. Performance was reviewed based on temperature control and system energy efficiency through temperature profile graphs and COP figures in particular. Following the laboratory investigation conducted in section 4.3, experimental validation of the model was sought to determine the validity of the modelled results.

4.4.1 Validation Method

The results from the constant condition 10VHC twenty-four hour experimental investigation was chosen as the validation scenario. This scenario was chosen due to the simplicity of operation and the limitations of the numerical model. Further, numerical model had been developed for typical system operation of 4acph, such as the 10VHC scenario. WVHC systems were not reviewed due to the laboratory tests operating a closed loop system and the model an open loop configuration.

The boundary conditions from the 10VHC laboratory investigation were specified in the model as per Table 4.8. The ambient data from the 10VHC test was formatted into thirty minute readings and input in the model. A twenty-four hour simulation with time steps of 46.2 seconds was initiated. Temperature profiles, energy consumption and COP figures were generated and compared.

Table 4.8 - Validation Boundary Conditions

| Parameter | Laboratory Boundary Conditions | Model Boundary Conditions |
|--|---|-------------------------------------|
| Chamber geometry (h × w × l) | 1.8 × 1.2 × 2.0 m | 1.8 × 1.2 × 2.0 m |
| Slab geometry (d × w × l) | 0.375 × 1.2 × 1.5 m | 0.375 × 1.2 × 1.5 m |
| Ambient temperature profile | See Figure 4.10 | Matched to lab. profile |
| Heating ('occupancy') schedule | On for 8hrs, Off for 16hrs | On for 8hrs, Off for 16hrs |
| Total Heat Gain (based on chamber area) | 187.5 W/m ² (from heater) – 68.2 W/m ² (heat lost) | 286.3W (119.3 W/m ²) |
| Ventilation schedule | 24hrs @4acph | 24hrs @4acph |
| System configuration | VHC | Fan Only, Slab |
| Test period | 24 hrs | 24 hrs |
| Initial slab and chamber temperatures | 17.2°C (slab) and 18.8°C (chamber) | 17.2°C (slab) and 18.8°C (chamber) |

4.4.2 Validation Initial Results

Figure 4.28 plots the modelled (M) and laboratory data for a twenty-four hour period; made up of eight hours with heating and sixteen hours without. From figure 4.28, initially an acceptable fit was observed between the modelled and laboratory data for both the slab and air inlet temperatures (4.5% and 7.8% variation during ‘occupied’ hours). Significant (48.7%) difference was observed between chamber experimental and modelled temperatures. A poor fit was observed in overall COP (12.6 (M) and 8.1), but a good fit for energy consumption (0.23 kWh/d (M) and 0.25 kWh/d).

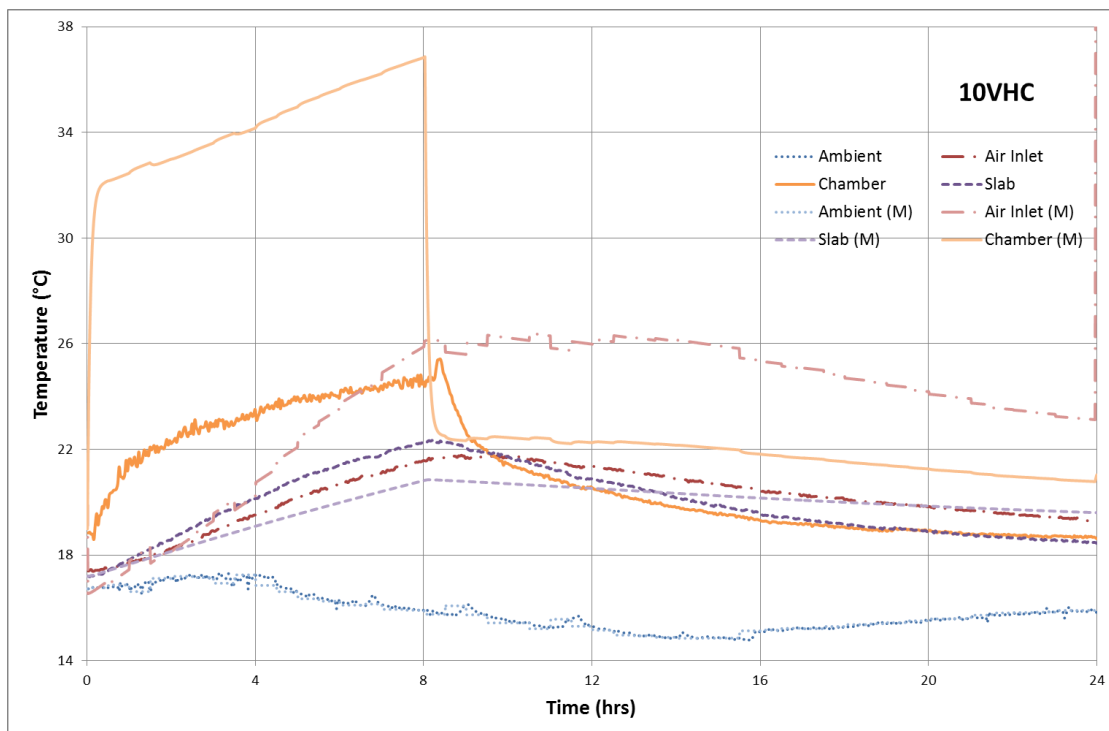


Figure 4.28 - 10VHC Initial Comparison Temperature Profiles

From analysis of figure 4.28 an investigation into the equations modelling heat transfer between the slab and room was conducted to identify reasons for the poor chamber temperature fit and improve the model. It revealed the slab to chamber interaction had not been effectively modelled. An early modelling assumption had discounted the impact conductive heat transfer on slab and chamber air temperatures. The model was updated to include a conductive heat transfer component:

Equation 4.8

$$q_{cond} = hA[T_{room,0} - T_{s,1}]$$

Where A is the soffit area and h the heat transfer coefficient determined from industry standards, 6.4 W/m²K at 4acph [136]. With this component included 10VHC simulations, as

per the boundary conditions outlined in Table 4.8, were re-run and the results observed in Figure 4.29.

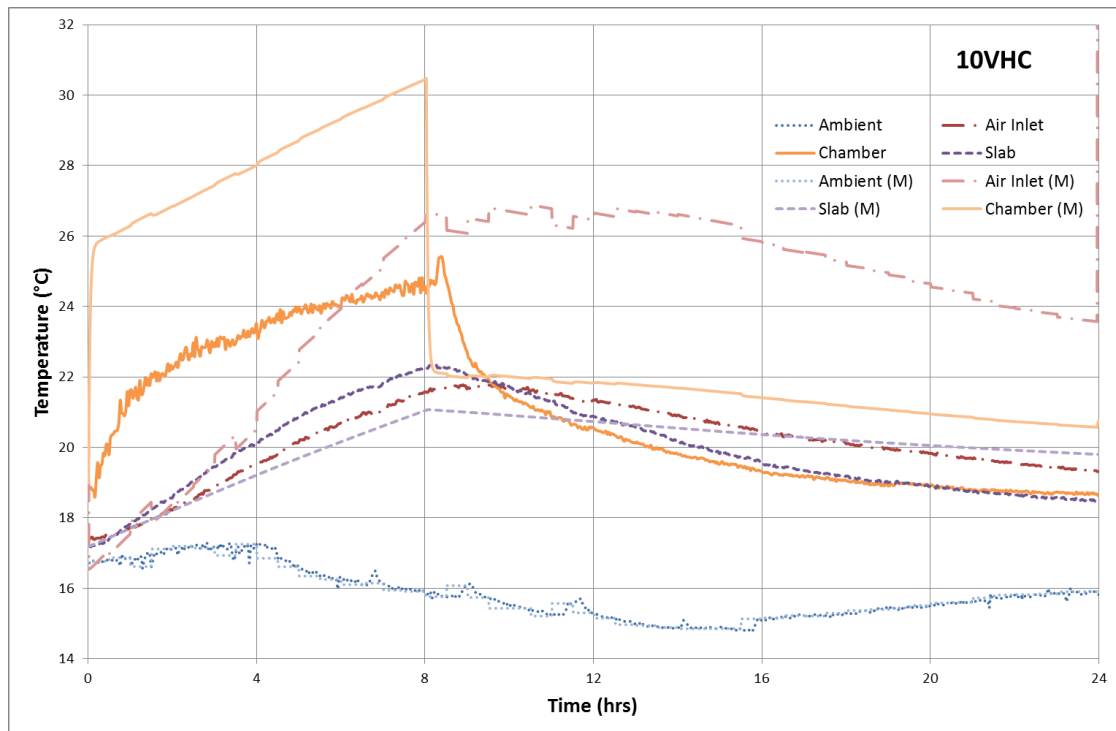


Figure 4.29 - 10VHC Scenario Validation Updated Temperature Profiles

The temperature profiles observed in figure 4.29 conveyed a similar fit for air inlet temperature (9.1% during ‘occupied’ period) and a tighter, but still poor, fit (22.0%) between modelled and laboratory chamber temperatures. The slab temperature fit improved (down to 3.9%). The fit between energy consumption remained good, following the conduction update, 0.25 and 0.23 kWh/d for laboratory and modelled scenarios respectively. The COP fit worsened, 8.1 compared with 13.5 in the laboratory and modelled scenarios respectively.

Linear optimisation was conducted to suitably fit the model to the laboratory data. The overall heat transfer coefficient, governing the internal slab heat transfer characterisation, (U), as well as the conduction heat transfer coefficient, (h), governing slab to chamber interaction were adjusted. A minimum of the combined percentage differences (ambient, air inlet, chamber and slab), during the ‘occupied’ period, was targeted by adjusting the U -value. Subsequently the combined percentage difference, during the ‘occupied’ period, was further minimised through adjustment of h . Table 4.9 displays the optimum heat transfer coefficients, the ‘occupied’ and twenty-four hour percentage differences.

Table 4.9 - Optimum Coefficients and Percentage differences of data

| Optimum Coefficients | | 'occupied' 8hr | | Total 24hr | |
|----------------------|-------|-----------------|-----|-----------------|------|
| U | 10.23 | Ambient %Diff | 0.7 | Ambient %Diff | 0.6 |
| h | 25.30 | Inlet Air %Diff | 0.4 | Inlet Air %Diff | 2.8 |
| | | Chamber %Diff | 1.6 | Chamber %Diff | 5.4 |
| | | Slab %Diff | 3.4 | Slab %Diff | 4.9 |
| | | Sum of %Diff | 6.0 | Sum of %Diff | 13.6 |

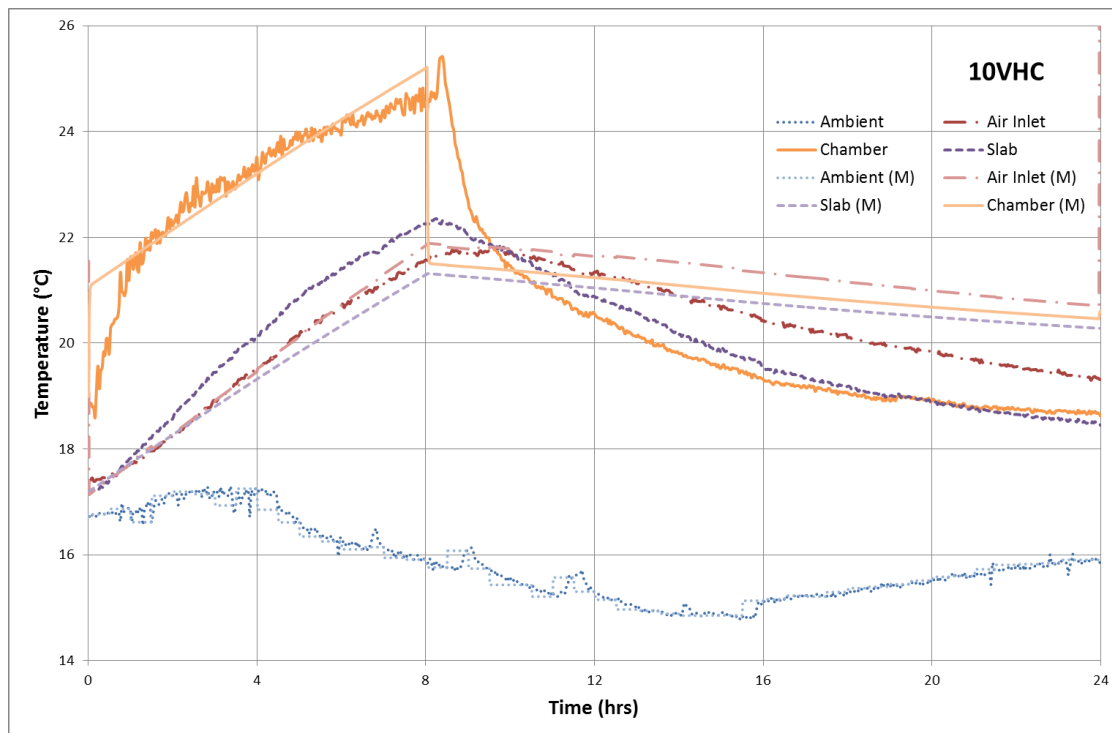


Figure 4.30 - 10VHC Scenario Validation Temperature Profiles

This fit demonstrated in Figure 4.30 suggested that under the boundary conditions tested the model was valid for modelling average chamber temperatures within 6% accuracy, for 'occupied' periods. The major discrepancy between modelled and laboratory chamber temperatures lies in the response time. The model does not sufficiently model the thermal inertia observed in the laboratory, however simulated temperatures sufficiently model a linear approximation of the laboratory reality (within 13.6% total difference).

The resulting COP comparison was improved (10.2 (M) against 8.1), but was still significantly different (26%). The energy consumption remained closely aligned.

4.4.3 Validation Summary

Following an update to the heat transfer calculation between the chamber and the soffit, and an optimisation of the heat transfer coefficients, a fit of 1.6% was found between the modelled and laboratory tested chamber temperatures, during occupied periods. Air inlet

temperatures displayed a good fit (0.4%), with average slab temperatures displaying an acceptable fit (3.4% difference).

Overall there was an acceptable fit between modelled and laboratory energy consumption (12%). The modelled performance overestimated system efficiency, seeing the percentage difference between modelled and laboratory COP figures increase by 26%.

The laboratory data available can be utilised in further research work to expand the functionality of the Excel model tool. Further research models can be validated from the laboratory data.

4.5 Conclusions

To investigate system performance, a prototype WVHC system was designed, constructed and installed in a laboratory chamber. The prototype featured six active cores, two full slab length and four shortened lengths, due to internal core obstructions. An eight pass double serpentine configuration of water pipes were embedded 50-60mm above the soffit level. For future prototypes the pipe bends should be fully cast into the slab to avoid the risk of damage. Additional concrete covered the pipes, embedded sensors and air network cross-overs. The slab was raised to 1.8m for testing and installed in the modified chamber. Due to the size of the prototype the outer 'ambient' region could not be sealed therefore laboratory ambient temperatures were used throughout the experimental investigations.

Two channels of investigation were conducted, fixed operation (*constant conditions*), to determine system performance without control, and variable operation (*variable conditions*), to determine system performance with temperature set-point control. Firstly each system was heated for eight hours, and then allowed to discharge for sixteen hours. Temperatures were monitored and a heat balance calculated, from which COP figures could be generated. Only the VHC system investigated in the laboratory resembled the modelled scenarios due to the variation in water systems, closed loop in the laboratory and open loop in the model.

Under fixed operation conditions the 10VHC experimental scenario offered the greatest COP of 8.1. Temperature reduction was observed for all the systems tested, against a PassiveHC reference test. Significantly, the closed loop water system provided inefficient cooling whilst operated under fixed conditions. Improvements to system efficiency were predicted for the WVHC system under temperature set-point control.

To operate the WVHC systems effectively temperature set-point control was investigated as the second channel of investigation. Through set-point control, comfort was improved and energy saved, versus the fixed system operation method. Water cooling was saved for the latter half of the day and used intermittently keeping the slab below 22°C. COP figures were improved against the previous best, 10VHC. The 32WVHCa21pman system achieved a COP of 10.6 for the twenty-four hour investigation. Investigation into automated temperature set-point control found that a fan set-point of 20°C coupled with a pump set-point of 22.5°C achieved the greatest automated thermal control and efficiency under the conditions tested, recording a COP of 8.2.

In contrast to the TES systems tested, published Cool-Phase® performance, calculating the efficiency of Monodraught's active-TES system, gives a COP equivalent, the ESEER. Based on night and day performance the Cool-Phase® system has an ESEER of 7.3 [150].

The use of a closed loop water tank provided heating benefits during the 'unoccupied' night period due to the recycled day time heat stored in the water tank. The work has demonstrated that appropriate intermittent temperature set-point control is suitable at efficiently operating a closed loop water tank system. From modelled evidence, an open loop mains water cooling system offers greater cooling benefits to the WVHC system. Future revisions of the WVHC prototype testing will investigate the performance of an open loop mains water supply system.

The model validation, based on the 10VHC *fixed operation* results demonstrated a fit of 1.6% and 0.4% between chamber and slab temperatures respectively. Heat transfer coefficient adjustment was required to find a suitable fit for the model. A poor fit (26%) was found for COP figures. Further investigation into appropriate heat transfer coefficients that accurately model VHC and WVHC performance would be useful both academically and industrially to aid computer modelling.

Enhancement to the traditional VHC system, delivering cooling of $120\text{W}/\text{m}^2$, has been demonstrated through effective control of the water pipe addition. Under varying cooling demand conditions it is anticipated variations to system configuration and control are required. Further investigation into an energy-efficient enhancement hierarchy, that maintains comfort temperatures, should be investigated in *Chapter 5*.

Chapter 5: Sensible Thermal Mass Component

CFD Modelling, Laboratory Validation and Optimum Operating Method

5 Sensible Thermal Mass Component

5.1 Introduction

Building on the findings from the fixed heat gain scenarios in *Chapter 4*, this chapter focuses on characterising system performance under different cooling demands. Two streams of investigation were undertaken on the isolated active-TES system: modelling of the ventilated hollow core (VHC) and water cooled hollow core (WHC) system, to contrast prototype performance against traditional ventilated hollow core geometry; and laboratory testing on the prototype component to further quantify performance.

Subsequently validation of the models created was conducted and the Optimum Operating Method (OOM) for the enhanced water and air cooled hollow core (WVHC) prototype from the performance coefficients generated. The OOM advises optimum system operation, under static control, for mitigating differing levels of heat gain.

Finally, the isolated VHC model was simulated in a room context, under typical office building conditions. This work built upon the theoretical simulation conducted in this chapter to

confirm the energy-efficient thermal control benefits of the active-TES system in a real world application.

In this work ANSYS Fluent has been used to develop computational fluid dynamics (CFD) models, replicating the air and water systems of the prototype hollow core slab. Steady state modelling has been carried out to determine the theoretical cooling capacity for each system. In the laboratory tests, conditions were maintained for eight to thirty hours until slab temperatures had stabilised. To enable continual cooling and steady state conditions in the laboratory, an open-loop mains water supply was connected to the rig. To replicate the isolated modelled scenario, the prototype slab was lowered onto a pallet, with heater under the soffit layer, instrumented and insulated. The open loop water pipe delivered 7-9°C cooling water at 3-4l/min.

5.1.1 Contributions to knowledge

Published work on active hollow core systems has been reviewed thoroughly [33]. In [37] Barton reported straight core heat transfer of $5.29\text{W/m}^2\text{K}$. With a typical temperature difference of 4°C through the slab, a typical cooling capacity of 20W/m^2 was reported. When inlet air temperature was conditioned to 12°C , in line with industry guidance [34], maximum cooling performance with a 10°C air temperature change was 50W/m^2 . Findings from [33, 39] predicted $50\text{-}70\text{kWh/m}^2$ HVAC operation was possible within a UK building. Previously, validation of CFD results has been carried out with test samples on a two-core VHC system [36, 38]

Barton [37] and Winwood et al [40] carried out CFD assessment on three and five VHC systems, typically found in industry. This chapter investigated a six-core VHC system to determine the additional benefits from activating as much of the thermal mass as possible. The findings from the six-core VHC and eight-pass-pipe WHC CFD modelling and validation in this chapter offer useful contributions to knowledge.

WHC systems (commonly labelled TABS) have been previously investigated, demonstrating suitability for room temperature control when pipes are embedded approximately 50mm from the soffit surface [24]. The benefit of water pipe addition can specifically condition the soffit layer of the thermal mass. To date no work has investigated the combined benefit of conditioning an air stream through the slab, and controlling the soffit layer temperature through embedded active water pipes. The construction, testing and analysis of the combined six-core, eight-pass-pipe WVHC component rig for model validation offers further

novelty. The component rig tested in this chapter was the first investigation of its kind to quantify performance of the combined WVHC system.

Despite previous studies on VHC decks [36, 37], the performance had been solely assessed on a temperature basis. This chapter develops performance coefficients, derived from the relationship between soffit thermal loads and average slab temperatures, for VHC and WVHC systems offers further contributions to knowledge. The figures enabled the development of a theoretical optimum operating method (OOM).

5.1.2 Chapter aims

The work of this chapter aims to accomplish the work below.

- 1) Compare laboratory sample hollow core with typical full-scale hollow core systems through CFD modelling.
- 2) Establish isolated VHC performance under controlled simulated and laboratory conditions to quantify performance over a range of conditions.
- 3) Simulate sample VHC in typical office room scenarios through CFD modelling.

5.2 CFD Investigation

The CFD investigation was carried out to compare the six-core prototype VHC performance against typical industry scale three and four-core active thermal mass slab, under a range of thermal loads. The CFD modelling offers estimation of VHC and WHC prototype performance, enabling the proposal of a system performance hierarchy.

5.2.1 Modelling methodology

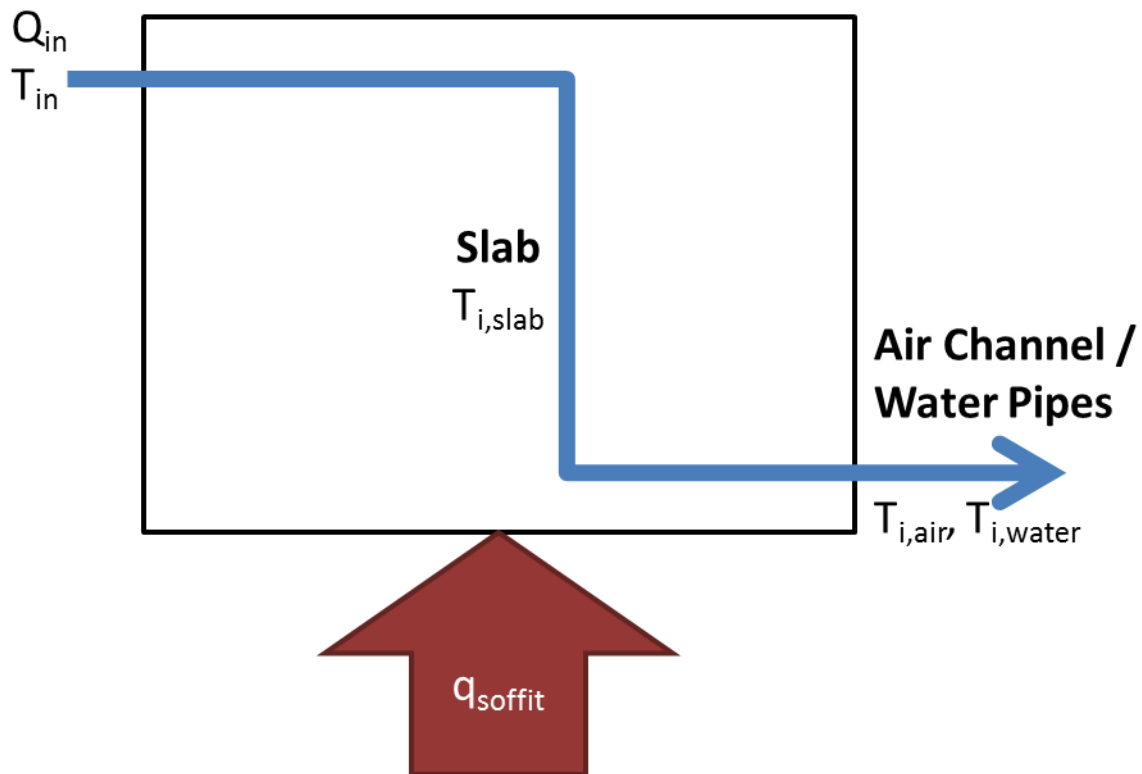


Figure 5.1 - Schematic diagram representing the modelling method

The modelling method followed in this chapter aimed to identify the cooling performance of the concrete hollow core component alone, under typical building thermal loads, but isolated from the building architecture. The final simulations (Section 5.6) reintroduce the room architecture, considering the thermal performance of the slab, when coupled with a room space. As shown in Figure 5.1, each model features a concrete slab with an embedded air channel or water pipe network. Using ANSYS Fluent, steady-state modelling was conducted on each model under turbulent flow and energy modes.

Each simulation was initialised with the slab and fluid (air or water) components temperatures set ($T_{i,slab}$, $T_{i,air}$ and $T_{i,water}$). The fluid inlet velocity (component of Q_{in}), fluid inlet temperature (T_{in}) and soffit heat flux (q_{soffit}) were set as boundary conditions. Once convergence was reached, steady-state slab and fluid temperatures were reported.

No radiative mode was activated in the component models since the heat exchanges in observance were within the slab, to and from the passing internal fluid. No external air or attached room was modelled in conjunction with the slab component model, therefore internal gains were modelled as a heat flux acting evenly across the soffit surface. Further, no heat transfer occurred at the slab wall boundary, only within the slab.

Differing slab and fluid configurations were modelled, with their internal heat transfer and resulting stable temperatures observed. Due to various soffit heat flux simulations being conducted on each model, a specific simulation was commonly referred to by model type and soffit heat flux, eg. 3-core 50W/m². The models investigated are introduced in the sections following.

5.2.1.1 Air Based

Three air systems were modelled: a traditional 9m span three-core hollow core slab, a 9m four-core slab and latterly a 1.5m six-core slab akin to the laboratory prototype available (Figure 5.2). The hollow cores were modelled as cylinders. Following independent mesh testing, these slabs were simulated with an air flow rate of four air changes per hour (acph). Air inlet temperature to the hollow core labyrinths was set at 18°C (291K). Due to differing soffit areas the 4acph flow rate equates to an air inlet velocity of 1.5m/s for the three and four-core slabs, and 0.22m/s for the prototype slab. Soffit heat fluxes ranging from -100W/m² to 178W/m² were investigated. This range was in line with the BSRIA Rules of thumb for thermal loads in commercial buildings, 100W/m² and 180W/m² being the upper heating and cooling loads respectively [143]. 178W/m² was simulated for ease of validation, instead of 180W/m², since this was the maximum output from the heat mat used in *Chapter 4*. The temperatures and hollow core heat fluxes from the steady state simulations were reported.

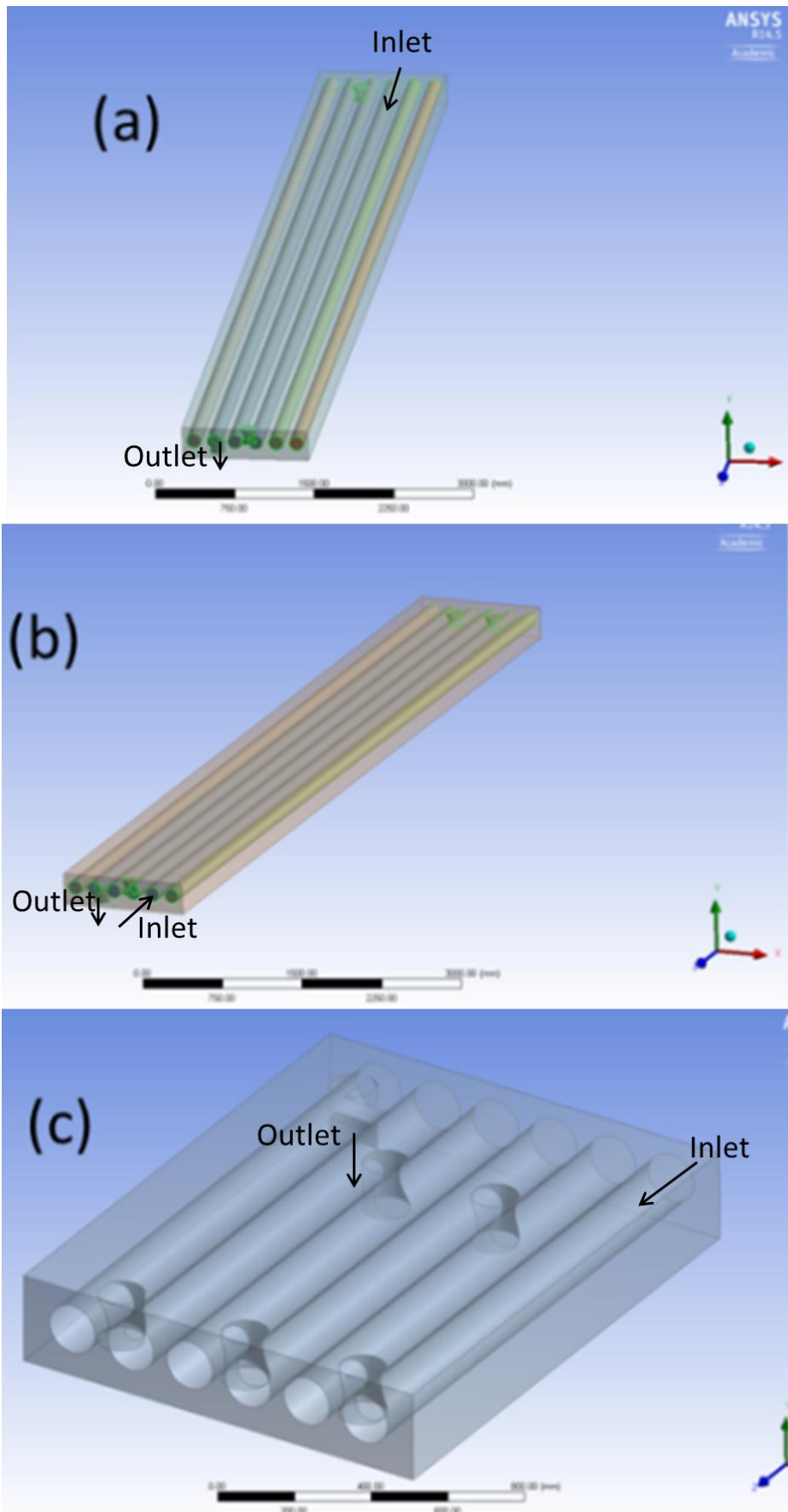


Figure 5.2 - (a) Typical 3 Core Slab, (b) Typical 4 Core Slab and (c) Prototype Air Slab

5.2.1.2 Water Based

For the prototype water based slab investigation (WHC), only the straight embedded part of the pipes was modelled as in Figure 5.3(b). A full pipe network model (figure 5.3(a)) was created but the simulations lacked sufficient certainty to warrant drawing conclusions. To mimic the flow of water through the slab, akin to the pipe network in figure 5.3(a), the outlet temperature from pipe 1 was matched with the inlet temperature to pipe 2 and so on, until a continual gradient of temperature was calculated. Water velocity of 0.58m/s was used throughout the simulations, an equivalent velocity to the 4l/min water flow rate from the investigation in *Chapter 4*.

To estimate a combined air and water performance average slab temperatures at the plane just above the water pipes was recorded and analysed along with temperatures from the same plane in the air hollow core model. Combined results were therefore estimated analytically.

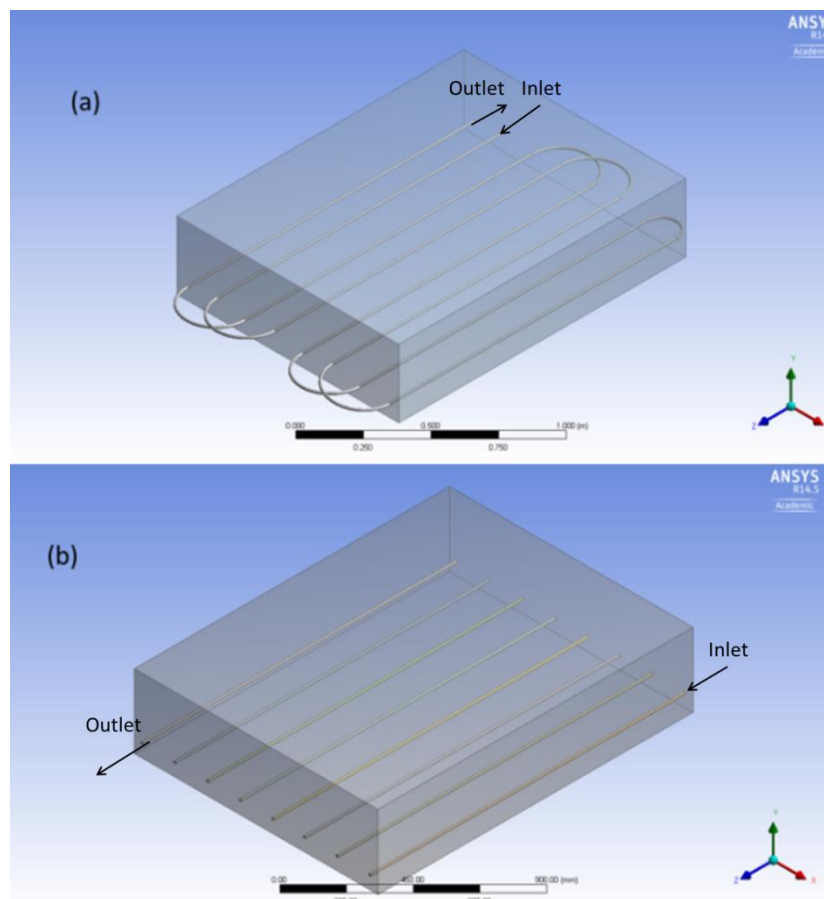


Figure 5.3 - (a) Prototype Pipe Network and (b) Simplified Embedded Pipe Network

5.2.2 Simulation Parameters

For each simulation the parameters were initialised with the boundary conditions in Table 5.1. Following simulations, the output parameters (as per Table 5.2) were exported along with temperature and heat flux graphics of the soffit and pipe networks for the 50W/m^2 soffit heat flux simulations (figure 5.1). The CFD temperature readings in Kelvin were converted to degrees centigrade during the analysis for ease of interpretation.

During the simulations the models were constructed from a solid concrete slab, coupled with an air or water network as per the designs in figure 5.2 and figure 5.3. The fluid (air or water) inlets were specified as pressure inlets, with flow velocity specified in meters per second. The outlets were specified as velocity outlets. During the energy mode simulations the inlet air temperature was specified, as well as an initial fluid and solid temperatures. A constant, evenly distributed thermal load was applied to the ceiling soffit. No heat loss was accounted for to the surrounding walls. The energy mode took into account conduction and convection heat transfer. The radiative mode was not included in the simulations since the major heat transfer in observance was through the solid slab or between the slab and internal fluid.

The mesh settings for each simulation was auto generated based on the 'medium' mesh settings in Table 5.3. Confirmation of the mesh suitability (within 0.63%) for the tests was confirmed through the mesh independent testing.

The input parameters, in table 5.1, were based on best practice industry guidelines, laboratory measurements and industry consultancy [34, 136, 144]. The air velocity was determined to achieve a minimum of four air changes per hour in a room with the equivalent floor area as the slab soffit. Water velocity was defined by the laboratory pumping rate. The turbulent flow viscous model was used for each model. The k-epsilon mode was used for turbulent flow with default parameters set for each fluid (water and air).

The initial slab temperature was assumed to be 25°C to replicate an overheated slab at the end of the day requiring heating, as observed in the worst case scenario in *Chapter 4*. The inlet air temperature was defined at 18°C , replicating the worst case scenario reported in *Chapter 4*. The water inlet temperature was specified at 15°C , in line with the ambient water temperature from *Chapter 4* trials. The internal heat gain acting upon the soffit (represented by a boundary heat flux) was tested at 0, 10, 20, 50, 100 and 178W/m^2 to replicate minimum and maximum heat gains within a typical office [143]. Theoretical heating conditions were simulated with air inlet temperatures at 32°C and soffit heat flux at 0, -25, -50 and -100W/m^2 , again in line with heating load guidelines. The increments were investigated to enable

subsequent analysis of the relationship between soffit heat flux and slab temperature, further, they are in line with rule-of-thumb guidance from BSRIA regarding thermal loads in commercial buildings.

Table 5.1 - Boundary Conditions for CFD Simulations

| | <i>units</i> | 3 Core Model | 4 Core Model | 6 Core Air Only Prototype | | Water Only Prototype |
|----------------------------------|------------------------|---------------------|---------------------|----------------------------------|------|-----------------------------|
| Air Velocity | <i>m/s</i> | 1.50 | 1.50 | 0.22 | 0.88 | - |
| Water Flow Rate | <i>m/s</i> | - | - | - | - | 0.58 |
| Initial Slab Temperature | <i>K</i> | 298 | 298 | 298 | 298 | 298 |
| | <i>°C</i> | 25 | 25 | 25 | 25 | 25 |
| Air/Water Inlet Temp | <i>K</i> | 291 | 291 | 291 | 291 | 288 |
| (for cooling) | <i>°C</i> | 18 | 18 | 18 | 18 | 15 |
| Soffit Heat Flux | <i>W/m²</i> | 0 | 0 | 0 | 0 | 0 |
| | | 10 | 10 | 10 | 10 | 10 |
| | | 20 | 20 | 20 | 20 | 20 |
| | | 50 | 50 | 50 | 50 | 50 |
| | | 100 | 100 | 100 | 100 | 100 |
| | | 178 | 178 | 178 | 178 | 178 |
| | | | | | | 500 |
| Air/Water Inlet Temp | <i>K</i> | - | - | 308 | 308 | 303 |
| (for heating) | <i>°C</i> | | | 32 | 32 | 28 |
| Soffit Heat Flux (Coolth) | <i>W/m²</i> | - | - | 0 | 0 | 0 |
| | | | | -25 | -25 | -25 |
| | | | | -50 | -50 | -50 |
| | | | | -100 | -100 | -100 |

Table 5.2 - Output Parameters

| 3 Core Model | 4 Core Model | Air Only Prototype | Water Only Prototype |
|---------------------|---------------------|---|--|
| | | Soffit Heat Flux (<i>W/m²</i>) | |
| | | Soffit Temperature (<i>K</i>) | |
| | | Slab TC's Plane Temp (<i>K</i>) | |
| | | Slab Wall Temperature (<i>K</i>) | |
| | | Slab Top Temperature (<i>K</i>) | |
| | | Air Inlet Temperature (<i>K</i>) | <i>for each pipe</i> |
| | | Air Midway Temperature (<i>K</i>) | Inlet Temperature (<i>K</i>) |
| | | Air Outlet Temperature (<i>K</i>) | Outlet Temperature (<i>K</i>) |
| | | Air Channel Wall Heat Flux (<i>W/m²</i>) | Pipe Wall Heat Flux (<i>W/m²</i>) |

5.2.3 Simulation Procedure

The following modelling procedure was followed throughout the investigation:

- 1) Construct the CFD models of traditional three and four-core hollow core slab.
- 2) Design and construct CFD model of the six-core prototype air and water hollow core slab.
- 3) Mesh the constructed models.
- 4) Conduct Mesh Independent Testing.
- 5) Set up modelling parameters in Fluent.
- 6) Simulate 'flow only' mode initiated for each model to aid convergence.
- 7) From the converged point initiate 'energy equation' and 'turbulent flow' modes for the models under constant air velocities, heat flows and initial temperatures as per Table 5.1.
- 8) Following achieved steady-state stabilisation of a numerical solution, post simulation; extract output data using CFD-post. Numerically, as presented in Table 5.2, record the temperatures and heat fluxes along with pictorial temperature mapping (Figure 5.4 - Figure 5.6).
- 9) Repeat steps 4 to 7 for each model and scenario conditions in Table 5.1.

5.2.4 Mesh Independent Study

Following creation of the models and specification of the boundary conditions a mesh independent study was conducted to confirm the certainty of the results. Three levels of mesh refinement were tested.

5.2.4.1 Mesh independent study Method

- 1) Following construction of the models a 'coarse' mesh, as defined in Table 5.3, was specified.
- 2) The boundary conditions for each model were specified, with a soffit heat flux of 50W/m^2 .
- 3) The model simulation was initiated and run until convergence RMS of less than 10^{-4} was achieved. The soffit temperature was also monitored until stabilisation had been achieved.
- 4) The steady-state soffit temperature was recorded.
- 5) Subsequently the mesh was globally refined to the 'medium' and 'fine' mesh conditions laid out in Table 5.3.
- 6) Steps 2 to 4 were repeated.

- 7) The soffit temperature results were compared and conclusions drawn on the mesh independence for each model.

Table 5.3 - Mesh Parameters

| Mesh Parameter | Fine | Medium | Coarse |
|---|----------------------|----------------------|----------------------|
| Use advanced sizing function | on: curvature | on: curvature | off |
| Relevance Center | Fine | Medium | Coarse |
| Initial Seed Size | Active Assembly | Active Assembly | Active Assembly |
| Smoothing | High | Medium | low |
| Transition | Fast | Fast | Fast |
| Span Angle Center | Fine | Medium | Coarse |
| Number of Nodes | 41801 | 7048 | 1425 |
| Number of Elements | 229973 | 35045 | 7264 |
| Average volume of an Element(m ³) | 2.0*10 ⁻⁶ | 1.3*10 ⁻⁵ | 6.3*10 ⁻⁵ |

5.2.4.2 Results

The results of the mesh independence tests were displayed in Table 5.4. In each case the 'medium' mesh was sufficient to achieve results within 0.63% of those achieved with the 'fine' mesh. This demonstrated a strong level of mesh independence at the 'medium' mesh level used throughout the CFD investigation. The 'coarse' mesh demonstrated poor mesh independence. Since sufficient parity between 'medium' and 'fine' settings was achieved no further refinement of the mesh was investigated.

Table 5.4 - Mesh Independent Results

| Boundary Conditions | | 3-core | 4-core | 6-core | 6-core | Water |
|--------------------------|------------------------|--------|--------|--------|--------|-------|
| inlet velocity | <i>m/s</i> | 1.5 | 1.5 | 0.22 | 0.88 | 0.563 |
| inlet temperature | <i>K</i> | 291 | 291 | 291 | 291 | 288 |
| Initial Slab | <i>K</i> | 298 | 298 | 298 | 298 | 298 |
| Soffit Heat Flux | <i>W/m²</i> | 50 | 50 | 50 | 50 | 50 |
| Mesh Conditions | | | | | | |
| Mesh | | | | Coarse | | |
| Soffit Temp | <i>K</i> | 328.7 | - | 321.3 | 304.5 | 292.2 |
| %Diff from Fine | <i>%</i> | 1.58 | N/A | 1.97 | 0.59 | 0.24 |
| Mesh | | | | Medium | | |
| Soffit Temp | <i>K</i> | 323 | 310 | 317.1 | 303.7 | 291.7 |
| %Diff from Fine | <i>%</i> | -0.19 | -0.32 | 0.63 | 0.33 | 0.07 |
| Mesh | | | | Fine | | |
| Soffit Temp | <i>K</i> | 323.6 | 311 | 315.1 | 302.7 | 291.5 |

5.2.5 Modelling Assumptions

During the construction and simulation stages various problems were overcome whilst meshing, building the geometry and setting the boundary conditions. The results presented in the next section are the outcome of a combination of solutions. In brief the problems and solutions found are summarised below.

Initially the graphical representation of the differing hollow cores required some approximations. The hollow core was considered to be constructed from 100% concrete with perfectly cylindrical cores, connected by cylindrical cross-overs. In the prototype model the cross-overs were placed appropriately to ensure the bulk air flow followed a similar path length to that of the prototype slab.

The most difficult construction graphically was the as constructed prototype fluid pipe network. Initially this was created to match the prototype system however due to instability in the final solution, only the embedded pipes were modelled. To simulate one continual flow through the pipes subsequent inlet temperatures were matched with the previous outlet temperature (Temp. of outlet pipe1 = Temp. of inlet to pipe2). This ensured a

temperature gradient along the embedded pipe path length approximating one continual pipe with eight passes through the slab.

With the different geometry of each slab model tested, different meshes were generated depending on the required need for precision. A medium mesh was favoured to enable faster simulation iterations.

In the three-core typical hollow core system, fully converged solutions, to a precision of 10^{-6} were not achieved. Internal surface roughness was increased from 0.5 to 0.8 to aid the heat transfer between the concrete and the air. To reach convergence (of at least 10^{-4}), flow only simulations were used to initiate the solution before the energy equation was activated.

Even with these tools a perfectly converged (10^{-6}) solution was not always found for the three-core model, particularly for scenarios with medium and high heat fluxes. In this case the results were outputted when the simulation reached the smallest achievable convergence tolerance, typically from 10^{-4} to 10^{-5} . These results therefore offer a representation of performance, but care should be taken with how much weight is put on the three-core findings under higher heat flux conditions.

The four-core model demonstrated greater stability however for heat fluxes above 50W/m^2 . A similar method for obtaining stable output data was utilised when a converged solution could not be obtained.

When water pipes were added to the prototype six-core air hollow core slab model, floating point errors caused the simulation to terminate. Despite efforts to clean up the model, simplify the pipe network and simulation parameters a solution could not be found. Combined fluid and air system performance was therefore estimated through post simulation analysis of separate fluid and air systems under identical conditions. Temperatures were taken at the plane just above the water pipes to act as suitable input into the base surface of the air based model.

5.2.6 Results

5.2.6.1 Temperature Findings

5.2.6.1.1 Cooling

A fixed heating duty was inflicted upon the ceiling soffit (bottom of slab) ranging from $0-178\text{W/m}^2$. Each different system in Figure 5.6 demonstrated a different capability of removing this heat and keeping the slab cool. Figure 5.4 and Figure 5.5 demonstrate the

temperature profile of the slabs under a 50W/m^2 heating load. Full boundary conditions can be found in table 5.1 and table 5.4. The slab was considered perfectly insulated on all surfaces therefore the only outlet for the heat is into the concrete thermal mass, which starts the simulation at 25°C (298K), or into the air or water moving through the air network or water pipes.

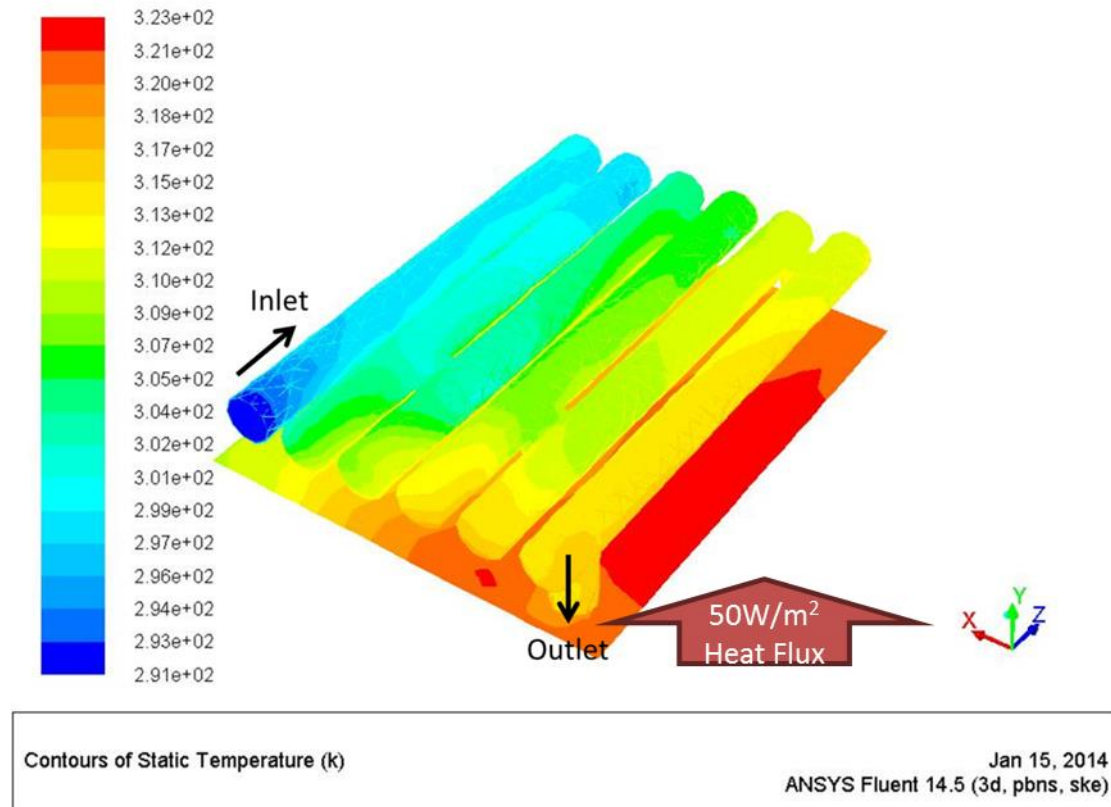


Figure 5.4 - Prototype Air Slab at 0.22m/s air velocity and with 50W/m^2 Soffit Heating

The water cooled slab was capable of keeping the slab cooler through the extreme conditions than the air based slabs. A 500W/m^2 heat flux was therefore imposed upon the slab to observe what occurs when the slab cooling capability was tested to an extreme.

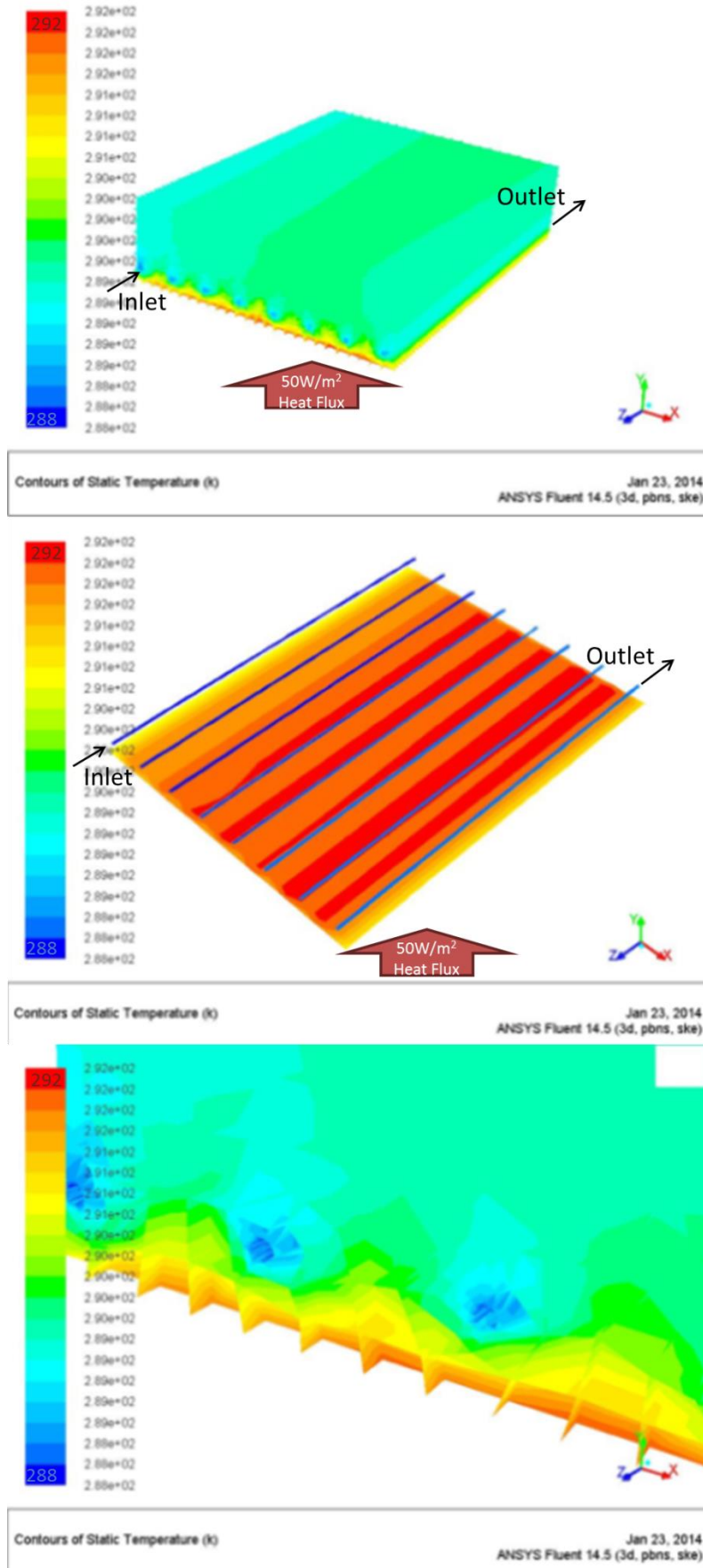


Figure 5.5 - Water Cooled Prototype Slab with 0.58m/s water velocity and 50W/m² soffit heating

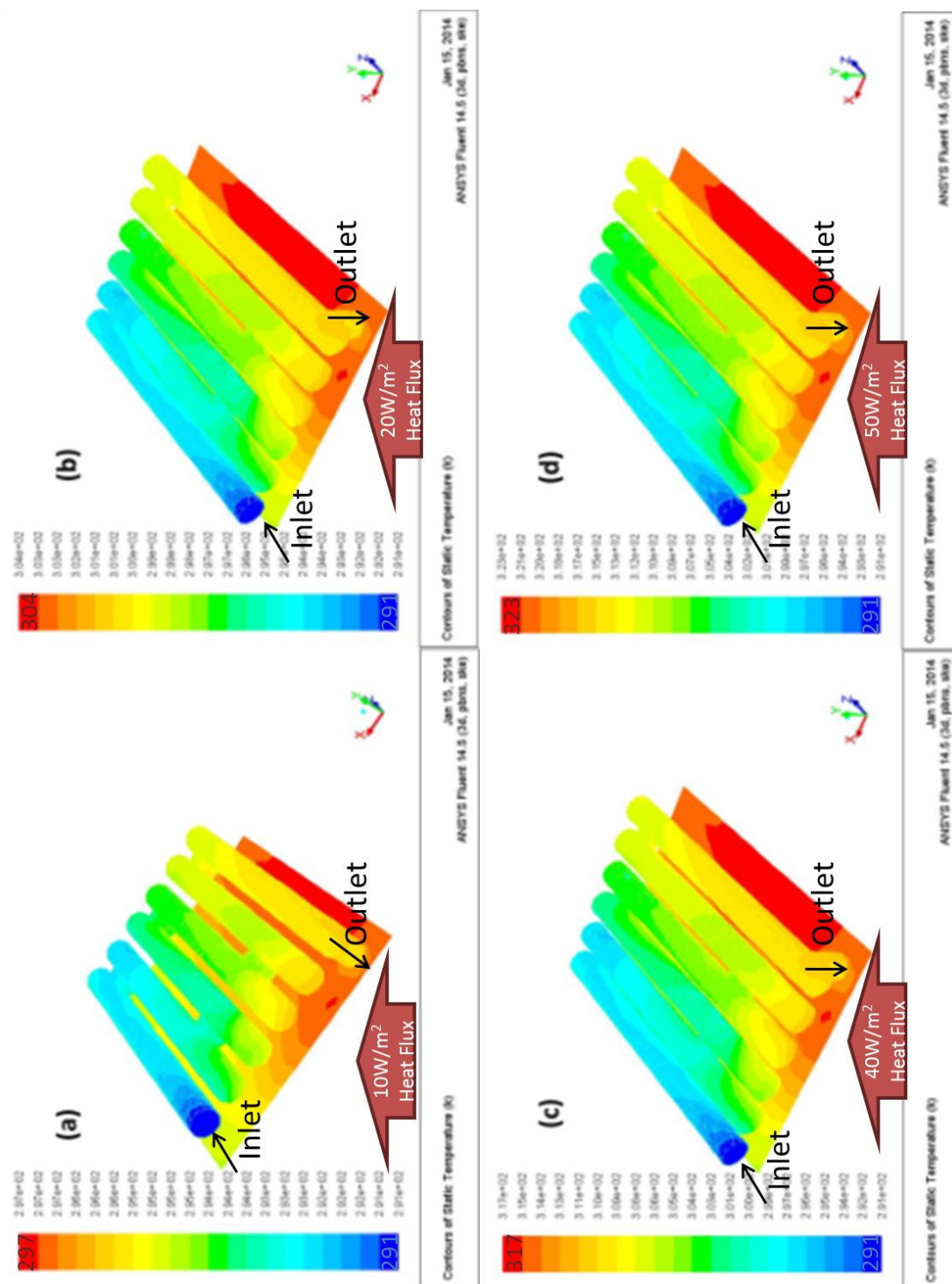


Figure 5.6 - Air Prototype Slab with 0.22m/s air velocity under (a) 10W/m² (b) 20W/m² (c) 40W/m² and (d) 50W/m² ceiling soffit heat flux

Figure 5.6 demonstrates the increasing soffit temperature as the soffit heat flux increased. It was necessary to refer to the colour scale of each image as the temperatures vary from case to case. In figure 5.6 (a) the colour temperature ranges from 18°C (blue) to 24°C (red). For figure 5.6 (b) they range from 18°C (blue) to 31°C (red). Figure 5.6 (c) and (d) range from 18°C (blue) to 44°C (red) and 50°C (red) respectively. At this low air velocity rate (0.22m/s) though

the air changes of the room below (if one were present) were in line with building regulations (4acph) an increased velocity was required to maintain slab control temperatures.

5.2.6.1.2 Heating

Following the cooling investigation, the capability of the prototype slabs to heat occupied spaces was tested. As before, to replicate the thermal demands from the room acting on the slab, heat fluxes of 0, -25, -50 and -100W/m² were imposed upon the ceiling soffit surface. The air inlet temperature set to 308K (35°C) and the water temperature set to 303K. (30°C) Figure 5.7 and Figure 5.8 graphically depict the differing temperature profiles of the slab under different heating strategies, all moderating the 50W/m² of cooling.

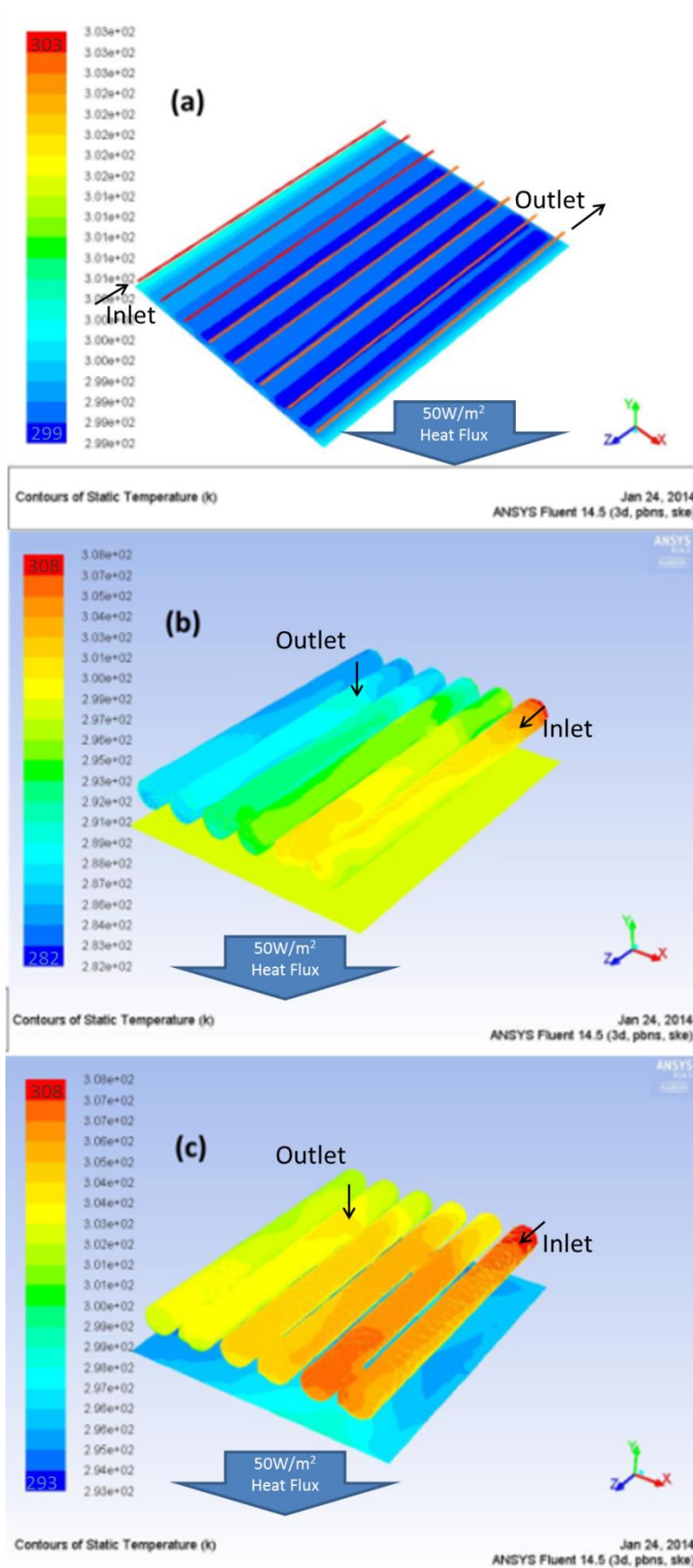


Figure 5.7 - Internal wall and soffit temperature contours and (a) Water Pipe network, (b) Air Network with Air velocity of 0.22m/s and of (c) 0.88m/s all with a -50W/m^2 heat flux on the Soffit

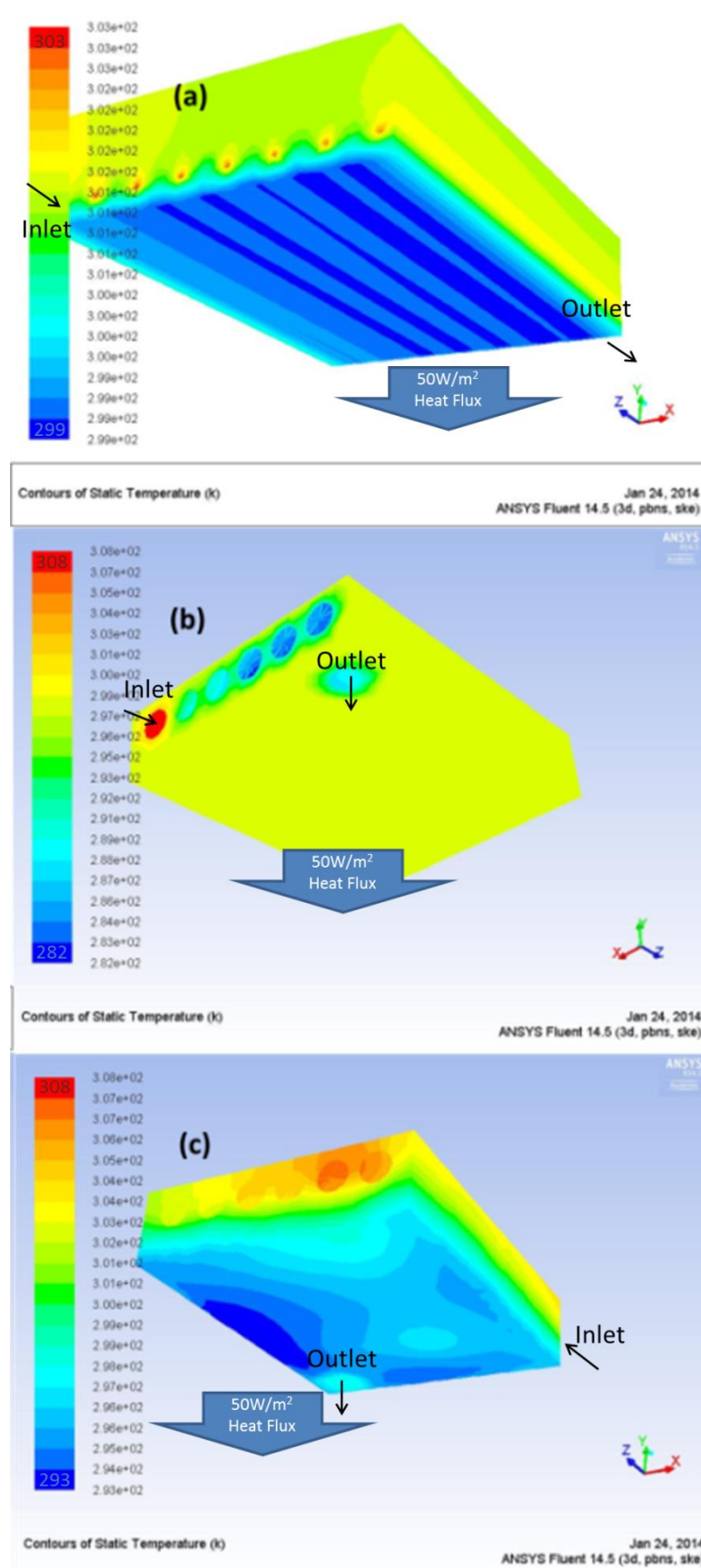


Figure 5.8 - Outer slab wall temperature contours of (a) Water Pipe network, (b) Air Network with Air velocity of 0.22m/s and of (c) 0.88m/s all with a -50W/m^2 heat flux applied to the Soffit

When interpreting Figure 5.7 and Figure 5.8 it was clear that the water pipe slab provides the greatest heating maintaining a soffit temperature greater than 25°C. An increase in air velocity reduced the heating capability.

5.2.6.2 Heat Flux Findings

Figure 5.9 depicts the varying heat flux profiles across the prototype slab (air velocity at 0.22m/s and soffit heat flux at 50W/m²). Air enters top left and exits top right. The heat flux (W/m²) between the air core and the slab ranges from 2.6 - 8.7W/m² in the majority of the air network. The red areas (6.9 - 8.7W/m²) highlight the areas of greater heat transfer, occurring after the air inlet and initial cross-overs.

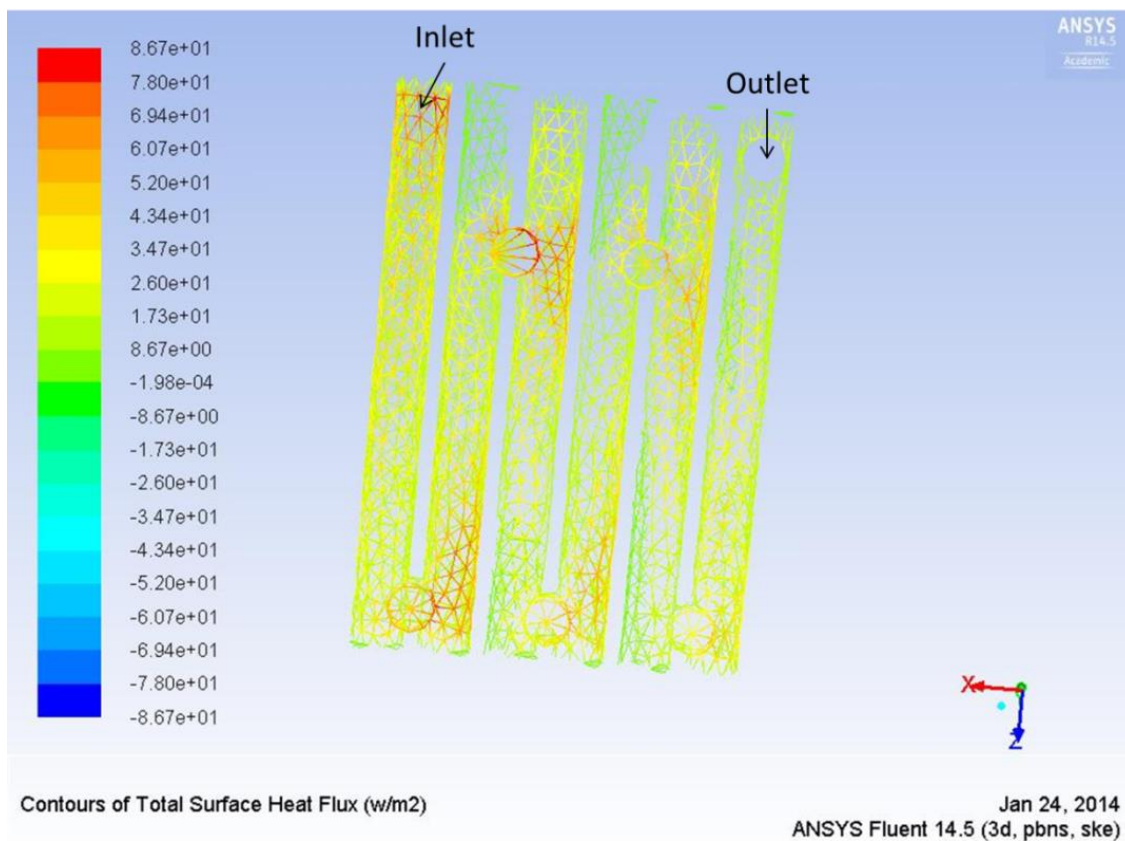


Figure 5.9 - Heat Flux Contours of the Air Cooled Prototype Slab with Air Velocity of 0.22m/s and Soffit Heat Flux of 50W/m²

5.2.6.3 *Compiled Findings*

Table 5.5 - Summary of Key Cooling Results at Steady State

| | | A) 3 Core | B) 4 Core | C) 0.22m/s Air Only | D) 0.88m/s Air Only | E) 0.58m/s Water Only | C&E) Theoretical Combined Prototype |
|------------------------------|-------------|--------------|--------------|---------------------------|---------------------------|--------------------------------|--|
| Soffit Heat Flux | W/m^2 | | | | 10 | | |
| Soffit Temperature | $^{\circ}C$ | 24.5 | 22.2 | 22.9 | 20.3 | 15.5 | 15.5 |
| Air/Water Inlet Temp | $^{\circ}C$ | 17.9 | 17.9 | 17.9 | 17.9 | 14.9 | - |
| Air/Water Outlet Temp | $^{\circ}C$ | 23.3 | 23.3 | 22.4 | 19.0 | 15.0 | - |
| Soffit Heat Flux | W/m^2 | | | | 50 | | |
| Soffit Temperature | $^{\circ}C$ | 50.1 | 39.2 | 43.4 | 30.3 | 18.6 | 18.6 |
| Air/Water Inlet Temp | $^{\circ}C$ | 17.9 | 17.9 | 17.9 | 17.9 | 14.9 | - |
| Air/Water Outlet Temp | $^{\circ}C$ | 35.6 | 23.1 | 41.0 | 23.6 | 15.2 | - |

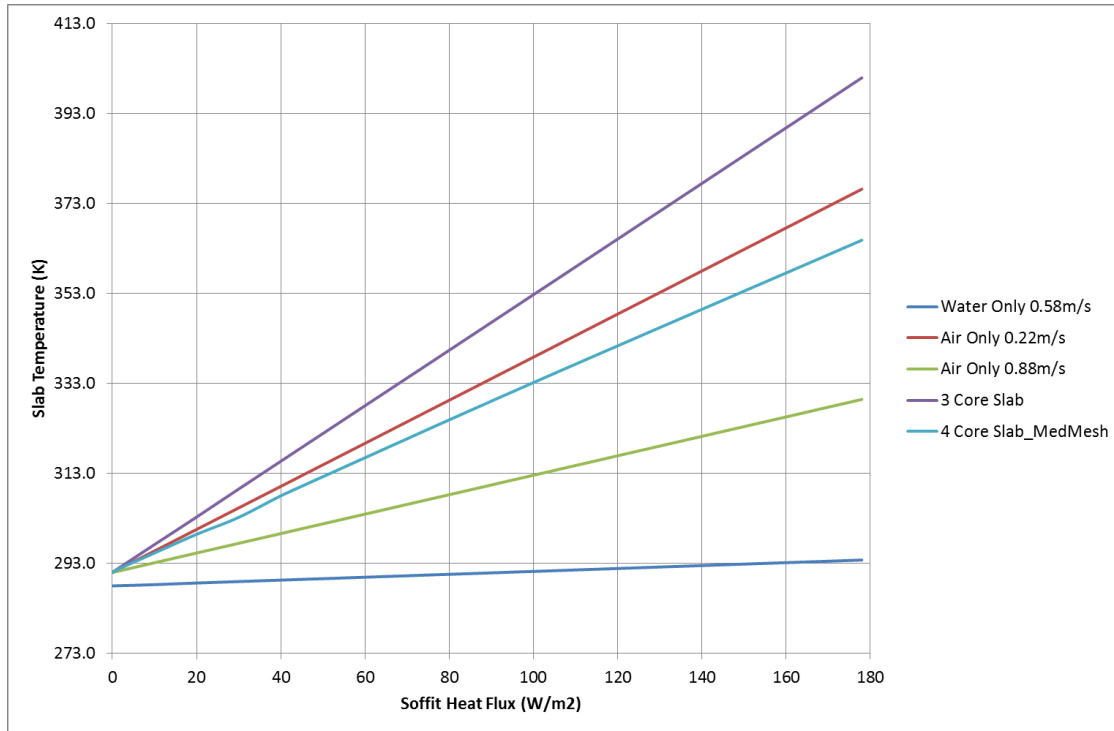


Figure 5.10 - Soffit Temperature versus Soffit Heat Flux where Slab is cooling the Room

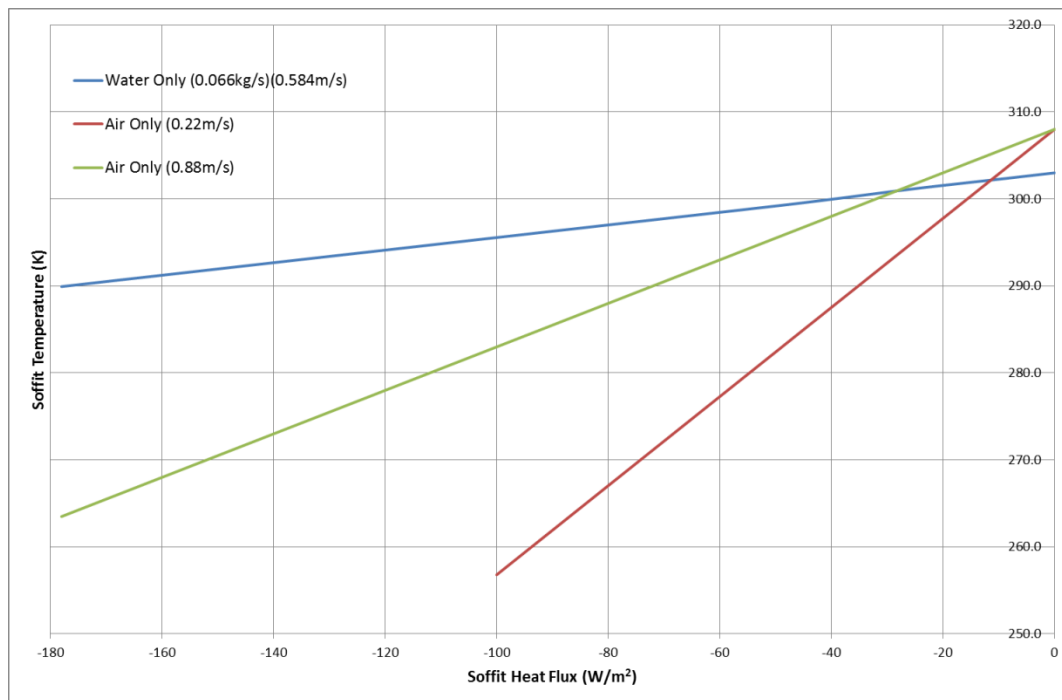


Figure 5.11 - Chart of Soffit Temperature versus Soffit Heat Flux where Slab is heating the Room

5.2.7 Discussion

5.2.7.1 Three-core versus four-core versus six-core Air Hollow Core

The typical three-core system demonstrates the greatest level of internal steady-state heat flux. This was because the ratio of soffit area to active core area was greatest. In all scenarios

the same level of heat transfer must be achieved since the soffit heat flux was constant through each simulation. In the four-core and prototype systems there were more cores active, therefore the heat transfer surface area was greater. In these situations the thermal load was dissipated across a larger surface area.

When operating the three-core system, the system with the fewest active cores and therefore the smallest relative active heat transfer area, an alternative property must be enhanced to achieve a thermal steady state. In the simulation solver this was achieved by varying the air temperature. The increase in temperature difference between inlet air temperature and outlet air temperature achieves the same overall dissipation of heat. However, this increase in air temperature increased the soffit temperature and resulted in poorer cooling performance capabilities.

Reported high heat flux figures did not correspond to good slab performance. When considering performance the three-core was the least suitable at managing the soffit temperature due to the smallest active core surface area.

When analysing the 50W/m^2 loads the six-core prototype was most capable at keeping soffit temperature down. When considering the soffit temperature, the prototype slab outperformed the three and four-core slabs. However, scenario D in Table 5.5, demonstrated that at increased flowrate the prototype slab performance was comparable with the four-core slab.

Another measure of whether the prototype was suitably representing the thermal behaviour of typical larger slabs was that the outlet air temperature matched the soffit temperature. In each case presented in Table 5.5 the prototype outlet air temperatures offered a closer match to their relevant soffit temperatures than a typical larger hollow core section.

5.2.7.2 Air Velocity Variations

To test the performance variations with respect to air velocity two simulation cases were investigated on the prototype slab. In line with what can be tested in the laboratory, the air velocities of 0.22m/s and 0.88m/s were set. These convert to approximately four air changes per hour (acph) and sixteen acph respectively.

At 10W/m^2 both were capable of keeping the soffit below 298K (25°C) although the higher air velocity case kept the soffit 3°C cooler. When the heating load was increased to 50W/m^2 both scenarios were overwhelmed and the slab stabilised at 316.6K (43.4°C) and 303.5K (30.3°C) for the low and high air change rates respectively.

This suggests that whilst increasing the flow rate four fold the thermal enhancement of the hollow core for high heating loads ($>50\text{W/m}^2$) was not sufficient to maintain comfort temperatures on the soffit surface. Commercial VHC installations typically operate at 1.5m/s , therefore a further doubling in air velocity may provide suitable cooling for systems loads up to 50W/m^2 , as reported in existing buildings [34]. Further testing and remodelling should investigate this assertion (see Section 5.6).

In practice, to increase cooling capacity, the air flowing through the core was cooled below 291K (18°C) to 285K (12°C) before being passed through the slab [34]. This variation was not simulated in this investigation, however further analysis in this section provided some estimation of performance in relation to air inlet temperature.

5.2.7.3 Air versus Water versus Combined Performance

Significant enhancement was achieved by the incorporation of fluid pipes into the slab. With water pumping through the slab at 288K (15°C) and 0.58m/s the pipes offered an almost tenfold increase of W/m^2 cooling delivered, compared to the air network. Due to the smaller surface area of the pipes this increase was necessary to deliver sufficient cooling to the slab. Unlike the air systems however minimal temperature differences were noted between the inlet and outlet due to the far greater thermal capacity of water compared to air.

Also, from figure 5.7, the position of the water pipes maintained the cooling capacity near to the soffit, creating a heat absorption layer at the pipe plane. This enabled the soffit temperature to be kept lower than the overall bulk slab. In practice this effect is useful when extreme radiant cooling is required.

At both 10W/m^2 and 50W/m^2 the water cooled system was capable of keeping the soffit temperature below 20°C (293K). Under the water system soffit temperatures were kept below 25°C (298K) until the heating load was increased to 178W/m^2 . Even then the water kept the soffit temperature to 28°C (301K). An extreme thermal load of 500W/m^2 was imposed to observe what occurred when the water system was overwhelmed and the slab saturated.

A combined system has been qualitatively considered by considering the temperature in the plane just above the fluid pipes as the soffit temperature for the air prototype system. Since the temperature at this plane, in the likely scenarios modelled (Soffit Heat Flux from $0 - 50\text{W/m}^2$), was within 2°C of the air inlet temperature (291K or 18°C) no additional simulation was considered.

It is reasonable to deduce therefore that the air passing through the slab was not required to do any cooling on the slab and can pass its cooling capacity directly to the room via air replenishment and convection. This offered an enhancement not considered in these CFD trials as the room beneath the slab has not been modelled. Therefore it was difficult to quantify the benefit at this stage.

In reality this combined operation utilised the cooling capacity from the pipes to manage the temperature of the slab and soffit; whilst the passing air temperature was kept cool ready for addition to the room space. Where warm outside air requires cooling it may be possible to achieve this through cooling in the slab, thus avoiding energy rich cooling in the preceding HVAC plant.

5.2.7.4 Enhancement Effect when Cooling

Figure 5.10 charts the soffit heat flux (W/m^2) against the soffit temperature (K). Following the precedent set in [23], the graph offers a graphical representation of how the different hollow core enhancements reduce the slab heating rate when the hollow core was operating in cooling mode. The gradient of the line can be considered as the Hollow Core Heating Performance Coefficient (k).

Since the relationship between soffit heat flux and temperature was linear, performance equations can be easily created for each system. The Y-intercept was equal to the inlet air or water temperature, making the plotting of alternative design conditions possible using the equation below and the appropriate k value from Table 5.6.

Equation 5.1

$$T_{soffit} = k \left(\sum Q_{internal} \right) + T_{inlet}$$

Table 5.6 - Hollow Core Heating Coefficients (k)

| | Air (Water) Velocity | Hollow Core Heating Coefficient (k) |
|---------------------------|-----------------------------|--|
| | <i>m/s</i> | |
| Prototype (4acph) | 0.22 | 0.479 |
| Prototype (16acph) | 0.88 | 0.216 |
| Three Core (4acph) | 1.50 | 0.618 |
| Four Core (4acph) | 1.50 | 0.415 |
| Water | (0.58) | 0.032 |

The three-core typical hollow core slab had the highest hollow core heating coefficient of 0.618. The prototype slab at 4acph (0.22m/s) offered the closest comparison to the four-core slab with $k=0.479$ (6-core) and 0.415 (4-core). The increased flow prototype slab offered greater cooling capacity bringing the heating coefficient down to 0.216. The water pipe enhanced slab had the lowest hollow core heating coefficient of 0.032 demonstrating an almost twentyfold enhancement on the typical three-core hollow core performance. A combined air and water system working in tandem may be able to achieve a k value of less than 0.05.

5.2.7.5 Enhancement Effect when Heating

Analysis of Figure 5.11 demonstrated the same relationship for each slab configuration as in the cooling scenario. The same k values (Table 5.6) can be considered for each relationship with appropriate air or water inlet temperatures used as the y -intercept.

Therefore just as in the cooling scenario above theoretical scenarios can be calculated from the equations when the slab was being used for heating as when the slab was being used for cooling. As before the water pipe enhancement offers the greatest capacity of heating surpassing the air controlled options.

Since heating and cooling performance offered the same coefficient, finding a valid equation for cooling operation will be sufficient to estimate performance during heating. For this reason, and due to the cooling needs of the technology offering greater scope for enhancement, the remainder of this system will investigate enhanced system design for cooling applications.

5.2.7.6 Determining an Optimum System Operation

It was possible from the performance equation and k -value of each hollow core configuration to determine when a soffit temperature exceeded 296K (23°C) or fell below 288K (15°C). At these points the hollow core technology alone was no longer capable of conditioning the room temperature.

When determining an optimum solution for each building scenario the equations relating the soffit temperature and heat flux can be used to determine the cooling strategy. Since each building differs in requirements, when the typical heating or cooling demand on a room was known appropriate set points for heating or cooling air and water can be calculated. Where extreme heating or cooling demands were required different technology enhancements can

be advised. A building-bespoke optimum solution of the technology and control strategy was therefore suggested.

Three variables are available for optimisation:

- 1) Air or water inlet temperature to slab
- 2) Air or water velocity
- 3) Technological enhancement

Velocity and temperature variation can be adjusted during the life of the hollow core building through changes to AHU set points. However there is an ongoing energy cost caused by utilising these methods. A technological enhancement must be carried out at the design stage that can minimise ongoing energy costs, despite the extra technical steps required. Table 5.7 shows the recommended slab configuration depending on the peak total internal gains.

Table 5.7 - Cooling Technology Recommendations

| Recommended Cooling Strategy | | | |
|---|------------------------|---|-------------------------------|
| Peak Total Internal Building Loads <i>W/m²</i> | Technology | Flow Rate | Slab Inlet Temperature |
| 0-5 | 3 Core or Prototype | 4 acph (1.5m/s) | 18°C |
| 5-10 | 3 Core or Prototype | 4 acph (1.5m/s) | 15°C |
| 10-15 | 3 Core or Prototype | 4 acph (1.5m/s) | 12°C |
| 15-30 | 3 Core or Prototype | 16 acph (6m/s) | 12°C |
| 30-40 | 4 Core or Water System | 4acph (1.5m/s) (or 0.58m/s of Water) | 12°C |
| 40-130 | Water System Only | 0.58m/s | 12°C |

Table 5.8 - Industry Expected Performance Recommendations

| Internal Building Loads | Recommended Cooling Strategy | | |
|-------------------------|------------------------------|--|------------------------|
| | Technology | Flow Rate | Slab Inlet Temperature |
| W/m ² | | | |
| 0-25 | 3 Core or Prototype | 4 acph (1.5m/s) | 18°C |
| 25-30 | 3 Core or Prototype | 4 acph (1.5m/s) | 15°C |
| 30-40 | 3 Core or Prototype | 4 acph (1.5m/s) | 12°C |
| 35-50 | 3 Core or Prototype | 16 acph (6m/s) | 12°C |
| 45-65 | 4 Core or Water System | 16acph (6m/s) (or 0.58m/s of Water) | 15°C |
| 50-75 | Water System Only | 0.58m/s | 12°C |

The findings in Table 5.7 contrast against the traditional VHC building figures quoted in Table 5.8 [151]. Traditionally a 1 - 2°C soffit temperature rise is expected during a peak summer afternoons. Night ventilation would then be utilised to avoid overheating. At peak periods the thermal mass will draw on accompanying technologies to bring the cooling benefit. In industry, air velocity can be increased to a maximum of 2m/s before fan noise must be considered (2.8m/s being an upper limit) [151]. Air cooling in the AHU is typically initiated first, followed by design and efficiency enhancements where capacity, size, weight, capital cost and COP is critical to selection.

The differences between theoretical capacity and industry expected figures were likely due to external influences effective in a building scenario. The theoretical figures have been calculated in an idealised scenario through simulation media with performance levels calculated based on the derived equations. These simulations were also calculated at steady state, assuming the peak load and all operating conditions maintained for an indefinite length of time. In building scenario weather patterns and internal gains change dynamically. Similarly dynamic control was also utilised to keep the soffit temperature below 296K (23°C). Further, in typical buildings perfect levels of insulation surrounding the slab, as in the model, is not possible. Heat loss from the slab, adjacent room or through open windows will result in improved cooling capacity. Section 5.6 investigates the performance of the slab when connected to a room space, although the slab and room are considered perfectly insulated.

5.2.8 Summary of Findings

The prototype slab with air velocities of 0.22m/s (4acph) offers a 20% enhancement (equivalent to a 6.7°C saving at 50W/m² against typical three-core performance) on the hollow core heating coefficient of typical three-core 9m hollow core with air velocity of 1.5m/s (4acph). The prototype slab path length was long enough to satisfy a key assumption in typical VHC control strategies that outlet air temperature was comparable to soffit temperature.

Increased air velocities can further enhance the capabilities of hollow core, offering a 60% increase (19.8°C saving) on the capability of the slab to maintain soffit temperatures when internal heat gains increased. At this air velocity the prototype performance was comparable to a typical four-core 9m hollow core section.

The addition of water pipes offered the most significant enhancement saving 19.8°C, an 88% enhancement of hollow core heating coefficient. These enhancements significantly widen the scope of hollow core design, installation and operation.

In the combined slab, utilising air and water, the water cools the slab and soffit allowing the cooling capacity in the air to focus on directly cooling the occupied room space, through air replacement and convection currents. Therefore the incorporation of the fluid pipes, enabling pipe cooling of the slab, may make the hollow core technology suitable for buildings where extended or continual occupancy hours occur.

Additionally it has been identified from the modelling completed in this section that further novel investigations into CFD slab performance would be beneficial. These include widening the investigation assessing the performance variation with respect to inlet air velocity speeds. This investigation will help validate or disprove the assumption made from the limited data available currently, that the velocity has an inverse square relationship to the hollow core performance coefficient. Better understanding of this relationship could lead to the generation of a technology calculator, commercially applicable for design engineers.

Investigating the effect of other performance variables such as surface roughness, air-stream baffles and cross over geometry will aid the understanding of how to best maximise the heat transfer between the air and the slab. During this further work investigation into the increased energy cost of increased turbulence should be considered against the measured benefits to offer commercial and academic benefit.

Further work is required to determine a hollow core heating coefficient for a combined system. Through subsequent experimental laboratory testing this will be possible. The laboratory tests investigated in the next section enabled validation of these modelled results. The hollow core system utilised in the laboratory testing was constructed in line with a combined air and water prototype design, as used in this modelling investigation and building on the preparation work done in *Chapter 3* and *4*.

5.3 Laboratory Investigation

Using the CFD investigation into the hollow core component performance in the VHC and WHC systems as a start point, a laboratory investigation was conducted to validate the modelling and develop performance predictions for the novel combined WVHC prototype. These performance predictions were then used to develop a system hierarchy and optimum operating method (OOM) for efficient implementation of a multifunctioning thermally active building system (TABS).

This section details the procedure carried out to construct a laboratory test rig suitable for validation against the CFD model and useful for system performance predictions. It outlines the tests carried out and methodology followed. Subsequently the results from the tests are presented and discussed.

Validation and system hierarchy are discussed in subsequent sections in this chapter. The system hierarchy outlines the theoretical capacity derived from the validated performance charts for each system. These capacities are then applied in an OOM.

5.3.1 Methodology

5.3.1.1 Rig Design and Construction

Building on the simulation work it was purposed to construct a test rig that could suitably emulate the modelled conditions and determine the prototype performance. The rig was designed to utilise the prototype constructed for the *Chapter 4* exploratory investigation. Slab component performance was to be tested in this investigation; therefore the slab was isolated in an insulated chamber capable of delivering: constant heat load, air supply to the air network, and an open loop water supply to the embedded pipes. The construction of the laboratory rig was accomplished as follows.

After the investigation reported in *Chapter 4* the recycled chamber was dismantled, the prototype disconnected and removed from the chamber. The Prototype slab was removed

from the specialist frame and lowered onto an insulated pallet. Before lowering the slab onto the insulated slab a dimmable heat mat was spread across the soffit surface (Figure 5.13). The rig was constructed to the millimetre measurements as shown in Figure 5.12.

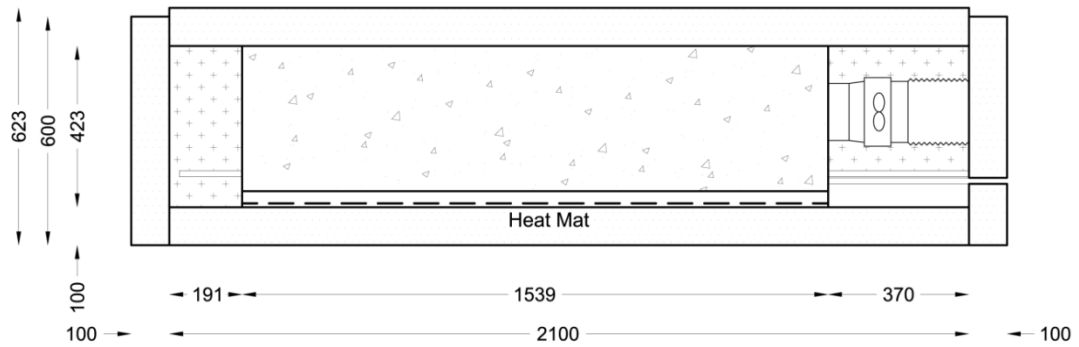


Figure 5.12 - Cross section of WVHC component Rig

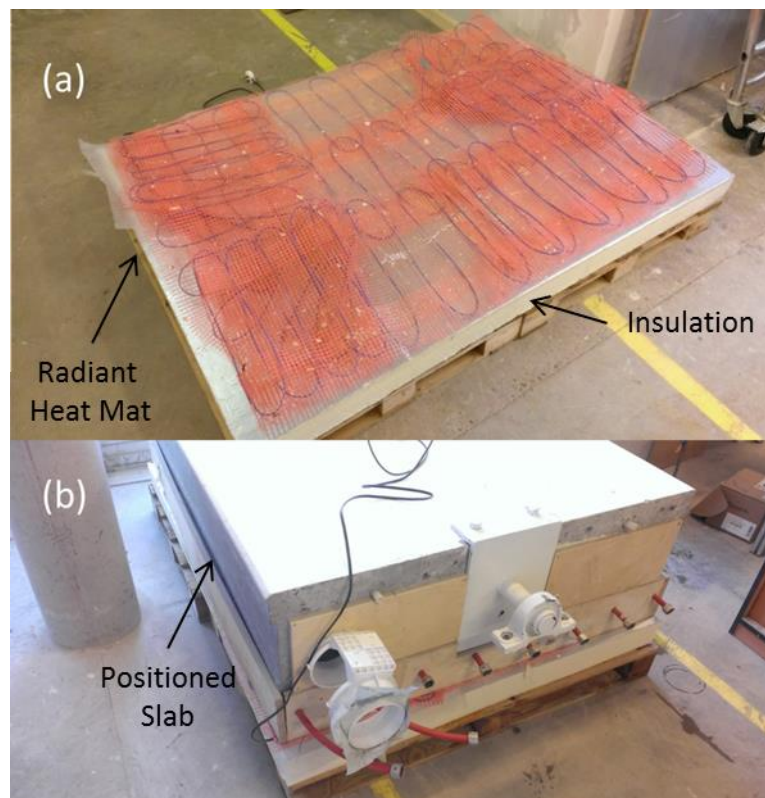


Figure 5.13 - Insulated Palette with (a) Heat Mat and (b) Prototype Slab

An axial fan with maximum fan power of 32W capable of delivering 2.5m/s was installed into the sealed fan bracket. Subsequently the fan was connected to a remote heat pump powered air conditioning system (AC). The AC installed was a Toshiba KYR35-GW/X1c system capable of maintaining room set points of 17 to 35°C.

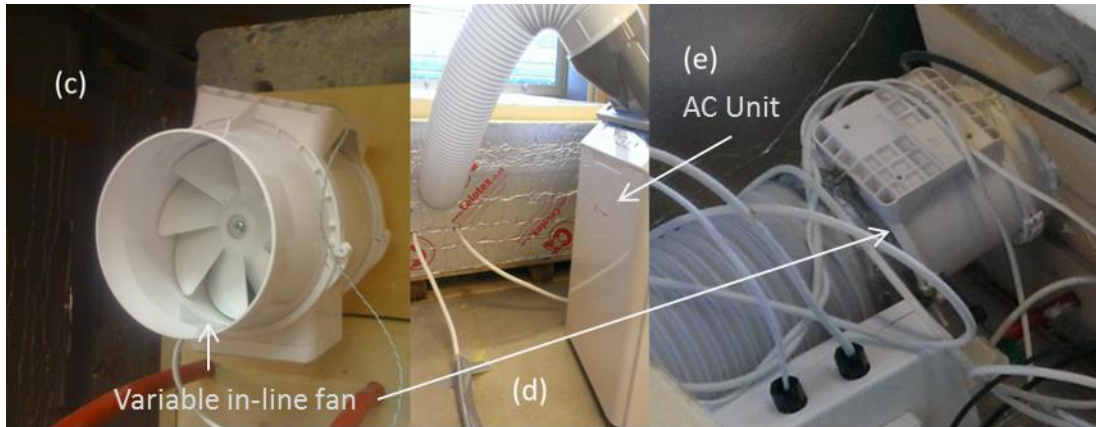


Figure 5.14 - Air system with (c) 32W Fan, (d) AC Unit and (e) connecting duct

An open loop mains water connection was made in Figure 5.15 (g). Flexible rubber hosing supplied water from the mains water connection into the rig via a FT-110 series turbine flow rate sensor (Figure 5.15 (h)). From the water flow meter the inlet water is connected into the embedded water network within the slab via Pex-al-Pex to Pex couplers (Figure 5.15(f)). The outlet-water return pipes water back to the drain to complete the open loop.

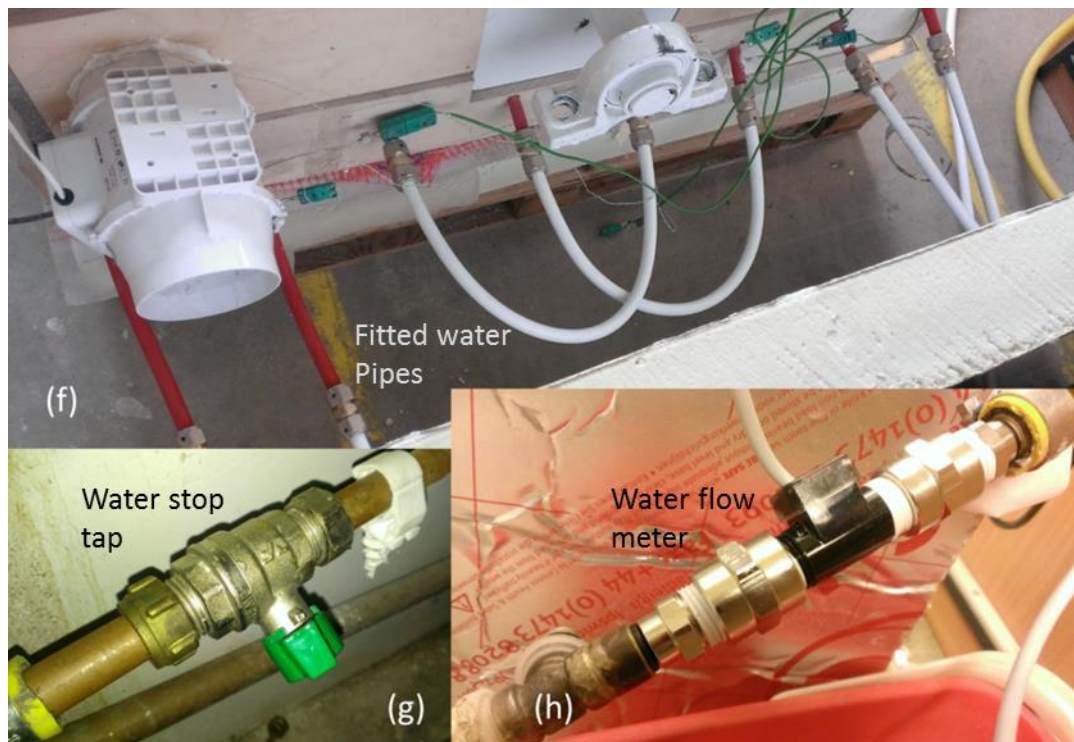


Figure 5.15 - Water System Installation

As explained in Chapter 4, over twenty K-type thermocouples are installed throughout the concrete slab. They were connected to the DT500 DataTaker which was subsequently connected to a PC running the DeLogger software. Additional to the temperature sensors,

the flow meter (Figure 5.15(h)) was connected giving frequency readings. A conversion factor of fifty-five between frequency (Hz) and flow rate (l/min) was issued in the component documents [152]. Instrumentation accuracy was limited as per the levels found in Table 11.1 in Appendix B – Instrument Accuracy and Measurement Errors.

Having connected the air, water and instrumentation the WVHC prototype slab was isolated away from the lab conditions with a surrounding layer of 100mm Celotex with U-value of $0.22\text{W/m}^2\text{K}$ [153] (Figure 5.16). The WVHC prototype performance was ready to be investigated under different system control, heat loads and fluid flow rates.

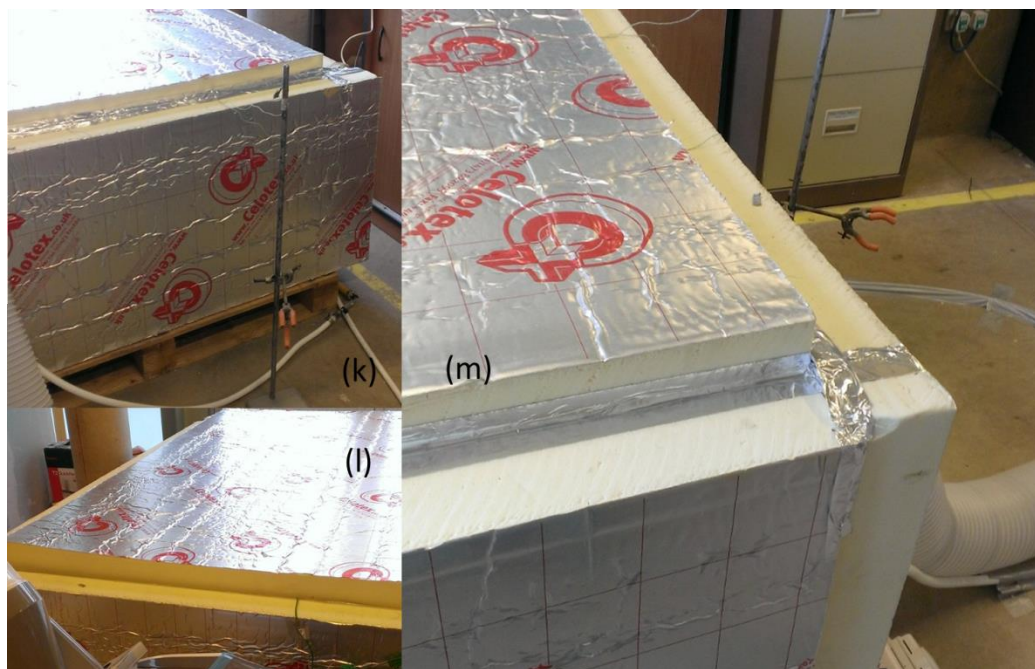


Figure 5.16 - Insulated Slab

5.3.1.2 Experimental Procedure

The installed hollow core prototype component rig had the capability of determining the saturation temperature of passive (PassiveHC), ventilated (VHC), water cooled (WHC) and combined water and ventilated (WVHC) hollow core systems. The different systems were tested at five heat loads; 0, 20, 50, 100 and 250W/m^2 . Ventilation rates were set based on fan powers; 10, 20 and 32W. A target water velocity of 0.58m/s was sought for water cooled systems and averaged between 0.55 and 0.71m/s . The conditions tested are summarised in Table 5.9.

Table 5.9 - Compiled Experiment Conditions Investigated

| System | Air Velocity | Water Velocity | Heat Flux |
|---------------|---------------------|-----------------------|---------------------|
| PassiveHC | 0.2m/s (4acph) | 0.39m/s | 0W/m ² |
| VHC | 1.2m/s | 0.56m/s | 20W/m ² |
| WHC | 2.5m/s | 0.71m/s | 50W/m ² |
| WVHC | | | 100W/m ² |
| | | | 250W/m ² |

The experimental investigation for each saturation test followed the procedure below:

- 1) Set scenario conditions (System, flow rates, heat load) from Table 5.10.
- 2) Maintain scenario conditions for eight to thirty hours until stabilised.
- 3) Unload recorded temperature and frequency data.
- 4) Repeat stages 1-3 with next scenario conditions from Table 5.10.

Table 5.10 - Exhaustive Experiment Conditions for each Scenario Investigated

| System | Air Velocity | Water Velocity | Heat Load | System | Air Velocity | Water Velocity | Heat Load |
|------------|--------------|----------------|------------------------|--------|--------------|----------------|------------------------|
| | <i>m/s</i> | <i>m/s</i> | <i>W/m²</i> | | <i>m/s</i> | <i>m/s</i> | <i>W/m²</i> |
| Passive HC | 0 | 0 | 20 | 20VHC | 1.2 | 0 | 50 |
| Passive HC | 0 | 0 | 50 | 20VHC | 1.2 | 0 | 20 |
| Passive HC | 0 | 0 | 250 | 20VHC | 1.2 | 0 | 100 |
| WHC | 0 | 0.55 | 20 | 20VHC | 1.2 | 0 | 250 |
| WHC | 0 | 0.56 | 0 | 20WVHC | 1.2 | 0.58 | 250 |
| WHC | 0 | 0.55 | 50 | 20WVHC | 1.2 | 0.6 | 0 |
| WHC | 0 | 0.56 | 100 | 20WVHC | 1.2 | 0.66 | 20 |
| WHC | 0 | 0.645 | 250 | 20WVHC | 1.2 | 0.69 | 50 |
| WHC | 0 | 0.389 | 250 | 20WVHC | 1.2 | 0.71 | 100 |
| WHC | 0 | 0.594 | 250 | 32VHC | 2.5 | 0 | 20 |
| VHC | 0.2 | 0 | 20 | 32VHC | 2.5 | 0 | 50 |
| VHC | 0.2 | 0 | 0 | 32VHC | 2.5 | 0 | 100 |
| VHC | 0.2 | 0 | 50 | 32VHC | 2.5 | 0 | 250 |
| VHC | 0.2 | 0 | 250 | 32WVHC | 2.5 | 0.653 | 20 |
| WVHC | 0.2 | 0.55 | 0 | 32WVHC | 2.5 | 0.702 | 50 |
| WVHC | 0.2 | 0.59 | 20 | 32WVHC | 2.5 | 0.613 | 250 |
| WVHC | 0.2 | 0.59 | 50 | 32WVHC | 2.5 | 0.54 | 250 |
| WVHC | 0.2 | 0.59 | 100 | | | | |
| WVHC | 0.2 | 0.63 | 250 | | | | |

5.3.2 Results and Discussion

5.3.2.1 50W/m² Temperature Profiles

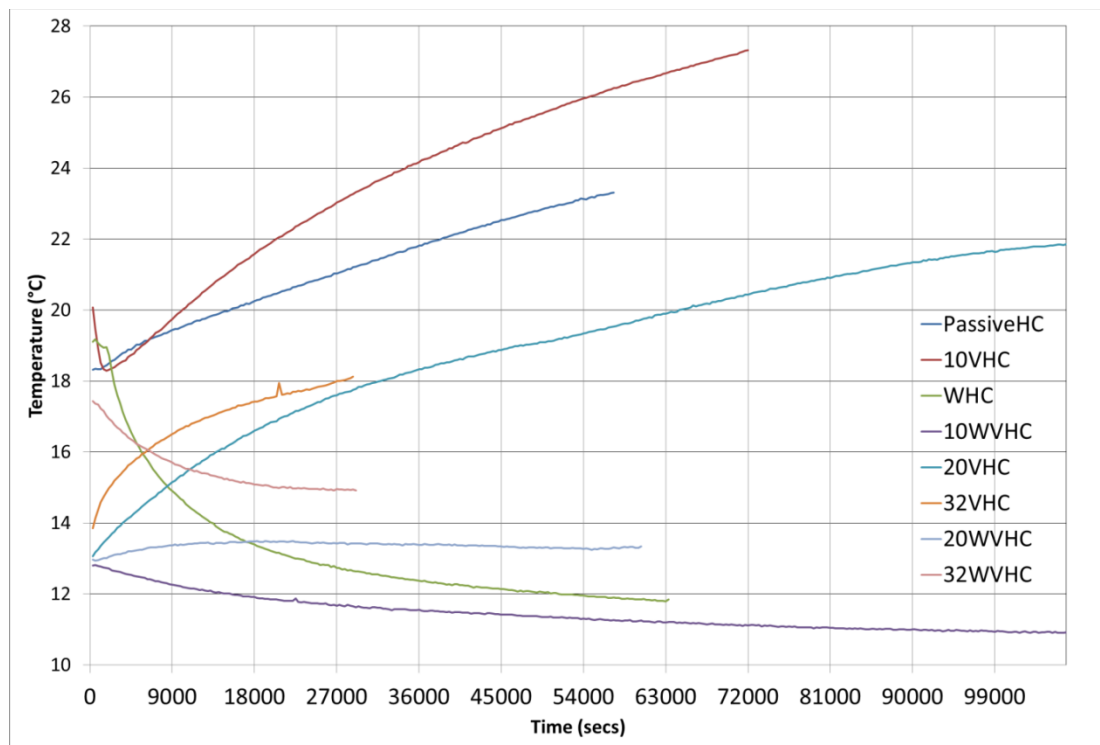


Figure 5.17 - Slab 5 Temperature Profiles for each System with 50W/m² Load

For each scenario the system conditions were specified initially and maintained throughout the test period to allow the system to stabilise. Due to time constraints each scenario was maintained for eight to thirty hours. Ambient conditions throughout the experiments averaged between 14 and 17°C. Water inlet temperature ranged from 7 to 8°C. Variation of less than 0.1°C per five minutes was achieved for all scenarios (Figure 5.17); with the exceptions of the PassiveHC and 10VHC systems where extended test periods would be beneficial.

For the 50W/m² heat load reviewed in Figure 5.17 the lowest final temperatures of 10.9°C and 11.8°C were achieved by the 10WVHC and WHC systems. (Temperatures measured 50mm from the soffit embedded in the centre of the slab, thermocouple 'Slab 5'). The greatest final temperatures, revealing the systems with poorest cooling performance were the 10VHC and PassiveHC systems with temperatures of 27.3°C and 23.3°C, although it is expected that under extended test conditions greater temperatures would be reached. This was due to insufficient cooling ventilation air passing through the slab and dissipating the thermal load.

It was evident from the slab temperature profiles that the water system offers cooling benefit, due to the reduction in temperature from the start point. The combined 20WVHC and 32WVHC systems exhibited stabilisation temperatures below the typical chilled ceiling operation temperature of 16°C. Operating below this temperature in a UK room setting would encourage the onset of soffit condensation [154]. The systems within slab target operating temperatures (18-22°C) were the 20VHC and 32VHC systems.

5.3.2.2 Heat Balances

To further characterise the cooling performance of the system components, heat balances for each scenario were analysed. Figure 5.18 represents the different heating and cooling flows as well as the heat transfer to the surrounding ambient laboratory. Fan and heater loads were measured with power meters throughout the investigation with isolated performance analysed. Slab, air and water cooling were calculated from component physical properties, time step temperature differences and, where applicable, respective flow rates in Table 5.11. Heat transfer through the insulation was calculated from the physical properties in Table 5.11 and the wall temperature difference calculated at each time step. Additional heat lost or gained was calculated as the balance between the other heat flows.

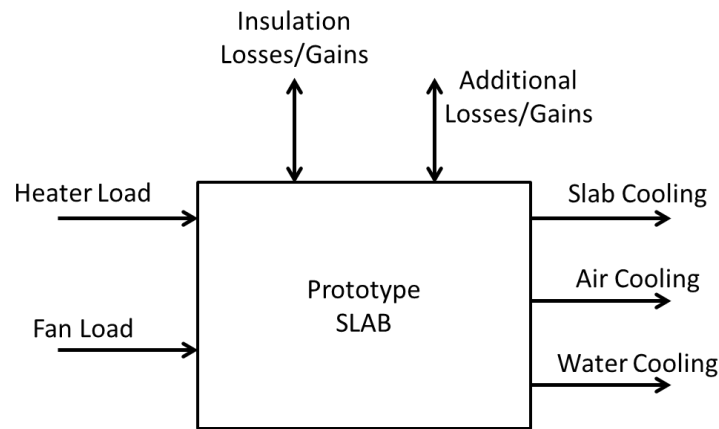


Figure 5.18 - Prototype Slab Heat Balance

Table 5.11 - Air, Water, Slab and Insulation Physical Properties

| | Air | | Water | | Slab | |
|---------------------------|-------|-------------------|------------------|-------------|--------------------|----------------|
| Air Velocity | 2.5 | m/s | Flow Rate | 4.0 | Volume | 0.53 |
| Air Inlet Diameter | 0.125 | m | Flow | $6.7e^{-5}$ | Density | 2300 |
| Air Density | 1.225 | kg/m ³ | Density | 1000 | Cp | 900 |
| Air Mass Flow | 0.037 | kg/s | Mass Flow | 0.067 | Insulation | |
| Air Cp | 1005 | J/kgK | Cp | 4182 | U - Celotex | 0.22 |
| | | | | | Wall Area | 8.841 |
| | | | | | | m ² |

Table 5.12 - Complete Heat Balance Summary

| | Air Velocity | Water Velocity | Fan Load | Heater Load | Insulation Losses | Slab Cooling Rate | Air Cooling Cond Rate | Water Cooling Rate | Heat Rate from Ambient Room |
|-----------|--------------|----------------|----------|-------------|-------------------|-------------------|-----------------------|--------------------|-----------------------------|
| | <i>m/s</i> | <i>m/s</i> | <i>W</i> | <i>W</i> | <i>W</i> | <i>W</i> | <i>W</i> | <i>W</i> | <i>W</i> |
| PassiveHC | 0.0 | 0 | 0 | 36 | -7.6 | -7.7 | 0 | 0 | -20.7 |
| PassiveHC | 0.0 | 0 | 0 | 90 | -4.2 | -58.3 | 0 | 0 | -27.5 |
| PassiveHC | 0.0 | 0 | 0 | 450 | -23.8 | -333.3 | 0 | 0 | -92.9 |
| WHC | 0.0 | 0.55 | 0 | 36 | 4.5 | 16.5 | 0 | -70.6 | 13.6 |
| WHC | 0.0 | 0.56 | 0 | 0 | 6.9 | 18.3 | 0 | -101.4 | 76.2 |
| WHC | 0.0 | 0.55 | 0 | 90 | 5.5 | 3.4 | 0 | -184.3 | 85.4 |
| WHC | 0.0 | 0.56 | 0 | 180 | 4.7 | -7.8 | 0 | -238.1 | 65.9 |
| WHC | 0.0 | 0.65 | 0 | 450 | -3.9 | 26.4 | 0 | -358.3 | -118.1 |
| WHC | 0.0 | 0.39 | 0 | 450 | -2.8 | -22.1 | 0 | -412.0 | -13.1 |
| WHC | 0.0 | 0.59 | 0 | 450 | -2.2 | -27.2 | 0 | -339.2 | -83.7 |
| VHC | 0.2 | 0 | 10.4 | 36 | -4.7 | -24.6 | 0 | 0 | -14.6 |
| VHC | 0.2 | 0 | 10.4 | 0 | -1.2 | -51.7 | 0 | 0 | 42.4 |
| VHC | 0.2 | 0 | 10.4 | 90 | -10.0 | -71.8 | 0 | -0.4 | -18.2 |
| VHC | 0.2 | 0 | 10.4 | 450 | -25.6 | -318.7 | -0.1 | -3.9 | -112.1 |
| WVHC | 0.2 | 0.55 | 10.4 | 0 | 5.3 | 47.7 | 8.0 | -113.6 | 42.3 |
| WVHC | 0.2 | 0.59 | 10.4 | 36 | 5.7 | 1.7 | 11.5 | -125.0 | 59.8 |
| WVHC | 0.2 | 0.59 | 10.4 | 90 | 3.4 | -1.5 | 7.7 | -172.8 | 59.7 |
| WVHC | 0.2 | 0.59 | 10.4 | 180 | 1.7 | -5.0 | 6.1 | -265.8 | 72.6 |
| WVHC | 0.2 | 0.63 | 10.4 | 450 | -0.8 | -21.8 | -12.5 | -413.2 | -2.5 |
| 20VHC | 1.2 | 0 | 20 | 90 | -4.1 | -9.9 | -141.2 | 0 | 45.1 |
| 20VHC | 1.2 | 0 | 20 | 36 | -2.9 | 62.1 | -126.8 | 0.2 | 11.4 |
| 20VHC | 1.2 | 0 | 20 | 180 | -0.2 | -75.6 | -130.5 | -0.9 | 7.2 |
| 20VHC | 1.2 | 0 | 20 | 450 | -13.2 | -65.1 | -380.8 | 0.3 | -11.2 |
| 20WVHC | 1.2 | 0.58 | 20 | 450 | 1.3 | -16.1 | -65.6 | -303.1 | -86.7 |
| 20WVHC | 1.2 | 0.60 | 20 | 0 | 3.2 | 37.2 | 5.0 | -167.1 | 101.9 |
| 20WVHC | 1.2 | 0.66 | 20 | 36 | 3.4 | -1.0 | 8.2 | -184.4 | 117.8 |
| 20WVHC | 1.2 | 0.69 | 20 | 90 | 4.1 | -12.8 | 12.2 | -224.7 | 110.9 |
| 20WVHC | 1.2 | 0.71 | 20 | 180 | 4.8 | -14.3 | -5.8 | -289.4 | 104.5 |
| 32VHC | 2.5 | 0 | 32 | 36 | -7.5 | 138 | -354.9 | 0 | 157.6 |
| 32VHC | 2.5 | 0 | 32 | 90 | -0.5 | -44.9 | -185.9 | -0.4 | 109.4 |
| 32VHC | 2.5 | 0 | 32 | 180 | -3.4 | -51.4 | -262.5 | -0.4 | 104.6 |
| 32VHC | 2.5 | 0 | 32 | 450 | -7.3 | -107.8 | -463.4 | -0.8 | 97.3 |
| 32WVHC | 2.5 | 0.65 | 32 | 36 | 3.6 | 19.6 | -11.8 | -218.6 | 139.6 |
| 32WVHC | 2.5 | 0.70 | 32 | 90 | 2.9 | -14.2 | -28.8 | -248.9 | 138.5 |
| 32WVHC | 2.5 | 0.61 | 32 | 450 | 0.5 | 0.2 | -118.4 | -288.5 | -75.7 |
| 32WVHC | 2.5 | 0.54 | 32 | 450 | 1.3 | -8.7 | -107.0 | -284.2 | -83.8 |

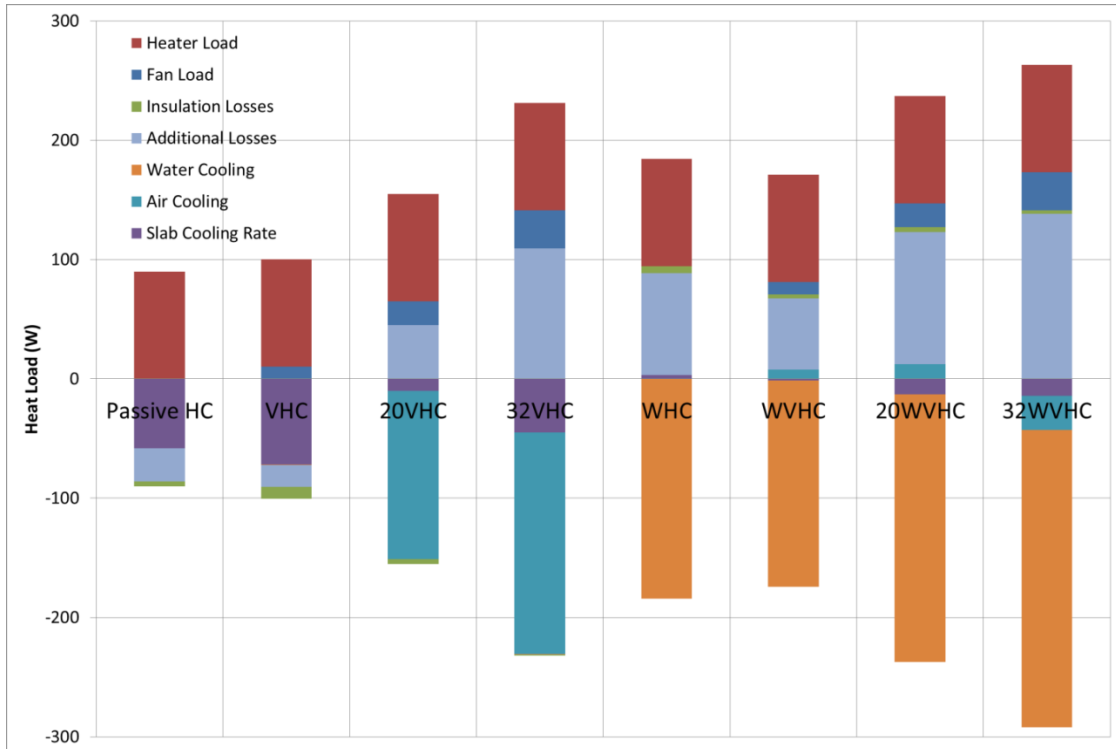


Figure 5.19 - Heat Balance Graph for 50W/m² Scenarios

For each system condition a final thirty minute average was calculated and analysed. A complete table of heat balance characterisation can be found in Table 5.12. Figure 5.19 characterises the final thirty minute performance of each system under a 50W/m² heat load.

During the water activated scenarios (WHC or WVHC systems) the system stabilised below ambient temperature. The heat transfer through the insulation layer reversed in direction. Through the ventilated slab systems (20VHC and 32VHC) the air cooling provided the majority of the cooling. For the WHC and WVHC systems the bulk of cooling was carried out by the water component.

5.3.2.3 Coefficient of Performance (COP)

Further analysis of the heat balance enabled the generation of COP figures for each scenario analysed.

Equation 5.2

$$COP = \frac{\text{Total Cooling}}{\text{Fan Power} + \text{Estimated Pump Power}}$$

The *total cooling* carried out by the slab, air and water components was summed from the heat balance components. Since water was transported to, through and from the rig under mains pressure no energy was consumed by the rig to transport the water, therefore an

estimated pump power calculation was calculated. *Estimated pump power* was calculated from data in Chapter 4 where the Conrad submersion pump was capable of delivering 4l/min from 160W of power. For the system analysis this was converted to a specific pump power of 228.6W/m/s. This figure, multiplied by the inlet water velocity, gave the *estimated pump power*. COP figures for each system, at different heat loads, are presented in Table 5.13 below.

Table 5.13 - COP Figures at different Heat Loads

| 0W/m ² | | 20W/m ² | | 50W/m ² | | 100W/m ² | | 250W/m ² | |
|-------------------|------------|--------------------|------------|--------------------|------------|---------------------|------------|---------------------|------------|
| <i>System</i> | <i>COP</i> | <i>System</i> | <i>COP</i> | <i>System</i> | <i>COP</i> | <i>System</i> | <i>COP</i> | <i>System</i> | <i>COP</i> |
| VHC | 5.0 | 32VHC | 6.8 | 20VHC | 7.6 | 20VHC | 10.4 | VHC | 31.0 |
| 20WVHC | 0.8 | 20VHC | 3.2 | 32VHC | 7.2 | 32VHC | 9.8 | 20VHC | 22.3 |
| WHC | 0.6 | VHC | 2.4 | VHC | 6.9 | WHC | 1.9 | 32VHC | 17.9 |
| WVHC | 0.4 | 32WVHC | 1.2 | 32WVHC | 1.5 | WVHC | 1.8 | 1/2WHC | 4.9 |
| | | 20WVHC | 1.0 | WHC | 1.4 | 20WVHC | 1.7 | WVHC | 2.9 |
| | | WVHC | 0.8 | 20WVHC | 1.3 | | | 20WVHC | 2.5 |
| | | WHC | 0.4 | WVHC | 1.1 | | | WHC | 2.5 |
| | | | | | | | | 32WVHC | 2.5 |

From review of the COP figures in Table 5.13 the VHC systems consistently outperformed the WHC and WVHC systems; due to the added energy required to pump the water through the system. The greater the thermal load, the better performing WHC systems were. Based on these findings, water activated systems should therefore only be operated as cooling support systems, when the air system is failing to maintain comfort temperatures.

Further, from the results in Table 5.13 the COP figures suggested increased efficiency for water based systems when water flow as reduced to a required minimum. In Table 5.13 the 1/2WHC system operated with a water velocity of 0.38m/s in contrast to the typical 0.55-0.71m/s. This reduction in water velocity achieved a COP of 4.9 for the 1/2WHC system; almost double that of the WHC COP of 2.5.

5.3.2.4 Final Slab Temperatures versus Heat Load

To further review the performance of the systems and contrast against modelled performance final slab temperatures were plotted against the imposed heat load for each system. Table 5.17 documents the average final slab temperatures recorded in the laboratory study. Subsequently lines of best-fit were fitted to the data (Figure 5.20). The gradient of this line can be regarded as the *performance coefficient* (k) (Table 5.15) and was useful for reviewing system performance. The *performance coefficient* enables an understanding and

development of a system hierarchy and enables the prediction of maximum system cooling capability.

Table 5.14 - Laboratory Final Temperatures

| Heat Flux W/m ² | Passive HC | 10VHC (0m/s) | 20VHC (1.2m/s) | 32VHC (2.5m/s) | WHC (0.55-0.56m/s) | 10WVHC | 20WVHC | 32WVHC |
|-------------------------------|------------|-----------------|-------------------|-------------------|-----------------------|--------|--------|--------|
| 0 | - | 18.7 | 18.7 | - | 9.9 | 10.0 | 13.3 | - |
| 20 | 29.1 | 22.0 | 23.0 | 21.0 | 10.6 | 10.2 | 13.4 | 15.8 |
| 50 | 23.3 | 27.4 | 23.3 | 19.0 | 12.2 | 11.4 | 13.7 | 15.3 |
| 100 | - | - | 24.9 | 24.8 | 12.1 | 13.7 | 14.9 | - |
| 250 | 48.9 | 48.3 | 42.0 | 34.2 | 19.4 | 16.5 | 18.6 | 18.9 |

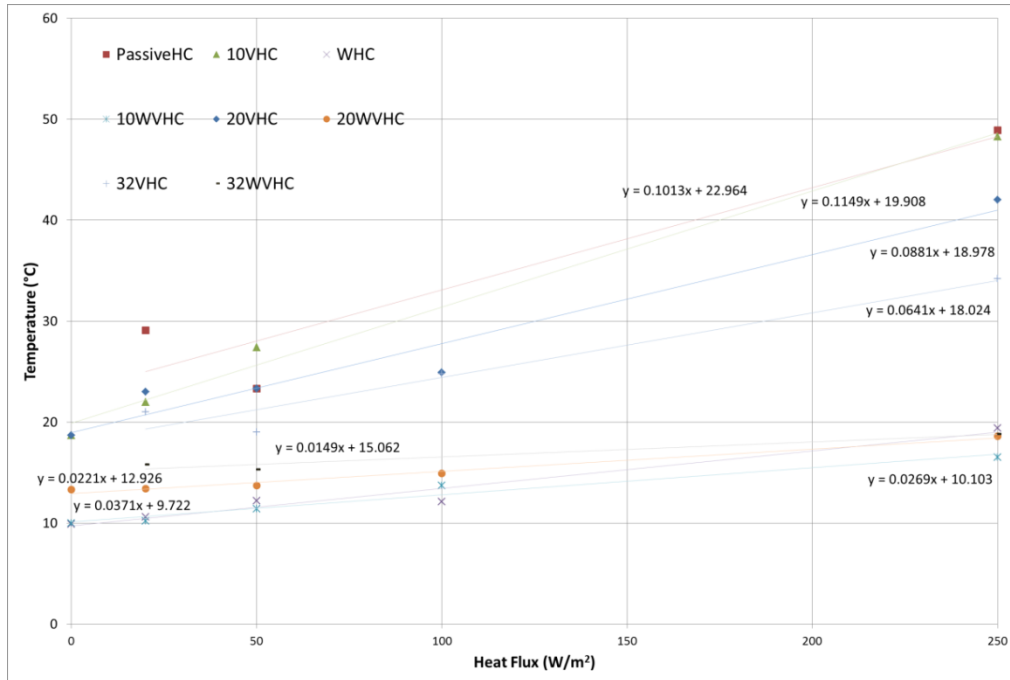


Figure 5.20 - Final Slab Temperature against Heat Load Plot

Table 5.15 - Performance Coefficients

| System | Performance Coefficient |
|------------|-------------------------|
| Passive HC | 0.1013 |
| 10VHC | 0.1149 |
| 20VHC | 0.0881 |
| 32VHC | 0.0641 |
| WHC | 0.0371 |
| 10WVHC | 0.0269 |
| 20WVHC | 0.0221 |
| 32WVHC | 0.0149 |

PassiveHC and 10VHC demonstrated the weakest cooling performance. It was expected that the 10VHC system would outperform the PassiveHC system however the reverse was observed. Significant error in the PassiveHC model may be the cause, however further investigation of fan behaviour at low wattage revealed that when fan power was less than 18W it was insufficient to overcome the initial inertia, and the fan blades did not rotate. It was therefore reasonable to conclude that the 10VHC system, with a 10W fan loading, was not sufficient to pass ventilation air through the hollow core network. The 10VHC system therefore operated as a passive slab, with an additional 10W thermal load emitted from the fan motor unit.

The 32WVHC system offered the most significant cooling performance, utilising the water and air cooling benefits in the system. From the performance coefficients a clear hierarchy of cooling performance was developed. Maximum theoretical cooling, capable of maintaining the slab at 22°C was also deduced using the equations generated in Figure 5.20.

Further review of the *performance coefficients* was useful for analysis of flowrate benefit. In the VHC systems, the greater the fan power, the better the performance of the system. From the initial modelling investigation it was deduced that there was an inverse square relationship between air velocity and performance coefficients. Analysis of the limited data available (velocities between 0.2&2.5m/s) suggested *air velocities* varied with respect to *performance coefficients* through the following relationship. Further investigation strength testing Equation 5.3 would be beneficial for the development of a complete engineering design tool for VHC systems.

Equation 5.3

$$\text{Air Velocity} = -3.913\ln(\text{Performance Coefficient}) - 8.2664$$

5.3.3 Summary of Findings

The laboratory testing of the hollow core prototype component enabled system performance to be quantified. Final slab temperature, heat balances, COP and performance coefficients have been measured and calculated from the data recorded.

It was found that a fan loading of 10W was insufficient to rotate the fan blades or deliver the intended 0.22m/s of air. The lowest final slab temperature of all the 50W/m² systems was achieved by the 10WVHC system (11.4°C). Ideal final slab temperatures (18-22°C) were achieved by the 20VHC (22°C) and 32VHC system (19.0°C).

VHC systems displayed greater energy efficient cooling with COP figures consistently higher than WHC and WVHC alternatives throughout the heat load conditions tested. 32WVHC displayed the greatest cooling capacity with a performance coefficient of 0.015. All WHC and WVHC systems achieved performance coefficients less than 0.04. The VHC only systems recorded performance coefficients ranging from 0.064 – 0.115.

Following comparison and validation with modelled performance a clear hierarchy of cooling performance was developed. Maximum theoretical cooling, capable of maintaining the slab at 22°C was also deduced in the following section, using the equations generated in Figure 5.20.

5.4 Performance Comparison and Validation

5.4.1 Initial Comparison

5.4.1.1 Method

Following the completion of the CFD modelling and laboratory testing of the component hollow core the results of each investigation were reviewed in an effort to validate the work. Two key indicators were used to carry out the comparative validation: *final slab temperatures* and *performance coefficients*. The *performance coefficients* assessed the performance of the technology throughout the increasing heat loads. The *final slab temperatures* were useful for assessing performance of the equivalent technologies under comparable conditions.

5.4.1.2 Performance Indicators

5.4.1.2.1 Final Slab Temperature

The CFD modelling was carried out at steady state; therefore the final temperatures occurred when the scenario conditions reached equilibrium. Initially temperatures compared were calculated as the average temperature at the soffit at the end of the simulation, when the model energy balance had stabilised.

The comparable figure measured in the laboratory tests was calculated from an average of the calibrated embedded slab temperatures over the final thirty minutes. In total, during prototype construction, nine K-type thermocouples were embedded on the original soffit layer, prior to the approximately 50 mm concrete addition. For each time step an average slab temperature was calculated from the nine thermocouple's calibrated readings.

To level out time variation, a final thirty minute average was calculated from the average slab temperatures. This *final average temperature* reading for each scenario tested was compared against the area average CFD soffit temperature.

5.4.1.2.2 Performance Coefficient

On a scenario to scenario basis this measure enabled performance comparison. To validate the simulation of system performance, review of the performance coefficients was undertaken. Performance coefficients were calculated as the gradient of the line plotting scenario *heat load* against *final slab temperature* for each system operation.

Equation 5.4

$$k = \frac{(T_{slab,\infty} - T_{ambient,0})}{Heat\ Load}$$

Heat load was specified by the user in the modelling investigation. For the laboratory tests the heat load was measured from a power meter linked to the radiant heat mat. The power delivered to the heat mat was assumed constant throughout the test period. The assumed constant power was subsequently divided by the soffit area (1.8m²) to determine the soffit heat load.

5.4.1.3 Results

Table 5.16 - Modelling Final Temperatures

| Soffit Heat Flux W/m ² | VHC (0.22m/s) | VHC (0.88m/s) | 3 Core (1.5m/s) | 4 Core (1.5m/s) | WHC (0.58m/s) |
|--------------------------------------|------------------|------------------|--------------------|--------------------|------------------|
| <i>Final Soffit Temperature (°C)</i> | | | | | |
| 0 | 17.9 | | 17.9 | 19.0 | 14.9 |
| 2 | 18.8 | 17.9 | 19.1 | 19.7 | 14.9 |
| 10 | 22.6 | 20.0 | 24.1 | 22.6 | 15.1 |
| 20 | 27.4 | 22.2 | 30.2 | 25.8 | 15.5 |
| 30 | 32.2 | 24.3 | 36.4 | 28.4 | 15.8 |
| 40 | 37.0 | 26.5 | 42.6 | 31.0 | 16.1 |
| 50 | 41.8 | 28.7 | 48.7 | 33.6 | 16.5 |
| 100 | 65.7 | 39.5 | 79.6 | 46.7 | 18.1 |
| 178 | 103.1 | 56.3 | 127.8 | 66.9 | 20.6 |

Table 5.17 - Laboratory Final Temperatures

| Heat Flux W/m ² | Passive HC | 10VHC (0m/s) | 20VHC (1.2m/s) | 32VHC (2.5m/s) | WHC (0.55-0.56m/s) | 10WVHC | 20WVHC | 32WVHC |
|--|------------|-----------------|-------------------|-------------------|-----------------------|--------|--------|--------|
| <i>Final TC Plane Average Temperature (°C)</i> | | | | | | | | |
| 0 | | 18.7 | 18.7 | | 9.9 | 10 | 13.3 | |
| 20 | 29.1 | 22 | 23 | 21 | 10.6 | 10.2 | 13.4 | 15.8 |
| 50 | 23.3 | 27.4 | 23.3 | 19 | 12.2 | 11.4 | 13.7 | 15.3 |
| 100 | | | 24.9 | 24.8 | 12.1 | 13.7 | 14.9 | |
| 250 | 48.9 | 48.3 | 42 | 34.2 | 19.4 | 16.5 | 18.6 | 18.85 |

Table 5.16 displays the final temperature results generated from the modelling investigation. Table 5.17 tabulates the final temperature results generated from the laboratory investigation. The differences in the scenarios modelled, due to unforeseen laboratory limitations, meant it was not possible to carry out a direct comparative validation, based on

equivalent scenario final temperatures. System performance was therefore reviewed based on performance coefficients calculated from respective heat loads and final slab temperatures reported in Table 5.6 and Table 5.15.

Table 5.18 - Performance Coefficient Comparison

| Modelled | | Laboratory | |
|------------------------|--------------------------------|----------------------|--------------------------------|
| <i>System</i> | <i>Performance Coefficient</i> | <i>System</i> | <i>Performance Coefficient</i> |
| VHC (0.22m/s) | 0.4787 | Passive HC | 0.1013 |
| VHC (0.88m/s) | 0.2161 | VHC (10Wfan) | 0.1149 |
| 3 Core (1.5m/s) | 0.6175 | VHC (20Wfan) | 0.0881 |
| 4 Core (1.5m/s) | 0.2674 | VHC (32Wfan) | 0.0641 |
| WHC (0.58m/s) | 0.0324 | WHC | 0.0371 |
| | | WVHC (10Wfan) | 0.0269 |
| | | WVHC (20Wfan) | 0.0221 |
| | | WVHC (32Wfan) | 0.0149 |

From Table 5.19 the performance of the WHC system was comparable. For the air based systems there was a distinct difference between the modelled and laboratory tested results. Further investigation was required to understand the source of such differences and make steps to reduce the effect of these differences, in an effort to validate the simulation of the prototype component. Although WVHC systems were not modelled their results were included in table 5.19 to offer a comparison in cooling performance between the different systems. Their performance was picked up in the Optimum Operating Method section after validation of the model.

5.4.2 Table of Differences

In an effort to reduce the differences between the model and laboratory findings, and ultimately validate the model, a *table of differences* was assembled. Categorized into *conditions*, *geometry* and *roughness*; Table 5.19 enables a systematic reduction of differences. From the *table of differences* a systematic approach was taken to difference reduction by refining assumptions and improving the similarity between the models.

Table 5.19 - Table of Identified Differences

| Identified Difference | Area of Modelling | Laboratory | Remedial Action |
|--|---|---|---|
| CONDITIONS | | | |
| Heat Transfer at the Boundary | Zero heat transfer or heat loss at the boundary | Heat lost through insulated walls | Heat loss quantified through heat balance and data plotted against effective thermal load |
| Flow Rate | Constant air (0.22,0.88 m/s) and water (0.56m/s) velocities | Varied air (0-2.4m/s) and water (0.4-0.7m/s) velocities | Select average velocities for comparison cases and re-model |
| Heat Delivery | Uniform heat flux ranging from 0-178W/m ² , acting on the soffit surface | Radiant heat mat effective load of 4-250W/m ² delivered 0-50mm from soffit | Performance assessed across a range of loads |
| Ambient, Initial and Inlet Temperatures | Constant air temperature of 18°C | Average ambient temperature of 15-18°C | Re-model with average lab temperatures |
| | Constant water temperature of 15°C | Average water temperature of 7-8°C | Re-model with average lab temperatures |
| Temperature Sensor Position | Soffit temperature analysed | Water pipe slab layer temperature analysed | Analyse using water pipe layer (0.58mm from soffit) temperatures |
| Time to Stabilise | No constraint | Time limited to 8-48hrs | No further action |
| GEOMETRY | | | |
| Slab Dimensions | Slab design measurements | Prototype dimensions | Re-model with prototype dimensions |
| Slab Geometry | Perfect circular cores | Mushroom shaped cores | Re-model with more accurate cores |
| | Hollow cores | Level of blocking due to metal pins | Re-model with more accurate cores |
| | Even cross-overs | 2 cross-overs only half exposed | Re-model with more accurate cross-overs |

| | | | |
|---------------------------------|--------------------------------------|--|---|
| | Full depth cross-overs | Cross-overs drilled to 70% core depth | Re-model with more accurate cross-overs |
| Surrounding Air | No surrounding air | 42mm air layer beneath soffit | Re-model with air layer |
| ROUGHNESS | | | |
| Roughness of Air Channel | Smooth surfaces, specified roughness | Rough concrete surface on inside of air channels | Adjust modelling parameters |
| Roughness of Soffit | Smooth surface | Rough surface | Adjust modelling parameters |

5.4.3 Laboratory Data Calibration

The first stage of difference reduction was to calculate an *effective thermal load* (eLoad) for each laboratory scenario. The eLoad (W/m²) was then plotted against *average final slab temperature* to generate new performance coefficients. The eLoad was calculated based from the final thirty-minute average heat balance.

Equation 5.5

$$\text{Effective Thermal Load } \left(\frac{W}{m^2}\right) = \frac{[\text{Fan Power}(W) + \text{Heater Power}(W) - \text{Wall Heat Transfer}(W) - \text{Heat Lost}(W)]}{\text{Soffit Area}(m^2)}$$

Heat lost was calculated from the heat balance per time step, taking into account the slab, air and water cooling power.

Equation 5.6

$$\text{Heat Lost}(W) = \text{Fan Power}(W) + \text{Heater Power}(W) - \text{Wall Heat Transfer}(W) - \text{Slab, Air and Water Cooling}(W)$$

Slab, air and water cooling power was calculated from their respective physical properties, average flow rates and the temperature change observed from one time step to the next. From substituting Equation 5.6 into Equation 5.5 the eLoad was equal to the effective cooling observed experimentally in the slab, air and water components. Any thermal load greater than that observed in the component temperature changes were reasonably considered lost to the atmosphere. To reasonably validate the laboratory work against the modelling, since no boundary heat transfer occurs in the laboratory model, the eLoad should be considered when calculating the performance coefficients. Table 5.21 documents the effective thermal loads for each scenario against their respective average final slab temperatures. Comparison

of final slab temperatures with Table 5.16 was still ineffective due to the different heating conditions modelled. Plots of eLoad against final temperature were therefore generated and respective performance coefficients generated.

Table 5.20 - Effective Thermal Load Final Temperatures

| Heater | (W/m^2) | 0 | 20 | 50 | 100 | 250 | |
|----------------|-------------|-------------|------|-------|-------|-------|-------|
| Load | | | | | | | |
| Passive | eLoad | (W/m^2) | | 4.3 | 32.4 | 185.2 | |
| | Temp | °C | | 29.1 | 23.3 | 48.9 | |
| 10VHC | eLoad | (W/m^2) | 28.7 | 15.1 | 40.1 | 179.3 | |
| | Temp | °C | 18.7 | 22.0 | 27.4 | 48.3 | |
| 20VHC | eLoad | (W/m^2) | | 35.8 | 83.9 | 115 | 247.6 |
| | Temp | °C | | 23.0 | 23.3 | 24.9 | 42.0 |
| 32VHC | eLoad | (W/m^2) | | 121.2 | 128.3 | 174 | 317.8 |
| | Temp | °C | | 21.0 | 19.0 | 24.8 | 34.2 |
| WHC | eLoad | (W/m^2) | 46.2 | 30.1 | 100.5 | 139.2 | 202.3 |
| | Temp | °C | 9.9 | 10.6 | 12.2 | 12.1 | 19.4 |
| 10WVHC | eLoad | (W/m^2) | 32.2 | 62.2 | 90.8 | 147.1 | 253.9 |
| | Temp | °C | 10 | 10.2 | 11.4 | 13.7 | 16.5 |
| 20WVHC | eLoad | (W/m^2) | 69.5 | 98.4 | 125 | 171.8 | 213.7 |
| | Temp | °C | 13.3 | 13.4 | 13.7 | 14.9 | 18.6 |
| 32WVHC | eLoad | (W/m^2) | | 117.3 | 146.3 | | 224 |
| | Temp | °C | | 15.8 | 15.3 | | 18.85 |

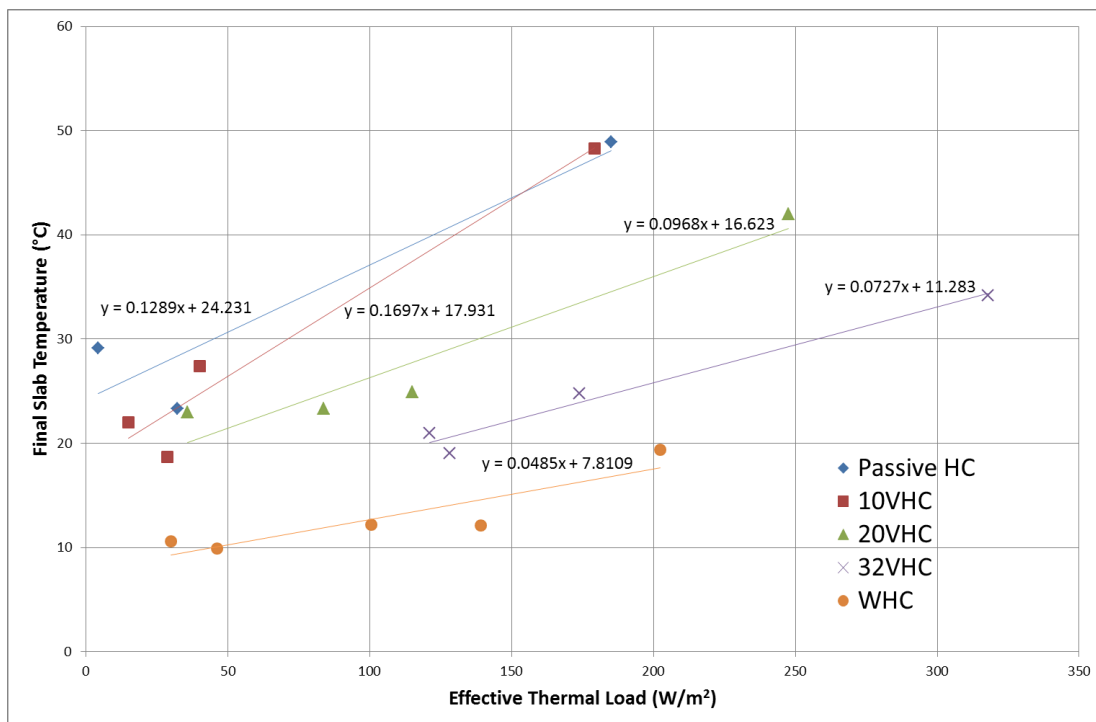


Figure 5.21 - Effective thermal load (eLoad) against final average slab temperatures

Table 5.21 - Effective thermal load (eLoad) performance coefficients

| Modelled | | Laboratory | |
|-----------------|-------------------------|---------------|-------------------------|
| System | Performance Coefficient | System | Performance Coefficient |
| VHC (0.22m/s) | 0.4787 | Passive HC | 0.1289 |
| VHC (0.88m/s) | 0.2161 | VHC (10Wfan) | 0.1697 |
| 3 Core (1.5m/s) | 0.6175 | VHC (20Wfan) | 0.0968 |
| 4 Core (1.5m/s) | 0.2674 | VHC (32Wfan) | 0.0727 |
| WHC (0.58m/s) | 0.0324 | WHC (0.55m/s) | 0.0485 |

Extracting the performance coefficients from Figure 5.21 Table 5.19 was updated to form Table 5.22. Most notably the difference between the modelled and laboratory tested water system performance increased. In general the air based system performance coefficients were closer, but were still far from a comparable match. Noticeably the same system hierarchy was observed in both investigations, with increased air speed offering better cooling (lower performance coefficients) whilst the water system remains the best cooling option. The almost tenfold enhancement from the water system was not observed in the laboratory cases.

Despite estimating an eLoad, comparative with the perfect thermal load modelled, the reduction in difference was not sufficient to consider the modelling valid. It was therefore concluded that re-modelling of the slab system was required.

5.4.4 Re-Modelling

5.4.4.1 Simulation Conditions

Essential to validating the modelling was to ensure the modelled conditions best replicated the laboratory conditions. Average ambient conditions and water inlet conditions were used for the modelling inputs. Average readings from the laboratory scenarios for the 20VHC, 32VHC and WHC systems were used during the validation process. Both *thermal load* and *eLoad* were calculated to aid the validation review. Further, the final reference temperature extracted from the modelling was calculated as the average slab temperature at the thermocouple plane, 0.58mm above the soffit.

Table 5.22 - 20VHC Conditions and Final Slab Temperatures

| 20VHC | | | | |
|---------------|---------------------|--------------|------------------------|-------------|
| | | | Lab | Re-Modelled |
| Thermal Loads | Ambient Temperature | Air Velocity | Final Slab Temperature | |
| W/m^2 | $^{\circ}C$ | m/s | $^{\circ}C$ | $^{\circ}C$ |
| 20 | 16.9 | 1.2 | 23.0 | 20.6 |
| 50 | 15.3 | 1.2 | 23.3 | 24.7 |
| 100 | 15.3 | 1.2 | 24.9 | 34.0 |
| 250 | 17.1 | 1.2 | 42.0 | 64.0 |
| 35.8 | 16.9 | 1.2 | 23.0 | 23.6 |
| 83.9 | 15.3 | 1.2 | 23.3 | 31.0 |
| 115 | 15.3 | 1.2 | 24.9 | 36.9 |
| 247.6 | 17.1 | 1.2 | 42.0 | 63.5 |

Table 5.23 - 32VHC Conditions and Final Slab Temperatures

| 32VHC | | | | |
|---------------|-------------|----------|------------------------|-------------|
| Thermal Loads | Ambient | Air | Lab | Re-Modelled |
| | Temperature | Velocity | Final Slab Temperature | |
| W/m^2 | $^{\circ}C$ | m/s | $^{\circ}C$ | $^{\circ}C$ |
| 20 | 18.1 | 2.5 | 21.0 | 20.9 |
| 50 | 16.5 | 2.5 | 19.0 | 23.4 |
| 100 | 16.6 | 2.5 | 24.8 | 30.4 |
| 250 | 18.1 | 2.5 | 34.2 | 52.6 |
| 121.2 | 18.1 | 2.5 | 21.0 | 34.8 |
| 128.3 | 16.5 | 2.5 | 19.0 | 34.2 |
| 174 | 16.6 | 2.5 | 24.8 | 40.6 |
| 317.8 | 18.1 | 2.5 | 34.2 | 62.0 |

Table 5.24 - WHC Conditions and Final Slab Temperatures

| WHC | | | | | |
|---------------|-------------|-------------|----------|------------------------|-------------|
| Thermal Loads | Ambient | Water | Water | Lab | Re-Modelled |
| | Temperature | Temperature | Velocity | Final Slab Temperature | |
| W/m^2 | $^{\circ}C$ | $^{\circ}C$ | m/s | $^{\circ}C$ | $^{\circ}C$ |
| 20 | 16.2 | 7.7 | 0.55 | 10.6 | 8.5 |
| 50 | 16 | 8.1 | 0.55 | 12.2 | 9.7 |
| 100 | 14.6 | 7.3 | 0.56 | 12.1 | |
| 250 | 16.5 | 10.2 | 0.59 | 19.4 | 17.9 |
| 30.1 | 16.2 | 7.7 | 0.55 | 10.6 | 8.8 |
| 100.5 | 16 | 8.1 | 0.55 | 12.2 | 11.4 |
| 139.2 | 14.6 | 7.3 | 0.56 | 12.1 | 11.8 |
| 202.3 | 16.5 | 10.2 | 0.59 | 19.4 | 16.5 |

Table 5.22, Table 5.23 and Table 5.24 tabulate the average laboratory conditions inputs in the re-modelling process and document the laboratory and re-modelling final slab temperatures. During the re-modelling both the actual thermal load and the effective

thermal loads were simulated. Those final slab temperatures where comparable alignment ($\pm 2^{\circ}\text{C}$) was found have been boxed.

For certain scenarios, the modelling has produced valid results, closely matching the final slab temperatures observed in the laboratory tests. This has not been the case for all scenarios. In the 32VHC system investigation there was a better final slab temperature fit when the actual thermal loads were modelled as opposed to the eLoads. System review of performance coefficients was therefore carried out for both the actual thermal load (aLoad) and the eLoad.

Table 5.25 - Performance Coefficient Comparison under same conditions

| Modelled | | | Laboratory | | |
|--------------------------|-------------------------|--------|--------------------------|-------------------------|--------|
| System | Performance Coefficient | | System | Performance Coefficient | |
| | aLoad | eLoad | | aLoad | eLoad |
| VHC (20Wfan) | 0.1914 | 0.1912 | VHC (20Wfan) | 0.0881 | 0.0968 |
| VHC (32Wfan) | 0.1412 | 0.1425 | VHC (32Wfan) | 0.0641 | 0.0727 |
| WHC (0.55m/s) | 0.0408 | 0.043 | WHC (0.55m/s) | 0.0371 | 0.0485 |

From review of the performance coefficients, when re-modelled under laboratory conditions, the figures in Table 5.25 demonstrated a close fit between the WHC systems. It was reasonable to consider that despite the differences between modelling and laboratory exact geometry, sufficient matching of performance coefficients has been reached to verify the WHC model a valid representation of WHC slab performance.

In the re-modelled systems the VHC coefficients of performance were approximately double of those found experimentally. Further difference reduction was therefore required to improve the validity of the VHC model.

5.4.4.2 Geometry Refinement

The initial VHC model had been constructed from slab design measurements, quoting the slab dimensions at 325 by 1,197 by 1,500mm [155]. Core diameter was specified at 140mm diameter and crossovers and outlet diameter at 125mm. During the laboratory investigation

specific measurements for the prototype slab were taken. They found a slight discrepancy between figures.

As measured, the prototype slab had the dimensions 358 by 1,165 by 1,500mm. The core cross section has a vertical height of 155mm and a width of 145mm. The crossovers and outlet diameter is 125mm. The prototype also has two cores foreshortened by 470mm leaving an effective air channel length of 1,030mm. The VHC model was therefore remodelled with the measured prototype geometry. The core cross section was approximated to be cylindrical with a diameter of 150mm.

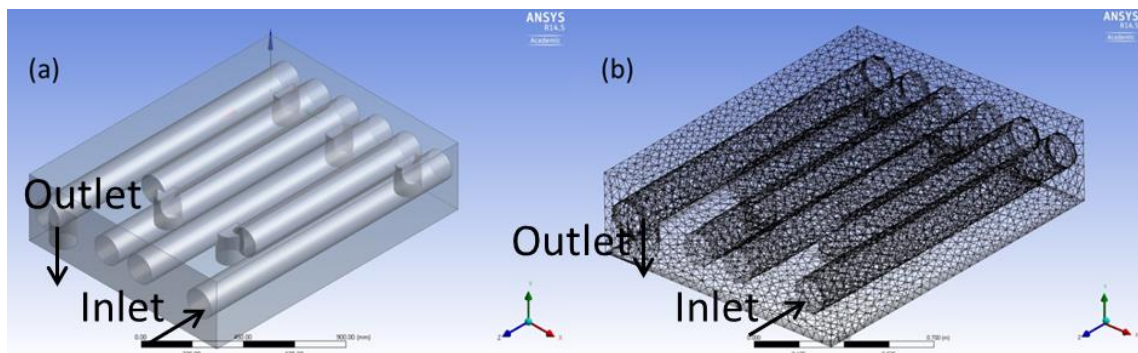


Figure 5.22 - Updated Geometry Model and Mesh

The updated geometry model was modelled and meshed as before (Figure 5.22). Under the same average laboratory conditions as before, with the updated geometry, the 20VHC system performance was investigated in comparison with the re-modelled lab data.

Table 5.26 - Matched Geometry Final Slab Temperature Comparison

| 20VHC | | | | |
|---------------|---------------------|--------------|------------------------|-------------|
| Thermal Loads | Ambient Temperature | Air Velocity | Lab | Re-Modelled |
| | | | Final Slab Temperature | |
| W/m^2 | $^{\circ}C$ | m/s | $^{\circ}C$ | $^{\circ}C$ |
| 20 | 16.9 | 1.2 | 23.0 | 20.2 |
| 50 | 15.3 | 1.2 | 23.3 | 23.4 |
| 100 | 15.3 | 1.2 | 24.9 | 31.6 |
| 250 | 17.1 | 1.2 | 42.0 | 57.7 |
| 35.8 | 16.9 | 1.2 | 23.0 | 22.7 |
| 83.9 | 15.3 | 1.2 | 23.3 | 28.9 |
| 115 | 15.3 | 1.2 | 24.9 | 34.0 |
| 247.6 | 17.1 | 1.2 | 42.0 | 57.4 |

Table 5.27 - Updated Geometry Performance Coefficients

| Modelled | | | Laboratory | | |
|-------------------------|-------------------------|--------|-------------------------|-------------------------|--------|
| System | Performance Coefficient | | System | Performance Coefficient | |
| | aLoad | eLoad | | aLoad | eLoad |
| VHC (20Wfan) | 0.1666 | 0.1663 | VHC (20Wfan) | 0.0881 | 0.0968 |

The difference reduction work matching the prototype geometry used in the laboratory improved the performance coefficients, however they remained approximately double that of the laboratory coefficients generated. As in the previous case, individual scenario final average temperatures were well matched ($\pm 2^{\circ}\text{C}$), though insufficient matching across the system operation meant further difference reduction was required.

5.4.4.3 Surface Roughness

As default, the surface roughness constant in the CFD simulation was specified at 0.5. In actual laboratory conditions the prototype surface is very rough. The roughness constant in the CFD simulation was therefore increased to 1 [156]. The 20VHC system was again simulated and results contrasted.

Across all the heat loads simulated there was no change in final slab temperature due to the roughness constant variation. This was likely due to the steady state simulation parameters. The roughness will likely affect heat transfer rate, but not the final temperature balance. Further difference reduction was subsequently investigated.

5.4.4.4 Air Gap

The final difference re-modelled was the introduction of a 42mm air gap beneath the soffit. In the previous modelling cases a specified heat flux acted upon the slab soffit. In the laboratory testing, due to the shutters surrounding the prototype, a 42mm gap between the bottom of the shutter and the slab soffit occurred. In the laboratory the radiant heat mat was situated within this air space.

To determine the effects of the air gap a 42mm was modelled. Initially heat flux was specified directly on the slab soffit as before although upon comparison of final slab temperatures the match was reduced. Heat flux was therefore specified on the base surface of the air layer however this had the same result with final slab temperatures greatly reduced on the previous modelling scenarios.

The laboratory thermal load was generated by radiation only the solid surfaces surrounding this system will absorb the radiation. The air gap therefore adds additional resistance for the heat flux due to the different forms of thermal energy delivery. The air gap therefore inhibited difference reduction and was duly removed.

5.4.5 Summary of Findings

In conclusion it was possible to validate that the WHC model results offer a suitable representation of laboratory performance. Similarly, under the eLoad of 35.8W/m^2 and the actual thermal load of 50W/m^2 the model generates suitable final slab temperatures. Above this thermal load the model simulates an invalid representation of VHC performance.

For thermal loads greater than 50W/m^2 , the CFD modelling underestimated the performance of the VHC system with respect to laboratory findings. This was likely due to the instability of the VHC systems at high thermal loads. Traditionally VHC systems are capable of maintaining comfort temperatures up to thermal loads of 50W/m^2 . Above this range, without additional conditioning, the VHC system is incapable of stabilising the temperature. In the laboratory tests the time dependency and safety considerations limited the final slab temperatures reached. Within the CFD modelling typical convergence tolerance (10^{-6}), when the heat load reached 100W/m^2 , was not reached.

5.5 Optimum Operating Method Generation

The intended generation of an Optimum Operating Method (OOM) was designed to offer an easy design tool for matching optimum operating of the prototype WVHC system for differing occupancy conditions and thermal loads. Research by Dounis [157] highlighted the traditional reliance on modelling systems to enable building system control. For the generation of this OOM a classical energy-efficient approach was taken where energy consumption is minimised whilst comfort temperatures are maintained [9].

Through analysis of the system COP and performance coefficients generated it was possible to determine a system hierarchy of energy cooling efficiency. This energy efficiency system hierarchy formed the basis for the OOM. The *maximum cooling capability* for each system was subsequently calculated from the performance equations in Figure 5.21. This suggested the limitation to which a system operating mode was capable of maintaining comfort temperatures. The limitation was calculated at the heating load that caused the average slab temperature to reach 22°C. Combining the *system hierarchy* and *maximum cooling capability* enabled the generation of an OOM, useful for building design and system operation.

5.5.1 System Hierarchy

Based on average COP figures calculated from figures in Table 5.13, an energy-efficient hierarchy was formulated in Table 5.28. This ranked the systems in order of energy-efficiency.

Table 5.28 - Average COP Figures

| System | COP |
|--------|-------|
| 10VHC | 11.33 |
| 20VHC | 10.88 |
| 32VHC | 10.43 |
| 32WVHC | 3.75 |
| 20WVHC | 1.46 |
| 10WVHC | 1.40 |
| WHC | 1.36 |

5.5.2 Maximum Theoretical Cooling Capacity

Based on the performance coefficients calculated from the eLoads (Table 5.22 and Figure 5.21) the *maximum theoretical cooling capacity* was calculated. The 'Goal Seek' function in Microsoft Excel was utilised to determine the internal heat gain (W/m^2), at which point slab temperature reaches 22°C. Under UK design guidance, this marks the temperature at which the slab is considered overheated[34]. Rearranging Equation 5.4 gives Equation 5.7 below.

Further, setting $T_{slab,\infty}$ to 22°C enables calculation of a theoretical maximum internal cooling capacity.

Equation 5.7

$$\text{Heat Load} = \frac{(T_{slab,\infty} - T_{ambient,0})}{k}$$

Table 5.29 - Maximum Theoretical Cooling Capacity

| | Performance Coefficient (k) | Air/Water Inlet Temperature | Max. Internal Cooling Capacity |
|--------|-----------------------------|-----------------------------|--------------------------------|
| | | °C | W/m ² |
| 10VHC | 0.1697 | 18.0 | 23.6 |
| 20VHC | 0.0968 | 18.0 | 41.3 |
| 32VHC | 0.0727 | 18.0 | 55.0 |
| 32VHC | 0.0727 | 15.0 | 96.3 |
| 32VHC | 0.0727 | 12.0 | 137.6 |
| WHC | 0.0485 | 7.8 | 292.8 |
| 32WVHC | 0.0321 | 11.4 | 330.2 |
| 20WVHC | 0.0349 | 10.0 | 343.8 |
| 10WVHC | 0.0311 | 8.7 | 427.7 |

Table 5.29 documents the calculated maximum cooling capacity for each system. The effectively passive operated 10VHC system exhibited a cooling capacity of 23.6W/m². By activating the prototype hollow core with air velocities of 1.2 and 2.5m/s (20VHC and 32VHC respectively) it was possible to deliver up to 55W/m² of cooling with 18°C ambient air.

The addition of water to the TABS prototype enabled almost six-times the cooling capacity. Through combination of VHC and WHC systems, cooling of 330 to 428W/m² was possible, should such demand be required by building service engineers. In practice, it is unlikely to find water delivery between 7 and 8°C. An increase in water delivery temperature would significantly reduce the maximum internal cooling capacity.

5.5.3 Optimum Operating Method

Combining the results from Table 5.28 and Table 5.29 it was possible to determine an optimum system hierarchy and appropriate operating conditions for each system (Table 5.30).

Table 5.30 - Optimum Operating Conditions and System Hierarchy

| Suitable Cooling Range | System Hierarchy | Air/Water Inlet Temperature | Average COP | Max. Internal Cooling Capacity |
|------------------------|------------------|-----------------------------|-------------|--------------------------------|
| W/m^2 | | $^{\circ}C$ | | W/m^2 |
| 0-30 | 10VHC | 18.0 | 11.33 | 23.6 |
| 30-40 | 20VHC | 18.0 | 10.88 | 41.3 |
| 40-55 | 32VHC | 18.0 | 10.43 | 55.0 |
| 55-95 | 32VHC | 15.0 | - | 96.3 |
| 95-135 | 32VHC | 12.0 | - | 137.6 |
| 135-330 | 32WVHC | 11.4 | 3.75 | 330.2 |
| 330-340 | 20WVHC | 10.0 | 1.46 | 343.8 |
| 340-425 | 10WVHC | 8.7 | 1.40 | 427.7 |
| - | WHC | 7.8 | 1.36 | 292.8 |

Table 5.30 represented the culmination of the hierarchical OOM. To use the table in system design calculate the seasonal peak cooling requirements. Matching these peak cooling requirements against the specified ranges in the far left column identifies the optimum system and conditions to employ to ensure comfort temperatures are maintained and energy efficiency maximised.

Due to their dominating COP figures the VHC systems were favoured until capacity was reached. Noticeably the OOM presented in Table 5.30 proposed a combined WVHC solution over the WHC system alone, due to the WHC system having the weakest COP figure.

From the solitary COP figure calculated for the 1/2WHC system (Table 5.13), operating minimum water flow rates was advisable to achieve the greatest energy-efficiency. When applied in whole building system water recycle, heat storage and grey water options should be considered to avoid unsustainable dependency on open loop mains water provision.

The OOM applicability was limited to conditions where ambient air temperatures were less than the target slab or room temperature. To achieve Table 5.30 performance, the quoted air and air and water average temperatures should be followed throughout operation.

5.6 Room Model

The analysis in *Chapter 5* thus far focuses on an isolated slab model. To further widen the applicable scope of the analysis, the developed CFD slab model was used to assess thermal performance of the lab system under typical office room conditions. Typical room conditions were taken from [158], with slab operation informed from industry practice [136].

5.6.1 Method

The following method was followed, using ANSYS Fluent as before:

1. Construct a room model that takes mechanically ventilated inlet air through the slab and delivers it to the room, before venting from the room.
2. Set typical room conditions for slab flow rate and office thermal loads for:
 - a. Interior space (75W/m^2),
 - b. General office (125W/m^2),
 - c. and Perimeter zone (180W/m^2).
3. Investigate grid (mesh) independence of the model.
4. Run steady-state simulations for each thermal load with:
 - a. $0.31, 0.77, 2.0, 2.5$ & 2.8m/s inlet flow rate (typical of active thermal mass operation),
 - b. 25°C initial temperature,
 - c. 18°C slab inlet temperature,
5. Monitor temperature, heat fluxes and room velocities.

5.6.2 Model

A 1.5 by 1.2 by 1.9m air chamber was created directly beneath the slab model, previously investigated in this chapter (Figure 5.22). The outlet vent from the slab feeds directly into the room beneath. A circular outlet vent, of diameter 0.125m , was positioned in the upper opposite corner, to ensure the air inside the chamber was well mixed before exhausting from the model. Figure 5.23 depicts the velocity air flow through the model. Even heat flux was specified from the floor plane, delivering a constant thermal load to the space. The boundary conditions are contained in Table 5.31, representative of typical active thermal mass, office room conditions.

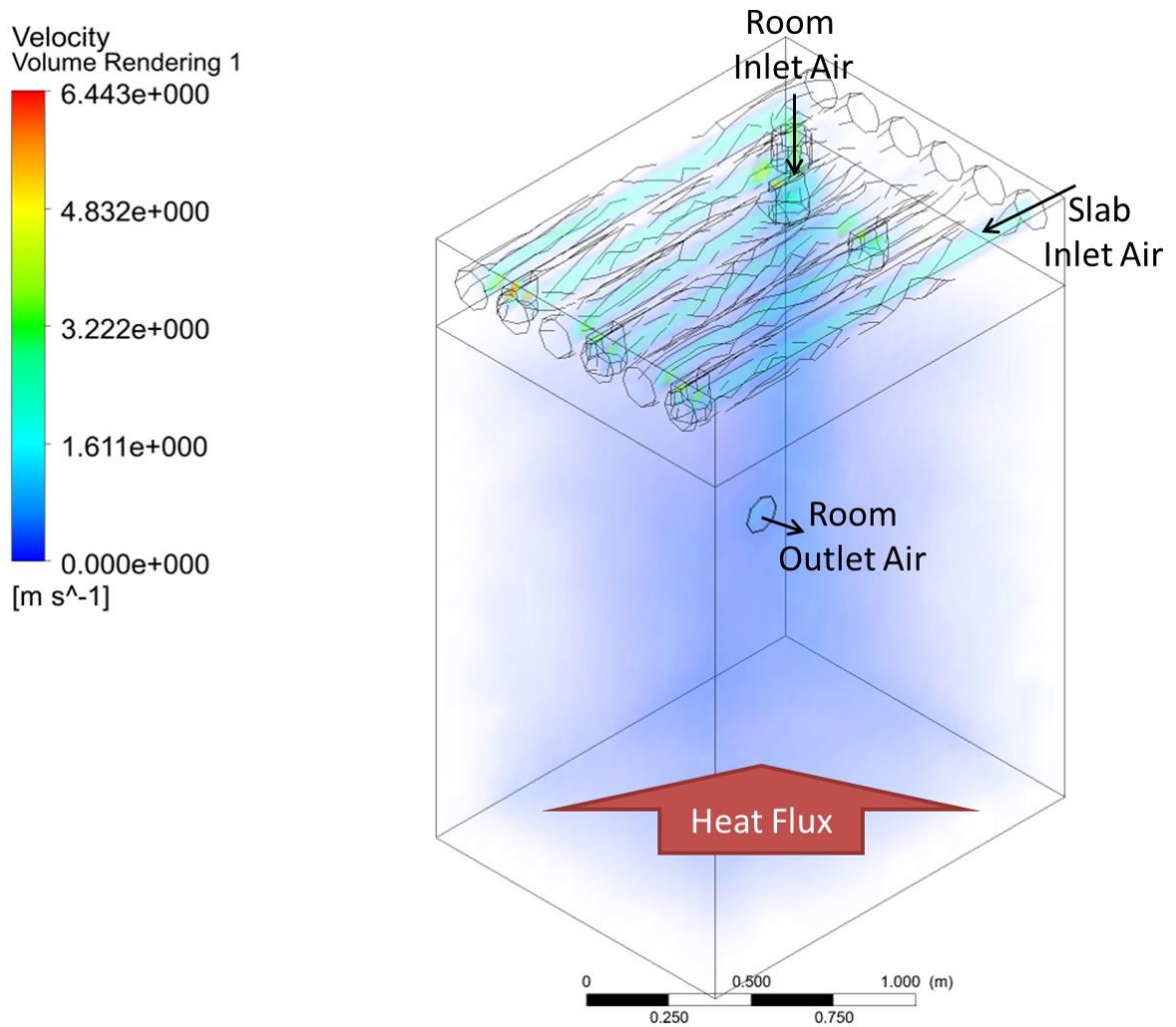


Figure 5.23 - Room model with slab ceiling

Air and slab temperatures were initialised at 25°C, representing an overheated slab and room. Inlet air temperature to the slab was set at 18°C throughout the simulations, representative of industrial operation to mediate slab temperature and maintain comfort conditions in the room. Five inlet air velocities were simulated over three heat fluxes. The inlet air velocities represented different modes of slab operation, from minimum fresh air requirements [159] up to upper velocities, based on industrial design guidance [136]. The three heat fluxes simulated represent the overall thermal load in interior, general and perimeter office zones [158]. Since the thermal boundary was specified at an exterior surface, the fixed heat flux condition was used throughout the modelling [160].

Table 5.31 - Room model boundary conditions

| | Minimum Air Flow | Typical Air Flow | |
|---|--------------------------------|------------------|------------------|
| Initial Air and Slab Temperature | 25 | 25 | °C |
| Inlet Air Velocity | 0.31 (4acph), 0.77 (10acph) | 2.0, 2.5, 2.8 | m/s |
| Inlet Air Temperature | 18 | 18 | °C |
| Floor Heat Flux | 75, 125, 180 | 75, 125, 180 | W/m ² |

5.6.2.1 Governing equations

Throughout the room model simulations the following governing equations have been used. Fluid flow in the model is governed by the standard k- ϵ model (Equation 5.8 and Equation 5.9), where k is the turbulent kinetic energy and ϵ is the rate of dissipation. A full break down of the fluid flow transport equation is given in [161]. A brief overview of each term can be found in Table 5.32.

Equation 5.8

$$\frac{\partial \rho}{\partial t}(\rho k) + \frac{\partial}{\partial x_i}(\rho k u_i) = \frac{\partial}{\partial x_j} \left[\left(\mu + \frac{\mu_t}{\sigma_k} \right) \frac{\partial k}{\partial x_j} \right] + G_k + G_b - \rho \epsilon - Y_M + S_k$$

Equation 5.9

$$\frac{\partial \rho}{\partial t}(\rho \epsilon) + \frac{\partial}{\partial x_i}(\rho \epsilon u_i) = \frac{\partial}{\partial x_j} \left[\left(\mu + \frac{\mu_t}{\sigma_\epsilon} \right) \frac{\partial \epsilon}{\partial x_j} \right] + C_{1\epsilon} \frac{\epsilon}{k} (G_k + C_{3\epsilon} G_b) - C_{2\epsilon} \rho \frac{\epsilon^2}{k} + S_\epsilon$$

Convective and conductive heat transfer is governed by the energy equation (Equation 5.10). A full explanation of terms can be found in [162]. General terms used are included in Table 5.32.

Equation 5.10

$$\frac{\partial}{\partial t}(\rho E) + \nabla \cdot (\vec{v}(\rho E + p)) = \nabla \cdot \left(k_{eff} \nabla T - \sum_j h_j \vec{J}_j + (\vec{\tau}_{eff} \cdot \vec{v}) \right) + S_\epsilon$$

Where radiant heat transfer has been included in the simulations, the P-1 radiant model was used based on the governing equation, Equation 5.11. Limited explanation is given in Table 5.32. Further detail of the terms used in the model can be found in [163].

Equation 5.11

$$q_r = \frac{1}{3(a + \sigma_s) - C\sigma_s} \nabla G$$

Table 5.32 - Overview of certain terms for Equation 5.8, Equation 5.9, Equation 5.10 and Equation 5.11

| Term | Brief Explanation |
|----------------------|---|
| G_k | Generation of turbulence kinetic energy due to the mean velocity gradients |
| G_b | Generation of turbulence kinetic energy due to the buoyancy |
| Y_M | Contribution of the fluctuating dilation in compressible turbulence to the overall dissipation rate |
| $C_{1\varepsilon}$ | 1.44 |
| $C_{2\varepsilon}$ | 1.92 |
| σ_k | 1.0 |
| σ_ε | 1.3 |
| K_{eff} | Effective conductivity ($k+k_t$, where k_t is the turbulent thermal conductivity) |
| \vec{J}_j | Diffusion flux of species j |
| S_h | Heat of chemical reaction and other defined volumetric heat sources |
| a | Absorption coefficient |
| σ_s | Scattering coefficient |
| G | Incident radiation |
| C | Linear-anisotropic phase function coefficient (explained further [163]) |

Further to Equation 5.8, in the k- ε viscous model buoyancy is included in the generation of the k component. The generation of turbulence due to buoyancy (G_b) is accounted for in the Equation 5.12 from [164]. Where Pr_t is the turbulent Prandtl number (0.85 in the model), g_i is the gravitational vector and β given by Equation 5.13.

Equation 5.12

$$G_b = \beta g_i \frac{\mu_t}{Pr_t} \frac{\partial \rho}{\partial x_i}$$

Equation 5.13

$$\beta = -\frac{1}{\rho} \left(\frac{\partial \rho}{\partial T} \right)_P$$

5.6.2.2 Radiant model independence

In comparison with the previous models utilised in Chapter 5, the room model includes a fixed heat flux across a fluid space, before interacting with any solid surface. Due to this addition, the P-1 radiant model was considered for the simulations (in addition to the fluid flow and energy equations previously used). Parallel simulations were conducted with and without the P-1 radiant model activated, and results compared.

Table 5.33 - Radiant independence model boundary conditions

| | Low heat flux | High heat flux | |
|---|---------------|----------------|------------------|
| Initial Air and Slab Temperature | 25 | 25 | °C |
| Inlet Air Velocity | 2.0 | 2.0 | m/s |
| Inlet Air Temperature | 18 | 18 | °C |
| Floor Heat Flux | 50 | 200 | W/m ² |

Table 5.34 - Radiant independence model simulation results

| | Low heat flux | | High heat flux | | |
|------------------------------------|---------------|-----------|----------------|-----------|------------------|
| | - | Radiation | - | Radiation | |
| Avg. Room Temperature | 20.3 | 20.8 | 26.9 | 28.6 | °C |
| Avg. Slab Temperature | 18.6 | 19.7 | 19.8 | 24.6 | °C |
| Avg. Room Inlet Temperature | 18.4 | 19.2 | 19.0 | 22.3 | °C |
| Avg. Soffit Heat Flux | 3.8 | 11.2 | 15.5 | 46.2 | W/m ² |

Notably, the inclusion of the radiant model delivered an, approximately three times greater, soffit heat flux (Table 5.34); resulting in increased slab, room and room inlet temperatures. Due to this discrepancy in results the model was deemed not radiant independent, and P-1 radiant heat transfer model included throughout the room model simulations.

5.6.2.3 Mesh independence testing

Prior to initialising the simulations mesh independence was tested over five mesh refinements, as specified in Table 5.35. The boundary conditions for the mesh independence testing were:

- Initial temperatures: 25°C
- Inlet air velocity: 2.0m/s
- Inlet air temperature: 18°C
- Floor heat flux: 75W/m²

Average room temperature, slab temperature and soffit heat flux were all monitored and displayed in Table 5.36, along with percentage deviations from the *ultra-fine* mesh settings results.

Table 5.35 - Mesh parameters

| Mesh Parameter | Ultra Fine | Fine | Medium | Medium Coarse | Coarse |
|---|------------------|------------------|------------------|------------------|-----------------|
| Use advanced sizing function | on: curvature | on: curvature | on: curvature | on: curvature | off |
| Relevance Center | Fine | Fine | Medium | Coarse | Coarse |
| Initial Seed Size | Active Assembly | Active Assembly | Active Assembly | Active Assembly | Active Assembly |
| Smoothing | High | High | Medium | Medium | low |
| Transition | Slow | Fast | Fast | Fast | Fast |
| Span Angle Center | Fine | Fine | Medium | Medium | Coarse |
| Number of Nodes | 82570 | 56371 | 11248 | 5882 | 1965 |
| Number of Elements | 459138 | 305058 | 56437 | 30634 | 8198 |
| Model Volume (m ³) | 3.995 | 3.995 | 3.995 | 3.995 | 3.995 |
| Average volume of an Element(m ³) | 8.7E-06 | 1.3E-05 | 7.1E-05 | 1.3E-04 | 4.9E-04 |

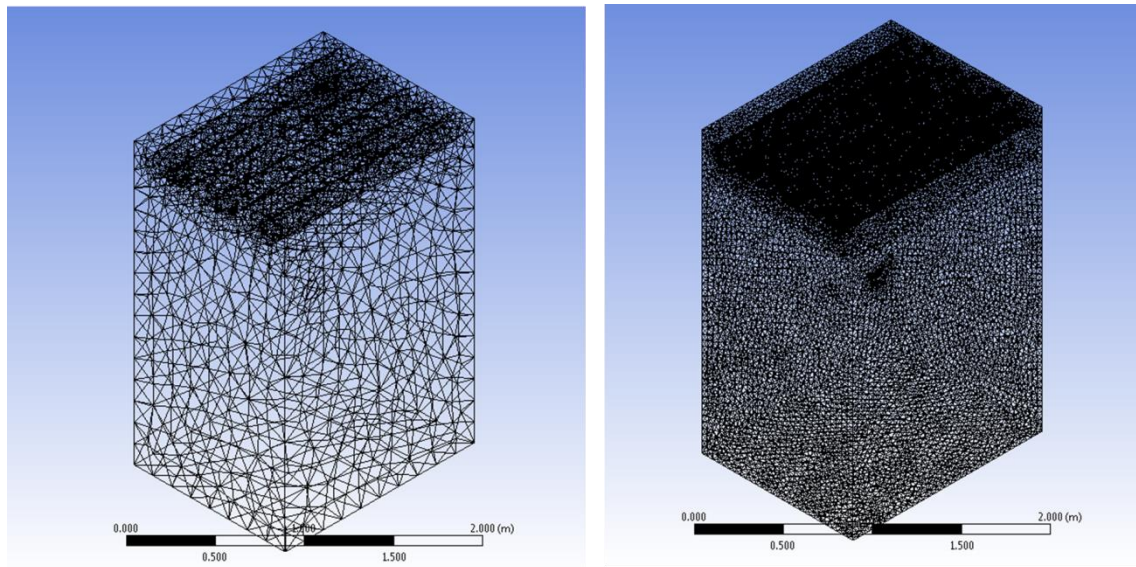


Figure 5.24 - Medium-coarse and ultra-fine meshed room model

Table 5.36 - Mesh independence results

| Mesh Parameter | Ultra Fine | Fine | Medium | Medium Coarse | Coarse |
|---|--------------|---------------|---------------|---------------|---------------|
| Av Room Temp (K) | 295.4 | 294.6 | 294.9 | 295 | 293.6 |
| Av Slap Temp (K) | 293.6 | 293.1 | 293.2 | 293.4 | 292.2 |
| Av Soffit Heat Flux (W/m ²) | 20.05 | 16.16 | 15.88 | 17.04 | 14.48 |
| Room Temp deviation | 0.00% | -0.27% | -0.17% | -0.14% | -0.61% |
| Slap Temp deviation | 0.00% | -0.17% | -0.14% | -0.07% | -0.48% |
| Soffit Heat Flux deviation | 0.00% | -19.40% | -20.80% | -15.01% | -27.78% |
| Av Deviation from Ultra Fine | 0.00% | -6.61% | -7.03% | -5.07% | -9.62% |

The mesh independence study identified the *medium-coarse* mesh as the preferred choice. This mesh setting demonstrated the optimum in solution accuracy and solving time. A good fit was observed from the temperature readings; however the soffit heat flux figure had a poor level of accuracy. Little weight should therefore be given to conclusions based on the soffit heat flux; therefore subsequent analysis majors on temperature figures.

To ensure mesh independence across the simulation range mesh independent tests were conducted with; an inlet velocity of 0.77m/s and 125W/m² heat flux, and 0.33m/s and 180W/m². In each the medium-coarse mesh results deviated less than 5% overall, from the ultra-fine mesh. The temperature figures deviated no more than 0.7%.

5.6.3 Simulation Results

5.6.3.1 Velocity Vectors

To communicate the nature of the air velocity path throughout the room model Figure 5.25, Figure 5.26, Figure 5.27 and Figure 5.28 have been produced. The graphical results displayed are for inlet to the slab at 2m/s, at 18°C, with a fixed 75W/m² load on the floor. Average inlet velocity to the room increased 30-34% under the differing slab inlet velocities investigated. This is due to the turbulent air flow through the slab air network. The narrowing bore diameter in the network constricts the flow, increasing the velocity. Within in the slab air network (Figure 5.27) the velocities increase following each cross-over. Increased heat transfer rates occur in these regions. There is a 7-10% increase in room outlet velocity against room inlet velocity.

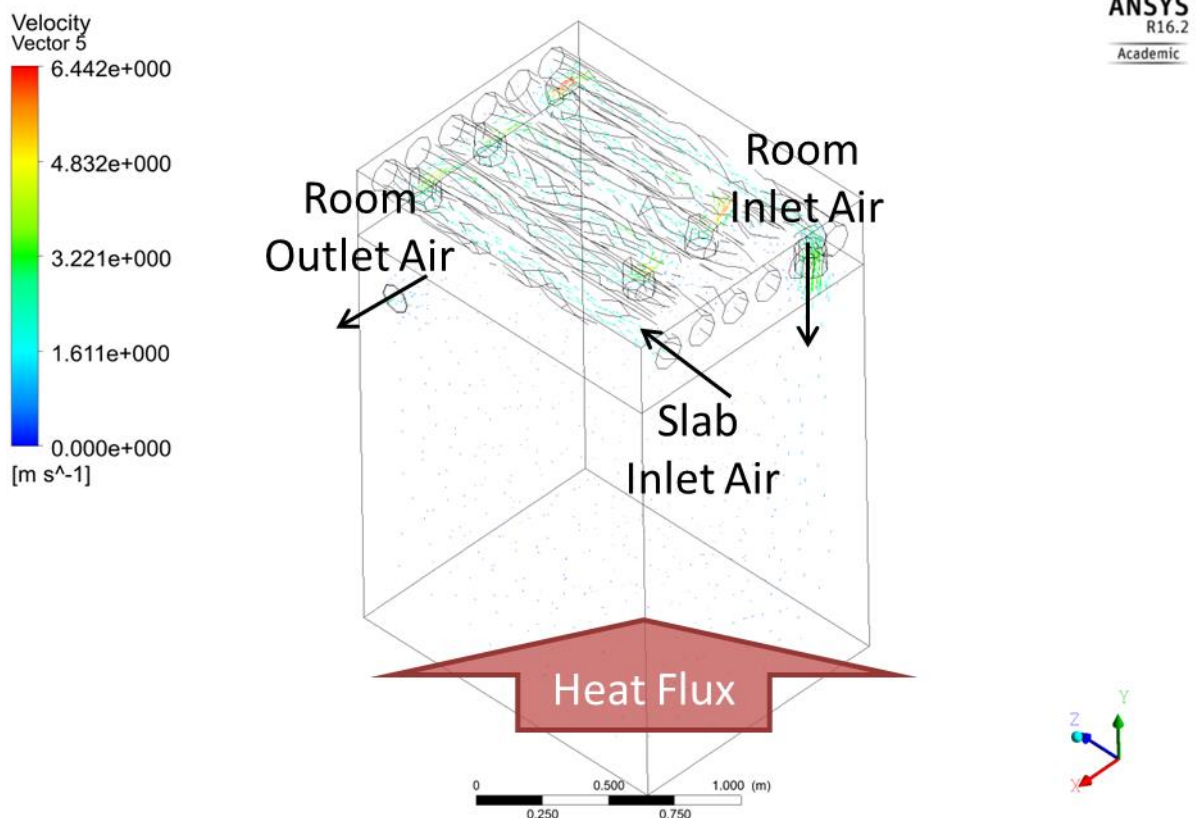


Figure 5.25 - Room model velocity vector isographic frame view

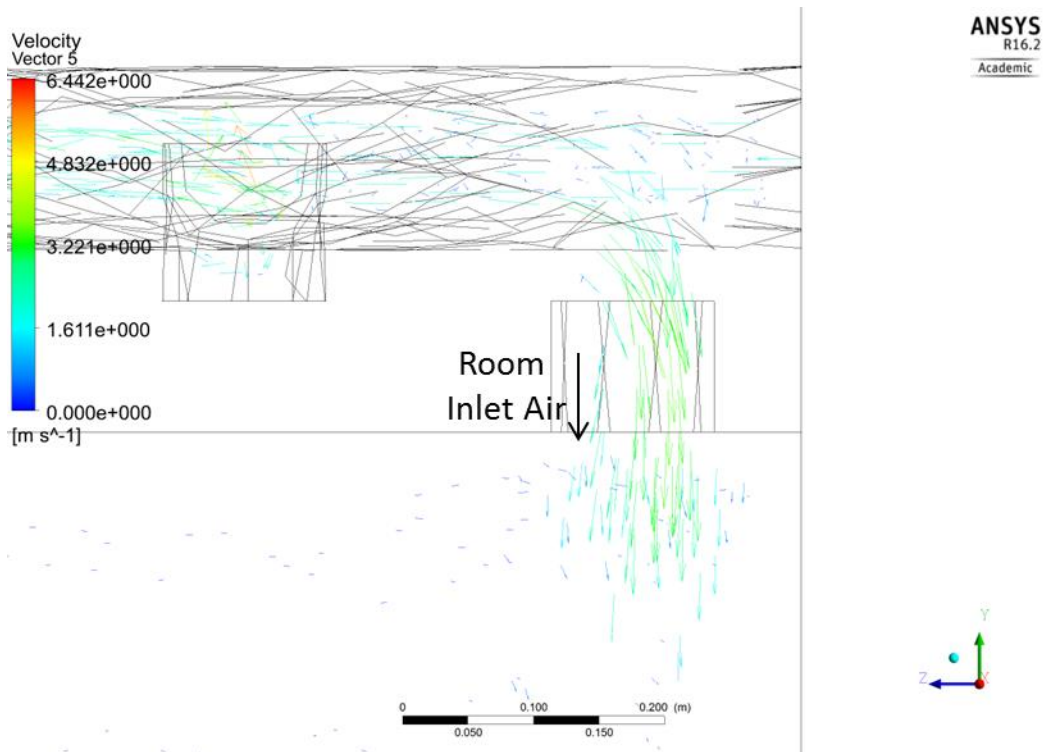


Figure 5.26 - Room inlet velocity vector frame view

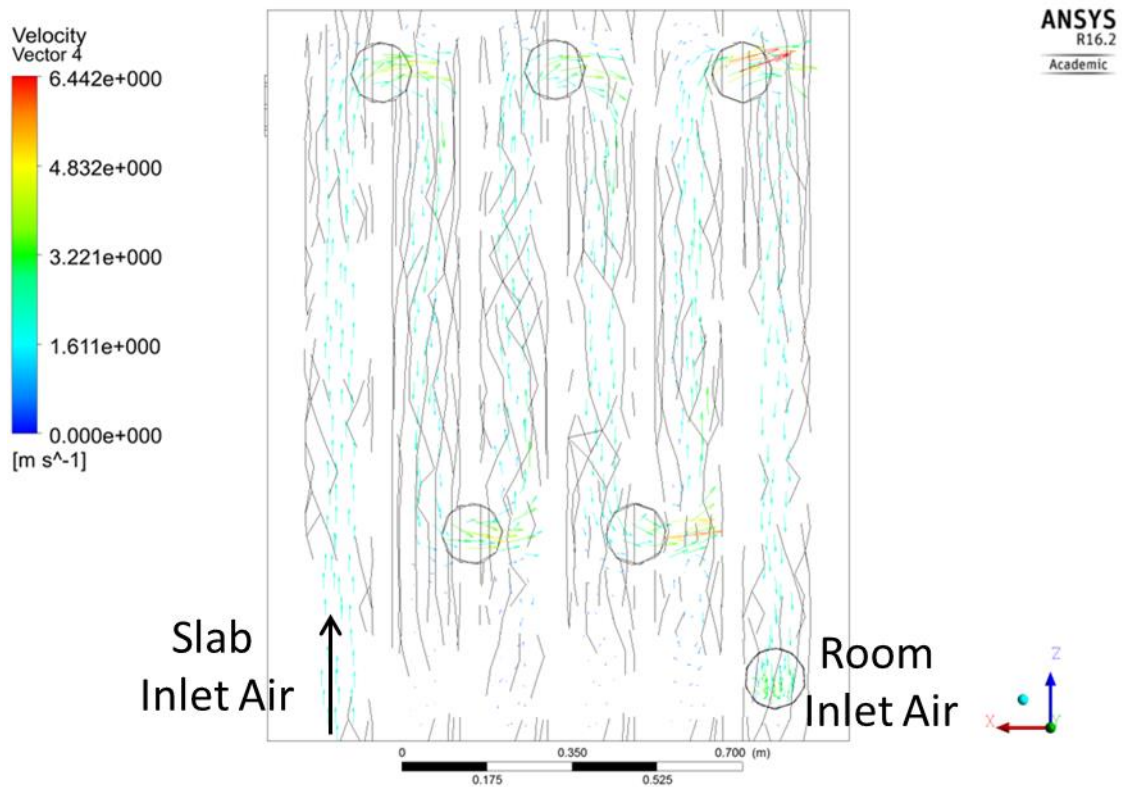


Figure 5.27 - Slab air network velocity vector frame view

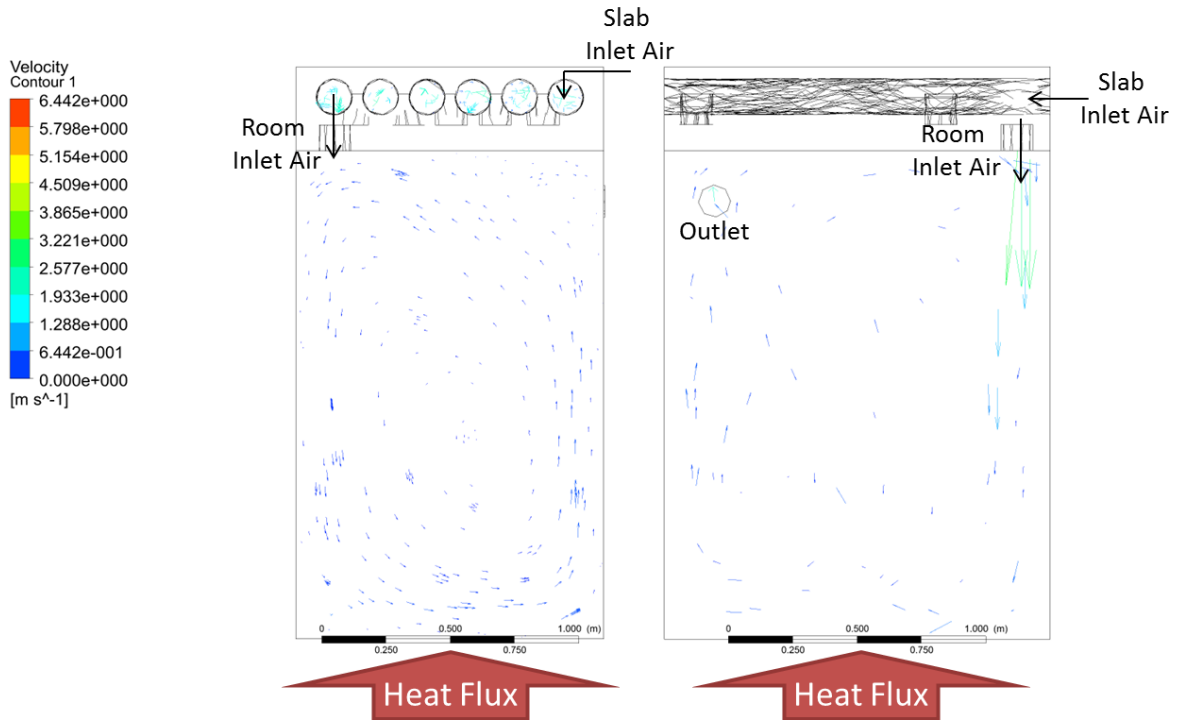


Figure 5.28 - Velocity contours (l) front on at a mid-point cross section and (r) whole room volume from the right side

From Figure 5.28 it is apparent that the air flow within the room space is dominated by the forced convection stimulated by room inlet air flow. Evidence of buoyancy effects is displayed in the velocity vector graphic to the right in Figure 5.28; however the forced convection is more dominant.

5.6.3.2 Temperature Distribution

Figure 5.29 graphically portrays the temperature distribution within the room model at a mid-point cross-section (3D view), under 2m/s velocity inlet and 75W/m² floor heat flux conditions. The room temperatures demonstrate a well-mixed environment, with temperatures deviating by 1-2°C in the bulk of the room. Increased temperatures were observed within the first 10cm of the floor due to the modelled position of the thermal load. Within the slab temperature deviation is observed with the three cores closest to the cool air inlet maintaining a temperature around 18°C. This concentration of temperature reduces the nearer to the soffit, with a uniform soffit temperature apparent.

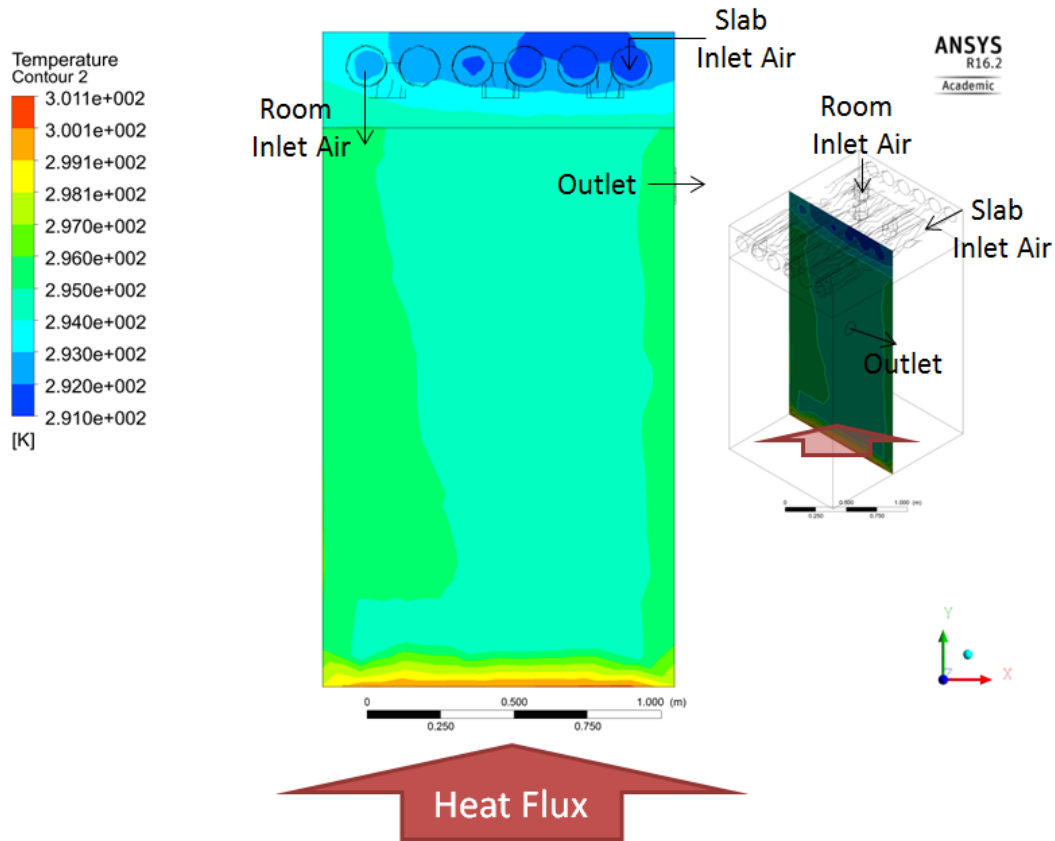


Figure 5.29 - Room model isotherms with inlet velocity at 2m/s and floor heat flux at 75W/m²

5.6.3.3 Results

Results from the fifteen scenarios simulated have been captured in Table 5.37. Soffit heat flux varied from 13 to 84W/m², depending on the floor heat flux and air velocity. The velocity defined by the minimum fresh air requirements (0.31m/s) was not able to maintain comfort room temperatures. Comfort temperatures were maintained, under all typical heat fluxes, when the inlet velocity was increased to 2.5 and 2.8m/s.

Table 5.37 - Room simulation results

| | Floor Heat Flux | Inlet Air Velocity | | | | | |
|-------------------------------------|---------------------|--------------------|---------|--------|--------|--------|-----|
| | | 0.31m/s | 0.77m/s | 2.0m/s | 2.5m/s | 2.8m/s | |
| Avg. Air Network Temperature | 75W/m ² | 30.1 | 21.3 | 18.6 | 18.4 | 18.3 | °C |
| | 125W/m ² | 38.6 | 23.7 | 19.2 | 18.8 | 18.6 | °C |
| | 180W/m ² | 45.8 | 26.4 | 19.8 | 19.2 | 18.9 | °C |
| Room Inlet Temperature | 75W/m ² | 37.3 | 24.1 | 19.4 | 19.0 | 18.8 | °C |
| | 125W/m ² | 50.5 | 28.3 | 20.4 | 19.7 | 19.4 | °C |
| | 180W/m ² | 62.0 | 33.0 | 21.6 | 20.5 | 20.1 | °C |
| Avg. Room Temperature | 75W/m ² | 42.7 | 28.1 | 21.8 | 21.0 | 20.7 | °C |
| | 125W/m ² | 59.1 | 34.9 | 24.4 | 23.1 | 22.5 | °C |
| | 180W/m ² | 73.6 | 42.3 | 27.3 | 25.3 | 24.5 | °C |
| Avg. Slab Temperature | 75W/m ² | 38.8 | 25.4 | 20.3 | 19.7 | 19.5 | °C |
| | 125W/m ² | 53.1 | 30.5 | 21.8 | 20.9 | 20.5 | °C |
| | 180W/m ² | 65.8 | 36.2 | 23.6 | 22.2 | 21.6 | °C |
| Avg. Room Velocity | | 0.039 | 0.100 | 0.266 | 0.345 | 0.390 | m/s |

The figures Table 5.38 display the volume temperature profiles from the side wall of the room model under each of the conditions investigated. For each temperature distribution the same colour limits were specified, ranging from 291K (18°C) to 350K (77°C). Light blue represents comfort conditions. Table 5.39 documents the temperature isotherms from the central plane (Figure 5.29 position) for each condition. The colour key ranges from 291K (18°C) to 302K (29°C), to capture the comfort range.

Table 5.38 - Side wall semi-transparent temperature gradients for each room model scenario

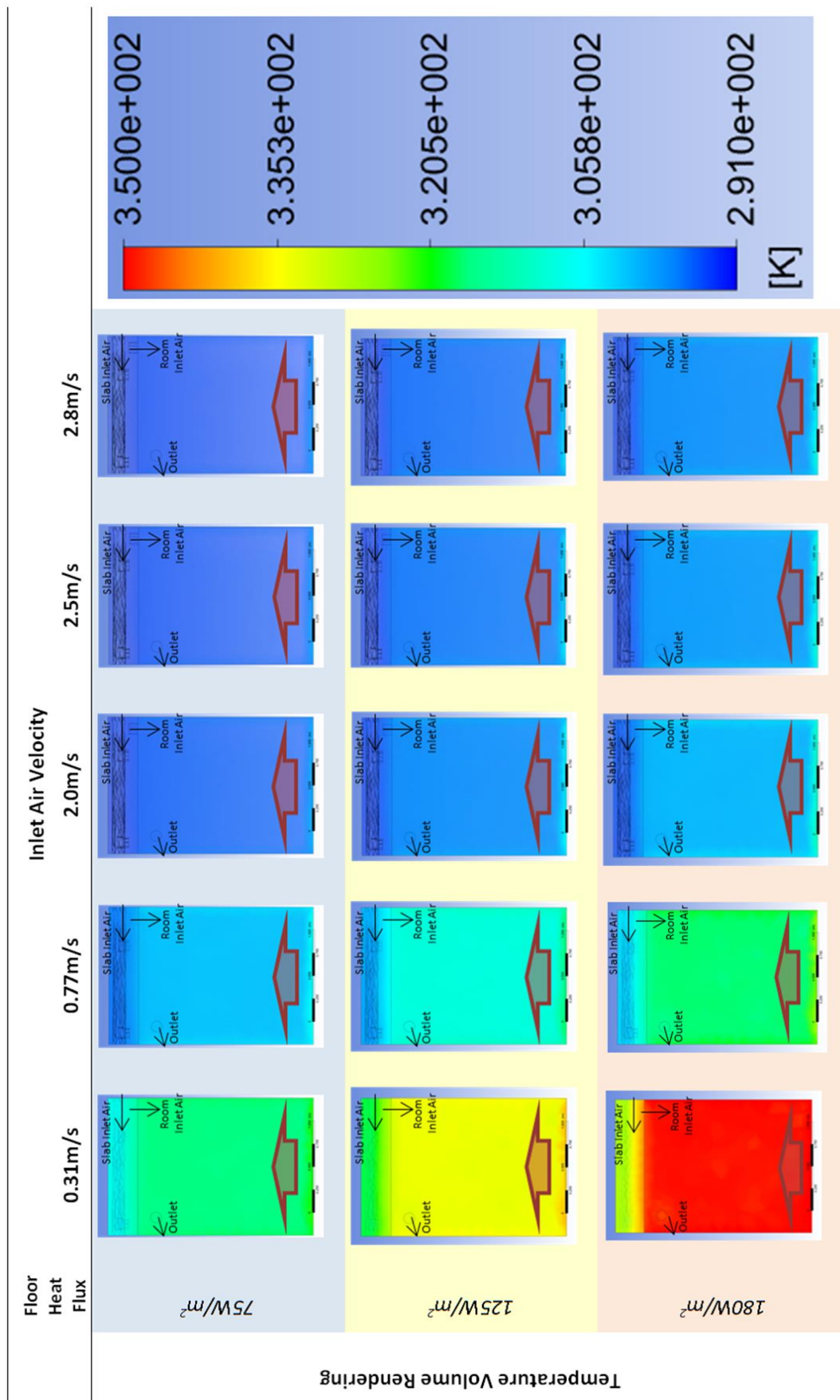
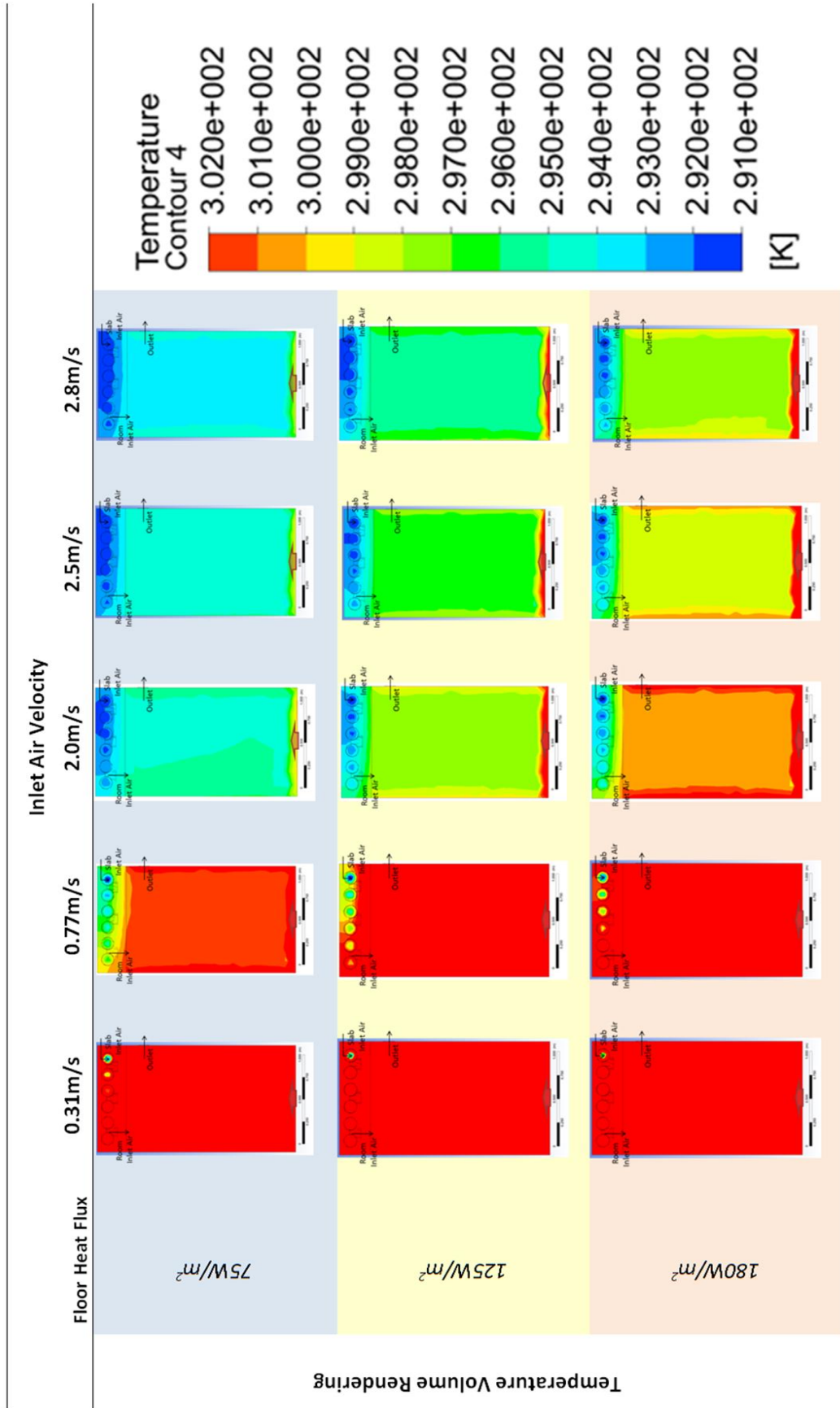


Table 5.39 - Central plane temperature gradients for each room model scenario



5.6.4 Discussion

The results demonstrate that increased ventilation rates effectively maintain comfort conditions under the typical office conditions tested. Figure 5.30 plots the internal thermal load against room temperature, with differing lines for each inlet velocity. Understanding the building requirements, the figure is suitable for sizing the fan requirements to deliver thermal comfort.

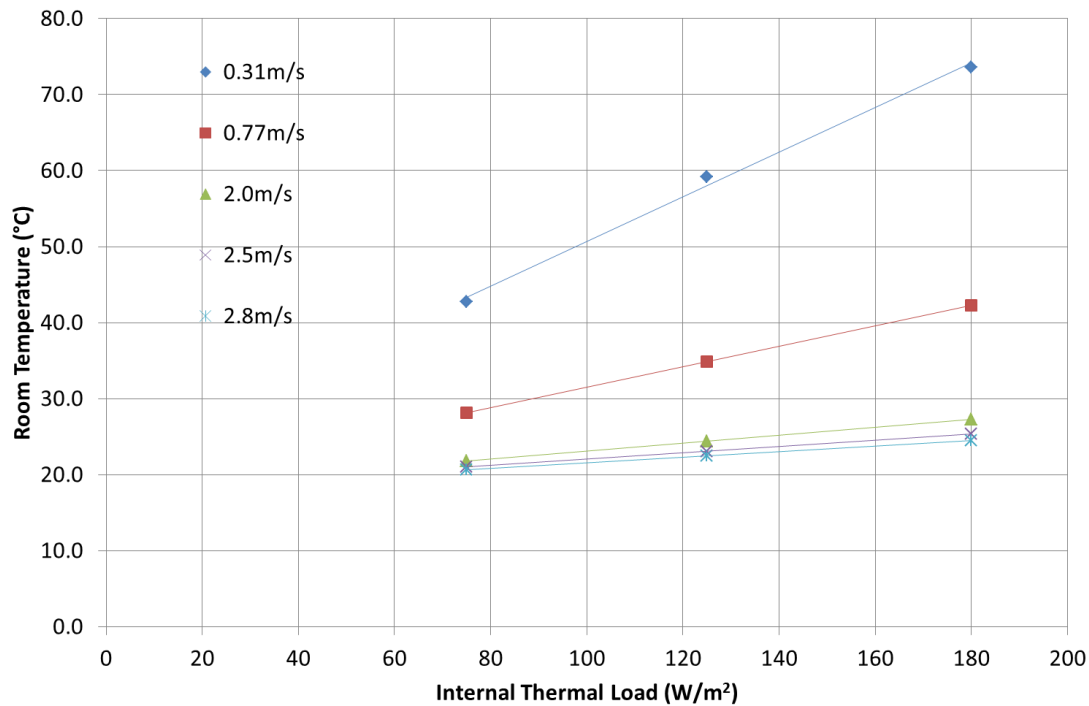


Figure 5.30 - Sizing graph: Internal thermal load against room temperature

Using the linear relationship for inlet velocity of 2.8m/s ($y=0.0365x+17.95$) it is possible to predict room temperatures at a range of thermal loads. For example room temperature would exceed 25°C were the internal thermal load surpass 200W/m². This sets a workable limit for building service engineers when considering applicability of a ventilated active thermal mass system. Beyond a thermal load of 200W/m², which can occur in highly glazed areas or server rooms for example, the active slab requires additional technology to maintain comfort conditions.

As previously discussed in this chapter, addition of embedded cool water pipes can isolate the slab-air network from the room heat, and ensure cool air continues to condition the room. This however is a costly addition and not suitable for retrofit. Typically in industry, AC plant featuring heat pump technology is included to pre-cool the air inlet, ensuring sufficient cooling is available when required. Alternatively, the addition of increased thermal mass and

heat transfer surface area offers increased thermal capacity, resulting in increased cooling and widening the scope of low-energy active thermal mass for high internal thermal load applications.

5.6.5 Summary

The CFD room modelling conducted has shown that at times of high solar gain, additional cooling is required – either through increased thermal mass, faster ventilation rates or addition of AC plant. Increased ventilation rates provided enough cooling capacity to avoid room overheating during the typical room conditions considered, however extreme room scenarios exist that would cause the cooling capacity of the system to be overwhelmed, and the room overheated.

Ventilation rates are increased as a first resort, due to the relatively low fan power (compared to AC) and the VSDs making control easy and efficient. There is a limit to increasing air speed, when fan noise becomes noticeable and occupants complain about excessive drafts. Where the fan speed reaches its limitations, industry design warrants AC plant to be sized to account for the periods of overheating.

Alternatively however, if additional thermal mass can be added that specifically targets high demand periods, and overheating periods reduced within building regulations, then the AC plant does not need to be fitted. At the very least, the AC plant can be drastically reduced – offsetting the additional thermal mass costs and reducing running costs.

The following chapters of this thesis investigate the options for incorporating additional thermal mass with the ventilated active thermal mass system, in contrast with increased thermal mass transfer using water-cooled addition to the active thermal mass.

5.7 Conclusions

This chapter investigated and validated the component performance of the prototype WVHC technology to quantify cooling performance and inform optimal design, installation and operation of the technology.

To accomplish these objectives CFD models of the air and water slab components were generated in ANSYS Fluent. The steady state performance of the six-core prototype VHC system was reviewed against traditional three and four-core active mass systems. The performance coefficients calculated for the prototype VHC and four-core traditional VHC were 0.25 and 0.27 respectively. A system hierarchy was suggested based on modelled performance however did not align with typical industrial benchmarks.

Laboratory tests were subsequently designed and conducted to validate the CFD modelling and develop a valid optimum operating method (OOM). The laboratory tests used the prototype WVHC slab from *Chapter 4*. It was intended to match modelled and laboratory conditions however fan limitations meant it was not possible to test low flow rates (<1m/s) as modelled. A reduced number of heat loads were tested due to time limitations.

Test conditions were maintained for eight to thirty hours for each system scenario tested to enable the system to reach steady state conditions. PassiveHC and 10VHC systems under a 250W/m² load failed to reach a stable slab temperature during the twenty-four hours period. Tests were aborted due to safety concerns. All other systems reached a stable temperature level of less than 0.1°C temperature rise per five minute interval.

To quantify performance, average final thirty-minute heat balances were calculated for each scenario tested. The results from these heat balances were used to determine COP figures for each scenario. With a thermal load of 50W/m² the VHC systems achieved COP figures between 6.9 and 7.6. The WHC and WVHC systems produced COP figures of 1.1 to 1.5 due to the additional theoretical pumping power calculated. Reducing pumping power to a minimum will enable better COP figures.

Final slab temperatures were plotted against the heat load for each scenario; performance coefficients for each system were calculated from their respective correlations. 20VHC and 32VHC systems generated performance coefficients of 0.064 and 0.088 respectively. WHC and WVHC systems achieved performance coefficients ranging from 0.015 to 0.037.

This analysis, along with subsequent testing, revealed that the fan required a fan power of 18W or more to rotate the blades and deliver an air velocity. The 10VHC system could therefore be considered akin to the PassiveHC system with an additional 10W thermal load acting on the slab. A relationship between air velocity and performance coefficients was established however further work to strength test the relationship is required before using the equation as a design tool.

Following the laboratory testing, validation of the CFD modelling was sought. Initial comparison revealed a poor match in performance coefficients; though was inconclusive since it had not been possible to closely replicate the modelled conditions in the laboratory. Systematic difference reduction was undertaken to enable validation.

The WHC component model of the prototype system was validated with comparable performance coefficients generated between the model and the laboratory results (0.043 & 0.049 respectively). The VHC component model was only validated for thermal loads up to $50\text{W}/\text{m}^2$ from final slab temperature investigation.

From the effective thermal load laboratory data the OOM was presented. The OOM was generated to maintain comfort conditions whilst maximising energy efficiency. The OOM suggested VHC systems were suitable for maintaining comfort conditions up to $135\text{W}/\text{m}^2$, where air velocities up to $2.5\text{m}/\text{s}$ and air temperatures of 12°C are achievable. WVHC systems, where previous air requirements and water velocities of $0.56\text{m}/\text{s}$ and temperatures of 8°C were achieved, were capable of maintaining a slab temperature of less than 22°C for soffit heat flux up to $425\text{W}/\text{m}^2$.

When applied to a room scenario, and heat flux applied from the floor, the VHC system was able to maintain comfort temperatures up to $200\text{W}/\text{m}^2$ under air inlet velocity at $2.8\text{m}/\text{s}$ and temperature at 18°C . This was sufficient cooling to maintain comfort temperatures under the typical thermal conditions imposed upon the space. Thermal loads above this threshold require additional cooling.

Despite their added benefit, practically installing embedded water pipes into ceiling systems is undesirable in the building industry due to the added risks and costs incurred. Alternative retrofit enhancement solutions should be investigated utilising added, active thermal mass PCM systems. *Chapter 6* investigated the component performance of PCM additions to active sensible TES systems.

As highlighted in *Chapter 2*, additional PCM is capable of enhancing the TES within a building due to the increased thermal capacity. In addition to investigating the performance of VHC and WVHC systems under differing cooling demands, it would be of interest to investigate an optimum PCM enhancement and the benefit it may bring to an active TES system under summer conditions.

Chapter 6: PCM Component

Modelling, Construction and Laboratory Testing

6 PCM Component

6.1 Introduction

Following the slab component investigation in *Chapter 5*, assessing the water and air enhanced hollow core system capacity; *Chapter 6* investigates the additional benefit available from phase change material (PCM) to the air water hollow core system. Building on the evidence from literature (*Chapter 2*), active-PCM enhancements and PCM varieties will be investigated via CFD modelling and experimental component investigation.

The purpose of the modelling stage of this investigation was to determine a suitable arrangement for PCM within the prototype hollow core system. An assessment of thermal capacity was planned to determine the theoretical benefit of each PCM configuration.

CFD modelling enables the assessment of a range of active PCM enhancements within the WVHC prototype system, without needing to construct all variations practically. Following the modelling stage fundamental analysis of available PCM samples was carried out to enhance the understanding of PCM behaviour through the experimental testing. DSC-TGA

analysis was carried out on two PCM samples to determine experimentally the latent heat of phase change, and the melt temperature.

Having conducted the DSC-TGA analysis, component trials were carried out on the preferred prototype PCM addition in an insulated chamber. The ability to moderate temperature swing was assessed against non-PCM designs. The experimentation stage served as a proof-of-concept study to demonstrate the PCM-diffuser benefit on air temperature.

6.1.1 PCM

Phase Change Materials (PCM) utilise the latent heat of crystallization to store high levels of thermal energy over their melt range. Therefore in a room setting PCM with a melt temperature between 18 and 25°C offer thermal storage enhancement at a room level. PCM with melt temperatures of 21 or 22°C traditionally offer the largest cooling capacity due to completion of their melt phase. PCM with melt temperatures of 25-28°C offer better overheating offset, due to their higher melt temperatures, although complete phase change in these cases are less common [54].

Following melt temperature latent heat is the most important physical property of a PCM. Latent heat figures above 200kJ/kg offer the top performance on the current market [165]. Thermal conductivity, density, specific-heat capacity and melt width are further physical properties that significantly affect performance.

6.1.2 Investigation context

Active thermal mass provides efficient heating and cooling to rooms throughout most of the year. The ideal application of PCM addition was identified as an additional cooling-source during peak-cooling-demand periods. Peak-cooling-demand typically occurs during the late afternoon in well insulated, densely populated office buildings; especially during hot, sunny periods.

During these times sensible active thermal mass offers sufficient room comfort until slab soffit temperatures exceed 23°C. It is intended that at this point the PCM will minimise room temperature rise and offer additional TES; aiding room comfort and avoiding expensive cooling. Offices are typically occupied between eight and ten hours a day, thus active periods in this region are desirable.

For optimum benefit of PCM applications a daily melt-freeze cycle is advised. In the investigations carried out, evidence for melt-freeze cycle progression will be monitored by liquid fraction observations. Benefit to room comfort will be monitored through air-

temperature variation and potential energy savings from the case to air heat flux available. Alongside room comfort, energy saving benefits and cooling value; practical installation and application considerations were factored into the investigation.

6.1.3 Contributions to knowledge

The work carried out in this chapter documented, for the first time, the assessment of four possible PCM enhancements to an active-sensible-TES system. Previously, work combining PCM and sensible TES found the PCM passive-layer additions hindered the thermal control [100, 166].

Work conducted [104, 119, 167] has previously investigated active-PCM technology to enhance air conditioning systems. An existing industrial system, Cool-Phase™, utilises this technology with natural ventilation to provide 6 to 10 kWh of thermal energy storage, capable of replacing AC units [132]. This investigation develops on these ideas, seeking to prove the concept of a commercially viable active-PCM addition to the sensible-TES system.

Also novel in this chapter was the experimental DSC assessment of a bio-based PCM, X25. The range of commercially available bio-based PCM was launched in 2013. To date, no academic work has been published using these PCM. The results have helped inform the subsequent investigation, where X25 was encapsulated in a novel active-PCM unit.

The prototype design, construction and installation of the chosen active-PCM unit were also documented; offering learning for future manufacturers of active-PCM units. Further, the findings from the laboratory testing, containing novel-PCM X25, offered further contributions to knowledge by giving understanding of melt times and the benefit of active-PCM-TES on air temperature.

6.1.4 Chapter aims

- 1) Identify preferred active TES location for PCM retrofit enhancement to the hollow core, through CFD simulation.
- 2) Identify cost-effective optimum PCM for encapsulation in the retrofit design, through CFD simulation.
- 3) Quantify the preferred PCM's physical properties through DSC analysis.
- 4) Physically test the retrofit solution under laboratory conditions to determine energy storage capacity.

6.2 PCM Component Modelling

6.2.1 Methodology

To investigate the benefits of adding PCM to a sensible active thermal mass system; the transient performance of six configurations were designed and modelled in ANSYS Fluent. To ensure speed and stability throughout the modelling process, thirty-millimetre cross-section models were simulated (Figure 6.2). The thirty-millimetre models were suitable for identifying the ideal PCM location and system type. Scale-up factors are used to calculate the thermal capacity of equivalent three-dimensional models.

6.2.1.1 Configurations

The six configurations tested were:

- (1) A: a 10kg PCM Air insert placed within the air channels of the hollow core slab.
- (2) B: a 10kg PCM Air diffuser placed below the hollow core slab air outlet.
- (3) B(2): a 4kg Double layer PCM air diffuser placed below the hollow core slab air outlet.
- (4) B(2)10: a 10kg Double layer PCM air diffuser placed below the hollow core slab air outlet.
- (5) C: a 10kg Soffit Layer of PCM covering the exposed slab
- (6) D: a 10kg PCM section in a water tank

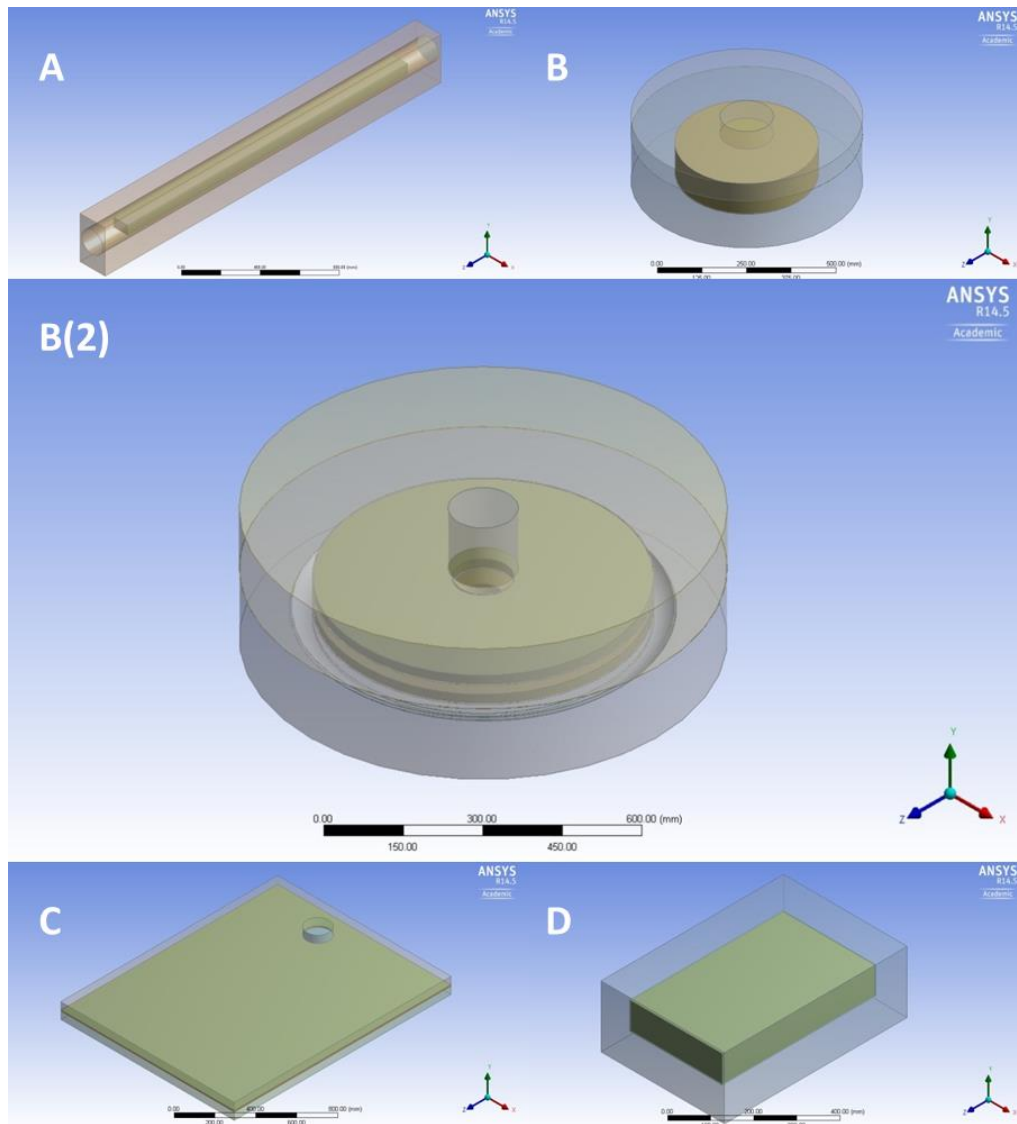


Figure 6.1 - 10kg Constant Mass Models of Configurations (A-D)

The models were designed to maintain the same PCM mass of 10kg in each configuration (Figure 6.1). All the configurations tested were encased in aluminium to avoid PCM leaking during the melt phase. From these models a thirty-millimetre cross-section of each was constructed and simulated. The cross-section models were used to aid stability and speed of simulations. The results generated are therefore suitable for performance comparison of the PCM configurations. Using the heat flux from the thirty-millimetre models, and the appropriate surface areas in Table 6.1, the thermal capacities for the three-dimensional constant-mass models were calculated.

The key difference to transpire between the 10kg models and the thirty-millimetre cross-section models is the air velocity in each scenario. Since the air inlet and PCM surface area varies significantly between the cross-section and constant-mass models it is not suitable to

use the average air temperature as a key performance indicator. A four acph simulation of the B(2) thirty-millimetre cross-section model was carried out to review the performance of the technology under lower velocities with results in the Appendixes. Across the models (A-D) the air-inlet areas are comparable, therefore comparable performance review is still possible.

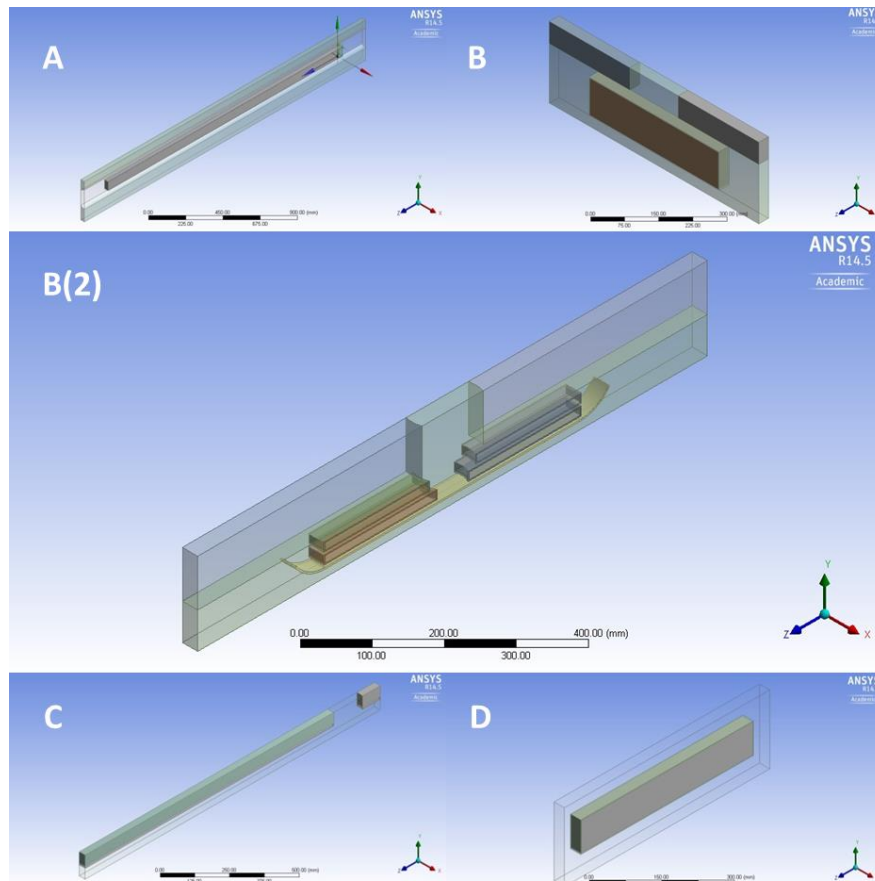


Figure 6.2 - 30mm Cross Section Models (A-D)

6.2.1.2 Table of Comparable Properties

To aid the comparable contrast between the thirty-millimetre cross-section models and the 10kg constant-mass models key volumes, masses and areas were documented in Table 6.1 and Table 6.2 for each scenario. Table 6.3 and Table 6.4 document summary ratios for each model. These demonstrated the exceptionally high air-change rates found in the thirty-millimetre cross-section models. Table 6.4 also includes volume multipliers that demonstrated the scale up required to go from the thirty-millimetre cross-section models to the 10kg constant-mass models.

Table 6.2 shows that all the models tested have a comparable inlet area ensuring a similar air flow-rate is supplied to each model. Table 6.4 reveals that the B(2)10 and C thirty-millimetre

cross-section models have the highest surface area to volume ratios. A and B(2)10 have the smallest air-change rates and A has the highest weight ratio of PCM to total twenty-four hour air mass.

Table 6.1 -10kg Constant-Mass Models Dimensions

| | | A: | B: | B(2): | B(2)10: | C: | D: |
|-----------------------------|-------|-----------|-----------|--------------|----------------|-----------|-----------|
| Slab Vol | m^3 | 0.088 | 0.019 | 0.061 | 0.090 | 0.089 | - |
| PCM Vol | m^3 | 0.013 | 0.013 | 0.005 | 0.013 | 0.012 | 0.013 |
| Air Vol | m^3 | 0.029 | 0.041 | 0.036 | 0.092 | 0.087 | - |
| Water Vol | m^3 | - | - | - | - | - | 0.035 |
| Slab Mass | kg | 251.8 | 53.9 | 173.8 | 257.0 | 254.9 | - |
| PCM Mass | kg | 10.21 | 10.18 | 4.07 | 10.16 | 10.04 | 10.21 |
| Air Mass | kg | 0.029 | 0.041 | 0.036 | 0.092 | 0.087 | - |
| Water Mass | kg | - | - | - | - | - | 35.45 |
| PCM Surface Area | m^2 | 0.665 | 0.377 | 0.819 | 1.347 | 3.582 | 0.434 |
| Inlet Air:Water Area | m^2 | 0.082 | 0.018 | 0.012 | 0.014 | 0.018 | 0.018 |

Table 6.2 - Thirty-millimetre Cross-sectional Models Dimensions

| | | A: | B: | B(2): | B(2)10: | C: | D: |
|-----------------------------|-------|-----------|-----------|--------------|----------------|-----------|-----------|
| Slab Vol | m^3 | 0.012 | 0.001 | 0.002 | 0.003 | 0.002 | - |
| PCM Vol | m^3 | 0.004 | 0.001 | 0.0003 | 0.0003 | 0.0003 | 0.001 |
| Air Vol | m^3 | 0.006 | 0.002 | 0.0019 | 0.004 | 0.0024 | - |
| Water Vol | m^3 | - | - | - | - | - | 0.002 |
| Slab Mass | kg | 34.6 | 2.6 | 6.8 | 9.3 | 5.8 | - |
| PCM Mass | kg | 3.062 | 0.972 | 0.263 | 0.263 | 0.228 | 1.02 |
| Air Mass | kg | 0.006 | 0.0021 | 0.002 | 0.004 | 0.002 | - |
| Water Mass | kg | - | - | - | - | - | 2.287 |
| PCM Surface Area | m^2 | 0.376 | 0.019 | 0.075 | 0.113 | 0.100 | 0.119 |
| Inlet Air:Water Area | m^2 | 0.004 | 0.005 | 0.004 | 0.004 | 0.004 | 0.006 |

Table 6.3 - Summary Ratios for 10kg Constant-Mass Models

| | | A: | B: | B(2): | B(2)10: | C: | D: |
|--|-----------------|--------|-------|-------|---------|-------|----------|
| PCM Surface Area to Volume Ratio | $m^2:m^3$ | 52.7 | 30.0 | 163.2 | 107.4 | 289.0 | 34.5 |
| acph | <i>per hour</i> | 15,444 | 2,338 | 1,824 | 806 | 1,091 | 1,005 |
| PCM:Total Air mass (in 24 hours) | $kg:kg$ | 0.001 | 0.004 | 0.003 | 0.006 | 0.004 | 0.000012 |
| Slab:Total Air mass (in 24 hours) | $kg:kg$ | 0.024 | 0.024 | 0.109 | 0.145 | 0.111 | - |
| Slab&PCM:Air mass (in 24 hours) | $kg:kg$ | 0.025 | 0.028 | 0.112 | 0.151 | 0.116 | 0.000012 |

Table 6.4 - Volume multipliers and summary ratios for the thirty-millimetre cross-section models

| | | A: | B: | B(2): | B(2)10: | C: | D: |
|--|-----------------|-------|--------|--------|---------|--------|----------|
| 30mm Volume Multipliers | | | | | | | |
| Slab | | 7.28 | 20.94 | 25.40 | 27.51 | 43.97 | - |
| PCM | | 3.33 | 10.47 | 15.48 | 38.67 | 43.94 | 10.00 |
| Air/Water | | 5.17 | 19.17 | 18.64 | 22.44 | 36.08 | 15.50 |
| Summary Ratios | | | | | | | |
| PCM SA:V | $m^2:m^3$ | 99.4 | 16.1 | 230.8 | 349.4 | 355.5 | 94.5 |
| acph | <i>per hour</i> | 3,888 | 11,411 | 10,281 | 4,899 | 9,950 | 5,315 |
| PCM:Total Air mass (in 24hrs) | $kg:kg$ | 0.006 | 0.0017 | 0.0005 | 0.0005 | 0.0004 | 0.000003 |
| Slab:Total Air mass (in 24hrs) | $kg:kg$ | 0.067 | 0.0044 | 0.0142 | 0.0194 | 0.0100 | - |
| Slab&PCM:Air mass (in 24 hours) | $kg:kg$ | 0.073 | 0.0061 | 0.0148 | 0.02 | 0.0104 | 0.000003 |

6.2.1.3 Test Conditions

The test conditions simulating peak-cooling-demand scenario used for all simulations, except in the different conditions test, were:

- Twenty-four hour transient simulations
- Initialised with slab, case and PCM parts at 18°C (to replicate post night cooling [168])
- Air or water initialised at 23°C (to breach cooling set-point [168])
- Heat load of 50W/m² distributed evenly across the soffit layer [12, 169]
- Constant inlet air velocity of 1.5m/s (or constant inlet water velocity of 0.56m/s [34]) both at 25°C (to breach peak set-point [168]).

As standard, A22H-PCM, manufactured by PCM Products, was used through the majority of the simulations. A22H physical properties can be found in Table 6.11. To observe the benefits of the PCM incorporation the PCM void was filled with aluminium to offer a base case.

For each scenario simulated the performance benefit, thermal capacity and enhanced thermal transfer was reviewed via the following time dependant monitors (Figure 6.3 and Figure 6.4):

- Slab Temperature
- Air (or Water) Temperature
- PCM Temperature
- PCM Case to Air Heat Flux
- PCM Liquid Fraction

Thermal mass enhancement for energy saving in UK offices

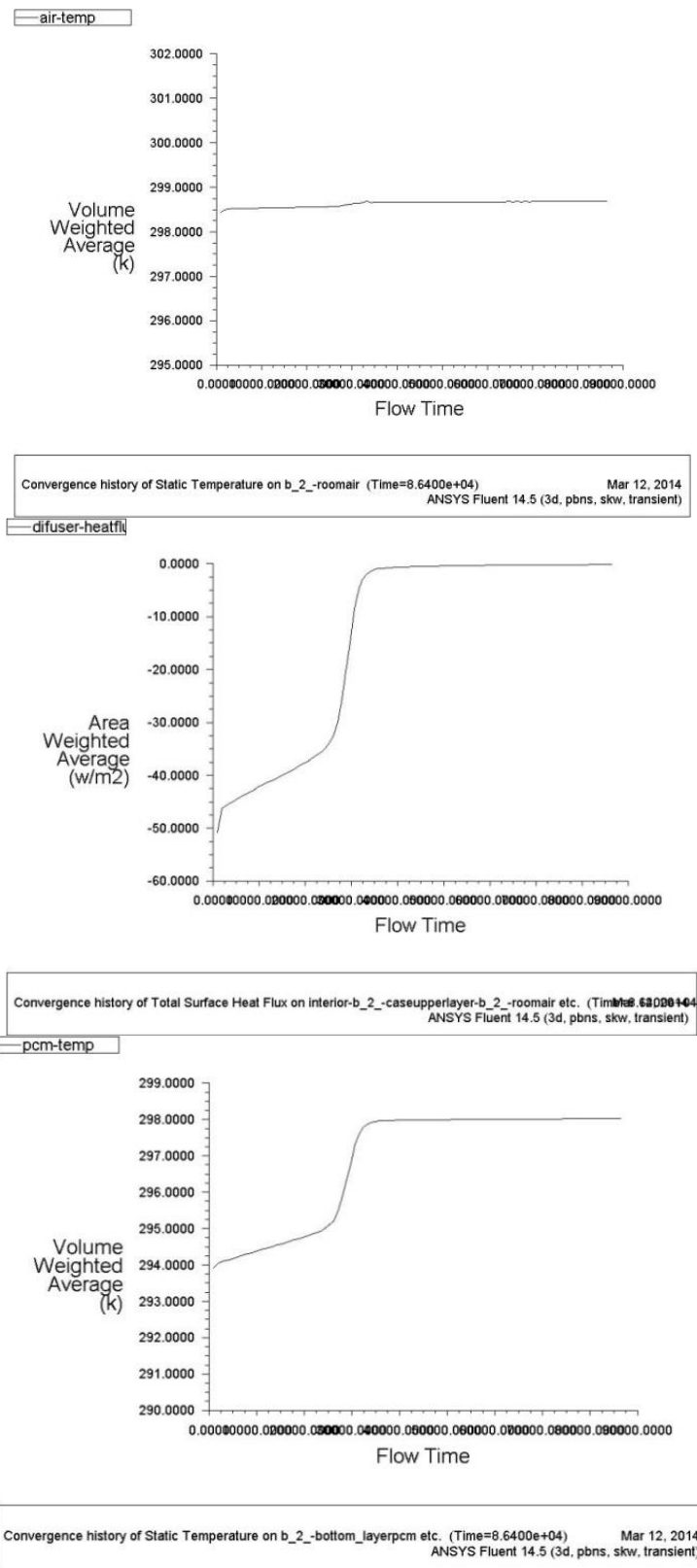


Figure 6.3 - Example of the first three CFD monitors reviewed

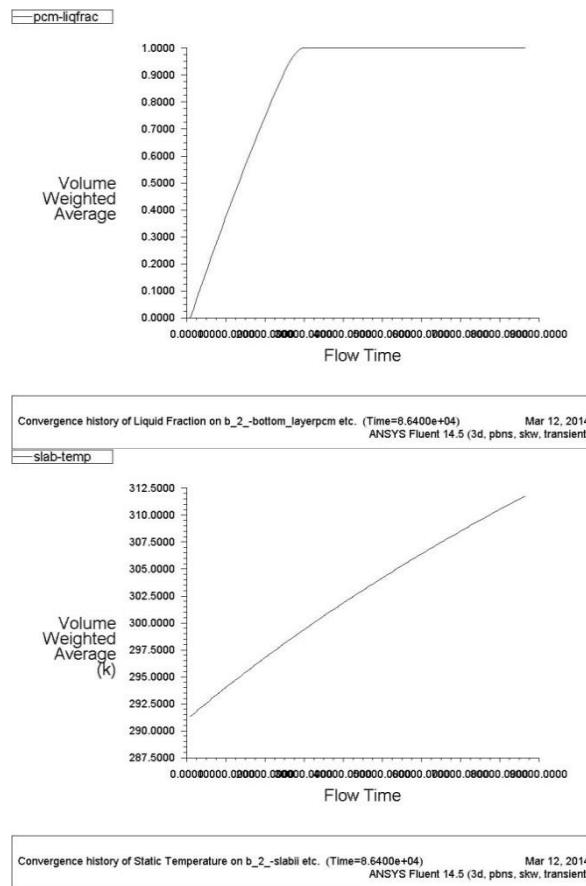


Figure 6.4 - Examples of the final two monitors reviewed over the twenty-four hour CFD simulations

From the twenty-four hour monitors produced data was extracted for specific performance at key time intervals:

- Initially (t=0 seconds)
- 5 minutes (t=300 seconds)
- Half an hour (t=1800 seconds)
- 2 hours (t=7200 seconds)
- 8 hours (t=28800 seconds)
- 24 hours (t=86400 seconds)

From this data graphs and calculations were carried out accordingly. The cooling power output (W), available at different time periods, was calculated by multiplying the heat flux (W/m^2) by the surface area (m^2). By further multiplying these figures by their time period (hours) a cooling energy figure in watt-hours (Wh) was generated.

6.2.1.4 Independence Testing

To determine the suitable parameters for the models, mesh and time-step independent tests were conducted to determine the suitable modelling parameters.

6.2.1.4.1 Mesh Independence Testing

For the mesh independence testing, steady state tests were conducted with different levels of mesh refinement on the A and B(2) models. In both cases the PCM temperature was monitored to compare results. The different mesh settings are specified in Table 5.3. The results and preferred settings, based on convergence speed and accuracy, are displayed in Table 6.6 and Table 5.3 respectively. For each simulation case (A-D) the preferred mesh settings were used.

Table 6.5 - Mesh Parameters

| Mesh Parameter | Fine | Medium | Coarse | Preferred |
|------------------------------|--------------------|--------------------|--------------------|--------------------|
| Use advanced sizing function | on: curvature | on: curvature | off | on: curvature |
| Relevance Center | Fine | Medium | Coarse | Medium |
| Initial Seed Size | Active Assembly | Active Assembly | Active Assembly | Active Assembly |
| Smoothing | High | Medium | low | Medium |
| Transition | Slow | Fast | Fast | Slow |
| Span Angle Center | Fine | Medium | Coarse | Fine |

Table 6.6 - PCM Temperature under differing Mesh Parameters

| | A | B(2) upper | B(2) lower |
|----------------------------|-------|---------------|---------------|
| PCM Temperature (K) | | | |
| Coarse | 298.3 | 298.0 | 298.2 |
| Medium | 298.2 | 298.1 | 298.2 |
| Fine | 298.3 | 298.0 | 298.2 |
| Preferred | 298.3 | 298.0 | 298.2 |

6.2.1.4.2 Time-step Independence Testing

To confirm the time-step independence, transient simulation was run on the A and B(2) models for two hours. The boundary conditions were maintained as outlined in the Test Conditions section (Section 6.2.1.3). Four step-size combinations were investigated (Table 6.7) and the PCM temperature monitored during this period. The two hour value for each parameter was reviewed for the different combinations investigated, with the preferred time-step parameters offering efficient simulation. Additionally, the PCM liquid fraction was reviewed in the B(2) investigation. Based on the Table 6.8 results, the good fit across the

time-step results suggests time-step independence for the conditions tested. For each case (A-D) the 24hr Test settings were used.

Table 6.7 - Time-step Independence Settings

| | | 24hr | 2hr | Half | Quarter | 5sec |
|------------------------|----------------|-------------|-------------|-------------|----------------|-------------|
| | | Test | Test | Step | Step | Step |
| Step Size | <i>(secs)</i> | 180 | 180 | 90 | 45 | 5 |
| Number of Steps | | 480 | 40 | 80 | 160 | 1440 |
| Max iterations | | 20 | 20 | 20 | 20 | 20 |
| Total Time | <i>(hours)</i> | 24 | 2 | 2 | 2 | 2 |

Table 6.8 - Time-step Independence Results

| | A | B(2) | |
|------------------|---------------------|---------------------|-----------------------|
| | <i>PCM Temp (K)</i> | <i>PCM Temp (K)</i> | <i>PCM Liq. Frac.</i> |
| 2hr Test | 294.0 | 294.3 | 0.263 |
| Half Step | 294.0 | 294.3 | 0.265 |
| Qtr Step | 294.0 | 294.3 | 0.266 |
| 5s Step | 294.0 | 294.3 | 0.263 |

6.2.1.4.3 Iteration Independence Testing

Following the time-step independence testing the independence of modelled results based on the maximum number of iterations was investigated. The two hour test conditions in Table 6.7 were used for investigations with the number of max iterations varied. For the boundary conditions; a fixed 50W/m^2 heat flux was maintained on the soffit and the 1.5m/s inlet air entered at 298K . The model was initialised with air temperature at 296K and all other parts at 291K [168, 169]. The maximum number of iterations was varied between 5 and 200. The B(2) model was used as a test case as it represented the most complex model under investigation. The liquid fraction and PCM temperature after two hours were recorded and comparisons observed.

Table 6.9 displays the results of the test on the B(2) model. A maximum of 20 iterations shall be used going forward with this investigation as it offers sufficient accuracy coupled with small simulation durations.

Table 6.9 - Iteration Independence Results

| Max. Iterations | Liquid Fraction | PCM Temp (K) |
|------------------------|------------------------|---------------------|
| 5 | 0.160 | 295.6 |
| 20 | 0.164 | 295.7 |
| 50 | 0.165 | 295.7 |
| 200 | 0.166 | 295.7 |

6.2.2 Results and Discussion

6.2.2.1 PCM Configuration

To identify the optimum PCM configuration in conjunction with the active-hollow core system; air temperature, heat flux, theoretical energy savings and PCM liquid fraction were reviewed from the thirty-millimetre cross-sectional models of the 10kg PCM Configurations.

Despite offering the greatest cooling energy over the first eight occupied hours (Table 6.10) the PCM Water Tank (scenario D) was not graphed against the air options. It was considered early into the review that despite the good performance the building industry would be reluctant to utilise additional water systems due to the added complexity and risk associated. Should a significant performance improvement have been noted (ten times or more) then the scenario would have been considered in more detail, however this was not observed.

6.2.2.1.1 Air Temperature

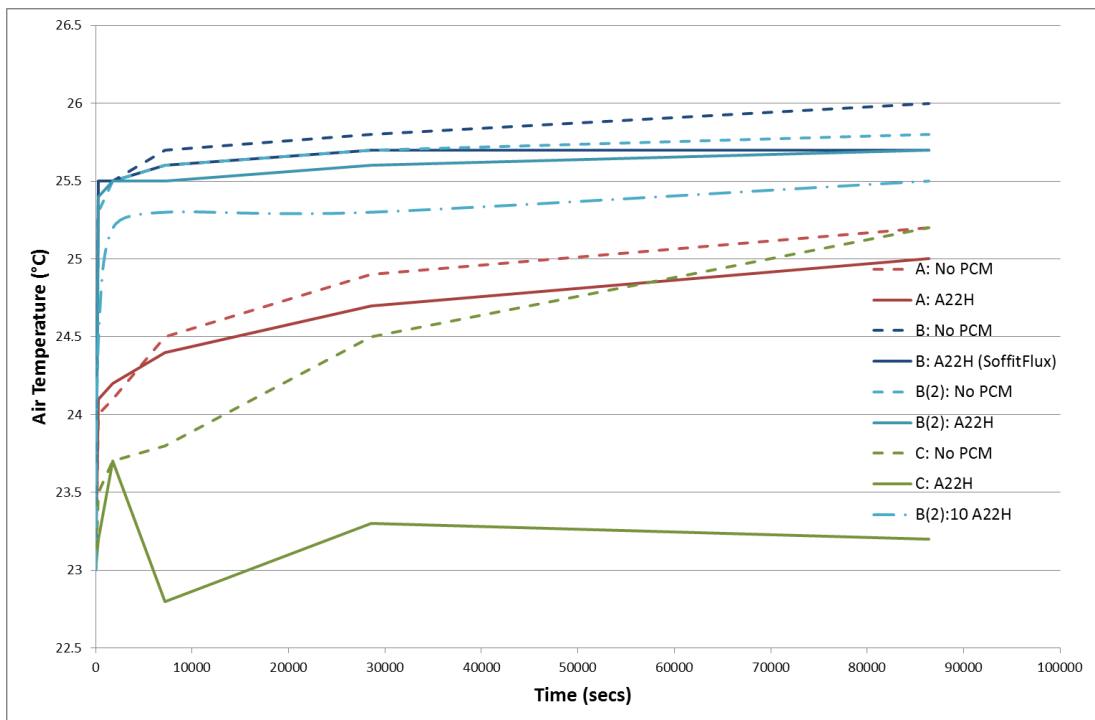


Figure 6.5 - Air Temperature vs Time Chart

As mentioned previously, due to the cross sectional models the benefits in the air temperature indicator were not as significant as expected. Never the less, even with the exceptionally high air change rate savings of between 0.2 and 2°C were observed in Figure 6.5. The greatest benefit was seen in scenario C. In scenario C the PCM soffit addition keeps the room air to its lowest temperature and also offered the greatest benefit over the non PCM comparison. This was in part achieved by blocking the thermal load from the ceiling soffit from interacting with the air temperature.

6.2.2.1.2 PCM Liquid Fraction

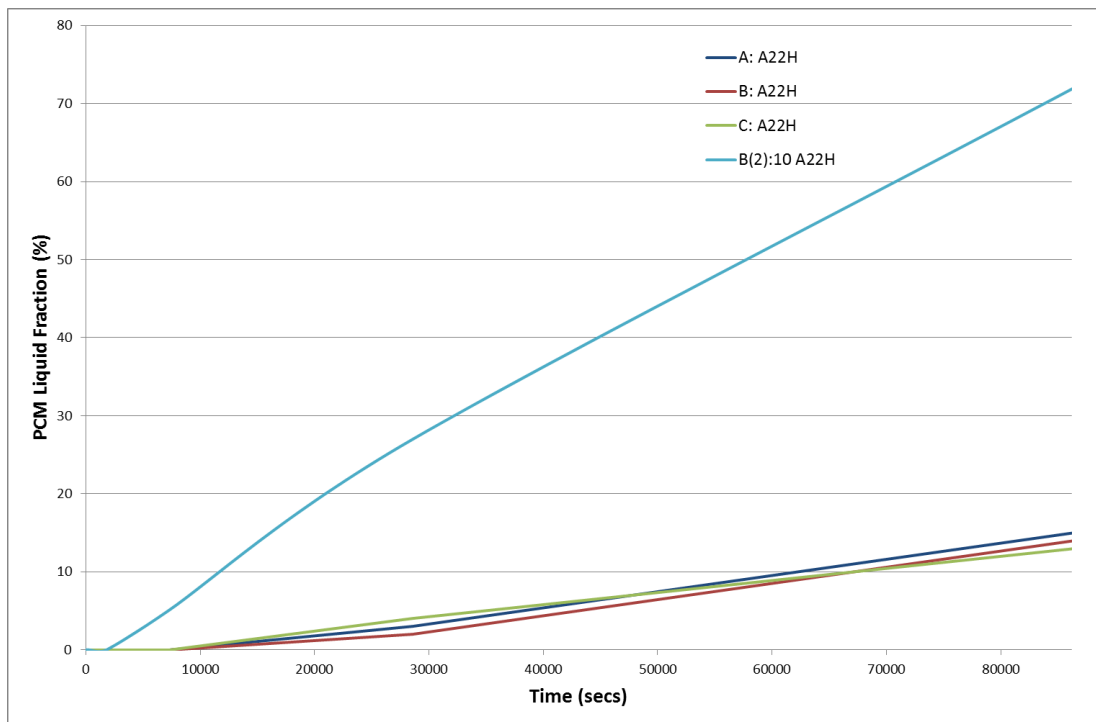


Figure 6.6 - PCM Liquid Fraction vs Time

From Figure 6.6 it is clear that the only air-based PCM scenario where there is a regular rapid charge and discharge of the PCM is in the B(2)10 model. Work found in the appendixes further demonstrates that in the light weight, 4kg B(2) scenario, it was possible to achieve complete regular daily melt-freeze cycling of the PCM (within eight hours).

6.2.2.1.3 Heat Flux

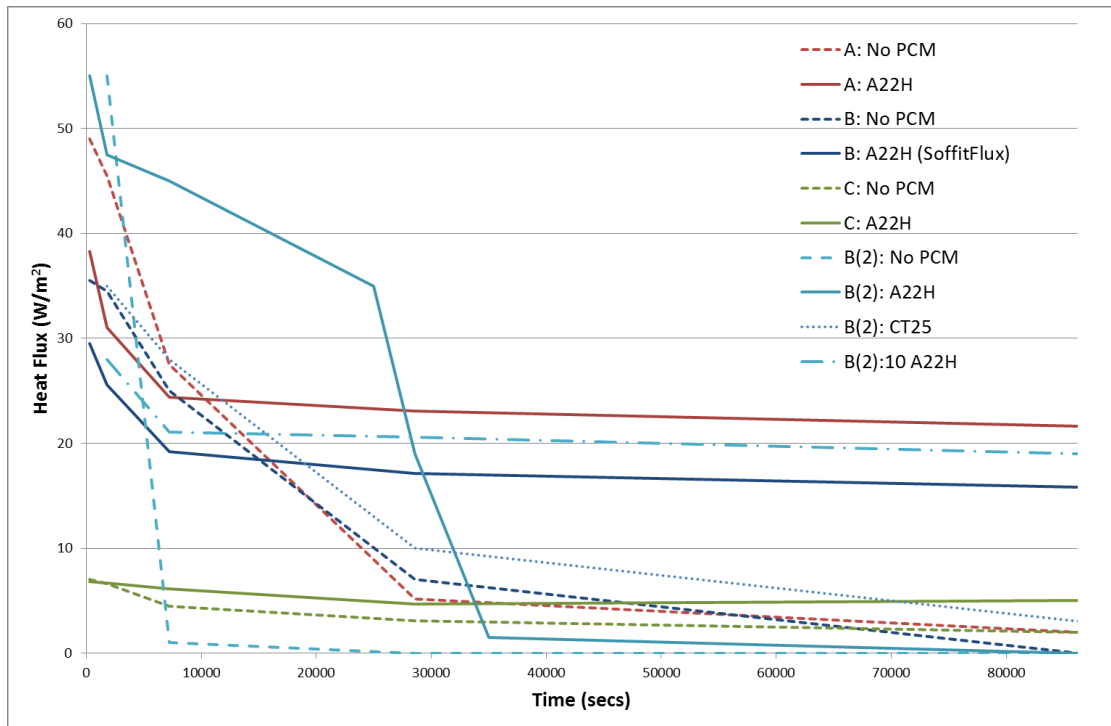


Figure 6.7 - Heat Flux vs Time Chart

Figure 6.7 charts the cooling heat flux of the different scenarios against a non-PCM Aluminium alternative over a twenty-four hour period (86,400 seconds). PCM benefits are seen during the process of cooling heat flux being delivered to the room. The initial high figures are caused through the sensible heat available during the temperature change. Once the phase change is reached the heat flux stabilizes, delivering cooling benefit to the room.

In each of the 10kg scenarios modelled (A, B, B(2)10 and C), the heat flux is stabilised throughout the twenty-four hour period. The 4kg (B(2)) model stabilises heat flux for eight hours (28,800 seconds), matching a typical office working week. B(2) X25 achieves only slightly better than many of the non-PCM references due to the peak room temperature of 25°C being too low to achieve a significant melt fraction.

From the heat flux graph the greatest sustained heat flux is demonstrated in the PCM insert model (A), followed by the 10kg double-layer diffuser (B(2)10) and the single-layer diffuser (B). The 4kg double layer diffuser (B(2)) shows greatest early heat flux provision but rapidly tappers once the PCM is fully melted.

6.2.2.1.4 Power Output and Energy Savings

Table 6.10 - Power Output

| | | A: | B: | B(2): | B(2)10: | C: | D: |
|---|---------|-------|------|-------|---------|-------|-------|
| Thirty-millimetre cross-section models | | | | | | | |
| Two hour Heat Flux | W/m^2 | 24.4 | 19.2 | 45.0 | 21.1 | 5.5 | 82.5 |
| 10kg constant-mass models | | | | | | | |
| PCM Surface Area | m^2 | 0.66 | 0.38 | 0.82 | 1.35 | 3.58 | 0.43 |
| Two hour Power Output | W | 16.1 | 7.3 | 36.9 | 28.5 | 19.7 | 35.5 |
| Two hour Cooling Energy Output | Wh | 37.0 | 17.1 | 74.4 | 67.4 | 39.2 | 96.7 |
| Eight hour Cooling Energy Output | Wh | 130.1 | 58.1 | 230.4 | 234.8 | 152.0 | 286.5 |

Table 6.10 contrasts the available cooling from each configuration during the first eight hours. Based on heat flux figures taken from Figure 6.7 for each thirty-millimetre scenario the heat fluxes were multiplied by the surface area in the constant-mass models. From these power outputs the energy output in watt-hours was generated.

From Table 6.10 the greatest cooling output was achieved in configuration D. As reasoned previously, despite the high cooling capabilities due to the increased risk and complexity of the water PCM system, not to mention the added energy losses through pumping and pipe losses, the air scenarios are favoured for further review. Therefore B(2) and B(2)10 are favoured. Based on eight hour days, five days a week for forty-eight weeks of the year; a 234.8Wh cooling saving per day could equate to over £8,000 of savings per year if the cooling demand is required and beneficial throughout the year.

6.2.2.1.5 Optimum Configuration

Based on these initial results a compromise solution must be found. Since PCM performance will be demanded during a peak couple of hours, rapid and sudden heat flux cooling capabilities are favoured over longer lasting options. To evaluate the optimum configuration two and eight hour review periods for cooling capabilities were observed.

Despite the excellent temperature reduction achieved by configuration C in Figure 6.5, the heat flux and cooling benefit on the room is minimal. Therefore the optimum solution suggested for further testing and modelling is the multi-layer diffuser (B(2) and B(2)10). Of

the air options considered this configuration offers the best consistent cooling capabilities throughout the conditions tested.

Appropriate PCM should be selected to best optimise the cooling performance when the PCM addition is most needed. It is possible then that a more suitable PCM (melt point circa 25°C) would give better cooling performance when the slab has been saturated. Further testing on PCM variation in different conditions was therefore carried out.

6.2.2.2 Different PCM

Table 6.11 contains the physical properties of the selected PCMs for further analysis in the B(2) model. To ensure the full capacity of each PCM is fairly contrasted the inlet air temperature was increased to 28°C with soffit and PCM temperature at 21°C and air temperature at 24°C initially, in line with scenario (v) in Table 6.13.

Table 6.11 - PCM Properties

| | A22H | X25 | A25H | RT24 |
|---|---------------------|------------|---------------------|----------------|
| Supplier | EPS/PCM Products | ***** | EPS/PCM Products | Rubitherm |
| PCM Type | Organic Wax | Bio-based | Organic Wax | Organic Wax |
| Latent Heat of Formation (kJ/kg) | 216 | 185 | 226 | 150 |
| Liquid Temperature (°C) | 22 | 25 | 25 | 25 |
| Solid Temperature (°C) | 21 | 22 | 24 | 21 |
| Density (kg/m³) | 820 | 859 | 810 | 880 |
| Specific Heat Capacity (kJ/kgK) | 2,860 | 2,100 | 2,150 | 2,000 |
| Thermal Conductivity (W/mK) | 0.18 | 0.18 | 0.18 | 0.2 |

As noted before, the air temperature benefit was minimal (<1°C) between the non-PCM and PCM simulations. This is due to the high air change rate causing a very low ratio of PCM mass to total air mass (Table 6.4). Laboratory testing will be utilised to determine overheating-offset capabilities, until then performance will be reviewed on liquid fraction, heat flux and watt-hours of cooling.

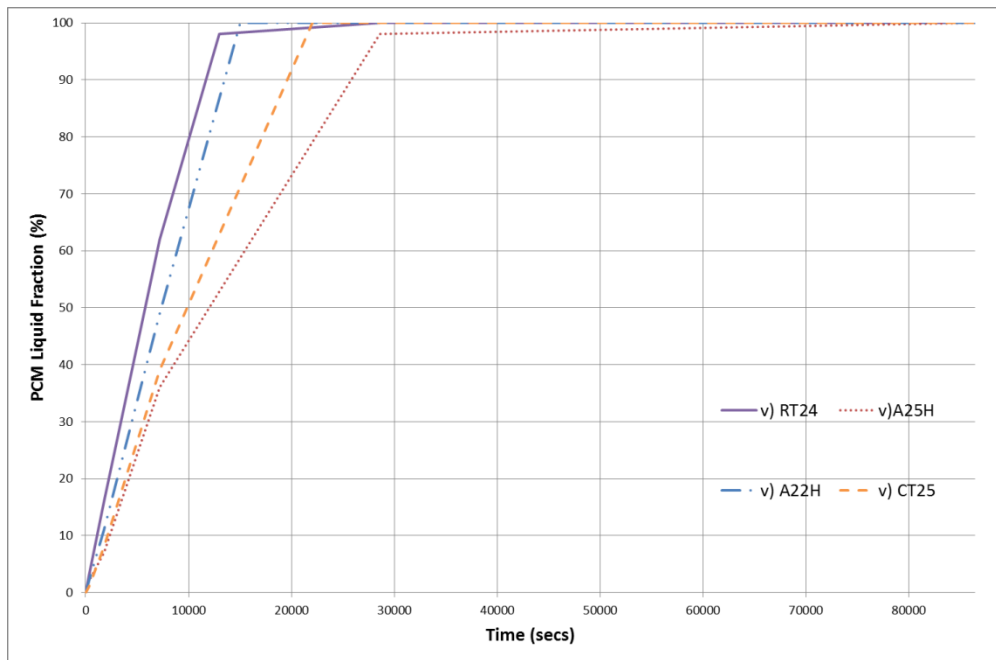


Figure 6.8 - PCM Liquid Fraction Comparison

From Figure 6.8 the liquid fractions over the twenty-four hour heating period are displayed. Based on the test conditions (initial temperature of 21°C rising to a maximum of 28°C) all the PCMs completed their melt cycles. RT24 reached 98% melt fraction fastest (taking 3.6 hours), then A22H melting in 4 hours, with X25 reaching 100% in 6 hours and finally A25H taking 8 hours to fully melt.

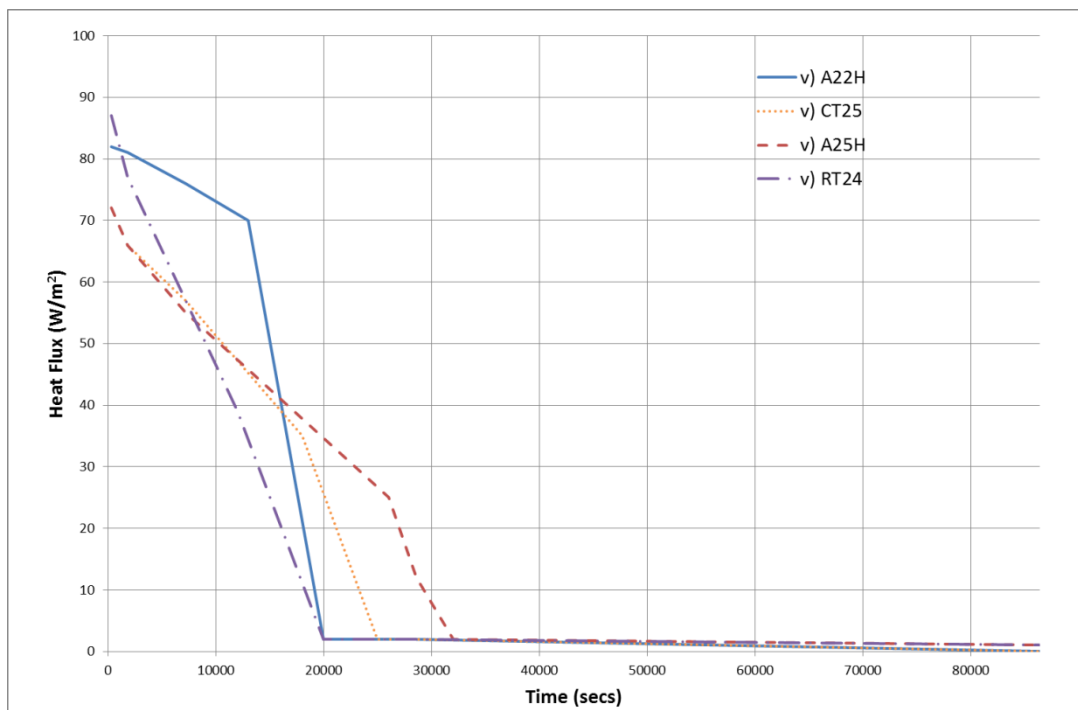


Figure 6.9 - Heat Flux of Differing PCM

From the heat flux monitors displayed in Figure 6.9, A22H maintained the greatest cooling heat flux during the first 4 hours until the majority of the phase change had been completed. X25 and A25H displayed comparable profiles. A25H offered the most sustained cooling heat flux. All of the PCMs significantly outperformed the non-PCM alternative in Figure 6.7.

Table 6.12 - Cooling Capacity Data (18-28°C)

| | | No PCM | A22H | X25 | A25H | RT24 |
|--------------------------------------|---------|--------|------|------|------|------|
| Thirty-millimetre B(2): Model | | | | | | |
| 2hr Heat Flux | W/m^2 | 1 | 76 | 57 | 55 | 57 |
| 10kg constant-mass Model | | | | | | |
| PCM Surface Area | m^2 | 0.82 | 0.82 | 0.82 | 0.82 | 0.82 |
| 2 hour Power | W | 0.8 | 62.3 | 46.7 | 45.1 | 46.7 |
| 2 hour Cooling Energy Output | Wh | 34 | 124 | 76 | 98 | 110 |
| 8 hour Cooling Energy Output | Wh | 37 | 282 | 220 | 286 | 204 |
| 8 hour PCM Cooling Value | $Wh/£$ | - | 12.8 | 15.7 | 13.0 | 5.3 |

From evidence found in Table 6.12, which followed the same method as Table 6.10 to calculate Power Output and Cooling Energy, A22H demonstrated the greatest two hour cooling performance; with an energy output of 124Wh. X25 and RT24 recorded comparable performance saving after eight hours, 220 and 204Wh respectively over the 21-28°C band simulated. A22H and A25H offered the greatest overall performance over eight hours of simulation, 282 and 286Wh respectively.

In Summary, A22H demonstrated the optimum two hour performance of the PCMs tested due to its high latent heat and ability to complete its phase change cycle quickly. A25H displayed the greatest eight hour cooling output. Based on the cooling value, calculated in Table 6.12, X25 displayed the greatest cooling output per pound (Wh/£), offering the commercial optimum for the prototype solution.

6.2.2.3 Different Conditions

As tabulated in Table 6.13 the PCM A22H and X25 performance was reviewed under differing conditions to determine their performance and value across a range of conditions. Each scenario represents a different occasion the PCM may face throughout a summers week:

- i) Typical of a peak week summers morning; slab cooled to 18°C via night cooling and air temperatures creeping up due to intense solar gains.

- ii) Similar to conditions (i) with increased internal solar gains and some pre-cooling carried out by the slab on the inlet air.
- iii) Typical of a peak summers afternoon during an extreme hot spell; slab has significantly overheated, the room air is already warm and the inlet air is being heated by the slab.
- iv) Typical of an average summers afternoon; AC plant has maintained slab temperatures to 21°C, room temperature is creeping up whilst the slab is struggling to cool warm inlet air.
- v) Typical of an extreme summer’s afternoon; high temperature (30°C+) ambient air is delivered to the slab and the slab cools to 28°C before the air enters the room.

In reality the PCM diffuser will undergo an even greater variety of room conditions however in the simulations initial conditions were maintained throughout the twenty-four hour simulation. Further simulations with purpose built software would be capable of testing the PCM diffuser under dynamic conditions.

Table 6.13 - Different Test Conditions

| | (i) | (ii) | (iii) | (iv) | (v) |
|---|------------|-------------|--------------|-------------|------------|
| Initial Room Air Temperature (°C) | 23 | 25 | 23 | 24 | 24 |
| Initial Slab Temperature (°C) | 18 | 18 | 28 | 21 | 21 |
| Inlet to Room Air Temperature (°C) | 25 | 23 | 25 | 22 | 28 |

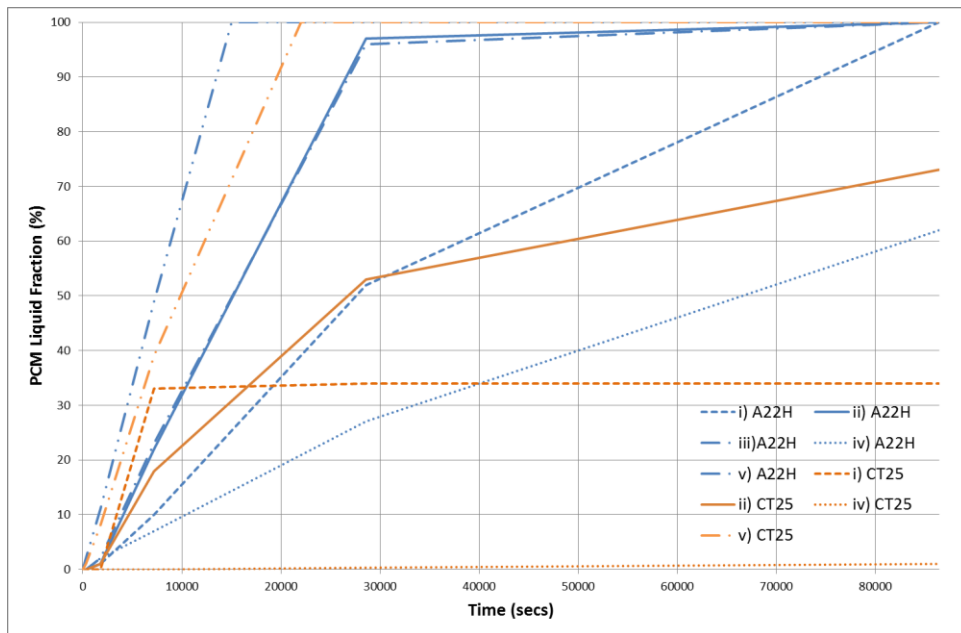


Figure 6.10 - PCM Liquid Fraction for B(2) Model under Different Conditions

Based on the liquid fraction in each of the conditions (Figure 6.10) the A22H achieved a higher or faster melt fractions than the X25 in all comparative cases. This means that the A22H is making more use of its latent heat capacity on a more regular basis; however the X25 has initialised the melt phase, but remains in it throughout the duration of the majority of simulations. Therefore the X25 has remaining capacity that can be utilised when overheating onset encroaches (scenario (v)).

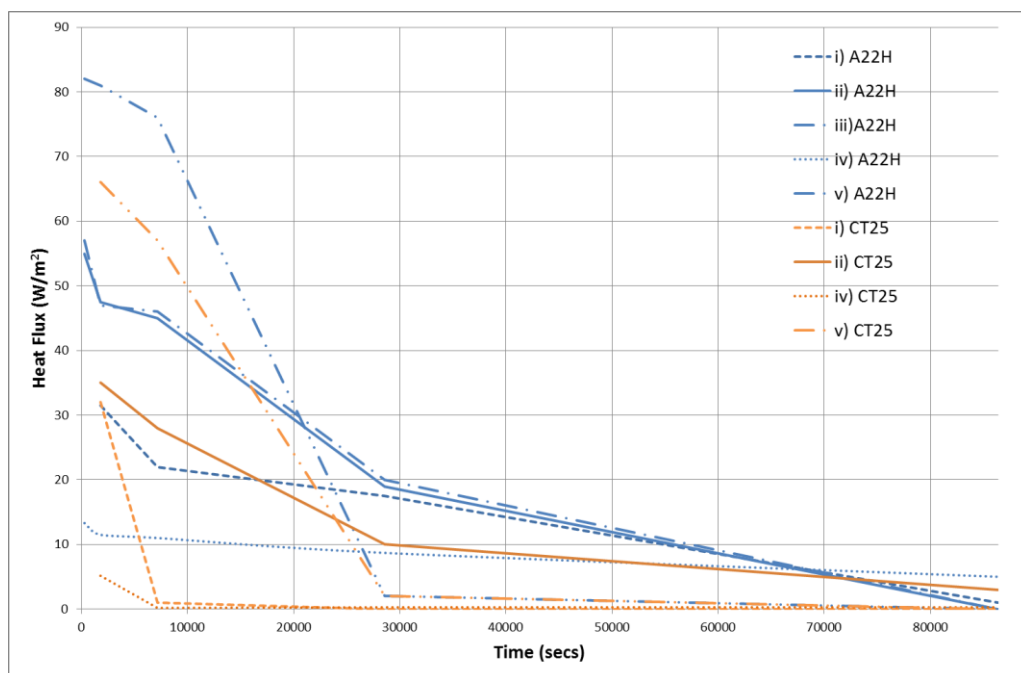


Figure 6.11 - Chart of Heat Flux against Time for B(2) models under different conditions

For each of the conditions tested (Figure 6.11), A22H offers a higher level of heat flux than X25. Similarly, the power outputs reported in Table 6.14 and Table 6.15 further confirm that A22H offers more cooling benefit in each summer condition. However when commercially considering the cooling value, X25 surpasses A22H in three out of four scenarios compared.

Table 6.14 - A22H Power Output at Different Conditions

| | | A22H | | | | |
|-------------------------------------|---------|-------|-------|-------|------|-------|
| | | i | ii | iii | iv | v |
| Thirty-millimetre Model | | | | | | |
| 2 hour Heat Flux | W/m^2 | 22 | 45 | 46 | 11 | 76 |
| Constant-mass Model | | | | | | |
| PCM Surface Area | m^2 | 0.82 | 0.82 | 0.82 | 0.82 | 0.82 |
| 2 hour Power | W | 18.0 | 36.9 | 37.7 | 9.0 | 138.3 |
| 2 hour Cooling Energy Output | Wh | 44.5 | 74.4 | 75.0 | 18.1 | 124.4 |
| 8 hour Cooling Energy Output | Wh | 140.8 | 230.4 | 235.8 | 66.1 | 314.5 |
| 8 hour PCM Cooling Value | $Wh/£$ | 6.4 | 10.5 | 10.7 | 3.0 | 14.3 |

Table 6.15 - X25 Power Output at Different Conditions

| | | X25 | | | |
|-------------------------------------|---------|------|-------|------|-------|
| | | i | ii | iv | v |
| Thirty-millimetre Model | | | | | |
| 2 hour Heat Flux | W/m^2 | 1.0 | 28.0 | 0.2 | 57.0 |
| Constant-mass Model | | | | | |
| PCM Surface Area | m^2 | 0.82 | 0.82 | 0.82 | 0.82 |
| 2 hour Power | W | 0.8 | 23.0 | 0.2 | 103.7 |
| 2 hour Cooling Energy Output | Wh | 31.9 | 50.9 | 6.1 | 98.5 |
| 8 hour Cooling Energy Output | Wh | 34.4 | 143.5 | 7.3 | 242.4 |
| 8 hour PCM Cooling Value | $Wh/£$ | 9.8 | 41.0 | 2.1 | 69.2 |

6.2.3 Summary of Findings

The simulations carried out offer a comparable performance assessment on the differing PCM enhancement configurations to a hollow core system. Based on the conditions tested an informed suggestion of which PCM to employ depending on desired outcome can be given. The total potential for energy savings and cooling value was quantified.

All of the configurations tested offered cooling benefit for the associated room. From the six configurations tested the 10kg two-layer diffuser (B(2)10) and the 10kg PCM contained Water Tank (D) offered the greatest levels of cooling during the first eight hours of the twenty-four hour simulations.

Configuration D was ruled out on practical grounds, due to the added risk and complexity it would bring to an actual installed system. In the risk-adverse building industry it is deemed a less feasible solution. Should the performance have greatly exceeded the best air based system the case would be stronger, but as D and B(2)10 had comparable benefits, B(2)10 has been suggested for prototype manufacture and laboratory testing.

Based on the simulation conditions investigated A22H offers the greatest two hour energy benefit due to the fast completion of the melt phase, A25H offers the greatest eight hour energy benefit in conditions (v) and X25 offers the greatest cooling value (Wh/£). The PCM to install will depend on the most pressing need for the given retrofit scenario. For laboratory testing X25 in a B(2)10 configuration will be tested to determine the thermal benefit and energy savings possible with the enhanced prototype slab, due to the preferable economic case.

6.3 PCM DSC Analysis

To contrast X25 diffuser performance, commercially available Energain® board was also shaped into a comparable diffuser. To characterise the Energain® and bio-based (X25) PCM used in the prototype diffusers, DSC-TGA analysis was carried out on each sample.

6.3.1 Method

The analysis was carried out by an SDT Q600 DSC-TGA machine (Figure 6.12) connected to a PC. The PCM samples were placed in two alumina crucibles inside the machine. Subsequently the balance was reset before placing the sample.

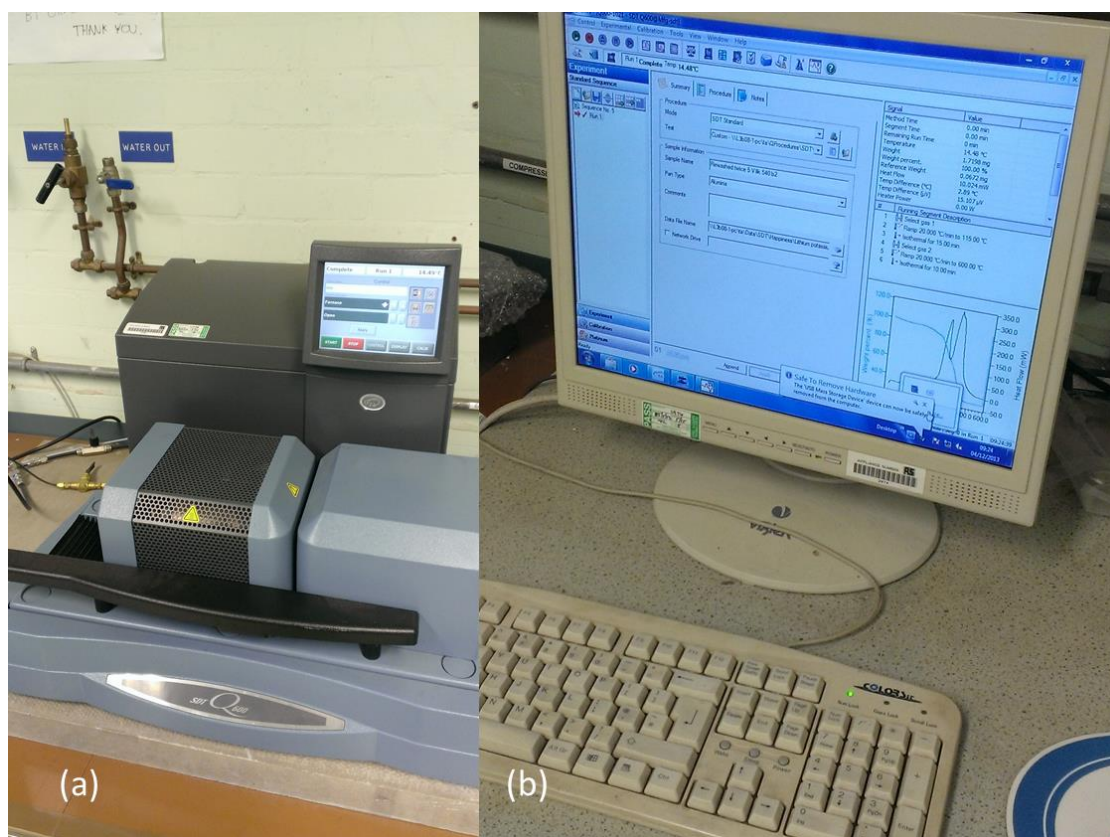


Figure 6.12 - (a) SDT Q600 DSC-TGA and (b) Accompanying PC

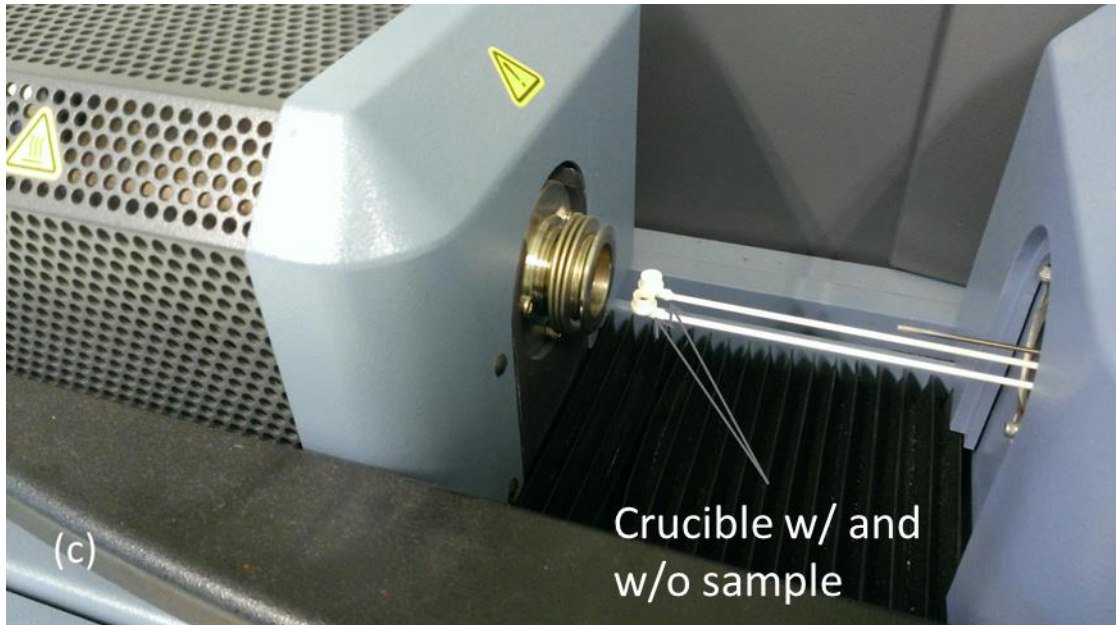


Figure 6.13 - Alumina Crucibles, Temperature Probe and Furnace Entrance

Due to the warm laboratory temperatures and the small sample size the onset of melting occurred at room temperature. Early DSC results demonstrated evidence of the melt phase finishing. To determine onset temperature the PCM samples were frozen and the laboratory window opened. The spatula and tweezers used to place the samples were cooled in ice. An ice filled beaker was used to transport the PCM samples from the freezer to the DSC-TGA machine. The combination of these cooling measures ensured onset temperatures could be determined from the DSC analysis.

For each sample, nitrogen gas was selected to maintain an inert atmosphere in the DSC furnace. The SDT Q600 DSC-TGA machine then increased the temperature by 1°C per minute until the furnace temperature reached 35°C . Once 35°C was reached the system cooled back to laboratory temperature.

The Energain[®] investigation was conducted in December, thus the laboratory temperature with window open was approximately 11°C . The DSC scan was conducted on a 14.6mg sample of Energain[®]. Energain[®] is made up of 40% ethylene polymer and 60% paraffinic PCM. Literature quotes the paraffin melt temp at 21.7°C and a latent heat capacity of 70kJ/kg [170].

The bio-based PCM (X25) DSC analysis, using the same heating rates as before, was carried out in June, therefore with the window open the laboratory temperature was 19°C . The

analysis was conducted on a 10.5mg sample of X25. Commercial publications state a melt temperature of 25°C and total latent heat of 186kJ/kg [85].

6.3.2 Results and Discussion

Figure 6.14 and Figure 6.15 display the major findings for each PCM sample from the DSC-TGA analysis. Full readings can be made available on request.

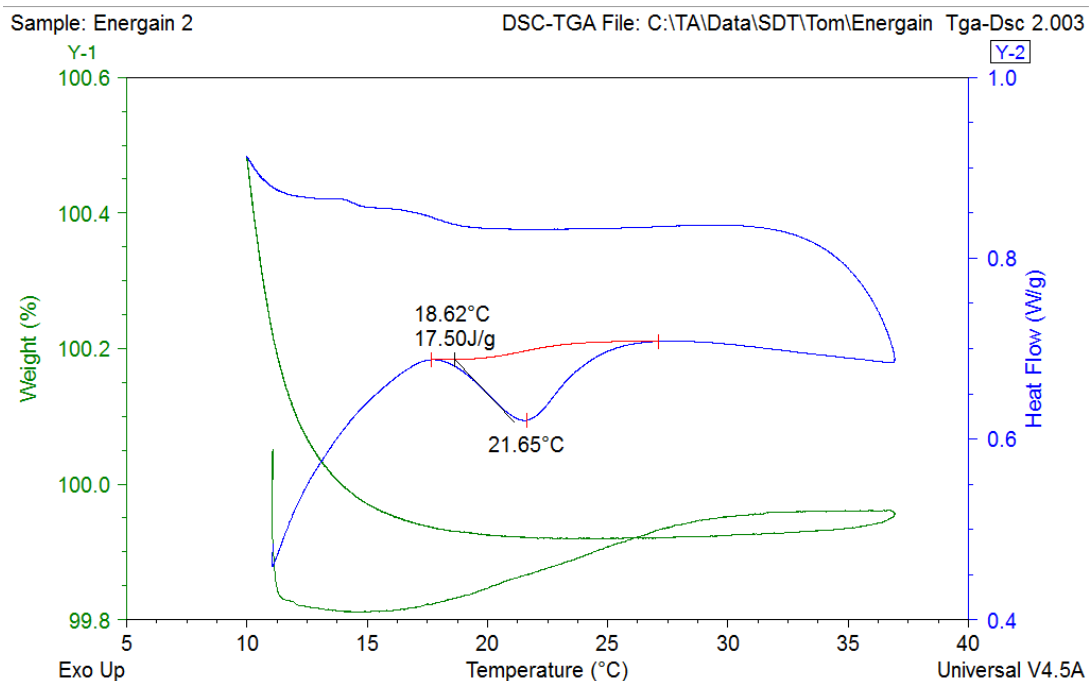


Figure 6.14 - DSC Test for Energain® Sample

Figure 6.14 displays both the DSC and TGA data. DSC measures the heat flow to and from the sample over a changing temperature. Again over a changing temperature the TGA assesses the weight variation. The TGA analysis is useful for monitoring and measuring the sublimation, combustion or evaporation of materials. Since both PCM samples tested assess the solid/liquid phase change, sample weight changes by less than 0.2mg. From analysis of the heat flow curve (W/g) the onset temperature is found to be 18.62°C, melt temperature was 21.65°C and latent heat was 17.50J/g.

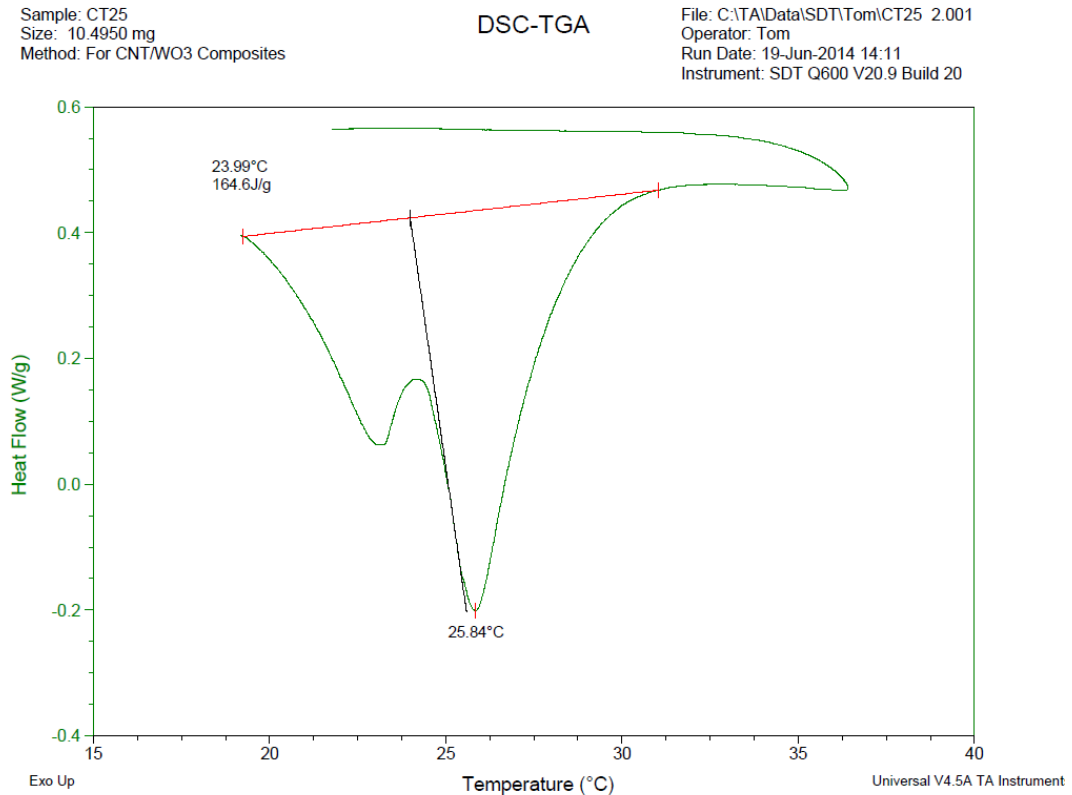


Figure 6.15 - DSC Test for X25

From Figure 6.15, two melt peaks were observed revealing X25 to be a eutectic PCM requiring further analysis (Figure 6.16) to determine the physical properties. The first peak has an onset temperature of 22.12°C, a melt peak at 23.14°C with total latent heat of 10.73J/g. The second, deeper, peak has an onset temperature of 24.70°C, a melt peak temperature of 25.84°C and a total latent heat of 34.82J/g.

Upon combined assessment of the double peaks the approximate onset temperature was 19.8°C, the average melt temperature was 24.49°C and the total latent heat was 164.6J/g. The literature data for each PCM sample is tabulated against laboratory findings in Table 6.16 to review findings.

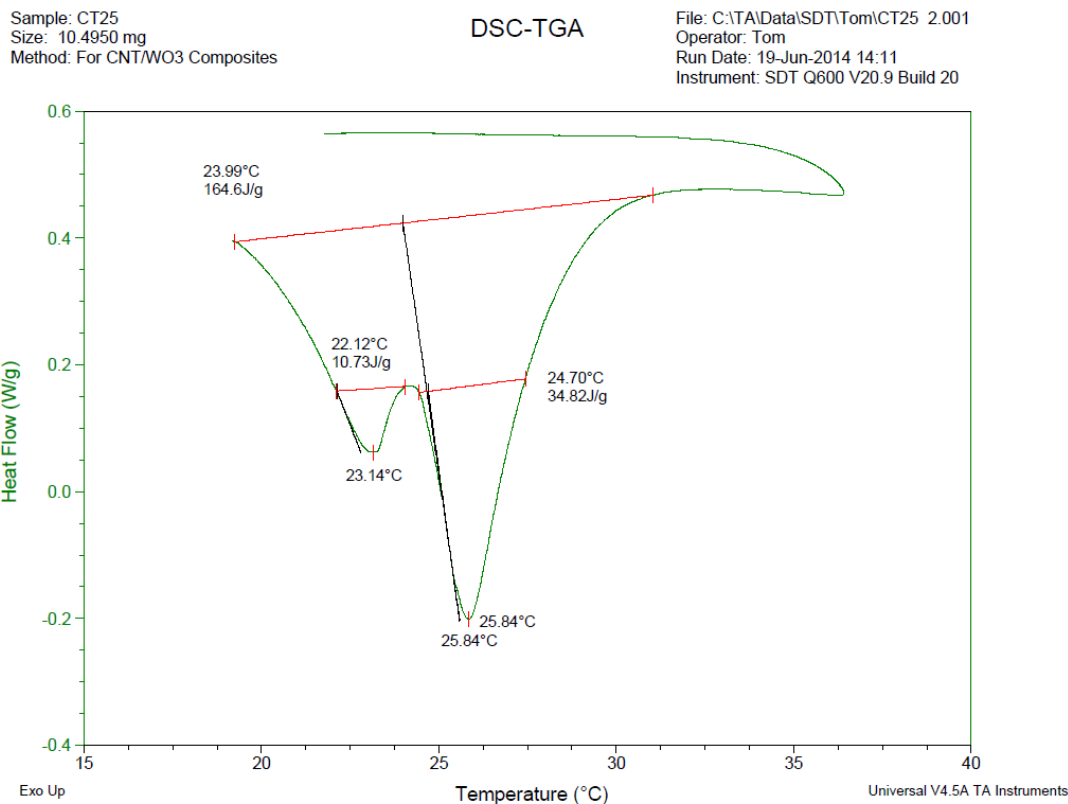


Figure 6.16 - X25 DSC Curve

Table 6.16 - Literature and Laboratory DSC Data

| | Literature Data | | Laboratory Data | | Units |
|--------------------------|-----------------|-------|-----------------|-------|-------|
| | Energain® | X25 | Energain® | X25 | |
| Onset Temperature | - | - | 18.6 | 19.8 | °C |
| Melt Temperature | 21.7 | 24.9 | 21.7 | 24.5* | °C |
| Latent Heat | 70.0 | 186.0 | 17.5 | 164.6 | kJ/kg |

*Average of two melt peaks at 23.14 and 25.84°C

Table 6.16 reveals a close match between literature and laboratory melt temperatures. The DSC assessments have also been useful for understanding when the melting phase begins. Significant discrepancy is evident between the literature and laboratory latent heat figures. Since Energain®, in bulk, is made up of a 40% polymer to 60% PCM ratio. It is possible that for the given sample analysed a greater percentage of polymer was present due to leaching during transportation, reducing the laboratory latent-heat reading. For the X25 assessment there is an 11.5% discrepancy. This may be due to the phase-change initiating below the DSC start temperature of 19°C.

6.3.3 Summary of Findings

The DSC tests generated onset and melt temperatures as well as determining the latent heat. Two melt peaks were found for the X25 sample. A good level of agreement was found between the literature and laboratory melt temperatures. Discrepancy was found between literature and laboratory latent heat figures.

6.4 Prototype PCM Diffuser Design and Construction

Based on the findings from the CFD modelling the B(2) design was favoured for prototype design and construction.

6.4.1 Design

Initially a circular diffuser was discussed with university technicians; however recognising the complexities a square diffuser was favoured as a suitable alternative. As modelled in ANSYS Fluent a two layer model was designed. The diffuser was constructed from five three-millimetre aluminium sheets cut and welded into three units to form the design in Figure 6.17 and Figure 6.18. Each unit was sealed and bolted to form the complete diffuser. Each layer was to be fitted with aluminium honeycomb and filled with 5kg of PCM.

6.4.1.1 Specification

The five aluminium sheets making up the bulk structure were ordered from LeanGate Metals with the dimensions:

- 2 Aluminium Sheets of 600x600x3mm for layer bases
- 2 Aluminium Sheets of 640x640x3mm for layer lids
- 1 Aluminium Sheet of 700x700x3mm for the angled diffuser base

Additionally 5m of $\frac{3}{4}$ by $\frac{3}{4}$ by $\frac{1}{8}$ " Aluminium angle was ordered to construct the layer walls along with 4m of $\frac{1}{4}$ " Aluminium round bar to separate each layer.

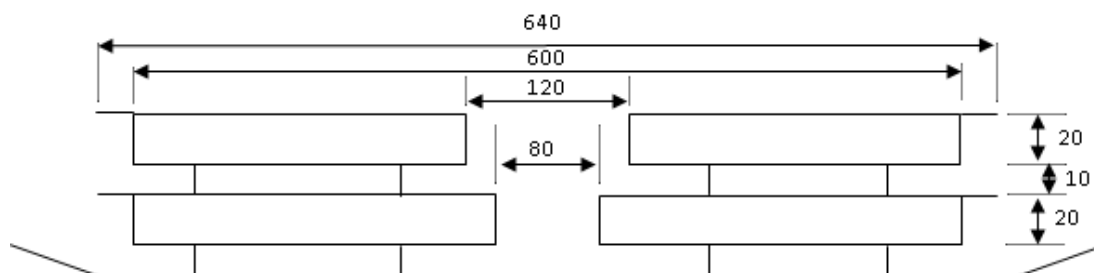


Figure 6.17 - Diffuser Specifications Cross Section (in mm)

The design specified a top layer of 600 by 600mm 20mm deep. The angle would be turned outwards to provide a lip to secure the 640 by 640mm lid. A square 120mm hole was to be removed from the upper layer lid and base with additional angle mounted to seal the hole. Beneath the upper layer structure, 10mm sections of round bar were to be welded to the underside of the upper layer and the top of the lower layer lid.

The lower layer lid was to have an 80 by 80mm central square hole removed from the 640 by 640mm section. As for the upper layer this would be secured to the lower 600 by 600mm section by bolting to the welded aluminium angle sides. An 80 by 80mm central square hole was to be removed from the lower layer and hole wall sealed with aluminium angle. As for the upper layer beneath the lower layer 10mm round bar sections were to be welded to both the second layer base and the 700 by 700mm angled diffuser base.

The 700mm square sheet was to be bent 30mm in from each edge to an angle of 30°. The remainder of the angled diffuser base was to remain intact to ensure diffuser air was deflected across the soffit surface.

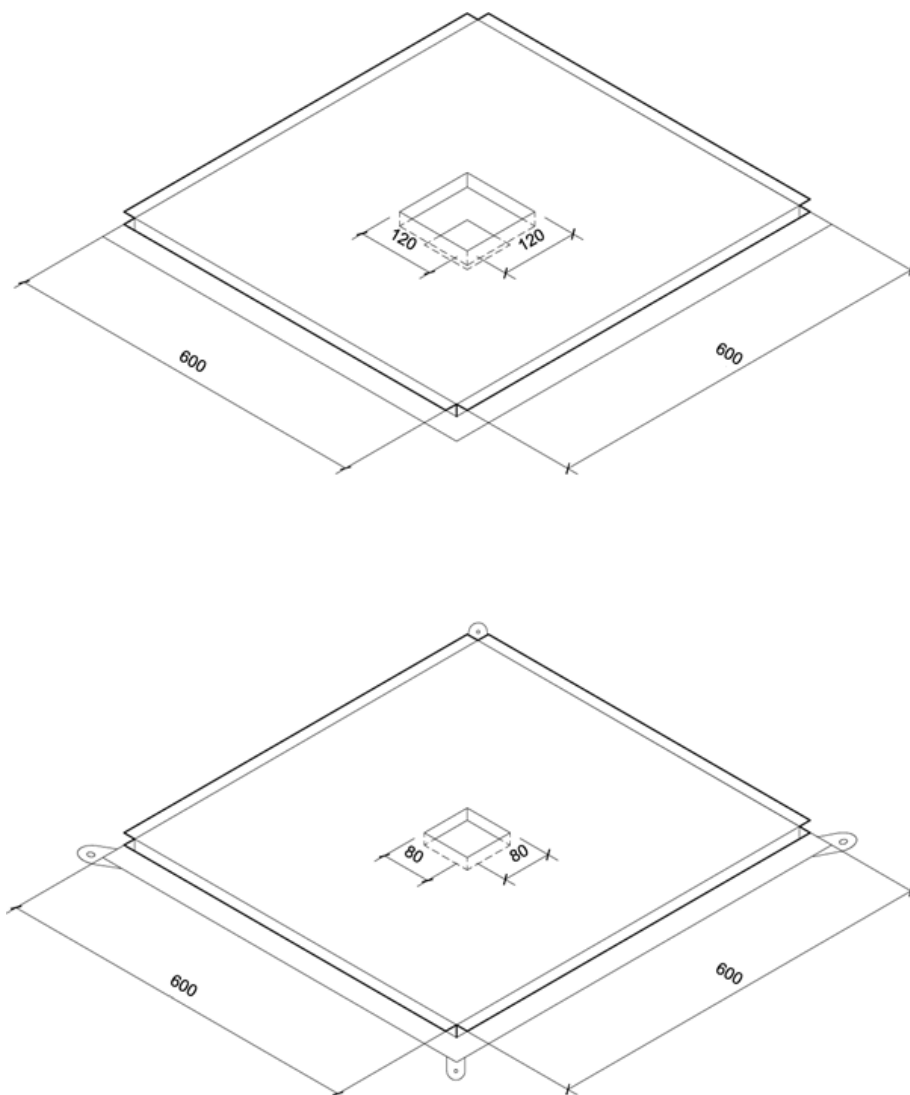


Figure 6.18 - PCM Diffuser Prototype Sketch (in mm)

6.4.2 Construction

As specified aluminium to construct the diffuser was sourced from LeenGate Metals. The required five sheets were pre-cut. However a mix up in dimensions meant the sheets delivered were four 600 by 640 by 3mm sheets and one 700 by 700 by 3mm aluminium sheet. An adjustment to the original design was therefore made to turn the aluminium angle in so the connection lip was on the inside of the rectangular diffuser and 600 by 640mm diffuser layers were constructed (Figure 6.19). The 30° bend in the 700mm square angled base sheet was maintained however the sheet was bent 30mm and 50mm from the sheet edge depending on the length of the edge above. The dimensions of the layer holes and layer spacing were kept as before.

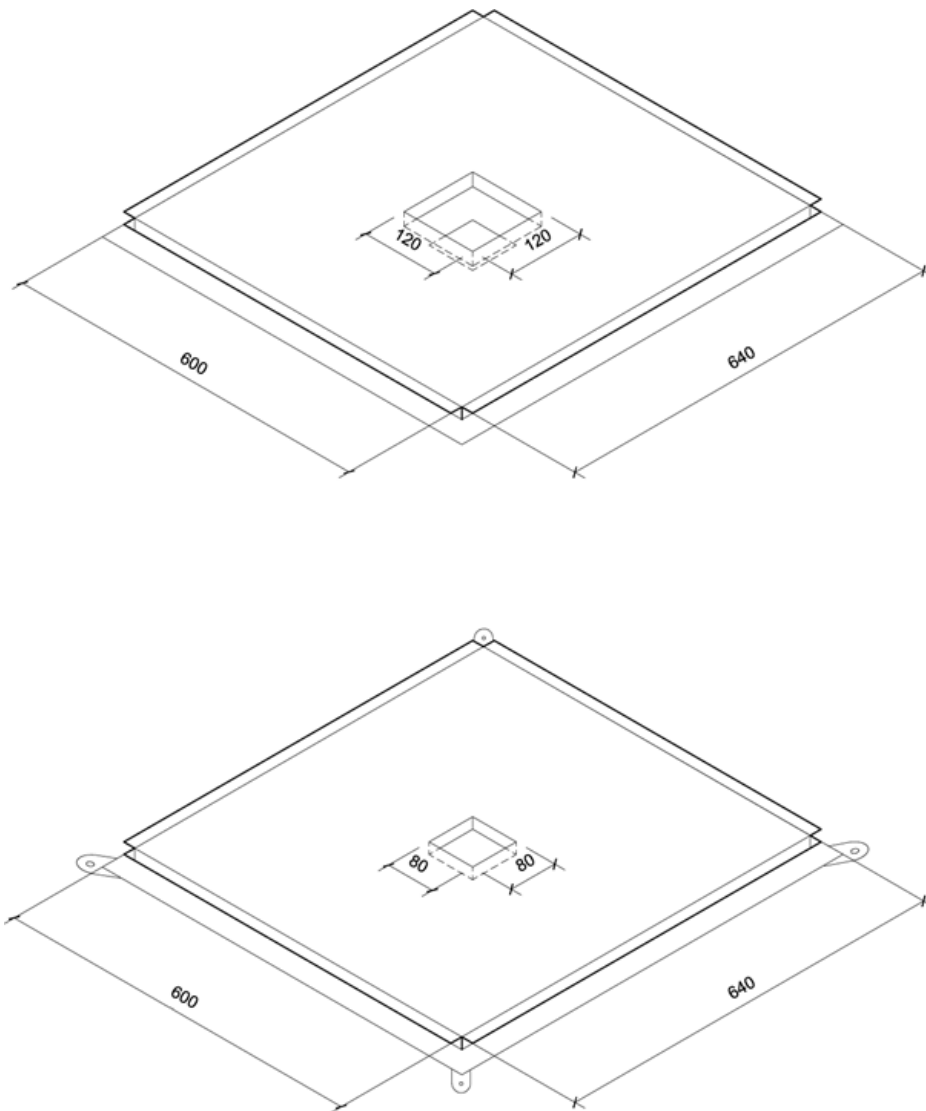


Figure 6.19 - Modified PCM Diffuser Dimensions following mis-delivery (in mm)

In the University of Nottingham workshop's, fully qualified technicians cut the required holes and the angle lengths. The bends were made as directed above. Following cutting, the angle sections were welded onto each layer base to construct a sealed tray. Due to the 10mm spacing it was not possible to weld the aluminium bar. Instead hollow spacers were fitted; the holes drilled and bolts inserted connecting the two layers (Figure 6.20). The same method was repeated to fit the bottom tray lid to the base of the upper tray and to fit the angled base sheet to the base of the bottom tray.

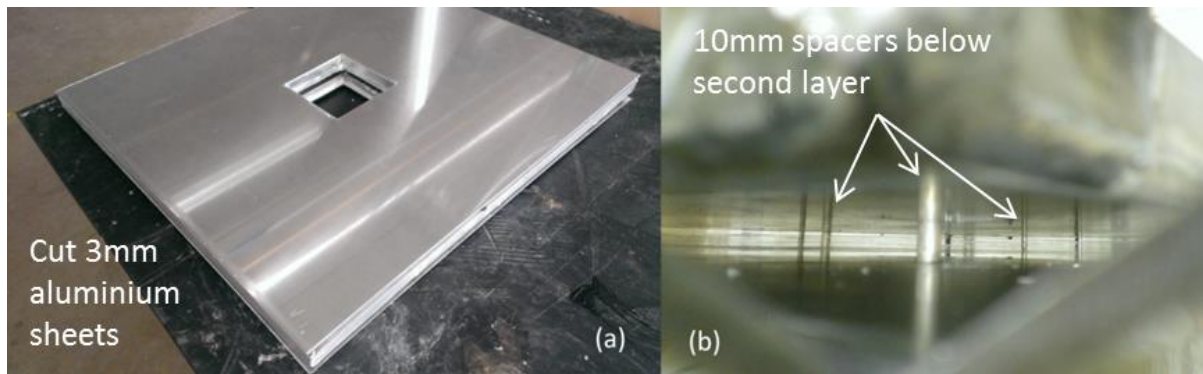


Figure 6.20 - (a) Upper Layer of Diffuser Cut (b) Spacers between Lower Layer and Angled Base

Additional aluminium tabs were welded to the bottom tray wall and the bottom tray lid to enable secure connection between the separate parts. Holes were drilled and tapped in the upper tray aluminium angle walls to secure the upper tray lid with the rest of the diffuser. A mild steel attachment was designed and fitted to the inner wall of the upper tray to secure the diffuser into the air outlet (Figure 6.21).

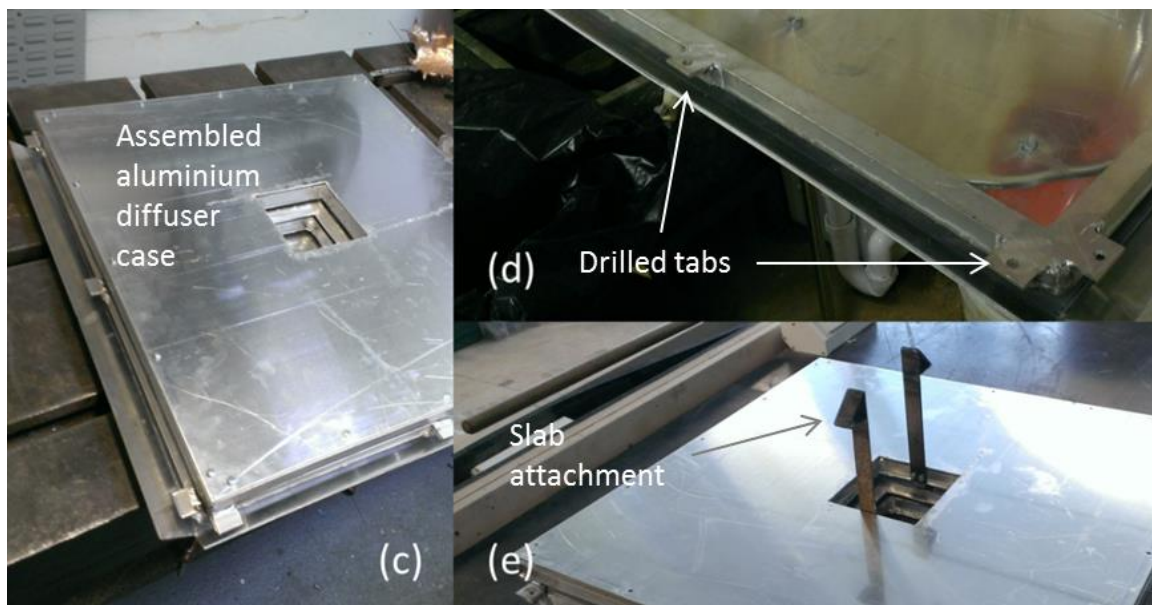


Figure 6.21 - (c) Diffuser with undrilled tabs, (d) Lower Layer with Drilled Tabs and (e) Mild Steel Diffuser Attachment

Having completed all the metal work the trays were prepared for PCM installation. Initially each tray was leak tested and subsequently sealed using an aluminium alloy. Additional sealant was inserted around vulnerable welds to ensure the trays remained water-tight. Following sealing, aluminium honeycomb sheets were measured, cut and inserted into both the upper and lower trays. The honeycomb was added to the tray volume to enhance the thermal conductivity to the PCM bulk (Figure 6.22).

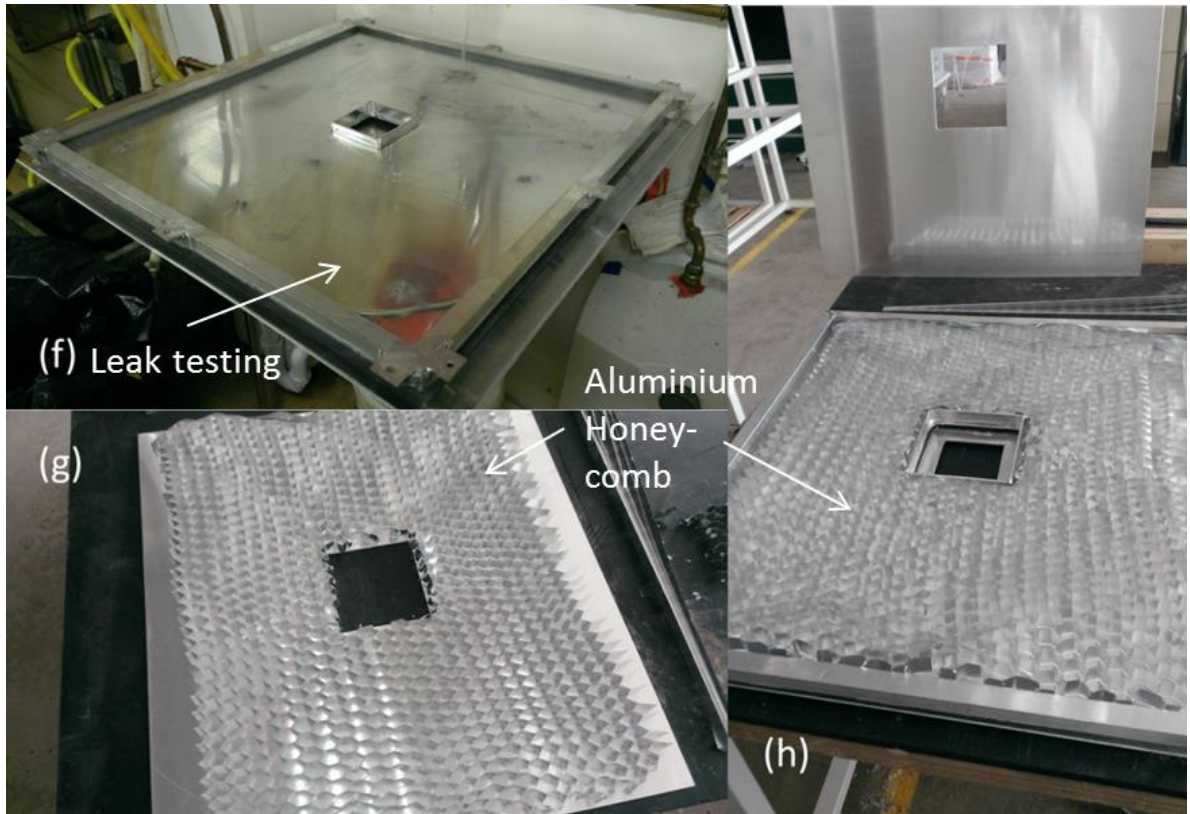


Figure 6.22 - (f) Leak Testing Lower Tray, (g) Measuring Honeycomb and (h) Fitting Honeycomb

The trays were then deemed ready for PCM charging. The PCM selected was X25. Based on cost benefit analysis of the modelling data, X25 offered optimum solution. The X25 sample installed was purchased in 4kg units. Since laboratory temperatures remained below X25 melt temperature the X25 samples were melted in a thermal chamber. The full containers were weighed before and after charging to determine the PCM loaded weight. A total of 7.53kg of PCM was loaded across the two diffuser trays (Figure 6.23).

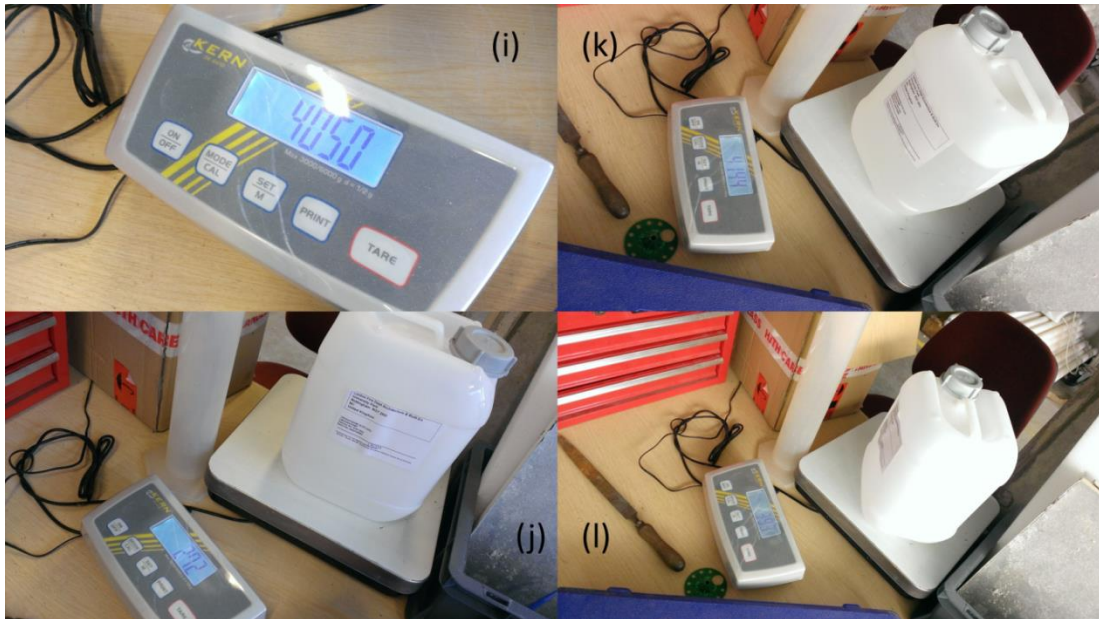


Figure 6.23 - (i) Lower Tray PCM Weight Before and (j) After Charging, and (k) Upper Tray Weight Before and (l) After Charging

Before the PCM solidified in the trays, type-K thermocouples were embedded in both trays midway into the PCM mass (Figure 6.24). Throughout the experimentation the temperature readings from these sensors, referenced against DSC curves, offered the only understanding of what phase the PCM was in at any given time. From industry quoted figures it can be assumed that for temperatures 18°C and below the PCM has been fully solidified whilst above 28°C the X25 is fully melted [85].

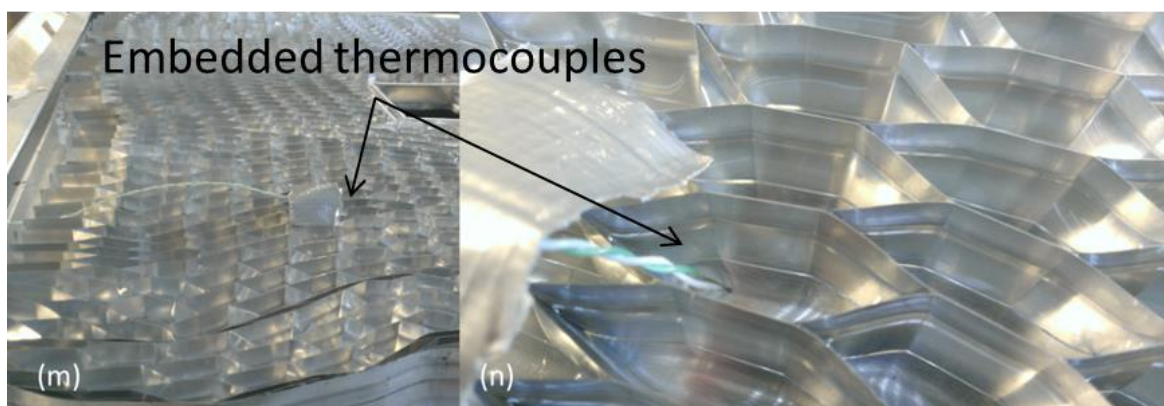


Figure 6.24 - (m) Charged Lower Tray, (n) Embedded Thermocouple

After charging each tray with the X25 PCM the trays were sealed and secured using the appropriate screws, nuts and bolts (Figure 6.25). With the PCM Diffuser prototype constructed and fully charged additional type-K thermocouples were placed between the PCM layers to give a measure of the air temperature passing through the diffuser. Finally the

diffuser was fitted inside a thermal chamber and chilled sufficiently to solidify the encapsulated PCM (Figure 6.26).



Figure 6.25 - (o) Fully Charged X25 Diffuser

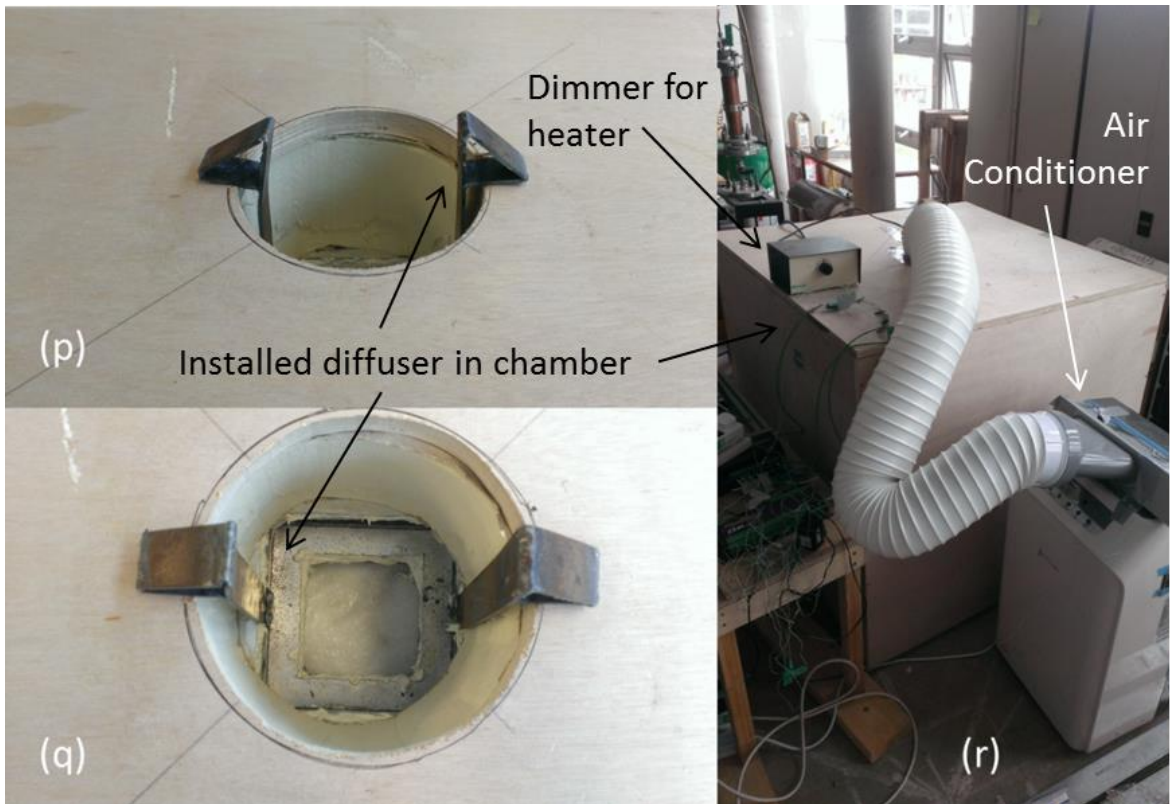


Figure 6.26 - (p) and (q) Diffuser Fitted inside Thermal Chamber and (r) Attached AC Duct Cooling Thermal Chamber

6.4.3 Additional Diffusers

In order to contrast the prototype X25 PCM diffuser performance two further diffusers were constructed for component testing in the thermal chamber.

6.4.3.1 Inert Diffuser

Following the same rectangular dimensions as the X25 diffuser an inert triple layer diffuser was constructed from 10mm thick Celotex insulation. Each layer was made up of one sheet of 640 by 600 by 10mm Celotex with upper and lower holes of 120mm and 80mm squares cut away respectively. As with the X25 diffuser, a 700 by 700mm angled base layer was constructed with the edges upturned (Figure 6.27).



Figure 6.27 - Inert Celotex Diffuser

6.4.3.2 Energain® Diffuser

To determine the benefit of the X25 PCM against a lightweight alternative an Energain® diffuser was constructed (Figure 6.28). To form the upper and lower tray layers an Energain® sheet was cut to the rectangular dimensions 600 by 640mm. The upper and lower Energain® layers had 120mm and 80mm central squares removed to allow the ventilation air to diffuse between the layers. Energain® sheets have a thickness of 5.26mm therefore each layer was 5.26mm thick with doubled over Energain® spacers separating the layers by 11.02mm. Based on the physical properties given in [170], the Energain® diffuser dimensions equate to a total PCM loading of 2.04kg. An inert angled Celotex base layer was combined to diffuse the air throughout the chamber.



Figure 6.28 - Energain(r) Diffuser

6.5 Prototype PCM Diffuser Proof of Concept Testing

Building on the work carried out in the PCM Component Modelling Section (section 6.2) that assessed the PCM enhancements to an air and water based active slab and the construction of the prototype PCM diffusers, the work done in this section investigates the component performance of the preferred dual-layer prototype PCM diffuser; B(2)10.

6.5.1 Method

- 1) Construct Diffusers (Figure 6.29):
 - a. an inert non-PCM Diffuser (to eliminate the diffuser variable)
 - b. a X25 PCM Prototype Diffuser (in line with findings from WP2)
 - c. an Energain® PCM Diffuser (to contrast X25 Diffuser performance)
- 2) Construct a thermal test chamber capable of mounting the diffusers, varying air inlet temperature and monitoring the temperature changes within (Figure 6.30 and Figure 6.31).
- 3) Carry out three hour cyclic tests for each diffuser configuration monitoring temperatures:
 - a. One hour heated air delivery (AC Heater set point 25°C)
 - b. One hour ambient air delivery (AC Fan Only)
 - c. One hour chilled air delivery (AC Chiller set point 18°C)
- 4) Retrofit a 50W/m² heat load to the thermal chamber
- 5) Carry out step (3) again for each diffuser with 50W/m² internal heat load
- 6) Conduct a heating and cooling saturation test:
 - a. With no diffuser
 - b. With the X25 prototype diffuser

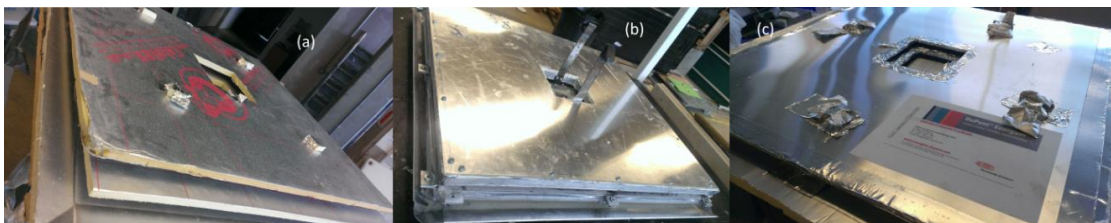


Figure 6.29 - Tested Diffusers (a) No PCM, (b) X25, (c) Energain(r)



Figure 6.30 - Thermal Chamber

Throughout the three-hour cyclic test the temperatures of air, PCM, chamber walls were monitored. The temperature set points on the AC unit during the heating and cooling periods were 25 and 18°C respectively. For the X25 diffuser studies, due to warm laboratory temperatures the heating set point was increased to 28°C. Additional reference scenarios without diffuser were tested with the same heat set point to determine relative benefits under the same conditions. Instrumentation accuracy was limited as per the levels found in Appendix B – Instrument Accuracy and Measurement Errors in Table 11.1.

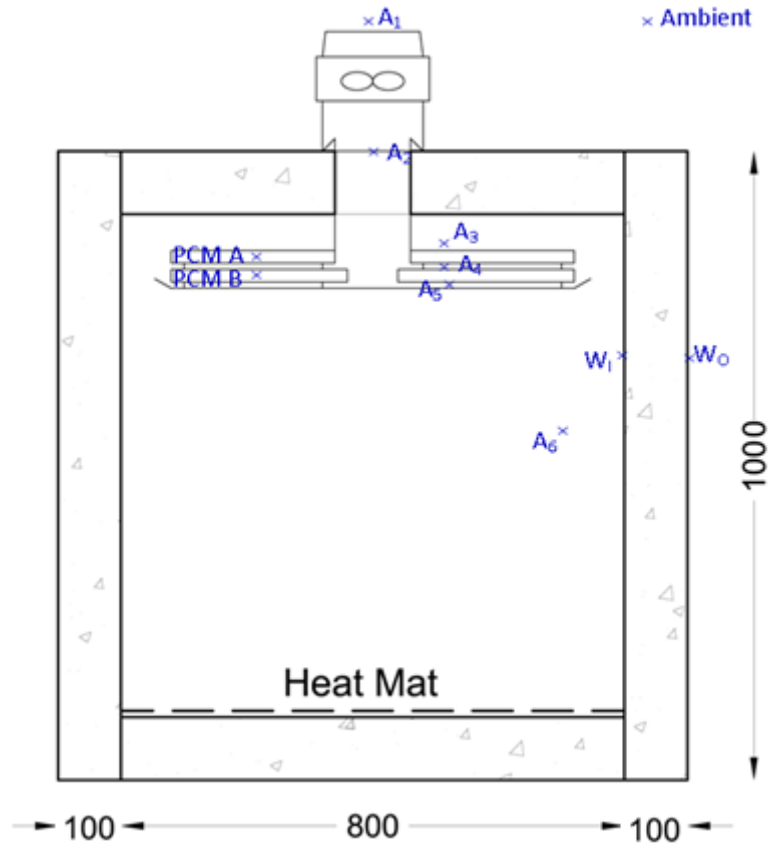


Figure 6.31 - Chamber and Thermocouple Setup (dimensions in mm)

6.5.2 Results and Discussion

Having conducted the experimental method, temperature profiles were generated for each test conducted. This enabled a review of diffuser performance under heating and cooling conditions. For the X25 diffuser the heater set point was increased from 25°C to 28°C due to the increased laboratory ambient temperature. Saturation temperature profiles are contrasted for the X25 diffuser and no diffuser tests. Finally a theoretical heat flux figure is calculated for the PCM diffuser cooling performance. Further experimentation with a heat flux sensor would validate this calculation.

6.5.2.1 Temperature Profiles

6.5.2.1.1 Three-hour Temperature Profiles

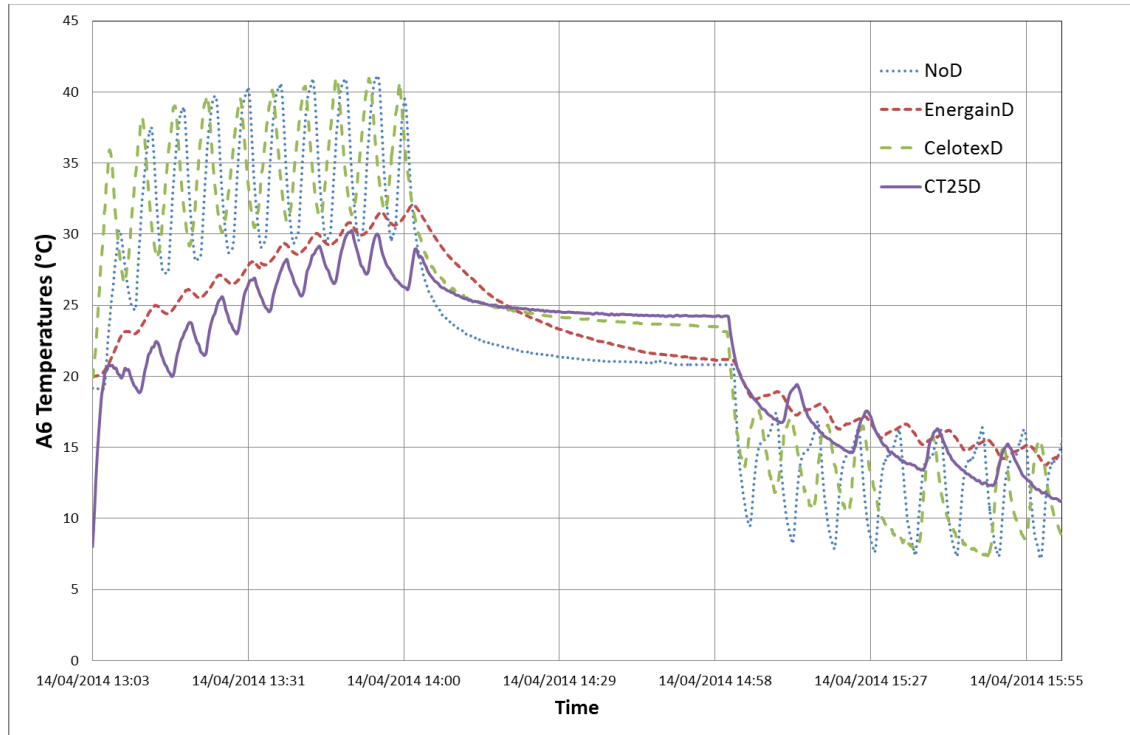


Figure 6.32 - Three hour Temperature Profiles without internal load

The three-hour temperature profiles displayed in Figure 6.32 display the variation in temperature during one hour of ventilated heating, one hour of ambient ventilation and one hour of ventilated cooling. For each system the fluctuation observed during heating and cooling periods is due to control of the AC system. The temperatures plotted were measured by the thermocouple at point A₆ in Figure 6.31.

Initially the Energain[®] performance was plotted against the base case empty chamber featuring no diffuser. To determine the source of the temperature savings, the Celotex (inert) diffuser was tested to ensure the Energain[®] performance had not given false readings due to the hot inlet air being diffused away from the temperature sensor. Comparing the blue dotted and green dashed line reveals that the Celotex diffuser reduced the temperature variation during the heating cycle but did not reduce the moving average chamber temperature.

The Energain[®] diffuser (EnergainD) and X25 diffuser (X25D) reduced the heating sinusoidal-average chamber temperature by 4.8 and 6.8°C respectively against the no-diffuser (NoD) reference at the end of the heating period. During the ambient stabilisation period only the

EnergainD noticeably delayed the temperature drop to ambient temperature. This was due to the ambient temperature in the EnergainD case being near to the melt temperature of 21.7°C. In the X25D study the ambient temperature was 24.2°C; 2.2°C above the quoted freeze temperature of X25.

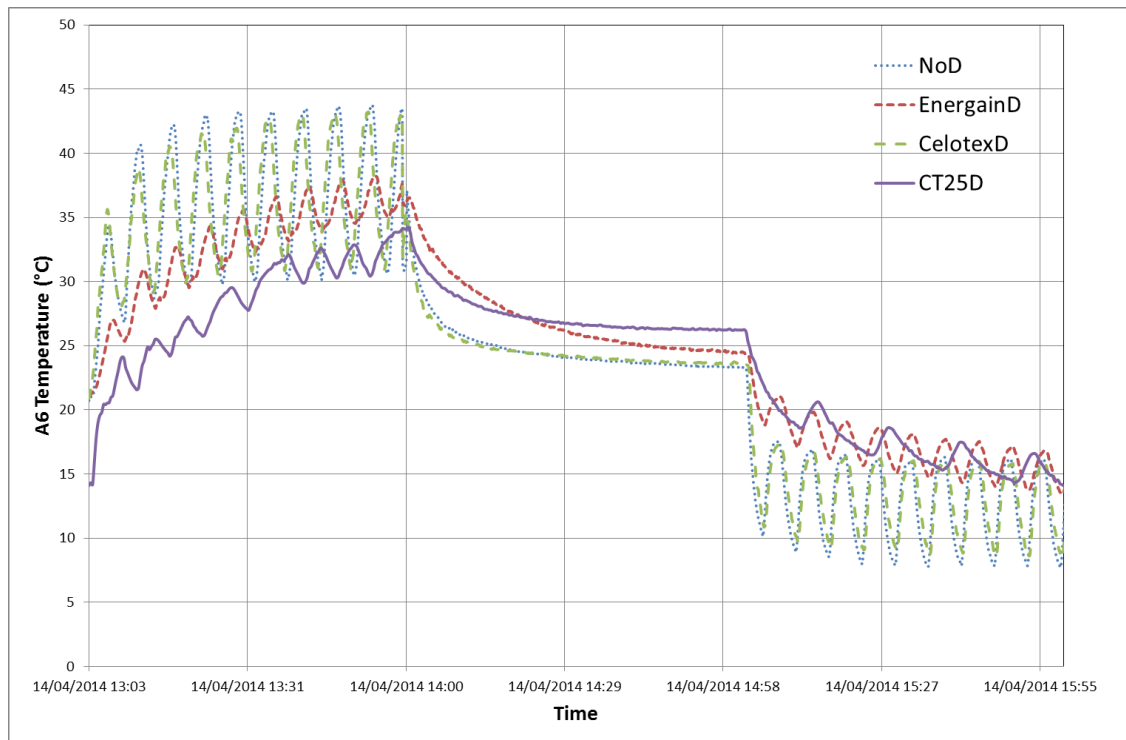


Figure 6.33 - Three Hour Temperature Profiles with internal Load of 50W/m²

To further test the diffuser performance, similar three-hour heating-ambient-cooling trials were carried out with a 50W/m² thermal load applied within the thermal chamber. The thermal load mimics building internal gains. Figure 6.33 plots the performance of the four diffuser scenarios over the hour-long heating, ambient fan and cooling operations.

With the additional internal heat load applied the EnergainD and X25D provided 0.5 and 3.8°C respective cooling against the NoD reference of 36.5°C after one-hour of heating. Temperature comparisons were calculated as the mid-temperature in the final sinusoidal temperature fluctuations observed due to the AC control. When contrasting the amplitude of the temperature fluctuation the PCM diffusers reduced the temperature swing from approximately 13.2°C in the NoD scenario to 2.3°C in the PCM scenarios.

During the ambient period the heater loading was maintained, therefore increased ambient temperatures are observed in Figure 6.33 when compared against the same period in Figure 6.32. During cooling the EnergainD and X25D tests, (charged with more heat from the heated

period and with the heat load still operational), maintained an average sinusoidal temperature 2.9 and 3.5°C respectively above the 11.8°C reference temperature.

Figure 6.32 and Figure 6.33 plots the cyclic benefit of the PCM diffuser. To assess the cooling and heating savings of the diffuser-technologies trialled, separate heating and cooling temperature profiles have been generated (Figure 6.34 to Figure 6.37). To minimise the disturbance due to AC control a moving average has been plotted for each technology.

6.5.2.1.2 Chamber Heating Analysis

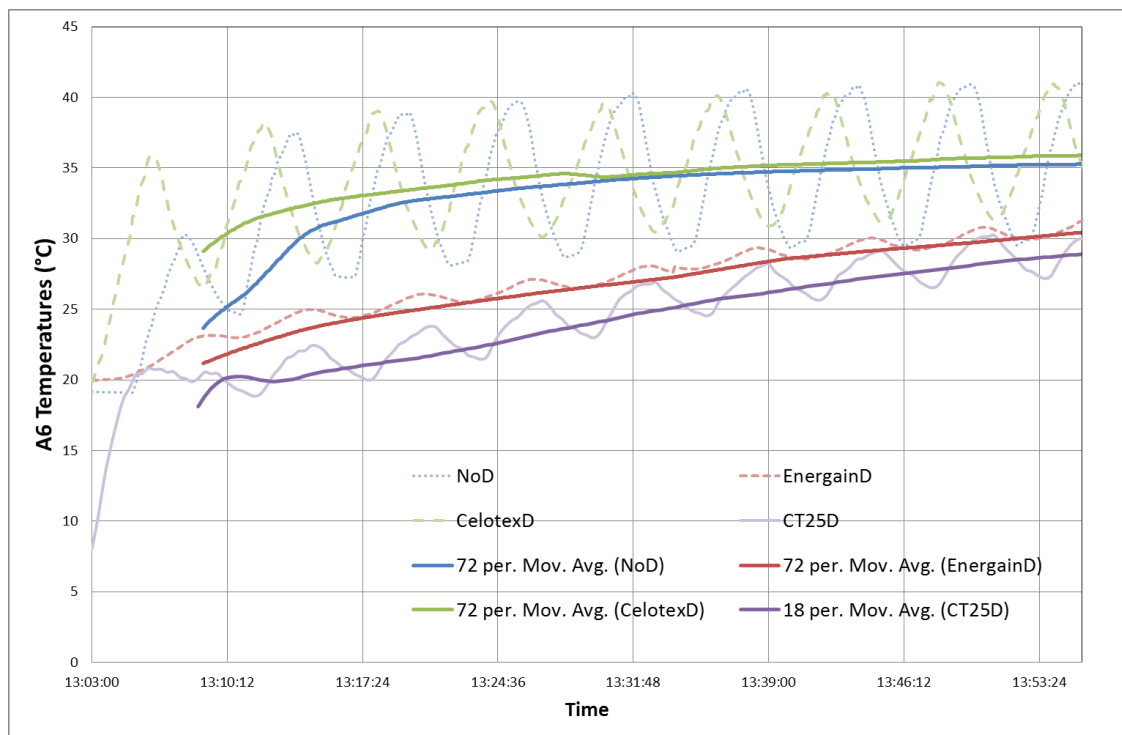


Figure 6.34 - AC-only Cooling-Saving Profiles

To assess the diffuser cooling and heating benefits the results from the three-hour temperature profiles have been plotted in isolation. Figure 6.34 charts the hour-long chamber process, without internal loads. Moving average best fit lines were plotted to smooth the inlet-air temperature fluctuations caused by the AC control.

The CelotexD offers no thermal benefit during overheating chamber conditions, even exceeding the NoD reference, with a final temperature of 36°C, to the NoD 35°C. The PCM diffusers offer thermal benefits, cooling the chamber space by 4.8 and 6.8°C. To further assess the diffuser benefits air inlet temperatures were plotted and their moving averages determined. From the difference between the chamber temperature (A6) and the air inlet temperature (A2) the cooling benefit throughout the chamber heating hour was deduced.

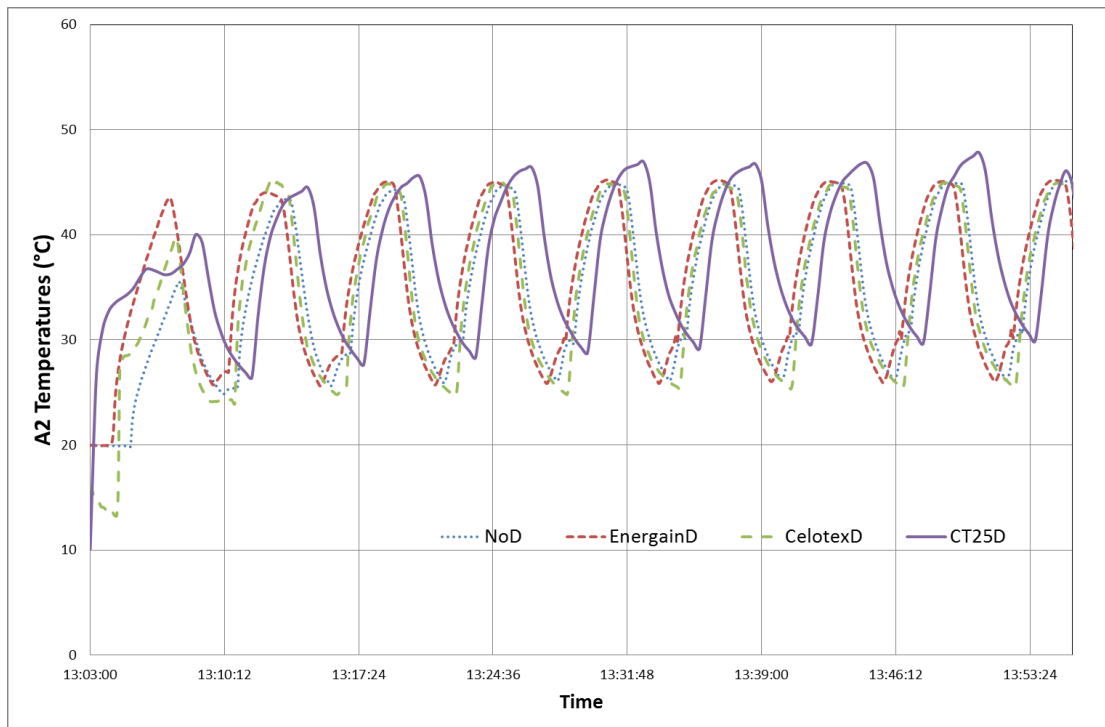


Figure 6.35 - Air Inlet (A2) Temperature Profiles during Chamber Heating

Figure 6.35 graphically plots the air inlet temperatures, recorded by thermocouple A2 in Figure 6.31, during the chamber heating hour. The similar temperature amplitude and frequency confirm each diffuser was inflicted with a similar thermal load from the AC unit. The X25D investigation was calculated in a hotter ambient laboratory. The AC heating profile therefore differs slightly in pattern due to the increased ambient conditions it was operating in.

Following Figure 6.35, Figure 6.36 was calculated based on the temperature difference between the inlet (A2) and chamber (A6) temperatures. The temperature difference achieved is proportional to the active cooling power of the diffuser. Figure 6.36 plots the temperature difference for each diffuser, and the appropriate moving average.

From the graph it is possible to deduce that, whilst NoD and the CelotexD see no significant variation between the inlet and chamber temperatures, the EnergainD reduces temperature by 5-12°C throughout the hour heating. The X25D, with greater thermal mass and a high melt temperature, reduces the temperature by 11 – 16°C.

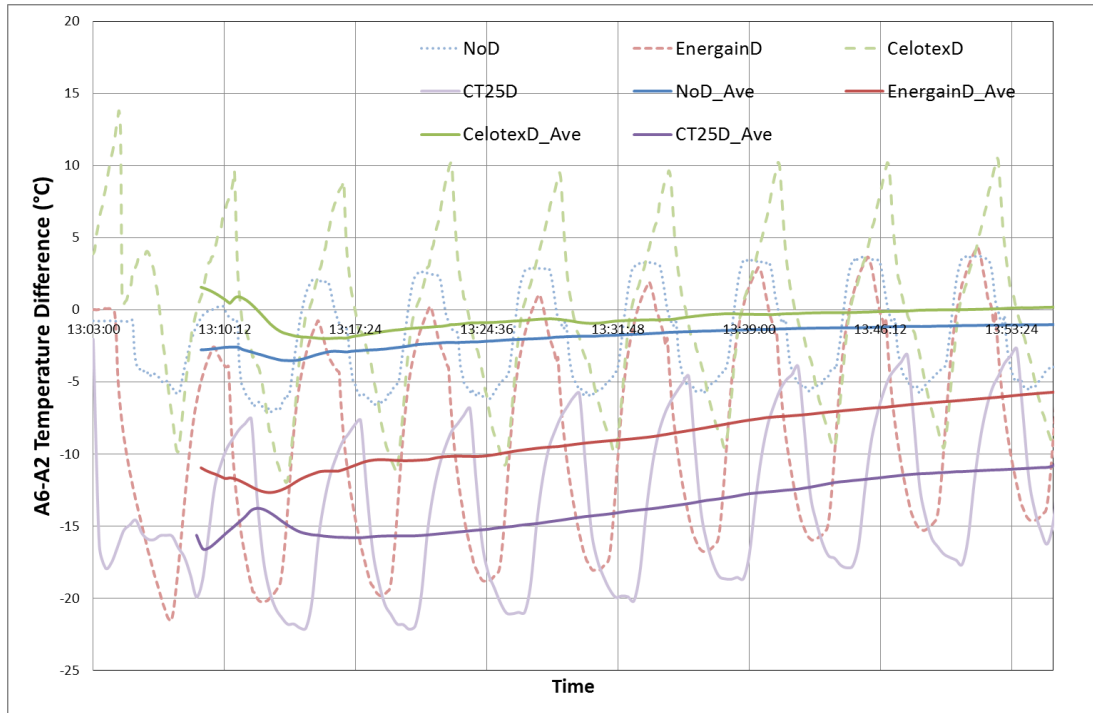


Figure 6.36 - A6-A2 Temp Profiles during Chamber Heating

The average temperature change throughout the hour was calculated and tabulated in Table 6.17. From the temperature difference, the energy transferred between the diffuser and the air was calculated. Known physical properties were used for air. Air velocity figures were not measured during the experiment. Prior measurements recorded an air velocity of 3.8m/s when the AC system was on low fan, and disconnected from the chamber. Prior to the chamber heating hour, when supplying air, via forced convection, to the chamber the peak velocity was measured at 2.8m/s. Commercially, a ventilation rate of 1.5 to 2.0m/s is commonly used. The figures in Table 6.17 and Table 6.18 were based on the industry standard of 1.5m/s.

At 1.5 m/s the X25D offers 230W/m² of cooling for the first hour. Comparatively, in a velocity range between 0.5m/s and 2.5m/s the X25D cooling power ranges from 76 to 380W/m², with no internal heat gain. The cooling flux (W/m²) was calculated from the normalised cooling power divided by the active surface area in the X25D of 1.25m². The normalised cooling power includes expected heat transfer effects from the ambient surrounds. The heat lost, through ambient heat transfer, is considered equal to the cooling power offered in the NoD scenario. The normalised cooling power therefore documents the cooling achieved by the diffuser. Negative numbers represent heat absorption into the thermal mass and positive numbers represent heat dissipation from the diffuser.

During the first chamber heating hour the PCM diffusers, EnergainD and X25D, offer 167 and 283W more cooling than the reference chamber. Further investigation beyond one hour of operation should be investigated to determine the long-term cooling power (section 6.5.2.2).

Following the same method, figures for temperature reduction and associated cooling power were calculated for the first hour of chamber-heating when a 50W/m² internal load was applied. Under these conditions the EnergainD suffered a more than 70% loss in cooling power. The X25D cooling power reduced less than 20% from the AC only investigation.

Table 6.17 - Cooling Power with flow rate of air at 1.5m/s

| | | NoD | CelotexD | EnergainD | X25D |
|---------------------------------|----|-------|----------|-----------|--------|
| AC only | | | | | |
| Average Temp. Difference | °C | -1.9 | -0.6 | -8.8 | -13.6 |
| Cooling Power | W | -45.3 | -13.3 | -212.3 | -328.0 |
| Normalised Cooling Power | W | 0.0 | 31.9 | -167.0 | -282.7 |
| with Internal Heater | | | | | |
| Average Temp. Difference | °C | -0.8 | -0.5 | -2.7 | -11.0 |
| Cooling Power | W | -19.3 | -11.0 | -63.8 | -265.0 |
| Normalised Cooling Power | W | 0.0 | 8.4 | -44.5 | -245.7 |

6.5.2.1.3 Chamber Cooling Analysis

To assess the benefit of PCM for reducing heating requirements, the hour under chamber cooling conditions was plotted in isolation (Figure 6.37). The average air inlet temperature across the simulations was between 10 and 11°C.

At the end of the hour long cooling period, the Energain® and X25 diffusers maintained chamber temperatures 2.0 and 1.0°C respectively above the NoD final temperature. The EnergainD offers better temperature stabilisation due to the greater use of latent heat under the test conditions. For X25D, the initial temperature of 24°C is in the midst of the melt range. In this position incomplete latent heat is available to maintain temperature conditions.

As conducted in the chamber heating case, the calculation of an hour long average temperature difference (between chamber and air inlet temperatures) has been tabulated in Table 6.18. Heating power and normalised heating power have been calculated from air physical properties with an inlet velocity of 1.5m/s. The same analysis has been conducted on the chamber cooling with internal gains data.

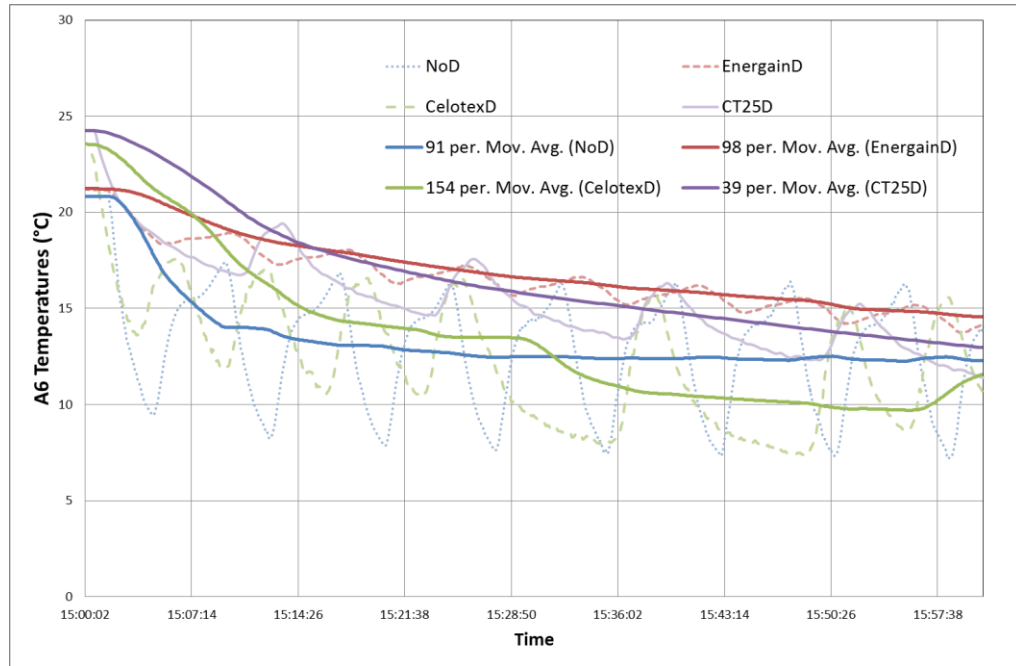


Figure 6.37 - Chamber cooling Temperature profiles (PCM heat benefit)

Table 6.18 - Chamber Cooling (PCM heating Benefit)

| | | NoD | CelotexD | EnergainD | X25D |
|---------------------------------|----|-------|----------|-----------|-------|
| AC only | | | | | |
| Average Temp. Difference | °C | 1.6 | -0.5 | 5.1 | 6.8 |
| Heating Power | W | 38.2 | -12.5 | 123.4 | 163.7 |
| Normalised Heating Power | W | 0.0 | -50.7 | 85.2 | 125.5 |
| with Internal Heater | | | | | |
| Average Temp. Difference | °C | -2.1 | -1.2 | 1.7 | 8.0 |
| Heating Power | W | -51.4 | -29.3 | 39.7 | 192.8 |
| Normalised Heating Power | W | 0.0 | 22.0 | 91.1 | 244.2 |

Between the chamber heating and cooling hours, an hour of ambient fan-only stabilisation was conducted. During this time, approximately half of the heat stored in both PCM diffusers mass was discharged. When the internal thermal load was applied the EnergainD stored additional energy during the stabilisation period before discharging that heat during the chamber cooling period. With internal thermal loads, the X25D showed normalised cooling power (Table 6.17) within 1% of the normalised heating power (Table 6.18), discharged during the chamber cooling period.

6.5.2.1.4 Internal Heating Load Contrast

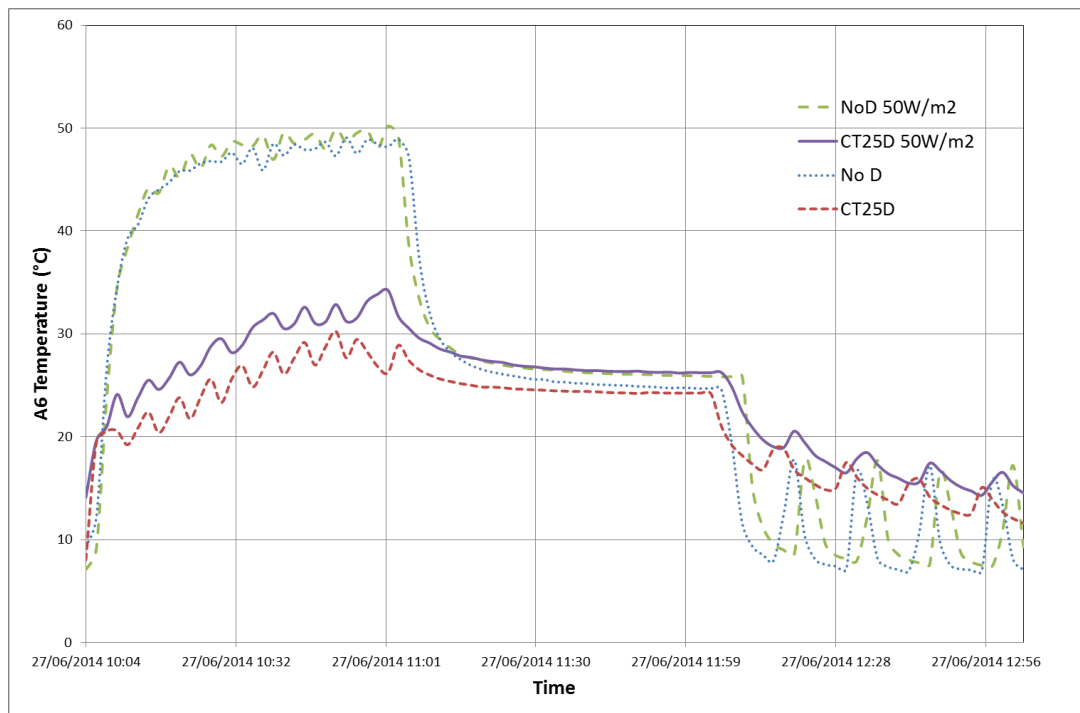


Figure 6.38 - Temperature Profiles with 0 and 50W/m² Loads

Figure 6.38 shows the direct comparison between no heating and an applied heating load of 50W/m². In the NoD case little change in temperature was observed during the heat loss stabilisation process between the no heating load and 50W/m² tests. In the X25D case a temperature increase of 2.8°C was observed between the no heating and applied 50W/m² heating load. A 20°C savings was observed between the different diffusers with zero heating load; whilst a 17.2°C savings was observed when 50W/m² was applied.

From analysis of Table 6.17 and Table 6.18 it is evident that internal gains reduce the capability of the PCM diffusers to cool the chamber, during chamber heating periods. Adding a heating load, or internal gain, benefited the X25D heating performance during the final hour, whilst the chamber was being cooled.

This was in line with previous studies where PCM addition to office spaces offered greater energy savings, alleviating morning heating more than afternoon cooling. In both cases, due to the position of the PCM in the ceiling, and the occupants on the ground, forced convection was required to achieve felt cooling benefits.

6.5.2.2 Saturation Temperature Profiles

The three hour cyclic tests demonstrated an improved performance for each of the PCM diffuser solutions. It is not clear from the charts however, how much phase change capacity

has been accomplished. To determine the theoretical capacity of the X25D, saturation tests were designed to observe the phase change curve under both cooling and heating operation.

Figure 6.39 and Figure 6.40 chart the relative performance of the X25D cases against the NoD reference case. For the heating case a 450W load was applied within the chamber. This was maintained throughout each case. Initially air at ambient temperature was supplied to the chamber via forced-ventilation through the diffuser. From review of the data the fan power increased the temperature of the inlet air by 1.5°C. Stabilisation of chamber temperatures occurs between 20:10 and 01:36 providing a useful window for analysis.

Prior to this period the temperatures climbed under thermal load, with the chamber temperature in the PCM case dropping when the latent phase was initiated. This occurs approximately 1hr45 after the experiment was initiated. In the diffuser chamber, temperatures between 32 and 35°C were maintained throughout the remainder of the stable heating period. The PCM gradually absorbs the heat whilst the ambient inlet air keeps PCM bulk temperatures below 27°C.

When the performance was reviewed after the consistent night operation the thermal load to the PCM diffuser was increased by applying a hot air inlet to the diffuser – unsettling the stabilisation that had been achieved overnight. From 09:22 the AC unit mode was changed from *'Fan only'* to include a heater with a set point of 28°C. The PCM B bulk temperature remains stable for a further hour before succumbing to sensible heat gain. The PCM A, protected from the internal radiant loads by the lower PCM layer, maintained stable temperatures for a further hour. Following the completion of the phase change in both layers the ambient temperature ramped up intensely until the heat load was terminated.

Such additional load was not required in the reference case. For the first seven hours the system operated as expected with the heat load reaching a stable maximum of 39°C, with ventilation air dissipating the heat outside of the chamber. At 01:20 the ventilation air to the chamber was disconnected and subsequently the chamber temperatures rose drastically, finally stabilising between 85 and 88°C. Prior to this overheating, during the stabilisation period for both diffusers, the X25D reduced temperatures by 3.4-6.6°C.

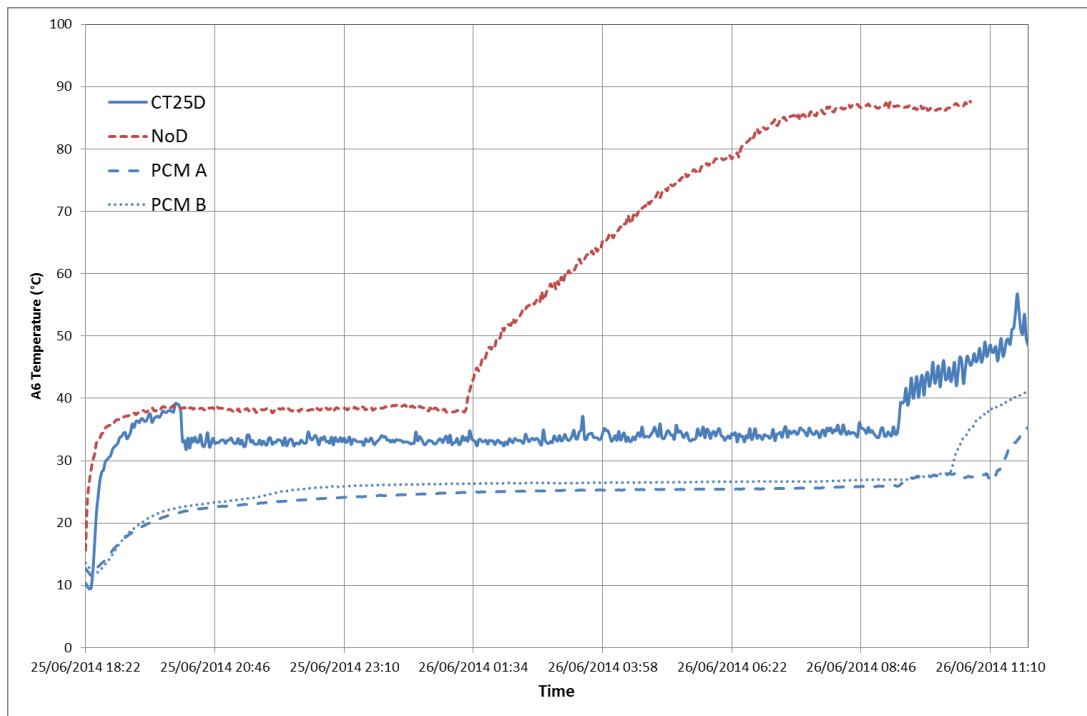


Figure 6.39 - Saturated Heat Temperature Profiles

A reverse PCM temperature profile was investigated with temperature profiled displayed in Figure 6.40, documenting the complete cooling of the system. The AC unit mode was set to cool with a set point of 18°C and temperatures monitored for each diffuser. In Figure 6.40 the red dashed line and the solid blue line represent the chamber air temperature (A_6) for the reference NoD and the X25D cases respectively. The spaced dashed and dotted blue lines represent the upper and lower PCM bulk temperatures (PCM A and PCM B in Figure 6.31) respectively.

The reference case was terminated after the temperature had stabilised below X25D air temperature. The observation of PCM freeze completion was not clear from the X25D air temperature line; therefore PCM bulk temperature readings were also included in the chart.

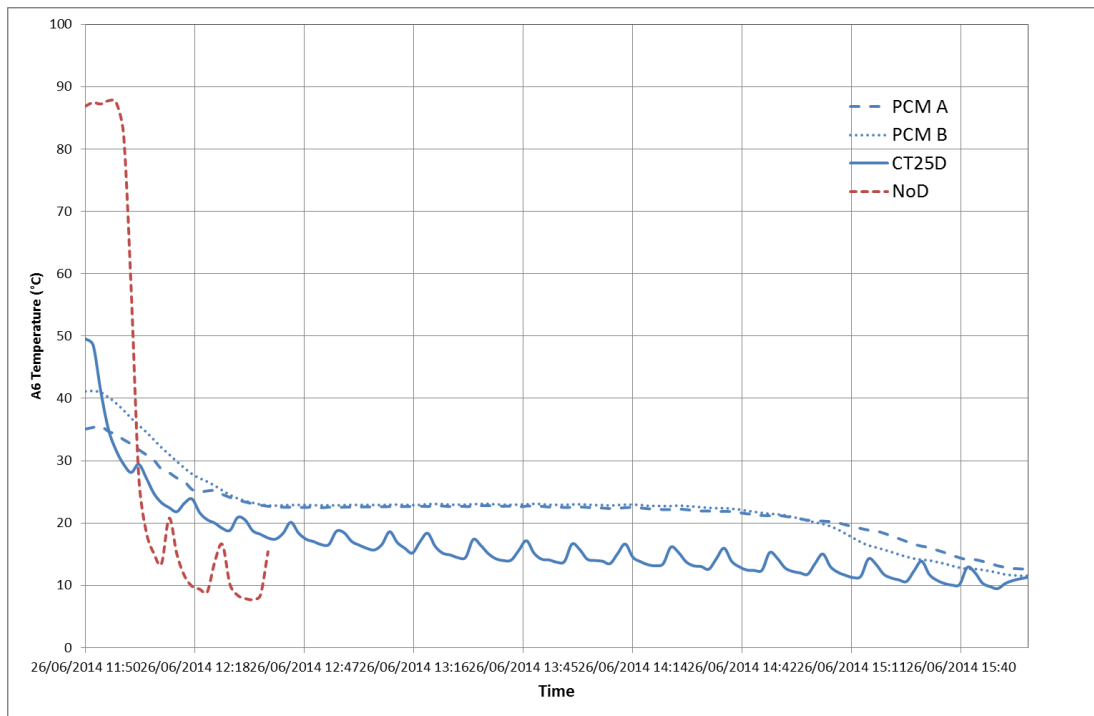


Figure 6.40 - Fully dissipated heat Temperature Profiles

To cool the thermal chamber below a comfort temperature of 18°C took just five minutes from 50°C, in the NoD case. For the X25D case the temperature first falls below 18°C after forty-five minutes although stabilises between 12 and 16°C for a further two hours. From the onset of PCM freezing until sensible heat transfer, takes two-hours-thirty-minutes in the X25D prototype.

6.5.2.3 Calculated Variable Heat Flux

Despite the differences in operation and the trends noted in Figure 6.39 the useful window of stable operation has been used to calculate an estimated heat flux (cooling flux) generated by the X25 PCM diffuser. Throughout the stabilisation period the chamber temperature reduction observed varies between 3.4-6.6°C against the NoD reference, with 5.1°C average chamber temperature for the duration of the stabilisation period (20:10 to 01:26).

Taking a typical inlet air velocity of 2.5m/s delivered from the AC unit and using literature figures for air heat capacity and density it was possible to calculate, that to maintain an average 5.1°C reduction a further 95W of cooling power was provided by the X25D, compared to NoD. In the experimental thermal chamber the active surface area of the PCM trays totals 0.93m². Therefore, based on the 2.5m/s air velocity, the average heat flux from the PCM during the stabilisation period is 102W/m².

Using this estimate of cooling power provided and the stated X25 physical properties [85], it was estimated that the X25D was capable of maintaining a cooling power of 95W for 4.4hours. After this time it is reasonable to assume that the latent capacity would be fully saturated, and the thermal mass of the diffuser would operate sensibly. This cooling capacity is only expected when the diffuser thermal mass has been fully frozen prior to the demand for cooling capacity.

6.5.2.4 Comparison with Modelled Heat Flux

During section 6.2, the modelled two hour heat flux for the B(2)10 system filled with 10kg of A22H PCM was 21.1W/m^2 . For the modelled B(2) system filled with 4kg of X25, two hour heat fluxes ranged from 28 to 57W/m^2 , depending on modelled conditions. During the modelling the inlet air velocity was held constant at 1.5m/s.

In comparison, the experimental heat flux measured value is 79% greater. To offer a closer comparison the inlet velocity used in the experimental calculations was reduced to 1.5m/s in line with the modelled conditions. Under these conditions the average experimental heat flux was 61W/m^2 , 7% greater than the modelled flux.

6.5.3 Summary of Findings

The component testing of the PCM prototype diffuser proves the concept that a thermally-active-PCM diffuser offers energy saving and comfort benefits through the moderation of daily temperature fluctuation. As observed, in the thermal chamber, 8.6°C of air temperature savings are possible during cooling. During PCM thermal energy transfer to the chamber, an increase in air temperature of 4.3°C was observed. When an internal heating load of 50W/m^2 was applied these savings reduced to 3.8 and 3.5°C . From the saturation investigation it has been possible to estimate a cooling heat flux of 102W/m^2 , with an air velocity of 2.5m/s, during intense cooling demand. At 1.5m/s the heat flux dropped to 61W/m^2 , 7% greater than the modelled heat flux.

For the X25 prototype diffuser tested it is estimated that the diffuser can deliver 95W of cooling power for 4.4 hours (0.4 kWh). From the heating saturation test, latent heat was returned to the thermal chamber air bulk for two-and-a-half hours. Further work using sensors to measure the heat flux from the diffuser to the air would validate the estimations made. In an effort to further prove the concept in a 'real world' setting the X25 prototype diffuser performance in a pilot scale test chamber, in combination with the WVHC prototype slab, will be investigated in *Chapter 7*.

6.6 Conclusions

In conclusion, the work carried out in *Chapter 6* identified a dual-layer diffuser as the optimum active PCM enhancement to the air and water prototype developed in *Chapters 3, 4 and 5*. This was achieved through CFD models that also suggested the bio-based PCM, X25, as the most cost effective option for prototype construction. In the dual layer (B(2)) modelled system the X25 PCM under modelled scenario (v) conditions achieved a two hour heat flux of 57W/m^2 .

Subsequent PCM DSC analysis of a X25 sample was conducted revealing two melt peaks at 23.14 and 25.84°C . An average of the two peaks (24.5°C) fitted closely with the literature melt temperature of 24.9°C . The measured combined latent heat of the two melt peaks was 11.5% less than the literature figure of 186kJ/kg .

A dual layer aluminium diffuser was designed and created capable of safely encapsulating the X25 PCM. The combined PCM load weight was 7.53kg across the two layers. Type-K thermocouples were embedded in the PCM layers to monitor temperature change throughout the laboratory investigations. Within the purpose built thermal chamber, the temperature moderating performance of the X25 diffuser (X25D) was measured against an empty chamber with no diffuser (NoD), a non-PCM inert Celotex diffuser (CelotexD) and an alternative PCM Energain® diffuser (EnergainD).

The X25D achieved the greatest cooling and heating savings reducing temperatures (under cooling demand conditions) by 8.6°C and by 4.3°C (under heating demand conditions). When an internal thermal load of 50W/m^2 was applied the temperature savings reduced to 3.8°C (under cooling demand conditions) and 3.5°C (under heating demand conditions). Heat saturation and fully-dissipated analysis revealed that the X25D was capable of holding its 95W cooling power for 4.4 hours, offering a thermal energy storage enhancement of 418Wh . In contrast with the market leading Cool-Phase® (which stores $6\text{--}10\text{kWh}$, in 210 to 390kg units [132] 0.03kWh/kg), the X25D was capable of storing 418Wh in a 25kg unit (0.02kWh/kg).

The laboratory findings were contrasted against the modelled findings. With laboratory air-inlet velocity matched to the modelling velocity of 1.5m/s , the laboratory heat flux was 7% greater than the modelled heat flux; 61W/m^2 compared to 57W/m^2 .

The work in this chapter has proved the concept that an active PCM diffuser is capable of delivering temperature moderation benefit to internal air environments. When internal loads

were tested in the chamber, results suggested greater heat transfer from the PCM for room heating, rather than room cooling. Further work should investigate retrofit in pilot scale systems. The work in *Chapter 7* proposes to determine the benefit of the PCM-diffuser in a typical room setting, when operated in conjunction with an active sensible-thermal-mass system.

Chapter 7: Pilot Scale Testing

System Testing and Economic Analysis of a Combined Thermal Mass Solution

7 Pilot Scale Testing

7.1 Introduction

The saturation component tests, carried out in *Chapters 5 and 6*, were useful tools for determining the theoretical performance of the different thermal mass enhancements investigated in this thesis. However in practical applications, thermal mass rarely has the luxury of idealised cooling and heating patterns and, therefore, to offer real world benefit thermal mass must endeavour to adapt to the conditions imposed upon it. The testing in *Chapter 7* sets out to discern the realised user benefit in a typical office scenario of the retrofit solution developed in *Chapter 6*. To comprehend office scenario performance, energy benefit, temperature reduction and associated financial savings were assessed.

Evidence from the research work in *Chapters 3*, coupled with suggestions from [12] revealed the greatest opportunity for VHC enhancement during spring and summer periods. Building on the component testing conducted in *chapters 5 and 6*, the prototype WVHC slab and PCM Diffuser will be tested in a thermal chamber under theoretical *peak-cooling-demand* and *diurnal-swing* conditions. The aim of the investigation was to quantify energy saving and

cooling benefit from the retrofit PCM diffuser developed in *Chapter 6*. Work by [24] inspired the form of the pilot scale test.

The prototype slab and diffuser were fitted in a thermal chamber with an identically sized empty adjacent test chamber, acting as a reference. Both were fitted with backup AC systems that maintained a maximum room temperature of 24°C. Energy monitors on each system recorded the energy consumption throughout the investigations into the VHC, WVHC and VPHC systems. It was proposed that the active thermal mass systems in the test chamber would provide the required cooling to maintain room temperatures below 24°C, therefore mitigating any energy consumption by the backup AC system.

From the determined energy savings and the known costs of manufacture and installation a comprehensive economic assessment was conducted. The economic assessment is intended to offer useful output for further academic research and industrial development.

7.1.1 Contributions to knowledge

Previous work observed the performance of TABS in a pilot scale laboratory test room [24], and active-PCM addition to buildings [104]. Work by [166] investigated the benefits of PCM incorporated into concrete decks. These works demonstrated the TES capacity enhancement but, in the case of [166], found the poor thermal conductance of PCM inhibiting on the concrete deck. In this chapter advances were made by incorporating an active-PCM element to overcome the poor thermal conductance of a passive PCM layer. Further, through the office scenario assessment of the prototype thermal mass enhancements, as designed and constructed in this thesis. For the first time the energy savings possible from WVHC prototype operation were assessed against an AC controlled equivalent reference thermal chamber.

Building on the research work [171, 172] to develop an active-PCM system for office temperature management, this chapter investigates a retrofit solution. The PCM diffuser, designed for enhancing existing active thermal mass systems was trialled on a pilot scale. A design by Gowreesunker [119] models the performance of PCM plate heat exchangers within an airport terminal diffuser; however no evidence from laboratory trials are identified. This trial marked the first innovative assessment of the energy savings benefits of the prototype PCM diffuser, integrated with a VHC system.

Finally, contributions to knowledge were presented in the economic assessment of the thermal mass enhancements. Due to the novelty of the technology, the work done in this

section marked the first investigation into the prototype thermal mass enhancement costs; it is useful for both further academic research budgeting and commercial implementation of the technologies investigated.

7.1.2 Chapter aims

- 1) Install the hollow core and active-PCM retrofit prototypes into two comparable test chambers.
- 2) Conduct thermal tests to establish the summertime benefit of each active thermal mass methodology.
- 3) Carry out building simulation to estimate annual energy consumption and assess the business case of the developed technologies.

7.2 Pilot Scale Prototype Testing

When investigating the realised benefit for office users and building managers three key metrics are often considered:

1. office temperature
2. energy consumption
3. installation and operational cost

The intention of office temperature is, for the benefit of the office user, to remain within the CIBSE comfort conditions for each season during occupied hours [9, 140]. For the benefit of the building manager *energy consumption* and associated *operational costs* are essential. Since over half of all commercial buildings are let *installation costs* are typically incurred by the building's owners.

During the saturation testing in *Chapters 5 and 6* the specific heat load was maintained and the temperature varied, to determine the temperature saving benefit under different conditions. This method was used to determine the cooling power capacity. For the purpose of the tests in this chapter average chamber temperature will be maintained within the CIBSE guidelines through the use of a backup heat-pump driven AC unit set to cool to 24°C. With comfort temperatures maintained the investigation will monitor office energy consumption, to determine the realised energy benefit for installing enhanced-thermal mass for energy-saving benefit in UK offices.

7.2.1 Installation Methodology

Initially, to accomplish the required *pilot scale prototype testing*, two equivalent test chambers were constructed in the University of Nottingham's Sustainable Research Building. The chambers were built from an insulated-timber-frame construction, clad with plaster board (Figure 7.1). Each chamber has a floor area of 1.8 by 2.4 metres, with an insulated ceiling three meters above the raised- insulated floor. 100mm Celotex insulation was used to line the floor, ceiling and walls.



Figure 7.1 - Constructed Test Chambers

One room (Room B) was designed as a reference chamber to be fitted with heat mat and air conditioning but no thermal mass. The second room (Room A) was fitted with thermal mass prototype systems. Before the thermal mass systems could be fitted, building services were connected to the room. Mains water was delivered to the room with a return drain pipe connected to the laboratory drainage system. Electrical sockets were installed within the chamber to power internal systems.

The prototype hollow core slab designed in *Chapter 3* and tested in *Chapter 4* and *5* was prepared and installed. Initially the slab was disconnected from the water and air lines in the *Chapter 5* rig and insulation removed (Figure 7.2). Extensions were prepared for the heavy duty slab trolley used in the *Chapter 4* investigation to raise the soffit surface to 2.1m above floor level. Additional steel box work braces were constructed and welded into place to increase the stability of the slab trolley.

Due to the weight and height of the hollow core prototype slab a thorough safety lift assessment, in accordance with LOLER was conducted prior to raising the prototype slab onto the reinforced mobile steel frame (Figure 7.2). The slab was raised on pallets by an appropriate fork lift truck and secured to the frame via half inch bolts and anti-rotation pins.

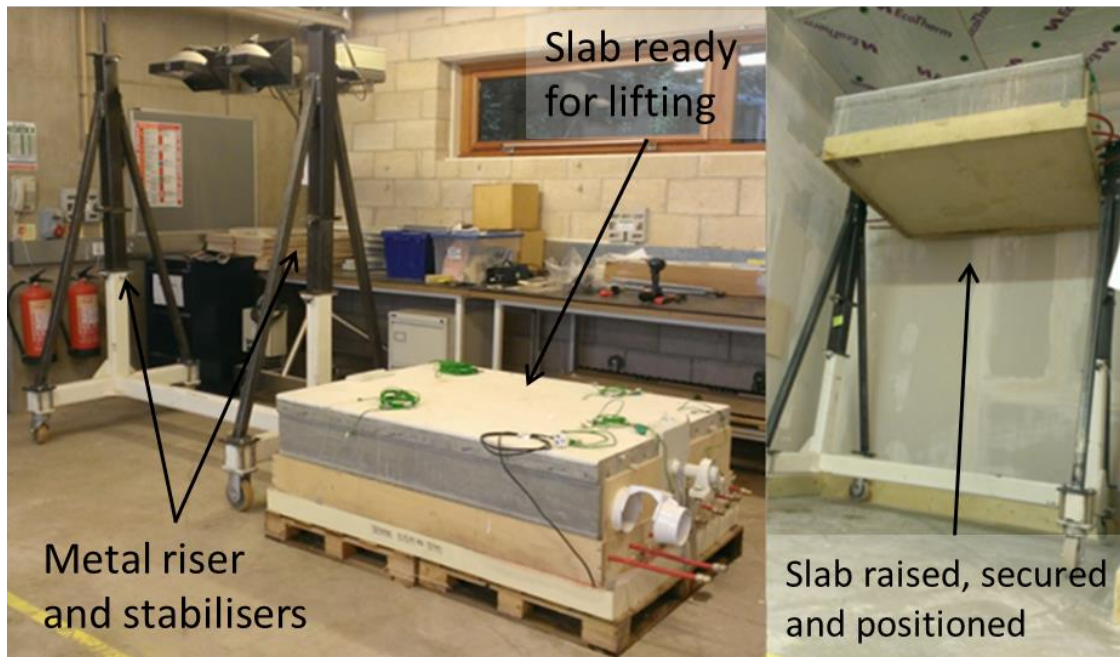


Figure 7.2 - Slab and Frame Before and After the Lift Procedure

With a chamber wall removed the raised slab was wheeled into position in the thermal chamber (Figure 7.2 (r)) where the floor was re-constructed around the heavy duty castors. The top and sides of the slab were insulated to ensure only the soffit surface area was exposed to the room.

The water and air networks were reconnected inside the chamber. The liquid thermocouples were resealed to avoid potential leaks in the system (as per section 3.2). The water network was connected to the internal chamber tap, via a flow meter and into the eight pass embedded water network. The return loop was connected to the drainage pipe with the open loop water pipe terminating in the laboratory drainage system. No water recycle was constructed in the system.

Once insulated and connected with required building services the remaining room thermocouples were installed. In both the thermal mass chamber (Room A) and reference chamber (Room B) the room sensors were placed on a central support positioned 0.2, 1.1 and 1.9m from the chamber floor (Figure 7.3). The thermocouples and flow meter were wired into a DT500 data logger (Figure 7.4) connected to a PC running DeLogger software. The room sensors from Room B are threaded through a small, sealed connection into Room A, where the data logger was positioned. Instrumentation accuracy was limited as per the levels found in Appendix B – Instrument Accuracy and Measurement Errors in Table 11.1.

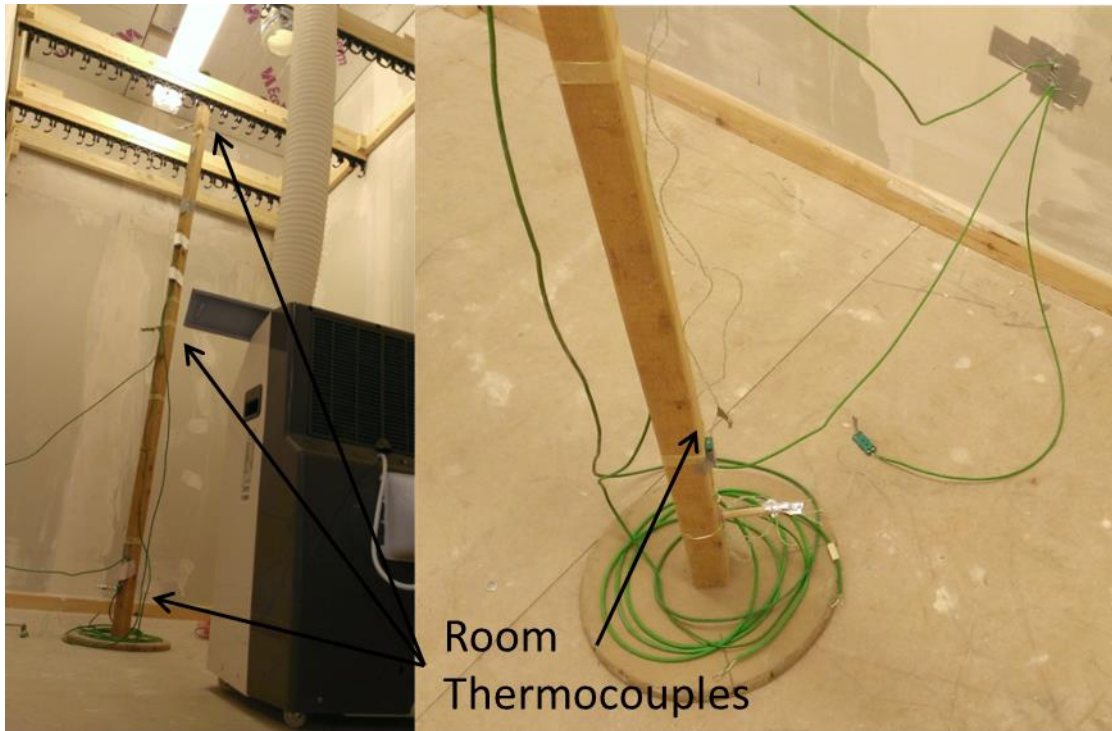


Figure 7.3 - Room B Temperature Sensors

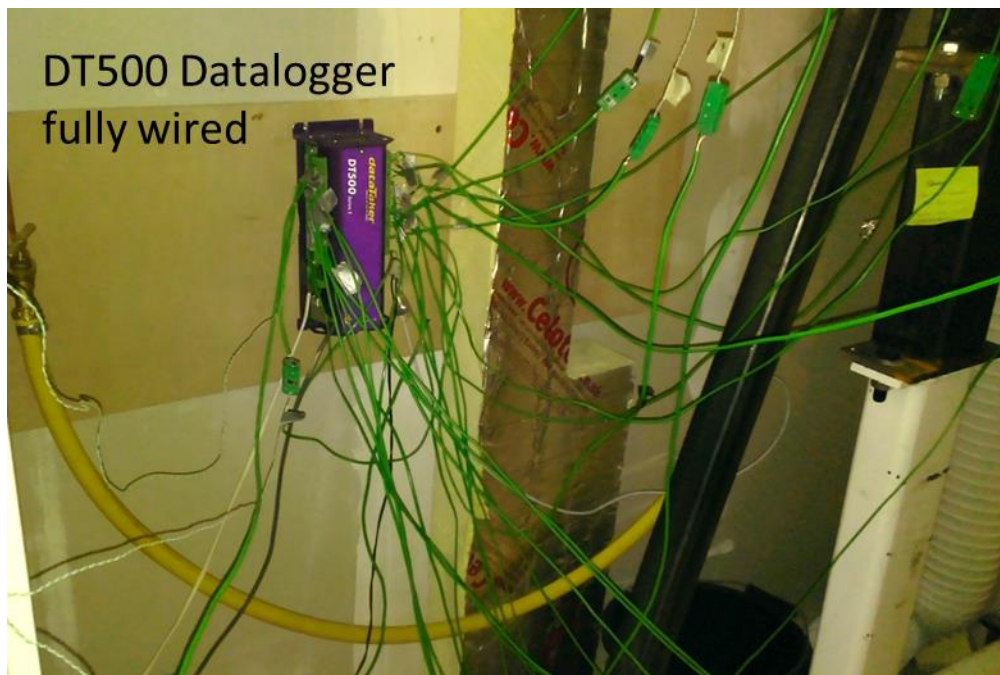


Figure 7.4 - Temperature and Flow Meter Sensors wired into the DT500 Data Taker

Equivalent radiant heat mats with a maximum power delivery of 450W were installed into each chamber. Each heat mat was connected to an electronic dimmer to adjust the delivered power. Energy meters were monitored to set the heat mat to deliver the required $50\text{W}/\text{m}^2$ of

heating, to replicate internal office gains. Each heat mat was connected to electronic timing switches to deliver eight hours of thermal load between 9am and 5pm (Figure 7.5).

Two KYR/45EW-1Rc portable air conditioners were installed, one in each room. Outlet vents were cut in each chamber (Figure 7.1) to fit the AC outlet air duct work. Internally the delivery air from the AC unit was delivered from roof mounts in Room B and via the prototype hollow core air network in Room A. Each unit can heat or cool to a room set point of 17-35°C (Figure 7.5). The installed heat pump systems quoted a cooling COP (W/W) of 3.04 and a heating EER (BTU/Wh) of 2.8. The system was capable of delivering 3.5kW of cooling and 3.7kW of heating. Due to the temperature dependant control of the AC units, the delivery air temperature fluctuates during operation.

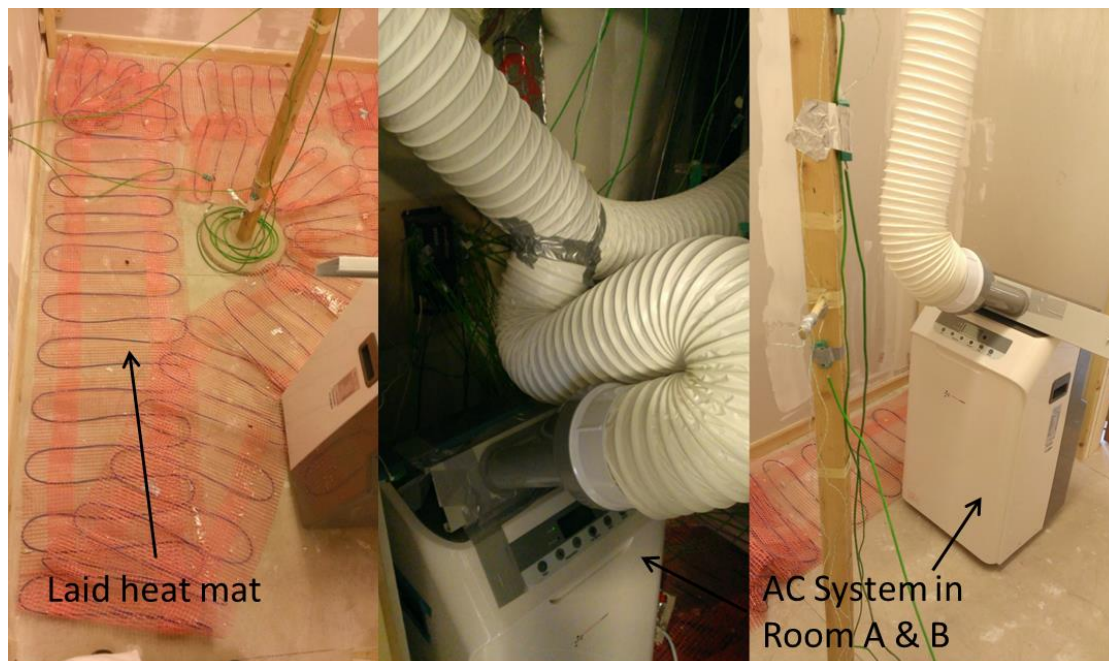


Figure 7.5 - Installed Heat mat (l) and AC Units in Room A (c) and Room B (r)

Prior to the VHC and WVHC trials, the energy meters and timing switches were appropriately connected. The DeLogger software was used to programme the data logger to harvest data every three minutes. Throughout the trials, current, maximum and minimum readings were recorded as well as the continual plotting of readings graphically.

Before the VPHC trials were started the X25 PCM Diffuser (X25D), used during the investigations in *Chapter 6*, was adapted to fit the prototype slab geometry. To connect the diffuser with the prototype slab, 40mm extensions were added to the steel sprung clip. The two layers were separated to enable the fitting of a wooden brace to secure the clip (Figure 7.6). The lower layer (PCM B) was secured and sealed to the upper layer via quarter inch

bolts. PCM A, PCM B, PCM air A (positioned between PCM layers A and B) and PCM air B (between PCM layer B and the base of the diffuser) thermocouples replaced Liquid 3-6 thermocouples in the data logger to monitor the performance of the PCM and the temperature of the air delivered to the room through the PCM diffuser (Figure 7.7).

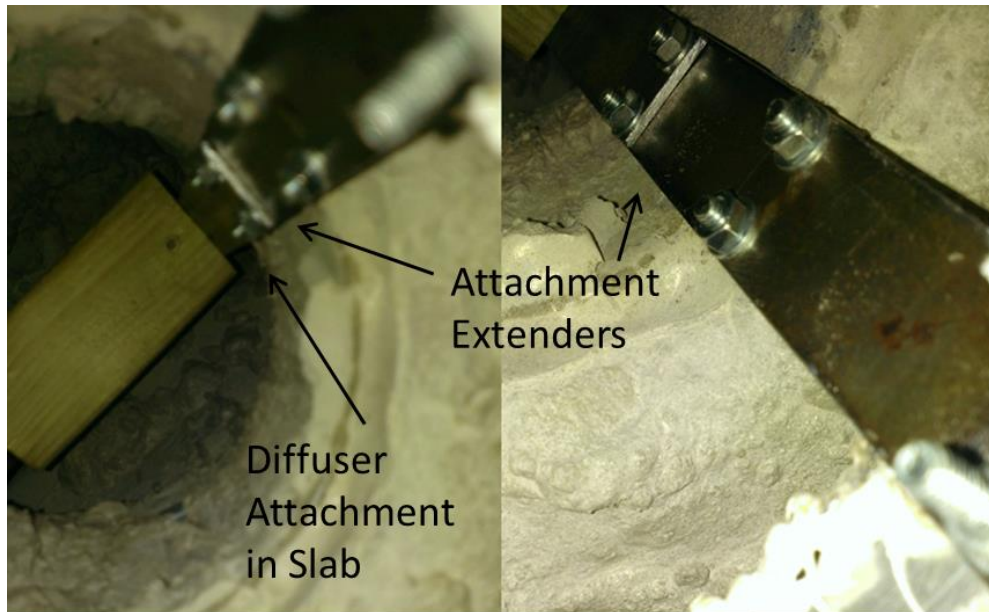


Figure 7.6 - Diffuser Clip Extensions secured with Wooden Wedge

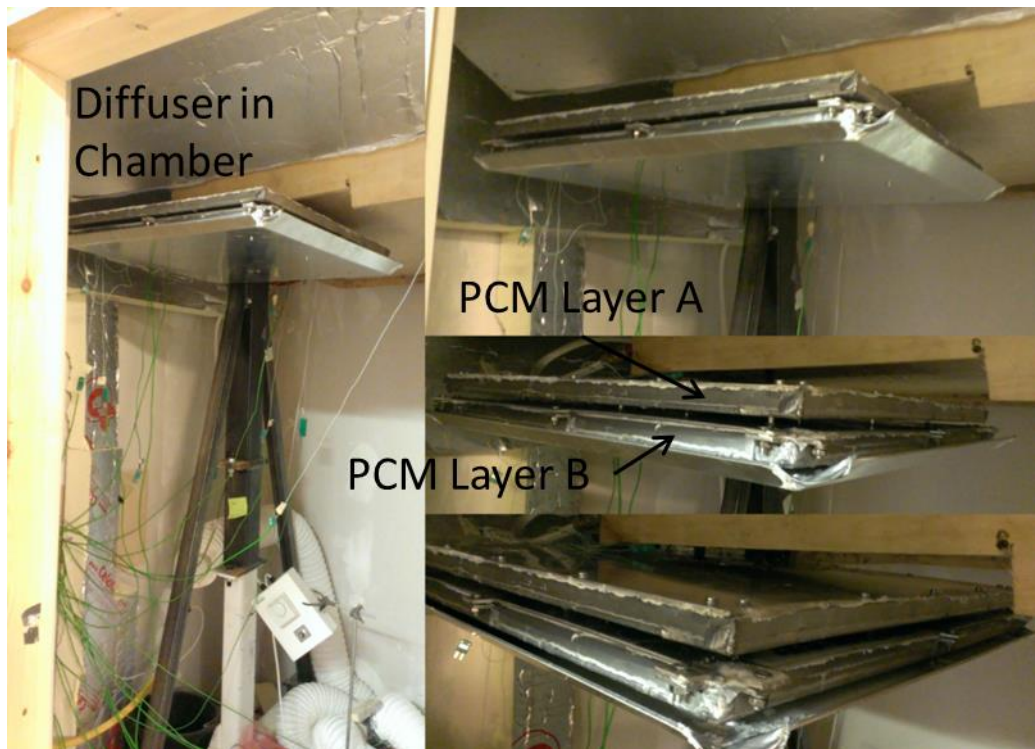


Figure 7.7 - Fitted Diffuser in Room A

The system under investigation determined the temperature sensors installed at any one time, since the data logger was limited to thirty inputs. The PCM diffuser was only installed during VPHC tests; the water system was active only when WVHC tests were in operation.

7.2.2 Test Method

Aspects of work by [24] has set a precedence for the test method conducted. In [24] a pilot scale chamber was constructed to investigate the performance of TABS systems. The room was heated to replicate occupancy internal heat gain, and then allowed the system to moderate. Temperature sensors were placed vertically in the space. The room was well insulated and energy use and temperature measured.

Since thermal mass works as a temperature mediator, the times of greatest thermal strain occur during extended peak periods [12]. This investigation has been undertaken to investigate the enhancement available during these conditions, both to energy savings and comfort (temperature). To investigate energy savings a back-up AC unit was used at a fixed temperature, the difference between the energy used to maintain a chamber temperature below 24°C in the two chambers being the 'energy savings'. To investigate temperature savings a fixed load, in line with the theoretical peak 2006 Part L load was applied [169] and temperatures of the chambers under each different system monitored.

Three scenarios were identified for investigation in the thermal chambers. They offer thermal mass enhancement through the traditional ventilated hollow core (VHC), the prototype combined water cooled and ventilated hollow core (WVHC) and the VHC system fitted with the innovative X25D (VPHC). As outlined in the *Installation Methodology* (section 7.2.1), each system has been installed into Room A of the two thermal chambers. An equivalent Room B, fitted with an AC system only, was used throughout as a reference chamber to determine the practical benefit of enhancement thermal mass. The three enhanced thermal mass systems were tested under three climactic conditions: *peak-cooling-demand*, *diurnal-swing* and *fixed-occupancy* conditions

In total four week-long tests were conducted under peak-cooling-demand conditions; three three-day diurnal-swing tests; and three fixed-occupancy tests were carried out on the VHC, WVHC and VPHC systems. A complete test log record is presented in Table 7.1.

Table 7.1 - Pilot-scale test chamber Test Log

| Date of Test Start | Date of Test Finish | Test Conditions | System Tested | Night Ventilation Strategy |
|--------------------|---------------------|-----------------|---------------|----------------------------|
| 28/05/2014 | 04/06/2014 | Peak Period | VHC | No Vent |
| 09/06/2014 | 16/06/2014 | Peak Period | WVHC | Lab Vent |
| 16/06/2014 | 23/06/2014 | Peak Period | VHC | Lab Vent |
| 02/07/2014 | 07/07/2014 | Peak Period | VPHC | No Vent |
| 07/07/2014 | 10/07/2014 | Diurnal Swing | VPHC | Night Cooling |
| 13/07/2014 | 14/07/2014 | Fixed Occupancy | VPHC | None |
| 15/07/2014 | 19/07/2014 | Diurnal Swing | WVHC | Night Cooling |
| 19/07/2014 | 20/07/2014 | Fixed Occupancy | WVHC | None |
| 20/07/2014 | 23/07/2014 | Diurnal Swing | VHC | Night Cooling |
| 24/07/2014 | 25/07/2014 | Fixed Occupancy | VHC | None |

7.2.2.1 Peak-cooling-demand Test Method

Office occupancy was simulated via a 50W/m² radiant load applied for eight hours in each room, in line with the TABS peak dissipation mode [12] and 2006 Part L standards [169]. Temperatures, water-flow rate and energy consumption were monitored throughout the week long simulations. The thermal mass was cooled to 18°C prior to each week long investigation to recharge the cooling capacity [168]. Table 7.2 documents the settings specified for each scenario tested. A night vent was fitted in the wall of Room A. Where applicable this was opened to ambient laboratory air during night periods enabling night ventilation of the active hollow core.

The AC unit and supply-air fan for Room A, and the AC unit in Room B were connected to energy meters. The energy meters monitor voltage (volts), current (amps), power (watts) and

energy consumed (kWh). Readings were taken before and after each week long investigation to determine the energy consumed to maintain room temperatures at or below 24°C [151, 168]. Since the rooms were comparable in size and construction the energy savings achieved by the enhanced thermal mass in Room A were calculated by the difference between the Room B and Room A energy meter readings.

Table 7.2 - Peak-cooling-demand Test Conditions

| Scenario | Reference Chamber | Thermal Mass Chamber | | |
|--------------------------------|-----------------------------|-----------------------------|-----------------------------|--------------------------------|
| | | VHC | WVHC | VPHC |
| a. Thermal Mass System | No Thermal Mass | Traditional VHC | WVHC Prototype Slab | VHC system with PCM Diffuser |
| b. AC Setup | Cool to 24°C | Cool to 24°C | Cool to 24°C | Cool to 24°C |
| c. Fan Setup | N/A | 32W Fan from 22°C | 32W Fan from 22°C | 32W Fan from 22°C |
| d. Water Setup | N/A | Water Off | Water On (0.5m/s) | Water Off |
| e. Water Schedule | N/A | N/A | 8hrs (9-5) Only | N/A |
| f. Occupancy (Heater) Schedule | 8hrs (9-5)on, off for 16hrs |
| g. Heater Load | 50W/m ² (216W) | 50W/m ² (216W) | 50W/m ² (216W) | 50W/m ² (216W) |
| h. Night Ventilation Strategy | N/A | i) No Vent ii) Lab Vent | Lab Vent | i) Vent Closed ii) Lab Vent |

7.2.2.2 Diurnal-swing Test Method

Following the *peak-cooling-demand* testing *diurnal-swing* testing was conducted to investigate how the thermal mass enhanced systems performed when twelve hours of night cooling were available. To enable the ‘night cooling’ the air conditioning units ran separate schedules during night time and ‘occupied’ periods. During occupied periods the AC and supply-air fan was connected to the energy meter and set to cooling mode, with a set point of 24°C, for eight hours. To offer ‘night cooling’, thirty minutes after the occupancy period had finished, the AC unit bypassed the energy meter and cooled to 18°C for twelve hours between 6pm and 6am.

The room temperature then passively equalized for three and a half hours until the occupied period started again at 9.30am. At the start of the ‘occupied’ period, the energy meter was

reconnected to the AC and supply-air fan. The ‘occupied’ AC setup was initiated to cool to 24°C for eight hours. The *diurnal-swing* testing was carried out for three consecutive 24 hour days with specific conditions for each system displayed in Table 7.3 below.

Table 7.3 - Diurnal-swing Test Conditions

| Scenario | Reference Chamber | Thermal Mass Chamber | | |
|--------------------------------|---|---|---|---|
| | | VHC | WVHC | VPHC |
| a. Thermal Mass System | No Thermal Mass | Traditional VHC | WVHC Prototype Slab | VHC system with PCM Diffuser |
| b. AC Schedule | 8hrs (9.30-5.30) | 8hrs (9.30-5.30) | 8hrs (9.30-5.30) | 8hrs (9.30-5.30) |
| c. AC Setup | Cool to 24°C | Cool to 24°C | Cool to 24°C | Cool to 24°C |
| d. Fan Setup | N/A | 32W Fan from 22°C for 8.5hrs | 32W Fan from 22°C for 8.5hrs | 32W Fan from 22°C for 8.5hrs |
| e. Water Setup | N/A | Water Off | Water On 8hrs (9-5) Only | Water Off |
| f. Occupancy (Heater) Schedule | 8hrs (9-5)on, off for 16hrs |
| g. Heater Load | 50W/m ² (216W) | 50W/m ² (216W) | 50W/m ² (216W) | 50W/m ² (216W) |
| h. Night Ventilation Strategy | AC Cool to 18°C for 12hours (6pm – 6am) | AC Cool to 18°C for 12hours (6pm – 6am) | AC Cool to 18°C for 12hours (6pm – 6am) | AC Cool to 18°C for 12hours (6pm – 6am) |

7.2.2.3 Fixed-occupancy Test Method

Finally to complement the saturation component tests, combined saturation tests were conducted in the test chambers. These tests enabled the contrast between the enhanced thermal mass technologies and the empty room, in particular how much *Peak Delay* and *Peak Reduction* was available.

In the same thermal chambers as the pilot scale tests, for the *fixed-occupancy* saturation tests, the temperature profiles of Room A (under VHC, WVHC and VPHC system operation) and Room B were monitored. Starting at 18-19°C each room was inflicted with a 50W/m² thermal load for eighteen hours. Tests were operated following the conditions in Table 7.4.

Table 7.4 - Fixed-occupancy Test Conditions

| | Scenario | | Reference Chamber | Thermal Mass Chamber | | |
|----|-----------------------------|------|---------------------------|---------------------------|---------------------------|------------------------------|
| | | | | VHC | WVHC | VPHC |
| a. | Thermal System | Mass | No Thermal Mass | Traditional VHC | WVHC Prototype Slab | VHC system with PCM Diffuser |
| b. | AC Schedule | | Off | Off | Off | Off |
| c. | AC Setup | | N/A | N/A | N/A | N/A |
| d. | Fan Setup | | N/A | 32W Fan | 32W Fan | 32W Fan |
| e. | Water Setup | | N/A | Water Off | Water On (2.5l/min) | Water Off |
| f. | Occupancy (Heater) Schedule | | 18hrs On | 18hrs On | 18hrs On | 18hrs On |
| g. | Heater Load | | 50W/m ² (216W) | 50W/m ² (216W) | 50W/m ² (216W) | 50W/m ² (216W) |
| h. | Night Ventilation Strategy | | None | None | None | None |

7.2.3 Results and Discussion

7.2.3.1 Peak-cooling-demand period Tests Temperature Profiles

As shown in Figure 7.8, Figure 7.9 and Figure 7.10, each week long investigation modelled five 'occupied' days segmented by sixteen hours of night ventilation. During this time the night ventilation was powered by the 32W axial supply fan. The fan air inlet was either recycled chamber air, in the case of 'no vent', or ambient laboratory air, in the case of 'lab vent'.

During 'occupied' periods the AC unit maintained room temperature, for both the reference chamber (Room B) and thermal mass chamber (Room A), below 25°C as recorded by the room thermocouples (24°C being the control set point for AC cooling). The ambient temperature steadily increased between each investigation due to the peak summer time laboratory conditions. During the VPHC investigation the ambient temperature remained above 23°C throughout the week, offering insufficient night cooling to recharge the slab or PCM. The high night time temperatures during the VPHC investigation resulted in the AC unit operating throughout the 'unoccupied' period as well as the 'occupied'.

The inclusion of the thermal mass in Room A moderated the temperature swing delivered from the AC unit; hence the temperature variation during the occupied periods was less in Room A, compared to Room B. The WVHC system was the only system capable of recharging the slab cooling potential, however, since the water was only run during the day, the high ambient temperature lab vent at night subsequently saturated the hollow core thermal mass. This was a poor operation method for peak periods where no cooling was available during night periods.

During the *peak-period* experiment the ambient conditions were above the air-supply-fan set-point of 22°C therefore no ambient cooling was available. For each system (Figure 7.8, Figure 7.9 and Figure 7.10), the benefits of the thermal mass systems were most noticeable during the first 'occupied' periods, since prior to the week test the thermal mass had been cooled to 18°C. After the first day the slab was saturated and the slab was unable to cool the air.

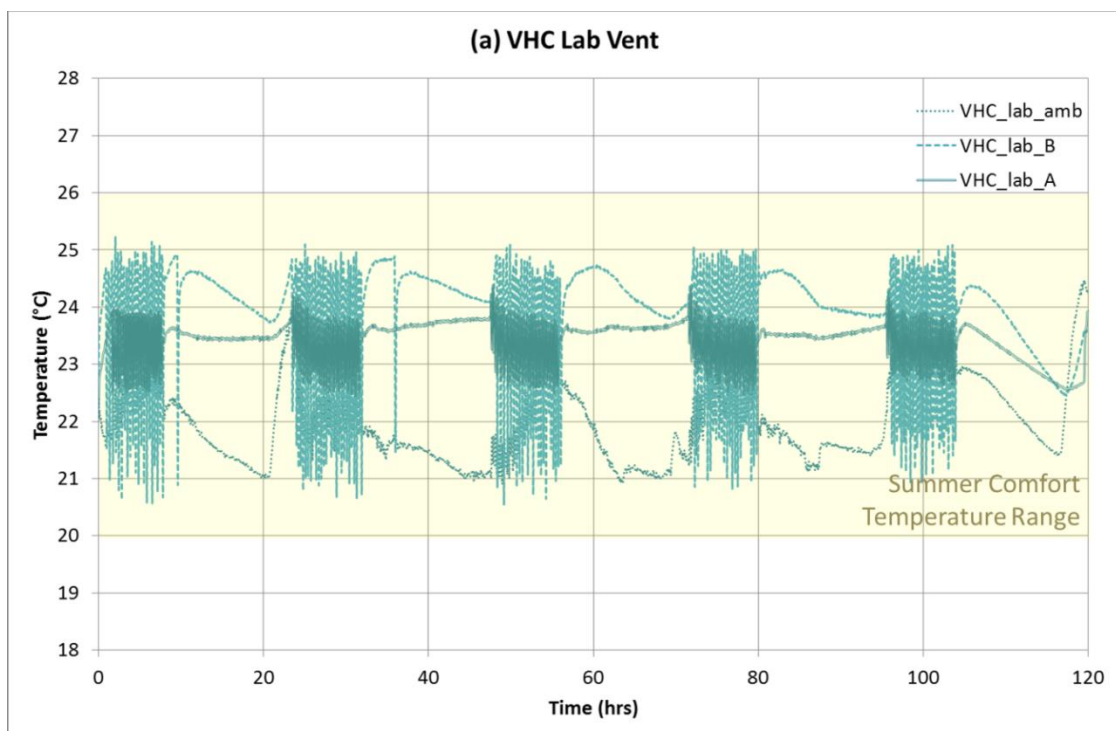


Figure 7.8 - VHC Peak Period Temperature Profiles

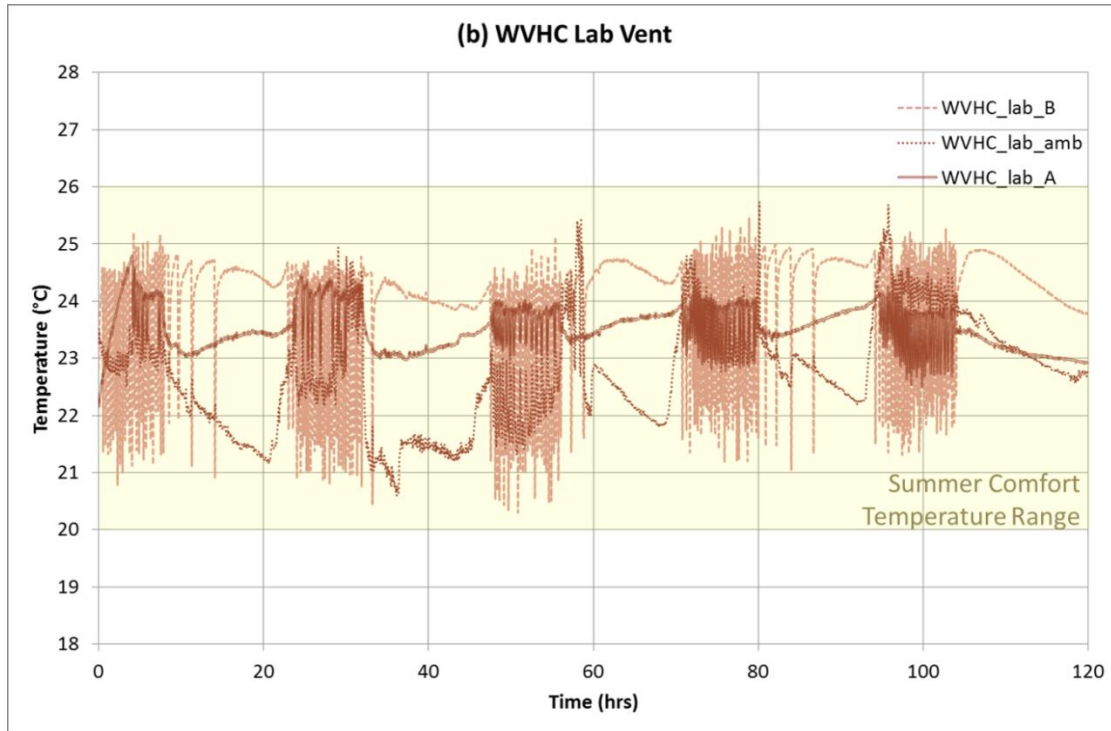


Figure 7.9 - WVHC Peak Period Temperature Profiles

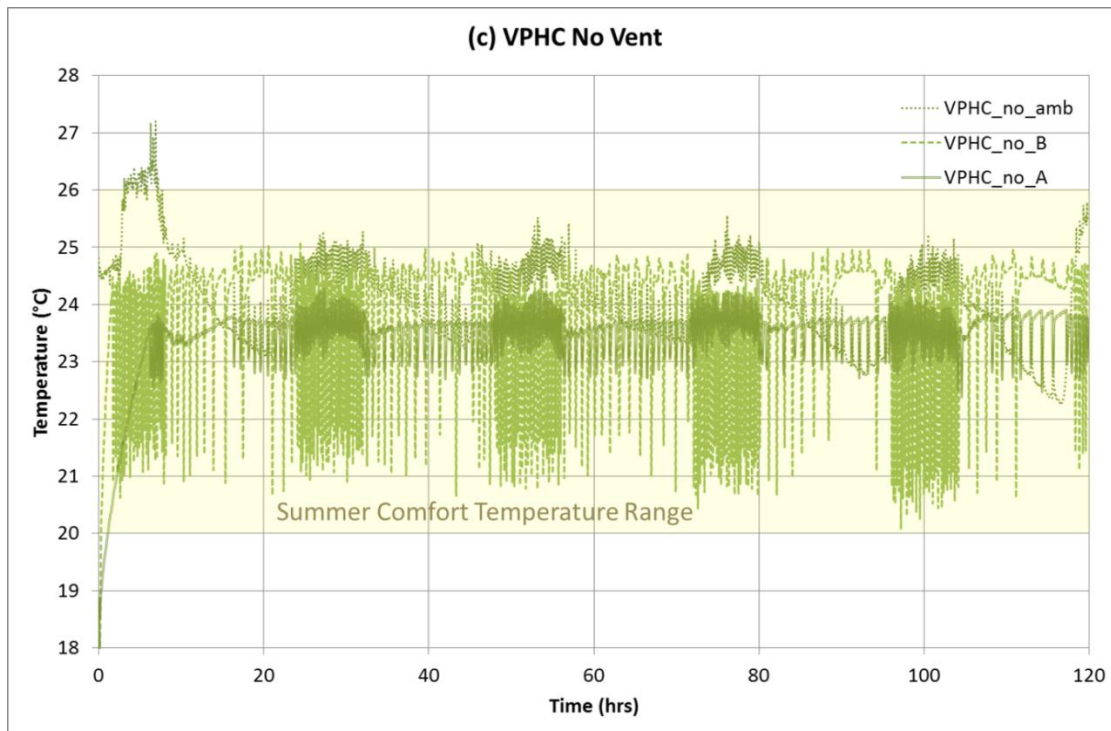


Figure 7.10 - VPHC Peak Period Temperature Profiles

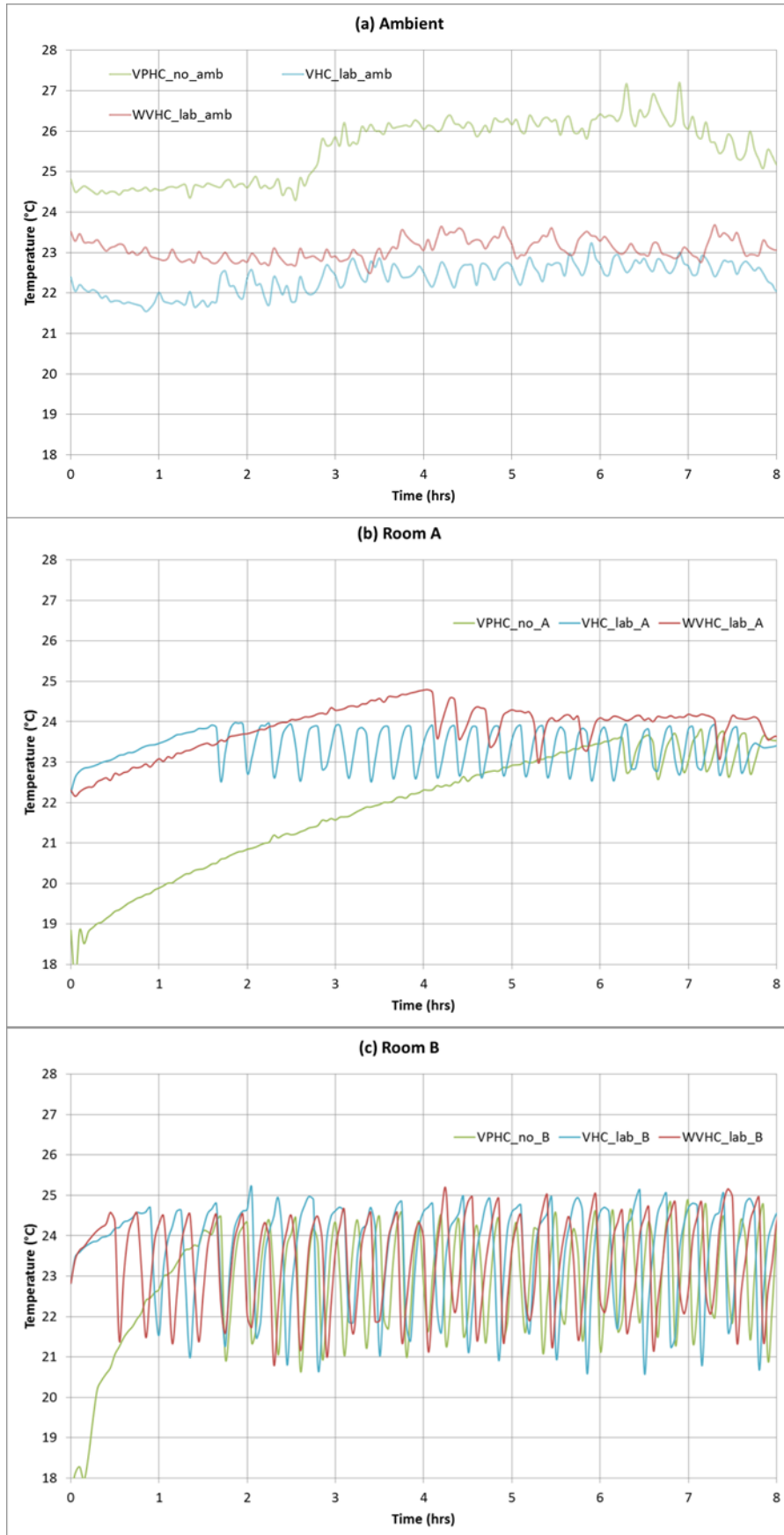


Figure 7.11 - Temperatures for First 8hours

The ambient temperatures charted in (a) of Figure 7.11 demonstrate the differing conditions each system was operating in. During the VHC lab vent and WVHC lab vent investigations the ambient temperature was 1-2°C below the operational peak. The ambient temperatures for the VPHC-no-vent investigation remained above the operational peak throughout the duration increasing the comparative thermal load. To account for the variation in ambient temperatures, comparison between the thermal mass systems has been carried out based on the benefit above the reference chamber since the reference chamber operated in the same ambient conditions it acts to normalise the ambient effects on the thermal mass system.

This method of normalisation was not fully effective due to the laboratory location. Room B was situated nearer to the main laboratory windows whilst Room A was placed nearer to the AC outlet of two other test facilities in the laboratory. The location of the ambient temperature sensor was therefore be more greatly affected by the AC outlet ducts than the window inlet. Because of this, lab windows were kept closed where possible to maintain a more homogenous temperature throughout the laboratory test space.

Due to the variation in ambient temperature it could be reasonably expected that the VPHC Room A temperature would rise fastest due to the increased load. Comparison of the Room A temperatures during the first eight hours revealed the time taken for the system to reach operational peak and the AC unit to initiate. The VPHC cooled the room without AC power for over 6 hours whilst the WVHC lab vent and VHC lab vent systems took 4 hours and 1.6 hours respectively.

7.2.3.2 Diurnal-swing Temperature Profiles

The temperature profile results from the three diurnal-swing tests are displayed in Figure 7.12, Figure 7.13 and Figure 7.14. Each graph plots the seventy-two hour ambient, Room A and Room B temperature profiles. Ambient temperature readings were taken from the centre of the laboratory space. Room A and B temperatures plotted are the average of the mid and upper thermocouple readings. During the diurnal-swing tests the lower Room A temperature readings became out of sync with the rest of the room temperature readings therefore were not included in the average room temperature analysis as they unduly biased the results.

Throughout the diurnal-swing tests the ambient temperature remained between 23°C and 29°C. The three-day experiment started with a twelve hour period of night cooling, followed by three and a half hours of stabilisation before the active thermal mass systems were initiated along with the radiant heaters simulating occupancy behaviour.

During the third night of the WVHC investigation the AC unit maintained 24°C for twelve hours before cooling to a target of 18°C for three and a half hours. Although different from the typical night cooling schedule the room temperature at the start of the third ‘occupied’ period was 21.1°C in comparison to 21.7 and 21.8°C on the previous two days. Although not ideal the minor room temperature difference was considered acceptable to continue the experimentation. The performance suffered during that day, only reaching half of expected WVHC slab performance, due to thermal mass not being fully recharged.

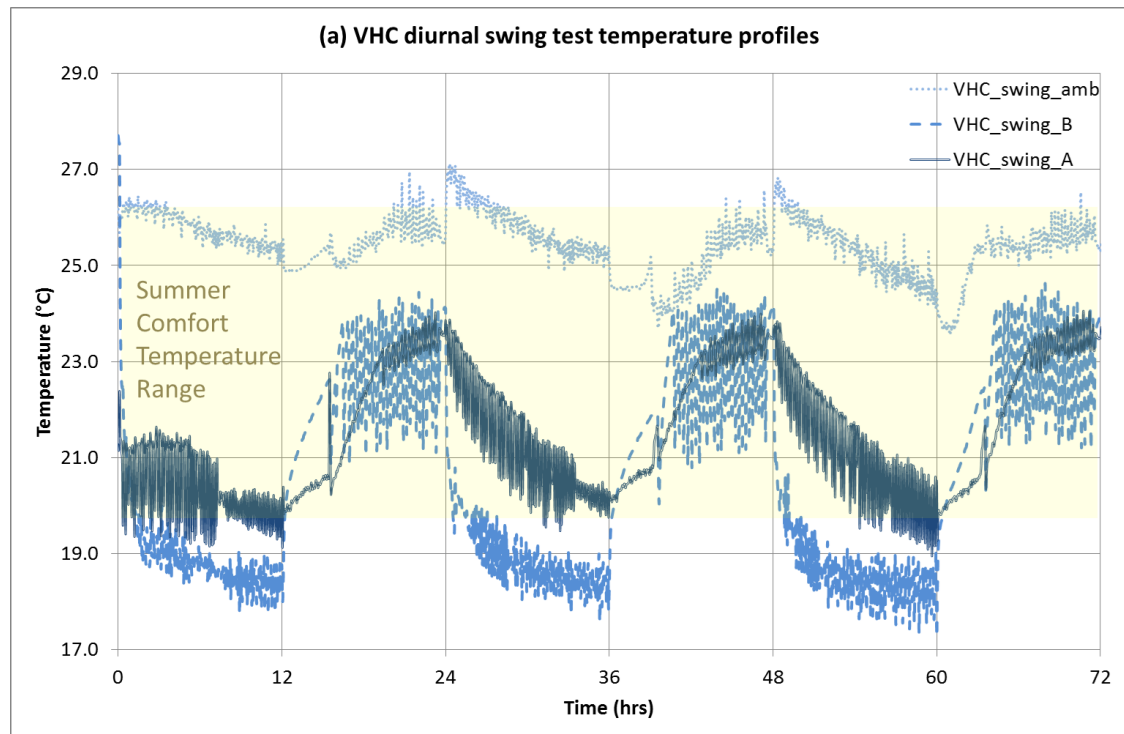


Figure 7.12 - VHC Temperature Profiles for the Diurnal Swing Tests

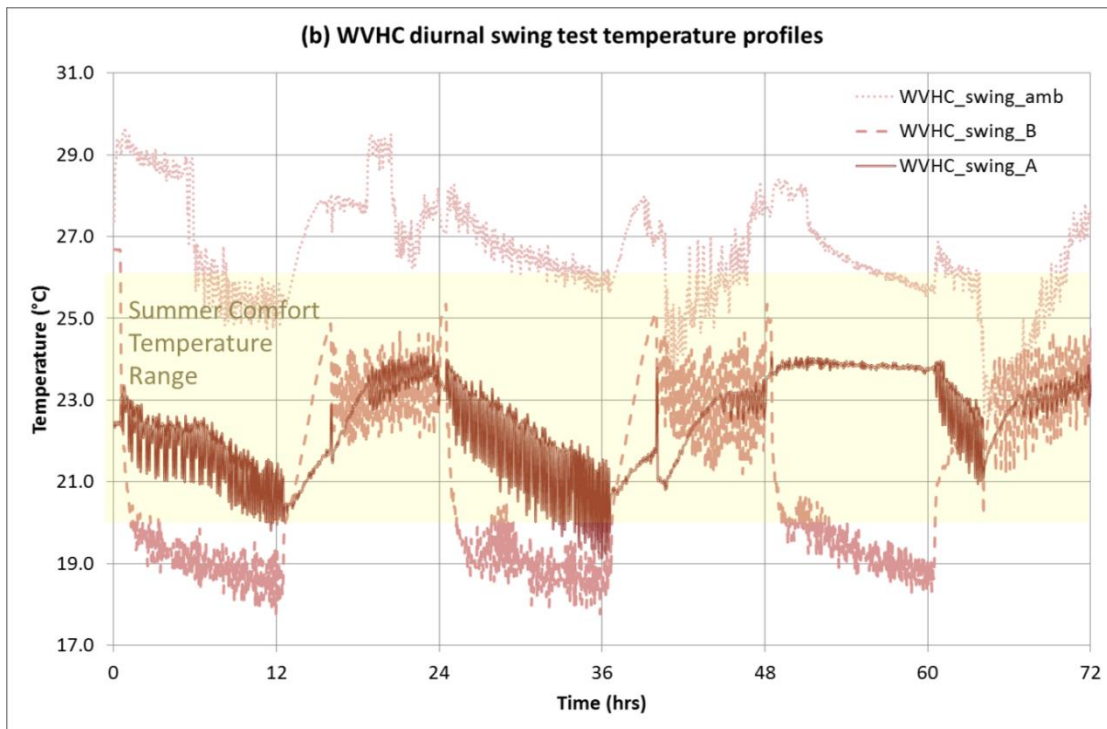


Figure 7.13 - WVHC Temperature Profiles from the Diurnal Swing Tests

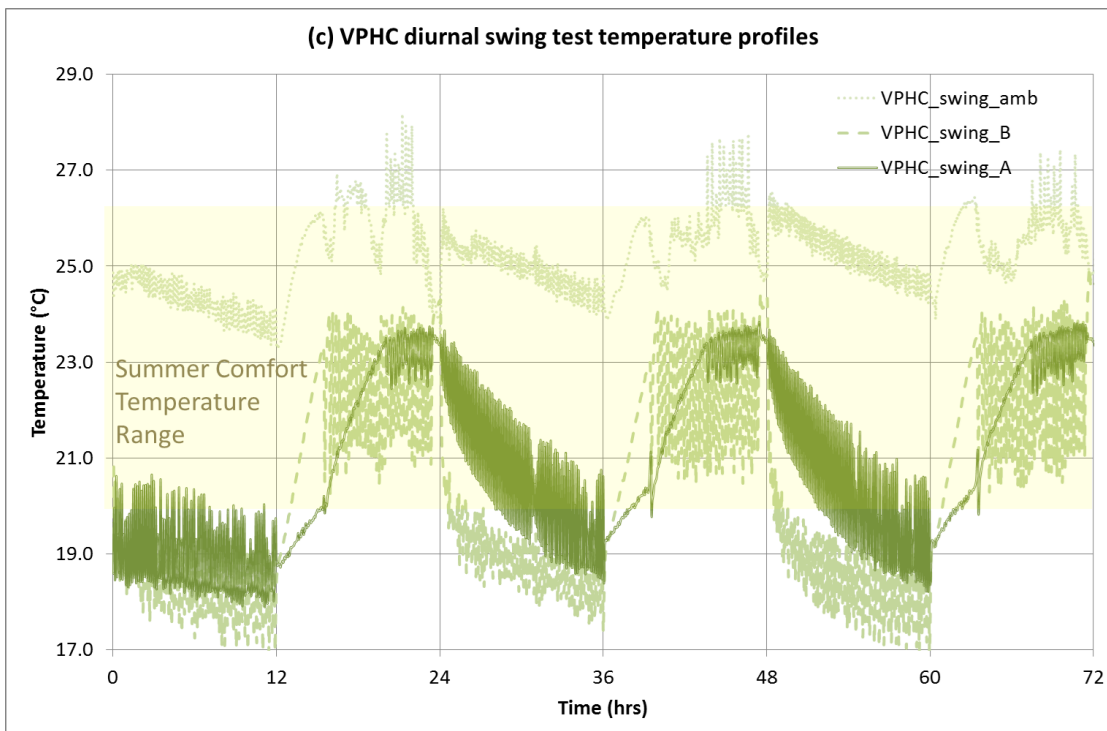


Figure 7.14 - VPHC Temperature Profiles from the Diurnal Swing Tests

Based on further analysis of the results presented in Figure 7.12 it is possible to suggest that in Room A the thermal mass systems offset AC cooling demand by 3.3 to 4.6 hours during the first day. In contrast to the *peak-cooling-demand* tests where the thermal mass was saturated by the second ‘occupied’ period the diurnal-swing night temperatures enabled the

thermal mass in Room A to offset AC cooling demand by 3.1 to 4.6 hours in day two and day three. The night cooling effect bought benefit through each day. When operating at its best the WVHC system offered 1.5 hours more passive cooling than the VHC system and the VPHC system offered 1 hour more passive cooling than the VHC system (based on analysis of Room A temperatures on day 2 in Figure 7.12).

The ambient, Room A and Room B temperature profiles, for the first 'occupied' period, were presented in Figure 7.15. Ambient temperatures during this period remained between 22 and 28°C. The analysis of these graphs was used to generate the data in Table 7.5. Based on these figures it is possible to compare the different system's performance under the *peak-cooling-demand* and *diurnal-swing* conditions.

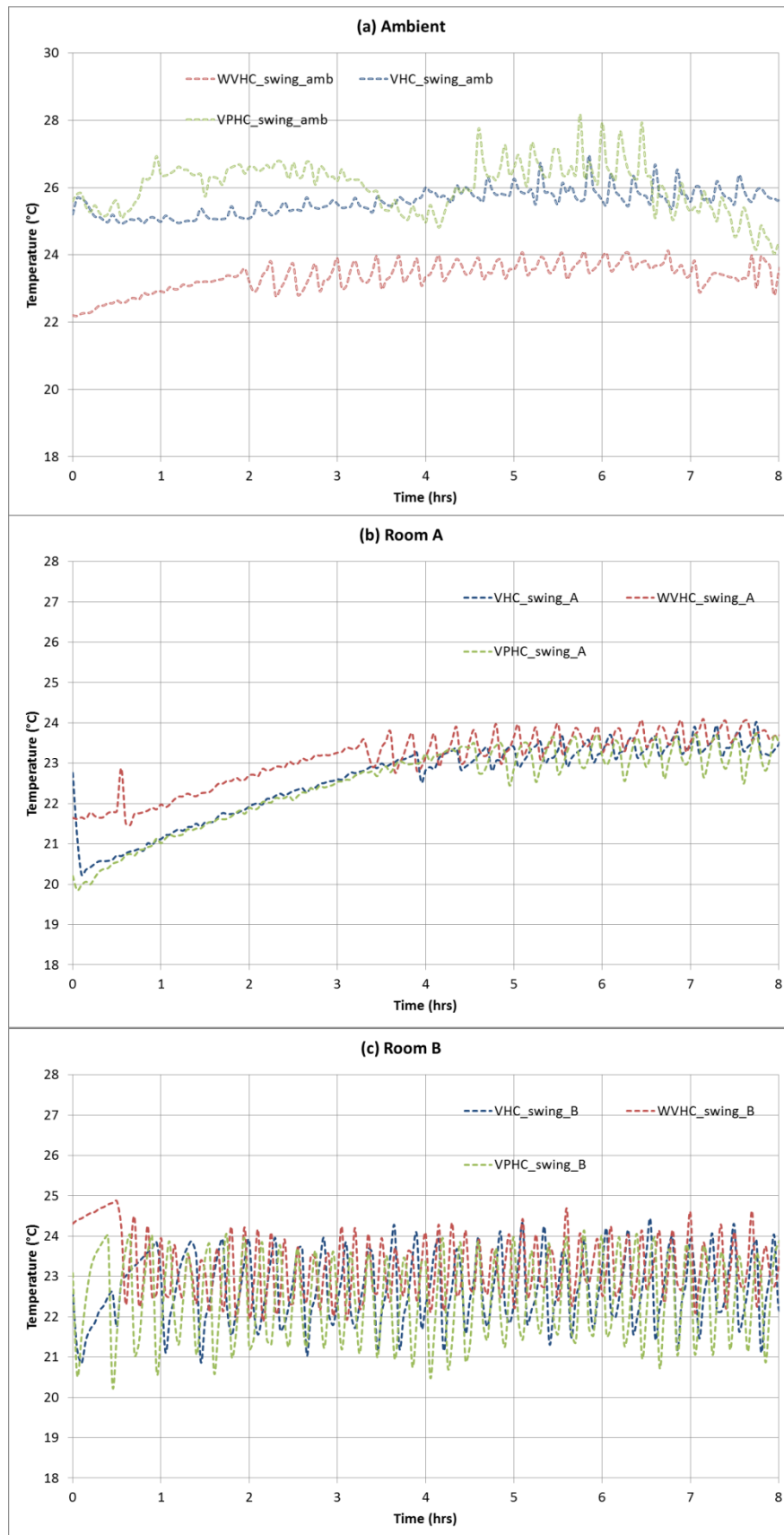


Figure 7.15 - First 8 'occupied' hour temperature profiles for diurnal swing tests

7.2.3.3 Peak Temperature Delay

Since each system started at differing temperatures the figures in Table 7.5 note the Peak Delay, the time taken for the temperature in Room A and Room B to rise from 22°C to 24°C. Table 7.5 and Table 7.7 also noted the time difference between Room A and Room B to compare technological performance negating ambient and initial temperature variance.

Table 7.5 - Day one Peak Temperature Delay

| | | VHC Peak Period | WVHC Peak Period | VPHC Peak Period | VHC Diurnal Swing | WVHC Diurnal Swing | VPHC Diurnal Swing |
|-----------------------------------|--------------|-----------------------|------------------------|------------------------|-------------------------|--------------------------|--------------------------|
| A: Peak Delay | <i>Hours</i> | 1.7 | 2.5 | 2.7 | 1.8 | 2.2 | 2.4 |
| B: Peak Delay | <i>Hours</i> | 0.9 | 0.5 | 0.7 | 0.7 | 0.5 | 0.4 |
| A-B: Peak Delay Difference | <i>Hours</i> | 0.8 | 2.1 | 2.0 | 1.2 | 1.7 | 2.0 |

The VHC-no-vent scenario offered the greatest additional *peak delay* (or ‘overheating offset’) due to the preferable ambient conditions. For the VPHC-no-vent, VHC-lab-vent and WVHC-lab-vent experiments no cooling was available from the ambient environment. During these *peak-cooling-period* conditions the VPHC and WVHC systems offered an additional 1.2 to 1.25 hours *peak delay* against the VHC system.

During day one of the *diurnal-swing* test 0.5 and 0.8 hours of *peak delay* was achieved by the WVHC and VPHC system respectively, against the VHC system performance. Table 7.6 presents the *peak delay* findings for day two and day three in the *diurnal-swing* tests.

Table 7.6 - Day two Peak Temperature Delay

| | | Day 2 | | | Day 3 | | |
|-----------------------------------|--------------|-------------------------|--------------------------|--------------------------|-------------------------|--------------------------|--------------------------|
| | | VHC Diurnal Swing | WVHC Diurnal Swing | VPHC Diurnal Swing | VHC Diurnal Swing | WVHC Diurnal Swing | VPHC Diurnal Swing |
| A: Peak Delay | <i>Hours</i> | 1.9 | 2.45 | 2.0 | 1.8 | 1.95 | 2.4 |
| B: Peak Delay | <i>Hours</i> | 0.6 | 0.1 | 0.3 | 0.5 | 0.6 | 0.3 |
| A-B: Peak Delay Difference | <i>Hours</i> | 1.2 | 2.3 | 1.6 | 1.3 | 1.3 | 2.1 |

Comparison of the *peak delay* difference between the *peak-cooling-demand* and *diurnal-swing* test shows little significant difference. This was likely due to the thermal mass being

cooled prior to both investigations. Day two and day three performances were where significant differences were noted. In the *diurnal-swing* conditions the *peak delay* difference was maintained, maintaining the energy saving benefit throughout the latter days of the test. In the *peak-cooling-demand* test the thermal mass was saturated, therefore there was no noticeable *peak delay* between Room A and Room B.

Based on the comparison between the *peak-cooling-demand* findings and the *diurnal-swing* findings, no additional benefit from the thermal mass enhancements was noted during the latter days of the *peak-cooling-demand* test. In practice it was during these periods that enhancements to active thermal mass systems were most needed. The enhancements in this investigation offered no additional benefit with respect to *peak delay* against the traditional VHC system. When tested under the *diurnal-swing* conditions the active-thermal-mass system enhancements offered 0.4 to 1.1 hour *peak delay* benefit against the VHC alternative, during the second 'occupied' day. Being able to maintain this *peak delay* from day to day is essential to offering energy savings. Without this additional benefit, as shown in the *peak-cooling-demand* results, additional thermal mass had an inhibiting effect on cooling the room down once saturated. The findings from this investigation reinforce the importance that effective, low energy, low cost, efficient night ventilation is a necessary system to be coupled with an active thermal mass technology to achieve low energy cooling.

7.2.3.4 Energy Consumption

The energy consumption figures recorded for each week long investigation were tabulated in Table 7.7. Under the *peak period* conditions only the WVHC offered energy saving benefits against the reference chamber. For the VPHC and VHC systems, increased AC power was required to maintain comfort temperatures during the week long simulation. The phenomena was due to saturated thermal mass impeding night cooling and requiring additional AC cooling to cool the mass, as well as the room air.

Under *diurnal-swing* conditions all the systems achieved energy savings against the reference chamber. The greatest energy saving benefit was achieved by the WVHC system saving 1.1 kWh per day, 0.7 kWh more than the traditional VHC system. The PCM diffuser saved an additional 0.4 kWh per day over the VHC savings. The savings achieved by the thermal mass systems, over the reference chamber, were due to effective utilisation of the 'night cooling' available. Pumping power was not included in the energy consumption figures.

Coefficient of Performance (COP) figures in Table 7.7 were calculated based on the AC, fan and pumping power, thermal load and chamber heat loss over the duration of the tests. The calculation revealed that for the enhanced thermal mass systems investigated, under *peak period* conditions the greatest COP was achieved by the WVHC system. VHC and VPHC system had comparable COP figures however the VPHC system cooled the greatest number of kWh due to high ambient conditions during the test. Under diurnal-swing conditions the VPHC system offered the greatest COP figures.

Table 7.7 - Energy Consumption Figures for Week Long Tests

| | | VHC Peak Period | WVHC Peak Period | VPHC Peak Period | VHC Diurnal Swing | WVHC Diurnal Swing | VPHC Diurnal Swing |
|-----------------------------|-----------------|-----------------------|------------------------|------------------------|-------------------------|--------------------------|--------------------------|
| A: Energy Consumed | <i>kWh</i> | 16.2 | 11.2 | 20.9 | 4.4 | 3.9 | 4.2 |
| B: Energy Consumed | <i>kWh</i> | 11.2 | 13.8 | 17.1 | 5.5 | 7.1 | 6.6 |
| Energy Cooled | <i>kWh</i> | 7.5 | 8.0 | 9.0 | 7.7 | 7.3 | 6.7 |
| A: Energy Consumed | <i>kWh /day</i> | 3.2 | 2.2 | 4.2 | 1.5 | 1.3 | 1.4 |
| B: Energy Consumed | <i>kWh /day</i> | 2.2 | 2.8 | 3.4 | 1.8 | 2.4 | 2.2 |
| Energy Cooled | <i>kWh /day</i> | 1.5 | 1.6 | 1.8 | 2.6 | 2.4 | 2.2 |
| A-B: Energy Consumed | <i>kWh /day</i> | 1.0 | -0.5 | 0.8 | -0.4 | -1.1 | -0.8 |
| A: COP | | 0.53 | 0.61 | 0.41 | 1.19 | 0.81 | 1.24 |
| B: COP | | 0.77 | 0.51 | 0.51 | 0.95 | 0.54 | 0.79 |

Table 7.8 presents additional COP figures calculated for the active-TES system during the respective test periods. Each figure has been calculated to offer further insight into the system performance:

- *COP A and B* have been calculated from the delivered energy from the heater, divided by the amount of energy the AC, fan and pump systems have used throughout the test period.
- The energy *efficiency improvement* of a thermal mass system against the reference AC unit has been quantified through the subtraction of COP B from COP A.
- The *COP A (w/heat loss) and COP B (w/heat loss)* figures were calculated throughout the experimentation period by using the same calculation as the COP A and B figures,

with the addition of chamber wall heat transfer to the bottom side of the division. Chamber wall heat transfer (heat loss or heat gain) between the chamber and ambient conditions has been calculated based on the inside and outside wall temperatures. A typical U-value for partition walls constructed from insulated plaster board and the geometry of the room was used. The exact energy transferred through the chamber wall differs throughout time, therefore including it in the COP calculation offered a measure of normalising the system COP figures found under different ambient conditions.

- The *COP A (day only w/heat loss)* calculated the system COP only taking into account the energy flows during the ‘occupied’ hours. This COP figure was deemed most appropriate representation of performance since during this period the performance of the system needs to operate optimally. For all these COP figures, pump energy was quantified linearly at 40W/l/min.
- The *COP A (day only w/heat loss and no pump energy)* figure in Table 7.8 was calculated to determine the comparative COP for the laboratory experiment, where no pumping duty was carried out due to the water flowing under mains pressure. The pumping duty calculation was removed for this figure.

Table 7.8 - COP Comparison across the test conditions and systems

| | VHC Peak Period | WVHC Peak Period | VPHC Peak Period | VHC Diurnal Swing | WVHC Diurnal Swing | VPHC Diurnal Swing |
|--|--------------------------------|---------------------------------|---------------------------------|----------------------------------|-----------------------------------|-----------------------------------|
| COP A | 0.53 | 0.61 | 0.41 | 1.19 | 0.81 | 1.24 |
| COP B | 0.77 | 0.51 | 0.51 | 0.95 | 0.54 | 0.79 |
| Efficiency difference (COP A - COP B) | -0.24 | 0.10 | -0.10 | 0.24 | 0.27 | 0.45 |
| COP A (w/heat loss) | 0.46 | 0.56 | 0.43 | 1.75 | 1.13 | 1.59 |
| COP B (w/heat loss) | 0.67 | 0.46 | 0.53 | 1.40 | 0.75 | 1.01 |
| COP A (day only w/heat loss) | 0.31 | 0.36 | 0.26 | 1.28 | 0.90 | 1.33 |
| COP A (day only w/heat loss and no pump energy) | | 0.46 | | | 1.49 | |

During *peak periods* the reference chamber offered more efficient cooling, with the exception of the WVHC system. The VPHC system demonstrated the poorest COP figures for the overall system. This was due to the PCM inhibiting room cooling (due to additional cooling from the AC system being required to cool the PCM) before the cooling benefit was

effective in the room. The addition of PCM to the system offered some benefit for the first day (in *peak temperature delay*) but once saturated inhibited room cooling, counteracting the intended PCM purpose.

When integrating PCM it is essential that an easily accessible energy efficient cooling source (as represented in the *diurnal swing* tests) is available to re-charge the PCM and avoid it counteracting its intended cooling purpose. Considering the bottom two rows in Table 7.8, under *diurnal swing* conditions, the VPHC offered marginal efficiency enhancement on the VHC system. The marginal improvement was anticipated due to the relatively small addition of thermal mass retrofit compared to the existing slab.

Without any accounting for pumping duty the WVHC system offers further system efficiency enhancement during occupied periods. The water pipes offered the greatest slab cooling; however when pumping duty was taken into account the efficiency of the system was outperformed by the VHC and VPHC systems.

Throughout the COP figures reported, the reported system efficiency was low compared to alternative heat pump technologies (COP>3) [146]. However COP figures are typically quoted for year round performance. The scenarios tested represent a summer seasonal efficiency ratio. Evidence from *Chapter 3* revealed that the poorest season for active-TES system efficiency was during peak summer conditions, therefore these results were in line with those findings.

7.2.3.5 Fixed-occupancy Temperature Profiles

To investigate the temperature saving benefit of the enhanced thermal mass systems further, *fixed-occupancy* (saturation) tests lasting eighteen hours were carried out on each of the three systems. The temperature profiles presented in Figure 7.16, Figure 7.17 and Figure 7.18 chart the ambient, average Room A and average Room B temperatures respectively, during the eighteen hour 50W/m² loading.

During the VPHC saturation test the ambient temperatures rose 3°C in 4 hours causing unexpected extra movement in the final 6 hours. This movement was reflected more significantly in Room B although evidence of a rise after hour twelve in the Room A profile was also noticeable. In the Room A temperature profile the VPHC profile tracked the VHC trend for the first 4 hours. Once above 24°C the rate of temperature increase in Room A reduced in the VPHC case. At its most extreme this deflection, caused by the melting PCM achieved a 0.9°C reduction in average room temperature. At the end of the eighteen hours,

due in part to the increased ambient temperature, the VPHC Room A temperature was 0.15°C below that of the VHC system.

The PCM addition extends the comfort temperature period by over two hours. The WVHC system demonstrates it has the greatest cooling capacity and was the most capable at delivering an on-going cooling capacity from the addition of open-loop mains water. At the end of the eighteen hour fixed-occupancy test the WVHC system registered a room temperature 3.7°C below the VHC system room temperature. Under these conditions the WVHC system was capable of maintaining comfort temperatures over an extended occupancy period.

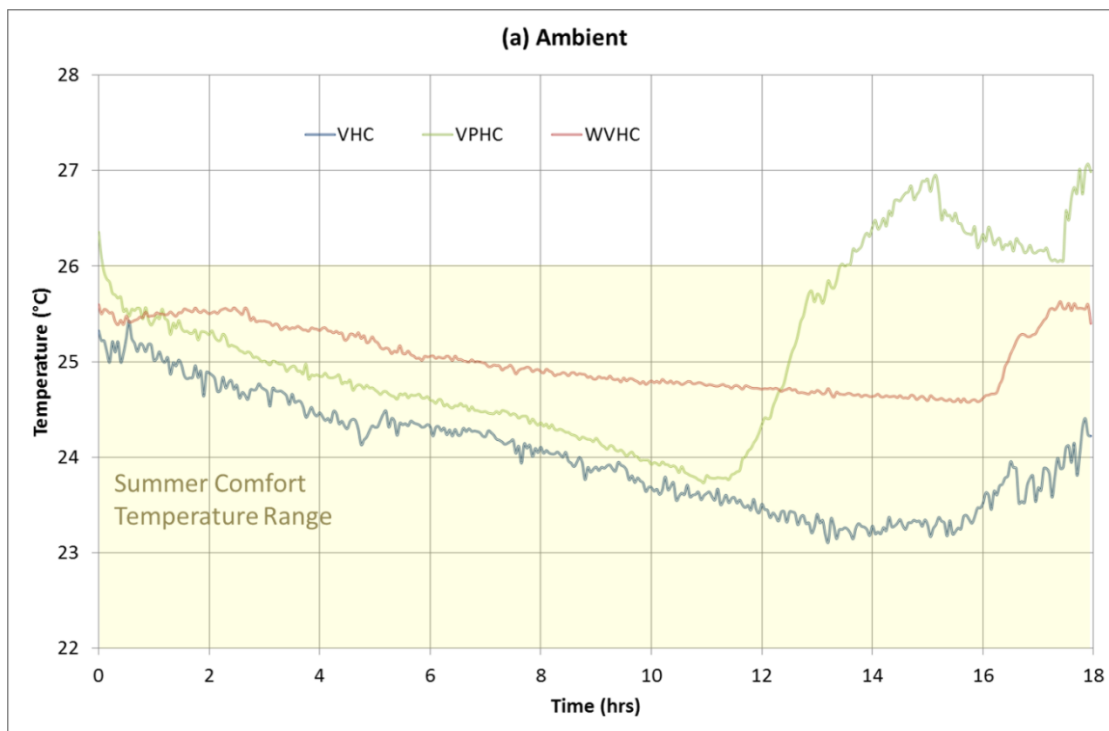


Figure 7.16 - Fixed-occupancy Ambient Temperature Profiles

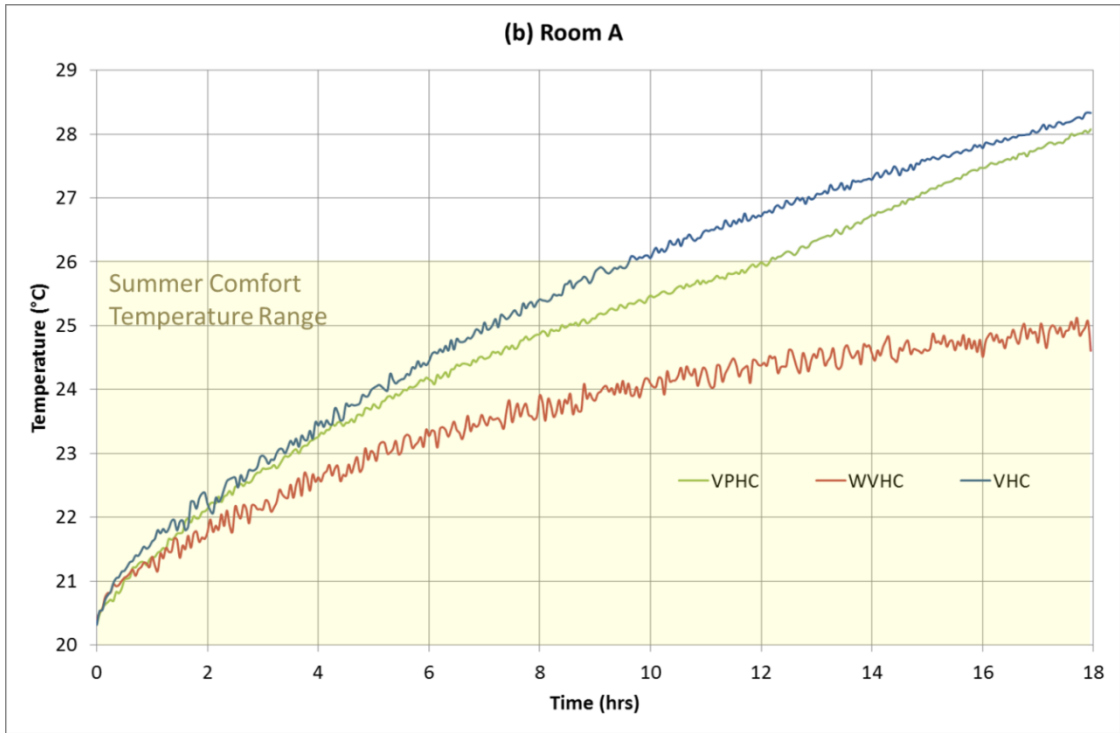


Figure 7.17 - Fixed-occupancy Room A Temperature Profiles

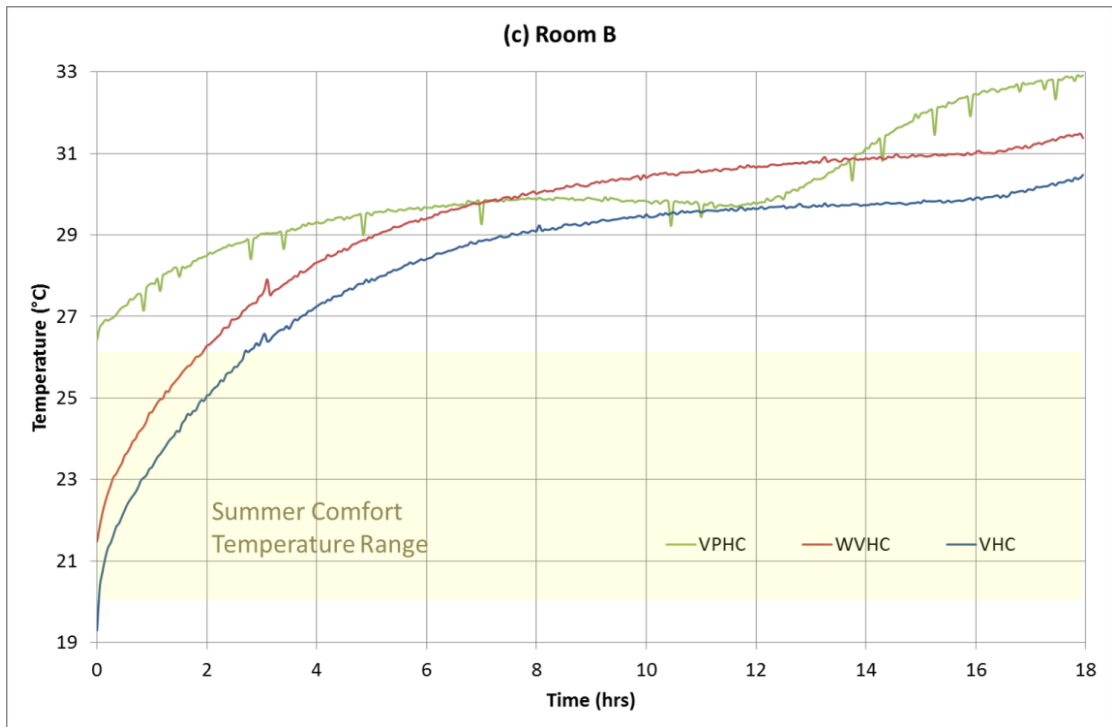


Figure 7.18 - Fixed-occupancy Room B Temperature Profiles

7.2.3.6 Occupied Average Temperature Difference

To further assess the temperature savings of the systems under the three conditions tested, the average occupied temperature difference was calculated. The results were displayed in Table 7.9. From these results it was clear that with the AC back up, as found in the *peak*

period and *diurnal swing*, minimal temperature difference was observed between the reference (B) and test chamber (A). On average, the WVHC system saved a small amount against the reference chamber temperatures during the *diurnal swing* conditions.

During the *fixed occupancy* conditions the temperature saving benefits of active thermal mass systems were observed. The differences in ambient and reference temperatures were accounted for. Under these conditions the WVHC and VPHC demonstrated a 2.8 and 1.0°C improvement respectively, against the VHC system. Therefore, where no backup AC system is present, WVHC or VPHC systems will offer greater comfort during hot periods.

Table 7.9 - Average Occupied Temperature Difference

| | VHC | WVHC | VPHC |
|------------------------|-------|--------|--------|
| | °C | | |
| Peak Period | 0.229 | -0.426 | -0.534 |
| Diurnal Swing | 0.001 | 0.365 | -0.149 |
| Fixed Occupancy | 2.93 | 5.72 | 3.94 |

7.2.3.7 Prototype Economic Analysis

7.2.3.7.1 Method

To assess the financial viability of the prototype system the energy savings, kgCO₂e and financial savings were calculated. The results were based on the figures from the diurnal swing tests therefore only represent the summer seasonal performance. It was not possible from this data to calculate annual energy savings, therefore subsequent payback calculations were not found. The figures for embodied carbon and energy prices were taken from UK average figures [173-175] and were presented in Table 7.10. It has been assumed, in line with the laboratory conditions that all energy consumption was from grid supplied electricity.

Table 7.10 - Data Inputs for Electrical Supply

| | Data Inputs | | |
|--|--------------|----------------|------------|
| Grid efficiency | 92.3% | | |
| Fuel type | <i>Coal</i> | <i>Nat Gas</i> | <i>Bio</i> |
| tCO₂e per kWh | 0.91 | 0.39 | 0.058 |
| Average fraction of UK fuel Mix | 0.34 | 0.256 | 0.059 |
| Price of Electricity | 0.1352 £/kWh | | |

7.2.3.7.2 Results

Table 7.11 displayed the economic savings anticipated per day for a chamber operating the installed technology during the *diurnal swing* conditions.

Table 7.11 - Daily Savings based on diurnal swing results

| | VHC | WVHC | VPHC | |
|-------------------------------|------|------|------|--------------------------|
| Energy Savings | 0.4 | 1.1 | 0.8 | <i>kWh/d</i> |
| Primary Energy Savings | 0.43 | 1.19 | 0.87 | <i>kWh/d</i> |
| tCO₂e Saved | 0.17 | 0.45 | 0.33 | <i>tCO₂/d</i> |
| Cost Saved | 0.05 | 0.15 | 0.11 | <i>£/d</i> |

7.2.4 Summary of Findings

7.2.4.1 Peak-cooling-demand Period Findings

Peak temperature delay and associated ‘energy savings’ were evident during the first day of the *peak period* investigation. However over the week investigated, without any provision of night cooling, the system was dependent on the AC heat pump technology to provide the required cooling to maintain stable room temperatures below 24°C.

The addition of X25D PCM unit to the VHC system (VPHC) increased the thermal mass capabilities in a key region when overheating threatens, without impinging on the soffit heat transfer to the room. However floor temperatures were greatly increased due to the dispersion of ventilation currents away from the floor level. Under the *peak period*, the limitations of the PCM diffuser were akin to that of the sensible thermal mass. When no night cooling was available, during hot night periods, the PCM hindered the cooling of the room during the daytime and stabilised the temperature around 25°C. The addition of PCM alone does not deliver sufficient cooling; only when coupled with sufficient night cooling does the PCM enhancement aid avoidance of daily overheating. The PCM offered increased capacity as the slab approached 23°C, but once saturated impeded the conditioning of the room.

Under the *peak period* conditions the water incorporated system (WVHC) offered the most energy efficient cooling method. If pumping duty was removed from the COP calculation, since the system operates under mains pressure, the COP increases 27%. In the thermal chamber the WVHC system performance exceeded the VHC and VPHC tests due to the continual addition of cooling capacity from the mains water. On an energy level the WVHC

system had the best respective savings against the reference thermal chamber. The greatest *peak temperature delay* was achieved by the VPHC and WVHC systems.

The VHC system used 1.0 kWh per day more than the reference chamber due to the additional cooling required to cool the saturated thermal mass and chamber air. The WVHC system used 0.5kWh per day less than the reference chamber, demonstrating a 1.5kWh per day energy saving enhancement on the VHC system. The VPHC system used 0.8kWh per day more than the reference chamber but 0.2kWh per day less than the VHC system.

During the test period the ambient temperatures remained between 23 and 26°C, higher night temperatures than even an extreme heat wave in the UK, disabling the typical night cooling delivered through night ventilation. During these constant high temperatures the need for cooling during night ventilation was accentuated and the *diurnal-swing test* designed to mimic a daily temperature swing in the laboratory test facility.

7.2.4.2 Diurnal-swing Conditions Findings

The benefit of night cooling was clearly demonstrated between the tests conditions investigated. The energy consumption decreased by 1.7 kWh per day, for the VHC system. Respectively, the WVHC and VPHC systems energy consumption reduced by 0.9 kWh and 2.8 kWh per day. COP figures improved significantly under *diurnal-swing* conditions. More significant benefit was observed in the VHC and VPHC systems, where night-time cooling was the only source of cooling during the investigations. The WVHC and VPHC systems recorded superior COP figures to the VHC thermal-mass system, when considered without pumping duty over the 'occupied' period only.

The *peak delay* achieved by all systems under *diurnal-swing* conditions ranged from 1.2 to 2.0 hours in comparison with 0.8 to 2.1 hours under *peak-cooling-demand* conditions. Although the hours delayed were similar for the first days, the thermal-mass systems under *diurnal-swing* conditions maintained similar *peak delay* for each test day throughout the test period, ensuring on-going benefit.

7.2.4.3 Fixed-occupancy Conditions Findings

The WVHC system demonstrated the greatest-temperature-saving benefit of the three enhanced thermal-mass systems; saving 3.7°C after 18 hours. The VPHC system achieved a peak temperature benefit (after 11 to 12 hours of 'occupancy' heat load) of 0.9°C less than the VHC system at the equivalent time.

On average, the thermal mass temperature savings against the reference chamber ranged between 2.9 and 5.8°C. The WVHC system saved 2.8°C, whilst the VPHC enhancement saved 1.0°C against the VHC system. Further, the VPHC system maintained summer comfort conditions for an additional two hours over the VHC system. The WVHC system maintained summer comfort throughout the *fixed occupancy* test period.

7.2.4.4 Limitations

Most significantly the pilot scale laboratory tests suffered from ambient temperature variation. The testing occurred during the summer months of June and July causing high indoor temperatures, where the laboratory was suffering from overheating. Efforts were made to improve the ventilation of the lab and reduce the ambient temperature, however this was countered by the behaviour of neighbouring researchers. Excess heat from neighbouring research bays was deposited into the ambient lab space increasing the peak laboratory temperatures. Within the restrictions of the test chambers location and facilities available the diurnal-swing test conditions artificially offered an ambient temperature swing between 18 and 28°C.

Within the laboratory space, at the Department of Architecture and Built Environment, was an environmental chamber capable of artificially generating a diurnal swing. However due to the scale and weight of the prototypes under investigation the chamber could not accommodate the enhanced thermal-mass systems. Insulated chambers were constructed, with portable AC units controlling internal temperatures, to undertake this work.

7.3 Economic Analysis

Numerous economic methods exist for assessing the commercial viability of capital investments. What is less simple is assessing the commercial viability of energy saving technologies since there is no direct economic gain, simply a reduction of economic loss. This assessment uses the available tools to offer economic conclusions, predicting when the savings made will offset the initial capital investment.

Work by Dincer [176] suggests assessing the economics of thermal energy storage (TES) systems by offsetting capital and operational costs against equivalent energy savings achieved by the TES system. Energy savings are either calculated against alternative technologies or a reference non-existent system. To determine capital cost, material and component costs should be obtained from the manufactures. Installation and maintenance costs require estimation for novel technologies.

Habeebullah [177] presents an objective cost function to determine the economic feasibility of a TES systems. The cost function incorporates capital cost of chillers and energy storage tanks. Operational costs are determined based on the operation period, the electrical energy consumed and the electrical tariff rate. To determine economic feasibility a capital recovery factor is incorporated to determine the annual repayment required to return the investment within a given period.

Henze [178] assesses the economic feasibility of various control strategies in a hotel AC system enhanced with TES. To provide financial assessment the work calculates the twenty year net present value (NPV) for each strategy. The twenty year NPV figure offers a comparable benchmark for each strategy.

Features from previous research have been utilised in the economic assessment of the enhanced TES systems reported here. Performance of each system was primarily compared against an equivalent room without TES; although the data generated was also useful for comparison between the TES systems. Two levels of economic analysis have been conducted. Initially, daily economic benefit has been assessed from the energy saving figures determined during the *diurnal-swing* investigation conducted for the VHC, WVHC and VPHC technologies reported previously in this chapter (section 7.2.3.7). Secondly building simulation software IES was used to simulate the performance of the chamber under year round conditions. From the simulated performance, economic conclusions were drawn.

7.3.1 Economic Analysis Method

To enable the economic assessment of the enhanced TES technologies, twenty year NPV figures for each system were calculated. To determine the NPV, capital costs and operational costs were calculated for each system. Economic performance during the life of the TES systems was heavily dependent on financial cost projections. Three tiers of interest rate and energy cost projections were therefore analysed; performance being reported for conservative, moderate and optimistic financial conditions.

During the assessment the economic feasibility was assessed on two scalar levels. Initially the economics of the laboratory test chamber room were investigated. Subsequently, based on the energy savings observed in the model the performance and costs were scaled up for a 3,000sqm commercial building, occupied 252 days a year.

7.3.1.1 Capital Cost Model

The capital cost estimated for both the chamber and the building was tabulated in Table 7.12.

Table 7.12 - Capital Costs

| | Chamber | Building |
|--------------------|---------|---------------------|
| Hollow Core | £0 | £50 m ² |
| AHU | £360 | £300 m ² |
| BMS | £0 | £3,000 |
| VHC | £255 | £45 m ² |
| WHC | £339 | £20 m ² |
| WVHC | £395 | £65 m ² |
| PHC | £132 | £154 m ² |
| VPHC | £387 | £199 m ² |

7.3.1.1.1 Chamber

The chamber costs calculated in Table 7.12 have been calculated from the laboratory rig costs incurred during the investigation. These are given in absolute cost (£). The hollow core was donated as an ex-display construction piece along with the original heavy weight trolley. The Toshiba KYR35-GW/X1c portable air conditioning system utilising heat pump technology functions as the AHU for the chamber costing £360. There was no BMS therefore no BMS cost was included.

The costs for the VHC, WHC and PHC systems included the different components required to activate the thermal mass in each configuration. The VHC required an additional fan and duct system as well as frame supports to raise the hollow core height. The WHC cost also incorporates the additional frame risers as well as the pipe cost and additional concrete. The PHC system was the material cost incurred to construct the X25 PCM Diffuser. No accounting for technician labour has been included as this was not incurred as a project cost.

The WVHC and VPHC systems were combined systems, therefore were an addition of VHC and WHC system costs or VHC and PHC respectively. In the case of the WVHC the cost of the metal frame risers has only been taken into account once.

7.3.1.1.2 Building

To offer typical, real-world figures the building costs (given in £/m²) were scaled up for a 3,000sqm building. Costs for VHC, WHC and WVHC were obtained from correspondence with the active thermal mass industry [151]. The industry advised that typically 70% of building surface area would be fitted with an active thermal mass system therefore the building floor area should be scaled down to 70% of the floor area.

The hollow core and AHU costs were obtained from the commercial modelling software Design Builder. The figure for BMS was deduced from expected savings due to BMS and the respective payback times available online. The PHC cost was calculated from the PCM Diffuser unit cost, including labour. The £/m² figure for the diffuser was calculated from the assumption that there would be one diffuser per active hollow core beam. The number of hollow cores, and thus diffusers was determined from the assumed hollow core size of 9m by 1.2m. As before the WVHC and VPHC system costs were a combination of their respective component costs.

7.3.1.2 Operational Cost Model

7.3.1.2.1 Chamber

The operational costs were determined from the energy consumption to the rig. These were monitored during the three day diurnal swing tests carried out in the laboratory. Whilst not necessarily representative of every day of the year, they contrast the daily performance of each technology against its counterparts in a comparable manner. The energy meters recorded fan and AHU energy consumed during occupied hours. Since the water for the WVHC investigation ran under mains pressure no additional energy was incurred in the rig,

however a theoretical pumping power based on 40W/l/min has been applied to the recorded flow rate to approximate pumping energy consumed.

From the measurements taken and the approximated pumping energy, a kWh per day figure was produced for each enhanced thermal mass system. From these the energy savings per day, against the reference chamber under the same conditions, was calculated.

Annual energy consumption was simulated in both reference chamber and thermal mass chamber models. Subsequently, based on the average UK electricity cost in 2013 from the Energy Savings Trust [175] in £/kWh, an annual operational cost was calculated for the first year. Subsequent year energy prices were subject to predicted market rate energy rises. In the UK energy prices in 2013 rose between 8.5 and 11.1% [179]. Three levels of inflation (8.5, 9.8 and 11.1%) were used in the economic assessment to determine the viability of the TES systems under differing economic forces.

7.3.1.2.2 Building

The operational cost model follows the same method as the chamber method however uses an energy consumption figure of kWh/d/m². This figure was derived from the energy consumption figures in the laboratory chambers during one day, divided by the chamber area of 4.32m².

7.3.1.3 Financial Savings Method

7.3.1.3.1 Payback Period

Initially a simple payback period was determined at both the *chamber* and the *building* scales. This was determined with three economic projections for energy price; *conservative* (+8.5%), *moderate* (+9.8%) and *optimistic* (+11.1%) in accordance with figures from [179]. The payback period was calculated when the project would first break even – following initial capital investment into the TES system and with taking energy savings as income.

7.3.1.3.2 Net Present Value

The payback period, though useful for assessment fails to account for the depreciating value of money where the savings in year 1 will be worth less than in year 2, in absolute terms [180]. Based on the current UK economic climate, despite gradual inflation, depreciating the value of money the rate of energy price inflation currently outstrips the depreciating value of money therefore causing a net increase in the value of savings each year, in most forecasts.

In net present value (NPV) analysis, the viability of investment was weighed against alternative investments based on the available interest rates projected. For this analysis three project interest rates have been identified to determine viability in differing economic climates. In the conservative case an interest rate of 10% was considered, in the moderate a rate of 5% and in the optimistic a rate of 2%. The lower the competitive interest rate the greater the novel TES viability.

Since NPV analysis is typically conducted to assess cash flow for investments where there is a monetary return on investment, some adjustments were made to accommodate the tool to consider energy saving, and thus financially saving, systems. Two methods were proposed and investigated in this *Economic Analysis*. In both cases, as well as identifying the breakeven point, a twenty year NPV figure was reported in Table 7.15 to Table 7.20.

7.3.1.3.2.1 NPV – Savings as Income Method

The first method incorporates annual financial savings as cash income. Whilst strictly inaccurate it enables the quantification of financial benefit from TES investment.

7.3.1.3.2.2 NPV – Technology Comparison Method

The second method calculates the actual NPV for buildings fitted with enhanced TES systems and those fitted without. The operational costs of running the system with and without TES each year were added to the initial capital investment debt. In each case the NPV gets consistently more negative as money will spent operating both air conditioning systems.

Following calculation of each NPV a comparison between the TES fitted building and reference building was calculated for each year. It was anticipated that a building fitted with an enhanced TES system would reduce the operating cost, thus the total cost of capital and operational costs, for the non-TES reference building, would be greater than the TES fitted building, over a given life span of the project, despite the additional capital cost.

By comparing the reference and TES NPV figures it was possible to determine after how long the TES fitted building would become more financially beneficial. The results from this NPV comparison were plotted in Figure 7.20 for each system tested. As before three economic conditions were investigated with varying rates of energy and interest rate inflation. The results of the investigation were tabulated and graphed in the next section.

7.3.1.4 Internal Rate of Return

Internal Rate of Return (IRR) figures have been calculated under the moderate financial conditions. The figure represents the rate of return the technology was capable of offering

during the first twenty years of installed-product life. The IRR was calculated based on a twenty year NPV of zero. Due to the two methods for calculating NPV in this assessment two IRR figures have been calculated also. Using goal seek analysis these figures were calculated by setting the NPV to zero and reading the respective interest rate.

7.3.2 Modelling Method

Two models were constructed in IES Virtual Environment (VE) to replicate the prototype laboratory set up. A representative model of the active thermal mass prototype tested in the laboratory was fitted above the chamber. The ApacheHVAC modeller was used in IES VE to replicate the air and water flows through the active thermal mass. The method for modelling this system followed the proprietary Actimass methodology agreed between Actimass and IES in January 2014 [134].

At time of writing, there was no specific method within IES to model the VPHC setup. To replicate PCM diffuser performance a Cool-Phase[®] thermal battery was used in the conditioned chamber. From numerical comparison the CPN4F thermal battery has a TES capacity 14.3 times that of the PCM diffuser [181, 182]. Therefore the chamber volume was scaled up 14.3 times, to offer proportional performance. Performance metrics were normalised per metre square and multiplied by the chamber or office floor surface area for economic analysis. The installed PCM differs from unit to unit so the results offer a 'predicted performance', but should be further investigated when modelling tools are available.

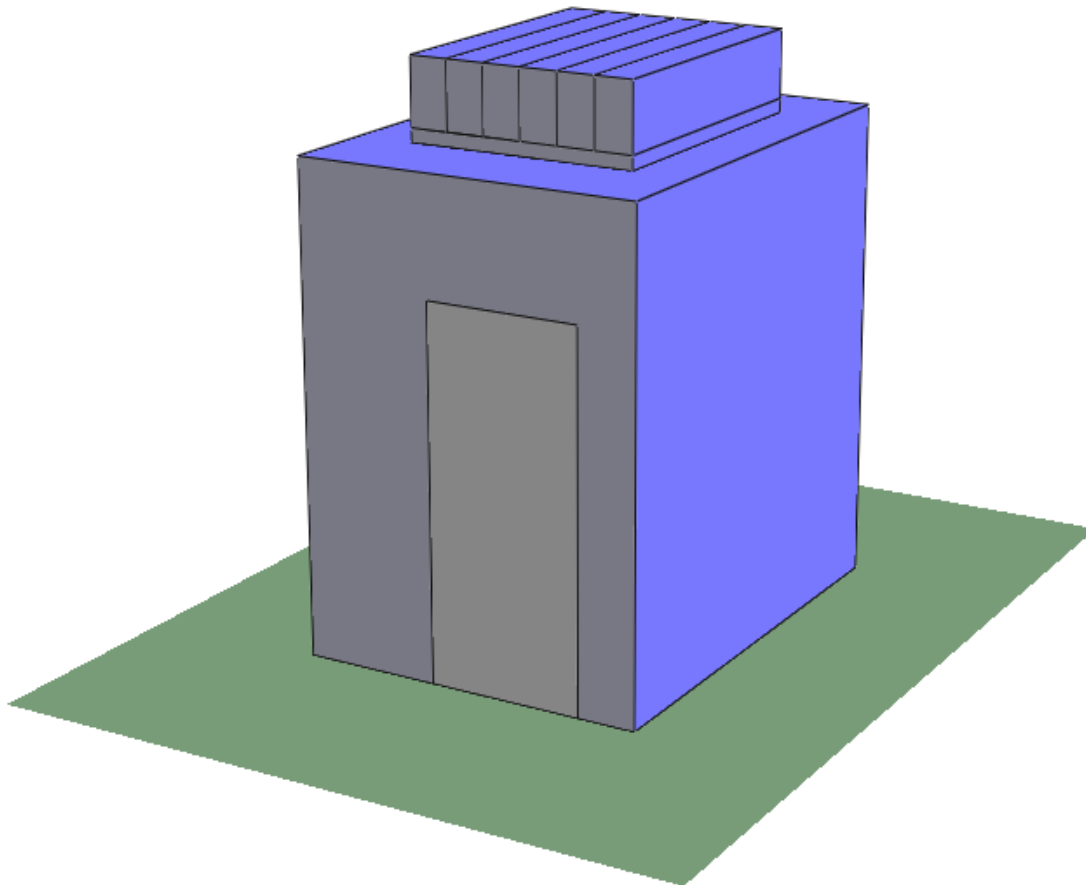


Figure 7.19 - IES Laboratory Chamber Model

Four annual simulations were conducted on the chamber. The replica laboratory chamber was constructed from replica materials as specified in IES construction manager. The U values of each component were specified in Table 7.13.

Table 7.13 - IES Model Construction

| Element | Description | U-Value |
|-----------------|----------------------------|-----------------|
| Chamber Walls | Stud partition | 0.1987 W/m^2K |
| Chamber floor | Standard floor (2002 regs) | 0.2499 W/m^2K |
| Chamber ceiling | Test chamber flat roof | 0.1812 W/m^2K |
| Door | Wooden Door | 2.1944 W/m^2K |

Firstly a reference simulation with the thermal mass removed (NoHC) was conducted. Secondly the traditional VHC system, without active water pipes; thirdly the combined WVHC was tested, with active water and air components in the ApacheHVAC network. Finally the VPHC representative model was simulated with a Monodraught Cool-Phase[®] thermal battery used to represent the PCM diffuser. Monodraught thermal batteries store 6 to 10 kWh in 4, 6

or 8 thermal battery modules [132]. The PCM diffuser stores 0.42 kWh of energy therefore a CPN4F module, in 14.3 times the volume reasonably represented the PCM component. The air stream was controlled by a heater and chiller during the hours of 9am to 5pm. The heater set point was 18°C with a 2°C dead-band and the chiller set point was 24°C with a 2°C dead-band, in line with the laboratory test conditions. The ventilation fan was fixed on at a rate of 4l/s. A 40W/m² internal heating load was applied throughout the simulations.

Annual simulations (1st Jan – 30th Dec) were conducted under the London Heathrow ASHRAE weather file. Despite simulating laboratory performance, the results generated from the modelling represented ‘predicted performance’ and should be treated as such. With further HVAC control the energy savings and system efficiency will be significantly improved.

For analysis of the systems, total annual system energy was exported for each simulation. An average UK business energy rate was used for the calculations (9.5p/kWh) ([183]). kgCO₂ emission savings from the simulations were also generated. The findings were subsequently analysed using the economic analysis method and conclusions drawn.

7.3.3 Results

7.3.3.1 Chamber Results

The energy, kgCO₂ and cost savings have been summarised per day, from the annual energy simulations conducted in IES. The IES annual energy consumption figures for each system were subtracted from the reference chamber performance. Subsequently the annual figure was divided by 252, the number of typical UK office working days, to give an average daily saving figure. These figures were multiplied by the respective terms in Table 7.10 to generate the saving figures in Table 7.14.

The initial investment costs in Table 7.15 followed the same method as section 7.3. Based on evidence from Table 7.15, under *moderate* financial market conditions, the WVHC technology offered the best economic case; despite the most expensive initial investment the payback period was shortest. The WVHC technology also offers the greatest twenty year savings-as-income NPV. The VPHC system demonstrated the poorest economic case due to the additional outlay for minimum additional savings. The theoretical mass-produced VHPC case, where PCM diffuser costs were reduced to £136.25 per unit, improved the twenty year NPV by £56.

Table 7.14 - Daily Savings based on diurnal swing results

| | VHC | WVHC | VPHC | |
|-------------------------------|------|------|------|---------|
| Energy Savings | 0.79 | 1.05 | 0.79 | kWh/d |
| Primary Energy Savings | 0.86 | 1.13 | 0.86 | kWh/d |
| kgCO2e Saved | 0.33 | 0.43 | 0.33 | kgCO2/d |
| Cost Saved | 0.08 | 0.10 | 0.08 | £/d |

Table 7.15 - Moderate Projection: Energy Price Rise by 9.8% annually; Interest Rate at 5%.

| CHAMBER | | | | | | |
|-----------------------------|--------------------|-----|----------------|-----------------------------|-------------|-----|
| System | Initial Investment | | Payback Period | NPV - Savings as Income | | |
| | | | years | Years to positive cash flow | 20 year NPV | |
| VHC | £ | 615 | 16 | 22 | -£ | 68 |
| WVHC | £ | 755 | 16 | 21 | -£ | 33 |
| VPHC | £ | 747 | 18 | 25 | -£ | 200 |
| VPHC (Mass Produced) | £ | 691 | 17 | 24 | -£ | 144 |

Following the same initial investment method as in the moderate financial market conditions, Table 7.16 presents an *optimistic* economic case for the three investigated TES technologies. As under *moderate* market conditions the WVHC system offers the strongest economic case in the *optimistic* projections. Payback was achieved within ten years for all TES technologies. Positive twenty year savings-as-income NPV figures were calculated for each technology.

Table 7.16 - Optimistic Projection: Energy Rise 11.1% Annually; Interest at 2%.

| CHAMBER | | | | | | |
|-------------|--------------------|-----|----------------|-----------------------------|-------------|-----|
| System | Initial Investment | | Payback Period | NPV - Savings as Income | | |
| | | | years | Years to positive cash flow | 20 year NPV | |
| VHC | £ | 615 | 15 | 17 | £ | 288 |
| WVHC | £ | 755 | 15 | 16 | £ | 436 |
| VPHC | £ | 747 | 17 | 19 | £ | 157 |

Table 7.17 presents the results from the chamber economic assessment under *conservative* market conditions. With energy price projected to rise 8.5% per year, and investment

interest available at 10%, a reduced twenty year savings-as-income NPV was found for each case, with WVHC remaining the most promising technology.

Table 7.17 - Conservative Projection: Energy Rise 8.5%Annually; Interest at 10%.

| CHAMBER | | | | | |
|---------|--------------------|----------------|-----------------------------|-------------|-----|
| System | Initial Investment | Payback Period | NPV - Savings as Income | | |
| | | years | Years to positive cash flow | 20 year NPV | |
| VHC | £ 615 | 17 | 52 | -£ | 324 |
| WVHC | £ 755 | 16 | 47 | -£ | 371 |
| VPHC | £ 747 | 19 | 70 | -£ | 456 |

7.3.3.2 Building Results

The up-scaled building level analysis followed the same modelling assumptions as in section 7.3. The 3,000 square metre building was assumed to have TES covering 70% of the building floor area. Table 7.18 presented the results of moderate economic projection with energy prices rising 9.8% annually and interest rates at 5%. *Initial additional investment* was calculated as the difference between installing the active-TES system and typical building hollow core. The results from two methods for calculating NPV were reported. The first method uses the TES chamber savings against a reference chamber, from the diurnal-swing tests; as used in the chamber financial assessment. The second used the technology-comparison-method or *comparison NPV*. This method assesses the actual economic running costs for the building both with and without TES; then using the difference between these cash flows determines the twenty year NPV. The latter method is preferable when the cumulative difference in savings in the TES building is greater than the initial additional investment.

On the building level the WVHC technology offered the strongest economic case, based on comparison-NPV figures. The WVHC financial case takes into account the total annual system energy used, including energy used to operate the water loop.

The fastest comparison-NPV payback occurred for the mass-produced VPHC system. Throughout the assessment this was the only system where comparison-NPV payback was less than three years. Although attractive, this scenario was based on the, as yet unrealised, condition that VPHC mass produced costs could achieve a unit cost of £136.25.

Table 7.18 - Moderate Projection: Energy Price Rise by 9.8% annually; Interest Rate at 5%.

| 3000m ² BUILDING | | | | | | | | | |
|-----------------------------|-------------------------------|---------|----------------|-----------------------------|-------------|--|-----------------------------|-------------|---------|
| System | Initial Additional Investment | | Payback Period | NPV - Savings as Income | | | NPV - Comparison | | |
| | £ | | years | Years to positive cash flow | 20 year NPV | | Years to positive cash flow | 20 year NPV | |
| VHC | £ | 94,500 | 22 | 32 | -£ 452,718 | | 7 | £ | 285,282 |
| WVHC | £ | 136,500 | 20 | 29 | -£ 373,762 | | 8 | £ | 364,238 |
| VPHC | £ | 317,382 | 24 | 37 | -£ 675,156 | | 18 | £ | 62,844 |
| VPHC (Mass Produced) | £ | 26,493 | 21 | 31 | -£ 389,371 | | 3 | £ | 353,733 |

Under optimistic market conditions (Table 7.19) comparison-NPV payback occurs within seven to fourteen years for each TES technology. The WVHC system offers a projected twenty-year-comparison NPV of over £690,000.

Table 7.19 - Optimistic Projection: Energy Rise 11.1% Annually; Interest at 2%.

| 3000m ² BUILDING | | | | | | | | | |
|-----------------------------|-------------------------------|---------|----------------|-----------------------------|-------------|--|-----------------------------|-------------|---------|
| System | Initial Additional Investment | | Payback Period | NPV - Savings as Income | | | NPV - Comparison | | |
| | £ | | years | Years to positive cash flow | 20 year NPV | | Years to positive cash flow | 20 year NPV | |
| VHC | £ | 94,500 | 21 | 23 | -£ 205,237 | | 7 | £ | 532,763 |
| WVHC | £ | 136,500 | 19 | 21 | -£ 47,464 | | 7 | £ | 690,536 |
| VPHC | £ | 317,382 | 23 | 26 | -£ 427,387 | | 14 | £ | 310,613 |

The conservative financial projections in Table 7.20 suggested significant negative savings-as-income NPV for each system. The VPHC system only predicted positive cash flow after of forty-eight years. The WVHC system continued to offer the strongest financial case although basic payback was only achieved after thirteen years.

For energy saving investments to be economically viable consistent growth in energy prices is required; without this growth the cumulative benefit of interest on investment outweighs the saving benefit. Further analysis is required to better quantify the performance risk when smart control is incorporated into the system.

Table 7.20 - Conservative Projection: Energy Rise 8.5% Annually; Interest at 10%.

| 3000m ² BUILDING | | | | | | | | |
|-----------------------------|-------------------------------|---------|-------------------------|-----------------------------|-------------|-----------------------------|-------------|--|
| System | Initial Additional Investment | | Payback Period years | NPV - Savings as Income | | NPV - NoHC Comparison | | |
| | £ | | | Years to positive cash flow | 20 year NPV | Years to positive cash flow | 20 year NPV | |
| VHC | £ | 94,500 | 24 | >100 | -£ 630,529 | 9 | £ 107,471 | |
| WVHC | £ | 136,500 | 21 | >100 | -£ 608,204 | 10 | £ 129,795 | |
| VPHC | £ | 317,382 | 26 | >100 | -£ 853,175 | 35 | -£ 115,175 | |

Figure 7.20 charts the comparative cash flow for each installation, using the comparison NPV method under moderate financial conditions (energy price rise of 9.8%, interest rates of 5%). Due to the low initial investment the mass-produced VPHC (VPHC (mp)) system offers positive comparative cash flow after three years. The VPHC (mp) system continues to offer the best investment, based on comparison-NPV, until the thirteenth year after investment and installation. During the twelfth and thirteenth years the increased energy savings offered by the WVHC system offset the greater investment and enable greater comparative cash flow. The VPHC system has the greatest initial investment. There was no evidence of the VPHC system becoming more financially preferable to the VHC system during the first fifty years, at the laboratory cost point. Improvements in modelling the PCM unit may improve predicted performance.

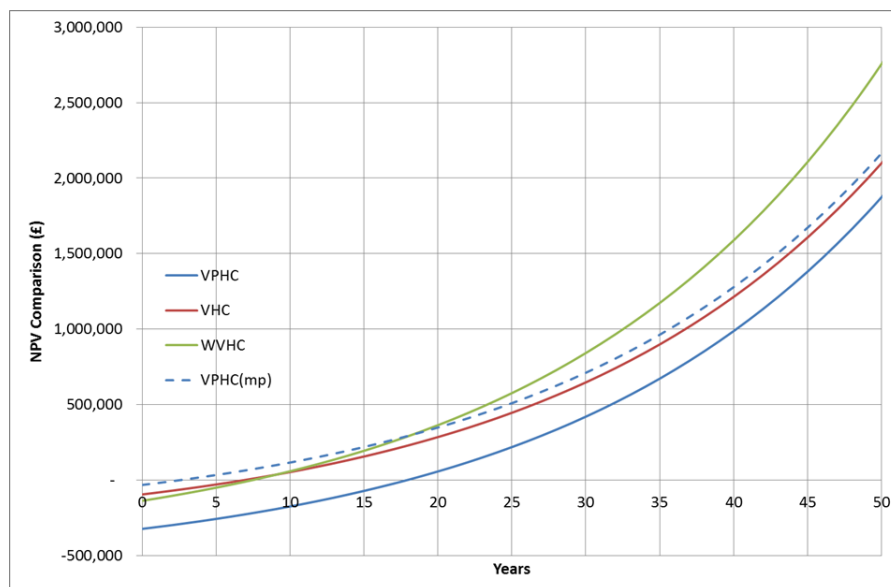


Figure 7.20 - Comparison NPV for each TES technology against Time (years) under moderate financial conditions

The IRR figures displayed in Table 7.21 have been calculated based on the savings-as-income and comparison NPV methods. The moderate financial projections were used to determine the figures. The greatest IRR was offered by the VPHC (mp) system.

Table 7.21 - Internal Rate of Return

| System | IRR | |
|----------------------|-------------------|------------|
| | Savings as Income | Comparison |
| | % | % |
| VHC | -1.2 | 21.3 |
| WVHC | 0.5 | 19.9 |
| VPHC | -2.9 | 6.6 |
| VPHC (Mass Produced) | -0.6 | 57.4 |

7.3.3.3 Suitability for the Green Deal

Although there were requests in place for the UK government to drop the ‘Golden Rule’ for non-domestic Green Deal suppliers this was not yet the case [13]. At the time of writing, for retrofit technologies to be accredited by the Green Deal; the technology must save the building occupant more money per annum than it costs the occupant in loan repayments. A twenty-five-year repayment period was typical for domestic property installations. Within the commercial market there were calls to shorten this period in line with commercial rent terms.

Based on the Historic Scotland Technical paper [180] the Green Deal was part financed by large corporations such as Marks & Spencer Plc, Tesco Plc or B&Q Plc. As of September 2011 these company’s lending rates were 6.4, 7.4 and 10.8% respectively. They are anticipated to operate as compound interest loans.

Of the two TES enhancements tested, the WVHC system would be practically difficult and costly to retrofit; ruling out its viability for the non-domestic Green Deal scheme. Analysis of the WVHC system revealed that the annual payments required to payback a Marks & Spencer Plc loan at 6.4% were approximately ten times the savings made via the system (without including pumping duty).

The VPHC system was more suitable for retrofit, since minimal adaptation to the building AHU plant or Building Energy Management System (BEMS) was required. In the VPHC (mp)

case, of £136.25 per unit, based on a 6.4% lending rate and five year repayment plan, the annual financial savings (based on moderate fuel price rise of 9.8% annually) were more than double the loan repayments. Based on the modelling assumptions the VPHC (mp) system was deemed suitable for the non-domestic Green Deal.

The VPHC system, based on the prototype production costs, did not meet the Green Deal's 'Golden Rule'. In order for the VPHC technology to meet the 'Golden Rule', based on the 6.4% loan interest rates, with a five year repayment plan and a moderate fuel price rise the cost of the technology must be reduced to £30 per square meter – approximately £300 per unit.

7.3.4 Summary of Findings

The findings from the model-based economic assessment follow a similar trend as the laboratory-based economic assessment. WVHC demonstrated the greatest financial case in each economic scenario. The theoretical VPHC(mp) provided the fastest return-on-investment observed, within three years. Taking into account the prototype costs, the VPHC system showed no evidence of greater financial savings than the VHC system. This was due to the minimal savings the modelled VPHC system demonstrated over the VHC system (less than 0.1Wh per day on a chamber scale).

The findings from the model-based economic assessment offered a more promising energy and financial savings outlook than those based on the laboratory findings for the VHC system, and an equivalent outlook for the WVHC and VPHC performance. In the VHC case, this was due to an energy saving increase against the reference case (NoHC) of 0.39 kWh per day, based on simulation findings. In the WVHC and VPHC case there were respective variation of 4.8% and 0.6% in daily energy savings from the laboratory to the simulated results.

Under the non-domestic Green Deal, none of the enhancement systems satisfied the 'Golden Rule'. When investigated, based on the modelling assumptions, the retrofit PCM diffuser satisfied the 'golden rule' when manufacturing costs could be reduced to approximately £300 per unit. Further, the financial case will benefit from improved control.

7.4 Conclusions

The work conducted in this chapter has assessed the energy saving and economic potential of prototype active-TES systems. To determine the available savings, pilot-scale laboratory tests were conducted on the VHC, WVHC and VPHC systems developed throughout this thesis. Two insulated chambers, one with TES and one without, were constructed in an open plan laboratory. Both chambers were fitted with variable-load radiant-heat mat, portable AC units, thermocouples and energy meters.

The laboratory setup was limited due to the ambient laboratory temperatures and the variable temperature delivered by the AC unit. The chambers were insulated and sealed, however efforts to enable night cooling via laboratory ventilation had an adverse effect due to the summer-time laboratory temperatures experienced. Week-long, *peak-cooling-demand* trials were conducted for each of the three TES configurations under investigation.

Under the *peak-cooling-demand* conditions the WVHC offered the only week long energy saving (0.5kWh per day against the reference chamber). The WVHC and VPHC systems offered *peak-temperature delay* enhancement up to 1.25 hours for the first occupied day. Subsequent days suffered from overheating with the AC units being required to cool the thermal mass as well as the chamber air. As a result the VHC and VPHC systems used more energy per day during the *peak-cooling-demand* week than the reference chamber.

A night-cooling strategy was implemented to synthetically represent *diurnal-swing* conditions between 18 and 28°C. Under these conditions a *peak-temperature delay* of 1.2 to 2.3 hours was maintained from day to day. Energy savings were achieved for all the TES systems. The VHC, WVHC and VPHC controlled chambers achieved respective energy savings of 0.4, 1.1 and 0.8kWh per day, against the reference room energy consumption. COP figures ranging from 1.3 to 1.5 were achieved during the *diurnal-swing* conditions.

Fixed-occupancy testing assessed the temperature reduction capabilities of the TES with an air recycle system. The 'occupancy' heater load of 50W/m² was applied for eighteen hours and temperatures monitored. In the TES chamber (Room A) the WVHC maintained room temperatures around 25°C, 3.7°C below the VHC case. At its peak the VPHC system reduced room temperatures by 0.9°C against the VHC system. At the end of eighteen hours the VHC and VPHC room temperatures were 28.3 and 28.1°C respectively. An average temperature saving of 2.8 and 1.0°C was observed by from the enhanced active-TES systems, WVHC and VPHC respectively, throughout the eighteen hour test period

Based on the research work conducted, the WVHC and VPHC systems offer energy saving and thermal comfort enhancement over the VHC system during *peak-cooling-demand* and *diurnal-swing* conditions. During *diurnal swing* conditions the VPHC benefit over the VHC was small (0.4kWh/day). The WVHC system offered a more holistic benefit saving; 0.7kWh per day and maintaining room temperatures below 25°C after eighteen hours of occupancy. Following laboratory trials uncertainty remained about the year round benefit of the technologies and whether the enhancement warrants the additional investment required.

An economic assessment was conducted to comprehend the financial case for each TES technology. Cost inputs were derived from industrial partner figures and project costs. To quantify the economic benefit the payback period, NPV and IRR were calculated for each system. The NPV was calculated for the 3,000 metre square theoretical office building via two methods: the savings-as-income and the technology comparison methods.

To find annual economic figures, IES VE annual simulations were conducted on a laboratory scale model for each TES system. From the model-based economic assessment WVHC offered the strongest case. If VPHC(mp) figures were achieved, a payback of three years was achievable at an IRR of 57%. Without improved manufacturing costs, there was no evidence that the VPHC system would become preferable economically, compared to the VHC system, within the first fifty years.

The WVHC system, as simulated, offered the strongest financial case throughout the scales and economic metrics. Under optimistic financial projections, on a building scale, a twenty year comparison-NPV of £690,000 was achieved. Under conservative projections the WVHC system registered just under £130,000 for the same comparison-NPV metric. Under moderate financial case projections the systems all achieved a positive twenty year comparison-NPV.

The VPHC exhibited slightly worse economic feasibility compared to the VHC system during the first twenty years. This was due to the VPHC costs for building level projections being calculated based on the prototype production costs. A 'mass produced' cost for VPHC technology (VPHC (mp)) was calculated and the economic case investigated. On a building level, under the moderate conditions, the VPHC (mp) twenty year comparison-NPV figure exceeded the VHC by 24%.

By plotting the NPV comparison figures against years since installation, a direct cash flow comparison was carried out between TES technologies. The VPHC (mp) system was most

cash-rich for the first twelve years. In the years after the WVHC system emerged as offering the greatest on-going savings. The IRR assessment revealed all the laboratory systems tested to have an IRR between 6.6 and 21.3%. The VPHC (mp) had an IRR of 57.4% using the comparison-NPV figures.

Suitability for the non-domestic Green Deal was assessed based on the modelled economic data. It was found that if the VPHC technology can reduce unit cost to approximately £300 (£30 per m²), the technology would be viable for profitability and five year payback of the business backed loans. The WVHC system was found unsuitable for the non-domestic Green Deal.

The work conducted in this chapter proves the concept that active-TES enhancement to VHC systems would save energy, reduce summer peak temperature and be financially viable, under the given market conditions. Further optimisation of TES enhancement through active systems and PCM addition would be of benefit. In the final chapter of this thesis the major findings of this work are summarised. Building on the conclusions drawn, an outline of advised further work is presented. Finally recommendations for the future of TES, PCM and sustainable technologies will be presented, with specific reference to the UK office context.

Chapter 8: Conclusions

Findings, Recommendations and Further Work

8 Conclusions

8.1 Introduction

The research presented throughout this thesis investigated the extent to which enhanced thermal energy storage (TES) can offer cost-effective energy saving benefit and thermal comfort. The work investigated both latent and sensible thermal mass solutions configured in passive and active systems. UK office conditions provided the context for the investigation.

The work conducted to date has been undertaken via building, chamber and component level modelling; and sample, component and chamber laboratory testing. The sensible TES systems investigated have included passive, air and water activated concrete hollow core (*Chapters 3, 4, 5 & 7*). The PCM TES systems investigated have included a passive PCM soffit, a PCM water tank, a PCM air-channel insert and an active PCM diffuser system (*Chapter 6*). One coupled PCM and concrete TES system was tested in a pilot scale chamber (*Chapter 7*).

Whole-building and single-chamber level modelling were conducted under annual UK temperature weather profiles (*Chapter 3 & 7*). Component modelling and testing was carried out in ambient laboratory conditions (*Chapter 5 & 6*); chamber level testing was carried out

in *peak-cooling-demand* and *diurnal-swing* conditions (*Chapter 7*). Novel PCM configurations were investigated using established and novel PCMs, Energain[®] and bio-based PCM (X25) (*Chapter 6*). The work culminated in an economic assessment of the final enhanced TES systems tested (*Chapter 7*).

Throughout the modelling, testing and validation conducted, the thesis has demonstrated evidence to support the initial hypothesis, “*enhanced active-thermal mass systems, which utilise the building envelope and retrofit additions, are cost-effective energy-efficient thermal-comfort technologies suitable for UK offices.*” The extent of the investigated technologies’ cost-effective, energy-efficient and thermally-comfortable nature was not as significant as anticipated. It is anticipated that further benefits are achievable with optimisation of the PCM type, configuration and associated control strategy. Further work is advised to realise this potential.

This final chapter documents the major findings from the UK office TES investigation conducted. Thermal comfort, energy savings and associated financial savings have constituted the assessed benefit for the work. Following the major findings, informed recommendations have been put forward presenting suitable uses of the enhanced TES technology investigated. To conclude this study, proposed future work is presented that would aid the extension of knowledge in the field of TES, PCM and their applications within the low-energy office context.

Industrial collaboration between the University of Nottingham, Tarmac Building Products, the Technology Strategy Board and Actimass has underpinned this work. The work conducted in this study has therefore centred on real-world application. The findings have already influenced commercial ventures, inspired further research-funding applications and proposed a viable low-energy retrofit solution. Patent applications have been lodged and a new product launched. The publications, to date, arising from this investigation are presented at the end of this chapter.

8.2 Major Findings

Prior to this investigation, previous work [100] had gone so far as investigating a combined concrete hollow-core TABS-PCM system. *Chapter 2* further detailed the state of the art for active-TES technologies. Overall, the work undertaken offered further knowledge into the performance of water and ventilated hollow core, and additional PCM configurations, as energy-saving active-TES technologies for UK offices. Figure 8.1 illustrates how this investigation has furthered knowledge in the field of building TES. The black parts of the tree have been taken from [129], with the orange dashed sections added as a result of this research work.

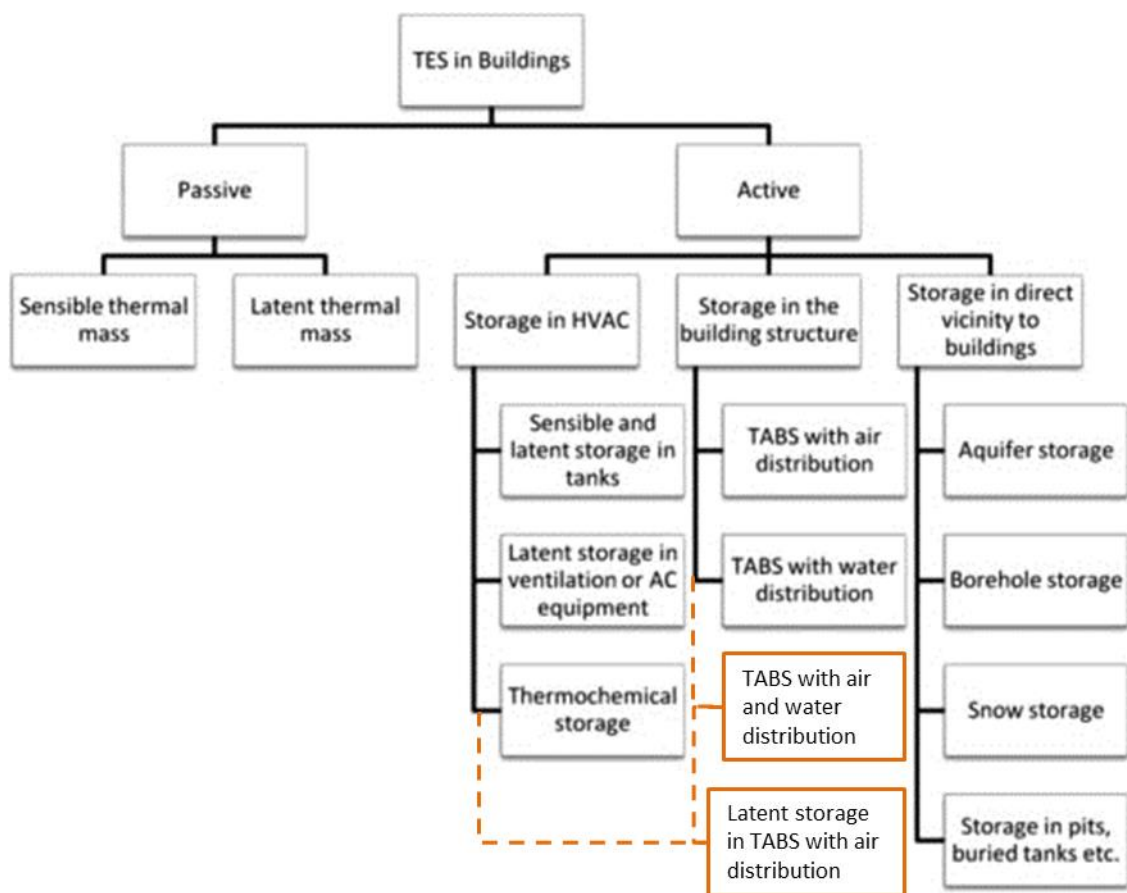


Figure 8.1 - TES technology tree [129] with thesis contributions added (orange)

In *Chapter 3*, the performance of a sensible thermal-mass system for energy-efficient UK office temperature management was investigated. Initially a prototype water and air activated TES system was designed. Subsequently the year-round energy performance was modelled based on a linear time-step modeller.

In *Chapter 4* the designed prototype construction was documented, then installed into a chamber and the cooling performance of the technology investigated. Control strategies

were investigated under fixed thermal loads and the linear time-step model validated against laboratory results. *Chapter 5* continued the investigation, using CFD to determine isolated system cooling performance under differing thermal loads.

Chapter 6 investigated PCM enhancement to the active-TES system. Five designs were modelled; the preferred system was designed, constructed and cooling benefit determined experimentally. *Chapter 7* concluded the work, investigating the combined active thermal-mass system cooling performance, under differing UK office conditions in a pilot scale test facility. Finally, economic analysis was conducted to determine the commercial viability of each technology configuration for the UK office market.

The modelled active sensible thermal-mass systems demonstrated capability of moderating internal temperature swing whilst saving energy annually. In an idealised modelled scenario VHC and WVHC annual COP figures of 6.7 and 6.3 were generated respectively. In laboratory tests the automated VHC and WVHC systems registered COP figures of 7.5 and 5.5, respectively. A peak COP of 10.6 was achieved and chamber comfort-temperatures maintained, with efficient control of the WVHC system under peak-occupancy heating load. In contrast, minimum COP figures from CIBSE for different air conditioning systems range from 0.7 to 4.65 [9].

Through testing, efficient control of the WVHC system was required when operating a closed water loop. *Chapter 4* revealed that under constant pumping the thermal capacity of the water tank was quickly saturated and cooling inhibited.

From the variable load investigation in *Chapter 5*, to aid the commercialisation of WVHC technology by identifying target buildings, an optimum operating method (OOM) was generated for the WVHC system. The OOM suggested the VHC system was capable of maintaining comfort levels, at a COP of 10.4, for internal cooling demands up to 55W/m^2 . Through increased ventilation rates, in the CFD room scenario modelled, the VHC systems maintained thermal comfort for internal heat loads up to 180W/m^2 . Additionally, supply of chilled cooling water with increased fan speed can, theoretically under isolated laboratory conditions, avoid slab overheating for soffit heat fluxes up to 425W/m^2 . Based on the respective COP figures calculated, it was more efficient to operate the WVHC system (3.8) than a VHC system alone (1.4).

To develop alternative enhancements suitable for retrofit, the *Chapter 6* investigation revealed (of the PCM additions to the WVHC system) a two-layer diffuser at the air-stream

room inlet was preferable. From simulation, the PCM X25 demonstrated the optimum energy density per pound; therefore was favoured for the commercially backed investigation. DSC analysis of X25 revealed a double-melt-peak at 23.1 and 25.8°C, suggesting a eutectic make up. Under isolated component testing the X25-PCM diffuser offered average cooling of 61W/m² for the first four hours and a total TES capacity of 0.42 kWh.

During *peak-cooling-demand* investigation, conducted for the *Chapter 7* energy assessment, only the open-loop WVHC system demonstrated better energy-efficient cooling than the VHC system. The VPHC system, incorporating the X25-PCM diffuser and the VHC network, used more energy to cool the chamber than the VHC system. The VHC and VPHC systems used more energy to maintain comfort temperatures than the adjacent-reference chamber due to the lack of night cooling and saturated thermal mass.

The *diurnal-swing* condition tests demonstrated energy savings for both the WVHC and VPHC systems against the VHC system (0.7 and 0.4kWh per day respectively). All three TES systems out-performed the reference chamber by 0.4 to 1.1kWh per day, due to effective night cooling of the active thermal mass. Under the *fixed-occupancy* conditions the average temperature reduction against the typical VHC system was 2.8 and 1.0°C respectively for the WVHC and VPHC systems.

The economic analysis revealed that a X25-PCM diffuser priced at approximately £300 per unit would be considered suitable for the UK's non-domestic 'Green Deal' scheme. When considered, the water pumping duty inhibited the WVHC system energy-saving and financial performance. Advanced control strategies are required to automate efficient operation of the dual active TES system.

8.3 Recommendations

Based on the major findings presented, recommendations for the future of TES, PCM and sustainable technologies are presented with specific reference to the UK office context.

TES and PCM would provide benefit in the energy-efficient UK offices. VPHC systems have demonstrated suitability for retrofit in buildings with existing air-based TES systems. Practical considerations regarding PCM unit installation and configuration with existing building HVAC technologies must be optimised. It is anticipated that retrofit of similar PCM diffusers would have energy-saving benefit for buildings with pre-existing MVHR systems.

PCM technologies for cooling applications should be incorporated in active systems. For simple retrofit, external inlet-outlet ventilation fans, operated by temperature-set-points and a timer, will offer night ventilation to dissipate the waste heat. By installing an active PCM system, the traditional poor heat transfer properties of PCM can be overcome. Control of the passing fluid will also improve control of the PCM TES system.

PCM should not be added passively to sensible thermal mass systems within the built environment. The poor thermal conductivity of PCM impedes the utilisation of the sensible thermal mass. Exposed passive-PCM solutions offer some benefit within the built environment, but with payback periods in excess of eleven years. Central to any PCM application is consideration of the melt temperature. Passive-PCM systems with a melt temperature of 22°C will offer more heating offset than cooling offset on an annual basis. PCM systems with melt temperatures 25°C and above will offer more cooling benefit; however will impede cooling if saturated.

Active TES systems provide thermally-comfortable energy-saving technologies suitable for the UK office environment. For VHC systems where space cooling demands exceed 55W/m² more than 1% of the time, variable speed drivers should be installed. Where space cooling demands are greater than 135W/m² for extended periods, the WVHC system is advised as an energy-efficient alternative to AC technology. Water systems should be used in conjunction with air-based systems, since air systems require less energy to activate the thermal mass.. For new builds, where additional capacity is required, WVHC systems should be considered; operated with an effective control strategy. A water tank or PCM water tank system for whole building operations should be sized appropriately based on the peak cooling-demand of the building.

Active TES should be considered for low energy office systems. PCM offers some retrofit capability, whilst sensible TES systems must be incorporated at the design stage. For heating loads up to 55W/m^2 the VHC system is the most energy efficient. PCM diffuser addition offers up to 61W/m^2 when required, although should be designed and installed appropriately to avoid being fully saturated during occupied hours and impeding space cooling. WVHC systems should be installed and operated optimally during peak-cooling-demand periods.

Without effective control active TES systems alone will not satisfy AC requirements year round in UK offices. Efficient building fabric design and active TES control strategies will minimise the use of back plant equipment. TES systems centre on temperature control, therefore any dehumidification required must be carried out via additional plant equipment. Heat recovery should be installed in conjunction with the active TES systems to significantly boost overall system efficiencies.

8.4 Further Work

The work conducted to date has unearthed novel findings in the application of both latent and sensible TES as part of a low-energy office strategy. The work acts as a starting point for many further investigations.

Further work is advised to investigate the application of active PCM and sensible TES systems outside the UK office context. The identification of suitable locations, climactic conditions, building constructions, HVAC systems and occupancy demands where TES systems would offer benefit should be conducted. The further work should also consider the building trends in the investigated nations to identify the knowledge gap in the building trade and the viability of commercial introduction.

Integration of the TES models developed in this work would provide a room-level tool for simulating active PCM TES systems in various locations. Development of a specific X25-PCM diffuser module, suitable for modelling in commercially available building simulation software, will enable widespread investigation of the prototype performance. With the module programmed the software will enable investigation of worldwide performance suggested previously. HVAC design will also enable the development of appropriate control strategies for VPHC retrofit.

Strength testing of the module should be conducted to ensure validity of simulated results. The results from this work should be fed into the collating work proposed by Dutil *et al* [107]. There is growing need for increased confidence in the simulation results from modelled PCM, especially within the built environment where PCM popularity is growing. Work to increase the confidence in modelled results is paramount.

Continuing the experimental validation of the work conducted in this thesis, the Optimum Operating Method (OOM) proposed should be tested under different circumstances and climactic conditions to develop an industry recognised design tool. Experimental findings supporting the suggested efficiency parameters for each internal thermal load will strengthen the design tool. Further, the OOM should be enhanced based on available cooling as well as the internal gains. The OOM should also take into account occupancy patterns and ambient temperatures past, present and future, to offer not only a design tool but a method for daily active TES system control.

Further work investigating the most energy efficient air and water velocities through the WVHC systems will enable further optimisation of WVHC control strategies. An investigation

assessing the energy consumed by increasing fan power or cooling the air in the AHU, versus the cooling benefit realised in the room would further benefit control strategy optimisation. The findings from these investigations would aid the development of the OOM into a system control tool. Brief assessment conducted over three water flow rates (0.8, 2.9 and 4.4l/min) found that 2.9l/min offered the greatest energy benefit. Further assessment of optimal water flow is of particular importance, since pumping duty currently hinders the economic and energy-efficient case for WVHC operation.

Controlled laboratory tests investigating the benefits of open and closed-loop WVHC systems would provide useful findings when upscaling the technology. Accompanying the investigation should be the determination of optimum water storage tank size, configuration and PCM utilisation to enable additional TES away from occupied zones. Optimising the control systems for a closed loop system will be integral to this work. Determining the appropriately sized the water tank per square metre of pipe-embedded hollow core represents a crucial output.

To conduct more advanced testing of the active-TES control strategies, the pilot scale test facilities at the University of Nottingham should be enhanced. A pilot-scale fan-coil plant, coupled with complete control of ambient temperature profiles and a heat recovery system should be added to the test facility. The addition and automation of the technology will enable the simulation of a wider range of test conditions. Under these wider test conditions modelling results can be validated and optimum automated control strategies tested. The findings from these enhanced test facilities will strengthen the commercial case and ease the take-up of the novel TES technologies.

When developing the control algorithms, predictive weather profiles and expected occupancy schedules should be incorporated into the system design. Since TES systems moderate temperatures between peak and low demand spells, control strategies that incorporate expected demand as well as past demand could significantly boost the energy efficiency of active TES systems. Utilising predictive control for occupancy patterns could eliminate the thirty-minute lag time typical in VHC systems, whilst maintaining minimal energy consumption. Such control strategies would be useful for control of rooms with intermittent occupancy such as lecture theatres or meeting rooms.

The latter part of the research work reported to date was conducted under a '*proof of concept*' collaboration between the TSB, industry and the university. Further '*research and*

development' investment has been granted to develop a commercial PCM diffuser design. The PCM diffuser design should be optimised to maximise heat transfer to and from the diffuser, when in greatest demand. Consideration throughout the design period should also be given to cost-effective manufacturing methods targeting a sale price of less than £300 per unit.

Following design development, the diffuser should be programmed in industry-standard building simulation software. Using the simulation software the performance of the optimised VPHC system can be assessed. Part of the investigation should determine what adaptations to BEMS control strategies should be made if the PCM diffuser was retrofitted throughout a VHC building. The model will also enable simulations of VPHC performance in differing seasonal conditions and construction types.

PCM technologies are traditionally favoured in lightweight constructions, therefore the results of simulating PCM diffuser performance in lightweight buildings, fitted with MVHR systems could open up further commercial exploitation of the technology. Following modelled findings, laboratory tests investigating the enhanced thermal mass systems in lightweight constructions will help validate the findings.

Finally, further investigation applying the active TES systems in an alternative manner within UK offices could discover further energy-efficient solutions. Modelling and laboratory investigations should be conducted assessing the performance of the VHC, WVHC and VPHC systems as displacement ventilation from the floor up, rather than under the top-down strategy investigated in this thesis. Further applying the active TES concept, it would be interesting to investigate the capabilities of activating wall thermal mass in conjunction with building air systems; developing an efficient method for retrofitting active-walls would be useful in upgrading ancient-solid-wall buildings into energy-efficient structures.

8.5 Concluding Remarks

PCM is not a silver bullet, but it can offer energy saving benefits to UK offices. Alone, PCM offers ten times the cooling capacity of concrete; however concrete is one hundred times cheaper and benefits from remaining structurally sound when heated. Sensible thermal mass should be favoured for new-build integrated systems; however there is still a niche for PCM applications in retrofit.

PCM offers exciting retrofit opportunities, yet exposed sensible thermal mass too will have a strong future in the energy-efficient building industry. Active PCM systems offer greater control than passive systems and utilise night cooling efficiently, an essential when operating an air-based TES system. During peak cooling-demand periods, when night ventilation is insufficient to replenish TES, a cooling-water system, backed up by heat-pump technology, can provide energy-efficient cooling.

Optimisation and development of applications will further aid the integration of PCM technologies in the built environment. The research conducted has highlighted aspects surrounding the implementation of PCM and TES systems into the UK offices. The evidence advocates that with appropriate design, TES systems are well suited to offer energy-efficient benefits to occupants and building managers.

The extent to which energy-efficient benefits are realised within UK offices depends on further development of the concepts proven in this work; preparing the novel technologies investigated for market integration. For a sustainable future, a holistic approach is required, optimised active TES offers one part of the energy-efficiency puzzle [74].

8.6 Publications

8.6.1 Journal Papers

Whiffen, T. R., and S. B. Riffat. "A review of PCM technology for thermal energy storage in the built environment: Part I." *International Journal of Low-Carbon Technologies* (2012): cts021.

Whiffen, T. R., and S. B. Riffat. "A review of PCM technology for thermal energy storage in the built environment: Part II." *International Journal of Low-Carbon Technologies* 8.3 (2013): 159-164.

Whiffen, T. R., G. Russell-Smith, and S. B. Riffat. "Active thermal mass enhancement using phase change materials." *Energy and Buildings* 111 (2016): 1-11.

8.6.2 Accepted Abstracts

Whiffen, T. R., Riffat, S. B. "Simulated Dynamic Thermal Mass Performance." *Nova Science Publishers* (2012)

Whiffen, T. R. "Energy Recycling – A Global Energy Solution." *Nova Science Publishers* (2012)

Whiffen, T. R., Riffat, S. B., Zheng, X., Su, Y., Tetlow, D. "A Critical Investigation into the Capability of PCM as Lightweight TES within the Built Environment." *Applied Energy Special Issue in Energy Storage* (2014)

8.6.3 Conference Participation

Whiffen, T. R., Riffat, S. B. "The Future of PCM Incorporation: An Introduction, Review and Forecast." *Sustainable Energy Technology Research Conference, Vancouver 2012* – Conference Paper

Whiffen, T. R., Riffat, S. B. "Cooling without the Cost" *Universitas21: Energy Conference 2013, Dublin* – Oral Presentation

9 References

1. Davey, E., *The Energy Efficiency Strategy: The Energy Efficiency Opportunity in the UK*, D.o.E.a.C. Change, Editor. 2012.
2. Tanaka, N., *Energy Technology Perspectives 2010. Scenarios and Strategies to 2050*. 2010: OECD/IEA.
3. US Energy Information Administration, *Petroleum Chronology*. 2000: http://www.eia.gov/pub/oil_gas/petroleum/analysis_publications/chronology/petrochrohotgraph.htm.
4. European Commission, *EU Energy in Figures: Statistical Pocketbook 2014*, Energy, Editor. 2014.
5. Wade, J., Pett, J., Ramsay, L.,, *Energy efficiency in offices: Assessing the situation*. The Association for the Conservation of Energy, 2003.
6. Fuerst, F., McAllister, P., Nanda, A., Wyatt, P.,, *An investigation of the effect of EPC ratings on house prices*, D.o.E.a.C. Change, Editor. 2013.
7. Huhne, C., *The Carbon Plan - Delivering our Low Carbon Future*, D.o.E.a.C. Change, Editor. 2013.
8. Houssin, D. *International Energy Agency Webinar*. 2013.
9. Butcher, K.J., *CIBSE Guide F - Energy Efficiency in Buildings (3rd Edition)*. 2012: CIBSE.
10. International Energy Agency (IEA), *Energy Technology Perspectives*. 2014.
11. CEN, *Ergonomics of the Thermal Environment, in Analytical determination and interpretation of thermal comfort using calculation of the PMV and PPD indices and local thermal comfort criteria*. 2005.
12. Lehmann, B., V. Dorer, and M. Koschenz, *Application range of thermally activated building systems tabs*. *Energy and Buildings*, 2007. **39**(5): p. 593-598.
13. White, R., Archer, G., Lord Whitty, Colville, O.,, *Building Efficiency: Reducing energy demand in the comercial sector*. 2013, Westminster Sustainable Business Forum, Carbon Connect,.
14. Jeffries, I., Rowlands-Rees, T.,, *Energy Efficiency Trends Annual Report 2012/13*. 2013, EEVS and Bloomberg New Energy Finance.
15. Roberts, S., *Altering existing buildings in the UK*. *Energy Policy*, 2008. **36**(12): p. 4482-4486.
16. Rodrigues, L.T., M. Gillott, and D. Tetlow, *Summer overheating potential in a low-energy steel frame house in future climate scenarios*. *Sustainable Cities and Society*, 2013. **7**: p. 1-15.
17. Coley, D. and T. Kershaw, *Changes in internal temperatures within the built environment as a response to a changing climate*. *Building and Environment*, 2010. **45**(1): p. 89-93.
18. Chiu, J.N.W., P. Gravoille, and V. Martin, *Active free cooling optimization with thermal energy storage in Stockholm*. *Applied Energy*, 2013. **109**(0): p. 523-529.
19. Badescu, V., N. Laaser, and R. Crutescu, *Warm season cooling requirements for passive buildings in Southeastern Europe (Romania)*. *Energy*, 2010. **35**(8): p. 3284-3300.
20. Mlakar, J. and J. Štrancar, *Overheating in residential passive house: Solution strategies revealed and confirmed through data analysis and simulations*. *Energy and Buildings*, 2011. **43**(6): p. 1443-1451.
21. Leaman, A. and B. Bordass, *Productivity in buildings: the 'killer'variables*. *Building Research & Information*, 1999. **27**(1): p. 4-19.
22. Tyagi, V.V. and D. Buddhi, *PCM thermal storage in buildings: A state of art*. *Renewable and Sustainable Energy Reviews*, 2007. **11**(6): p. 1146-1166.

23. Russell, M.B. and P.N. Surendran, *Influence of active heat sinks on fabric thermal storage in building mass*. Applied Energy, 2001. **70**(1): p. 17-33.
24. Weitzmann, P., *Modelling building integrated heating and cooling systems*, in *Department of Civil Engineering*. 2004, Technical University of Denmark: Lyngby. p. 314.
25. Technical Committee CEN/TC 288, *Heating Systems in buildings - design of embedded water based surface heating and cooling systems*, in *Part 3: Optimizing for use of renewable energy sources*. 2006.
26. Wang, X. and J. Niu, *Performance of cooled-ceiling operating with MPCM slurry*. Energy Conversion and Management, 2009. **50**(3): p. 583-591.
27. Meierhans, R.A. *Slab cooling and earth coupling*. in *ASHRAE Transactions*. 1993.
28. Hauser, G., C. Kempkes, and B.W. Olesen, *Computer simulation of hydronic heating/cooling system with embedded pipes*. TRANSACTIONS-AMERICAN SOCIETY OF HEATING REFRIGERATING AND AIR CONDITIONING ENGINEERS, 2000. **106**(1): p. 702-712.
29. Feng, J.D., *Design and Control of Hydronic Radiant Cooling Systems*. 2014.
30. Basu, C., S. Schiavon, and F. Bauman, *Sizing Thermally Activated Building Systems (TABS): A Brief Literature Review and Model Evaluation*. 2012.
31. Basu, C., *Critical Simulation Based Evaluation of Thermally Activated Building Systems (TABS) Design Models*. 2012.
32. Winwood, R.B., R. and R. Edwards, *Advanced fabric energy storage I: Review*. BUILDING SERVICES ENGINEERING RESEARCH TECHNOLOGY, 1997. **18**(1): p. 1-6.
33. Xu, X., et al., *Research and application of active hollow core slabs in building systems for utilizing low energy sources*. Applied Energy, 2014. **116**(0): p. 424-435.
34. Littlewood, J., *Recommended Specification for Non-Domestic Buildings* 2011.
35. Olesen, B.W. and K.C. Parsons, *Introduction to thermal comfort standards and to the proposed new version of EN ISO 7730*. Energy and Buildings, 2002. **34**(6): p. 537-548.
36. Ren, M. and J. Wright, *A ventilated slab thermal storage system model*. Building and Environment, 1998. **33**(1): p. 43-52.
37. Barton, P., C. Beggs, and P. Sleigh, *A theoretical study of the thermal performance of the TermoDeck hollow core slab system*. Applied Thermal Engineering, 2002. **22**(13): p. 1485-1499.
38. Green, N., *Characterising the thermal energy transfer within a ventilated hollow core slab system*. 2010, University of Bath: Bath.
39. Winwood, R., R. Benstead, and R. Edwards, *Advanced fabric energy storage IV: Experimental monitoring*. Building Services Engineering Research and Technology, 1997. **18**(1): p. 25-30.
40. Winwood, R., R. Benstead, and R. Edwards, *Advanced fabric energy storage II: Computational fluid dynamics modelling*. Building Services Engineering Research and Technology, 1997. **18**(1): p. 7-16.
41. BRE, *NEW PRACTICE FINAL REPORT, The Elizabeth Fry Building, University of East Anglia*, in *The Government's Energy Efficiency Best Practice programme*. 1998.
42. Chae, Y.T. and R.K. Strand, *Thermal performance evaluation of hybrid heat source radiant system using a concentrate tube heat exchanger*. Energy and Buildings, 2014. **70**(0): p. 246-257.
43. Bring, A., *BRIS-computer program developed by National Swedish building research for calculation of room climate and heating and cooling effects*. National Swedish Building Research Summaries, 1974.
44. Angenbroe, G. and H. Vedder. *Accurate Modelling of Air-Supplied Heat Storage in Hollow Core Slabs*. in *CIIMA 2000, World Congress on Heating, Ventilation and Air Conditioning*. 2000.

45. Taylor, B.J., D.A. Cawthorne, and M.S. Imbabi, *Analytical investigation of the steady-state behaviour of dynamic and diffusive building envelopes*. Building and Environment, 1996. **31**(6): p. 519-525.
46. Russell, M. and P. Surendran, *Influence of active heat sinks on fabric thermal storage in building mass*. Applied Energy, 2001. **70**(1): p. 17-33.
47. Chae, Y.T. and R.K. Strand, *Modeling ventilated slab systems using a hollow core slab: Implementation in a whole building energy simulation program*. Energy and Buildings, 2013. **57**(0): p. 165-175.
48. Corgnati, S.P. and A. Kindinis, *Thermal mass activation by hollow core slab coupled with night ventilation to reduce summer cooling loads*. Building and Environment, 2007. **42**(9): p. 3285-3297.
49. Karlström, S., *Analysis of Thermally Active Ventilated Hollow Core Concrete Elements in a FEMLAB Environment Compared to Measurements*. 2004.
50. Zmeureanu, R. and P. Fazio, *Thermal performance of a hollow core concrete floor system for passive cooling*. Building and Environment, 1988. **23**(3): p. 243-252.
51. Bonte, M., et al., *Underground Thermal Energy Storage: Environmental Risks and Policy Developments in the Netherlands and European Union*. Ecology and Society, 2011. **16**(1).
52. Demirbas, M.F., *Thermal Energy Storage and Phase Change Materials: An Overview*. Energy Sources, Part B: Economics, Planning, and Policy, 2006. **1**(1): p. 85-95.
53. Dincer, I.R., M. A., *Thermal Energy Storage Systems and Applications*. 2 ed. 2011, Chichester: Wiley & Sons.
54. BASF, *Micronal(r) PCM - Intelligent Temperature Management for Buildings*. 2012.
55. Phase Change Energy Solutions, *Beyond Insulation™ Bio PCM*. 2010, Phase Change Energy Solutions: Asheboro, NC.
56. Monodraught Ltd, *Monodraught Cool-Phase Mark 2 Brochure*, M. Ltd, Editor. 2011: High Wycombe.
57. Tay, N.H.S., M. Belusko, and F. Bruno, *An effectiveness-NTU technique for characterising tube-in-tank phase change thermal energy storage systems*. Applied Energy, 2012. **91**(1): p. 309-319.
58. Akio, S., *Recent advances in research on cold thermal energy storage*. International Journal of Refrigeration, 2002. **25**(2): p. 177-189.
59. Dieckmann, J., *Latent heat storage in concrete*, T.U. Kaiserslautern, Editor. 2008: Kaiserslautern, Germany.
60. Regin, A.F.S., S.C. Saini, J.S., *Heat transfer characteristics of thermal energy storage system using PCM capsules: A review*. Renewable and Sustainable Energy Reviews, 2008. **12**: p. 2438–2458.
61. Zhou, D., C.Y. Zhao, and Y. Tian, *Review on thermal energy storage with phase change materials (PCMs) in building applications*. Applied Energy, 2011(0).
62. Baetens, R.J., Bjørn Petter. Gustavsen, Arild, *Phase change materials for building applications: A state-of-the-art review*. Energy and Buildings, 2010. **42**: p. 1361–1368.
63. Cabeza, L.F., et al., *Materials used as PCM in thermal energy storage in buildings: A review*. Renewable and Sustainable Energy Reviews, 2011. **15**(3): p. 1675-1695.
64. Sharma, A., et al., *Review on thermal energy storage with phase change materials and applications*. Renewable and Sustainable Energy Reviews, 2009. **13**(2): p. 318-345.
65. Zalba, B., et al., *Review on thermal energy storage with phase change: materials, heat transfer analysis and applications*. Applied Thermal Engineering, 2003. **23**(3): p. 251-283.
66. Mehling, H.C., L. F. , *Heat and cold storage with PCM: An up to date introduction into basics and applications*, ed. D.M. Mewes, E. h. F. 2008, Berlin, Germany: Springer.

67. Dean, J.A., *The Analytical Chemistry Handbook*. 1995, New York: : McGraw Hill, Inc. .
68. Buddhi, D.S., R. L. Seghal, P. N. Bansal, N. K. , *A simplification of the differential thermal analysis method to determine the latent heat of fusion of phase change materials*. . J Phys D Appl Phys 1987, 1987. **20**: p. 1601-5.
69. Zhang, Z., et al., *Preparation and thermal energy storage properties of paraffin/expanded graphite composite phase change material*. Applied Energy, 2012. **91**(1): p. 426-431.
70. Zhang, Y.P.J., Y., *A simple method, the T-history method, of determining the heat of fusion, specific heat and thermal conductivity of phase-change materials*. . Measur Sci Technol 1999. **10**: p. 201–5.
71. Hong, H., S.K. Kim, and Y.-S. Kim, *Accuracy improvement of T-history method for measuring heat of fusion of various materials*. International Journal of Refrigeration, 2004. **27**(4): p. 360-366.
72. Peck, J.H., et al., *A study of accurate latent heat measurement for a PCM with a low melting temperature using T-history method*. International Journal of Refrigeration, 2006. **29**(7): p. 1225-1232.
73. Dolado, P., et al., *Experimental validation of a theoretical model: uncertainty propagation analysis to a PCM-Air thermal energy storage unit*. Energy and Buildings, 2011(0).
74. Abhat, A., *Low temperature latent heat thermal energy storage: Heat storage materials*. Solar Energy, 1983. **30**(4): p. 313-332.
75. Peippo, K., P. Kauranen, and P.D. Lund, *A multicomponent PCM wall optimized for passive solar heating*. Energy and Buildings, 1991. **17**(4): p. 259-270.
76. Kuznik, F.V., J. Noel, J. , *Optimization of a phase change material wallboard for building use*. Appl Therm Eng, 2008. **28**: p. 1291–8.
77. Xu, X.Z., Y. P. Lin, K. P. Di, H. F. Yang, R. , *Modeling and simulation on the thermal performance of shape-stabilized phase change material floor used in passive solar buildings*. . Energy Buildings 2005. **37**: p. 1084–91.
78. Neeper, D.A., *Thermal dynamics of wallboard with latent heat storage*. Solar Energy 2000. **68**(5): p. 393–403.
79. Drake, J.B., *A study of the optimal transition temperature of PCM wallboard for solar energy storage*. , in Report ORNL/TM-10210. 1987, Oak Ridge National Laboratory.
80. Lane, G., *Solar heat storage: latent heat materials. background and scientific principles, vol. I*. . 1983, Florida: CRC: Press Inc.
81. Tyagi, V.V.K., S.C. Tyagi, S.K. Akiyama, T. , *Development of phase change materials based microencapsulated technology for buildings: A review*. Renewable and Sustainable Energy Reviews, 2011. **15**: p. 1373–1391.
82. Rubitherm Technologies GmbH. 'The Company'. Available from: <http://www.rubitherm.com/english/index.htm>.
83. Environmental Process Systems Ltd, *Product Summary*, E.P.S. Ltd, Editor. 2004.
84. BASF, *Micronal (r) PCM: Intelligent Temperature Management for Buildings*, BASF, Editor. 2008: Ludwigshafen, Germany.
85. Croda, *Phase Change Materials, ChrodaTherm Bio-based Phase Change Material*, C.I. Chemicals, Editor. 2013.
86. PCM Products, *Plus-Ice Phase Change Materials*, P.C.M.P. Ltd, Editor. 2012.
87. Lu, W. and S.A. Tassou, *Experimental study of the thermal characteristics of phase change slurries for active cooling*. Applied Energy, 2012. **91**(1): p. 366-374.
88. Ma, X., et al., *Investigation of energy transportation capability of a phase change slurry through a cold storage-cooling coil system*. International Journal of Energy Research, 2009. **33**(11): p. 999-1004.

89. Halawa, E. and W. Saman, *Thermal performance analysis of a phase change thermal storage unit for space heating*. Renewable Energy, 2011. **36**(1): p. 259-264.
90. Belusko M, B.F., *Design methodology of PCM thermal storage systems with parallel plates*, in *EuroSun Conference*. 2008: Lisbon, Portugal.
91. Royon, L., G. Guiffant, and P. Perrot, *Forced convection heat transfer in a slurry of phase change material in an agitated tank*. International Communications in Heat and Mass Transfer, 2000. **27**(8): p. 1057-1065.
92. Agyenim, F., et al., *A review of materials, heat transfer and phase change problem formulation for latent heat thermal energy storage systems (LHTESS)*. Renewable and Sustainable Energy Reviews, 2010. **14**(2): p. 615-628.
93. Huang, L., et al., *Subcooling in PCM emulsions—Part 1: Experimental*. Thermochemica Acta, 2010. **509**(1-2): p. 93-99.
94. Mehling, H. and L. Cabeza, *PHASE CHANGE MATERIALS AND THEIR BASIC PROPERTIES Thermal Energy Storage for Sustainable Energy Consumption*, H.Ö. Paksoy, Editor. 2007, Springer Netherlands. p. 257-277.
95. Zhou, G., et al., *An assessment of mixed type PCM-gypsum and shape-stabilized PCM plates in a building for passive solar heating*. Solar Energy, 2007. **81**(11): p. 1351-1360.
96. BOURZAC, K. "Melting" Drywall Keeps Rooms Cool. Technology Review, 2010.
97. de Gracia, A., et al., *New equipment for testing steady and transient thermal performance of multilayered building envelopes with PCM*. Energy and Buildings, 2011. **43**(12): p. 3704-3709.
98. Saman, W., F. Bruno, and E. Halawa, *Thermal performance of PCM thermal storage unit for a roof integrated solar heating system*. Solar Energy, 2005. **78**(2): p. 341-349.
99. Koschenz, M. and B. Lehmann, *Development of a thermally activated ceiling panel with PCM for application in lightweight and retrofitted buildings*. Energy and Buildings, 2004. **36**(6): p. 567-578.
100. Pomianowski, M., P. Heiselberg, and R.L. Jensen, *Dynamic heat storage and cooling capacity of a concrete deck with PCM and thermally activated building system*. Energy and Buildings, 2012. **53**(0): p. 96-107.
101. Soares, N.S., A. Vicente, R. Costa, J. , *Numerical simulation of a PCM shutter for buildings space heating during the winter*, in *World Renewable Energy Congress 2011*. 2011, Low-Energy Architecture: Linköping, Sweden.
102. Jaworski, M., *Thermal performance of building element containing phase change material (PCM) integrated with ventilation system – An experimental study*. Applied Thermal Engineering, 2014. **70**(1): p. 665-674.
103. PCM Products, *Plus-ICE(TM) Phase Change Materials Thermal Energy Storage Design Guide*. 2011.
104. Susman, G., *The application of phase change materials to cool buildings*, in *School of Engineering and Design*. 2012, Brunel University.
105. Susman, G., et al., *Tests of prototype PCM 'sails' for office cooling*. Applied Thermal Engineering, 2011. **31**(5): p. 717-726.
106. Rodrigues, L.T., *An investigation into the use of thermal mass to improve comfort in British housing*. 2010, University of Nottingham.
107. Dutil, Y.R., Daniel. Lassue, Stéphane. Zalewski, Laurent. Joulin, Annabelle. and J.K. Virgone, Frédéric. Johannes, Kevyn. Dumas, Jean-Pierre. Bédécarrats, Jean-Pierre. Castell, Albert. Cabeza, Luisa. F. , *Modeling phase change materials behaviour in building applications: selected comments*, in *World Renewable Energy Congress 2011*. 2011, Energy End-use Efficiency Issues: Linköping, Sweden

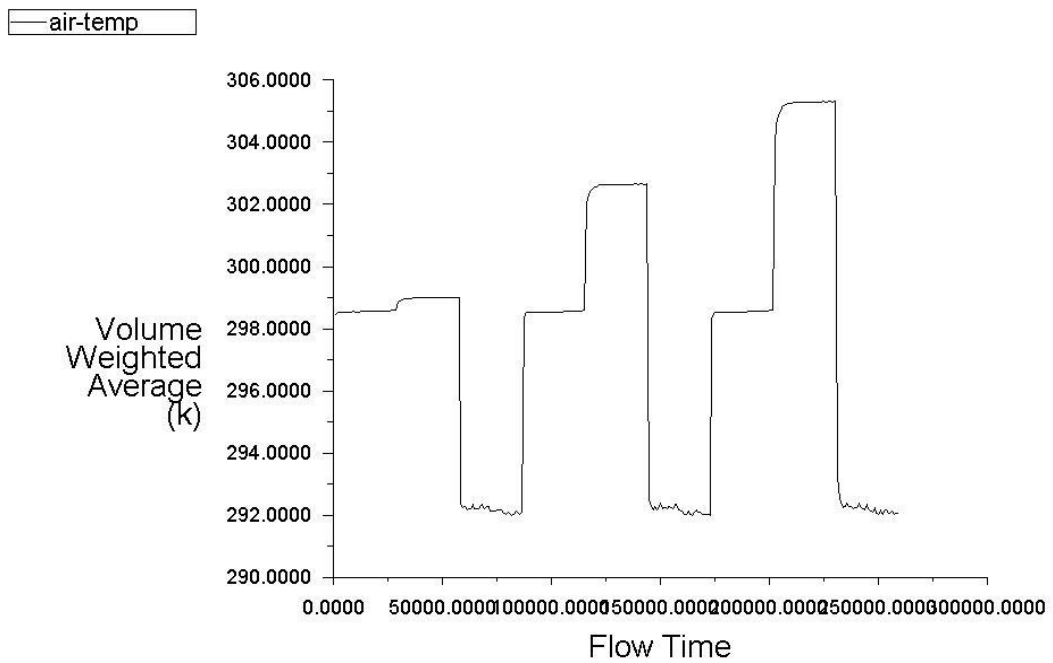
108. Verma, P., Varun, and S.K. Singal, *Review of mathematical modeling on latent heat thermal energy storage systems using phase-change material*. Renewable and Sustainable Energy Reviews, 2008. **12**(4): p. 999-1031.
109. Fluent, *Chapter 21. Modeling Solidification and Melting*. 2001.
110. Shatikian, V., G. Ziskind, and R. Letan, *Numerical investigation of a PCM-based heat sink with internal fins*. International Journal of Heat and Mass Transfer, 2005. **48**(17): p. 3689-3706.
111. IES and Monodraught Ltd, *IES Modelling Procedure for the COOL-PHASE(r) low energy cooling and ventilation system Performance Component*. 2013.
112. Ibáñez, M., et al., *An approach to the simulation of PCMs in building applications using TRNSYS*. Applied Thermal Engineering, 2005. **25**(11-12): p. 1796-1807.
113. Tindale, A., *Programming Phase Change Materials for Energy Plus*, T.R. Whiffen, Editor. 2013.
114. Design Builder, *Design Builder Design Guide*. 2013.
115. Qiu, L., M. Yan, and Z. Tan. *Numerical Simulation and Analysis Of PCM on Phase Change Process Consider Natural Convection Influence*. in *Proceedings of the 2012 International Conference on Computer Application and System Modeling*. 2012. Atlantis Press.
116. Kim, J.S. and K. Darkwa, *Simulation of an integrated PCM–wallboard system*. International Journal of Energy Research, 2003. **27**(3): p. 215-223.
117. Athienitis, A.K., et al., *Investigation of the thermal performance of a passive solar test-room with wall latent heat storage*. Building and Environment, 1997. **32**(5): p. 405-410.
118. Darkwa, K. and P.W. O’Callaghan, *Simulation of phase change drywalls in a passive solar building*. Applied Thermal Engineering, 2006. **26**(8–9): p. 853-858.
119. Gowreesunker, B., S. Tassou, and M. Kolokotroni, *Coupled TRNSYS-CFD simulations evaluating the performance of PCM plate heat exchangers in an airport terminal building displacement conditioning system*. Building and Environment, 2013. **65**: p. 132-145.
120. Gatzka, B. and G. Valentin, *PCMEXPRESS - PLANNING AND SIMULATION PROGRAMME FOR THE USE OF PHASE CHANGE MATERIALS (PCM) IN BUILDINGS: DEMONSTRATING ITS USE IN RESIDENTIAL AND OFFICE BUILDINGS IN IRELAND*. 2011.
121. Oyeleke, J., *Controlled Tests and Modelling of a Semi-Active PCM Cooling System*, in *People and Buildings*. 2011, Network for Comfort and Energy Use in Buildings: Arup UK.
122. Heim, D. and J.A. Clarke, *Numerical modelling and thermal simulation of PCM–gypsum composites with ESP-r*. Energy and Buildings, 2004. **36**(8): p. 795-805.
123. Tetlow, D., Y. Su, and S.B. Riffat. *EnergyPlus simulation analysis of incorporating microencapsulated PCMs (Phase Change Materials) with internal wall insulation (IWI) for hard-to-treat (HTT) houses in the UK*. in *10th International Conference on Sustainable Energy Technologies, Istanbul, Turkey*. 2011.
124. BASF, *Reducing CO2 in Buildings, Energy Efficient Whitehall*. 2011.
125. Menassa, C.C., *Evaluating sustainable retrofits in existing buildings under uncertainty*. Energy and Buildings, 2011. **43**(12): p. 3576-3583.
126. Alanne, K. and J. Paatero. *Seasonal Heat Storages and residential micro-generation*. in *Proceedings of the 1st International Conference on Micro-Generation and Application, Ottawa Canada*. 2008.
127. Ure, Z., *PCM/13/05/025/ZU, Re: Product Cost Request*, T.R. Whiffen, Editor. 2013.
128. Whiffen, T.R., *Cost Comparison Chart*. 2014.
129. Heier, J., C. Bales, and V. Martin, *Combining thermal energy storage with buildings – a review*. Renewable and Sustainable Energy Reviews, 2015. **42**(0): p. 1305-1325.

130. Shaw, M.R., K.W. Treadaway, and S.T.P. Willis, *Effective use of building mass*. Renewable Energy, 1994. **5**(5–8): p. 1028-1038.
131. Rijkssen, D., C. Wisse, and A. Van Schijndel, *Reducing peak requirements for cooling by using thermally activated building systems*. Energy and Buildings, 2010. **42**(3): p. 298-304.
132. Monodraught Ltd, *Cool-Phase Natural Cooling and Low Energy Ventilation System*. 2014.
133. Actimass, *Water Cooled Hollow Core Control Strategy*, in *Slab Control - Combined System*. 2013 Revision.
134. IES, *Actimass Simulation Training*, T.R. Whiffen and G. Russell-Smith, Editors. 2014.
135. Walker, C., *Methodology for the evaluation of natural ventilation in buildings using a reduced-scale air model*. 2006, Massachusetts Institute of Technology.
136. Russell-Smith, G., *Data Inputs for Accredited Thermal Modelling*, T.R. Whiffen, Editor.
137. Russell-Smith, G., *Water Based Slab Calcs*. 2009.
138. Ghatti, V. and S.M. Autif, *STUDY OF CONVECTIVE HEAT TRANSFER IN A RADIATIVELY COOLED BUILDING USING COMPUTATIONAL FLUID DYNAMICS*, in *American Solar Energy Society Conference*. 2002, Solar 2002
139. UK Office Direct Ltd. *Air Conditioner Size Calculator*. 2002 [cited 2012; Available from: http://www.ukofficedirect.co.uk/calculating_what_air_conditioner_cp.aspx].
140. CIBSE, *Environmental Design CIBSE Guide A*. 7th Edition ed. CIBSE GUIDE. 2006: Chartered Institution of Building Services Engineers.
141. Renewable Heat Incentive. *Renewable Synergy UFH Calculator Manual*. 2012 [18th Septemer 2012]; Available from: http://www.renewable-heat-incentive.com/rs_red/pdf/Renewable%20Synergy%20UFH%20calculator%20manual.pdf.
142. Demanuele, C., et al., *Using localised weather files to assess overheating in naturally ventilated offices within London's urban heat island*. Building Services Engineering Research and Technology, 2012. **33**(4): p. 351-369.
143. BSRIA, *2013 The BSRIA Blue Book*, A. Eastwell, Editor. 2012.
144. Whiffen, T.R., *Air Speed Tests*, a.s. tests.xlsx, Editor. 2012.
145. Celotex, *The Celotex Handy Guide*. 2014.
146. Butcher, K.J., *CIBSE Guide B - Heating, Ventilating, Air Conditioning and Refrigeration*. 2005, CIBSE.
147. Whiffen, T.R., *Water Pump Speed Test Data*, w.p.s.t. data.xlsx, Editor. 2012.
148. Whiffen, T.R., *Heat Loss Calculations*, q.p.c.p.c.a.h.l.r. 1h40.xlsx, Editor. 2013.
149. DECLG, *National Calculation Methodology (NCM) modelling guide (for buildings other than dwellings in England and Wales)*, Department of Communities and Local Government, Editor. 2008.
150. Monodraught Ltd, *Cool-Phase: Low energy cooling and ventilation system*. 2014.
151. Russell-Smith, G., *Project Review Meeting* T.R. Whiffen, Editor. 2014: Nottingham.
152. Gems, *Operating & Installation Instructions*, G.S.a. Controls, Editor.
153. Insulation Shop. *100mm Celotex GA4000 Characteristics*. 2014; Available from: http://www.insulationshop.co/100mm_celotex_ga4000_pir_insulation.html.
154. Miriel, J., L. Serres, and A. Trombe, *Radiant ceiling panel heating-cooling systems: Experimental and simulated study of the performances, thermal comfort and energy consumptions*. Applied Thermal Engineering, 2002. **22**(16): p. 1861-1873.
155. Littlewood, J., *Prototype Slab*. 2012.
156. Engineering Toolbox. *Absolute Roughness - k - for some common materials*. 2014; Available from: http://www.engineeringtoolbox.com/surface-roughness-ventilation-ducts-d_209.html.

157. Dounis, A.I. and C. Caraiscos, *Advanced control systems engineering for energy and comfort management in a building environment—A review*. Renewable and Sustainable Energy Reviews, 2009. **13**(6–7): p. 1246-1261.
158. BSRIA, *2015 The BSRIA Blue Book*, A. Eastwell, Editor. 2015.
159. Butcher, K.J., *CIBSE Guide A - Environmental Design (7th Edition)*. 2006, CIBSE.
160. Inc., F., *Inputs at Wall Boundaries*. 2006.
161. Fluent Inc., *Ansys Fluent Help, 12.4.1 Standard k-e Model*. 2006.
162. Fluent Inc., *Ansys Fluent Help, 13.2.1 Heat Transfer Theory*. 2006.
163. Fluent Inc., *Ansys Fluent Help, 13.3.3 P-1 Radiation Model Theory*. 2006.
164. Fluent Inc., ed. *Effects of Buoyancy on Turbulence in the k-e models*. 2006.
165. Whiffen, T.R. and S.B. Riffat, *A review of PCM technology for thermal energy storage in the built environment: Part II*. International Journal of Low-Carbon Technologies, 2012.
166. Pomianowski, M., P. Heiselberg, and R.L. Jensen, *Full-scale investigation of the dynamic heat storage of concrete decks with PCM and enhanced heat transfer surface area*. Energy and Buildings, 2013. **59**(0): p. 287-300.
167. Lazaro, A., et al., *PCM-air heat exchangers for free-cooling applications in buildings: Experimental results of two real-scale prototypes*. Energy Conversion and Management, 2009. **50**(3): p. 439-443.
168. Levermore, G., *Building control systems—CIBSE guide H*. 2000, Butterworth-Heinemann Oxford, UK.
169. Ren, M., et al. *Meeting the current and future UK challenges for sustainable building designs—Case studies*. in *Building Simulation*. 2007.
170. Dupont™, *Data Sheet - Measured Properties*, dupont_energain_datasheet.pdf, Editor. 2007.
171. Turnpenny, J.R., D.W. Etheridge, and D.A. Reay, *Novel ventilation cooling system for reducing air conditioning in buildings.: Part I: testing and theoretical modelling*. Applied Thermal Engineering, 2000. **20**(11): p. 1019-1037.
172. Etheridge, D., K. Murphy, and D. Reay, *A PCM/heat pipe cooling system for reducing air conditioning in buildings: review of options and report on field tests*. Building Services Engineering Research and Technology, 2006. **27**(1): p. 27-39.
173. Department of Energy and Climate Change, *UK Energy Statistics*, D.o.E.a.C. Change, Editor. 2014.
174. ElectricityInfo.org. *Fuel Mix of UK Domestic Electricity Suppliers*. 2015.
175. Energy Savings Trust, *Our Calculations*. 2013.
176. Dincer, I., *On thermal energy storage systems and applications in buildings*. Energy and Buildings, 2002. **34**(4): p. 377-388.
177. Habeebullah, B.A., *Economic feasibility of thermal energy storage systems*. Energy and Buildings, 2007. **39**(3): p. 355-363.
178. Henze, G., *Economic Analysis of Thermal Energy Storage Systems*. Journal of Architectural Engineering, 2002. **8**(4): p. 133-141.
179. Bolton, P., *Energy Prices*, H.o. Commons, Editor. 2014.
180. Heath, N., Clark, T., Pearson, G., *Green Deal Financial Modelling of a Traditional Cottage and Tenement Flat*, H. Scotland, Editor. 2012.
181. Monodraught Ltd, *Cool-Phase(r) Natural Cooling and Low Energy Ventilation System*. 2014.
182. Monodraught Ltd, *IES Modelling Procedure for the COOL-PHASE(r) low energy cooling and ventilation system Performance Component*, IES, Editor. 2013.
183. Business Energy. *Business Electricity - Contract and Pricing Information*. 2015 [25/03/2015].

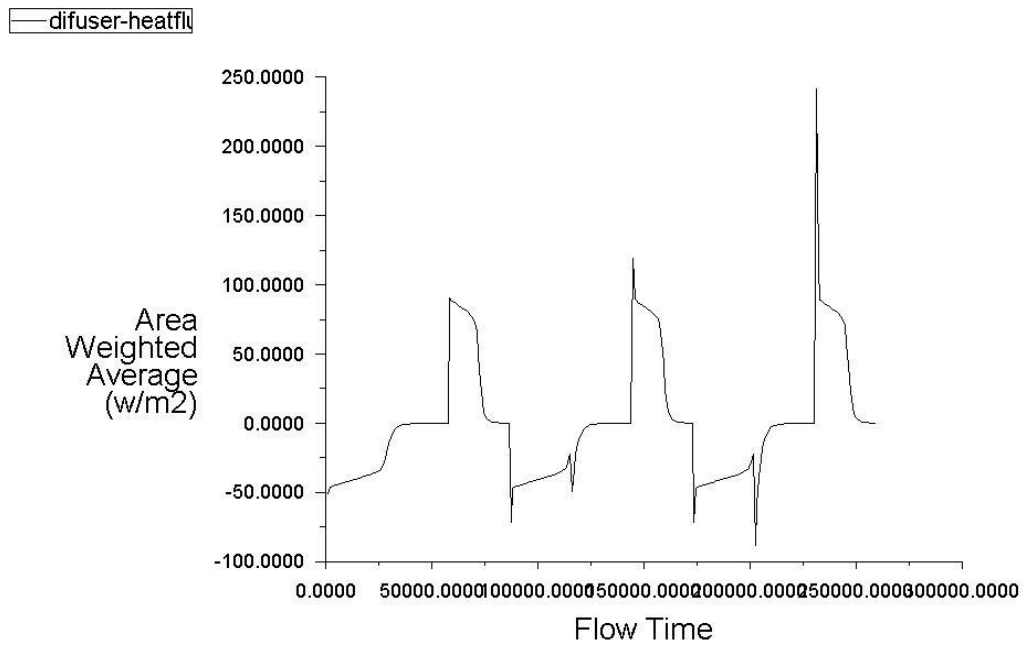
10 Appendix A

Theoretical 3-day Long simulation



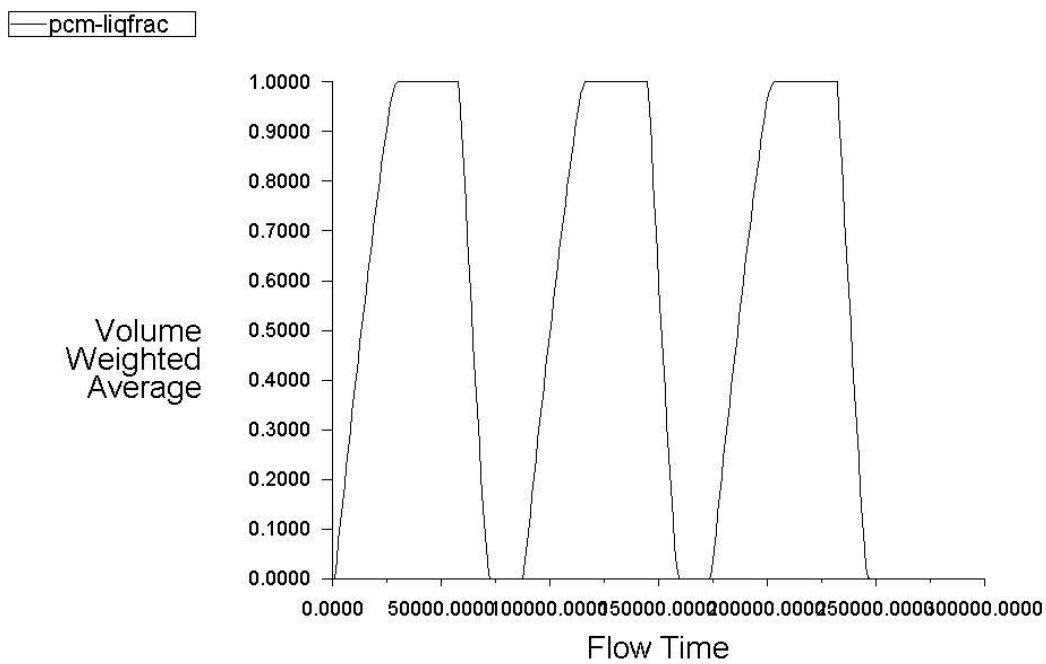
Convergence history of Static Temperature on b_2_-roomair (Time=2.5974e+05) Mar 13, 2014
ANSYS Fluent 14.5 (3d, pbns, skw, transient)

Figure 10.1 - 3day Air Temperature



Convergence history of Total Surface Heat Flux on interior-b_2_-caseupperlayer-b_2_-roomair etc. (Time=2.597261e+05) Mar 13, 2014
ANSYS Fluent 14.5 (3d, pbns, skw, transient)

Figure 110.2 - 3 Day Diffuser Heat Flux



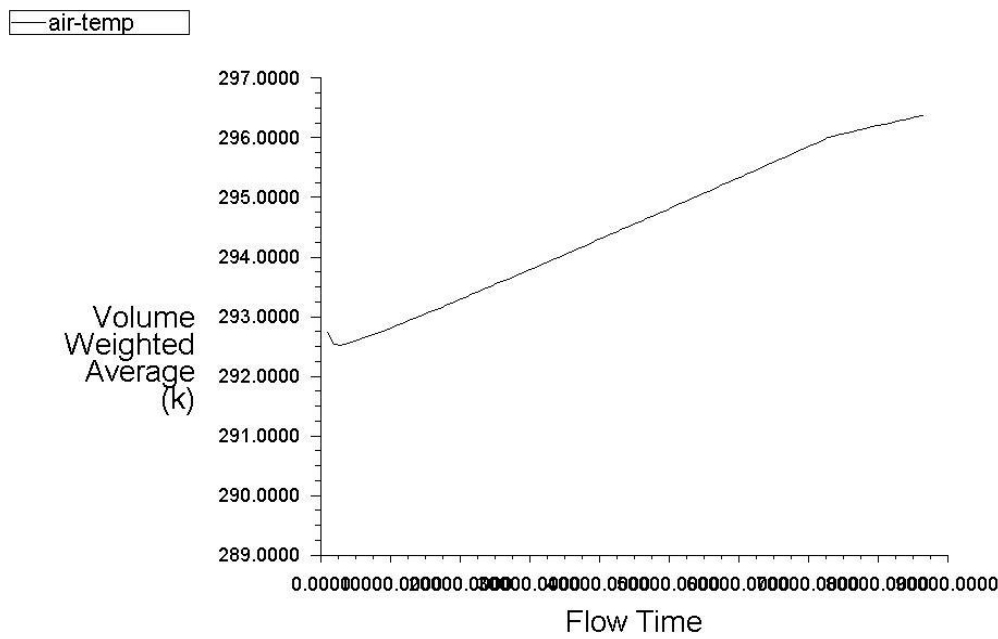
Convergence history of Liquid Fraction on b_2_-bottom_layerpcm etc. (Time=2.5974e+05) Mar 13, 2014
ANSYS Fluent 14.5 (3d, pbns, skw, transient)

Figure 10.3 - 3 day Liquid Fraction Monitor

All this revealed that the flow rate of air through the model was quick, so the air changes were really high, therefore a suitable flow rate was tested on the 4kg B(2) model.

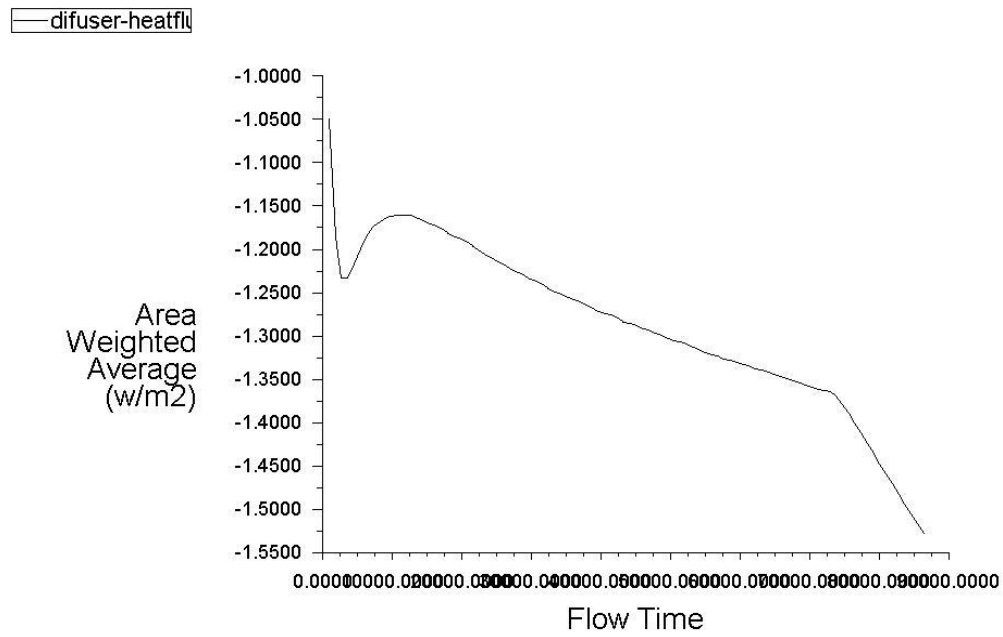
4acph B(2) Investigation

Due to the slower rates of air flow the heat flux is greatly reduced. Greater time given to the simulation would portray more of the benefits. It can be noted in the final 4hours the onset of melting and the utilisation of the Latent benefit is seen in a levelling off of the room temperature.

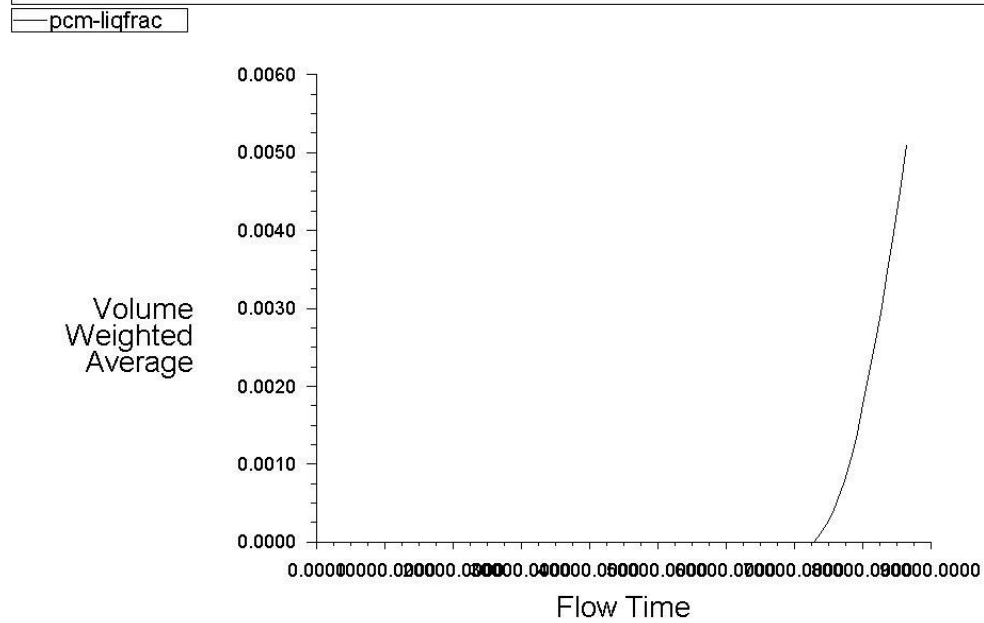


Convergence history of Static Temperature on b_2_-roomair (Time=8.6400e+04) Mar 21, 2014
 ANSYS Fluent 14.5 (3d, pbns, skw, transient)

Thermal mass enhancement for energy saving in UK offices



Convergence history of Total Surface Heat Flux on interior-b_2_-caselowerlayer-b_2_-roomair etc. (Time=8.6400e+04) Mar 21, 2014
ANSYS Fluent 14.5 (3d, pbns, skw, transient)



Convergence history of Liquid Fraction on b_2_-bottom_layerpcm etc. (Time=8.6400e+04) Mar 21, 2014
ANSYS Fluent 14.5 (3d, pbns, skw, transient)

11 Appendix B – Instrument Accuracy and Measurement Errors

Throughout the investigations reported in this work the instruments and measurement devices used have a limited degree of precision. Table 11.1 presents the accuracy of the instruments used throughout the investigations and the incurred measurement errors.

Table 11.1 - Instrument Accuracy

| Instrument | Suitability Range | Units | Sensitivity | Accuracy | Calibration |
|--|----------------------|-------|----------------|----------|---|
| K-type Thermocouple | -100 to +250°C | °C | 41µV/°C | ±1.5°C | Ice to boiling test conducted on reference thermocouple. All other thermocouples calibrated against the reference thermocouple. |
| Turbine Flow Sensor (Gems FT-110) | 1 to 10 l/min | Hz | 55Hz per l/min | ±3% | Flow rate calibrated against time taken to fill a one litre measuring cylinder. |
| Anemometer: Skywatch® Xplorer1 | 0.8 to 41.7 m/s | m/s | - | ±3% | Compared against measurements taken by alternative anemometers in university on same apparatus. |
| Energenie Power Meter | 0.1 to 3120 W | W | - | ±2% | - |
| | 200 to 276 V | V | - | ±1.5% | |
| | 0.005 to 13 A | A | - | ±2% | |
| | 45 to 65 Hz | Hz | - | - | |